NASA
Technical
Paper
2287

March 1984

Topics in the Optimization of Millimeter-Wave Mixers

Peter H. Siegel,
Anthony R. Kerr,
and Wei Hwang

NASA
Technical
Paper
2287

1984

Topics in the Optimization of Millimeter-Wave Mixers

Peter H. Siegel
Goddard Institute for Space Studies
New York, New York
and
Columbia University
New York, New York

Anthony R. Kerr
Goddard Institute for Space Studies
New York, New York

Wei Hwang
Columbia University
New York, New York

National Aeronautics
and Space Administration

Scientific and Technical
Information Branch

CONTENTS

CONTENTS

CONTENTS

CONTENTS

CONTENTS

CONTENTS

CONTENTS

CONTENTS

CHAPTER 1. INTRODUCTION

1.1 Research Objectives and Thesis Outline

The primary objective of this research is to gain a better understanding of the factors affecting the performance of room temperature single ended Schottky diode mixers operating above 100 GHz. The project is specifically aimed at the analysis and subsequent optimization of an existing mixer design [89] whose nominal operating frequency range is 140-220 GHz.

At the time this thesis was begun only one accurate analytical study of mixer performance had ever been performed above 100 GHz. This study, by Held and Kerr [63], cleared up many of the problems which had plagued earlier analyses and in the end the authors were able to predict, fairly accurately, the performance of an existing Schottky diode mixer operating at 115 GHz.

Even at 115 GHz however, questions had arisen regarding the accuracy of the diode equivalent circuit and the exact nature of the noise generation process. It was natural to ask whether or not the Held and Kerr analysis could be applied to a higher frequency mixer.

Above 100 GHz, reported mixer performance varies widely from laboratory to laboratory (and in fact there is a considerable difference in performance amongst devices produced in the same laboratory using diodes fabricated on the same semiconductor wafer). The reasons for these differences have never been adequately explained. In addition few guidelines exist to aid researchers in their efforts to produce better mixer diodes, nor is there any clear understanding of the relationships between mixer performance and the diode mounting circuit at these frequencies. The desire to solve some of these problems and to extend the work of Held and Kerr [63] were the motivating factors for this thesis.

As in any research project of this size several related topics were also investigated. These include:

(1). The development of a flexible computer program for the analysis of microwave and millimeter-wave mixers which would serve as the main analytical tool for this thesis.

(2). The development of a semi-automated microwave network analyzer to be used for making accurate low frequency measurements to characterize a particular mixer block design.

(3). The development of an improved procedure for measuring mixer performance in the millimeter-wave band which, unlike most previous methods, differentiates between the response at the upper and lower sidebands.

(4). The development of a varactor diode frequency doubler for the 140-220 GHz waveguide band to facilitate the measurements of mixer performance.

(5). The development of a computer program for the analysis of millimeter-wave varactor diode frequency multipliers.

(6). The development of a new type of rectangular waveguide transformer which can be used in place of conventional electroformed varieties greatly reducing the fabrication time for both mixers and multipliers.

Finally, although Schottky diode mixers have been in existence for twenty years no definitive set of design criteria has yet been established. It is hoped that the results presented in this thesis will at least lay the groundwork for the attainment of this most important goal.

The main body of this thesis is divided into six chapters. The topics covered can be briefly summarized as follows:

Chapter 2 describes the essential mixer theory, and the computer program for mixer analysis, on which the rest of this thesis is based.

Chapter 3 describes the measurement techniques used to characterize the mixer block (diode mount) over a wide (6 octave) frequency range. Such a characterization is necessary for an accurate analysis. The measured mount impedances of a 140-220 GHz mixer are given as a function of backshort position over the frequency range 140-1320 GHz.

Chapter 4 outlines an improved procedure for measuring mixer performance in the millimeter-wave band. Measurements of the noise temperature, conversion loss and IF output VSWR of the 140-220 GHz mixer are compared with the values predicted using the mixer analysis program described in Chapter 2.

Chapter 5 investigates the dependence of millimeter-wave mixer performance on the diode and mount characteristics. Extensive analysis of the 140-220 GHz mixer is performed, using the computer program of Chapter 2, in order to derive some guidelines for the optimization of the mixer diode and mounting structure.

Chapter 6 addresses the problem of obtaining swept frequency sources of power in the millimeter-wave region.

A flexible computer program for the analysis of varactor frequency multipliers, based on the mixer analysis program of Chapter 2, is described. The program can be used to predict the performance of frequency multipliers once the circuit and diode characteristics are known. The design of a high efficiency solid state frequency doubler for the 140-220 GHz band is also presented. When coupled with a lower frequency oscillator enough power is generated to drive the 140-220 GHz mixer.

Chapter 7 introduces a new type of rectangular waveguide transformer which greatly reduces the fabrication time required for millimeter-wave mixers and frequency multipliers. A theoretical analysis of the transformer is undertaken and design curves are presented.

The appendices contain computer program listings and specific computations which supplement the material in the chapters.

In the next section we will take a brief historical look at the origins of the modern day mixer and survey the state of the art in Schottky diode mixers for the 100 to 300 GHz range.

1.2 An Historical Introduction to Mixers

1.2.1 The Origin of the Superheterodyne Detector

More than 80 years have passed since R.A. Fessenden [48,69,70], while general manager of the National Electric Signaling Company in 1902, patented the principles of the heterodyne receiver. At that time the heterodyne action (literally, the "other force", indicating that energy was obtained from a source other than the incoming signal) was employed to convert an incoming radio frequency (RF) signal directly into the audio band. The received signal induced a current to flow in the coil of an antenna. A locally produced current having a slightly different frequency (local oscillator or LO) was then combined with the signal current using a transformer and the resulting beat frequency (intermediate frequency or IF) was used to drive a diaphragm. The diaphragm played the role of the nonlinear element, responding to the square of the applied current when the IF was in the audio band.

It was not long before E.H. Armstrong [7,8], working at Columbia University, described the now familiar concept of superheterodyning (derived from supersonic heterodyne) in which the beat frequency produced by the signal and LO was fixed above the audio band. Here it was amplified, demodulated amplified again and finally applied to the audio membrane. In the 1920's the nonlinear frequency converting element was a vacuum triode tube. Superheterodyning had the advantage of eliminating the audio frequency interference associated with atmospherics which greatly increased the receiver sensitivity. Actually, the concept of superheterodyning was first mentioned in a discussion at the end of a paper by J.L. Hogan [70] of National Electric, in 1913. It was also, according to W. Schottky [145], contained in two patents preceding that of Armstrong, one by L. Levy in 1917 and the other by W. Schottky himself working at the Siemens Laboratory in Germany in June 1918.

1.2.2 The Crystal Mixer

Although the principle of the superheterodyne receiver was employed extensively in the 1920's, the term "mixer" did not come into popular use until the mid 1930's, after the advent of the pentagrid converter valve [117,123,156]. This tube, for operation in the megahertz range, contained a local oscillator grid and a separate grid for the injection of the signal. When the LO was housed separately the vacuum tube in which the signal was superposed was generally known as a mixer tube.

In the push towards higher frequencies transit time effects between the vacuum tube grids imposed severe restrictions on the use of these components as mixer elements. At 3 GHz, even the best tubes were extremely noisy, having noise temperatures more than a hundred times higher than present day mixers at the same frequency [129]. During World War II a tremendous effort was made to find alternate mixer elements and the crystal rectifier became the central figure in the quest. Before the war, mixers using crystal rectifiers had very nearly the same noise temperatures as triode or pentagrid converter tubes, but by 1945 this figure had dropped by more than an order of magnitude even at 30 GHz, a frequency ten times higher than that of the old vacuum tube devices [129]. The best mixers at this time contained point contact diodes which consisted of a thin tungsten wire, or "whisker", which made a pressure contact with a boron-doped silicon crystal [165]. The point contact crystal rectifier replaced the vacuum tube in almost all microwave receivers, and over the next decade was pushed well into the millimeter-wave band.

1.2.3 Point Contact Mixers in the 100-300 GHz Range

Although H.C. Whitby, working at the Telecommunications Research Establishment, built a superheterodyne receiver in the millimeter-wave band in 1945 [174], it was some time before the 100 GHz mark was passed. The earliest published results of which the author is aware for a superheterodyne receiver operating above 100 GHz were reported in 1954 by C.M. Johnson [75] at the Radiation Laboratory of Johns Hopkins University. Using silicon diodes with tungsten point contacts, Johnson was able to obtain third, fourth, and fifth harmonic mixing with a 31 GHz klystron. However, at 124 GHz he measured single sideband mixer noise temperatures in excess of two million degrees and a best conversion loss of 19 dB.

In the early 1960's klystrons and traveling wave tubes operating above 100 GHz became commercially available [29] and spurred the development of fundamental mixers in this region of the spectrum. In 1963, R. Meredith and F.L. Warner [110] at Britain's Royal Radar Establishment produced a 140 GHz mixer with a germanium-titanium point contact diode using a carcinotron as the local oscillator. Their best reported single sideband mixer noise temperature was approximately 10,000 K with a corresponding conversion loss of 12.3 dB.

By 1958, both D.A. Jenny [74] working at RCA laboratories and G.C. Messenger [111] of Philco Corporation had recognized the superior high frequency characteristics of the type III-V semiconductors, namely gallium arsenide, over silicon and germanium. The first use of the new compound semiconductor above 100 GHz was probably in 1963 by M. Cohn, F.L. Wentworth and J.C. Wiltse [27] at the Advanced Technology Corporation (ADTECH). For a 140 GHz second harmonic mixer with a GaAs point contact diode, they reported a single sideband noise temperature of 37,000 K with 15 dB of conversion loss. In 1966, when R.J. Bauer, M. Cohn, J.M. Cotton and R.F. Packard [12] summarized the work at ADTECH on millimeter-wave detectors from 70-420 GHz, GaAs was firmly established as the most appropriate semiconductor for use in high frequency mixer diodes. Bauer achieved conversion losses below 6 dB with a 146 GHz fundamental mixer using a GaAs point contact diode, unfortunately however, he quotes no noise temperature data at this frequency. Some results from a 1.4 millimeter (210 GHz) receiver using second harmonic mixing were reported four years later by W.A. Johnson, T.T. Mori and F.I. Shimabukuro [79] at the Aerospace Corporation. Using a highly doped GaAs point contact diode with a gold-copper alloy whisker, Johnson measured a conversion loss of 22 dB. At 94 GHz these same diodes yielded a best conversion loss of 5.7 dB in a fundamental mixer constructed by M. McColl, M.F. Millea, J. Munushian and D.F. Kyser [108] also at Aerospace.

Most of the high frequency mixers at this time used sharply pointed phosphor bronze whiskers making point contact diodes with the semiconductor crystal. Generally, after contact, a forward voltage was applied to the diode, heating the area in the vicinity of the point and forming a weld. What is actually believed to have happened is that copper atoms from the phosphor bronze whisker diffused into the n-type GaAs. Since copper is an acceptor in GaAs, a sort of hybrid metal-semiconductor p-n junction was formed [18]. These diodes were usually mounted in a permanent structure developed by W.M. Sharpless [146] of Bell Telephone Laboratories (BTL) in 1956 and known as the Sharpless wafer. The wafer contained a coaxial low pass filter to prevent the RF energy from being coupled into the IF and DC bias circuits, and was mounted across a waveguide whose nominal height was reduced for better matching of the signal to the diode. A tuning plunger in the reduced height waveguide served to resonate out the capacitance of the diode and the inductance of the wafer mount so as to improve the RF matching to the diode. Despite the progress which had been made in the years since the first point contact devices [108,146-148] they still had serious stability and reproducibility problems.

1.2.4 The GaAs Schottky Diode Mixer

Although the theoretical behavior of the Schottky barrier diode had been generally understood 25 years earlier, no one had succeeded in producing a device which realized the ideal junction characteristics. With the development of a high vacuum metal film deposition technology, due largely to the work of R.J. Archer and M.M. Atalla [6] of Bell Telephone Laboratories (BTL) in 1963, most of the fabrication problems inherent in the point contact diode were overcome. In the microwave band, the most significant advancement came in 1965 when D.T. Young and J.C. Irvin [184] also of BTL, produced the first "honeycomb" diode. Instead of a single point contact, a planar array of diodes with micron sized anodes was produced using photolithography. These new Schottky barrier diodes were put to immediate use at the longer millimeter wavelengths (30-60 GHz) [23,26,37,38,98,158] but no results were reported for receivers above 100 GHz until the early 1970's.

By 1972 there were at least three millimeter-wave astronomy antennas capable of operating above 100 GHz in the United States; a 15 foot dish at the Aerospace Corporation, the University of Texas at Austin's 5 meter telescope, and the 36 foot antenna operated by the National Radio Astronomy Observatory (NRAO) at Kitt Peak [126]. Low noise broadband receivers were made for these instruments by groups at NRAO, Bell Telephone Laboratories (BTL) and Aerospace. Both the BTL and NRAO receivers contained GaAs Schottky barrier diodes with Sharpless wafer type mounts. The diodes were developed largely by C.A. Burrus [18] at BTL who was able to obtain 2 micron diameter junctions using standard photolithographic techniques. The resulting mixers had conversion losses in the neighborhood of 7 dB [19] and typical single sideband mixer noise temperatures between 1000 and 2000 degrees at 110 GHz [101]. The Aerospace mixers also contained GaAs Schottky barrier diodes although the noise temperatures at this time were considerably higher than the NRAO and BTL designs [180]. There was however, at least one mixer at Aerospace in 1972, containing a Mott barrier diode, that had a single sideband mixer noise temperature of 950 K at 110 GHz [109]. One other group which included B.J. Clifton and others at the MIT Lincoln Laboratory, had started to make GaAs Schottky barrier diodes in the early 1970's. Although they eventually produced some excellent image enhanced mixers in the 40-60 GHz band [24], most of their work above 100 GHz was centered in the submillimeter region of the spectrum.

By 1973, R.J. Mattauch at the University of Virginia, having improved upon the early BTL technology, was producing millimeter-wave GaAs Schottky barrier diodes for NRAO. It was at this time that various groups began to attain the low noise temperatures which had been predicted for the Schottky diode mixers. S. Weinreb and A.R. Kerr [176] at NRAO, made the first measurements on cooled mixers in the millimeter-wave band. Cooling to 18 K and using 5 micron diameter diodes made by R.J.Mattauch, they reported a best single sideband noise temperature of 280 K and 7.2 dB conversion loss at 85 GHz. At room temperature with an LO of 115 GHz and using a 3 micron diode, they obtained noise temperatures near 600 K and losses approaching 6 dB [87].

In 1974, G.T. Wrixon [182] at BTL, reported using conventional and electron beam lithography to produce low capacitance diodes for mixers in the 140-230 GHz range. For a 230 GHz mixer design he drew upon integrated circuit technology and mounted the whiskers on a quartz stripline filter which partially extended into the input waveguide for coupling to the RF signal. The diode chip was screwed in through a hole in the opposite wall of the waveguide in the contacting procedure. Wrixon obtained a best single sideband noise temperature of approximately 10,000 K (using his noise figure data) at 230 GHz with the new mount. For two other mixers, both of which used conventional Sharpless wafer mounts, he measured single sideband noise temperatures of 3500 K and 1100 K at 175 and 140 GHz respectively.

In 1975, A.R. Kerr [82], at the NASA Goddard Institute for Space Studies, reported single sideband noise temperatures of 500 K and conversion losses of 5.5 dB for a 115 GHz mixer with a 2.5 micron University of Virginia (U.Va.) diode made by R.J. Mattauch. Kerr also replaced the Sharpless wafer mount with a more sophisticated quartz stripline structure. The diode chip was mounted on one piece of quartz and the whisker on another. The two were slid together and glued in place on a third longer quartz strip after contact had been made. The whole structure was then mounted across a 4:1 reduced height waveguide. The extra rigidity allowed cooling of the mixer to 15 K where the noise temperature dropped to 300 degrees at 115 GHz.

By 1977, many groups were reporting impressive results with similar mixer mounting configurations. W.J. Wilson [179] at Aerospace, using a 2.5 micron U.Va. diode, produced a mixer with a 700 K single sideband noise temperature and 6.2 dB of conversion loss at 115 GHz. A month later A.R. Kerr, R.J. Mattauch and J.A. Grange [89] reported a new mixer design for the 140-220 GHz band. The more complicated three piece quartz mount was replaced by a simpler structure. In this design, the diode chip was mounted on a quartz stripline filter and the whisker on a ground steel post. The post was gold plated, pressed into the mixer block, and advanced towards the diode by a differential micrometer for contacting. The whisker hung across a 4:1 reduced height waveguide, which was asymmetrically split along the E-plane. The entire contacting procedure was monitored both optically and with a capacitance bridge. Using diodes made at U.Va., Kerr measured single sideband noise temperatures near 1000 K and a conversion loss of 6.2 dB at 170 GHz. Finally, in September of 1977, P. Zimmermann and R.W. Haas [185] of the Max Planck Institute in West Germany, published data on a 106-116 GHz mixer containing a 2 micron diode, made by G. Wrixon. They reported a noise temperature of 600 K and 6.2 dB of conversion loss at 107 GHz.

Since 1977 there have been improvements in both diode quality and mixer mount construction. Smaller diodes with lower capacitance and series resistance have been fabricated and have led to better high frequency performance. At Bell Telephone Laboratories R.A. Linke, M.V. Schneider and A.Y. Cho [102] have used molecular beam epitaxy to produce mixer diodes with very accurately controlled doping profiles. There have also been some significant advances made in the design and production of high efficiency frequency multipliers which can now provide milliwatts of power in the 200-300 GHz band. This has stimulated further work on Schottky diode mixers and has resulted in devices with successively lower noise temperatures.

There are now many laboratories making Schottky diode mixers in the 100-300 GHz region. At the time of writing, the best room temperature results which have been reported for a Schottky diode mixer above 100 GHz have come from the group at NASA GISS [30]. They built a mixer, using

U.Va. 2.5 micron diodes, which had a single sideband noise temperature of 440 K and a conversion loss of 5.3 dB at 115 GHZ. To my knowledge, the absolute lowest noise temperature which has yet been reported for a Schottky diode mixer at this same frequency, is 70 K. This result was obtained by A.V. Raisanen, N.R. Erickson, J.L.R. Marrero, P.F. Goldsmith and C.R. Predmore [131] at the University of Massachusetts Five College Radio Astronomy Observatory (FCRAO) for a mixer cooled to 18 K.

At 150 GHz the mixer analyzed in this thesis (see Chapter 4) had a noise temperature of 500 K (SSB) and 5.7 dB conversion loss. At 180 GHz the noise temperature increased to 760 K with the same loss (the analysis in Chapter 5 indicates that the mixer performance is even better when the operating point is changed slightly).

Above 200 GHz the best results to date have been reported by J.W. Archer and R.J. Mattauch [5] at NRAO using a 1.5 micron diode and an improved RF backshort design. Archer measured a single sideband noise temperature of 770 K and 6.2 dB of conversion loss at 230 GHz for this room temperature mixer. Cooled to 20 K, the mixer noise temperature dropped to 300 degrees and the conversion loss to 5.9 dB.

In the 300 GHz range N.R. Erickson [44] at FCRAO has obtained single sideband noise temperatures under 3000 K and conversion losses between 8.5 and 9 dB in a room temperature mixer. When cooled to 20 K, the noise temperature of this mixer fell to under 1000 degrees [45]. Results from many other laboratories can be found in Figs.1-1 and 1-2.

We have now reached the point where, by experience, we can obtain near optimum performance from Schottky diode mixers in the millimeter-wave band. However, even at 100 GHz the reported mixer performance varies widely and the best results are usually not reproducible from one diode to another, even when mounted in the same block. It seems reasonable to assume that any further improvements must come out of a more thorough understanding of the device behavior and the subsequent optimization of the diode and mixer mount characteristics. Providing the tools to undertake such a task is one of the major goals of this work.

References

1 Raisanen et. al. [132]
2 Raisanen et. al. [131]
3 Zimmermann and Haas [185]
4 Cong et. al. [30]
5 Kerr [82]
6 Wilson [180]
7 Keen et. al [81]
8 Linke in ref. [20]
9 Kerr et. al. [89]
10 Siegel [this thesis]
11 Vizard et. al. [173]
12 Erickson in ref. [5]
13 Archer and Mattauch [5]
14 Wrixon [182]
15 Erickson [44]
16 Vizard in ref. [141]
17 Lidholm in ref. [141]
18 Frerking et. al. [51]
19 Lidholm and de Graauw [99]
20 Archer [3]

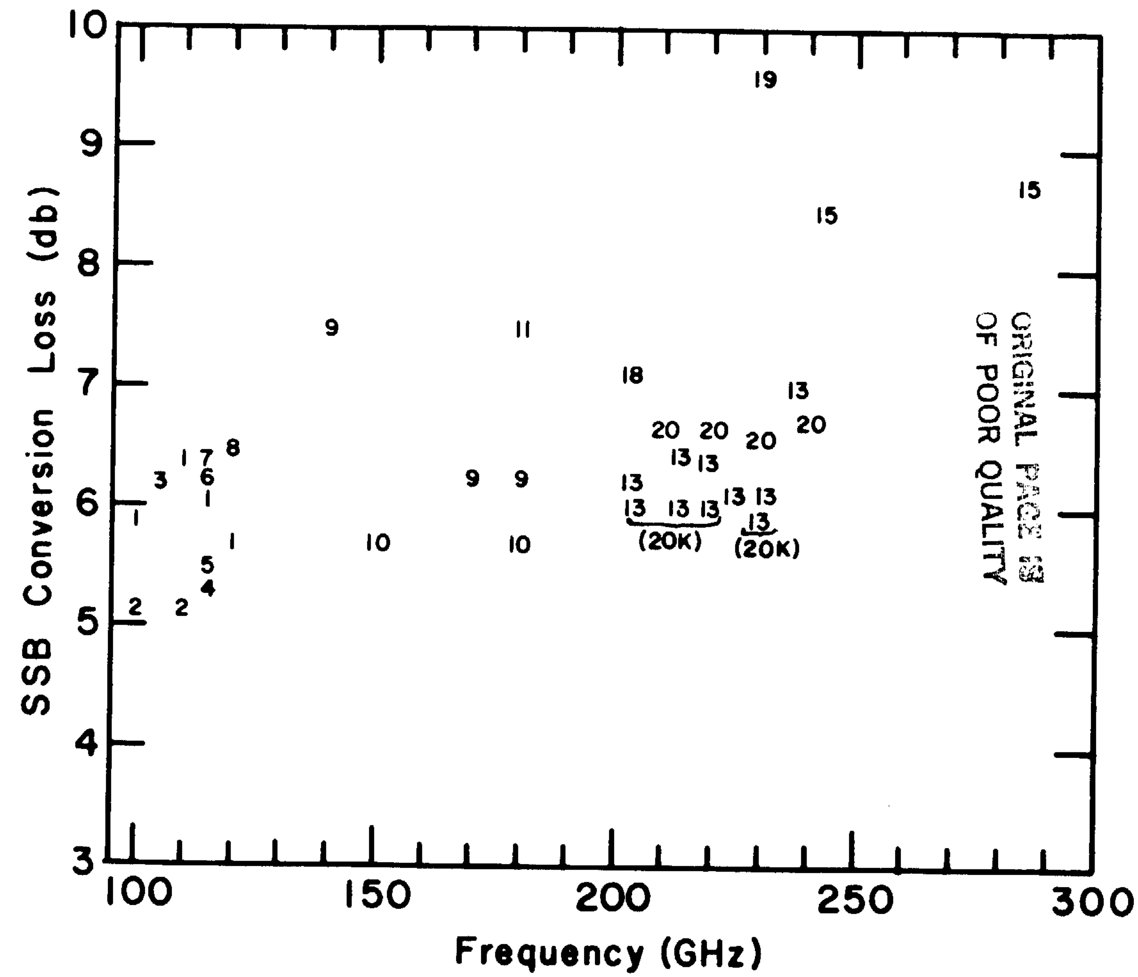

Fig. 1-1 Reported single sideband conversion losses of fundamental Schottky barrier diode mixers in the 100-300 GHz region. References for the plotted points appear in the list at the left. All results are for room temperature unless otherwise indicated.

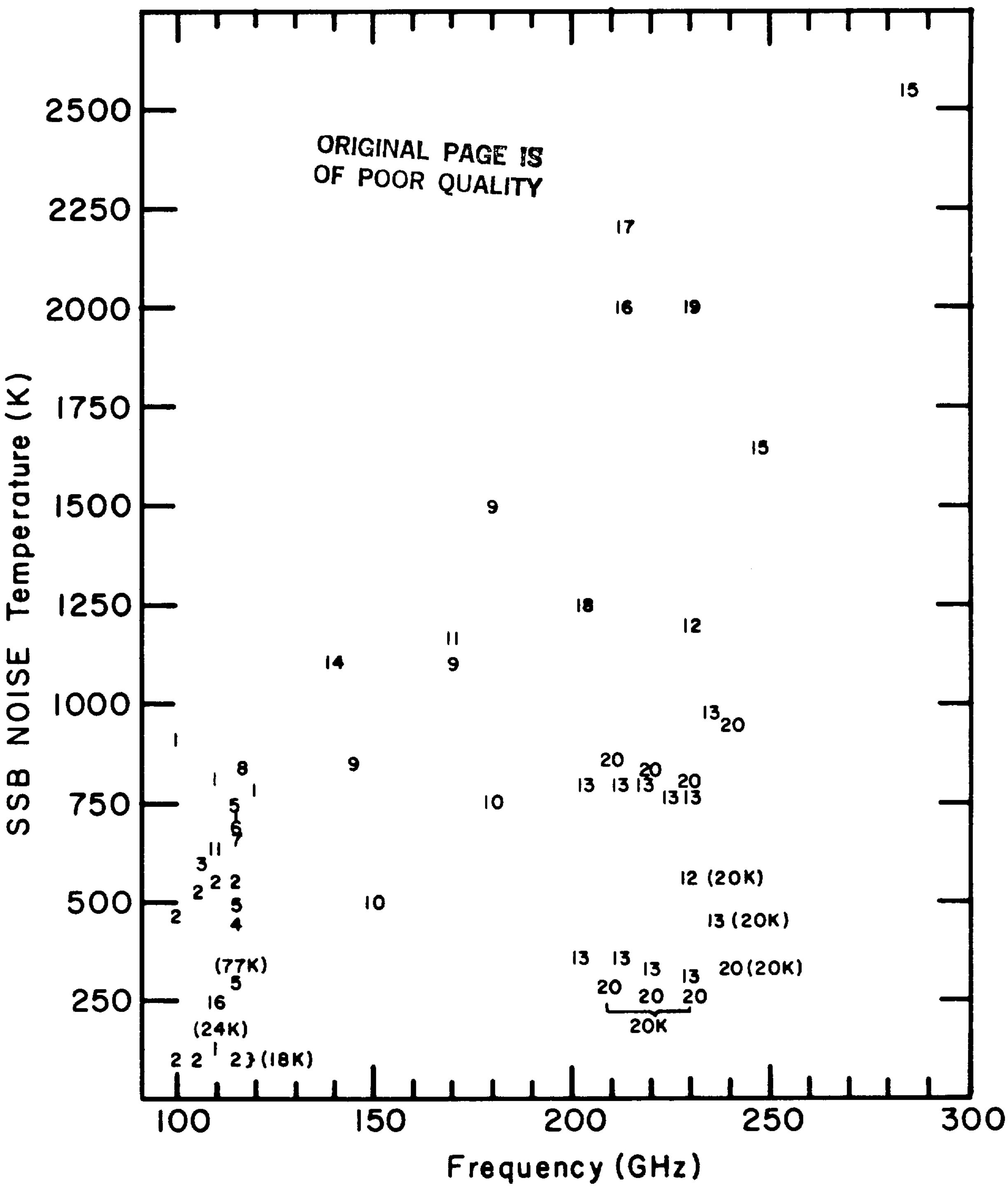

Fig. 1-2 Reported single sideband noise temperatures of fundamental Schottky barrier diode mixers in the 100-300 GHz region. References for the plotted points are given in the list in Fig. 1-1. All results are for room temperature unless otherwise indicated.

CHAPTER 2. MIXER THEORY AND ANALYSIS

2.1 Introduction

In this chapter we discuss the theory and analysis of room temperature single-ended Schottky diode mixers. A user oriented computer program is described which will perform a complete large and small signal analysis on a mixer with known diode and mount characteristics. Examples illustrating the use of the computer program are given, including a study of the effects of the series inductance and diode capacitance on the performance of some simple mixers. The program is an essential part of the mixer optimization process described in this thesis.

The mixer theory is presented in a form similar to that of Held and Kerr [63]. First, the large signal voltage and current waveforms produced in the diode by the local oscillator are determined using a nonlinear circuit analysis. The Fourier series coefficients of these waveforms are then used in a linear small signal analysis to obtain the mixer input and output impedances and the conversion losses between the mixer ports. Finally, the down converted thermal and shot noise components produced in the diode are determined and an equivalent input noise temperature for the mixer is derived.

A computer program which implements the mixer theory presented in this thesis has been described previously [151,152]. The nonlinear circuit analysis is based upon the multiple reflection technique of Kerr [83] and can handle a diode with any given I-V and C-V relationships. The diode series resistance is taken to be frequency dependent due to the skin effect but is considered independent of voltage. Arbitrary diode embedding impedances are allowed and although the diode mount is assumed lossless, it may have external loads connected at any number of sideband and LO harmonic frequencies. The large signal analysis produces the diode voltage and current waveforms and the available mixer LO power. The small signal analysis calculates the conversion loss between any pair of sideband frequencies and the mixer input and IF output impedances. The noise analysis determines both the thermal noise produced in the diode series resistance and the shot noise from the periodically pumped current in the diode conductance. The effects of intervalley scattering and hot electron noise can be included only as approximations.

To facilitate the use of the mixer analysis program the implementation of the Fortran code is described in detail and a number of examples are given. These include a study of the effects of the series inductance and diode capacitance on the performance of two simple mixer circuits containing (i) a conventional Schottky diode, (ii) a Schottky diode in which there is no capacitance variation and (iii) a Mott diode. A listing of the mixer analysis program and sample execution appear in Appendix 1.

2.2 Large Signal Analysis

2.2.1 Introduction

The most difficult step in analyzing a mixer is to determine the diode waveforms produced by the local oscillator. The procedure is complicated by both the highly nonlinear behavior of the diode and the distributed nature of the elements comprising the mixer mount.

One of the first attempts at solving the large signal problem is contained in the monograph by Torrey and Whitmer [165]. They obtained analytical solutions by assuming a sinusoidal voltage at the diode terminals, i.e. that no harmonic voltages were present beyond the local oscillator frequency. In their analyses, Torrey and Whitmer considered both a purely resistive diode and one represented by a nonlinear conductance shunted by a constant capacitance. The more complicated variable capacitance case was looked at qualitatively. Later investigators [13,40,103,112], dealt with the variable capacitance diode quantitatively, however they continued to make the simplifying assumption of a sinusoidal driving voltage.

Barber [10] pointed out the necessity for removing this waveshape constraint at the LO frequency but did not consider higher harmonics or varying capacitance in his analysis.

Fleri and Cohen [49] solved the large signal problem for a diode in a very simple lumped element embedding network. In their approach a numerical Runge-Kutta integration algorithm was used to solve the network state equations for the diode voltage and current. Gwarek [58] extended this method to allow more general embedding circuits. In his formulation the embedding network is represented as a simple lumped element circuit in series with a string of voltage sources, one at each harmonic of the local oscillator. The amplitudes and phases of these generators are adjusted to keep the apparent terminal impedance of the circuit equal to that of the actual embedding network. Although the scheme works well for many mixer circuits, it is strongly dependent on the guessed values of the lumped elements and does not converge for all embedding impedances.

Egami [41] used a harmonic balance technique to find the terminal voltage and current waveforms for a diode with a nonvarying capacitance. In his method the mixer equivalent circuit is separated into two parts, one containing the linear embedding network, and the other containing the nonlinear diode elements. The currents and voltages in each half are then matched or balanced at all the LO harmonic frequencies using an iterative procedure. Fourier analysis is used to shuttle between the time domain solution of the nonlinear diode network and the frequency domain solution of the linear embedding circuit. The method worked well with one or two LO harmonics, however convergence proved difficult when three or more harmonics were considered.

Recently, Hicks and Khan [65,66] have reported excellent results with a variation of the harmonic balance technique. Their method is a generalization of a procedure described by Gupta and Lomax [57]. A pair of dual algorithms is used to update the estimates of either the diode voltage or the diode current after each iteration. Convergence is reached when a stationary solution is obtained. The method requires the specification of a convergence parameter calculated from the properties of the embedding network and guessed values of the impedances of the nonlinear element at each harmonic frequency. The Hicks and Khan algorithms have been used successfully on a variety of nonlinear circuit problems.

The large signal analysis technique which is used in this thesis was developed by Kerr [83] and solves the nonlinear problem as a series of reflections between the diode and the embedding network. Like the harmonic balance methods, the algorithm operates in the time domain when considering the diode and in the frequency domain when dealing with the embedding network. Although this multiple reflection technique sometimes requires more computing time than either the methods of Gwarek [58] or Hicks and Khan [65,66], solutions have been obtained for all the mixer circuits which have been studied and no initial guesses are required.

2.2.2 Large Signal Equivalent Circuit

The large signal equivalent circuit of a Schottky diode mixer is shown in Fig.2-1. The embedding network is represented as a linear black box whose input impedances $Z_e(\omega)$ need be known only at the LO and its harmonic frequencies*. The diode junction is modelled in the usual way by a varying conductance $g(i_g)$ shunted by a voltage dependent capacitance $c(v_d)$. The series resistance $R_s(\omega)$ accounts for the resistance of the undepleted epitaxial

---

* In the small signal analysis we will require a knowledge of the embedding impedances at the sideband frequencies as well.

MIXER EQUIVALENT CIRCUIT

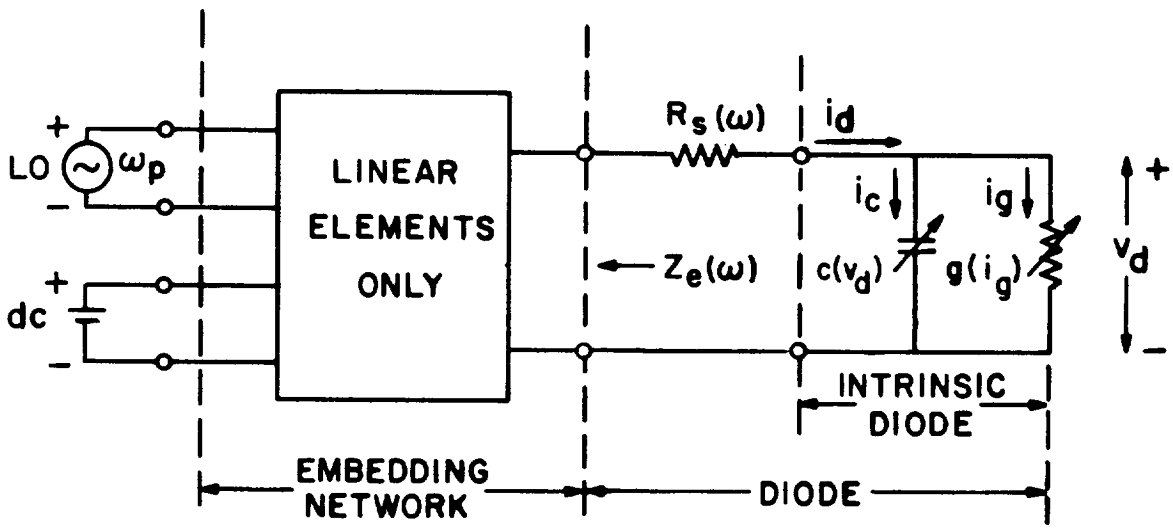

Fig. 2-1 The large signal equivalent circuit of a single diode mixer. The embedding network contains all the linear elements composing the diode mount. The frequency dependent series resistance is considered separately from the intrinsic diode.

layer and of the bulk semiconductor material. It is a function both of frequency and of diode geometry.

At room temperature and for forward voltages greater than $\approx 3kT/q$ the diode I-V relation is described by the thermionic emission theory * :

$$i_g = i_s \left[\exp\left(\alpha v_d\right) - 1\right], \tag{2.1}$$

where

$$\alpha = q/\eta kT \tag{2.2}$$

and η is the ideality factor which is temperature dependent. i_s is the saturation current which, for a Schottky diode, is given by [59,161]:

$$i_s = A\ R^{**}\ T^2 \exp[-q(\phi_b)/\eta kT], \tag{2.3}$$

---

* Strictly speaking the voltage dependence of the semiconductor barrier height modifies the I-V relation of (2.1) such that $i_g = i_s \exp(\alpha v_d)\ [1-\exp(-\eta\alpha v_d)]$ [135]. Under normal operating conditions the error will not greatly affect the mixer performance.

where R** is the modified Richardson constant, A is the junction area and ϕ_b is the actual semiconductor barrier height (including the effect of image force lowering). The diode capacitance current $i_c(t)$ is:

$$i_c = c\ (dv_d/dt)\ , \tag{2.4}$$

where $c=dq/dv_d$ is the incremental diode junction capacitance.

The junction capacitance and applied voltage are related by:

$$c = c_0(1-v_d/\phi_{bi})^{-\gamma}\ , \tag{2.5}$$

where c_0 is the capacitance at zero bias and ϕ_{bi} is the built in potential. γ reflects the doping profile in the epitaxial layer and is equal to one-half for an abrupt junction and one-third for a linearly graded junction.*

The built in potential ϕ_{bi} is [161] (see Fig.2-2):

$$\phi_{bi} = \phi_b - V_n + \Delta\phi \ , \tag{2.6}$$

where V_n is the potential from the semiconductor Fermi level to the conduction band edge and the last term accounts for image force lowering.

The differential conductance of the diode is obtained from (2.1):

$$g = di_g/dv_d = \alpha i_s \exp(\alpha v_d) = \alpha(i_g+i_s) \cong \alpha i_g \ . \tag{2.7}$$

---

* γ is, in reality, a weak function of applied voltage due to nonuniformities in the doping profile and to the fact that in small area diodes edge effects contribute substantially to the overall parallel plate junction capacitance [31,105,175].

Energy Band Diagram of a Metal-Semiconductor Junction

E_c = conduction band
E_v = valance band
$E_{F_{SC}}$ = Fermi level in semiconductor
E_{F_m} = Fermi level in metal
E_g = energy gap
V_n = potential from Fermi level to E_c
ϕ_{bi} = built in potential
χ = electron affinity
ϕ_m = metal work function
$\Delta\phi$ = image force lowering
ϕ_b = barrier height
Δ = potential drop across interfacial layer

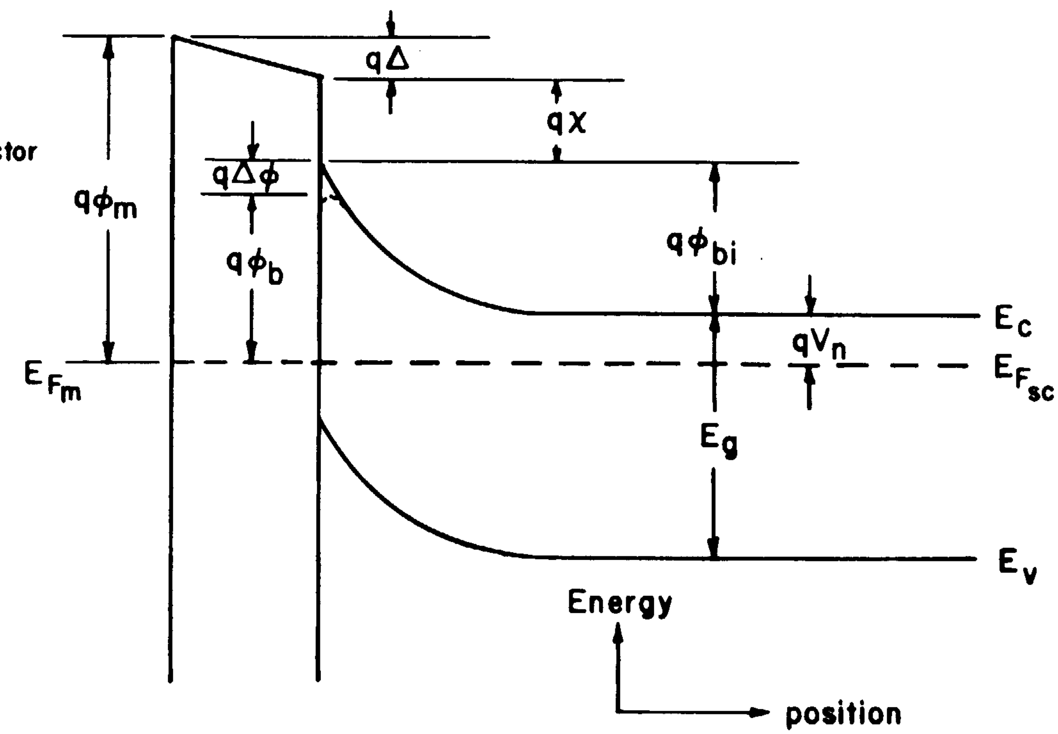

Fig. 2-2 The energy band diagram of a Schottky barrier diode [161] defining the barrier height and other physical parameters which are used in the text.

Since we will be using a form of harmonic balance technique we want to express v_d and i_d in the frequency domain. Using the Fourier series expansion:

$$v_d(t)=\sum_{n=0}^{\infty} V_{d_n} \exp(jn\omega_p t) \ , \tag{2.8}$$

$$i_d(t)=\sum_{n=0}^{\infty} I_{d_n} \exp(jn\omega_p t) \ , \tag{2.9}$$

where ω_p is the radian frequency of the local oscillator.

Using the above Fourier coefficients and referring to Fig.(2-1) we can express the constraints imposed on the steady state diode voltage and current by the embedding network as:

$$-V_{d_n}/I_{d_n}= Z_e(n\omega_p) + R_s(n\omega_p) \ , \ n=2,3,\ldots\infty \tag{2.10}$$

$$(V_{LO}-V_{d_1})/I_{d_1}= Z_e(\omega_p) + R_s(\omega_p) \ , \tag{2.11}$$

$$(V_{DC}-V_{d_0})/I_{d_0}= Z_e(0) + R_s(0) \ , \tag{2.12}$$

where V_{LO} and V_{DC} are the Thevenin equivalent LO and DC voltages seen by the diode.

Once we have the correct values of $v_d(t)$ and $i_d(t)$, V_{d_n} and I_{d_n} as calculated from (2.8) and (2.9) will satisfy (2.10-2.12). Then the small signal behavior of the mixer can be determined. As mentioned in Section 2.2.1 a method of solution which works well for a broad range of embedding impedances is the multiple reflection technique of Kerr [83] which will now be described.

2.2.3 The Multiple Reflection Technique

In the multiple reflection technique [83] the circuit of Fig. 2-1 is modified by the insertion of a long transmission line of arbitrary characteristic impedance Z_0 between the diode and the embedding network as shown in Fig. 2-3. At any given moment there will be waves propagating in both directions along the transmission line. In steady state these waves will all be of constant amplitude and will contain frequency components at DC and many LO harmonics. By choosing the length of the transmission line to be an integral number of wavelengths at the LO, and hence the LO harmonic frequencies, the steady state waveforms of the modified network (Fig. 2-3) will be the same as those in the original circuit of Fig. 2-1.

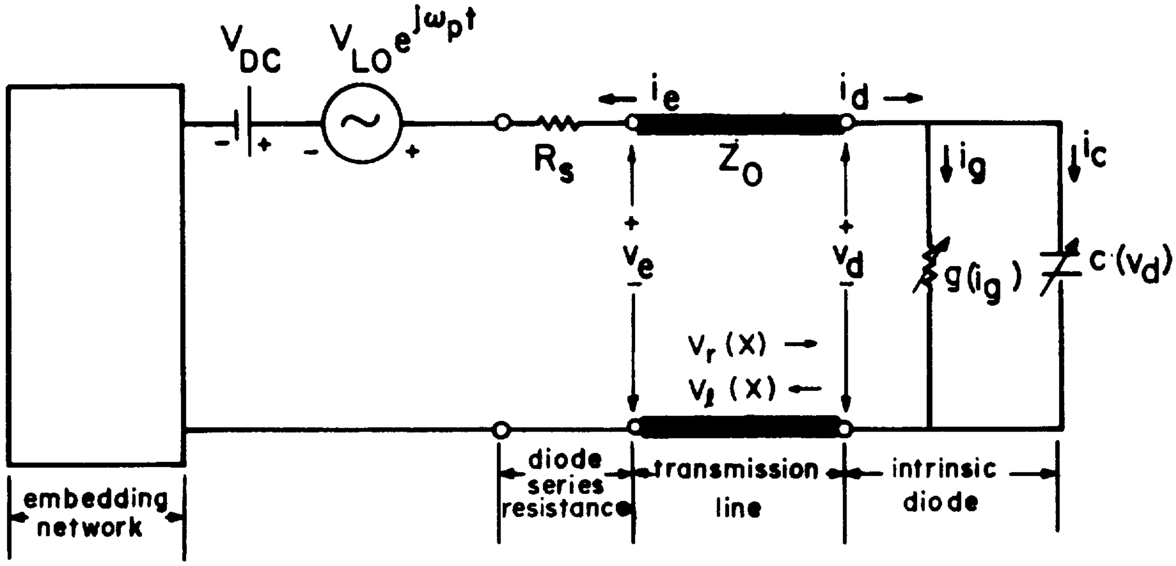

Fig. 2-3 The equivalent circuit of the mixer modified by the insertion of a long transmission line of characteristic impedance Z_0 between the intrinsic diode and the embedding network. The transmission line is an integral number of wavelengths long at the LO and harmonic frequencies so that the steady state voltage and current at the two ends are equivalent to those (v_d and i_d) of the circuit of Fig.2-1. V_{LO} and V_{DC} are the Thevenin equivalent LO and DC source voltages applied to the diode.

The transmission line serves two purposes; (i) it allows us to think in terms of reflected waves when considering the embedding network (which we will deal with in the frequency domain) and in terms of voltage and current when considering the diode (which we will deal with in the time domain), and (ii) if the transmission line is made long enough it eliminates the problems associated with transients generated upon reflections at the two ends. This construction then enables us to determine the diode waveforms for the circuit of Fig. 2-3 by alternately solving two much simpler circuits, each of which is in steady state with the transmission line.

The first circuit contains the transmission line and the diode and is solved in the time domain. The second circuit contains the transmission line and the embedding network and is solved in the frequency domain. After each of what will be termed a reflection cycle the terminal voltage and current in the two circuits are compared. If the waveforms are the same then the large signal problem has been solved, that is we have v_d and i_d equal to v_e and i_e in Fig. 2-3. On the other hand, if the terminal conditions in the two networks differ, the waveforms on the transmission line are changed in a predetermined fashion and the circuit analysis is repeated. The mathematical details follow.

Consider the circuit of Fig. 2-3. In general there will be a set of right and left traveling waves (v_r, v_l) on the transmission line. These waves are related to the total voltage and current [$v(x), i(x)$] at point x on the line by:

$$v(x) = v_r(x) + v_l(x), \tag{2.13}$$

and

$$i(x) = i_r(x) - i_l(x) = [v_r(x)-v_l(x)]/Z_0. \tag{2.14}$$

Since the transmission line is an integral number of wavelengths for all frequency components being considered, we have at the two ends (once we are in steady state):

$$v(x=0) = v(x=l) \text{ and} \tag{2.15}$$

$$i(x=0) = i(x=l). \tag{2.16}$$

Assume that the transmission line in Fig. 2-3 is terminated in an impedance Z_0 until time t=0 when the diode is first connected to the circuit. At time $t=0^+$ a right propagating wave will exist on the transmission line (V_R, I_R) made up of components at DC (subscript 0) and at the LO frequency (subscript 1). At the diode (x=l):

$$V_{R_0}(x=l)=I_{R_0}(x=0)Z_0 = V_{DC}Z_0/[Z_0+R_s(0)+Z_e(0)] \equiv V_0, \quad (2.17)$$

for the DC component and

$$V_{R_1}(x=l)=I_{R_1}(x=0)Z_0 = V_{LO}Z_0/[Z_0+R_s(1)+Z_e(1)] \equiv V_1, \quad (2.18)$$

at the LO frequency. V_{R_n} and I_{R_n} are the Fourier coefficients of v_r and i_r in (2.13)-(2.14), and $Z_e(n)$ and $R_s(n)$ are the embedding impedance and series resistance at harmonic n (frequency $n\omega_p$).

In the time domain, the transmission line and diode can be replaced by the equivalent circuit of Fig.2-4a where the voltage components, V_{R_0} and V_{R_1}, are given by (2.17) and (2.18). The state equation for this circuit is:

$$dv_d/dt = \{ [v_s(t)-v_d(t)]/Z_0 - i_g(t) \}/c(t), \quad (2.19)$$

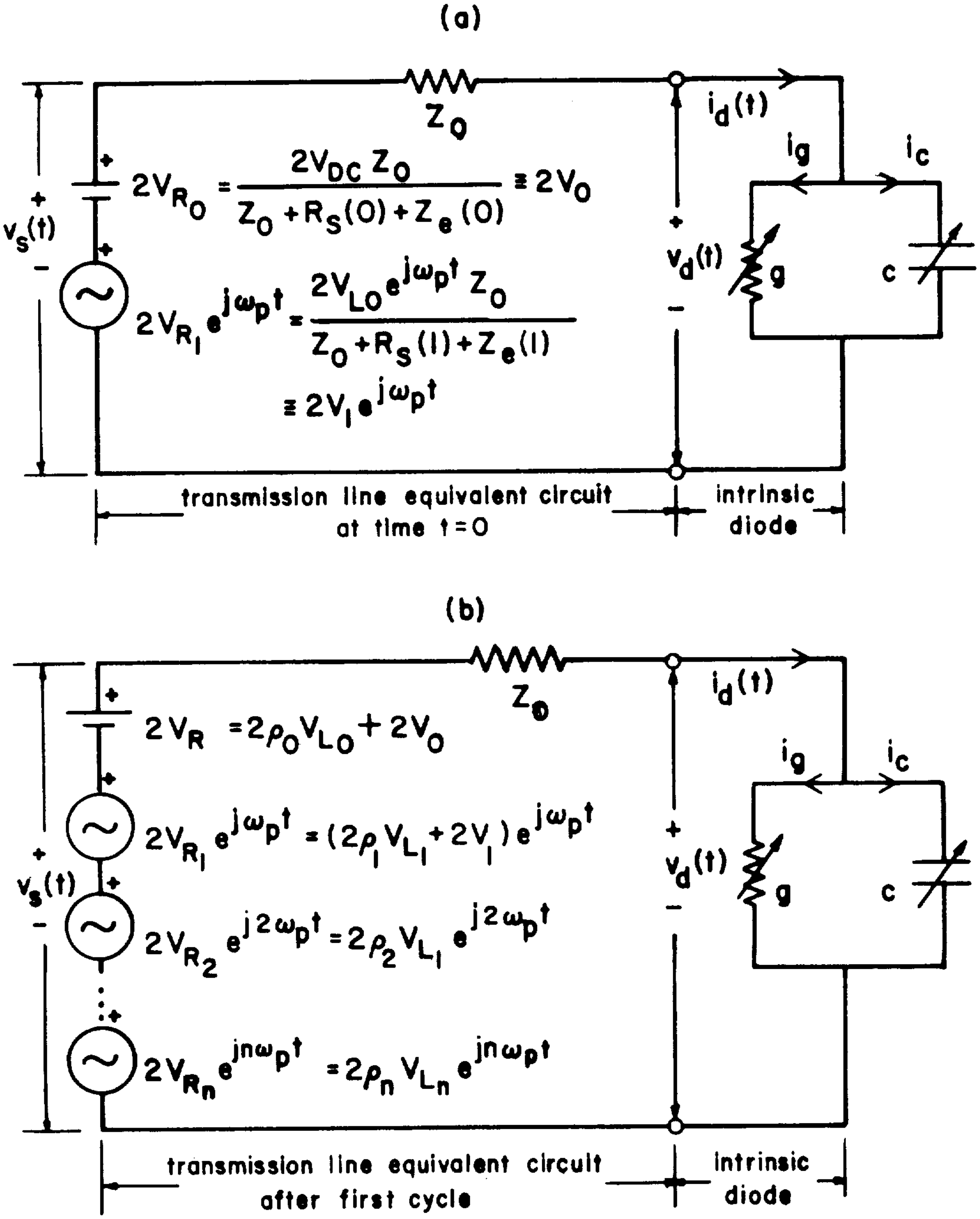

Fig. 2-4 The circuits which must be solved in the time domain to find the voltage and current at the diode terminals, (a) at time t=0 when the right propagating wave contains components only at DC and the LO frequency and (b) for all successive iterations. The voltage sources together with Z_0 make up the equivalent circuit of the transmission line, which is in steady state with the diode.

where $v_s(t)$ represents the sum of the voltage sources in the equivalent circuit of the transmission line. Given an initial value of $v_d(t=0)$, using (2.1)-(2.6) and allowing enough cycles (m) for steady state to be achieved, (2.19) can be solved numerically for $v_d(t)$ over an LO cycle, i.e. from $t=2\pi m/\omega_p$ to $t=2\pi(m+1)/\omega_p$.

Since the diode is nonlinear, the resulting steady state voltage waveform $v_d(t)$ will contain components at all the LO harmonic frequencies. This gives rise to a new left traveling wave on the transmission line of Fig.2-3. The amplitude of this wave is found by solving (2.13) and (2.14) for $v_l(x)$:

$$v_l(x) = [v(x)-i(x)Z_0]/2. \tag{2.20}$$

At the diode then:

$$v_l(x=l) = [v_d(t)-i_d(t)Z_0]/2. \tag{2.21}$$

From (2.15) this wave is incident on the embedding network and in the frequency domain:

$$V_{L_n} = [V_{d_n} - I_{d_n} Z_0]/2, \quad n=0,1,2\ldots\infty, \tag{2.22}$$

where V_{d_n} and I_{d_n} are the Fourier series coefficients of the diode voltage and current over one LO cycle (period $T = 2\pi/\omega_p$). That is:

$$V_{d_n} = 1/T \int_{-T/2}^{+T/2} v_d(t)\, \exp(-jn\omega_p t)\, dt\ , \tag{2.23}$$

and

$$I_{d_n} = 1/T \int_{-T/2}^{+T/2} i_d(t)\, \exp(-jn\omega_p t)\, dt\ . \tag{2.24}$$

At the embedding network, part of this wave will be reflected. The reflected components are calculated at each LO harmonic frequency from the voltage reflection coefficient, ρ_n:

$$\rho_n = [Z_e(n)+R_s(n)-Z_0]/[Z_e(n)+R_s(n)+Z_0]. \tag{2.25}$$

The component reflected from the embedding network becomes the new right propagating wave on the transmission line of Fig.2-3 and can be expressed as:

$$V_{R_n} = \rho_n V_{L_n}, \text{ for } n>1, \tag{2.26}$$

$$V_{R_1} = \rho_1 V_{L_1} + V_1, \text{ for } n=1 \text{ and} \tag{2.27}$$

$$V_{R_0} = \rho_0 V_{L_0} + V_0, \text{ for } n=0. \tag{2.28}$$

As this wave reaches the diode the circuit of Fig.2-4b applies where the additional voltage components produced by the diode on the previous cycle have now been included. The network state equation (2.19) can then be reformed and solved for $v_d(t)$ over an LO cycle. The procedure is repeated until the absolute value of the voltage divided by the current at the two ends of the transmission line are identical at all the LO harmonic frequencies, or from (2.10)-(2.12):

$$-V_{d_n}/I_{d_n} = V_{e_n}/I_{e_n} = [Z_e(n)+R_s(n)] \text{ for } n>1, \tag{2.29}$$

and

$$(V_{LO}-V_{d_1})/I_{d_1} = [Z_e(1) + R_s(1)] \text{ for } n=1.$$

To summarize; the algorithm for the calculation of the large signal diode voltage and current proceeds as follows:

(1). With a given value of V_{DC}, V_{LO} and $v_d(t=0)$, (2.19) is solved for $v_d(t)$, $t=2\pi m/\omega_p$ to $2\pi(m+1)/\omega_p$ and $i_d(t)$ is determined from (2.1)-(2.6).

(2). The Fourier coefficients of $v_d(t)$ and $i_d(t)$ (V_{d_n} and I_{d_n}) are found from (2.23)-(2.24).

(3). The amplitude of the left traveling wave, V_{L_n}, now incident on the embedding network is calculated from (2.22).

(4). This wave is partially reflected from the embedding network so that a new right traveling wave, V_{R_n}, is launched towards the diode. The amplitude of this wave at each LO harmonic is obtained from (2.25)-(2.28).

(5). Fig.2-4b now applies at the diode. A new state equation is formed from (2.19) and solved for $v_d(t)$ and again $i_d(t)$ is determined from (2.1)-(2.6).

(6). The Fourier coefficients of $v_d(t)$ and $i_d(t)$ are found from (2.23)-(2.24) and $|V_{d_n}/I_{d_n}|$ is calculated at each harmonic $n>1$.

(7). If (2.29) is satisfied at all the LO harmonic frequencies then the solution has converged and the correct $v_d(t)$ and $i_d(t)$ have been found. If (2.29) is not satisfied then steps (3)-(6) are repeated.

2.3 Small Signal Analysis

2.3.1 Introduction

Once the nonlinear large signal analysis is complete and the steady state voltage and current waveforms at the diode have been determined, a linear small signal analysis can be used to find the mixer conversion loss and port impedances. The small signal analysis presented in this thesis follows that of Held and Kerr [63] which is an extension of the original theory of frequency conversion given by Torrey and Whitmer [165].

In the analysis, a conversion admittance matrix is formed which relates the small-signal sideband currents and voltages of the diode. The elements of this matrix are derived from the Fourier series coefficients of the large signal diode conductance and capacitance waveforms. The conversion loss and port impedances can then be determined from the admittance matrix and the embedding impedances of the mixer mount at the various sideband frequencies.

2.3.2 Sideband Frequency Notation

If a mixer is pumped at a frequency ω_p and has an intermediate frequency ω_0, the only small signals which can produce an IF response are at the sideband frequencies ($n\omega_p \pm \omega_0$, n=0,1,2...). Following Saleh [138] it is useful to define the sideband frequencies by:

$$\omega_n = \omega_0 + n\omega_p \quad n=(\ldots-2,-1,0,1,2\ldots) . \tag{2.30}$$

For n<0 the sideband frequencies are seen to be negative. A brief comment on the meaning of these negative frequency terms is given in the footnote.*

Saleh's frequency notation leads to a considerable

---

* Electrical quantities are frequently described by a single complex quantity associated with some frequency, assumed positive. For example, an instantaneous voltage of frequency ω may be described by a complex amplitude V such that $v(t)=1/2[V\exp(j\omega t) + V^*\exp(-j\omega t)]$. We can just as meaningfully work with a negative frequency ($-\omega$) and the complex conjugate of the complex amplitude V^*, provided the convention is clearly understood. Impedances and admittances are then simply the conjugates of their conventional positive frequency values, i.e. $Z(-\omega) = V^*/I^* = Z^*(\omega)$.

simplification of the mixer theory. Using this notation all upper sideband frequencies ($\omega_0 + n\omega_p$) are considered positive, while all lower sideband frequencies ($\omega_0 - n\omega_p$) are negative. The sideband frequency index n is used as a subscript with the various electrical quantities and hence the upper sideband is written: $\omega_{+1} = \omega_0 + \omega_p$, the intermediate frequency becomes: ω_0 and the lower sideband is given by: $\omega_{-1} = \omega_0 - \omega_p$. V_{+1}, V_0 and V_{-1} then represent the voltages at these frequencies.

2.3.3 Conversion Admittance Matrix

Using the sideband notation described in the previous section let $\underline{\delta I}$ and $\underline{\delta V}$ denote the vectors of the small signal sideband currents (δI_n) and voltages (δV_n) at the terminals of the intrinsic diode (the diode excluding its series resistance):

$$\underline{\delta I} = [\ldots, \delta I_1, \delta I_0, \delta I_{-1}, \ldots]^t \qquad (2.31)$$

and

$$\underline{\delta V} = [\ldots,\delta V_1,\delta V_0,\delta V_{-1},\ldots]^t. \tag{2.32}$$

Torrey and Whitmer [165] have shown that $\underline{\delta I}$ and $\underline{\delta V}$ are related via a conversion admittance matrix $\underline{Y}$ defined by:

$$\underline{\delta I} = \underline{Y}\ \underline{\delta V}. \tag{2.33}$$

Using a row and column numbering for the admittance matrix which corresponds with the sideband notation of Section 2.3.2, $\underline{Y}$ can be written out as:

$$\underline{Y} = \begin{array}{ccccc} & \vdots & \vdots & \vdots & \\ \cdots & Y_{11} & Y_{10} & Y_{1-1} & \cdots \\ \cdots & Y_{01} & Y_{00} & Y_{0-1} & \cdots \\ \cdots & Y_{-11} & Y_{-10} & Y_{-1-1} & \cdots \\ & \vdots & \vdots & \vdots & \end{array} \tag{2.34}$$

The element values of the small signal admittance matrix were determined by Torrey and Whitmer [165] and are*:

$$Y_{mn} = G_{m-n} + j(\omega_0 + m\omega_p)\, C_{m-n}. \tag{2.35}$$

G_{m-n} and C_{m-n} are the (m-n)th Fourier coefficients of the diode conductance g(t) and capacitance c(t) waveforms defined in (2.5) and (2.7) and derived from the large signal diode voltage and current waveforms, $v_d(t)$ and $i_d(t)$:

$$G_{m-n} = 1/T \int_{-T/2}^{+T/2} g(t)\ \exp[-j(m-n)\omega_p t]\ dt\ , \tag{2.36}$$

$$C_{m-n} = 1/T \int_{-T/2}^{+T/2} c(t)\ \exp[-j(m-n)\omega_p t]\ dt\ , \tag{2.37}$$

---

* The derivation of (2.35) is somewhat lengthy but straight forward. The total (small plus large) signal current and voltage are expanded in a Taylor series about the large signal operating point of the diode. Higher order terms are neglected and it is found that $\delta i_g(t) = g(t)\,\delta v_d(t)$ and $\delta i_c(t) = c(t)\ \partial[\delta v_d(t)]/\partial t + \delta v_d(t)\,[\partial c(t)/\partial t]$. After transforming into the frequency domain, putting the equations into the form of (2.33) and using orthogonality we obtain (2.35).

where the integration is over one period (T) of the LO cycle.

The matrix $\underline{Y}$ can be regarded as the admittance matrix of a multifrequency multiport network in which there is one port for every sideband frequency ω_n (as shown in Fig.2-5). If the embedding impedances* Z_{e_n} and diode series resistance R_{s_n} corresponding to the sideband frequencies ω_n are now connected in parallel with the intrinsic diode, an augmented network is formed (shown by the broken line in Fig.2-5).

The ports of the augmented network correspond to the terminals of the intrinsic diode at the various sideband frequencies and do not represent physically accessible ports in the real mixer. The augmented network can be described by the admittance matrix $\underline{Y}'$ defined by:

---

* Z_{e_n} ($n=-\infty$ to $+\infty$) represents the embedding impedance of the mixer at sideband frequency ω_n. To perform the mixer analysis, the embedding impedances must be known up to LO harmonic frequency $2n\omega_p$ and at the 2n sideband frequencies, $m\omega_p \pm \omega_0$ ($m=1$ to $n/2$). The sideband impedances can be measured along with the LO harmonic impedances (see Chapter 3).

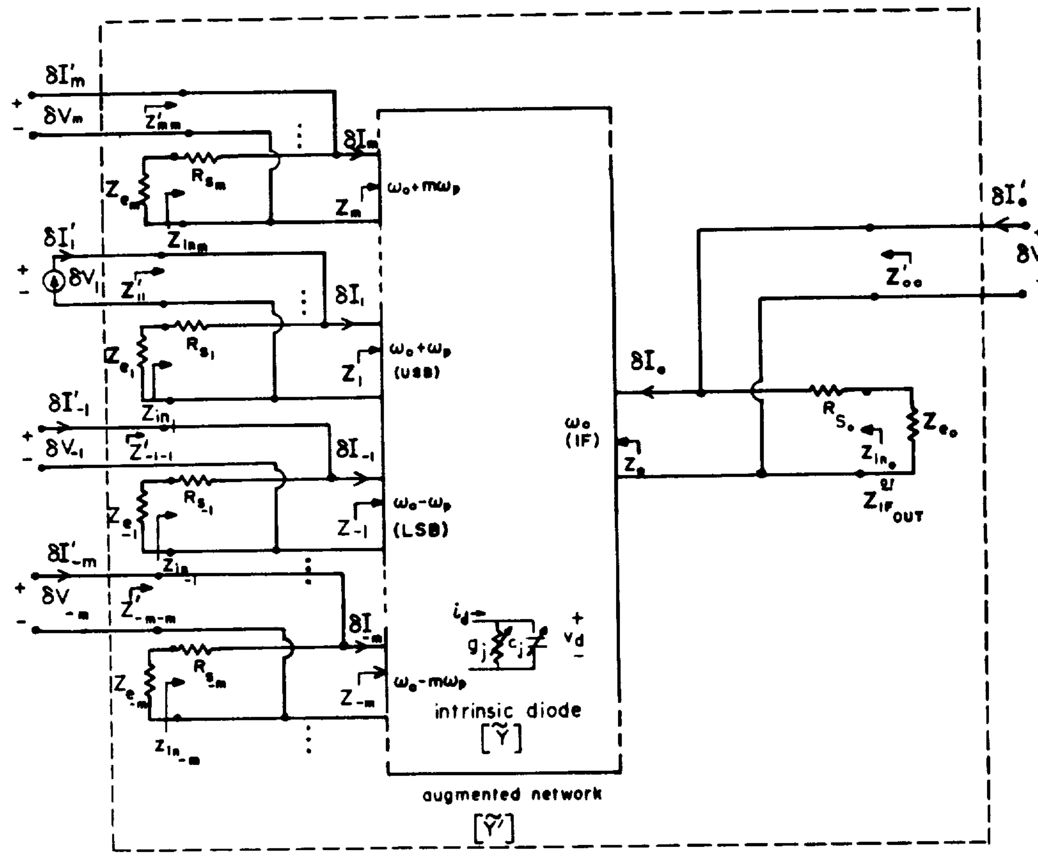

Fig. 2-5 The small signal representation of the mixer as a multifrequency linear multiport network. δV_m and δI_m are the small signal voltage and current components at sideband m (frequency $\omega_0 + m\omega_p$) at the intrinsic diode. The conversion matrix $\underline{Y}$ represents the intrinsic diode and the augmented network represented by $\underline{Y}'$ includes the sideband embedding impedances and diode series resistance. $\delta I'_{\pm 1}$ is the equivalent signal current generator which is connected at port ± 1 during normal mixer operation, the other ports being open circuited.

$$\underline{\delta I}' = \underline{Y}'\underline{\delta V}, \tag{2.38}$$

where

$$\underline{\delta I}' = [\ldots,\delta I_1',\delta I_0',\delta I_{-1}',\ldots]^t \tag{2.39}$$

and

$$\underline{\delta V} = [\ldots,\delta V_1,\delta V_0,\delta V_{-1},\ldots]^t. \tag{2.40}$$

δV_m and $\delta I_m'$ are the small signal voltage and current at sideband $\omega_m=\omega_0+m\omega_p$ (port m) of the augmented network. The elements of the augmented admittance matrix $\underline{Y}'$ are:

$$Y_{mn}' = Y_{mn} \text{ for } m\neq n \quad , \tag{2.41}$$

and

$$Y_{mm}' = Y_{mm} + [Z_{e_m}+R_{s_m}]^{-1} \quad \text{for } m=n. \tag{2.42}$$

Inverting (2.38):

$$\underline{\delta V} = \underline{Z}' \ \underline{\delta I}', \tag{2.43}$$

where

$$\underline{Z}' = (\underline{Y}')^{-1}. \tag{2.44}$$

The impedance matrix $\underline{Z}'$ enables us to calculate the conversion loss and the input and output impedance of the mixer and will also be used in Section 2.4 to compute the mixer noise properties.

2.3.4 Mixer Port Impedances

The impedance Z_m of any port of the intrinsic diode (see Fig.2-5) can be found by open circuiting the corresponding embedding impedance Z_{e_m} and then forming the $\underline{Z}'$ matrix defined in (2.44). The desired port impedance is given by the mm-th element of the newly formed $\underline{Z}'$ matrix, that is:

$$Z_m = Z'_{mm,inf} \quad , \tag{2.45}$$

where the subscript inf indicates that $\underline{Z}'$ has been formed with Z_{e_m} open circuited. The corresponding mixer input impedance seen by the embedding circuit includes the diode series resistance and is therefore given by:

$$Z_{in_m} = Z_m + R_{s_m} = Z'_{mm,inf} + R_{s_m} . \tag{2.46}$$

In particular the IF output impedance is:

$$Z_{IF_{out}} = Z_{in_0} = Z_0 + R_{s_0} = Z'_{00,inf} + R_{s_0} . \tag{2.47}$$

Throughout the remainder of this thesis it will be assumed that the IF load impedance is conjugate matched to the IF output impedance of the mixer, thereby minimizing the conversion loss. Once the mixer performance with a matched IF is known it is a simple matter to calculate the performance with any other IF termination. The value of the conjugate matched IF load impedance is, using (2.47):

$$Z_{e_0} = Z^*_{IF_{out}} = (Z'_{00,inf} + R_{s_0})^* \tag{2.48}$$

where $Z'_{00,inf}$ is the center element of the $\underline{Z}'$ matrix with Z_{e_0}=infinity. Rather than reforming the $\underline{Z}'$ matrix each time an input impedance is calculated, the intrinsic diode port impedance Z_m can be found from:

$$Z'_{mm} = (Z_{e_m}+R_{s_m}) \;||\; Z_m \;, \tag{2.49}$$

where Z'_{mm} is the mm-th element of the mixer impedance matrix formed with the IF load impedance conjugate-matched to the IF output impedance. The corresponding mixer input impedance is then:

$$Z_{in_m} = R_{s_m} + (Z_{e_m}+R_{s_m})Z'_{mm}/[(Z_{e_m}+R_{s_m})-Z'_{mm}] \;. \tag{2.50}$$

2.3.5 Conversion Loss

We will define the conversion loss of a mixer as the ratio of the available power* from a signal source of impedance Z_{e_j} at the input port j to the actual power delivered to a load impedance Z_{e_i} at the output port i. This definition corresponds to the conversion loss which is normally measured. Notice that the diode series resistance is not included as part of the source or load impedance. Referring to the left side of Fig.2-6, the available signal power at port j is**:

$$P_{avail}=1/2\ [\delta I_j \delta I_j^*]\ \mathrm{Re}[Z_{e_j}]\ , \tag{2.51}$$

where the port impedance $(R_{s_j}+Z_j)$ has been conjugate matched to the source impedance Z_{e_j}. Expressing (2.51) in

---

* That is, the power into a matched load.

** Note that the ports i and j are not the same as those defined in the multiport representation of the mixer (Fig. 2-5)

EQUIVALENT CIRCUIT FOR
CONVERSION LOSS CALCULATION

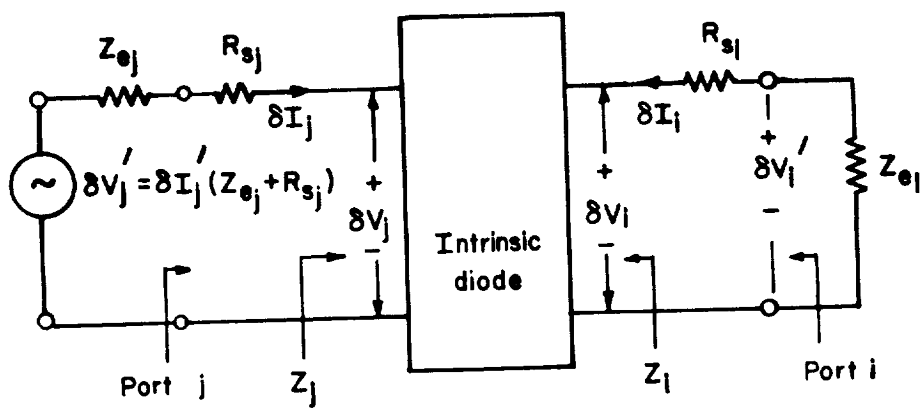

Fig. 2-6 The equivalent circuit of the mixer used for calculating the conversion loss from sideband j to sideband i. $\delta V_j'$ is the Thevenin equivalent of the current source $\delta I_j'$ connected to port j. In order that the calculated conversion loss correspond with that actually measured, the loss in the diode series resistance must be taken into account.

terms of $\delta I'_j$ (see Fig.2-6) we have:

$$P_{avail}=1/8\ |\delta I'_j|^2\ |Z_{e_j}+R_{s_j}|^2/\mathrm{Re}[Z_{e_j}]\ . \qquad (2.52)$$

The power delivered to the load impedance Z_{e_i} is (referring to the right side of Fig.2-6):

$$P_{del}=1/2\ [\delta V'_i\ \delta V'^*_i]\ \mathrm{Re}[1/Z_{e_i}]\ , \qquad (2.53)$$

where $\delta V'_i$ is the voltage across the load impedance, excluding the diode series resistance. In terms of V_i (2.53) becomes:

$$P_{del}=1/2\ [\delta V_i \delta V^*_i]\ \mathrm{Re}[Z_{e_i}]/|Z_{e_i}+R_{s_i}|^2\ . \qquad (2.54)$$

Recalling (2.43) with the condition that there is a source present only at the input port j we have:

$$\delta V_i = Z'_{ij}\ \delta I'_j\ , \qquad (2.55)$$

where Z'_{ij} is the ij-th element of the augmented impedance matrix $\underline{Z}'$.

Substituting (2.55) into (2.54) and taking the ratio with (2.52) we obtain the expression for the conversion loss from sideband j to sideband i in the mixer*

$$L_{ij} = P_{av}/P_{del} = \frac{|Z_{e_i}+R_{s_i}|^2 \; |Z_{e_j}+R_{s_j}|^2}{4|Z'_{ij}|^2 \; \mathrm{Re}[Z_{e_i}] \; \mathrm{Re}[Z_{e_j}]} \quad . \qquad (2.56)$$

---

* L_{ij} is the loss measured into a known load impedance Z_{e_i}. In the mixer analysis program described in Section 2.6 it is assumed that at the IF the load impedance is conjugate matched to the mixer output impedance $Z_{IF_{out}}$ for the calculation of L_{ij}.

2.4 Mixer Noise Theory

2.4.1 Introduction

The noise observed in a Schottky diode comes mainly from four sources: (1) shot noise due to the statistical nature of the current flow across the depletion layer, (2) thermal noise due to the random motion of the charge carriers in the undepleted semiconductor material, (3) lattice scattering noise from electron-phonon collisions and in GaAs intervalley scattering, and (4) hot electron noise associated with the thermal relaxation time of the charged carriers after they have crossed the Schottky barrier. At room temperature the noise contribution due to lattice scattering or hot electrons is usually small enough to be approximated by a slight increase in the temperature of the diode series resistance [63]. At cryogenic temperatures or in mixer diodes operated with substantial forward current flow, scattering and hot electron noise may make up a significant part of the overall noise [9,63,94] and a more complex analysis then is performed here is required to take account of their partially correlated components.

Strutt [160] analyzed the noise properties of vacuum tube diode mixers in 1946. He correctly treated the down converted shot noise components as correlated and also took into account the contribution of the thermal noise from the diode series resistance. Although Strutt did not consider any LO harmonics in his mixer model his method was essentially correct. Later authors, namely van der Ziel and Watters [170], van der Ziel [169], Kim [90], Dragone [39] and Uhlir [167] extended and refined the mixer noise theory to include additional harmonics and arbitrary sideband terminations.

An incorrect assumption that the mixer shot noise components were uncorrelated arose in the late 1950's and was perpetuated in the literature [62]. Held and Kerr [63] ended the confusion in 1978 when they extended and experimentally verified the earlier noise analyses of [39,90,160,169,170].

The noise theory which appears in this section follows that of Held and Kerr [63]. It is directly compatible with the small signal analysis of Section 2.3 and has been incorporated into the mixer analysis program which will be described in Section 2.6.

2.4.2 Noise Equivalent Circuit

The equivalent circuit of the Schottky diode, including noise sources, is shown in Fig.2-7a. T is the equivalent temperature of the series resistance and includes the effects of lattice scattering and pump heating. k is Boltzmann's constant and q is the electronic charge. In Fig.2-7b the thermal and shot noise are both represented as equivalent current sources in parallel with the intrinsic diode. $\delta i_T{}^2$ and $\delta i_S{}^2$ are the mean square values of the thermal and shot noise currents in the frequency range f to f+Δf. These current sources can be regarded as generating a multitude of quasi-sinusoidal frequency components, each with its own amplitude and phase. In the multifrequency multiport equivalent circuit of the mixer (Fig.2-5) the noise sources can be included by connecting an equivalent noise current generator to the appropriate port of the augmented network.

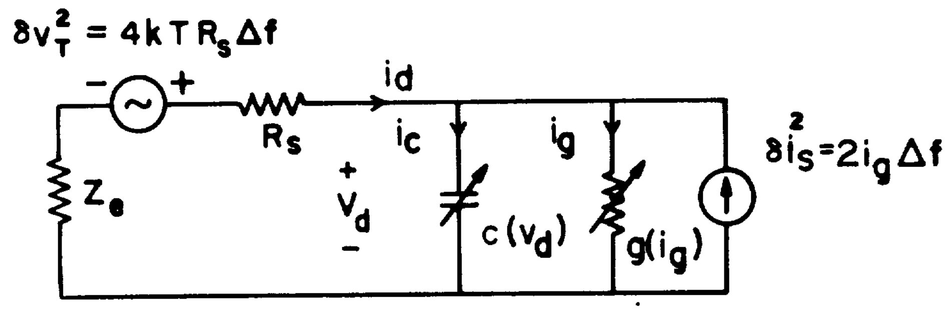

(a)

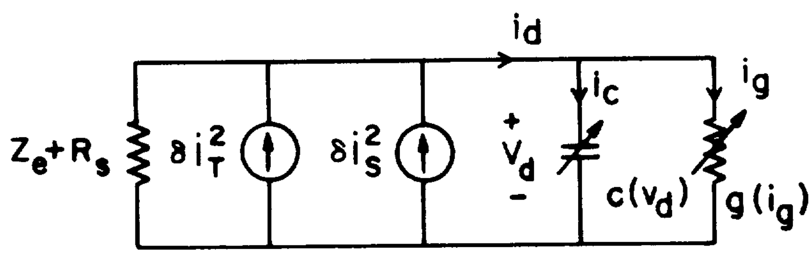

(b)

Fig. 2-7 (a) The equivalent circuit of a mixer including noise sources. T is the temperature of the diode series resistance including pump heating. (b) The equivalent circuit with the thermal noise source converted into a current source. δi_T^2 and δi_S^2 are the mean square values of the noise currents.

The mean square value of the shot noise current source in Fig.2-7b is well known* and is given by:

$$\delta i_S^{\,2} = 2qi_g\Delta f. \qquad (2.57)$$

The thermal noise voltage source has a mean square value** of $4kTR_s\Delta f$, which becomes upon transformation into a current source:

$$\delta i_T^{\,2} = 4kTR_{s_n}\Delta f/|Z_{e_n}+R_{s_n}|^2. \qquad (2.58)$$

At the intermediate frequency (n=0) we are assuming the mixer is conjugate matched $Z_{e_0}=(Z_0+R_{s_0})^*$ therefore, as

---

* Schottky [144] first predicted and calculated this theoretical form of what he termed the "shot effect" in 1918.

** This result was first calculated theoretically by Nyquist [119] in 1928 and experimentally verified by Johnson [77] in the same year. Actually, Johnson had demonstrated the existence of thermal noise somewhat earlier, hence the term "Johnson noise".

seen by the load Z_{e_0} the mean square value of the equivalent thermal noise current source connected to the IF port of the augmented network is given by:

$$\delta i_T^{\ 2} = 4kTR_{s_0}\Delta f/Z_0^{\ 2} = kTR_{s_0}\Delta f/|Z_{e_0}-R_{s_0}|^2, \qquad (2.59)$$

where the series resistance at the IF has been separated from both the embedding and diode port impedances.

2.4.3 Shot Noise

The shot noise in a mixer arises from the current in the diode conductance produced by the local oscillator and DC bias. It can be considered as white (Gaussian) noise, amplitude modulated by the LO waveform. Dragone [39] and Uhlir [167] have investigated the properties of this modulated noise and shown that there is partial correlation between the quasi-sinusoidal components at the various sideband frequencies. The correlated components at these sidebands are down converted in the diode to the intermediate frequency where they add vectorially.

Let $\delta I'_{S_n}$, representing the quasi-sinusoidal component at frequency ω_n of the periodically pumped shot noise current source in Fig.2-7b, be connected at port n of the augmented mixer as in Fig.2-8. We define $\underline{\delta I'_S}$ and $\underline{\delta V_S}$ as the vectors of the input shot noise currents and voltages at the ports:

$$\underline{\delta I'_S} = [\ldots \delta I'_{S_1}, \delta I'_{S_0}, \delta I'_{S_{-1}} \ldots]^t \tag{2.60}$$

and

$$\underline{\delta V_S} = [\ldots \delta V_{S_1}, \delta V_{S_0}, \delta V_{S_{-1}} \ldots]^t. \tag{2.61}$$

Recalling (2.43) the output noise voltage at the IF is:

$$\delta V_{S_0} = \underline{Z}'_0 \delta I'_S \quad , \tag{2.62}$$

where $\underline{Z}'_0$ is the center row of the augmented impedance matrix $\underline{Z}'$ defined in (2.44). It follows that

$$\delta V_{S_0} \delta V^*_{S_0} = \underline{Z}'_0 \underline{\delta I'_S} (\underline{Z}'_0 \underline{\delta I'_S})^\dagger = \underline{Z}'_0 (\underline{\delta I'_S}\,\underline{\delta I'_S}^\dagger) \underline{Z}'^\dagger_0 \quad , \tag{2.63}$$

ORIGINAL PAGE IS
OF POOR QUALITY

MIXER EQUIVALENT CIRCUIT
WITH SHOT NOISE SOURCES

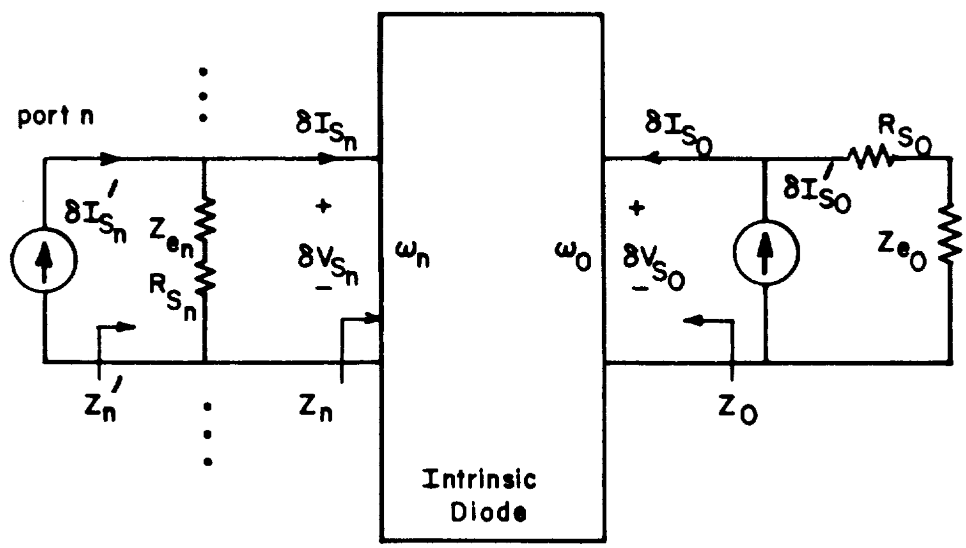

Fig. 2-8 The mixer small signal equivalent circuit with a shot noise current source at each sideband frequency port. The load impedance is conjugate matched to the IF output impedance in the noise calculations.

where † indicates the conjugate transpose of a matrix.

Taking the ensemble average* of (2.63) yields the shot noise voltage produced at the IF frequency:

$$\langle |\delta V_{S_0}|^2 \rangle = \underline{Z}_0' \langle \underline{\delta I}_S' \ \underline{\delta I}_S'^{\dagger} \rangle \underline{Z}_0'^{\dagger} \quad . \tag{2.64}$$

$\langle \underline{\delta I}_S' \underline{\delta I}_S'^{\dagger} \rangle$ is the shot noise current correlation matrix and has the general element $\langle \delta I_{S_m}' \ \delta I_{S_n}'^{*} \rangle$. Dragone [39] and Uhlir [167] have shown that:

$$\langle \delta I_{S_m}' \ \delta I_{S_n}'^{*} \rangle = 2qI_{m-n} \ \Delta f \ , \tag{2.65}$$

where I_{m-n} is the (m-n)th Fourier coefficient of the diode conductance current. As in (2.36) and (2.37) we have:

$$I_{m-n} = 1/T \int_{-T/2}^{+T/2} i_g(t) \ \exp[-j(m-n)\omega_p t] \ dt \ , \tag{2.66}$$

---

* Taking the ensemble average is equivalent to considering a small but finite bandwidth as must be used in any physical measurement. The finite bandwidth contains a multitude of quasi-sinusoidal noise components with random amplitudes and phases.

where the integration is over one LO period (T), t=0 to $t=2\pi/\omega_p$.

2.4.4 Thermal Noise

Thermal noise generated in the diode series resistance has components which are uncorrelated at the various sideband frequencies. Let $\delta I'_{T_n}$, representing the quasi-sinusoidal component at sideband frequency ω_n of the thermal noise current source in Fig.2-7b, be connected to port n of the augmented mixer as in Fig.2-9. If δV_{T_n} is the sideband noise voltage produced by $\delta I'_{T_n}$, then the noise voltage produced at the IF port of the augmented network by the thermal noise at all the sidebands can be found using (2.43):

$$\delta V_{T_0} = \underline{Z}'_0 \, \underline{\delta I'_T} \quad , \tag{2.67}$$

where

$$\underline{\delta I'_T} = [\ldots \delta I'_{T_1}, \delta I'_{T_0}, \delta I'_{T_{-1}} \ldots] \quad , \tag{2.68}$$

MIXER EQUIVALENT CIRCUIT
WITH THERMAL NOISE SOURCES

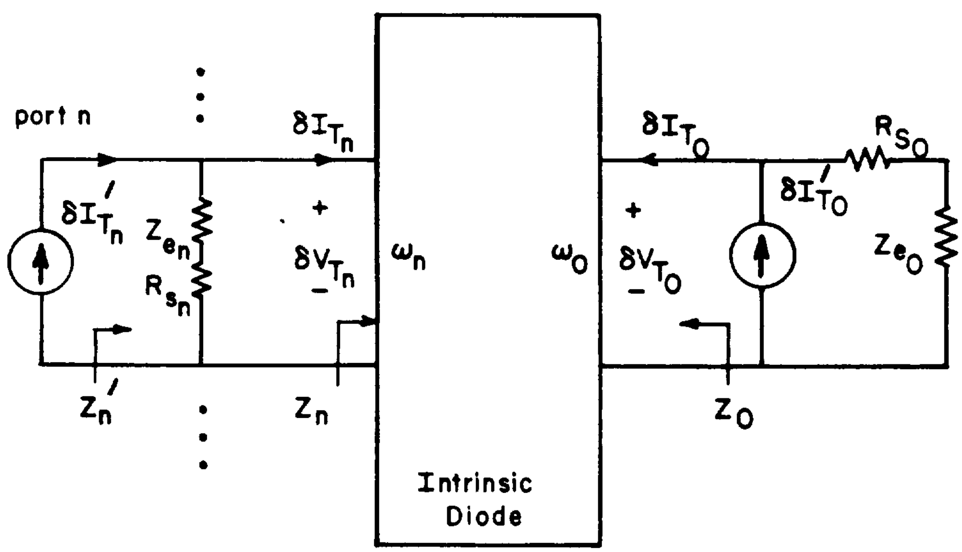

Fig. 2-9 The mixer small signal equivalent circuit with a thermal noise current source at each sideband frequency port. The load impedance is conjugate matched to the IF output impedance in the noise calculations.

is the vector of input thermal noise currents at the sideband ports of Fig.2-5, and $\underline{Z}_0'$ is the center row of the augmented impedance matrix $\underline{Z}'$. As in the shot noise analysis we write:

$$\delta V_{T_0}\delta V_{T_0}^{*}=\underline{Z}_0'\underline{\delta I}_T'(\underline{Z}_0'\underline{\delta I}_T')^{\dagger}=\underline{Z}_0'(\underline{\delta I}_T'\underline{\delta I}_T'^{\dagger})\underline{Z}_0'^{\dagger} \quad . \tag{2.69}$$

Taking the ensemble average gives the thermal noise voltage produced at the IF frequency:

$$\langle|\delta V_{T_0}|^2\rangle=\underline{Z}_0'\langle\underline{\delta I}_T'\underline{\delta I}_T'^{\dagger}\rangle\underline{Z}_0'^{\dagger} \quad . \tag{2.70}$$

The square matrix $\langle\underline{\delta I}_T'\underline{\delta I}_T'^{\dagger}\rangle$ is the thermal noise current correlation matrix. Since the thermal noise components at the various sideband frequencies are uncorrelated, the elements $\langle\delta I_{T_m}'\delta I_{T_n}'^{*}\rangle=0$ unless m=n, i.e. the matrix is diagonal. Recalling (2.58) and (2.59) we have:

$$\langle\delta I_{T_m}'\,\delta I_{T_n}'^{*}\rangle = 0 \text{ , for } m\neq n \text{ ,} \tag{2.71}$$

$$\langle\delta I_{T_m}'\,\delta I_{T_m}'^{*}\rangle=4kTR_{s_m}\Delta f/|Z_{e_m}+R_{s_m}|^2 \text{ , for } m=n\neq 0 \text{ ,} \tag{2.72}$$

$$\langle\delta I'_{T_0}\delta I'^{*}_{T_0}\rangle = 4kTR_{s_0}\Delta f/|Z_{e_0}-R_{s_0}|^2 \text{ , for } m=0. \tag{2.73}$$

2.4.5 Total Mixer Noise

The total output noise voltage of the mixer is obtained by combining the shot and thermal noise components. From (2.64) and (2.70):

$$\langle|\delta V_{N_0}|^2\rangle = \underline{Z}'_0[\langle\underline{\delta I}'_S\underline{\delta I}'^{\dagger}_S\rangle+\langle\underline{\delta I}'_T\underline{\delta I}'^{\dagger}_T\rangle]\ \underline{Z}'^{\dagger}_0 \quad . \tag{2.74}$$

It follows that the noise power delivered to the matched IF load Z_{e_0} from the mixer itself is (as in (2.54)):

$$P_{del} = \langle|\delta V_{N_0}|^2\rangle\ \mathrm{Re}[Z_{e_0}]/|Z_{e_0}+R_{s_0}|^2 \ . \tag{2.75}$$

The single sideband equivalent input noise temperature T_{SSB} of a mixer is defined as the temperature in Kelvin to which the signal port conductance of a noise free but otherwise identical mixer would have to be raised in order to produce at the output port the same noise power in a specified band as the actual mixer when its source impedances are noise free, i.e. at absolute zero [71]. Thus

$$T_{SSB} = P_{av}/k\Delta f = P_{del}L_{01}/k\Delta f \ , \tag{2.76}$$

where L_{01} is the conversion loss from sideband 1 to sideband 0 (signal to IF).

Substituting (2.75) and (2.56) into the expression above we obtain*:

$$T_{SSB} = \frac{\langle|\delta V_{N_0}|^2\rangle |Z_{e_1}+R_{s_1}|^2}{4k\Delta f|Z'_{01}|^2 \ \mathrm{Re}[Z_{e_1}]} \quad , \tag{2.77}$$

where Z'_{01} is an element of the augmented impedance matrix $\underline{Z}'$.

---

* Many people prefer to use the single channel noise figure rather than the noise temperature to characterize a mixer. The noise figure requires the specification of a reference temperature, usually taken to be 290 K, and is related to the single sideband mixer noise temperature as follows:

$$F_{SSB} = 1 + (L_s/L_i) + (T_{SSB}/290) \ ,$$

where L_s and L_i are the signal and image conversion loss, respectively (footnote continues on next page).

When describing the performance of a mixer whose physical port is coupled to both the signal and image frequencies, it is sometimes convenient to talk in terms of a double sideband noise temperature T_{DSB}. T_{DSB} is defined as the temperature in Kelvin to which the signal and image port conductances of a noise free but otherwise identical mixer would have to be raised in order to produce at the output port the same noise power in a specified band as the actual mixer when its source impedances are noise free, i.e. at absolute zero [71].

---

* (continued from previous page)

There is some confusion amongst workers regarding the relationship between noise figure and input noise temperature [168,181]. For a single response receiver it is clear that [72 eq. 24] :

$$F = 1 + T/290 .$$

This relationship is also valid for a double response receiver if the signal appears equally in both channels:

$$F_{DSB} = 1 + T_{DSB}/290.$$

If we now consider what happens when a double response receiver has the above signal present in only one channel we find [116]:

$$F_{SSB} = (1 + T_{DSB}/290) [1 + L_s/L_i] .$$

Finally, assuming the total signal power (summing both channels) of the double response receiver appears in only one channel we obtain using (2.78):

$$F_{SSB} = \{1 + T_{SSB}/[290 (1+L_s/L_i)]\} (1+L_s/L_i) ,$$

which reduces to the first equation in this footnote.

T_{DSB} is related to the single sideband mixer noise temperature T_{SSB} by [141]:

$$T_{DSB} = T_{SSB}/(1 + L_s/L_i), \tag{2.78}$$

where L_s and L_i are the signal and image conversion losses respectively.

2.5 Summary of Mixer Theory

The performance of a mixer can be characterized by its conversion loss and equivalent input noise temperature. These quantities depend upon the large signal waveforms at the diode and on the embedding impedances of the mixer at the small signal sideband frequencies. The diode waveforms can be found using the multiple reflection technique described in Section 2.2.3.

Once a steady state solution has been obtained, the Fourier coefficients of the conductance and capacitance waveforms can be extracted and used to find the conversion admittance matrix which relates the small signal sideband currents and voltages of the intrinsic diode. An augmented matrix can then be formed describing the multiport network which consists of the intrinsic diode, the diode series resistance and the sideband embedding impedances. The inverse of this matrix is the augmented impedance matrix $\underline{Z}'$, whose elements are used to calculate the conversion loss at the various sideband frequencies and the input impedances of the mixer ports.

In the noise analysis two components are considered:

shot noise in the diode junction and thermal noise in the series resistance. These are represented by equivalent noise current sources in parallel with the intrinsic diode. The periodically varying shot noise has correlated components while the thermal noise does not. Correlation matrices are formed and evaluated for both shot and thermal noise sources. The shot noise correlation matrix has elements related to the Fourier series coefficients of the diode conductance current, while the thermal noise correlation matrix depends only upon the embedding impedances at the sideband frequencies. The two matrices together yield the total output noise voltage from which the equivalent input noise temperature of the mixer can be calculated. Throughout the noise analysis the IF load impedance is assumed to be conjugate matched to the IF port impedance. The theoretical analysis is complete at this point.

2.5.1 Effect of Considering a Finite Number of Harmonics

In transforming the procedures of Sections 2.2-2.4 into a workable computer program there is a practical limit to the number of harmonics of the local oscillator which can be considered. This means that the small signal admittance matrix $\underline{Y}$ will be truncated above some finite harmonic number, which is equivalent to short circuiting the intrinsic diode at all higher sideband frequencies. In the nonlinear analysis restricting the number of harmonics is the same as terminating the intrinsic diode in an impedance Z_0, the characteristic impedance of the hypothetical transmission line, at all higher frequencies. The validity of these approximations is ultimately dependent upon the harmonic content of the large signal diode waveforms. For the diodes considered in this thesis it has been found (see Chapter 4) that using six LO harmonics is sufficient to give accurate predictions of the mixer performance.

In the next section we will discuss a computer pro-

---

* Using six LO harmonics in the large signal analysis means only the first three harmonic sideband <u>pairs</u> are used in the small signal analysis (see eq. 2.34).

gram which implements the large and small signal analyses described in Sections 2.2-2.4.

2.6 Mixer Analysis Program

2.6.1 Introduction

In order to optimize a mixer design one must be able to predict its performance with reasonable accuracy. The mixer theory given in Sections 2.2-2.4 was incorporated into a user oriented computer program which can readily accommodate a variety of mixer problems.

The program requires as inputs (1) the embedding impedances seen by the diode at each harmonic of the local oscillator and at the harmonic sidebands, (2) the diode I-V and C-V characteristics and (3) the operating conditions for the mixer, i.e. the bias voltage applied to the diode and the desired rectified current or input LO power. Other variables which may be input to change specific program operations will be discussed later in this section.

The program output includes (1) the large signal current and voltage waveforms at the diode, (2) the available mixer LO power, (3) the conversion loss between any pair of sideband frequencies, (4) the input impedance at each sideband and the IF output impedance, and (5) the equivalent input noise temperature referred to the upper and lower or any other sideband.

The remainder of this section outlines the computer program and the steps required for running it. A complete annotated listing can be found in Appendix 1. A chart indicating the general flow of the mixer analysis program is shown in Fig.2-10 and a list of the main program variables and their counterparts in the theory developed in Sections 2.2-2.4 is contained in Fig.2-11.

2.6.2 Program Implementation: Large Signal Analysis

The mixer analysis program begins with a call to subroutine LGSIG to perform the large signal analysis using the multiple reflection technique described in Section 2.2.3. The embedding network impedances $Z_e(n)$ (ZER,ZEI) and the sideband impedances Z_{e_m} (ZEMBSB) are input in the BLOCK DATA subprogram or formed, up to the highest desired LO harmonic (NH), assumed even, in subroutine ZEMBED. Note that for the lower sidebands (m<0) the complex conjugate of the actual embedding impedance must

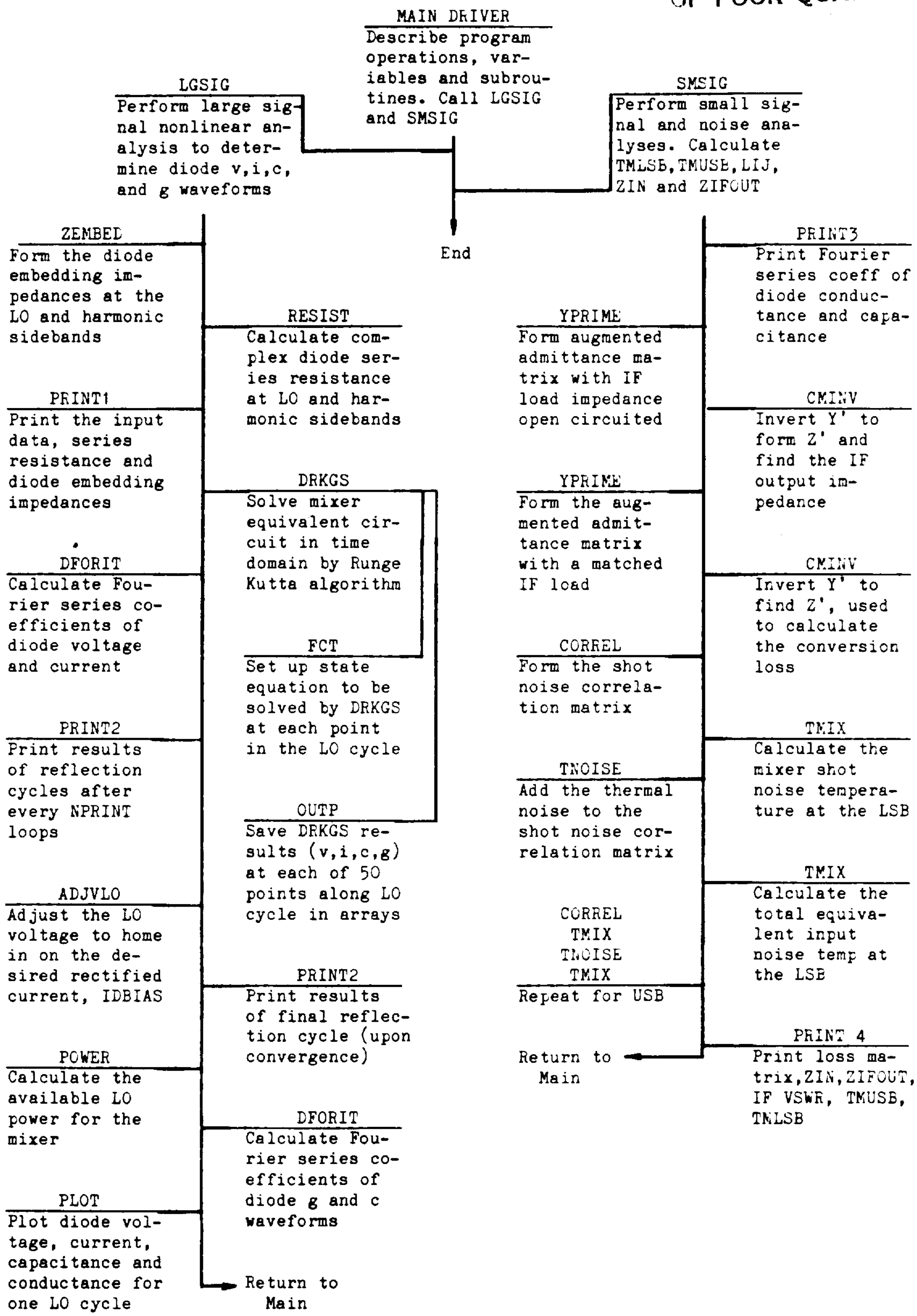

Fig. 2-10 Flow diagram of the mixer analysis program.

Text Variable	*Program Name*	*Text Variable*	*Program Name*
c	C	Y_{mn}	A(NHD2P1-m,NHD2P1-n)
c_0	CO	$\underline{Y}'$	A
C_{m-n}	FC(m-n+1)	$\underline{Z}'$(o/c IF)	A
g	GJ	$\underline{Z}'$(matched IF)	A
G_{m-n}	FG(m-n+1)	$Z_e(0) + R_s(dc)$	ZEMBDC
i_c	ICJ	$Z_e(n\omega_p)$	ZER(n) + j ZEI(n)
i_d	IGJ+ICJ	$Z_e(n\omega_p) + R_s(n\omega_p)$	ZEMB(n)
I_{d_n}	ID(n)	Z_{e_m}	ZEMBSB(NHD2P1-m)
i_g	IGJ	$Z_{IF_{out}}$	ZIFOUT
I_{m-n}	FG(m-n+1)/ALP	Z_{in}	ZIN
i_s	IS	Z_0	ZO
k	BOLTZ	Z'_{ij}	A(NHD2P1-i,NHD2P1-j)
L_i(LSB)	LIJ(NHD2P1,NHD2P2)	Z'_{mm}	A(NHD2P1-m,NHD2P1-m)
L_s(USB)	LIJ(NHD2P1,NHD2)	$Z'_{mm,inf}$	A(NHD2P1-m,NHD2P1-m)
L_{ij}	LIJ(NHD2P1-i,NHD2P1-j)	α	ALP
q	QEL	γ	GAM
R_s(dc)	RS	$\lvert\Gamma\rvert$	REF
$R_s(n\omega_p)$	RSLO(n)+ jXSLO(n)	η	ETA
R_{s_m}	RSSB(NHD2P1-m)	ϕ_{bi}	PHI
T	TK	ρ_0	RHODC
T_{SSB}	TMLSB or TMUSB	ρ_n	RHO(n)
v_d	Y(1)	ω_0	WIF
V_{d_n}	VD(n)	ω_p	WP
V_{DC}	VDC	$d\,v_d/dt$	DERY(1)
V_{LO}	VLO	$<\underline{\delta I}'_S\ \underline{\delta I}'^{+}_S>$	COR
V_{L_0}	VLDC	$<\underline{\delta I}'_T\ \underline{\delta I}'^{+}_T>$	COR
V_{L_n}	VL(n)	$<\lvert\delta V_{N_0}\rvert^2>$	VSQ
V_{r_0} or V_0	VRDC	$<\lvert\delta V_{S_0}\rvert^2>$	VSQ
V_{r_1} or V_1	VR(1)	$<\lvert\delta V_{T_0}\rvert^2>$	VSQ
V_{r_n}	VR(n)		

Fig. 2-11 Correspondence between the mixer analysis program variables and the variables used in the theory of Chapter 2.

be entered in accordance with the frequency subscript notation of Section 2.3.2. The real and imaginary parts of the embedding impedance $Z_e(n)$ at harmonic n become elements n of the arrays ZER and ZEI. The DC term is considered separately. The embedding impedance Z_{e_m} at sideband m becomes, in the notation of Section 2.3.2, array element (NH/2+1-m , where m=-NH/2...-1,0,1,...NH/2) of ZEMBSB.

After the embedding impedances have been formed RESIST is called to calculate the diode series resistance* at each LO harmonic (RSLO,XSLO) and at the sideband frequencies (RSSB) using the equations developed in Appendix 2. The array element notation for RSLO and XSLO is the same as that used for ZER and ZEI, that is $R_s(n)$ at harmonic n becomes array element n of RSLO and XSLO. Similarly the notation used for RSSB follows that of ZEMBSB, R_{s_m} at sideband m becomes array element (NH/2+1-m) of RSSB. Lastly the series resistance at the LO harmonics is added to the embedding impedance to form a complex array ZEMB.

---

* The diode series resistance is frequency dependent due to the skin effect and contains a reactive component. It is calculated, for a diode of given electrical properties and known geometry, in Appendix 2.

Following the call to subroutine RESIST, the embedding impedance (which now includes the diode series resistance) at DC (ZEMBDC) and ω_p (ZEMB(1)) are artificially set to Z_0 (ZO) the characteristic impedance of the hypothetical transmission line in the equivalent circuit of Fig.2-3. This has no effect on the final steady state solutions, as long as the Thevenin equivalent voltage sources at DC (VDC) and ω_p (VLO) are adjusted accordingly. This modification speeds up the nonlinear analysis by reducing the number of constraints imposed on the diode waveforms by the embedding network. The reflection coefficients (RHO) between the transmission line and the embedding circuit are now calculated at the remaining LO harmonics using (2.25).

The initial conditions for the circuit of Fig.2-3 are set up with VDC fixed by the desired DC bias voltage at the diode terminals. VDBIAS is the voltage across the diode plus series resistance as would be applied in an actual measurement. At this time the equivalent circuit of Fig.2-4a applies and the right propagating wave (VR) on the transmission line is formed using (2.17)-(2.18). The call to PRINT1 causes the input parameters to be printed.

Before beginning the full nonlinear circuit analysis the LO voltage source must be set so that the desired mixer operating conditions are met. In the program of

Appendix 1 and the measurements presented throughout this thesis the mixer is operated under a fixed DC bias voltage (VDBIAS) and rectified current (IDBIAS), the LO power being adjusted until this current is obtained. We begin by guessing at a value for VLO (the Thevenin equivalent LO voltage source) and run through a few reflection cycles to obtain an approximation to what will be the final DC rectified current (IDCOS(1)). If this calculated current is not equal to the actual mixer operating current (IDBIAS) within some specified accuracy (IDCACC) then the LO voltage source is changed by subroutine ADJVLO and the process is repeated. Alternatively one could operate the mixer with a fixed LO power level while the DC current was allowed to vary, as would be the case if one wanted to analyze a solid state harmonic generator for instance. This modification can be incorporated into the mixer analysis program and is considered in Chapter 6 in the discussion of varactor multipliers. The program loop variable for homing in on the correct LO voltage is JVLO and NCURR reflection cycles are run before the computed DC current (IDCOS(1)) is compared with IDBIAS.

When the correct value of VLO has been obtained the multiple reflection algorithm is allowed to continue until the convergence criteria given by (2.29) have been met within a specified accuracy ZQACC. The programming steps within this algorithm are as follows.

The IBM SSP routine DRKGS is called to calculate the diode voltage $v_d(t)$ [Y(1)] in the time domain by solving the differential equation of (2.19). The period of the voltage waveform is scaled so that one LO cycle occurs in 2π seconds. Subroutine FCT (required by DRKGS) sets up the state equation (2.19) with the equivalent transmission line voltage sources $v_s(t)$ being represented by the variable VS. DRKGS is called once per LO cycle and the integration step size is automatically adjusted to give the desired accuracy ACC (10^{-6} was found to be sufficient in all cases studied). Subroutine OUTP (also required by DRKGS) keeps track of the integration results, assigning the value of $v_d(t)$ [Y(1)] at intervals of 1/50-th of an LO cycle to the array VDDATA. The total diode current $i_d(t)=i_g(t)+i_c(t)$, capacitance c(t), and conductance g(t) at each of the 50 LO cycle steps are calculated from $v_d(t)$ using (2.1)-(2.7) and stored in appropriate arrays.

On returning to LGSIG, the Fourier transforms of $v_d(t)$ and $i_d(t)$ are determined using the IBM SSP routine FORIT. The resulting coefficients, V_{d_n} (VDCOS,-VDSIN) and I_{d_n} (IDCOS,-IDSIN) can be used to calculate the components of the left propagating wave on the transmission line (VL) using (2.22). The negative sign is present because DFORIT returns the coefficients for the trigonometric Fourier series representation whereas the equations in Section 2.2 use the single ended exponential series representation. The convergence criterion (2.29) is tested by forming $|V_{d_n}/I_{d_n}|/[Z_e(n)+R_s(n)]$ (ZQMAG) at each LO harmonic. If all the elements of ZQMAG are not unity within the specified accuracy (ZQACC) then the right propagating wave on the transmission line (VR) is formed from RHO and VL using (2.25)-(2.28). DRKGS is then called to start the next reflection cycle and the state equation (2.19) is reformed and resolved. In this and subsequent cycles the circuit of Fig.2-4b applies.

When (2.29) is satisfied the solution is considered to have converged and the results of the nonlinear analysis are printed in PRINT2. The available LO power required to maintain the DC operating current (IDBIAS) is now calculated in subroutine POWER using the equations developed in Appendix 3. Subroutine FORIT is again called to calculate the Fourier series coefficients of the diode capacitance (CJCOS/2, -CJSIN/2) and conductance (GJCOS/2, -GJSIN/2) waveforms (to be used in the small signal analysis). The factor of one-half converts from the single to the double ended Fourier series representation used in the small signal analysis. The large signal waveforms are then plotted using subprogram PLOT over an LO cycle, completing the nonlinear analysis.

2.6.3 Program Implementation: Small Signal Analysis

After the large signal analysis is finished subroutine SMSIG is called from the driving program to perform the linear small signal analysis following the theory in Section 2.3. The Fourier coefficients of the large signal diode conductance and capacitance waveforms are converted into complex form [FG=0.5*(GJCOS-jGJSIN), FC=0.5*(CJCOS-jCJSIN)] and printed in subroutine PRINT3. Calculation of the conversion loss matrix (XLMAT) and the mixer input and output impedances then begins with the formation of the small signal admittance matrix $\underline{Y}$ (A in the program) of equation (2.34) using (2.35). The IF load impedance is open circuited at this stage and the augmented admittance matrix $\underline{Y}'$ is formed in subroutine YPRIME from (3.41-3.42). The $\underline{Y}'$ matrix is then inverted to obtain the $\underline{Z}'$ matrix (also called A in the program) using the IBM SSP routine MINV slightly modified to handle a complex matrix. The IF output impedance (ZIFOUT) is the sum of the center element $Z'_{00,\mathrm{inf}}$ (A(NHD2P1,NHD2P1)) of this matrix and the diode series resistance R_{s_0} (RSSB(NHD2P1)) (see (2.47)). The IF load impedance (ZEMBSB(NHD2P1)) is now conjugate matched to the IF output impedance (ZIFOUT) and the augmented admittance matrix is reformed and inverted to find the $\underline{Z}'$ matrix (still called A in the program) of the mixer with a matched IF load. The elements of the conversion loss matrix (LIJ) and the input impedances at the sideband ports (ZIN) can now be calculated from (2.50) and (2.56).

2.6.4 Program Implementation: Noise Analysis

The noise analysis follows the theory of Section 2.4. It begins with the formation of the shot noise correlation matrix $\langle \underline{\delta I_S'} \underline{\delta I_S'}^{\dagger} \rangle$ from (2.65) in subroutine CORREL. The shot noise component of the equivalent input noise temperature referred to the lower sideband (array element NHD2P2) is calculated in subroutine TMIX using (2.77) with $\langle |\delta V_{N_0}|^2 \rangle$ replaced by $\langle |\delta V_{S_0}|^2 \rangle$ from (2.64). Next the total mixer noise correlation matrix is found in subroutine TNOISE by adding the shot noise correlation matrix (2.65) to the thermal noise correlation matrix (2.71)-(2.73). Subroutine TMIX is then called to find the total equivalent input noise temperature referred to the lower sideband (TMLSB) using (2.77). The thermal noise component (THLSB) is found by subtracting the shot noise contribution (SHLSB) from the total noise temperature. The process is repeated from the call to subroutine CORREL to find the shot (SHUSB), thermal (THUSB) and total mixer noise (TMUSB) temperatures referred to the upper sideband (array element NHD2). The results of the conversion loss and noise analyses are printed using PRINT4, completing the mixer analysis program.

For a more detailed description the reader is referred to the comments in the program listing of Appendix 1 and the flow chart of Fig.2-10.

2.6.5 Running the Mixer Analysis Program

A listing of the mixer analysis program appears in Appendix 1 along with the output from a run. Using the IBM Fortran IV-H compiler, the execution time for this particular listing is less than 3 seconds on an Amdahl 470/V6 computer. The comments in the listing provide a step by step explanation of the Fortran code. In addition, an alphabetical description of all of the variables and subprograms appears at the start of the main driver routine. To run the program the following information must be supplied by the user through the BLOCK DATA subprogram:

(1) The embedding network impedances at the LO frequency and the higher harmonics as real and imaginary parts (ZER,ZEI), in ohms (the number of harmonics being used is input via the element NH in COMMON/LOOPS/).

(2) The sideband impedances in complex form (ZEMBSB), in ohms, where sideband m corresponds to array element (NH/2+1-m) and there are NH+1 array elements in all. Sideband 0 (element ZEMBSB(NHD2P1)) will be conjugate matched by the program to the IF impedance of the diode in SMSIG and may be arbitrarily set at this stage. Note that for all lower sidebands (m<0) the elements of ZEMBSB must be input as the complex conjugates of their actual values.

(3) The LO frequency (FP) and intermediate frequency (IF), in hertz.

(4) The DC bias voltage applied to the diode plus series resistance (VDBIAS), in volts.

(5) The desired rectified current (IDBIAS), in amperes.

(6) The physical temperature of the mixer (TK), in Kelvin.

(7) The diode ideality factor (ETA).

(8) The diode built in or contact potential (PHI), in volts.

(9) The diode reverse saturation current (IS), in amperes.

(10) The diode capacitance at zero bias (CO), in farads.

(11) The diode capacitance law exponent (GAM).

(12) The measured diode series resistance at DC (RS) or the diode physical properties and chip geometry from which RS will be calculated. These parameters are: the anode radius (AR) in cm, the average distance from the anode to the edge of the chip (CR) in cm, the chip thickness (CT) in cm, the chip width (CW) and length (CL) in cm, the substrate (NDS) and epitaxial layer (NDE) doping in cm^{-3}, the carrier mobility (MOB) in $cm^2/V\text{-}s$, the density of states in the conduction band (NC) in cm^{-3}, the potential in (eV) from the donor level to the valence band edge (ED) and the whisker plus ohmic contact resistance (RW), in ohms. (See Appendix 2 for the calculation of the diode series resistance at DC and all the higher harmonic frequencies.)

The values of the remaining variables which are input via the BLOCK DATA subprogram are more or less dependent on the particular problem being solved and have been optimized for the listing in Appendix 1. The following information may prove useful in choosing values for these variables when running other examples.

The characteristic impedance (ZO) of the hypothetical transmission line inserted between the diode and the embedding network for the nonlinear analysis has a significant effect on the number of reflection cycles required for convergence. A value of 50 ohms results in a fairly rapid rate of convergence for examples in which the embedding impedances above the first harmonic approach short circuits, however a higher value (200 ohms) works better when the impedances are closer to open circuits.

The initial value of the local oscillator voltage (VLO) and the initial increment (VLOINC) used to zero in on the desired DC rectified current can be chosen so as to avoid many time consuming loops in the large signal analysis. If many runs are desired, as in the examples in Chapter 4, with only slight variations in the circuit parameters VLO will change very little in successive runs and VLOINC should be made fairly small.

The number of LO cycles needed to reach a steady state (NLO) for the circuit of Fig.2-3 need not be greater than one for most mixer problems (bear in mind that the solution will continue settling in successive reflection cycles) but if additional settling time is required NLO can be increased in the BLOCK DATA routine.

The calculated DC current (IDCOS(1)) is compared to the desired value IDBIAS after NCURR reflection cycles. If by this point IDCOS(1) has not had a chance to fully settle VLO will be incorrectly adjusted. Either NLO or NCURR in COMMON/LOOPS/ should then be increased.

The results of any of the reflection cycles can be printed by changing the parameter NPRINT, which causes printing every NPRINT cycles, in the BLOCK DATA program. Upper limits on other program loops such as the total number of nonlinear analysis cycles (NITER) or VLO adjustments (NVLO) can be increased or decreased as desired by changing the variables in COMMON/LOOPS/.

The local oscillator cycle was divided into 50 parts (51 points) in the examples which appear in this thesis to yield a reasonable number of data points for plotting the diode waveforms and to avoid aliasing*. If the number of points (NPTS, assumed odd) is altered some of the array dimensions must also be changed. In LGSIG and OUTP the variables in COMMON/DATA/ all have dimension NPTS.

If other than six harmonics of the local oscillator are to be considered in the analysis the variable NH

---

* The sampling theorem indicates that if NH harmonics are considered it should be necessary to consider only 2NH+1 points in the diode waveforms. This would be true if the waveforms produced by the Runge-Kutta integration contained only NH harmonics. However the integration solves the circuit of Fig.2-4b quite faithfully and, because of the exponential nonlinearity of the diode, harmonics above NH are present in the waveform. These are ignored in successive reflection cycles of the nonlinear analysis. If only 2NH+1 points are considered in the waveforms, the phenomenon of aliasing [17] occurs, by which higher frequency components are mixed with harmonics of the sampling frequency thereby causing errors in the computed Fourier coefficients.

(assumed even) must be set to that the number in the BLOCK DATA subprogram. Also the following array dimensions must be changed in LGSIG,SMSIG,FCT and BLOCK DATA to the value NH, if they represent LO harmonics, or to NH+1, if they refer to the sidebands: ZER, ZEI, RSLO, XSLO, ZEMB, RHO, VL, VR, ZQMAG and ZQPHA must be dimensioned NH and ZEMBSB, RSSB, CJCOS, CJSIN, GJCOS, GJSIN, VDCOS, VDSIN, IDCOS, IDSIN, GJMAG, GJPHA, CJMAG, CJPHA, FG, FC, A, COR, T, ZIN, XLMAT, WK1 and WK2 must be dimensioned NH+1. In addition some of the print formats may need to be altered.

The program can easily be altered to handle diodes with a capacitance voltage relationship which differs from that given in (2.5). If a doping profile is available, numerical curve fitting can be used to obtain C vs. V which can then be incorporated into the program by making CJ an internal function, CJ(Y(1)). Such an approach is illustrated in Section 2.7 where the program is used to analyze a mixer containing a Mott diode with a measured doping profile.

This concludes the description of the mixer analysis program. In the next section we examine some simple mixer circuits which have been analyzed using an earlier version of the program [151]. The accuracy of the mixer analysis program as listed in Appendix 1 is verified in Chapter 4 where it is used to predict the performance of an actual mixer operating in the 140-220 GHz band. It is again employed in Chapter 5 for optimizing a particular mixer design, and in Chapter 6 modifications are discussed which allow the program to be used for the analysis of diode multipliers.

2.7 Analysis of Some Simple Mixer Circuits

2.7.1 Introduction

As an example of the use of the mixer analysis program we examine the effects of the series inductance and diode capacitance on the performance of two simple mixer circuits. The embedding networks were chosen to simulate mixers in which there is inductance due to the diode package or contact whisker. Higher harmonics of the local oscillator are either short circuited or open circuited outside of the series inductance. The two mixer circuits were analyzed with three different diodes: (i) a more or less realistic Schottky diode, (ii) a Schottky diode with a constant junction capacitance, and (iii) an actual Mott diode. An earlier version of the mixer analysis program [151] was used for the study and the results are repeated in Appendix 4 of this thesis. It is shown that parametric effects due to the voltage variable capacitance may have either a beneficial or detrimental effect on the mixer performance depending on the circuit and diode parameters.

2.7.2 Computed Results and Discussion

The two mixer circuits which were analyzed are shown in Figs.2-12 and 2-13. The high pass filter in the first circuit (Fig.2-12) shorts out all higher harmonics, allowing only the signal, image and LO frequency to propagate outside the series inductance, L_s. The low pass filter in the second mixer circuit (Fig.2-13) presents an open circuit to the diode plus series inductance at the higher LO harmonics and sideband frequencies. Both circuits were analyzed with diodes having different C-V relationships. In one case the C-V law of eq. (2.5) was used with $\gamma=1/2$, representing a typical GaAs Schottky barrier diode. A second Schottky diode with no capacitance variation ($\gamma=0$ in eq. 2-5) was also looked at. Finally, a realistic Mott diode with the C-V relationship of Fig. 2-14 was used in the two mixer circuits*.

In each case the diode was forward biased at 0.4 volts and the LO power level was adjusted in the program to give a rectified current of 2 mA. The signal frequency

---

* The C-V relationship used for the Mott diode was obtained from an experimentally determined doping profile kindly supplied by M. V. Schneider of Bell Telephone Laboratories, Holmdel, N.J.

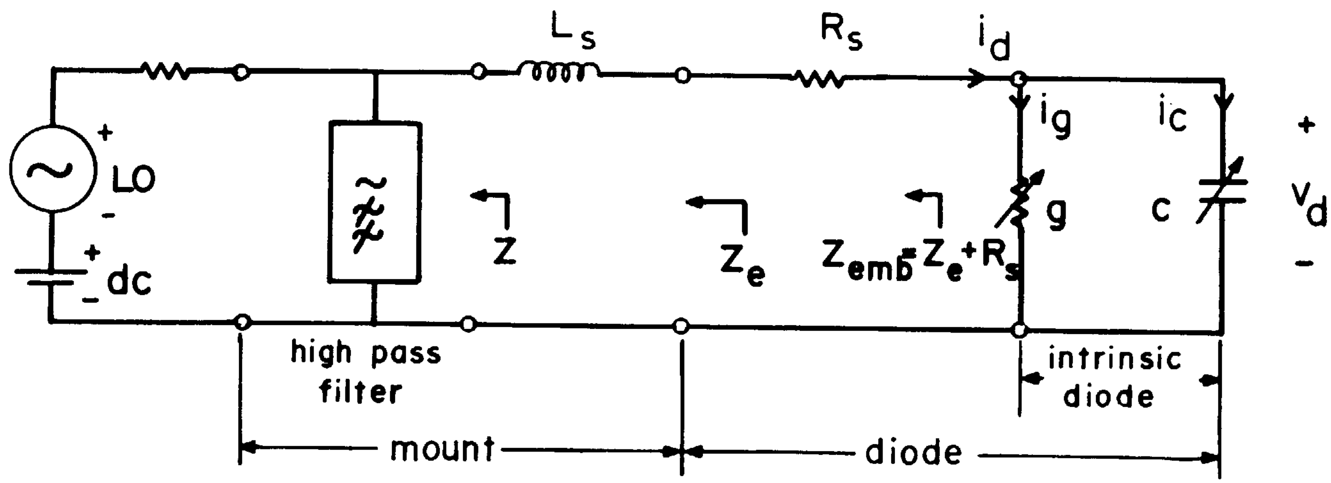

<u>Fig. 2-12</u> The equivalent circuit of a simple mixer. The filter passes all frequencies above the signal and image, thus <u>shorting</u> out the higher LO harmonics and sideband frequencies.

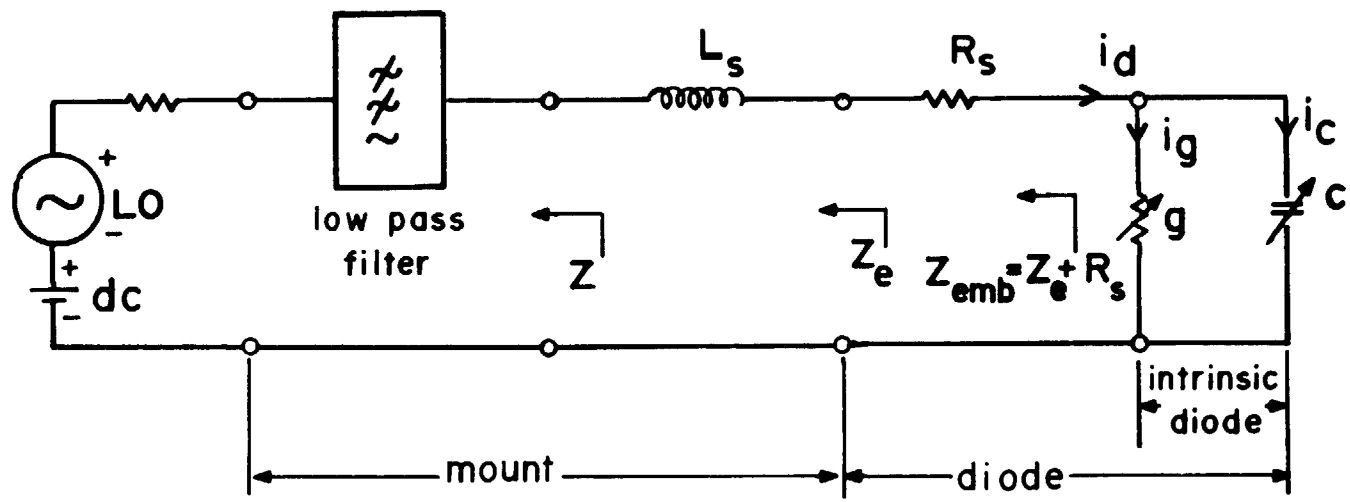

Fig. 2-13 The equivalent circuit of a simple mixer. In this circuit the filter stops all frequencies above the signal and image, thus open circuiting the higher LO harmonic and sideband frequencies.

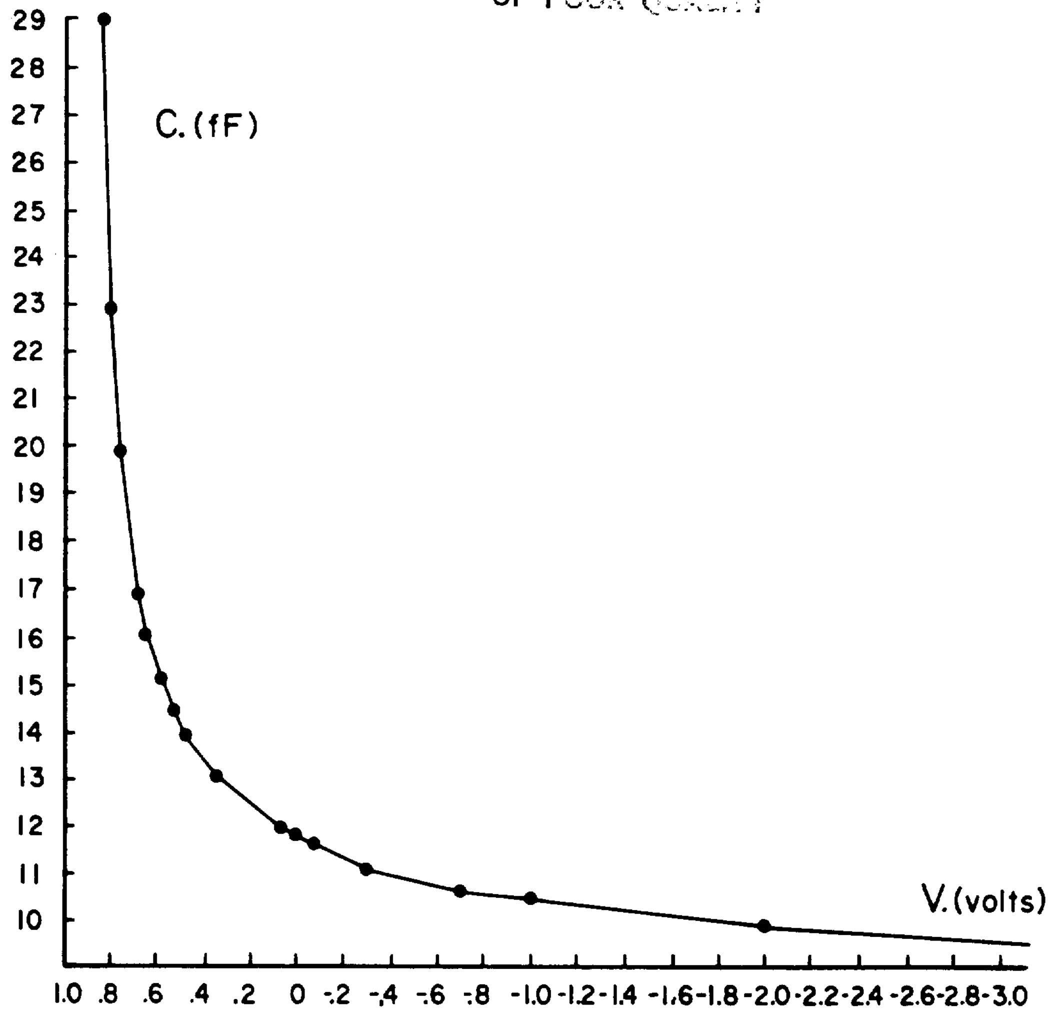

Fig. 2-14 A piecewise-linear approximation to the capacitance-voltage relationship of the Mott diode. The slope and C-axis intercept are supplied to the mixer analysis program for the calculation of the diode capacitance at any given voltage.

(taken to be the upper sideband) was chosen to be 119 GHz and the LO and intermediate frequencies were 115 and 4 GHz respectively. Values for the remaining diode parameters were in all cases: R_s=4.4 ohms (independent of frequency, i.e. the skin effect was not considered in the analysis), i_s=1.4 x 10^{-15} amps, η=1.13, ϕ_{bi}=0.9 volts, and T_k=296 Kelvin.

In the first example the effect of the series inductance on the mixer performance was studied by allowing L_s to vary from 0.01 to 0.25 nH while fixing the zero bias capacitance (c_0) of each diode at 11.8 fF (the actual value obtained for the Mott diode). The conversion loss (upper sideband to IF), equivalent single sideband input noise temperature, and the real part of the IF output impedance are plotted against values of L_s in Appendix 4, Section A4.1.

The minimum noise temperature is achieved with the constant capacitance diode, however this should not be assumed to be a general result as we will see shortly. Except for the diode with constant capacitance, the minima in the noise temperatures and conversion losses for each mixer circuit do not occur at the same value of L_s.

A broader view of the performance of the two mixer circuits is obtained from the plots which appear in

Appendix 4, Section A4.2. In these plots we see the effects of the zero bias capacitance on the overall mixer performance. Only the two Schottky diodes were used in the study.

The zero bias capacitance c_0 was allowed to vary from 1 to 20 fF for each of nine values of series inductance between 0.04 and 0.2 nH. In all cases increasing the series inductance sharpens the noise temperature and conversion loss minima and shifts them towards smaller values of c_0. Better performance is obtained with larger values of L_s and there is a corresponding increase in the IF output impedance. An interesting result of this analysis is that the parametric effects of the junction capacitance do not necessarily degrade the mixer performance.

Amongst the results there are some points which appear to be randomly scattered. This is due to the fact that for low values of series inductance, each increment in L_s causes a large change in the resonant frequency of the diode with the external circuit. If these resonances fall near LO harmonics the diode waveforms can be strongly affected as can the embedding impedances seen by the the small signal sidebands near these harmonics.

This concludes Chapter 2.

CHAPTER 3. MIXER MOUNT CHARACTERIZATION

3.1 Introduction

As we saw in Chapter 2 a mixer can be fully characterized by the electrical properties of its diode and its mount (embedding) impedances at the local oscillator (LO) and sideband harmonic frequencies. The number of harmonics which must be considered in any accurate mixer performance analysis will vary with the particular diode and mounting structure. However, as we shall demonstrate in Chapter 5, the impedance at the second and even the third LO harmonic can have a significant effect on the mixer performance.

In order to analyze and ultimately optimize a given mixer design the embedding impedances must either be derived theoretically or measured. Although the difficulties involved in the theoretical characterization of a given mixer mount are great, progress has been made in this direction [11,42,43,52,67]. At the present time, and at least for the near future, accurate millimeter-wave impedance measurements cannot be performed easily above

100 GHz.

In this chapter we discuss the techniques which have been employed to determine the mount impedances of an actual 140-220 GHz mixer [89] at frequencies up to the sixth harmonic of the local oscillator. This mixer will later be analyzed (Chapter 4) using the computer program of Chapter 2. Also described in this chapter is an automated microwave network analyzer system which can be set up around a small laboratory computer for gathering the impedance data and removing instrumentation errors. At the end of the chapter the measured diode mount impedances are presented for LO frequencies of 150 and 180 GHz as a function of mixer backshort setting at the first six LO harmonics and the first three pairs of associated sidebands (the IF frequency is 4 GHz).

3.2 Frequency Scaling

Frequency scaling is a technique which is often employed in the design of millimeter-wave components. The inherent linearities of the Maxwell field equations allow the physical size of low loss waveguide components to be scaled inversely with frequency without affecting their electrical properties* [159].

Eisenhart and Khan [43] described a method by which the embedding impedances of a waveguide mixer could be measured in the microwave band using a vector network analyzer. A 50 ohm coaxial cable is buried within the diode support structure (usually some type of stripline or microstrip filter) and emerges at the position of the anode of the diode. Here the center conductor of the coax is contacted by the whisker while the outer conductor

---

* Waveguide loss is a function of frequency through the skin effect and does not scale linearly with physical dimensions. In the modelling that has been done in this thesis we have assumed that waveguide loss contributes a negligible amount to the embedding impedance. If more accuracy is required the loss can be modelled by appropriately choosing the material of which the scaled device is constructed.

becomes the return path through the semiconductor bulk. When a test signal from the network analyzer is sent down the cable and the reference plane is moved forward to the position of the anode, then a measurement of the reflected wave versus frequency yields the mount impedance seen by the diode (see Fig. 3-2).

If we scale up the size of an actual millimeter-wave mixer (that is the mixer mount, not the actual diode), moving the operating frequency into the microwave band, then we can use the Eisenhart and Khan technique to measure the embedding impedances at the LO and many higher harmonic frequencies.

3.3 Mixer Model

The mixer design which was chosen for this investigation was described by Kerr, Mattauch and Grange [89] and is depicted in Fig.3-1. The operating band is nominally 140-220 GHz. An array of 2 micron diameter gold on platinum GaAs Schottky barrier diodes is photolithographically produced on the face of a 5x5x9 mil (1 mil= 0.001 inch) chip. The chip is soldered to, and forms part of, the first low impedance section of a 5 mil thick quartz microstrip filter structure which rests at the bottom of a 10x11x77 mil channel. The microstrip channel breaks through the middle of the wide side of a one-quarter height WR-5 waveguide (51x6 mils) and the diode face is mounted flush with the wall. Electrical contact to an anode of the diode is made by a half-mil diameter phosphor bronze whisker, bent into a V shape for added spring. The whisker is held on a 20 mil diameter post which is press fitted into a hole in the waveguide wall opposite the diode during the contacting process. A contacting backshort slides in the quarter height waveguide behind the diode and an electroformed step transformer, which brings the reduced height waveguide up to

ORIGINAL PAGE IS
OF POOR QUALITY

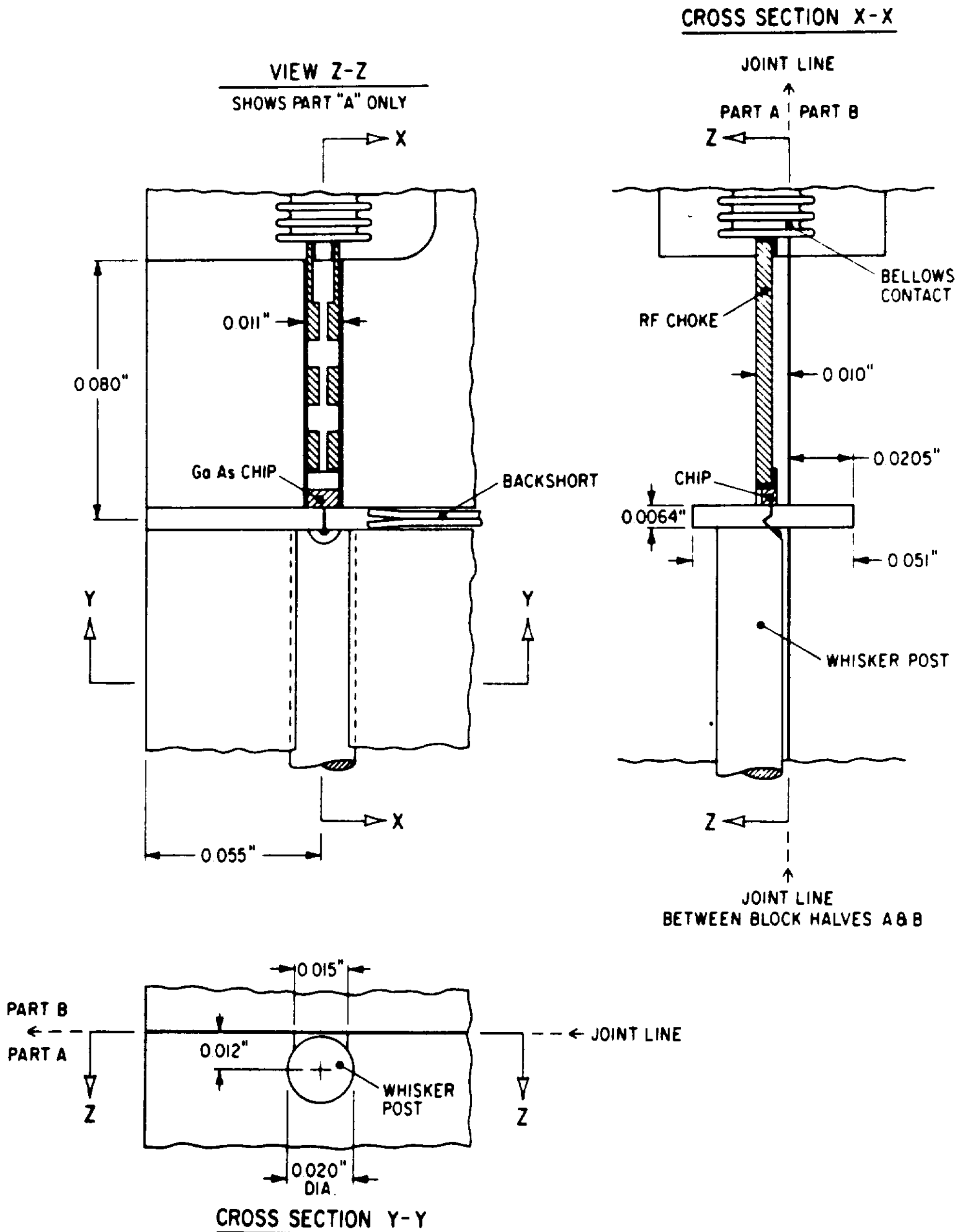

Fig. 3-1 A machinists drawing of the 140-220 GHz Schottky diode mixer [89] which is analyzed using the techniques of Chapters 2-4.

standard size (51x25.5 mils) is located on the input side of the diode. The electrical properties of the diode do not enter into the characterization of the mixer mount and will not be considered until Chapter 4.

A scale factor of 100 was chosen so as to reduce the mixer operating frequency to 1.4-2.2 GHz and allow impedance measurements up to the sixth local oscillator harmonic with a Hewlett Packard 8410A network analyzer. A model of the area in the vicinity of the diode was constructed containing the microstrip filter and diode chip, a sliding backshort, the full to one-quarter height waveguide step transformer, and the whisker and post. The GaAs diode chip was modelled with an aluminum block since the bulk GaAs is a good conductor even at a few hundred gigahertz*. The microstrip filter is composed of a fuzed quartz substrate with copper tape on its surface forming the low and high impedance sections. A 50 ohm coaxial cable, 85 mils in diameter, runs under the copper tape (in a channel cut in the quartz substrate) and through the diode block. A scaled up whisker contacts the center

---

* Although it is possible to scale the material properties of the GaAs chip more accurately it was felt that the effect on the overall embedding impedances would be very small.

conductor of the cable and a motor driven sliding short is contained in the reduced height waveguide. A broad band sliding load, constructed of Ferrosorb* conical absorbers, was inserted into the full height waveguide ahead of the step transformer to produce a matched condition for all waveguide modes. Additional absorbing material (Eccosorb** MF 124) was placed at the far end of the microstrip filter channel. The completely assembled model is shown in Figs.3-2 and 3-3.

---

* Ferrosorb is a product of the Microwave Filter Co., Syracuse, N.Y.

** Eccosorb MF 124 is a product of Emerson & Cuming, Canton, Mass.

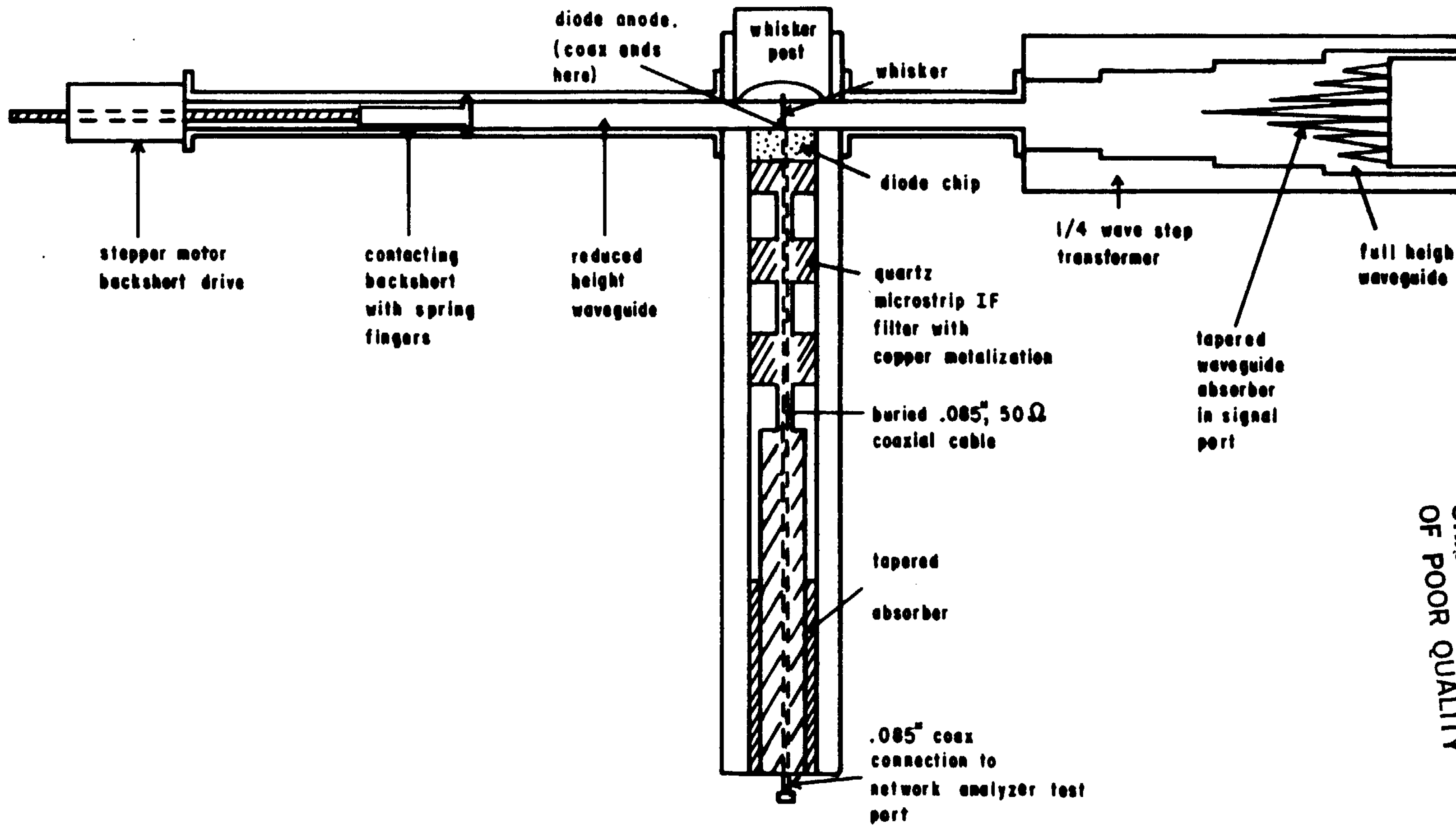

ORIGINAL PAGE IS
OF POOR QUALITY

Fig. 3-2 A view of the lower half of the 100x scale model of the mixer shown in Fig.3-1 (view z-z). The coaxial measurement cable is shown (dotted lines) under the surface of the microstrip filter. Dimensional tolerances were kept to ±10 mils (±0.1 mil in the actual mixer).

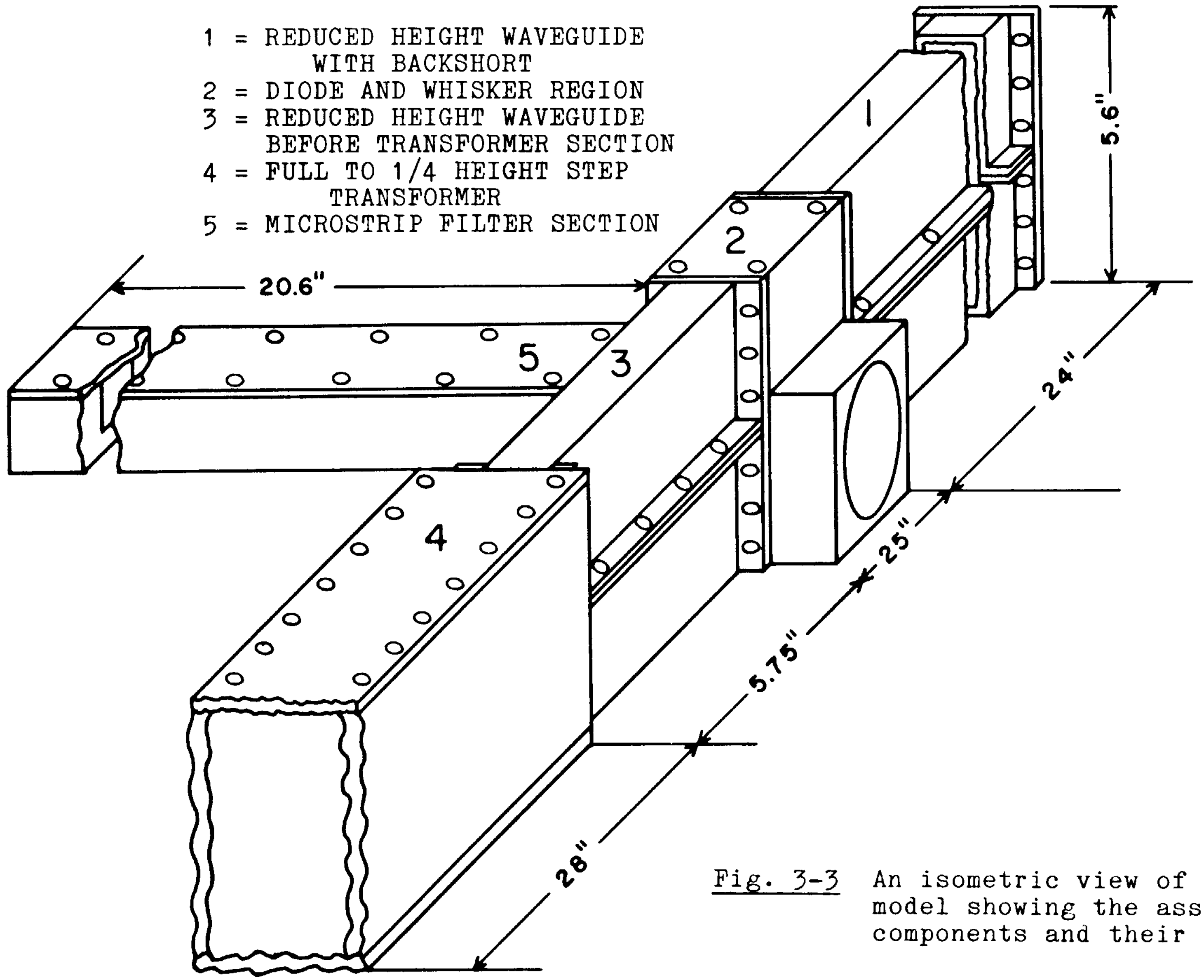

Fig. 3-3 An isometric view of the mixer model showing the assembled components and their dimensions.

3.4 Impedance Measurements

The mixer model embedding impedances, looking from the diode terminals into the waveguide mounting structure, were measured in 10 MHz intervals from 1.4-13.2 GHz at 65 different backshort positions. In this way the 140-220 GHz mixer mount was characterized over six LO harmonics for any desired intermediate frequency. Some representative Smith chart plots of these impedances will be given in Section 3.6.

To facilitate the data collection a semi-automated network analyzer was set up around an Apple II computer and a Hewlett Packard 8742A/8410A/8414A reflectometer test set. The network analyzer compares a known reference signal (the reflected wave from a short circuit at the end of a reference cable) with the reflected wave at the end of the coaxial cable in the mixer model. The reference plane of the reflectometer is extended by means of external cabling so as to fall at the position occupied by the anode of the diode. The complex ratio of the incident and reflected waves at the reference plane yields the embedding impedance of the mixer mount:

$$Z_e = Z_0 \, [\Gamma_v + 1]/[\Gamma_v - 1] \, , \tag{3.1}$$

where Z_0 is the characteristic impedance of the test set (50 ohms) and Γ_v is the complex reflection coefficient of the mixer mount.

A block diagram of the semi-automated network analyzer test set* appears in Fig.3-4. A 1 mV/MHz voltage controlled YIG (yttrium iron garnet) tuned oscillator coupled to a digitally programmable 0-10 volt D/A converter provides the microwave signal for the network analyzer. The signal frequency is monitored and adjusted using an HP5342A microwave counter and the D/A converter in a feedback loop which utilizes an IEEE-488 bus to communicate with the controller, an Apple II computer. The computer records the impedances measured with the network analyzer at each desired frequency point in the interval between 1.4 and 13.2 GHz and then advances the backshort in the mixer model (via a stepper motor) to its next position (corresponding to a distance of 2 mils in the actual mixer). Measurement results are output via a

---

* This test set is more fully described in references [149-150]. It incorporates a 3 short calibration scheme to remove inherent instrumentation errors (see Section 3.5.2).

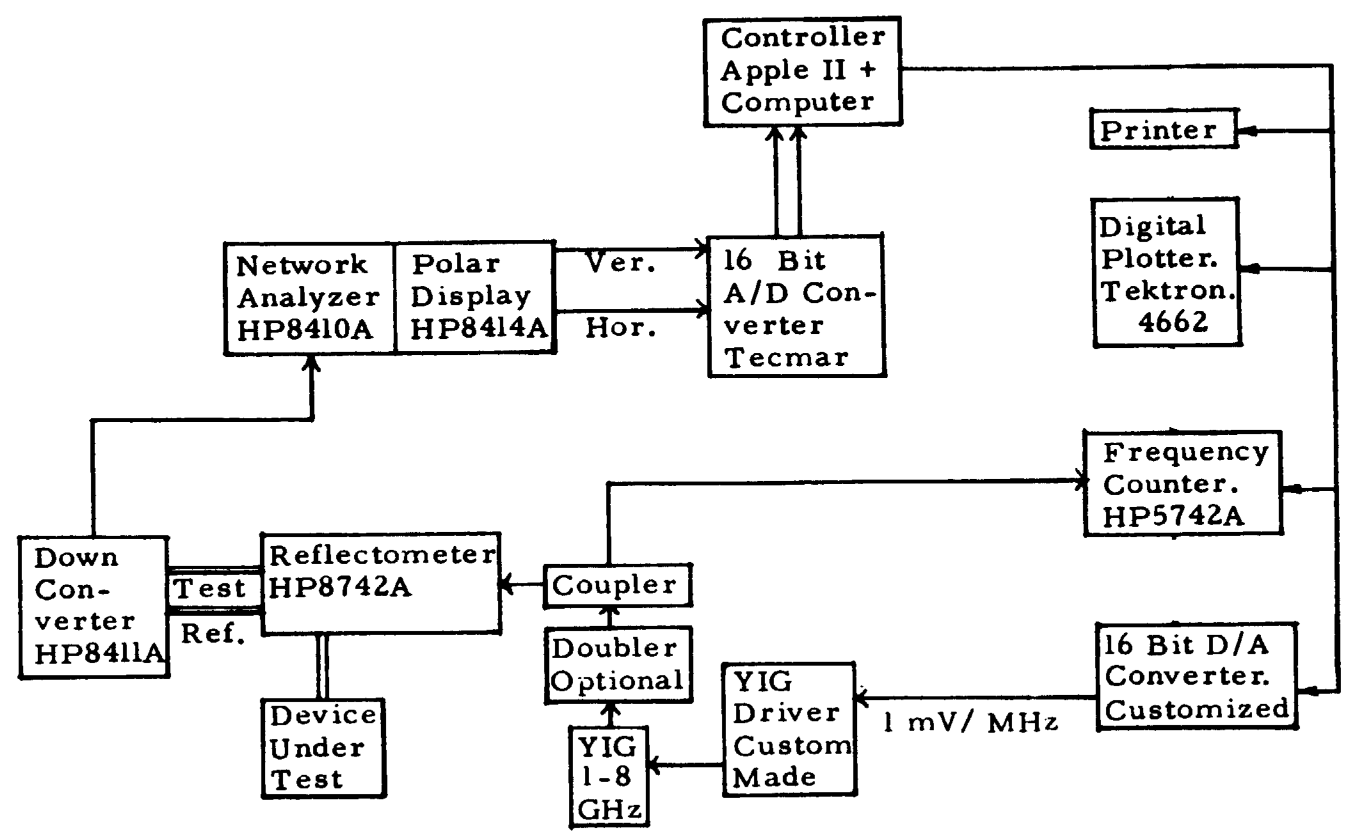

Fig. 3-4 A block diagram of the semi-automated reflectometer test set used for making stepped frequency impedance measurements on one port devices, specifically the 140-220 GHz mixer model.

printer and a digital plotter. The impedances are stored on diskettes and later transfered to a large mainframe computer for use in the mixer analysis program described in Chapter 2.

3.5 Measurement Uncertainties

3.5.1 Corrections to the Mixer Model

The 100x scale model accurately represents the actual 140-220 GHz mixer except in the region around the anode of the diode. In this area the coaxial cable poorly mimics the diode and its associated depletion region. The differences are highlighted in Figs.3-5a and 3-5b.

Fortunately the variations between the model and a true scaled version of the 140-220 GHz mixer occur over distances which are very short compared with a wavelength, even at the higher LO harmonics, and we can represent them by lumped elements. The largest discrepancy is in the value of the fringing capacitance from the whisker to the conducting portion of the diode chip face. This capacitance, shown in Fig.3-5, is in parallel with the diode junction and hence with the embedding network impedances. There is also a small inductive difference between the actual mixer and the model due to the variation in whisker tip angles.

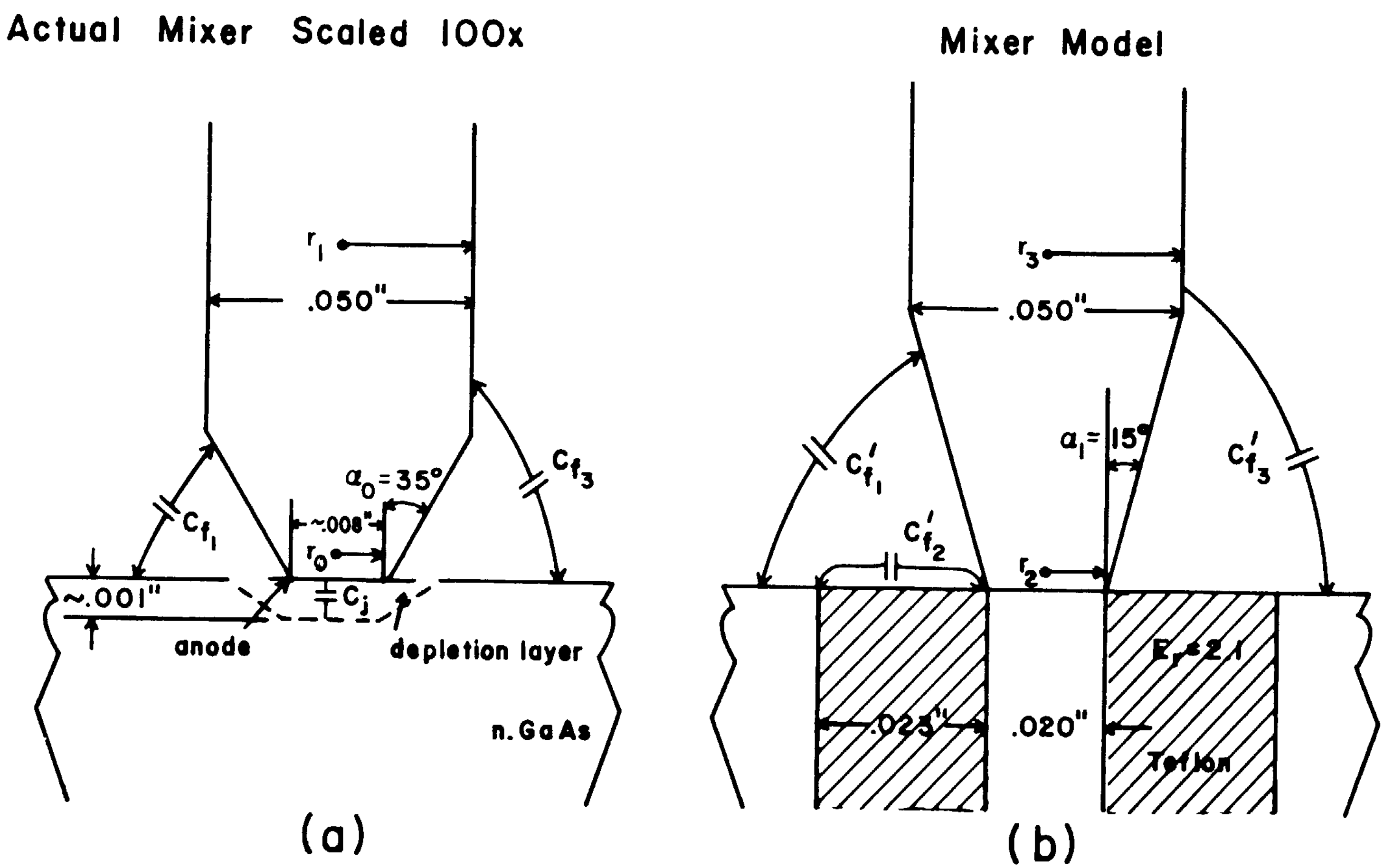

Fig. 3-5 A view of the region in the vicinity of the diode in (a) the actual 140-220 GHz mixer (shown blown up 100x) and (b) the 100x scale model. Electrical variations between the model and the actual mixer are due to differences in the fringing capacitances associated with the whisker and diode chip, and differences in the inductance of the two whiskers.

The excess inductance L_e of the mixer model can be calculated using the results in [88]*:

$$L_e = \mu_0 \cot\alpha_1 \, [r_3 - r_2 - r_2 \log r_3/r_2] \,/\, 2\pi \qquad (3.2)$$

$$- \mu_0 \cot\alpha_0 \, [r_1 - r_0 - r_0 \log r_1/r_0] \,/\, 2\pi ,$$

where α_0 and α_1 are the conical tip half angles, r_1 and r_3 are the whisker radii, r_0 and r_2 are the tip radii, and μ_0 is the free space permeability.

Using the dimensions in Fig. 3-5 we find the excess inductance of the mixer model (above that of the actual scaled mixer) to be: L_e=11.5 pH. This translates into a correction of L_e= -0.115 pH for the 140-220 GHz mixer. Hence if Z_e is the impedance measured on the scale model:

$$Z_{e_{corrected}} = Z_e + j\omega L_e , \qquad (3.3)$$

where L_e = -0.115 pH in this case.

---

* There is a small frequency dependent term in L_e due to skin effect which has been neglected in (3.2). At 180 GHz the error is less than 0.5 percent.

The capacitive difference between the actual mixer and the scale model is harder to calculate than the inductive difference. However, it was easily measured with a low frequency bridge as follows.*

Two scale models of the region in the vicinity of the diode, one of the actual mixer, and the other of the mixer model, were constructed (see Fig.3-6). A Boonton bridge with a resolution of 0.05 fF was used to measure the difference in fringing capacitance between the two models at a frequency of 1 MHz. As expected (a theoretical determination of the relative capacitances was also made) the fringing capacitance of the scaled mixer model was larger than that of the scaled mixer by some 500 fF. This difference reduces to 0.25 fF for the actual 140-220 GHz mixer and must be added in parallel with our measured embedding impedances to correct for the effects of the coaxial cable. Hence if Z_e is the impedance measured with the network analyzer on the 100x scale model of the mixer and C_e is the capacitive difference measured with the Boonton bridge then:

---

* This measurement can be made accurately only so long as the differences between our model and the actual scaled mixer occur over distances which are short compared to a wavelength.

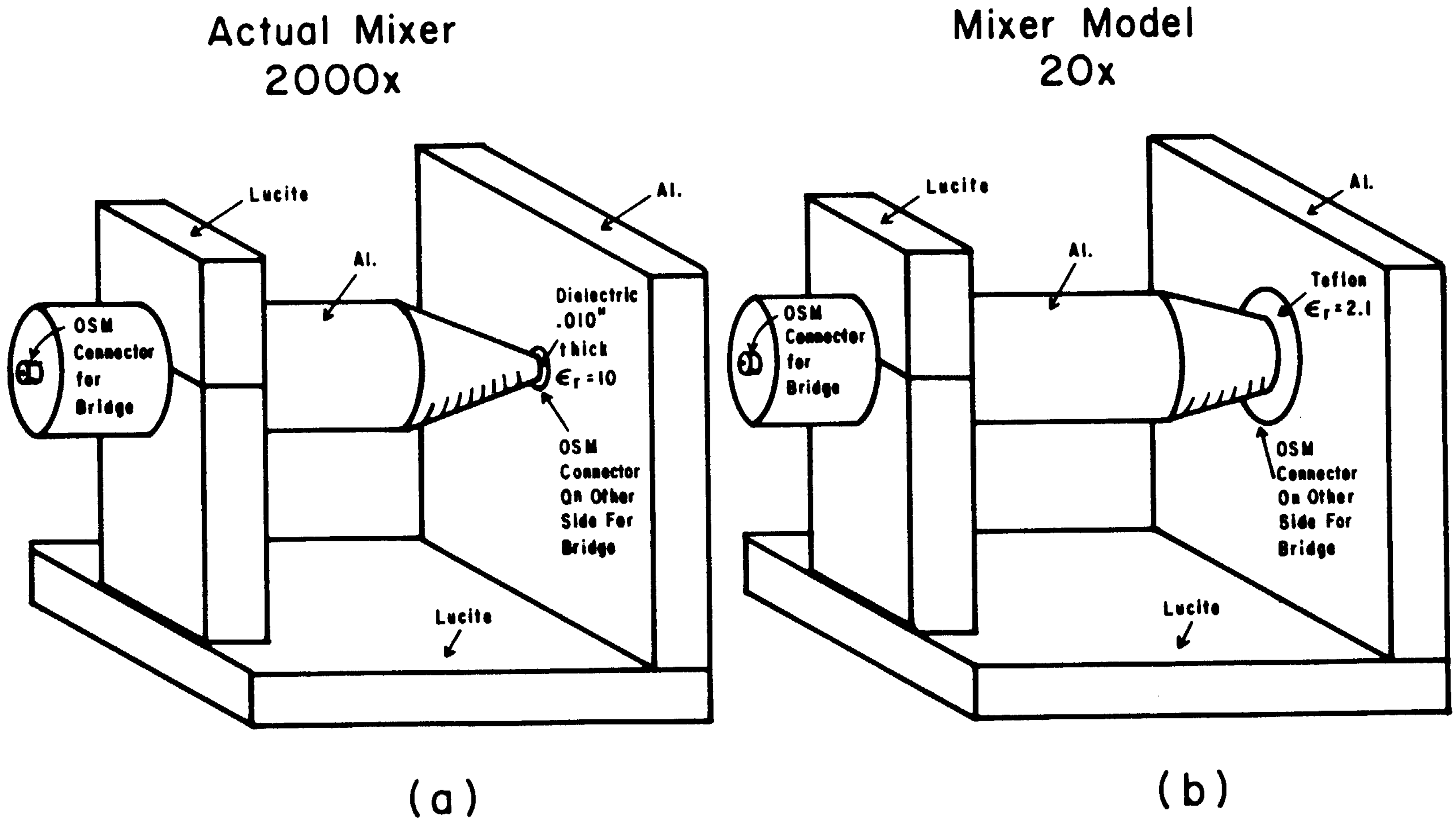

Fig. 3-6 Two scale models which were used to measure the difference in the fringing capacitance between (a) the actual mixer (scaled up 2000x) and (b) the mixer model (scaled up 20x). A Boonton bridge (model 75D) operating at 1 MHz was employed since the area over which the variation in capacitance occurs extends for much less than an LO wavelength. The bridge terminals are located; one on the back of each whisker and one on the rear of the plate representing the diode face.

$$Z_{e_{corrected}} = Z_e || (1/j\omega C_e) = Z_e/(1+j\omega Z_e C_e) \;, \tag{3.4}$$

where C_e is $-.25$ fF in this instance.

Combining both the inductive and capacitive corrections, we have:

$$Z_{e_{corrected}} = j\,\omega\,L_e + Z_e/(1 + j\,\omega\,Z_e C_e) \;. \tag{3.5}$$

Two other factors may cause the impedances measured on the scale model to differ from those of the actual mixer. First, due to practical considerations, the backshort in the scale model (see Fig. 3-2) is not an exact replica of the one in the actual mixer (Fig. 3-1). Second, the rather substantial loss at 140-220 GHz associated with the exposed length of reduced height waveguide, which increases as the sliding short is pulled back from the diode, is not accurately represented in the scale model.

The error in the measured embedding impedances caused by differences between the backshorts in the scale model and the actual mixer are difficult to determine. This is due largely to the problems encountered in trying to characterize the backshort over the nominal mixer operating range (140-220 GHz). So long as good electrical contact between the sliding short and the waveguide walls is maintained in both the scale model and the actual mixer, any differences in the measured and actual impedances will be small (at least at the LO frequency).

The effect on the mixer performance of the loss of the reduced height waveguide can be readily observed. As the backshort is moved further from the diode (i.e., more and more reduced height waveguide is exposed), the minimum values of the measured mixer noise and conversion loss increase. We can model this effect by making a correction to the measured embedding impedances at the LO, upper and lower sideband frequencies.

The embedding impedances together with a lossless backshort section can be represented by the 2 port network in Fig. 3-7. Z_e is the measured impedance at the LO frequency and Z_b is the impedance of the backshort and reduced height waveguide. The 2 port is described by 3 independent parameters z_{11}, z_{22} and $z_{12}z_{21}$. We may write:

$$Z_e = z_{11} - z_{12}z_{21}/(z_{22} + Z_b) \ , \tag{3.6}$$

where Z_b is a function of the waveguide impedance Z_c, the propagation constant of the TE_{10} mode β, and the length of reduced height waveguide between the diode and the short

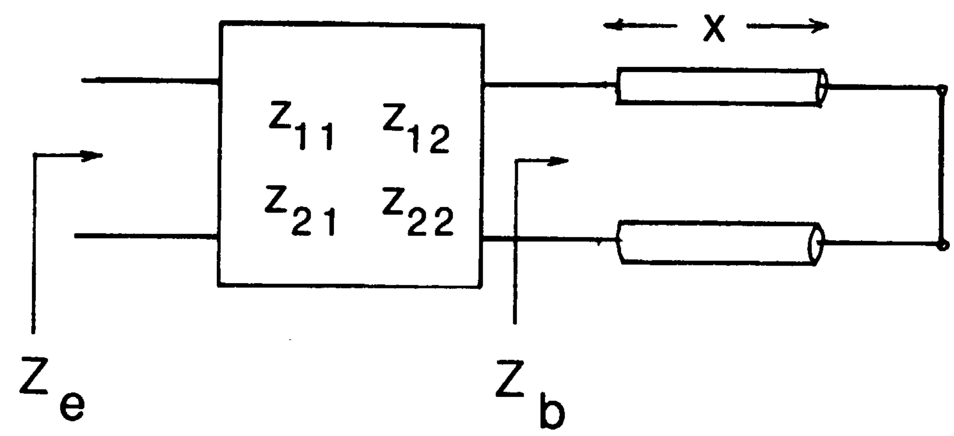

Fig. 3-7 A simple two port representation of the diode embedding network in which the backshort has been separated out from the rest of the circuit.

circuit plane, x. Hence

$$Z_b = jZ_c \tan \beta x \ , \tag{3.7}$$

with

$$Z_c = (\mu/\varepsilon)^{1/2} \ (\pi b/2a) \ , \quad \text{and} \tag{3.8}$$

$$\beta = (2\pi f_{LO}/c) \ [1-(f_{LO}/f_c)^2]^{1/2}. \tag{3.9}$$

f_c is the cutoff frequency of the reduced height waveguide with height b and width a.

In the actual mixer the reduced height waveguide has some loss per unit length α and so (3.7) becomes:

$$Z_b' = Z_c \tanh \ (\alpha + j\beta\ )x \ , \tag{3.10}$$

and we have:

$$Z_e' = z_{11} - z_{12}z_{21}/(z_{22} + Z_b') \ . \tag{3.11}$$

If we use three measured values of Z_e and Z_b we can find z_{11}, z_{22} and $z_{12}z_{21}$ from (3.6) at a particular frequency. Z_e' can then be determined from (3.10) and (3.11).

At 180 GHz α was taken to be 11.7 dB/foot (1.34 nepers/foot). This value of α is 3 times the theoretical loss so as to approximately compensate for waveguide surface roughness. The corrected values of the embedding impedances, Z_e', at the LO, signal and image frequencies were then calculated from (3.6)-(3.11) for each mixer backshort position. These impedances were then used in the mixer analysis program in place of the corresponding measured values, Z_e. The resulting changes to Z_e and hence in the mixer performance were very small.

The magnitude of the corrections to the measured impedances due to inductive and capacitive differences between the model and the actual mixer and waveguide loss can be inferred from Fig. 3-8.

IMPEDANCE VS. BACKSHORT POSITION AT 180.00 GHZ
SOLID LINE= MEASURED NORMALIZED DATA
DASHED LINE=CORRECTED DATA

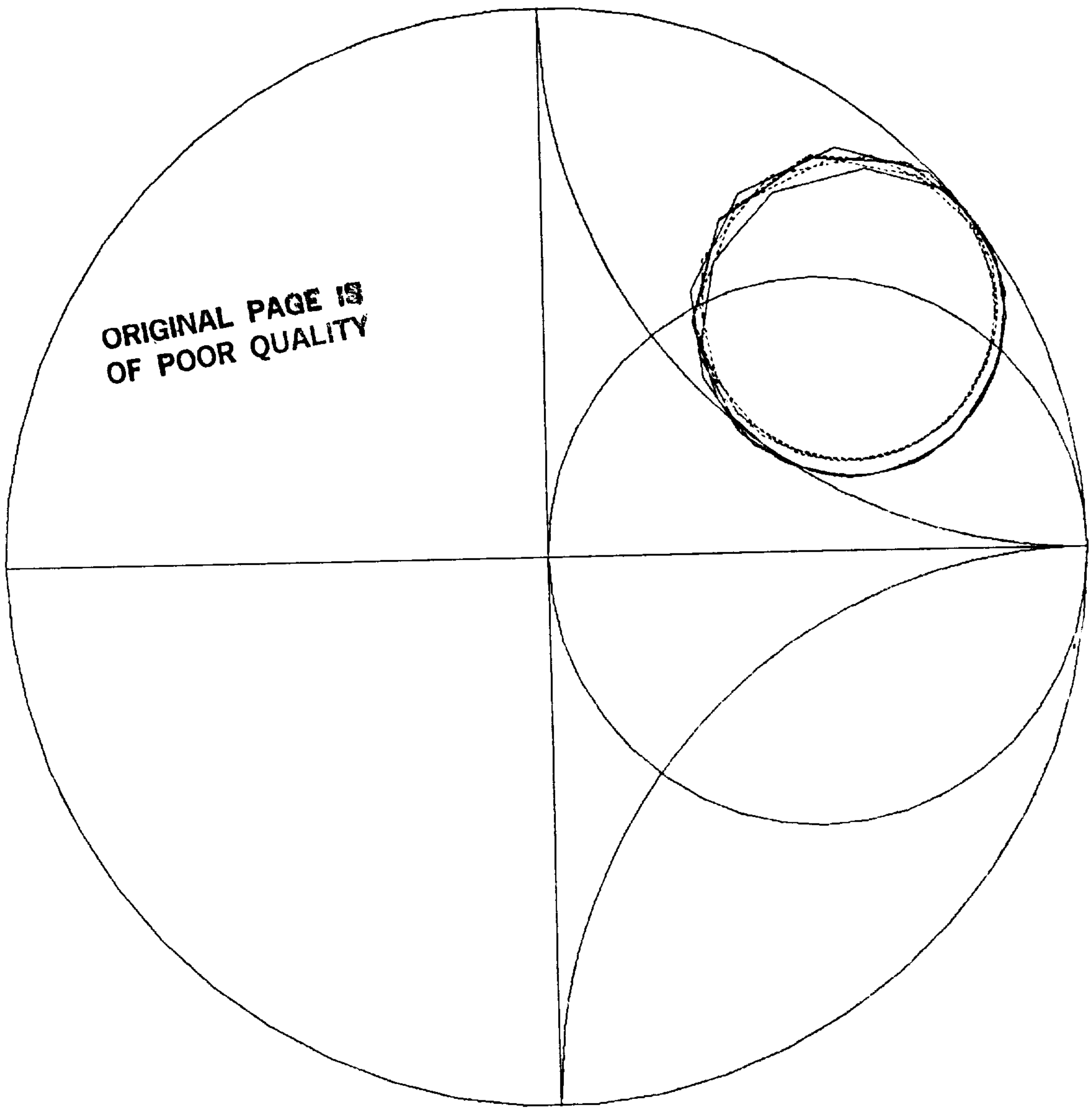

Fig. 3-8 The measured (solid line) and corrected (dashed line) diode embedding impedances as a function of backshort position at an LO frequency of 180 GHz. The dashed line shows the impedances corrected for waveguide loss and for capacitive and inductive differences between the mixer and the scale model.

3.5.2 Impedance Measurement Errors

Besides the errors inherent in the mixer modelling, that is the nonlinear scaling of the waveguide loss, backshort differences, and the distortion introduced by the presence of the test cable, there are additional measurement uncertainties due to imperfections in the microwave network analyzer. These errors have been well characterized and many schemes have been proposed for calibrating them out (see for example [46,47,60,61,64]). For the measurements in this thesis a calibration scheme which could be easily incorporated into the semi-automated network analyzer test set was used and will now be described.

Standard microwave network analyzers use directional couplers to sample the forward and reflected waves from the device under test and then down convert to a low intermediate frequency to take the required phase and amplitude ratios. The resulting measurement suffers from three major sources of error: (1) the limited directivity of the couplers, (2) the impedance mismatch at the test signal port and from the connectors in the system, and (3) a lack of gain and phase flatness between the test and reference channel signals. These errors can be calibrated out of the reflectometer system at a particular frequency by measuring three different one port devices whose complex reflection coefficients are known a priori.

An imperfect network analyzer can be represented by a two port scattering matrix, containing the three sources of instrumentation error, in series with the device under test (DUT) and an ideal reflectometer as shown in Fig.3-9. From the figure:

$$b_1' = a_1' S_{11} + a_2' S_{12} , \quad \text{and} \tag{3.12}$$

$$b_2' = a_1' S_{21} + a_2' S_{22} . \tag{3.13}$$

In the figure $b_2'=a$ and $a_2'=b$ which after substitution in (3.12-3.13) leaves:

$$a_1' = (a-bS_{22})/S_{21} , \text{ and} \tag{3.14}$$

$$b_1' = (a-bS_{22})S_{11}/S_{21} + bS_{12} . \tag{3.15}$$

Using the definition of the reflection coefficient, $\Gamma_v = b/a$ and $\Gamma_v' = b'/a'$ and solving for Γ_v in (3.14-3.15) we find:

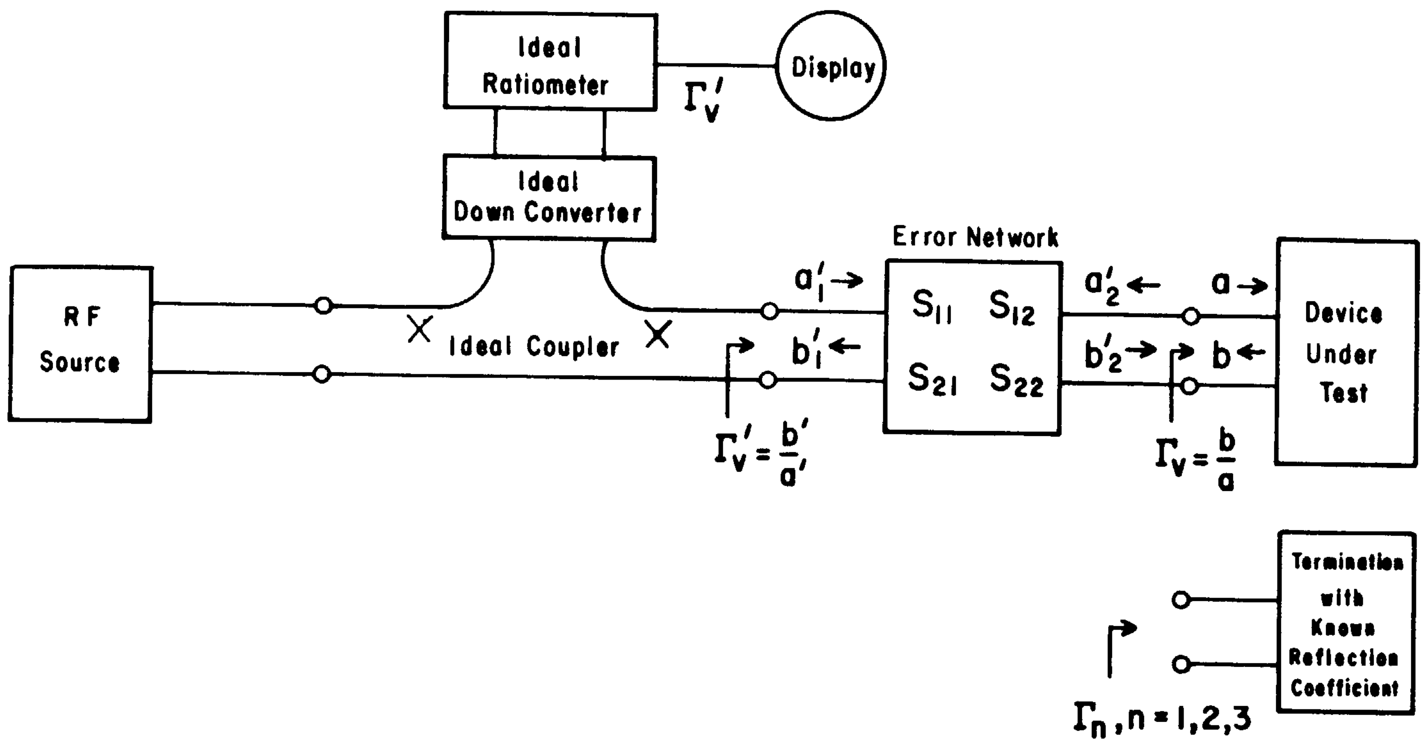

Fig. 3-9 An imperfect reflectometer represented by an ideal directional coupler, down converter and ratio meter in series with a two port error network and the device under test. The two port network, characterized by its scattering parameters, accounts for the three major sources of error in the reflectometer. These can be calibrated out if a measurement is made on each of three different terminations with known reflection coefficients.

$$\Gamma_v = (\Gamma_v' - S_{11})/[S_{12}S_{21} + S_{22}(\Gamma_v' - S_{11})] \ . \tag{3.16}$$

Equation (3.16) gives the actual reflection coefficient of the device under test in terms of the reflection coefficient measured through the imperfect reflectometer and three complex unknowns $S_{11}, S_{12}S_{21}$ and S_{22}.

Suppose we replace the DUT in Fig.3-9 with a one port device whose reflection coefficient Γ_1 is known exactly at the frequency of interest. When a measurement is made with our imperfect reflectometer we would find:

$$\Gamma_1 = (\Gamma_1' - S_{11})/[S_{12}S_{21} + S_{22}(\Gamma_1' - S_{11})] \ , \tag{3.17}$$

where the prime indicates the measured value of the reflection coefficient. Similarly if we repeat the procedure two more times we will obtain two more equations among the three unknowns $S_{11}, S_{12}S_{21}$ and S_{22}. Some simple but laborious algebra now yields:

$$S_{11} = \frac{\Gamma_1\Gamma_3(\Gamma_2'\Gamma_3' - \Gamma_1'\Gamma_2') + \Gamma_2\Gamma_3(\Gamma_1'\Gamma_2' - \Gamma_1'\Gamma_3') + \Gamma_1\Gamma_2(\Gamma_1'\Gamma_3' - \Gamma_2'\Gamma_3')}{\Gamma_1\Gamma_3(\Gamma_3' - \Gamma_1') + \Gamma_2\Gamma_3(\Gamma_2' - \Gamma_3') + \Gamma_1\Gamma_2(\Gamma_1' - \Gamma_2')} \tag{3.18}$$

$$S_{22} = \frac{S_{11}(\Gamma_2-\Gamma_1)+\Gamma_2'\Gamma_1-\Gamma_2\Gamma_1'}{\Gamma_2\Gamma_1(\Gamma_2'-\Gamma_1')} \text{ , and} \tag{3.19}$$

$$S_{12}S_{21} = [\Gamma_1'(1-S_{22}\Gamma_1)-S_{11}]/\Gamma_1 \quad . \tag{3.20}$$

Since all the reflection coefficients Γ_n and Γ_n' , n=1,2,3 are either known or measured, substitution into (3.16) results in a value for the actual reflection coefficient of the DUT, Γ_v.

There is some art in choosing the three one port devices to be used as the standards in the measurement. A number of simple terminations are possible, including open or short circuits, offset shorts or matched loads. The choice depends on the magnitude of the reflection coefficient which is expected from the DUT, one's physical ability to replace the device under test with the standards and the availability and accuracy of the terminations.

Reference to (3.18) indicates that choosing one of the calibration standards to be a matched load (Γ_1=0) will give S_{11} directly ($S_{11}=\Gamma_1'$). S_{22} and $S_{12}S_{21}$ must then be determined using the two additional standards, usually a short and an open circuited transmission line. However on many occasions this choice of calibration standards is impractical, especially when one remembers that the standards must all be implemented in the same transmission line structure as the DUT. The calibration does not account for connectors or adaptors which are used to attach the reference terminations to the test cable but not used on the device under test.

When the magnitude of the reflection coefficient to be measured is greater than about 0.05* [16,32] a simple means of implementing the three calibration standards is to use only short circuits [33]. This choice has the advantage of allowing the user to manufacture highly accurate reference terminations in almost any type of transmission line structure.

For the three short calibration scheme we have:

$$\Gamma_1 = 1e^{(j\pi)} = -1 , \tag{3.21}$$

$$\Gamma_2 = 1e^{(j\theta_1)} , \text{ and} \tag{3.22}$$

$$\Gamma_3 = 1e^{(j\theta_2)} , \tag{3.23}$$

---

* This restriction stems from experience and as Dalley [32] suggests, seems to indicate that at least one standard should have a reflection coefficient close to that of the device under test.

where $\theta_1=2\beta L_1$, $\theta_2=2\beta L_2$ and L_1 and L_2 are the physical changes in length between the reference short circuit and each of the offset short circuits. β is the propagation constant of the line. L_1 and L_2 vary with frequency and the wave velocity in the transmission line according to:

$$L = \theta_{radians} c/(4\pi f[\mu_r \varepsilon_r]^{1/2}) \quad , \qquad (3.24)$$

where c is the velocity of light, f the measurement frequency and μ_r and ε_r the relative permeability and permittivity of the short circuited transmission line. Empirically the best results are obtained when θ, θ_1 and θ_2 are separated by 120 degrees at the frequency of interest [32], i.e. when the phases of the calibration standards lie equally spaced on the unit circle. When the values of Γ_1, Γ_2 and Γ_3 in (3.21-3.23) are substituted into (3.18-3.20) considerable simplification results such that:

$$S_{11} = \frac{\Gamma_1'\Gamma_2'(1-e^{j\theta_1})-\Gamma_2'\Gamma_3'e^{j(\theta_1-\theta_2)}-\Gamma_1'\Gamma_3'(1-e^{j\theta_2})}{(\Gamma_2'-\Gamma_1')e^{j(\theta_1-\theta_2)}+(\Gamma_2'-\Gamma_3')(1-e^{j\theta_1})} \, , \qquad (3.25)$$

$$S_{22} = [\Gamma_1'-S_{11}+(S_{11}-\Gamma_2')e^{j\theta_1}]/(\Gamma_2'-\Gamma_1') \quad , \text{ and} \qquad (3.26)$$

$$S_{12}S_{21} = (S_{11}-\Gamma_1')(1+S_{22}) \quad , \qquad (3.27)$$

where the primed quantities are the indicated values of the reflection coefficients of the calibration standards. Notice that we do not get the same correspondence between a single measurement and one of the S parameters as we would have if one of the standards had been a matched load.

In summary, when θ_1 and θ_2 are appropriately chosen and the device under test is in turn replaced by each of the three reference short circuits, (3.25-3.27) can be solved for S_{11}, S_{22} and $S_{12}S_{21}$, and (3.16) then gives the corrected reflection coefficient. Hence at each frequency four complex quantities must be measured in order to calibrate out the three major sources of error in a standard reflectometer test set.

The 3 short calibration procedure was used for all the impedance measurements presented in this thesis. The magnitude of the correction can be inferred from Fig.3-10 where a set of measured and corrected impedances is shown as a function of frequency for a single backshort setting.

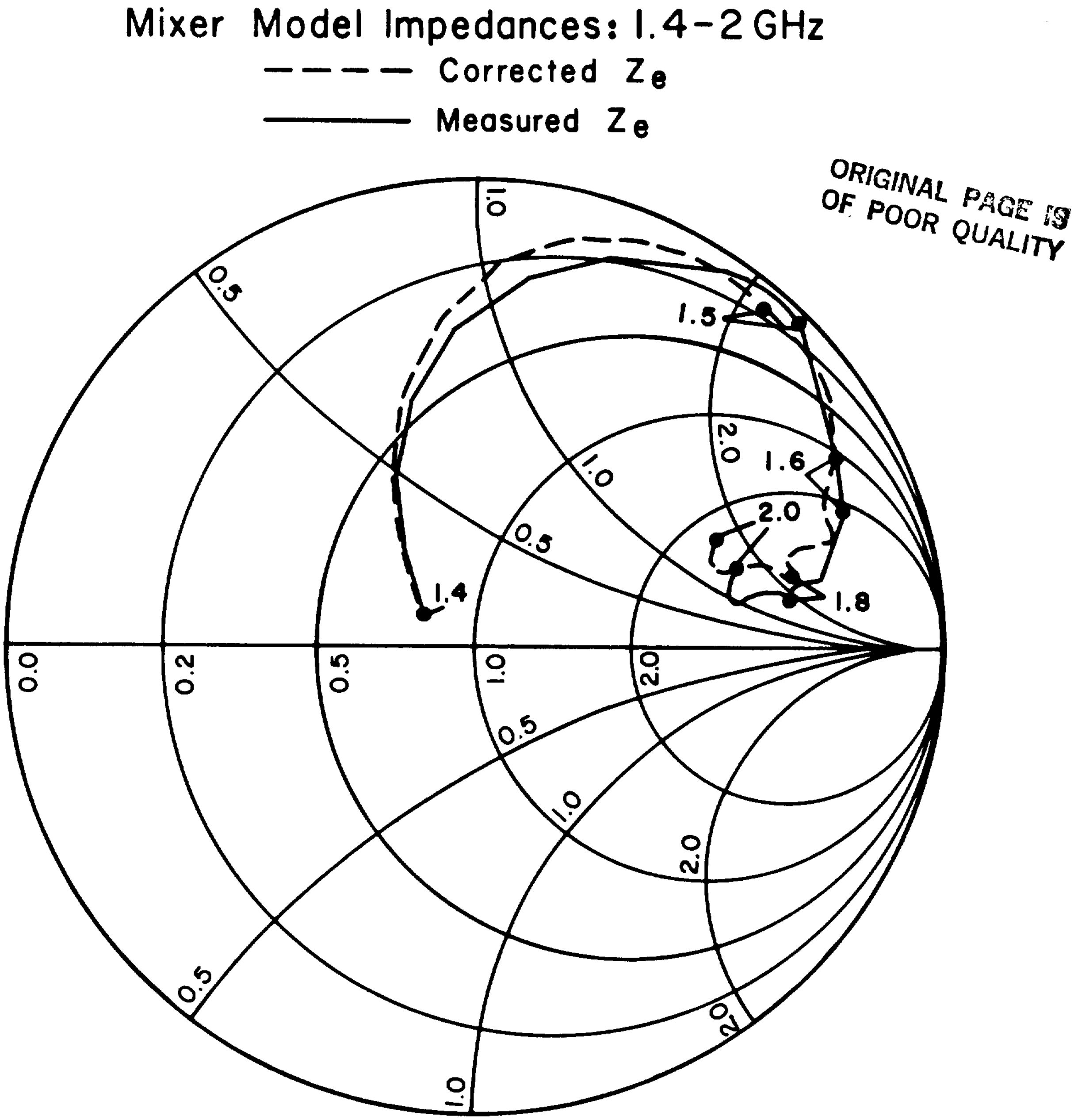

Fig. 3-10 A Smith chart plot showing the differences between the measured and corrected reflection coefficients (normalized to 50 ohms) for the 140-220 GHz mixer model at one backshort position. The data was collected over the frequency range 1.4-2 GHz. The corrected reflection coefficients (dotted) were calculated using (3.25-3.27) in (3.16).

3.6 140-220 GHz Mixer Impedances

The test set depicted in Fig.3-4 and the 3 short calibration scheme described in Section 3.5.2 were used to measure the embedding network impedances of the 140-220 GHz mixer up to the sixth LO harmonic. The data was then corrected for differences between the actual mixer and the scale model (including the loss in the reduced height waveguide) as discussed in Section 3.5.1. Smith chart plots of the corrected impedances (normalized to 50 ohms) versus backshort position at two representative LO frequencies, 150 and 180 GHz, are presented in Figs.3-11 to 3-22. Similar plots for the corresponding sideband frequencies appear in Figs.3-23 to 3-34 where an intermediate frequency of 3.95 GHz has been chosen. We see immediately that the impedances at the harmonic frequencies are neither open nor short circuits as has usually been assumed in past analyses. These impedances are used in the next chapter to compare the predictions of the mixer analysis program of Chapter 2 with measured mixer performance.

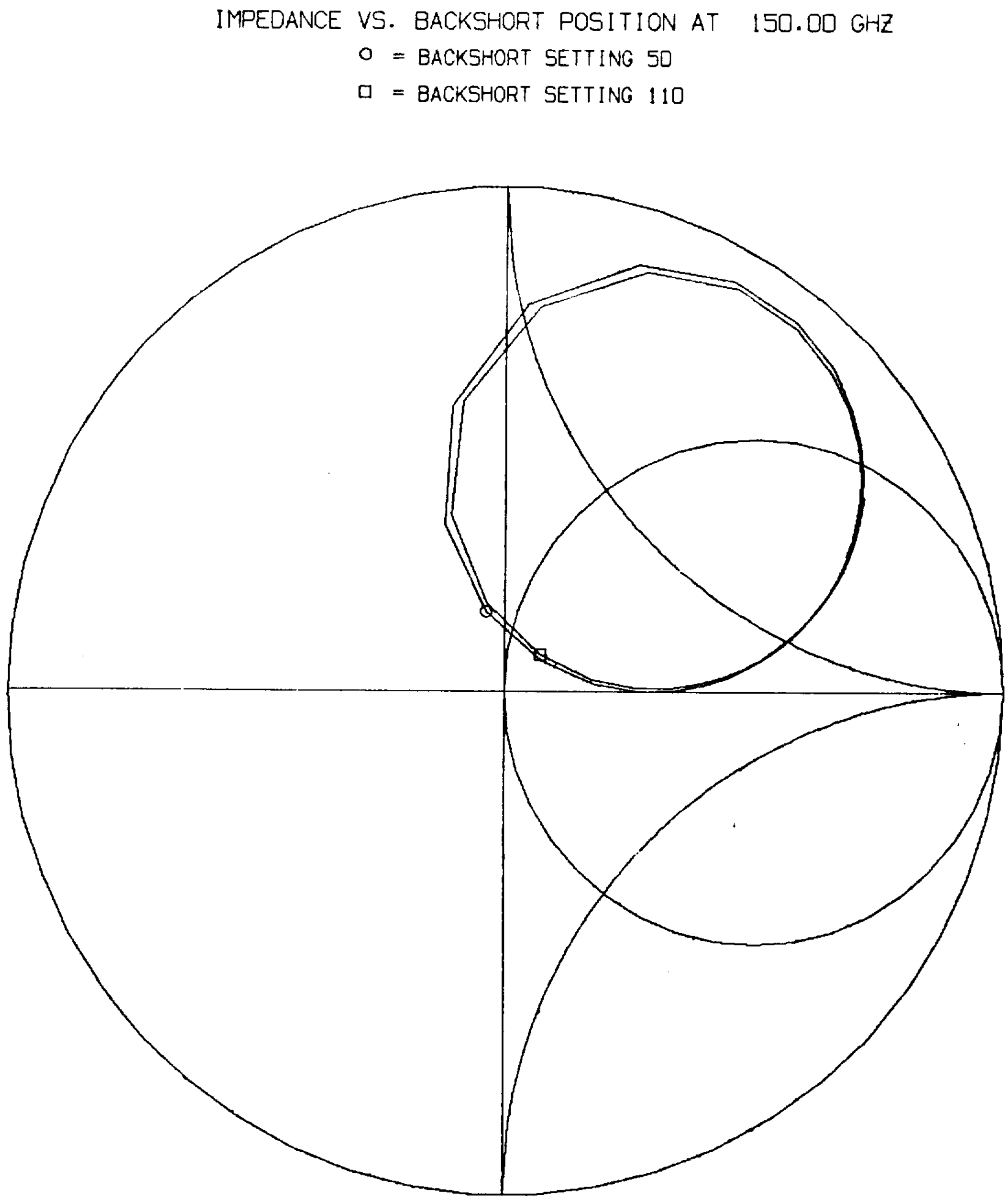

Fig. 3-11 A Smith chart plot of the measured diode embedding impedances as a function of backshort position at an LO frequency of 150 GHz. The data has been corrected both for instrumentation errors and for differences between the actual mixer and the mixer model following the procedures outlined in Section 3.5. The plotted symbols indicate the two backshort positions at which the mixer had the lowest conversion losses (see Fig. 4-11 of Chapter 4).

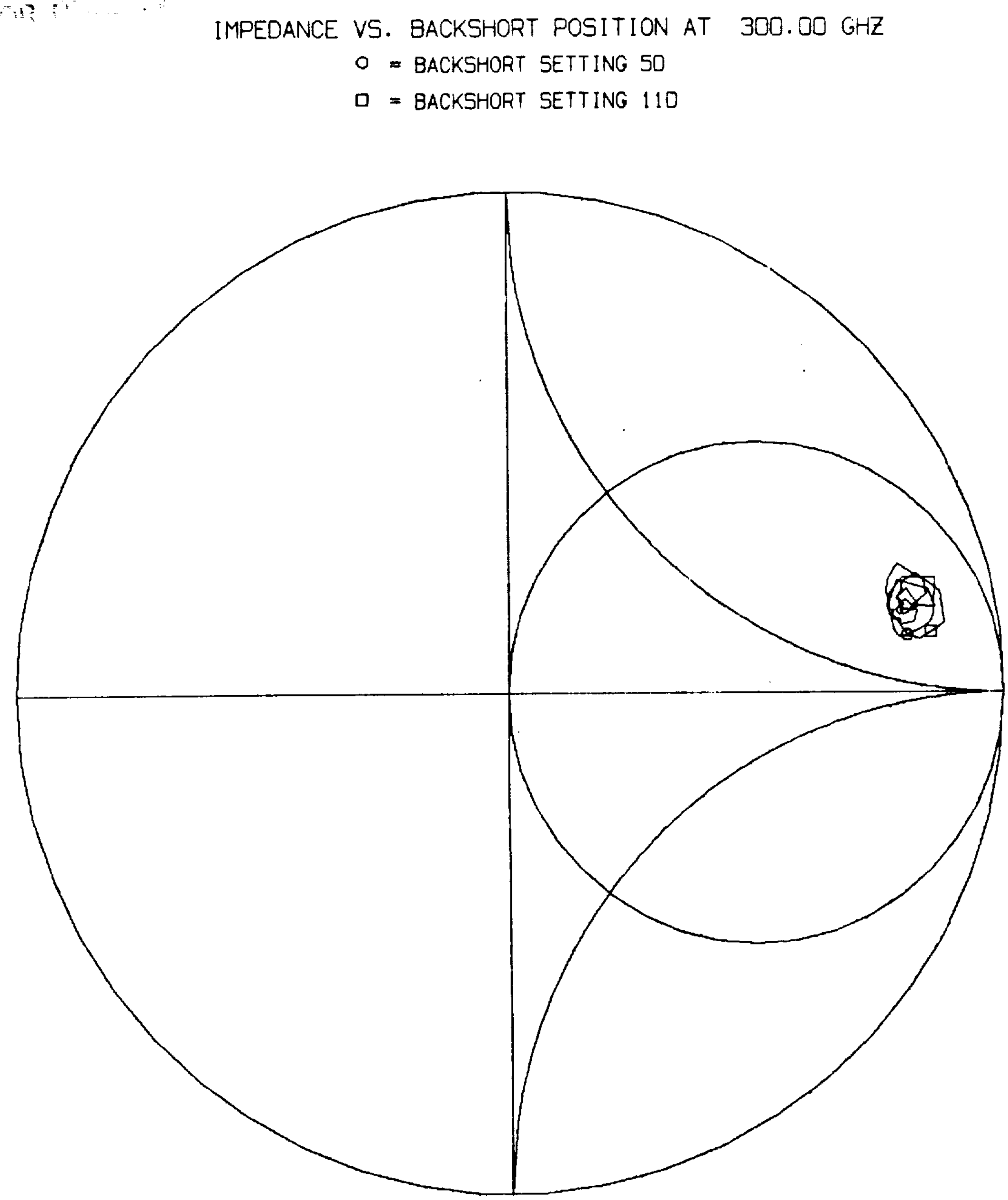

Fig. 3-12 A Smith chart plot of the measured diode embedding impedances as a function of backshort position at 300 GHz.

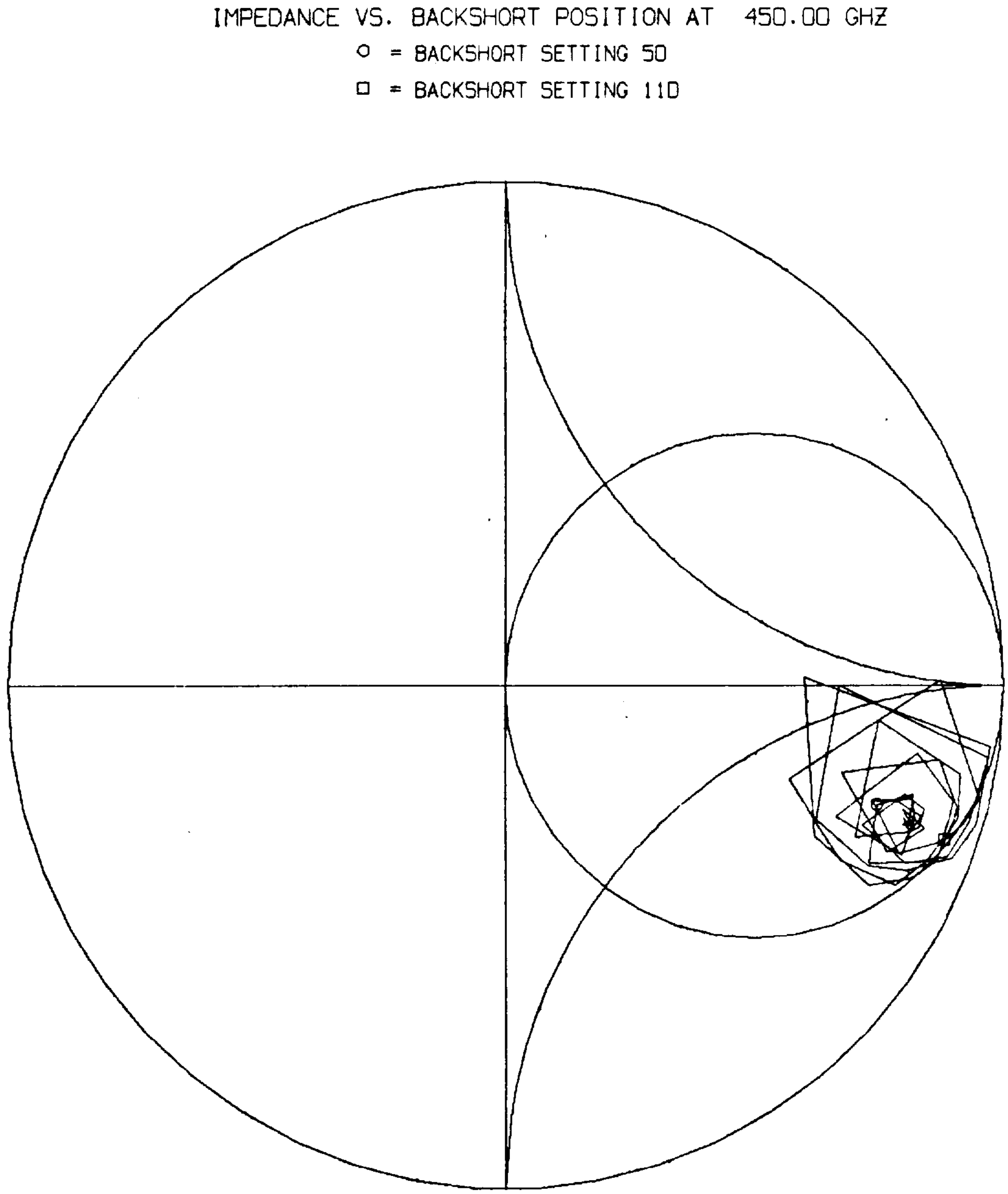

Fig. 3-13 A Smith chart plot of the measured diode embedding impedances as a function of backshort position at 450 GHz.

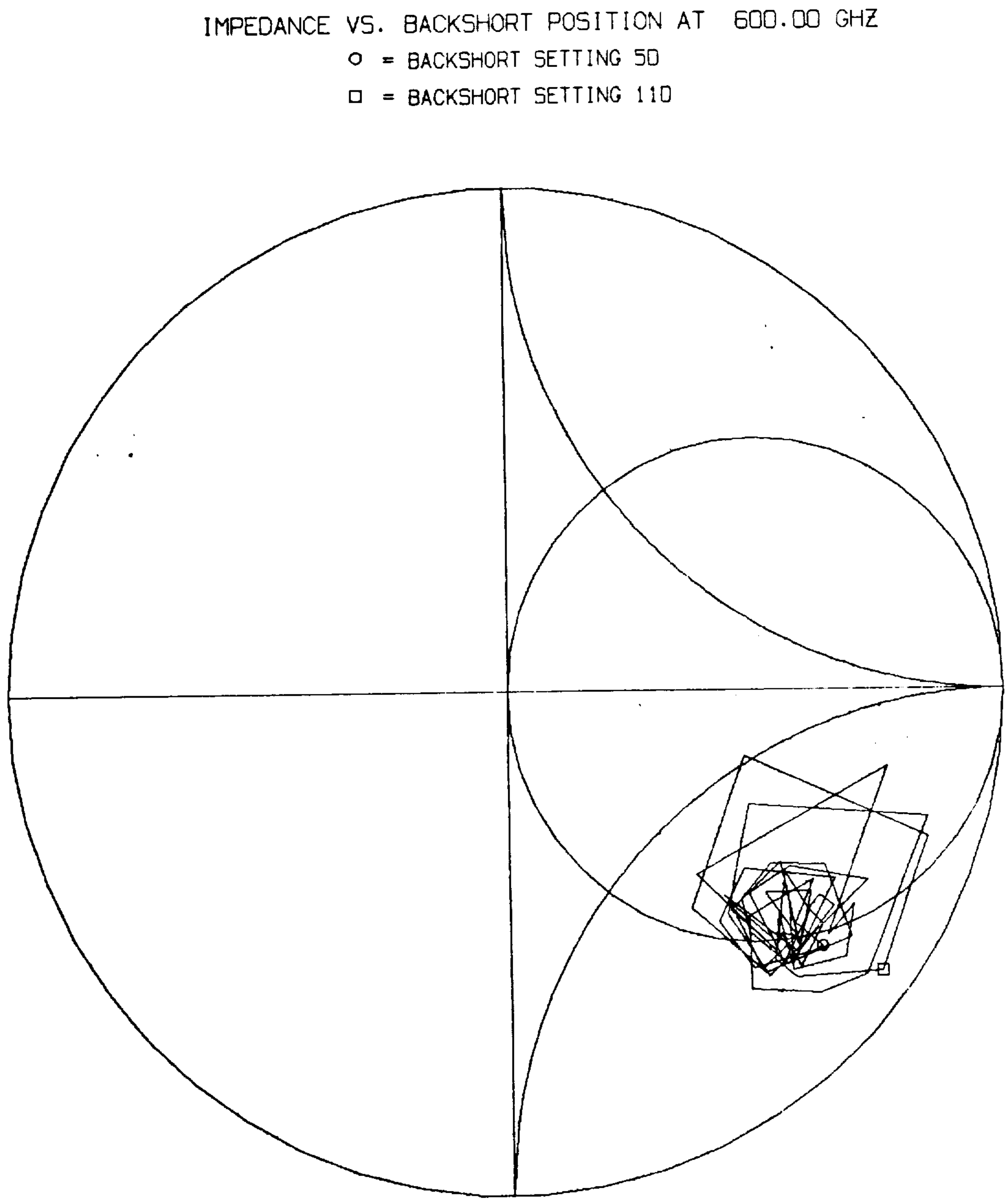

Fig. 3-14 A Smith chart plot of the measured diode embedding impedances as a function of backshort position at 600 GHz.

IMPEDANCE VS. BACKSHORT POSITION AT 750.00 GHZ

○ = BACKSHORT SETTING 50

□ = BACKSHORT SETTING 110

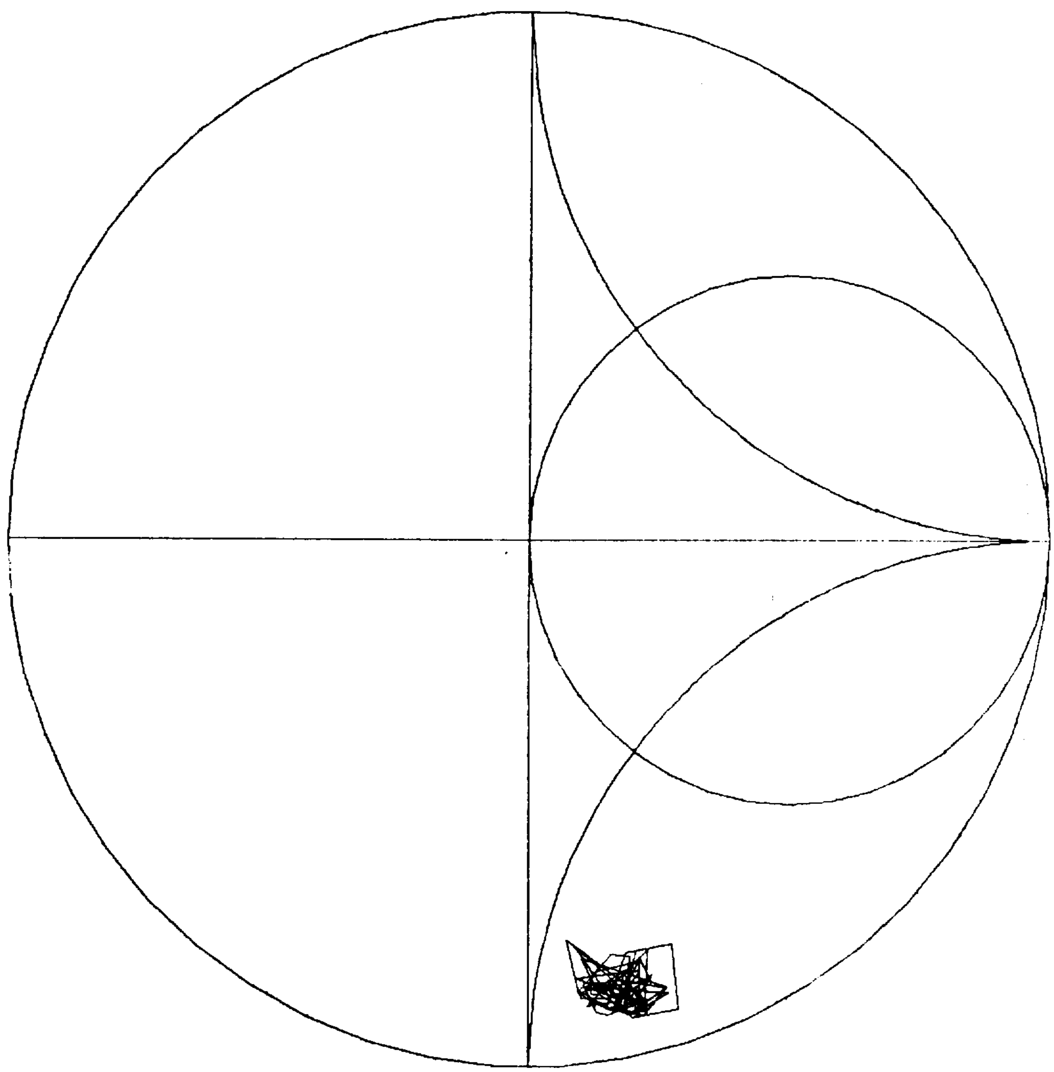

Fig. 3-15 A Smith chart plot of the measured diode embedding impedances as a function of backshort position at 750 GHz.

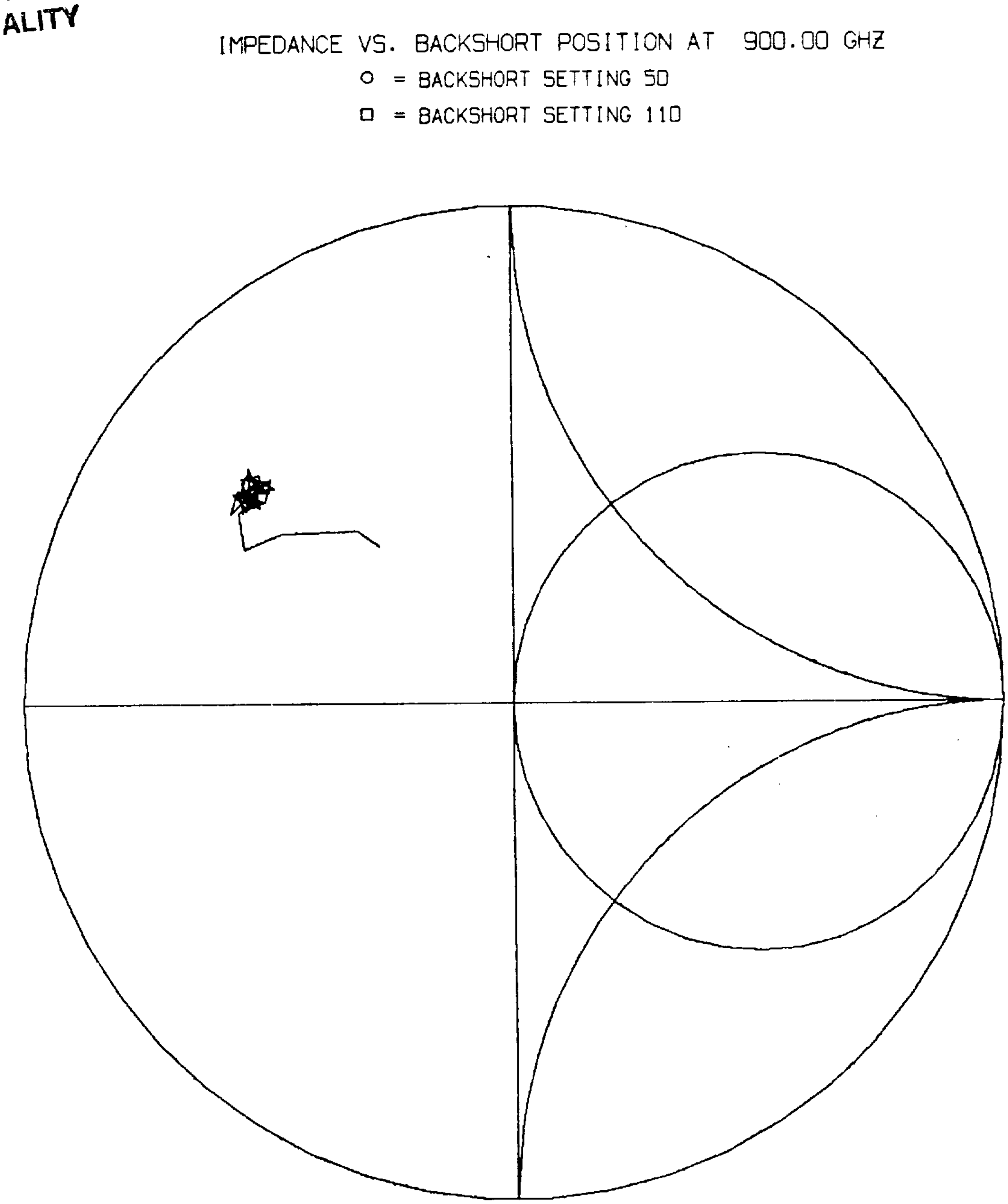

Fig. 3-16 A Smith chart plot of the measured diode embedding impedances as a function of backshort position at 900 GHz.

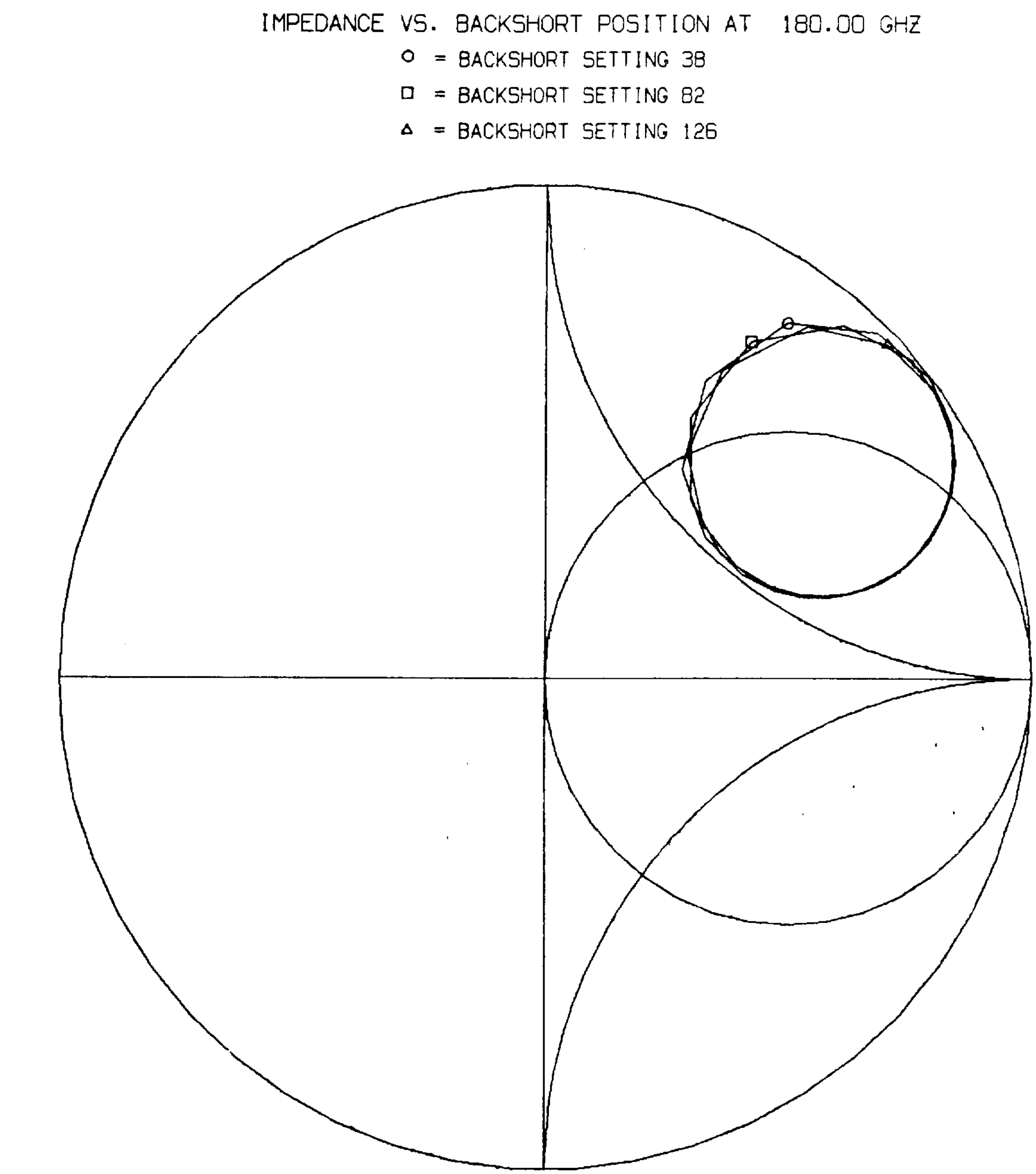

Fig. 3-17 A Smith chart plot of the measured diode embedding impedances as a function of backshort position at an LO frequency of 180 GHz. The plotted symbols indicate the three backshort positions at which the mixer had the lowest conversion losses (see Fig. 4-10 of Chapter 4).

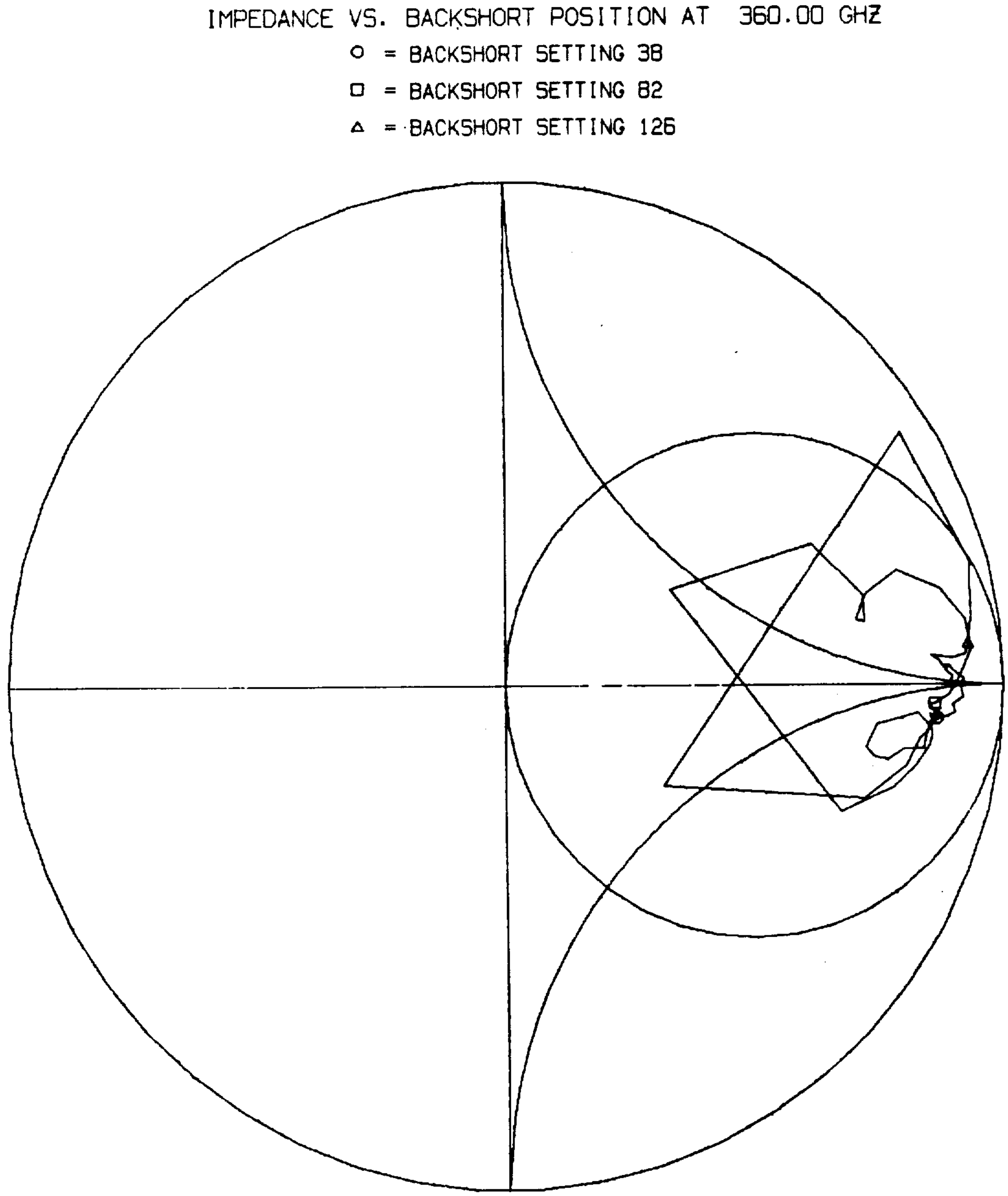

Fig. 3-18 A Smith chart plot of the measured diode embedding impedances as a function of backshort position at 360 GHz.

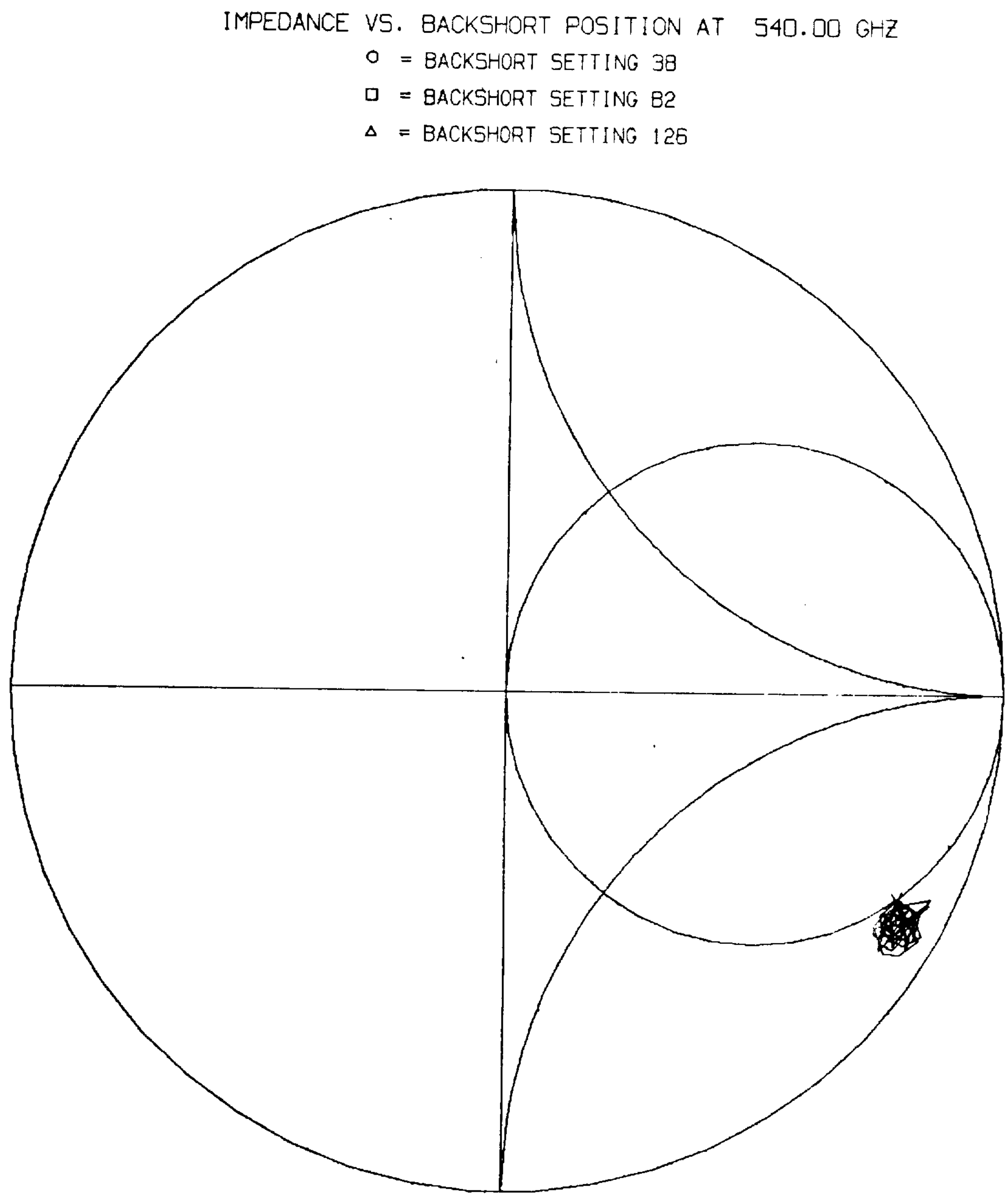

Fig. 3-19 A Smith chart plot of the measured diode embedding impedances as a function of backshort position at 540 GHz.

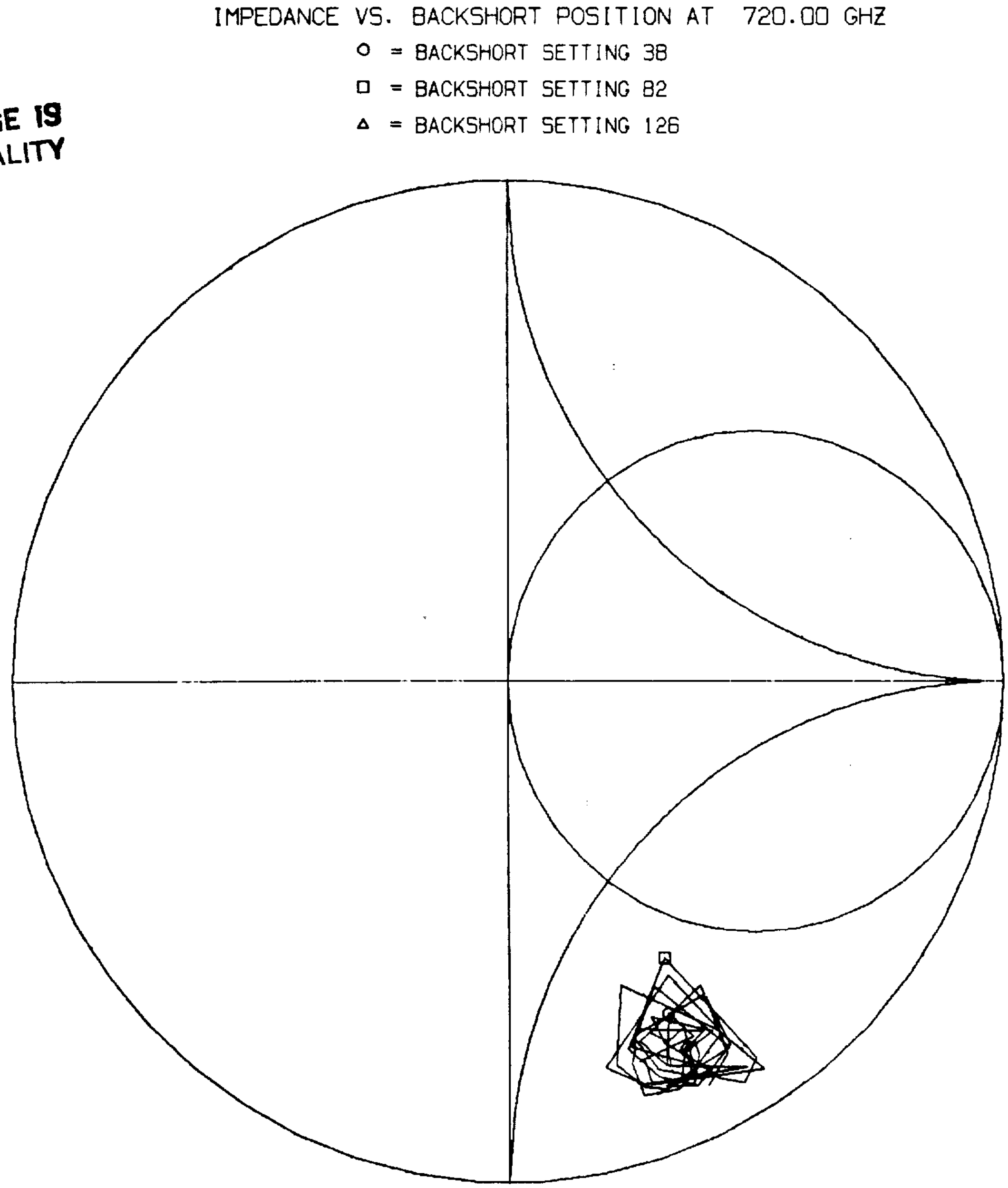

Fig. 3-20 A Smith chart plot of the measured diode embedding impedances as a function of backshort position at 720 GHz.

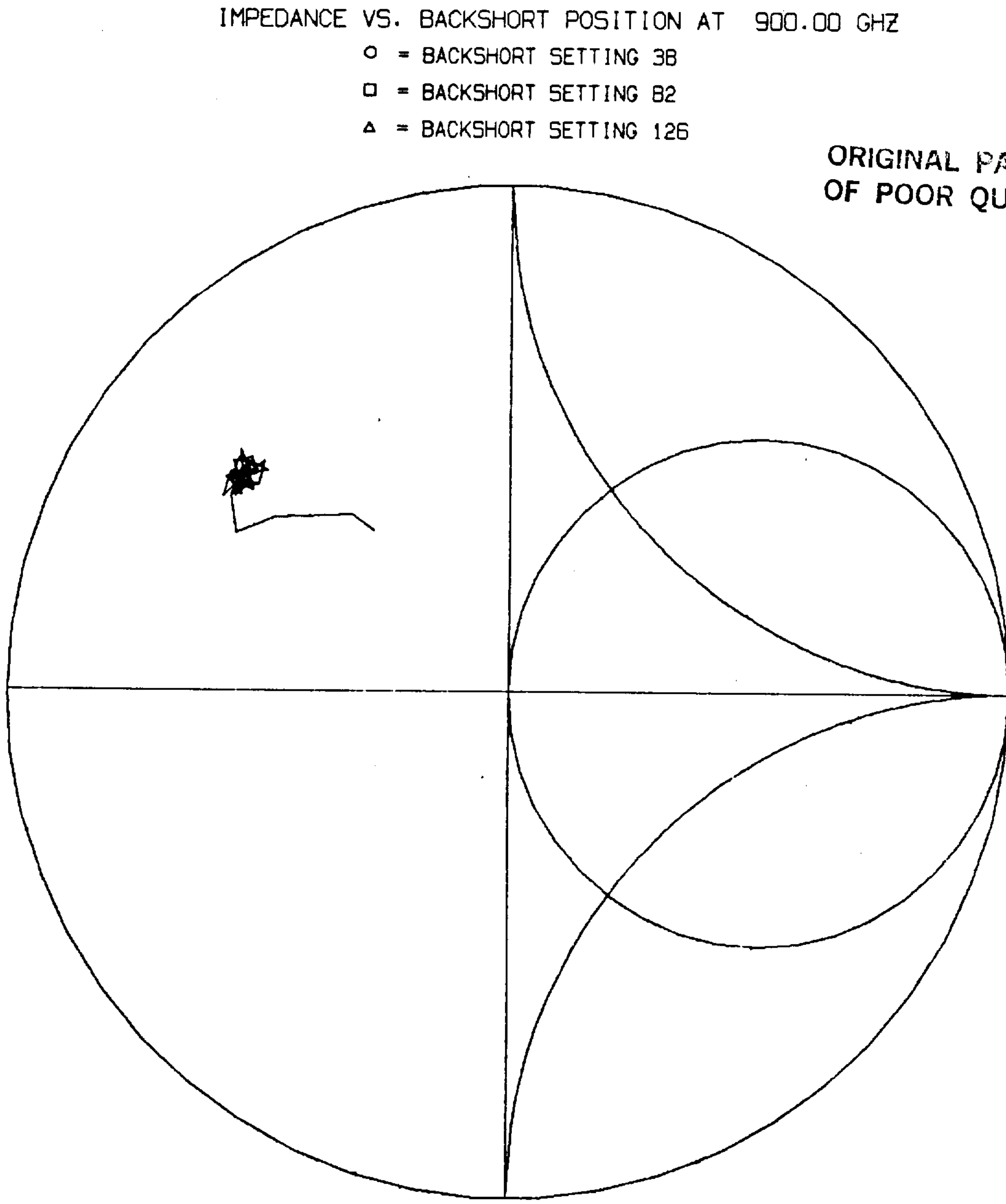

ORIGINAL PAGE IS OF POOR QUALITY

Fig. 3-21 A Smith chart plot of the measured diode embedding impedances as a function of backshort position at 900 GHz.

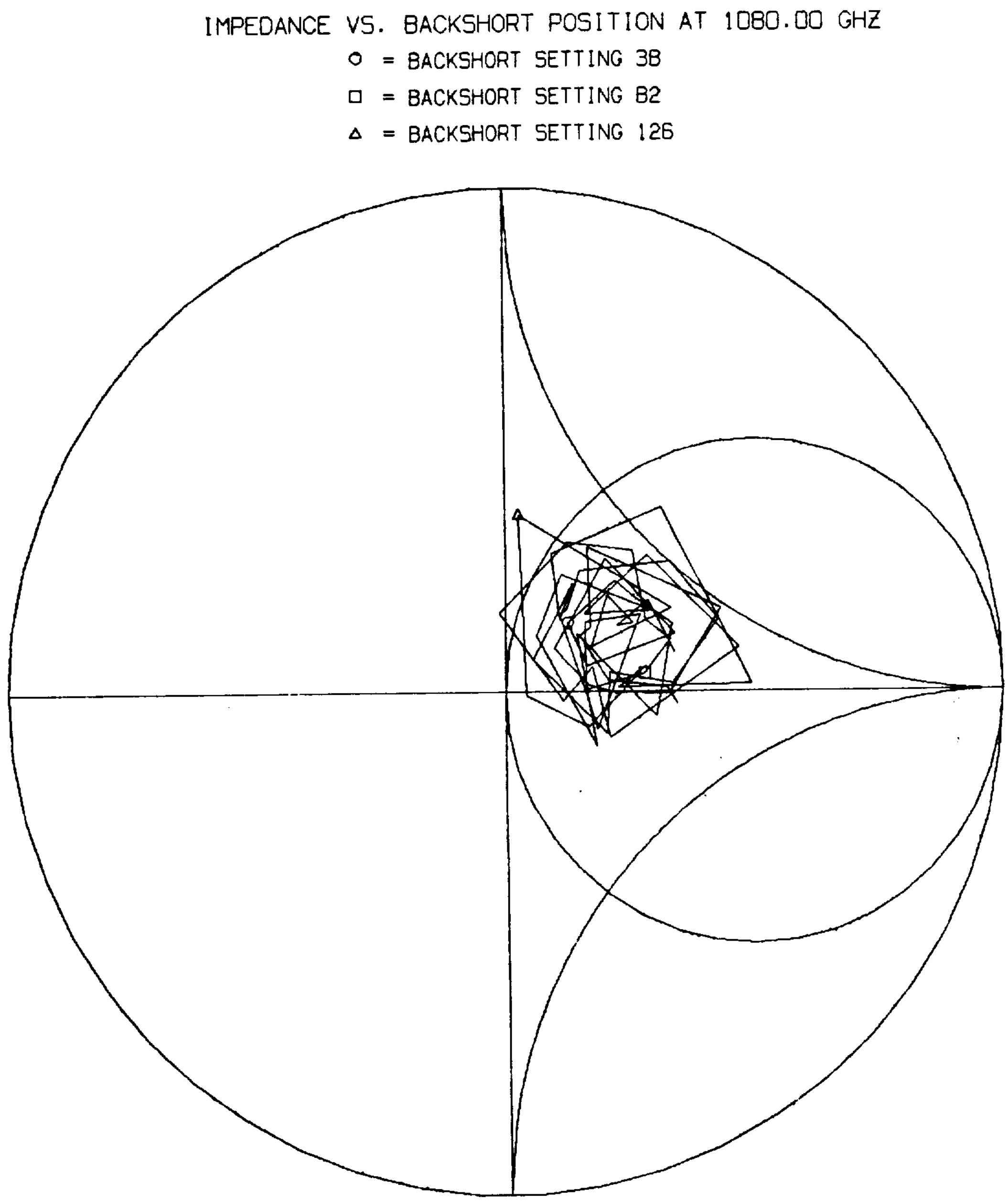

Fig. 3-22 A Smith chart plot of the measured diode embedding impedances as a function of backshort position at 1080 GHz.

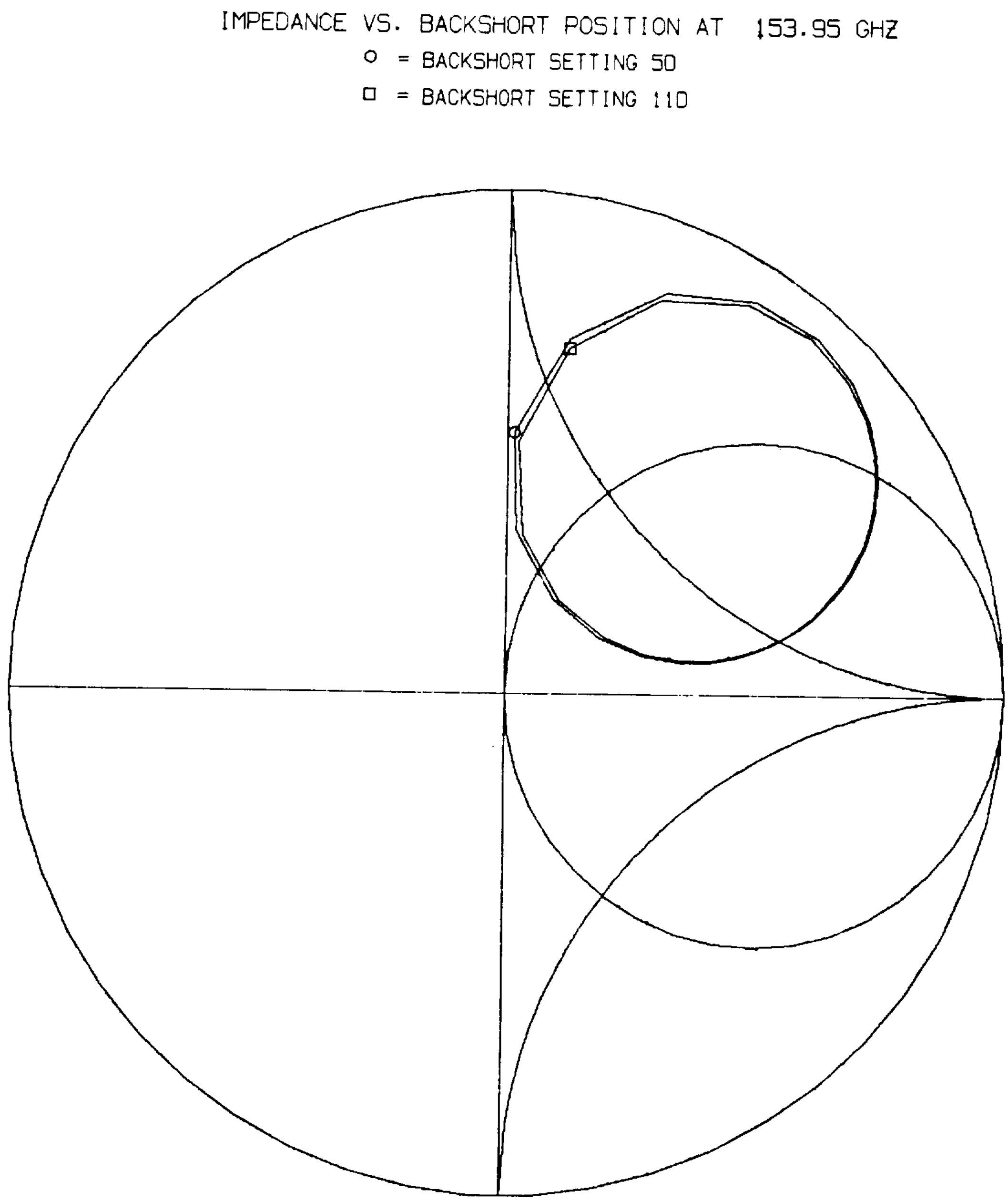

Fig. 3-23 A Smith chart plot of the measured diode embedding impedances as a function of backshort position at 154 GHz (the upper sideband). The LO frequency is 150 GHz and the IF is 3.95 GHz.

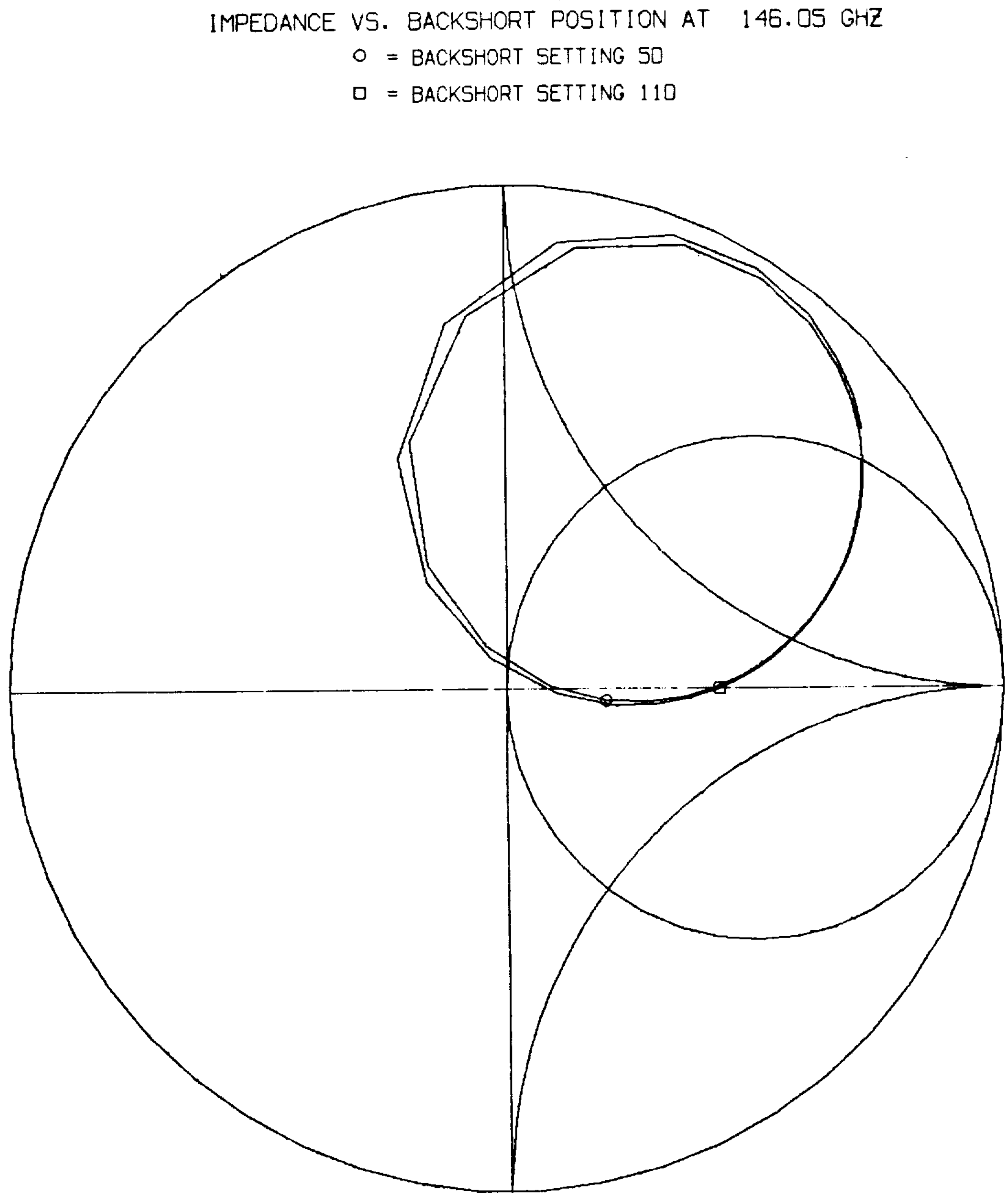

Fig. 3-24 A Smith chart plot of the measured diode embedding impedances as a function of backshort position at 146 GHz (the lower sideband).

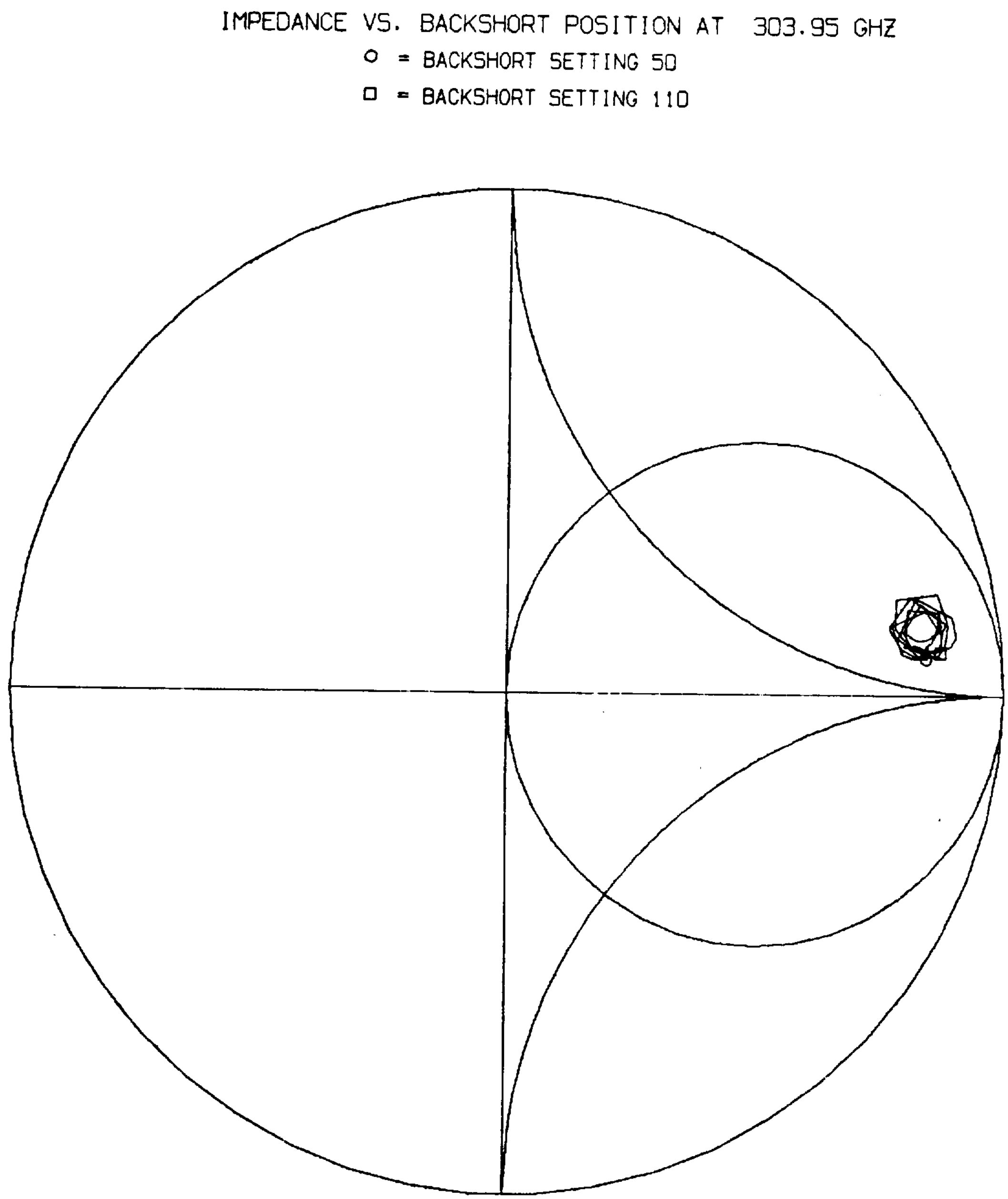

Fig. 3-25 A Smith chart plot of the measured diode embedding impedances as a function of backshort position at 304 GHz.

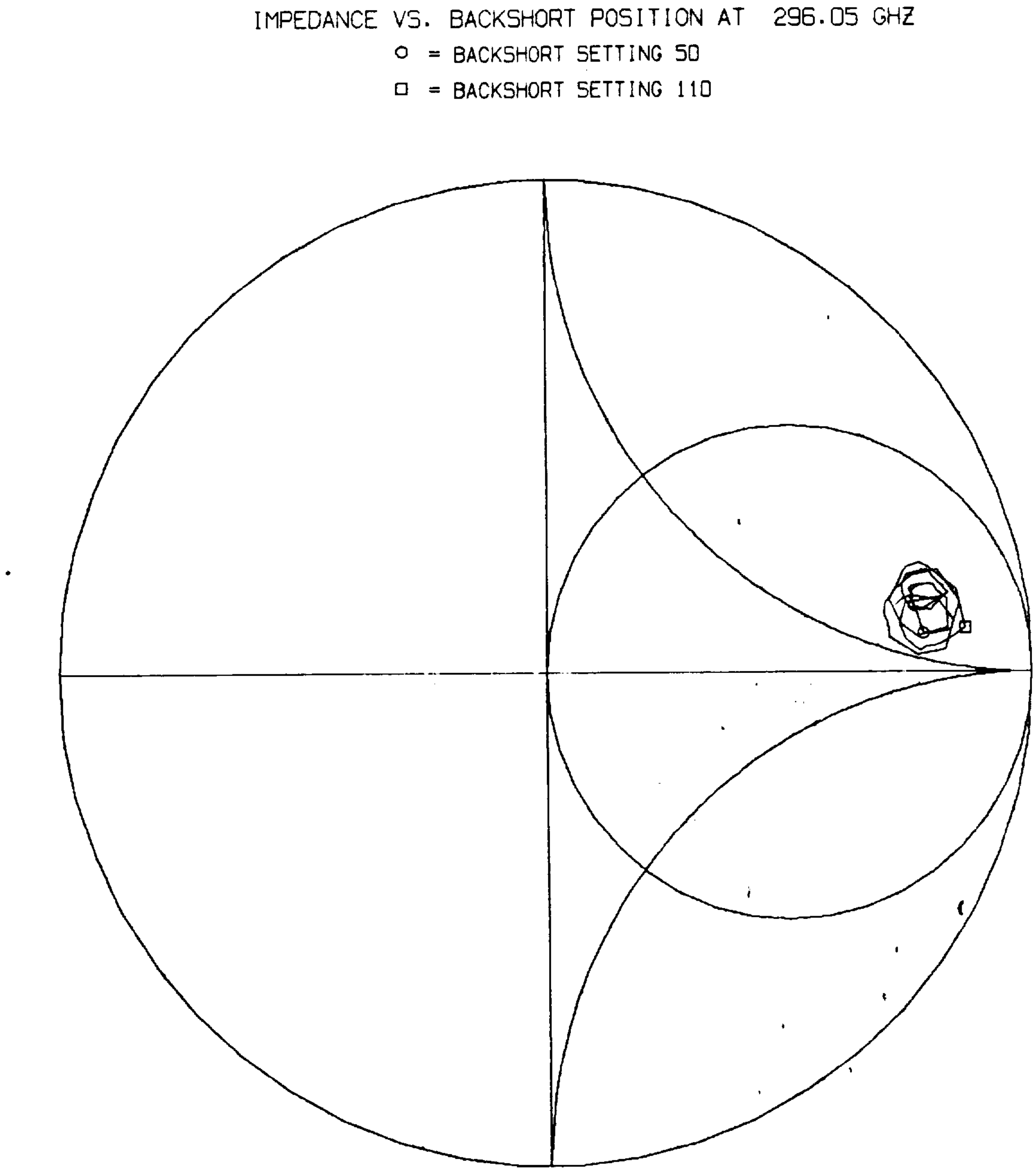

Fig. 3-26 A Smith chart plot of the measured diode embedding impedances as a function of backshort position at 296 GHz.

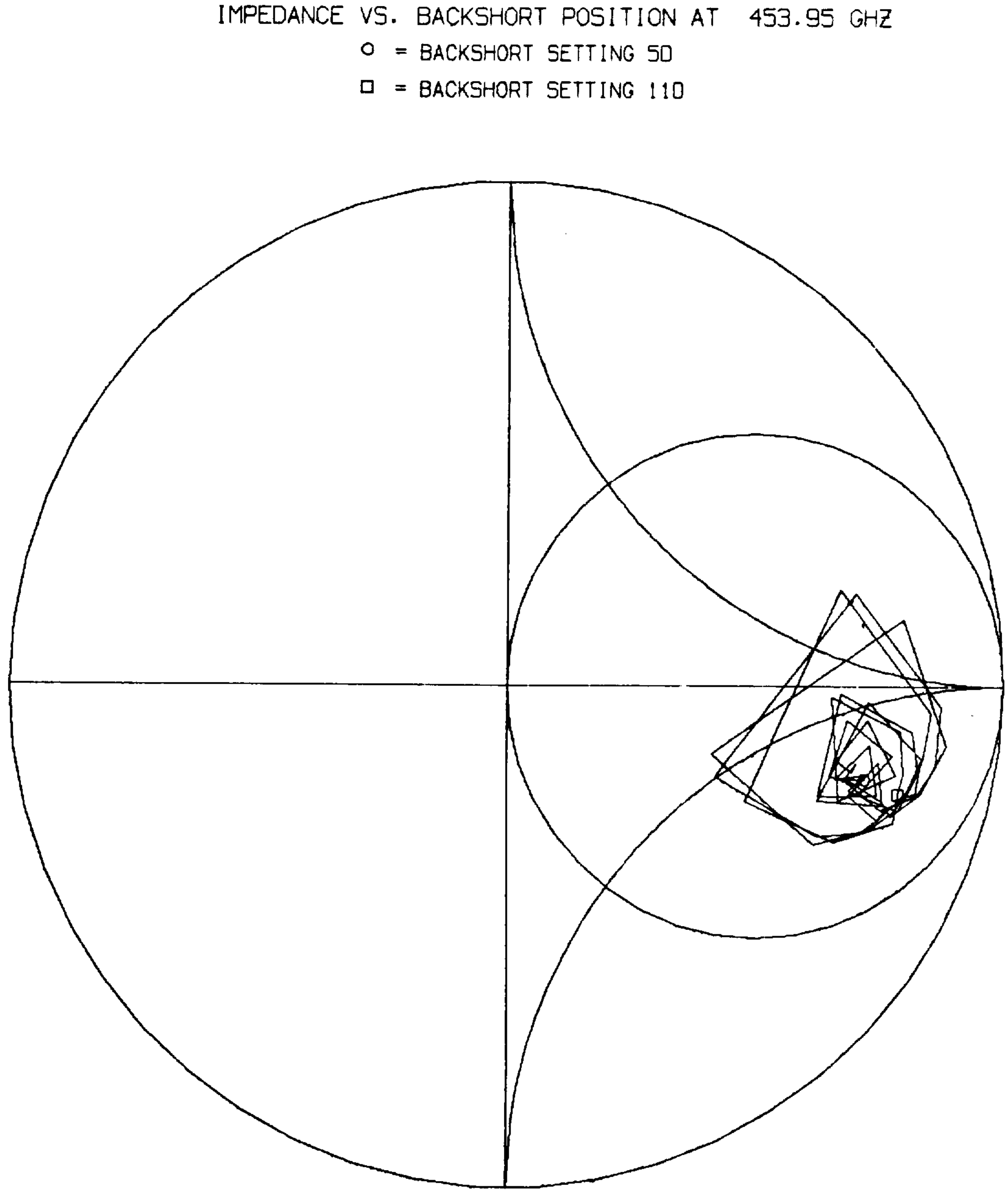

Fig. 3-27 A Smith chart plot of the measured diode embedding impedances as a function of backshort position at 454 GHz.

IMPEDANCE VS. BACKSHORT POSITION AT 446.05 GHZ

○ = BACKSHORT SETTING 50

□ = BACKSHORT SETTING 110

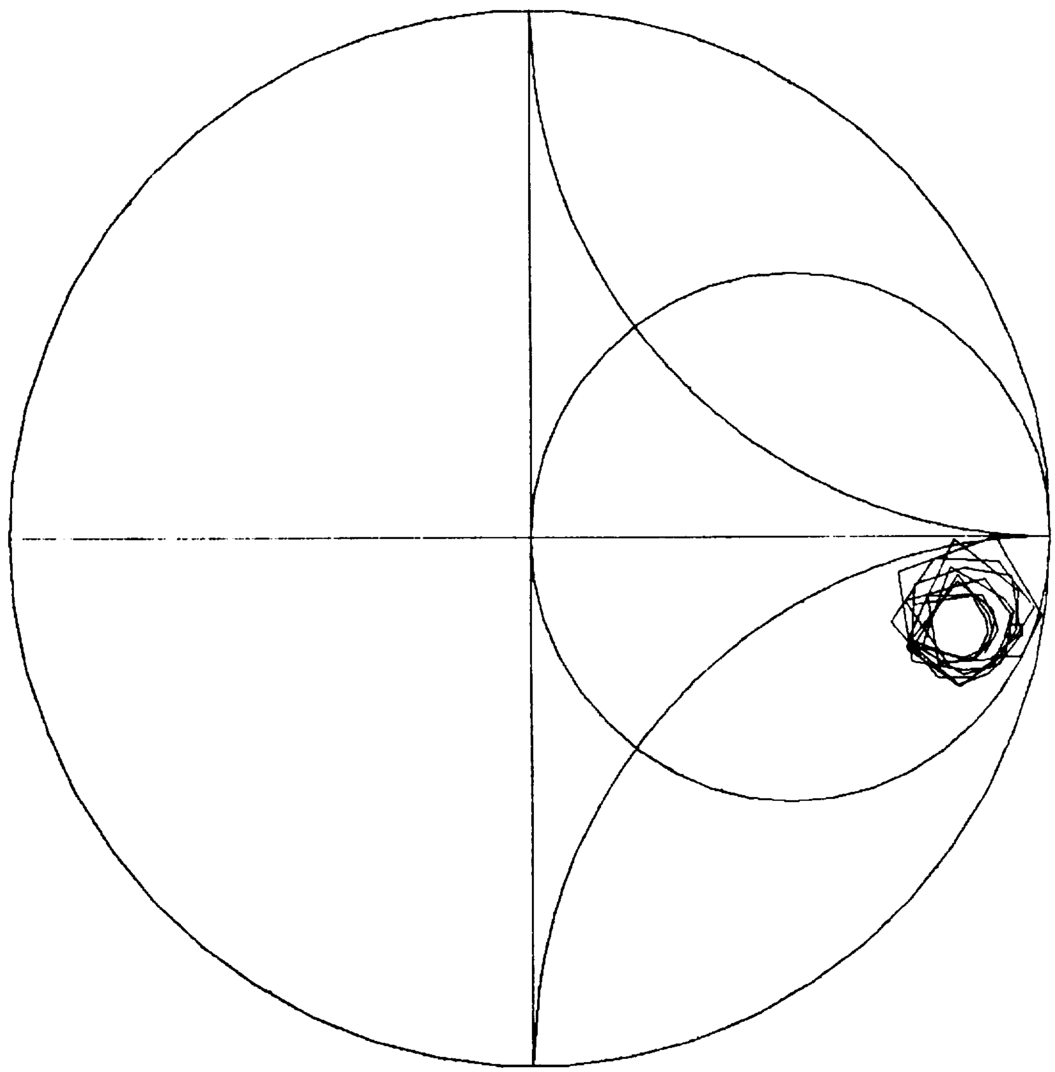

Fig. 3-28 A Smith chart plot of the measured diode embedding impedances as a function of backshort position at 446 GHz.

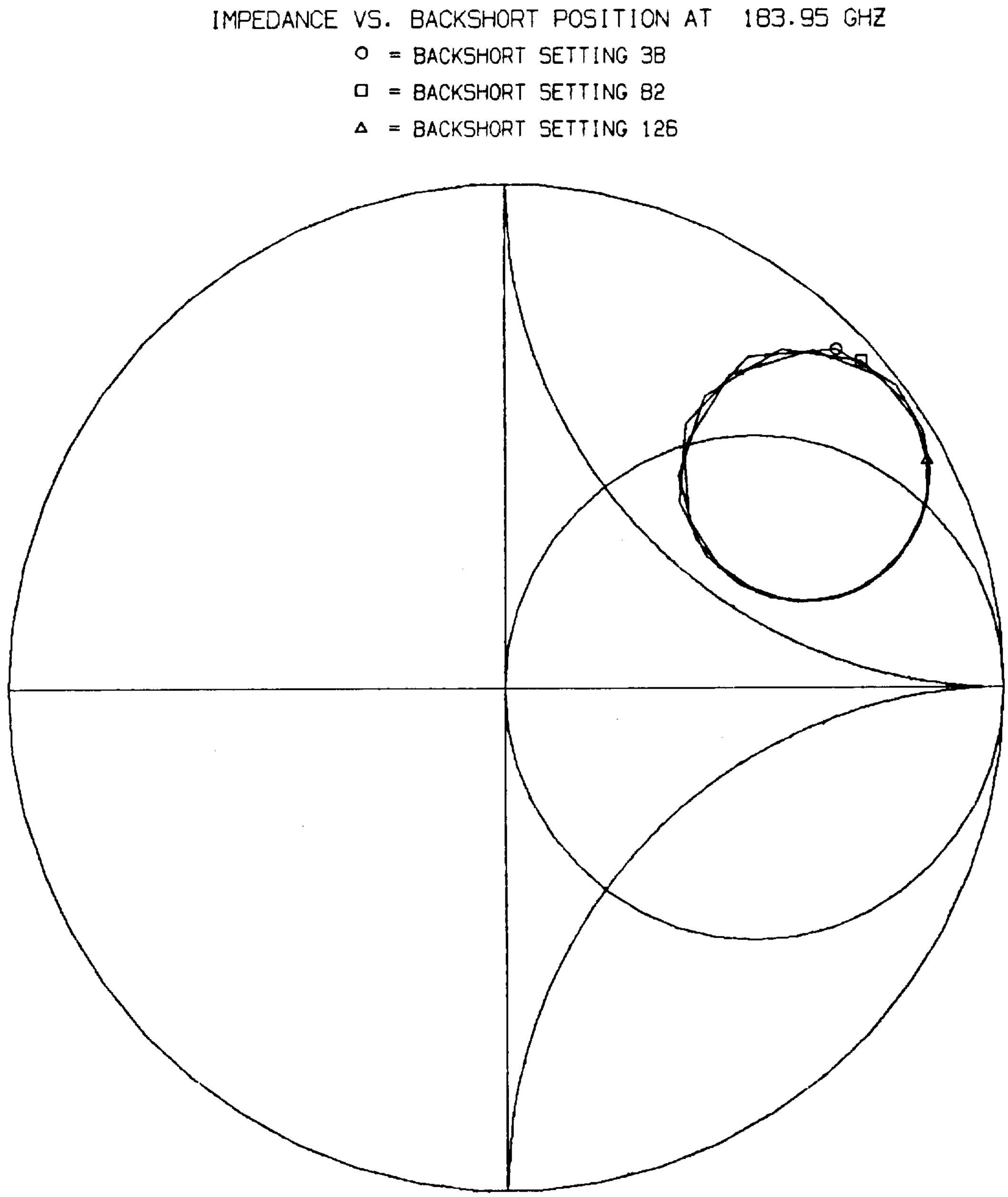

Fig. 3-29 A Smith chart plot of the measured diode embedding impedances as a function of backshort position at 184 GHz (the upper sideband). The LO frequency is 180 GHz and the IF is 3.95 GHz.

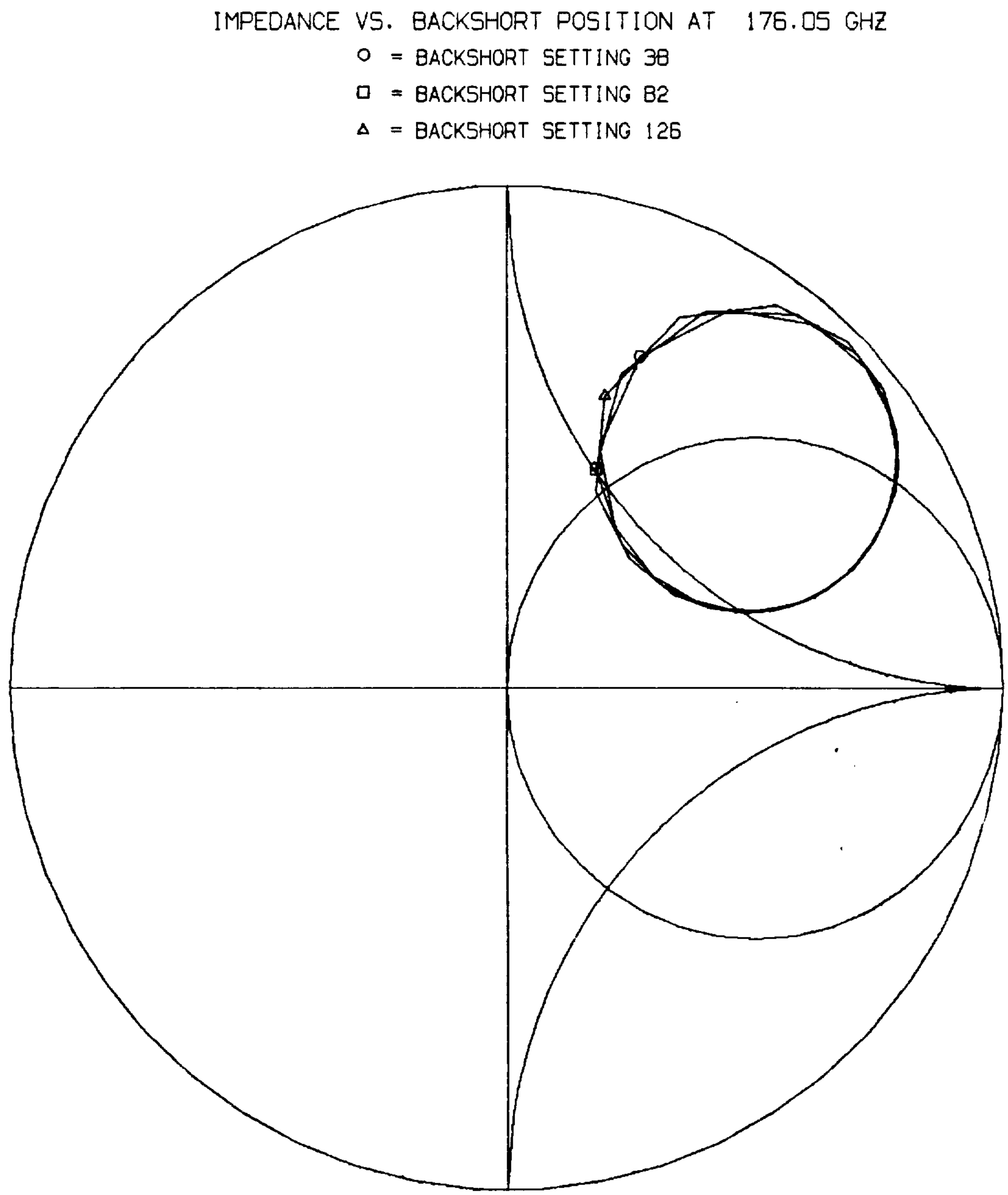

Fig. 3-30 A Smith chart plot of the measured diode embedding impedances as a function of backshort position at 176 GHz (the lower sideband).

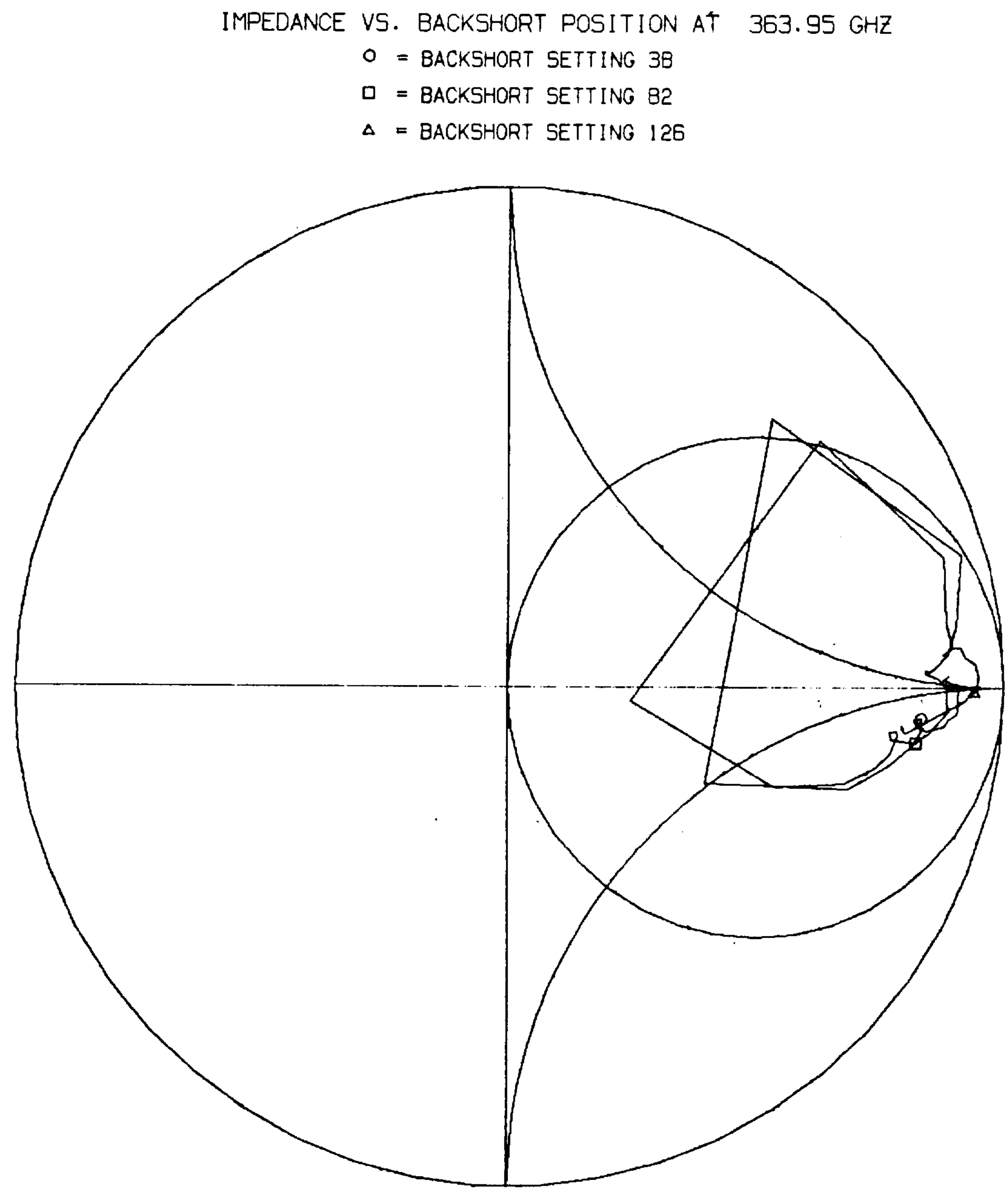

Fig. 3-31 A Smith chart plot of the measured diode embedding impedances as a function of backshort position at 364 GHz.

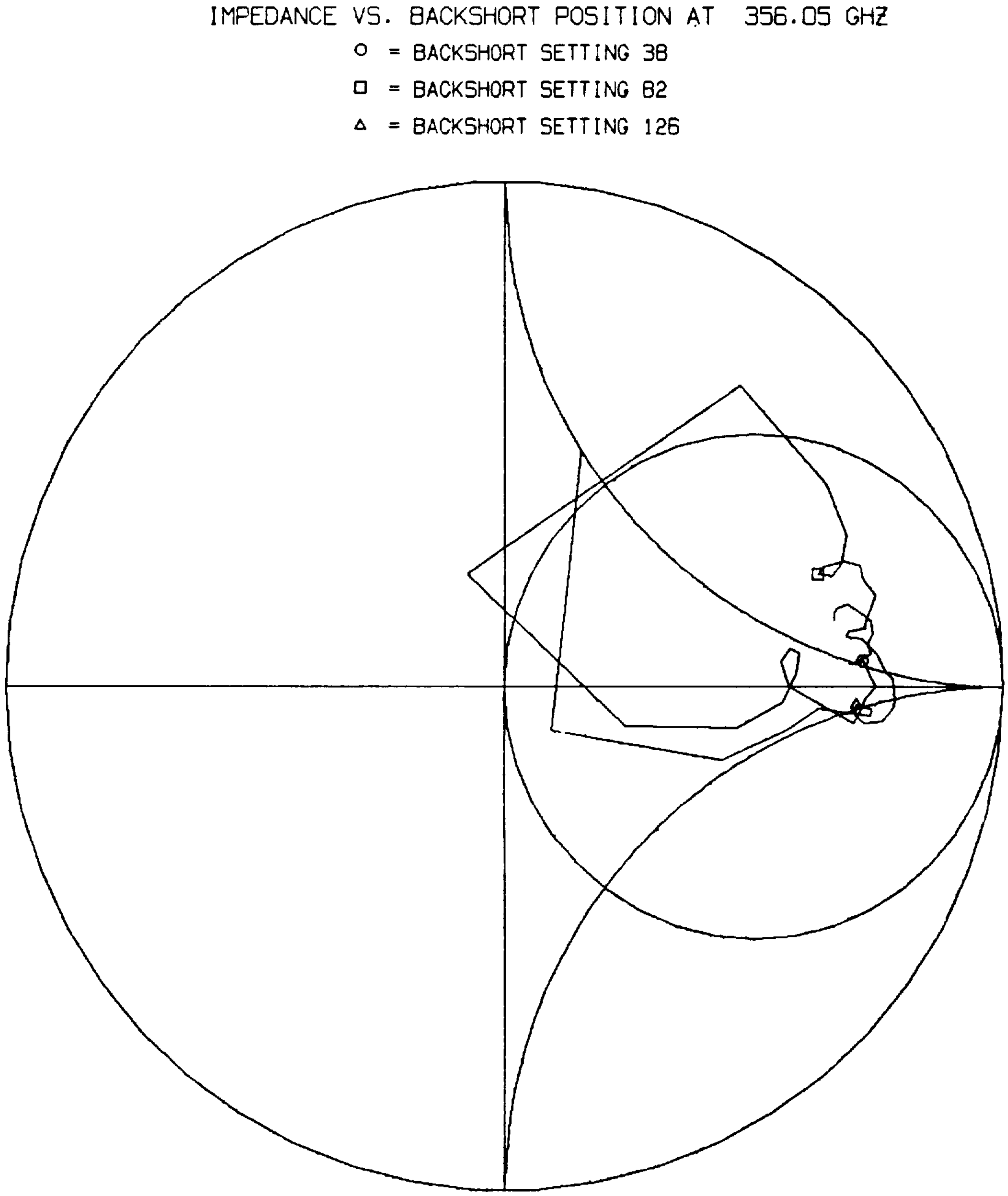

Fig. 3-32 A Smith chart plot of the measured diode embedding impedances as a function of backshort position at 356 GHz.

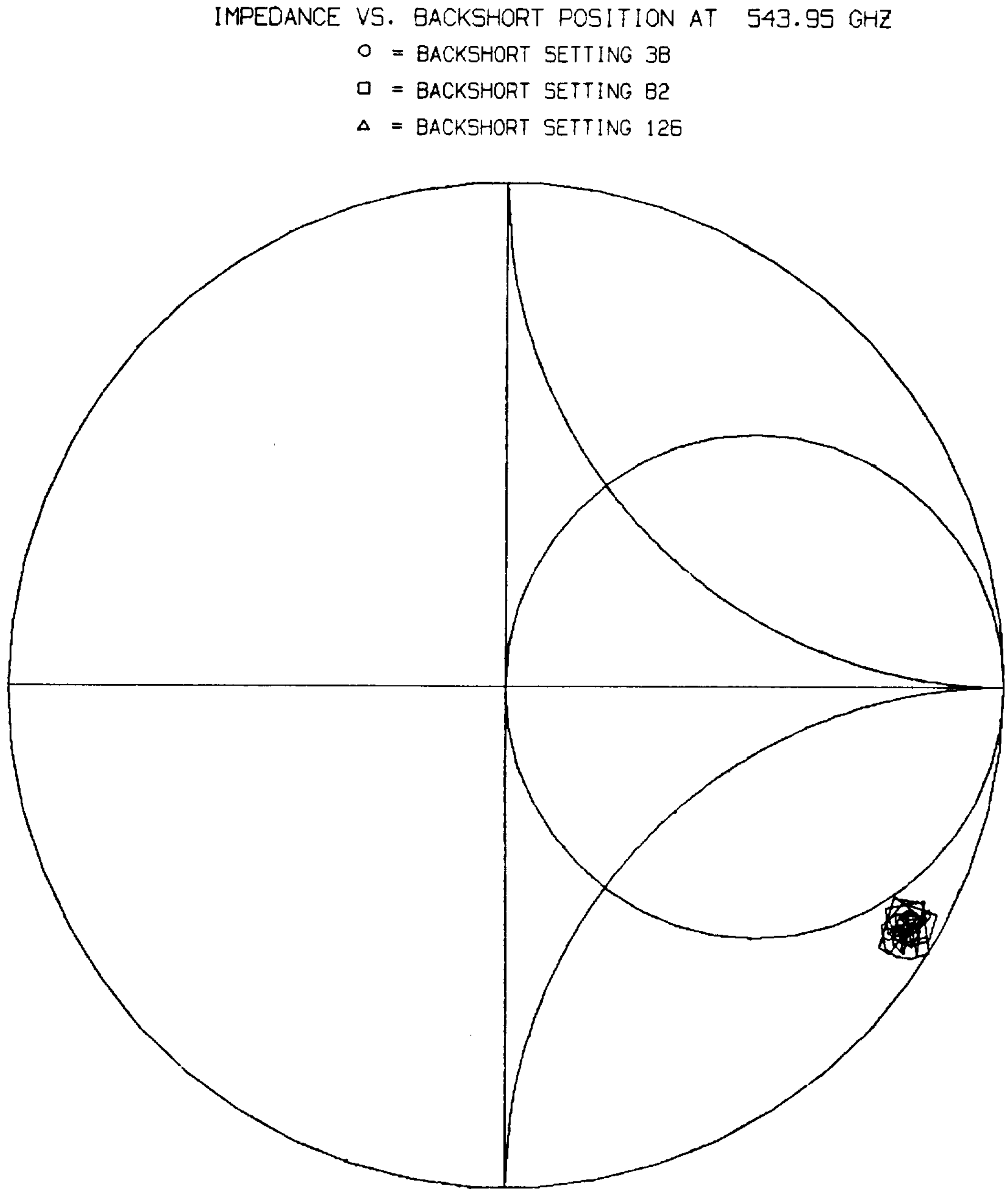

Fig. 3-33 A Smith chart plot of the measured diode embedding impedances as a function of backshort position at 544 GHz.

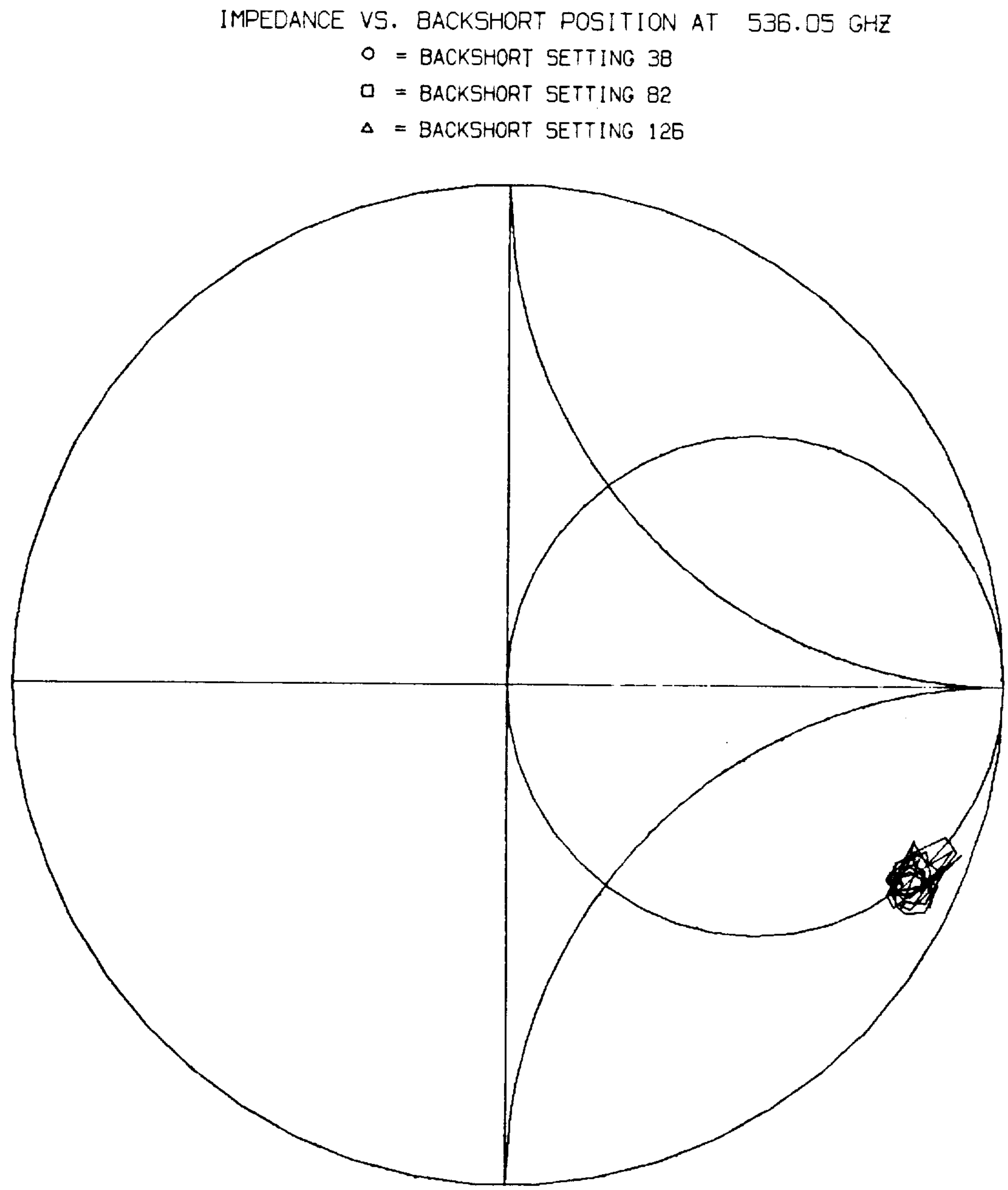

Fig. 3-34 A Smith chart plot of the measured diode embedding impedances as a function of backshort position at 536 GHz.

CHAPTER 4. MIXER MEASUREMENTS AND PERFORMANCE

4.1 Introduction

An essential step in any mixer optimization program is the accurate measurement of mixer performance, namely the signal and image conversion loss, the intermediate frequency output impedance, and the equivalent input noise temperature. At millimeter wavelengths these measurements are difficult and techniques vary widely from laboratory to laboratory.

The procedures used in this thesis to measure the conversion loss, IF impedance and noise temperature of a 140-220 GHz mixer are described in Sections 4.2-4.4. The results show clearly the importance of measuring the mixer conversion loss from both the upper and lower sidebands when a high IF frequency is used. In Section 4.5, the electrical characterization of the Schottky diode in the 140-220 GHz mixer is considered for incorporation into the computer program of Chapter 2. The measured and computed mixer performance at 150 and 180 GHz are then compared and discussed.

4.2 Conversion Loss

In broadband mixer operation it is generally assumed that the signal and image conversion losses are roughly equal. This is certainly not the case when the IF is a noticeable fraction of the signal frequency or when the mixer circuit has a high Q. It is therefore desirable to measure both the upper (L_{01}) and lower (L_{0-1}) sideband conversion losses under similar operating conditions.

A 150-220 GHz conversion loss test set is shown in Fig.4-1. The signal source is a Siemens RWO 110, 75-110 GHz backward wave oscillator coupled with a solid-state frequency doubler (described in Chapter 6) which can be swept across both the upper and lower sidebands. After calibrating out the loss from the waveguide switch, attenuator and resonant ring filter, the power meter reads the absolute signal level incident at the RF port of the

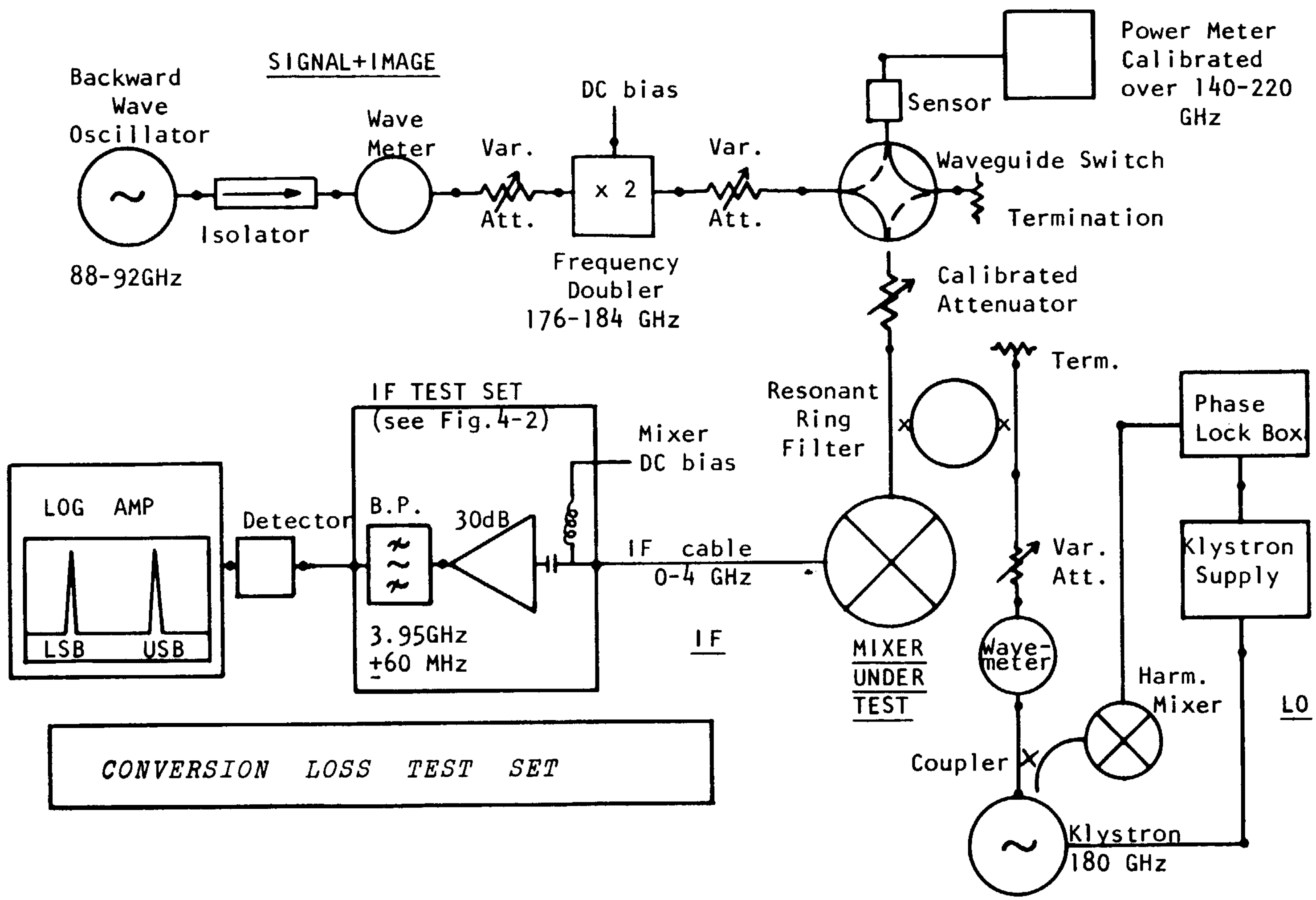

Fig. 4-1 A block diagram of the measurement test set used to determine the upper (USB) and lower (LSB) sideband conversion loss of a mixer under given bias conditions. The mixer operating frequency is 180 GHz and the IF is 3.95 GHz. The IF test set is detailed in Fig.4-2.

mixer*. A phase locked klystron supplies the local oscillator power which is combined with the signal in the resonant ring filter. The resonant ring suppresses any klystron noise which may appear at the signal or image frequency. The mixer output port is terminated in a 50 ohm coaxial line which couples into an IF amplifier (Varian model VSG-7421B, 3.7-4.2 GHz, gain 28dB) and bandpass filter. For the mixer under investigation the IF was chosen to be 3.95 GHz and the filter passband is 120 MHz. The output power level, after conversion from the upper and lower sidebands, is measured with a scalar network analyzer (Wiltron model 560). When the gain through the IF test set is known, the single sideband mixer conversion loss from the signal and image into a 50 ohm load at the IF port can be determined.

The overall measurement accuracy is governed mainly by uncertainties in the determination of the absolute signal power level incident at the input port of the

---

* The effects of mismatch between the mixer input impedance and the signal source impedance are minimized by the calibrated attenuator which is set to 20 dB during the measurements. However, loss in the mixer input waveguide and the reduced height waveguide containing the backshort will be part of the overall measured conversion loss. If not properly accounted for this will result in the measured conversion losses being slightly higher than those calculated using the mixer analysis program of Chapter 2.

mixer. In these measurements the thermocouple type power sensor (Anritsu model MP84B1 with ML83A readout) has a maximum VSWR of 1.6 and was calibrated by the manufacturer at 140 and 170 GHz. The calibrated attenuator (Hughes type 45728H) is set to 20 dB when the signal power is incident on the mixer and to 0 dB for reading the incident power with the Anritsu sensor. The absolute accuracy of the attenuation setting is $\pm 3\%$ or ± 0.6dB . The scalar network analyzer is accurate to better than ± 0.2 dB over the range 10 to -40 dBm. Thus the worst possible error in the measured conversion loss is approximately ± 1 dB.

4.3 Mixer Output Impedance

The mixer output port VSWR can also be found using the conversion loss test set described in the previous section. The additional components required in the IF portion of the measurement system are shown in Fig.4-2. A microwave oscillator supplies a 3.89-4.01 GHz swept signal which can be launched towards the IF port of the mixer through a directional coupler. The 2 screw tuners are used to reduce the directivity error in the coupler and mismatches in the other components of the test set. The isolator is necessary because the IF amplifier gain is a function of its source impedance.

With the mixer DC bias set to zero and no incident LO or signal power (equivalent to setting the large signal diode conductance to zero), IF power from the microwave oscillator (3.95 GHz) is applied through the directional coupler to the output port of the mixer. The reflected power, upon passing through the amplifier and filter, is measured with the scalar network analyzer. The mixer DC bias is then set to its normal operating level and LO power is applied until the desired rectified current is obtained in the diode. With the IF power still incident

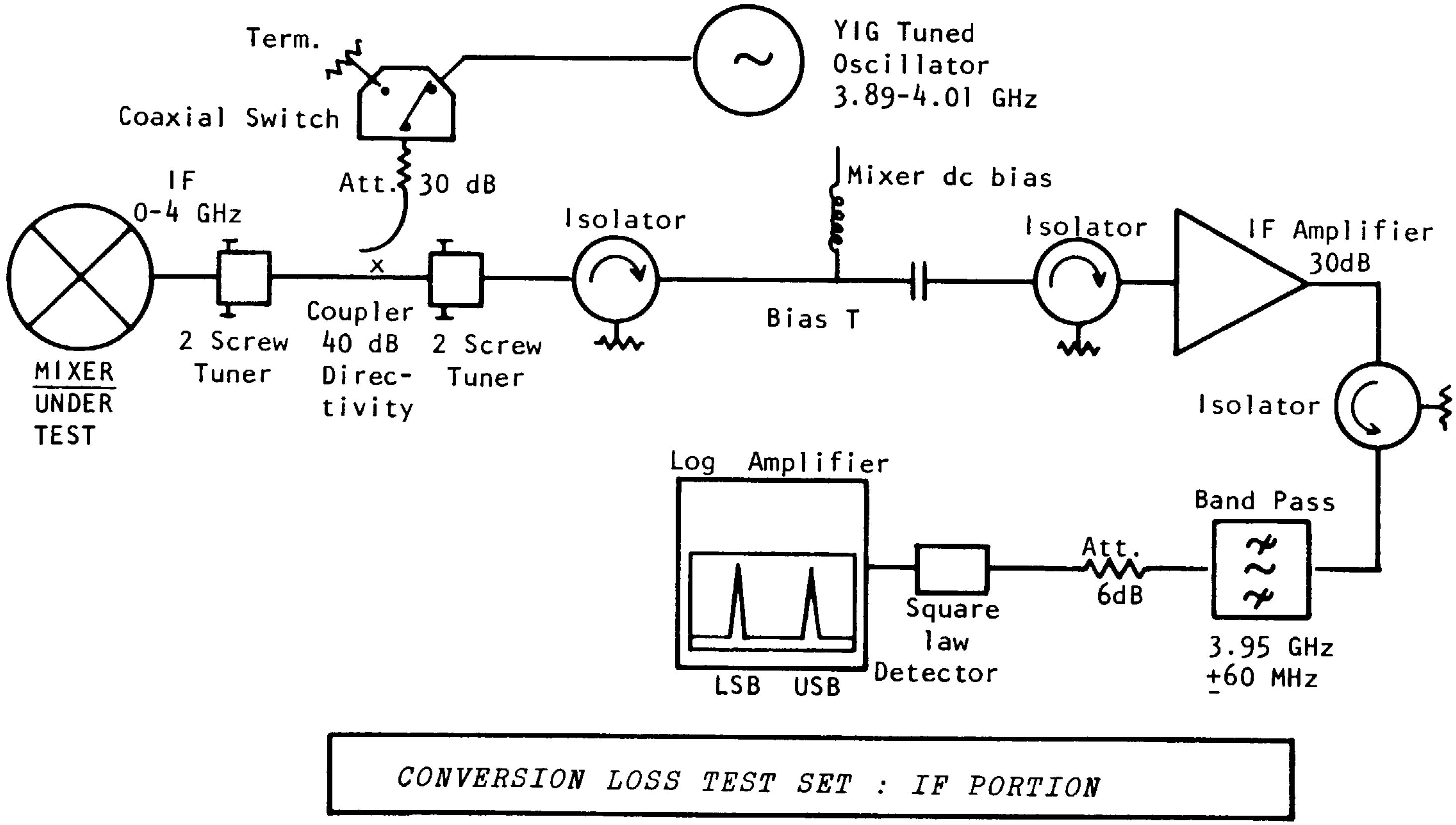

Fig. 4-2 The IF test set used for measuring the mixer conversion loss and output port impedance. While the loss is being measured the coaxial switch is set on the 50 ohm termination.

from the low frequency oscillator the subsequent change in the reflected power is measured on the network analyzer. This yields the magnitude of reflection coefficient at the IF port of the mixer and hence the output VSWR.

The measured conversion loss from the upper and lower sidebands can now be corrected to give the conversion loss into a matched IF load in accordance with the definition in (2.56). Referring to Fig.4-3 we have:

$$L_{corrected} = [1-|\Gamma|^2]\, L_{measured} \text{ , where} \tag{4.1}$$

$$|\Gamma|^2 = \frac{\text{Measured power reflected from IF port}}{\text{Measured power incident on IF port}}$$

$$= |Z_{IF_{out}} - 50|^2 \,/\, |Z_{IF_{out}} + 50|^2 \text{ .} \tag{4.2}$$

Loss Corrections for Matched Load

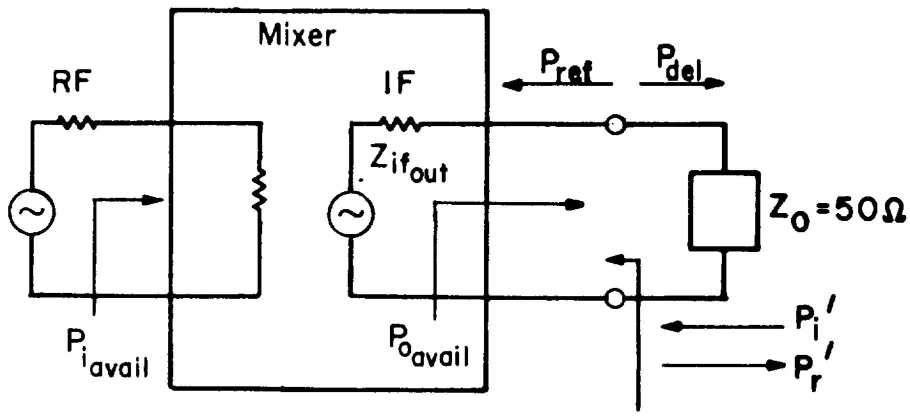

$$|\Gamma|^2 = \left|\frac{P_r'}{P_i'}\right| = \left|\frac{P_{o_{avail}}}{P_{ref}}\right| = \left|\frac{Z_{IF_{out}} - 50}{Z_{IF_{out}} + 50}\right|^2$$

$$P_O = \frac{P_{del}}{1 - |\Gamma|^2}$$

$$\text{LOSS (into matched load)} = \frac{P_{i_{avail}}}{P_{O_{avail}}}$$

$$\text{LOSS (measured)} = \frac{P_{i_{avail}}}{P_{del}}$$

$$\therefore \text{LOSS} = \text{LOSS (measured)} \frac{P_{del}}{P_O} = \text{LOSS (measured)} \left[1 - |\Gamma|^2\right]$$

Fig. 4-3 An illustration showing the corrections which must be made to the measured mixer conversion loss (into the 50 ohm test set) in order to obtain the conversion loss into a matched load at the mixer output port.

4.4 Noise Temperature

The equivalent input noise temperature is usually the most important mixer performance parameter. At room temperature it is often the largest part of the overall receiver noise (mixer plus IF amplifier). In the millimeter-wave bands the input noise temperature is most conveniently measured with a broadband noise source. The quantity being measured is thus a double sideband noise temperature, T_{DSB}. The single sideband noise temperature T_{SSB} can be derived using (2.78) if the signal and image conversion losses (L_s and L_i) are known.

Using the results of Sections 4.2 and 4.3 only one additional measurement is required to determine T_{SSB} referred to both the upper and lower sidebands. The noise measurement test set is depicted in Fig.4-4 and is similar to one described by Weinreb and Kerr [176]. The IF portion is the same as that used in the conversion loss measurements with an additional down conversion from 3.95 to 1.1 GHz. The 1.1 GHz signal is then amplified, passed through a step attenuator, rectified and finally measured with a DC voltmeter.

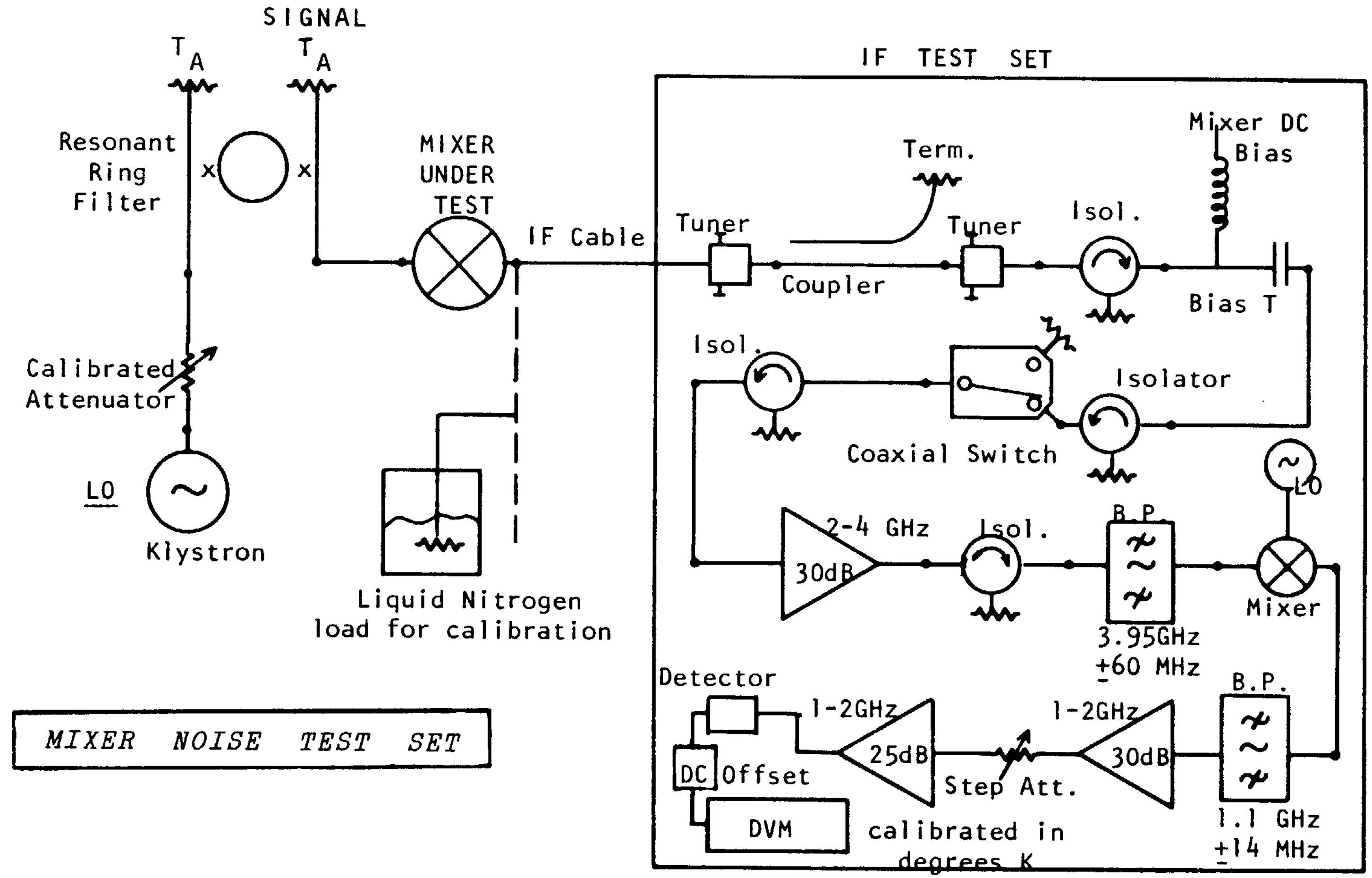

Fig. 4-4 A block diagram of the test set used for the mixer noise measurements. The system is similar to one described by Weinreb and Kerr [176]. Before any measurements are made the DVM is calibrated to read in degrees using the coaxial switch to toggle between a room temperature load and a 77K load at the end of the IF test set cable. The directional coupler is not required unless a separate measurement of the IF VSWR is desired.

For the initial calibration the IF cable is connected to a 50 ohm load immersed in liquid nitrogen (T_{LN}=77K) and the coaxial switch is used to toggle between this cold load and a 50 ohm room temperature termination. Using the step attenuator and fine DC gain and offset controls the voltmeter can be calibrated to read in degrees.

The mixer, with a room temperature termination at the signal port, is now connected to the IF cable and the DC bias and LO power level are set so as to maintain the same rectified current in the mixer diode as was used in the conversion loss measurements. The voltmeter reading is now a function of the mixer noise temperature, conversion loss, and output VSWR, and the noise contribution from the klystron, as modified by the resonant ring and the other waveguide components in the RF portion of the test set. The various contributions to T_{IF_A} are shown in Fig. 4-5. Beginning at the far left in the figure we have:*

$$T_1 = T_K/L_1 + T_A[1-1/L_1], \tag{4.3}$$

---

* In the equations which follow all the noise temperatures are actually noise powers, the $k\Delta f$ being understood.

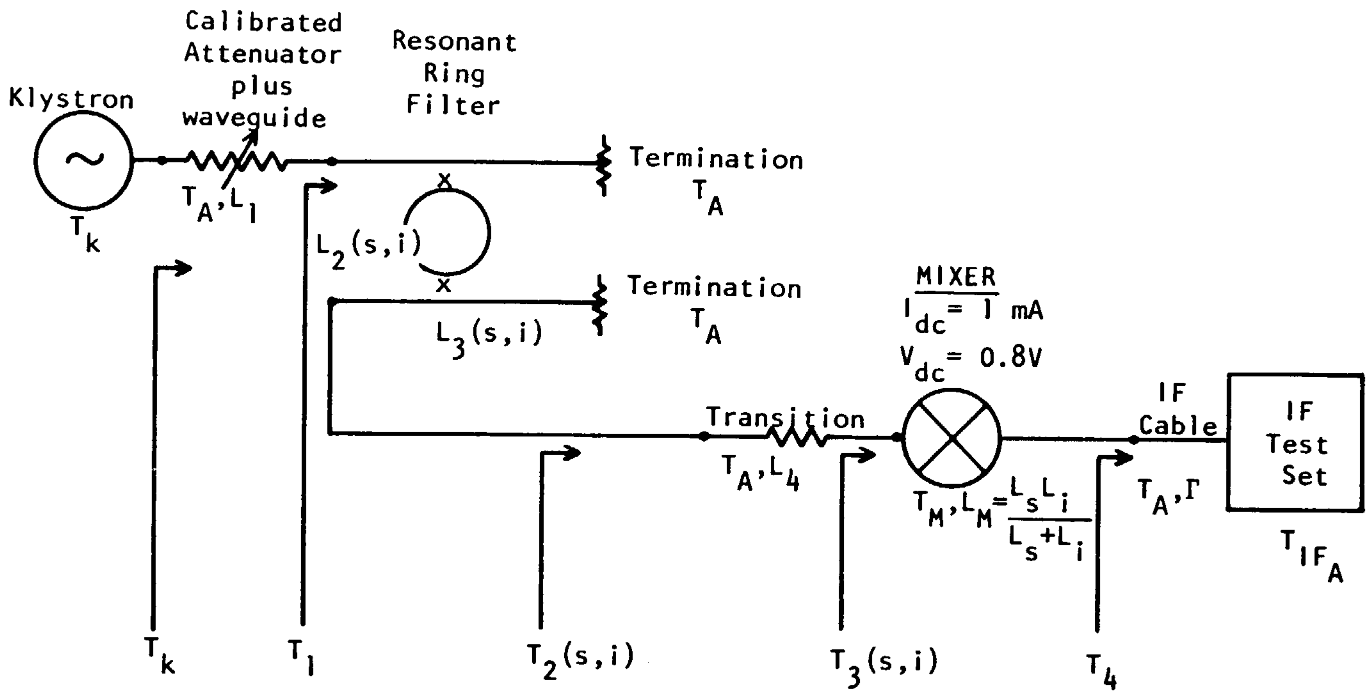

Fig. 4-5 The various contributions to the measured mixer output noise temperature T_{IF_A}. The attenuator is adjusted to maintain a constant rectified current in the diode as the backshort position is varied.

where T_K is the klystron noise temperature and L_1 is the loss in the calibrated attenuator (attenuation setting plus waveguide loss). The attenuator is used to keep the diode rectified current in the mixer constant as the backshort position is changed.

At the output of the resonant ring the noise temperature $T_2(s,i)$ for the signal or image is:

$$T_2(s,i)=T_1/L_2(s,i)+T_A/L_3(s,i)+T_A[1-1/L_2(s,i)-1/L_3(s,i)] \tag{4.4}$$

$L_2(s,i)$ is the loss, at the signal or image frequency, from the LO port to the mixer port due to the finite rejection in the resonant ring. $L_3(s,i)$ is the loss in the signal path of the resonant ring at the signal and image frequencies, and T_A is the thermal noise temperature of the signal port termination (a waveguide load at room temperature). The term $T_A\ [1 - 1/L_2(s,i) - 1/L_3(s,i)]$ in (4.4) is the noise contribution from the resonant ring itself. It is that noise temperature, T_{ring}, which makes the noise temperature at the output of the ring equal to T_A when the LO and signal ports are maintained at a temperature T_A. That is:

$$T_A/L_2(s,i) + T_A/L_3(s,i) + T_{ring} = T_A \ . \qquad (4.5)$$

Between the resonant ring (output waveguide in WR-7, 110-170 GHz) and the mixer (input waveguide in WR-5, 140-220 GHz) there lies a waveguide transition with equal loss, L_4, at both the signal and image frequencies. The noise temperature in front of this transition (at temperature T_A) is:

$$T_3(s,i) = T_2(s,i)/L_4 + T_A[1 - 1/L_4]. \qquad (4.6)$$

$T_3(s,i)$ is the temperature which is input at the mixer signal or image port and includes the noise from the klystron and the room temperature waveguide load.

If the mixer has a double-sideband equivalent input noise temperature T_M and has a conversion loss L_s at the signal frequency and L_i at the image, then at the IF port we have (see Fig. 4-5) an available output noise temperature (i.e. into a matched IF load):

$$T_4 = [T_3(s) + T_M]/L_s + [T_3(i) + T_M]/L_i , \qquad (4.7)$$

where T_3 has been separated into its signal and image contributions.

Because the IF output port of the mixer is not matched to the 50 ohm cable of the noise test set only $(1 - |\Gamma|^2)$ of the available mixer output noise, T_4, will actually be measured. To this must be added the contribution from the 50 ohm cable (at temperature T_A) which is reflected off the mixer output port. Thus the temperature measured on the calibrated voltmeter in the noise test set is:

$$T_{IF_A} = T_4[1 - |\Gamma|^2] + |\Gamma|^2 T_A, \tag{4.8}$$

where T_4 is given by (4.3)-(4.7).

Under some circumstances the contribution to T_{IF_A} from the klystron will be negligible and (4.8) can be solved directly for T_M once all the waveguide component losses have been measured. A high frequency klystron however, can be very noisy and may cause a substantial error in T_M if its noise contribution is not taken into account. T_K can be determined by removing the resonant ring and allowing all the klystron noise at the signal and image frequencies to flow directly into the mixer (that is after passing through the calibrated attenuator). In this case the individual noise temperature components sum up as shown in Fig. 4-6.

The calibrated attenuator is set so that the LO power entering the mixer is the same as in the previous measurement (i.e. the diode maintains the same rectified current). Loss L_O includes the loss through the attenuator and the associated waveguide components. Adding up the noise temperatures in exactly the same manner as before, the temperature measured by the IF test set, T_{IF_K}, is:

$$T_{IF_K} = \{T_M+T_K/L_O+T_A[1-1/L_O]\}(1-|\Gamma|^2)/L_M + T_A|\Gamma|^2, \quad (4.9)$$

where $L_M = L_sL_i/(L_s+L_i)$, is the double sideband conversion loss and T_M is the double sideband equivalent input noise temperature of the mixer.

Solving (4.8) and (4.9) for T_M we have after some laborious algebra:

$$T_M = \{ L_OL_M(T_{IF_K}-T_A|\Gamma|^2)/[1-|\Gamma|^2] - T_A(L_O-L_1L_4L_x/L_M) - L_1L_4L_x(T_{IF_A}-T_A|\Gamma|^2)/[1-|\Gamma|^2] \} / \{L_O-L_1L_4L_x/L_M\} \quad (4.10)$$

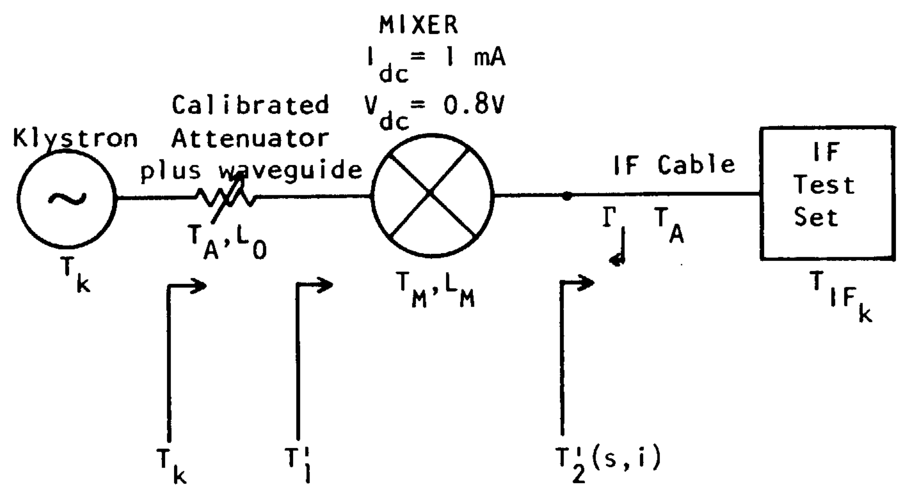

Fig. 4-6 The various contributions to the measured output noise temperature when the resonant ring filter is removed from the noise test set. This measurement, coupled with that illustrated in Fig. 4-5 yields enough information to calculate the klystron noise temperature. The attenuator is adjusted to maintain a constant rectified current in the diode as the backshort position is varied.

where

$$L_x = [L_s L_i L_2(s) L_2(i)] \;/\; [L_s L_2(s) + L_i L_2(i)] \; . \qquad (4.11)$$

If desired, equation (4.9) can now be solved for T_K, the klystron noise temperature. Typical values of T_K were between 10,000 and 13,000 degrees for the 180 GHz klystron used in the mixer measurements in this chapter.

The quantity T_M in (4.10) is the double sideband noise temperature; to calculate the single sideband noise temperature we use equation (2.78)*:

$$T_{SSB} = T_M \;/\; (1 + L_s/L_i) \qquad (4.12)$$

---

* To relate the measured double sideband noise temperature T_M to the upper and lower sideband noise temperatures calculated in the mixer analysis program (TMUSB and TMLSB) we use:

$$\mathrm{TMUSB} = T_M \;/\; (1 + L_{01}/L_{0-1}) \quad \text{and} \qquad (4.13)$$

$$\mathrm{TMLSB} = T_M \;/\; (1 + L_{0-1}/L_{01}) \; , \qquad (4.14)$$

where L_{01} and L_{0-1} are the measured conversion losses at frequencies $(\omega_{LO}+\omega_{IF})$ and $(\omega_{LO}-\omega_{IF})$ respectively. Note that in (4.14) the roles of signal and image have been reversed; L_{0-1} now represents the loss from the signal frequency to the IF, and L_{01} that from the image to the IF.

4.4.1 Output Noise Temperature

The calculation of the single sideband equivalent input noise temperature from the measurement described in Section 4.4 requires a knowledge of the upper and lower sideband conversion losses. Any errors in these measured losses will therefore appear in the calculated mixer noise temperatures. It is helpful to define an additional noise parameter, which can be measured without knowing L_s or L_i, to be used in comparing the measured and computed mixer performance. A convenient choice is the available mixer output noise temperature (that is, the output noise temperature measured with a matched load at the IF port). The output noise temperature, T_o, is given in (4.8):

$$T_o = T_4 = (T_{IF_A} - |\Gamma|^2 T_A)/[1-|\Gamma|^2], \qquad (4.15)$$

where T_{IF_A} is the temperature measured by the calibrated IF test set. Note that T_{IF_A} in (4.15) includes a contribution from the klystron (roughly 3-4 K in our case).

We can calculate the excess noise in T_o due to the klystron if we use the value of T_K obtained from (4.9). The output noise contribution from the klystron is then:

$$T_{o_{excess}} = (T_K - T_A)/L_1 L_4 L_x, \tag{4.16}$$

where L_x is given in (4.11) and T_4 has been written as T_A plus the excess noise from the klystron. A close approximation to T_o is then*:

$$T_o = (T_{IF} - |\Gamma|^2 T_A)/[1-|\Gamma|^2] - T_{o_{excess}} \ . \tag{4.17}$$

---

* T_o is not formed in the mixer analysis program. It is given by:

T_o = (TK+TDSB)/LDSB

where TK is the physical temperature of the signal and image terminations, TDSB = TMUSB/(1+LUSB/LLSB) {or TDSB = TMLSB(1+LLSB/LUSB)}, and LDSB = (LUSB*LLSB)/(LUSB+LLSB).

4.5 140-220 GHz Mixer Diode Characterization

Before we can compare the measured and predicted mixer performance in the 140-220 GHz band we must characterize the actual mixer diode for use in the computer program of Chapter 2. The parameters which must be determined are listed in Section 2.6.5. Some of these are available from the diode I-V curve; others are not so easily found. The methods used in this thesis to determine each of the diode parameters required for the mixer analysis program are discussed in this section.

(1) Diode Material Properties. The material properties of the diode used in the 140-220 GHz mixer were supplied by the manufacturer (R.J. Mattauch, University of Virginia, Charlottesville, Va.). The diode is designated type 1E2 and has the following characteristics:

Substrate: n-type GaAs doped with 2×10^{18} atoms/cm^3 of silicon. The resistivity is approximately 10^{-3} ohm-cm.

Epitaxial layer: 0.08 microns thick and doped with 2×10^{17} atoms/cm^3 of tellurium. The electron mobility is taken to be 2500 cm^2/V-s

Anodes: Electroplated gold over platinum, 2 microns in diameter and with a center to center spacing of 3 microns.

Chip dimensions: 5x9 mils on the front face and 5 mils thick, with an ohmic contact at the back face (see Figs. A2-1 thru A2-3 in Appendix 2).

(2) Diode I-V Law. The current-voltage relationship is assumed to be an exponential one and to follow the form of equation (2.1). This is born out by the plot of log i_d versus v_d which appears in Fig.4-7.

(3) Diode Ideality Factor. η is obtained from the diode log I-V plot, where $\alpha = q/\eta kT$ is the slope of the plotted line in the linear region ($v_d < 0.9$) of Fig. 4-7. We will see in Chapter 5 that the mixer performance is a very sensitive function of η. A variation in η of only a few percent can cause the mixer output noise temperature to change by as much as 20%. A value for η of 1.2 was found to give the best agreement between the measured and computed mixer performance. This is within the experimental error associated with the determination of η from the log I-V curve.

(4) Diode Saturation Current. i_s is found from the log I-V curve by extrapolating v_d back to the y-axis. For Schottky diodes, i_s is not constant with reverse bias but gradually increases; however, the error introduced by assuming i_s to be constant is negligible. Using Fig. 4-7 we find $i_s = 3.8 \times 10^{-17}$ A.

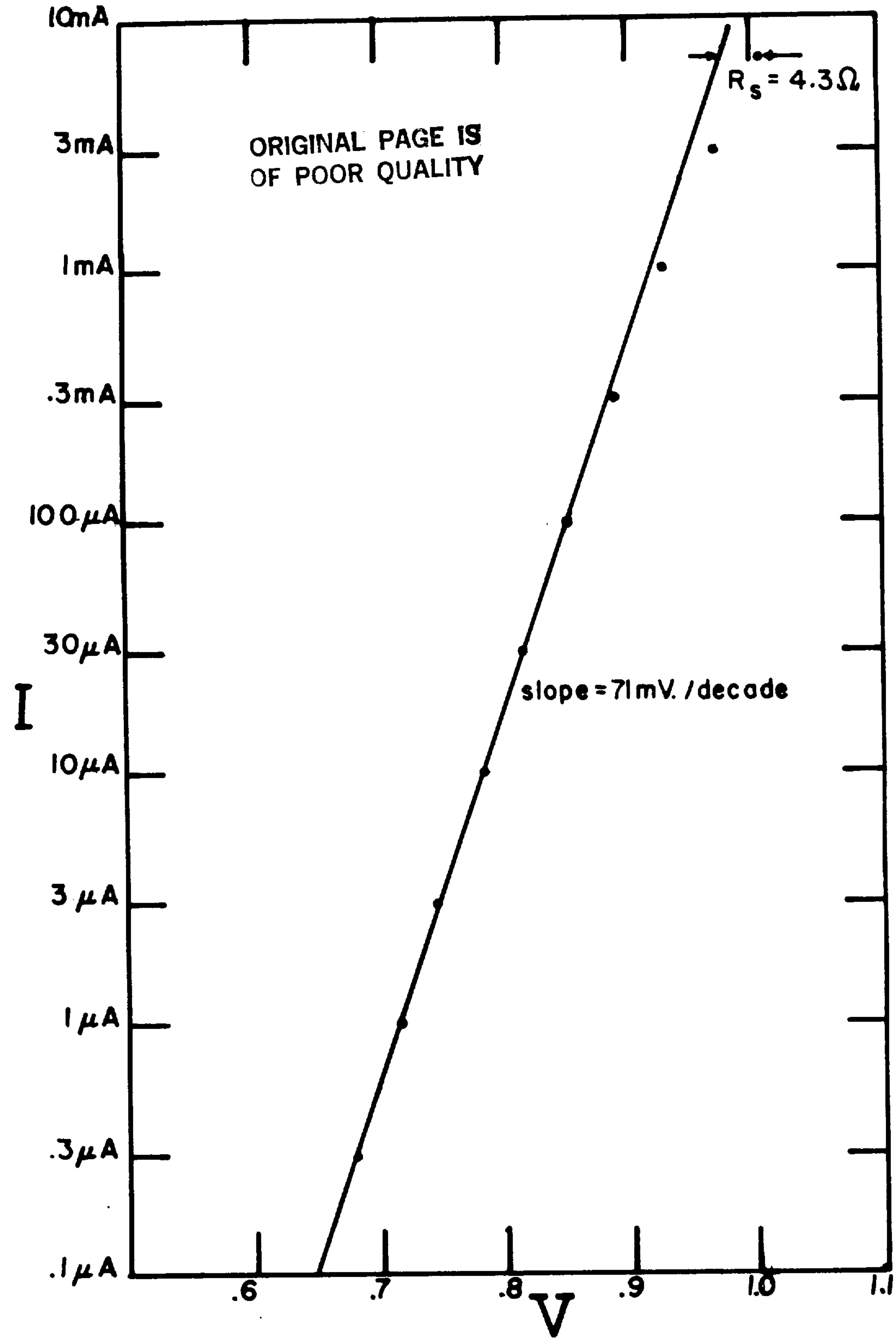

Fig. 4-7 A plot of log i_d versus v_d for the mixer diode used at 140-220 GHz. The diode was made by R.J. Mattauch at the University of Virginia and is a type 1E2.

(5) Diode C-V Law. The capacitance-voltage relationship is one of the more difficult diode properties to characterize accurately. The very thin epitaxial layer of the diodes used in the 140-220 GHz mixer are fully depleted at zero bias and it was not possible to obtain accurate C-V measurements in the forward conduction region. A doping profile was unavailable and the anode radius is so small that the parallel plate capacitor approximation for the depletion layer is not strictly valid; fringing fields may contribute a significant amount to the overall capacitance. In this thesis it has been assumed that the C-V law takes the form of equation (2.5) where the value of γ must be determined by a best fit to the measured mixer performance data (see (8)).

(6) Diode Zero Bias Capacitance. c_0 is measured with a capacitance bridge as the diode anode is being contacted by the whisker in the mixer assembly process. The capacitance of the diode package is monitored as the whisker is brought closer and closer to the anode. When contact is made the diode junction capacitance is added in parallel and, as shown in Fig.4-8, the reading jumps by an amount equal to c_0 (6.2 fF in this case).

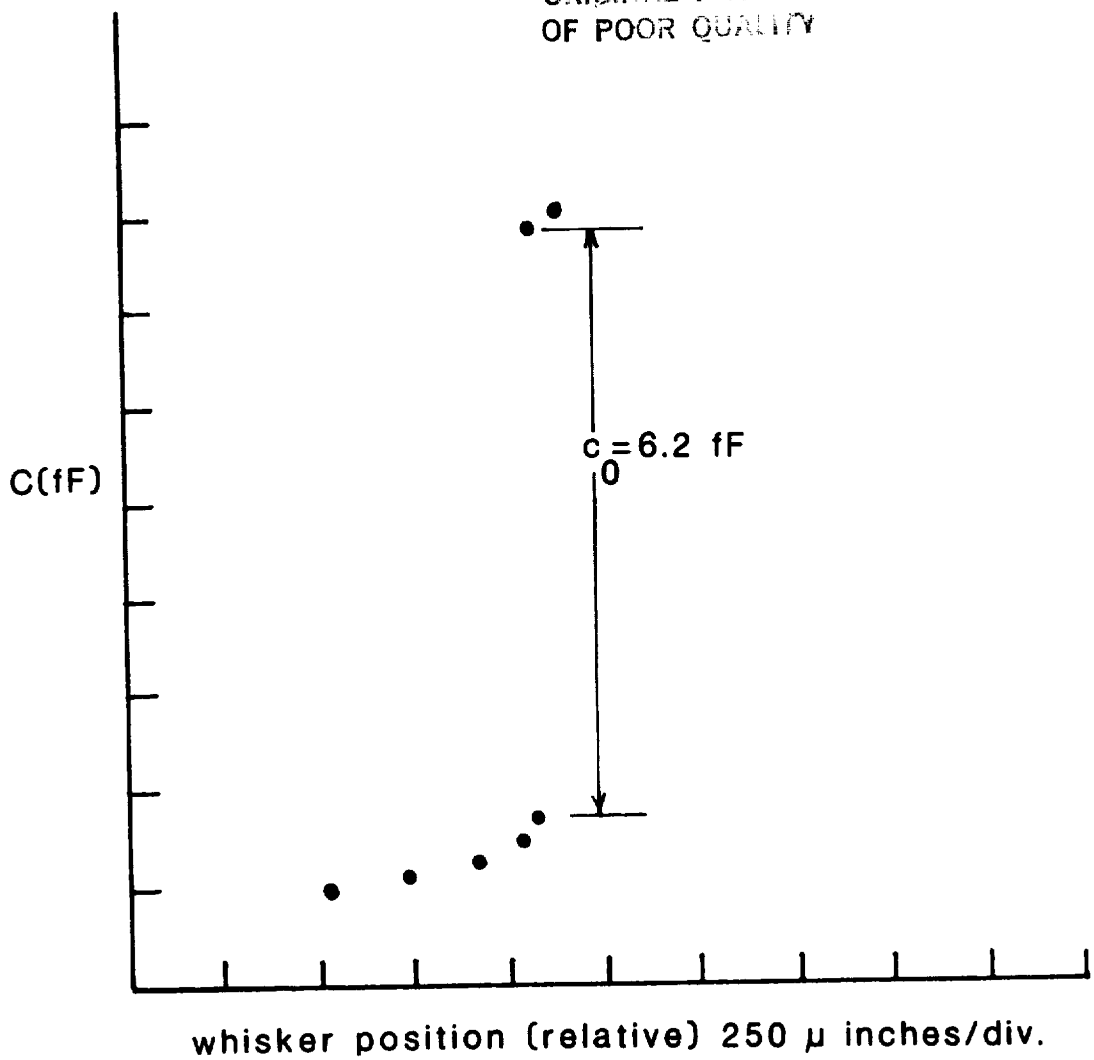

Fig. 4-8 A plot of the relative capacitance versus whisker position during the diode contacting procedure. As the whisker is advanced towards the diode the capacitance between the body of the diode chip and the whisker and mixer block (grounded) increases. At contact, the diode junction capacitance is added in parallel with the fringing capacitance and the measured value jumps by c_0. A Boonton model 75D 1 MHz capacitance bridge with a resolution of 0.05 fF is used for the measurement.

(7) Diode Barrier Height. The Schottky diode barrier height ϕ_b (asymptotic value minus image force lowering term), required for the determination of the built in potential ϕ_{bi}, is a function of the diode material properties, the preparation of the semiconductor surface and the metal deposition process. The surface state density at the metal-semiconductor interface was indeterminate and because of the very thin epitaxial layer of these diodes the author was unable to obtain the barrier height with certainty using a C-V measurement. Additional problems arise in modelling ϕ_b because it is weakly dependent upon the applied voltage. An approximate value for the barrier height of 1.06 V is suggested by measurements made by R.J. Mattauch at the University of Virginia on similar diodes. With this choice of ϕ_b and a value of $\Delta\phi$ (the image force lowering term) of 0.01 V, the built in potential $\phi_{bi} = 1.05$ V. Our choice of $\phi_{bi} = 1.05$ V is justified by the fact that with this value of ϕ_{bi}, the computed and measured mixer performance are in excellent agreement over a wide range of embedding impedances.

(8) C-V Law Exponent. As mentioned in (5) above, γ is determined by fitting the computed with the measured mixer performance. A value of 0.5 implies an abrupt junction, while a value of 0.3 implies a linearly graded doping profile. The problem is further complicated by the fact

that γ is voltage dependent [62]. It will be shown in Chapter 5 that the mixer performance is only moderately sensitive to the variations in the value of γ. In addition, for the instantaneous voltage range over which this mixer operates (v_d varies between roughly 0.4 and 1.0 V in an LO cycle) γ does not appear to be a strong function of v_d. This assertion is based on the close agreement between the measured and computed performance when γ is taken to be constant at 0.5.

(9) Diode DC Series Resistance. $R_s(dc)$ can be determined from the diode log I-V curve if the effects of pump heating, as observed by Weinreb and Decker [63,86], are included. The diode series resistance can also be calculated fairly accurately [36]. Using the equations in Appendix 2, the calculated value of $R_s(dc)$ for this diode is 4.8 ohms (including 0.5 ohms contributed by the whisker and microstrip filter). The DC log I-V curve (Fig. 4-7) yields a value of $R_s(dc)$ of 4.3 ohms to which must be added 2 ohms to compensate for diode heating [62,86]. For the results presented in this thesis $R_s(dc)$ was taken to be 6.3 ohms, the value determined from the log I-V curve plus 2 ohms to account for diode heating.

At high frequencies the DC resistance is modified by the skin effect. In the mixer analysis program the additional contribution to $R_s(dc)$ is calculated from the diode material properties and geometry (see Appendix 2). At 180 GHz, the skin effect adds roughly 2.5 ohms to R_s(dc), with an equal amount appearing as a reactive term. At the sixth harmonic (1080 GHz) R_s is increased by about 6.7 ohms over the DC value.

(10) Noise Generation Mechanisms. The noise in the Schottky diode is assumed to come from thermal noise generated in the diode series resistance and shot noise arising from the diode conductance current. The effects on the noise temperature of lattice and intervalley scattering and hot electrons have not been included in the mixer analysis program. It has been suggested [63] that these noise contributions can be accounted for by a slight increase in the temperature of the diode series resistance. The excellent agreement we have obtained between the measured and computed mixer noise temperature at 150 and 180 GHz suggests that the hot electron and intervalley scattering noise contributions are much smaller than the shot and thermal noise components in our mixer diode.

(11) Diode Conduction Properties. The diode conduction mechanism has been assumed to be due entirely to thermionic emission over the top of the metal-semiconductor barrier. As such, no account has been taken in the theory for quantum mechanical tunneling. At room temperature and with normal conduction current densities the thermionic

emission theory is certainly a good approximation. However, in cryogenically cooled diodes the contribution from tunneling may become significant [172] and a more complete noise theory than is given in this thesis is required to account for the partially correlated components. In addition, at very high frequencies (certainly by 1000 GHz) there are other effects, namely ballistic transport [50], intervalley scattering [124], dielectric relaxation [21], plasma resonance [21] and charge carrier inertia [21], which may cause the current-voltage relationship to deviate significantly from the form given in equation (2.1). The only evidence we have so far that these effects are small at 200 GHz is the excellent agreement between the theoretically predicted and the measured mixer performance. These results will be presented in the next section.

4.6 140-220 GHz Mixer: Comparison of Theory and Measurements

In this section we examine the ability of the mixer analysis program of Chapter 2 to predict the conversion loss, noise temperature and output VSWR of an actual 140-220 GHz mixer. Using the results discussed in Sections 4.2-4.5, a comparison of the measured and predicted mixer performance at 150 and 180 GHz will be made as a function of backshort setting.

The diode equivalent circuit, with the parameter values used in the mixer analysis program, is shown in Fig. 4-9. The LO harmonic and sideband embedding impedances at a particular mixer backshort position are taken from the Smith chart plots at the end of Chapter 3 (note that the impedances given in the plots must be multiplied by 50 ohms before they are used in the program).

The impedance data covers a range of backshort positions beginning about 10 mils from the diode and going out 130 mils (approximately one guide wavelength at the low end of the waveguide band). The complete mixer analysis is performed at each of 66 equally spaced (every 2 mils)

Diode Parameter Values

$R_s(dc) = 6.3\Omega$

$\alpha = q/\eta kT = 32.24$

$T = 300K$

$\eta = 1.2$

$i_s = 3.77 \times 10^{-17} A.$

$\phi_{bi} = 1.05 V.$

$\gamma = 0.5$

$C_o = 6.2 \times 10^{-15} F.$

BIAS POINTS

$V_{dc} = 0.8 V$

$I_{dc} = 1 mA.$

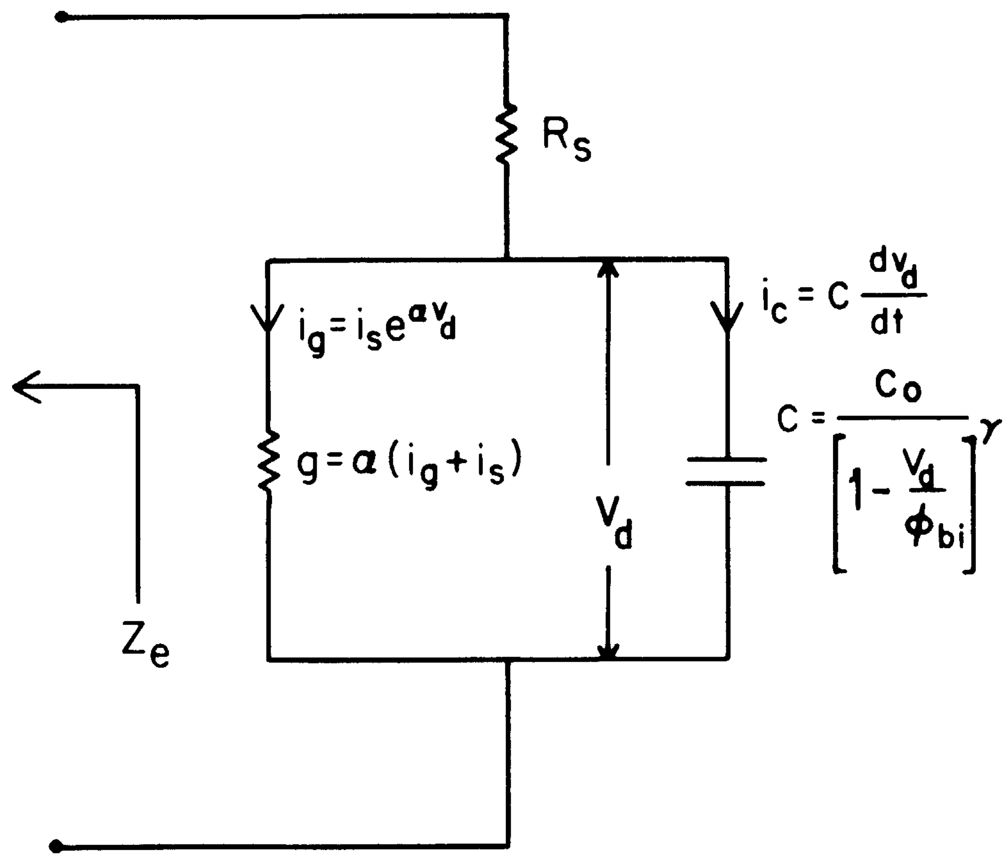

Fig. 4-9 The diode equivalent circuit with the derived parameter values used in the mixer analysis program to compare the measured and computed performance at 150 and 180 GHz.

backshort settings. The upper and lower sideband conversion loss, input and output noise temperature and IF VSWR are then plotted as a function of backshort position.

The computed results are superposed with the measured mixer performance in Figs. 4-10 and 4-11. The error bars on the measured points are obtained by assuming an uncertainty of $\pm$ 1 dB for the conversion loss and $\pm$3K in the reading of T_{IF_A} [$\pm 3/(1-|\Gamma|^2)$ for T_o]. All measurements were performed at a bias setting of 0.8 V and a diode rectified current of 1 mA. Where no measured points appear there was insufficient LO power available to obtain the required diode rectified current.

The values of η, γ and ϕ_{bi} used in the mixer analysis program were all chosen to give a best fit to the measured mixer performance within their allowed experimental tolerances. This is justified by the fact that all three independent mixer performance parameters, conversion loss, noise temperature and IF output VSWR, show good agreement between measurements and computations over a wide range of embedding impedances.

Examining the 180 GHz results first (Fig. 4-10) we see that the agreement between the measured and computed mixer performance is excellent except for a few points

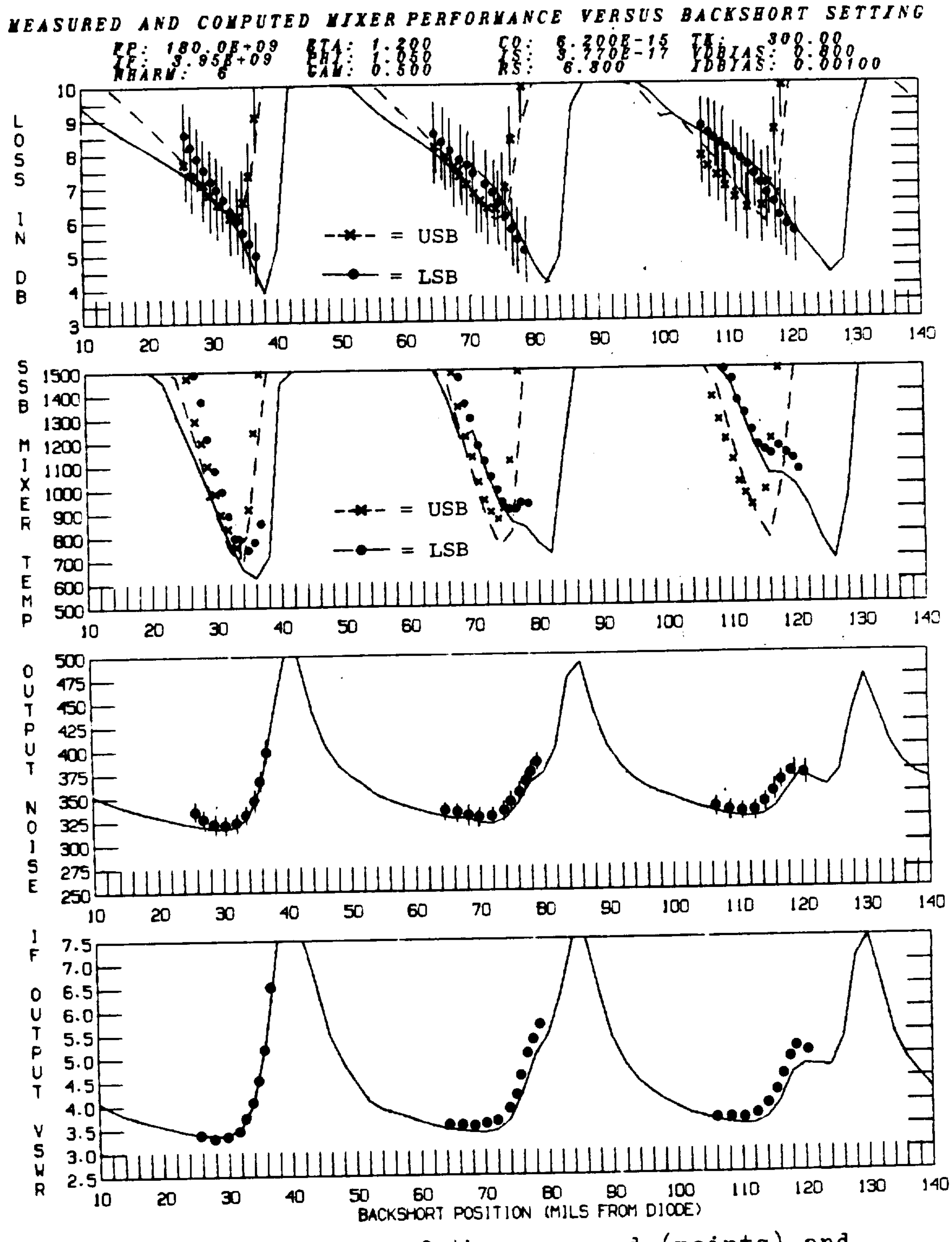

Fig. 4-10 A comparison of the measured (points) and computed (lines) mixer performance at 180 GHz. Error bars reflect uncertainties in the input signal power level and in the IF readings (error bars for the input noise temperature are typically +400,-200K and are not shown).

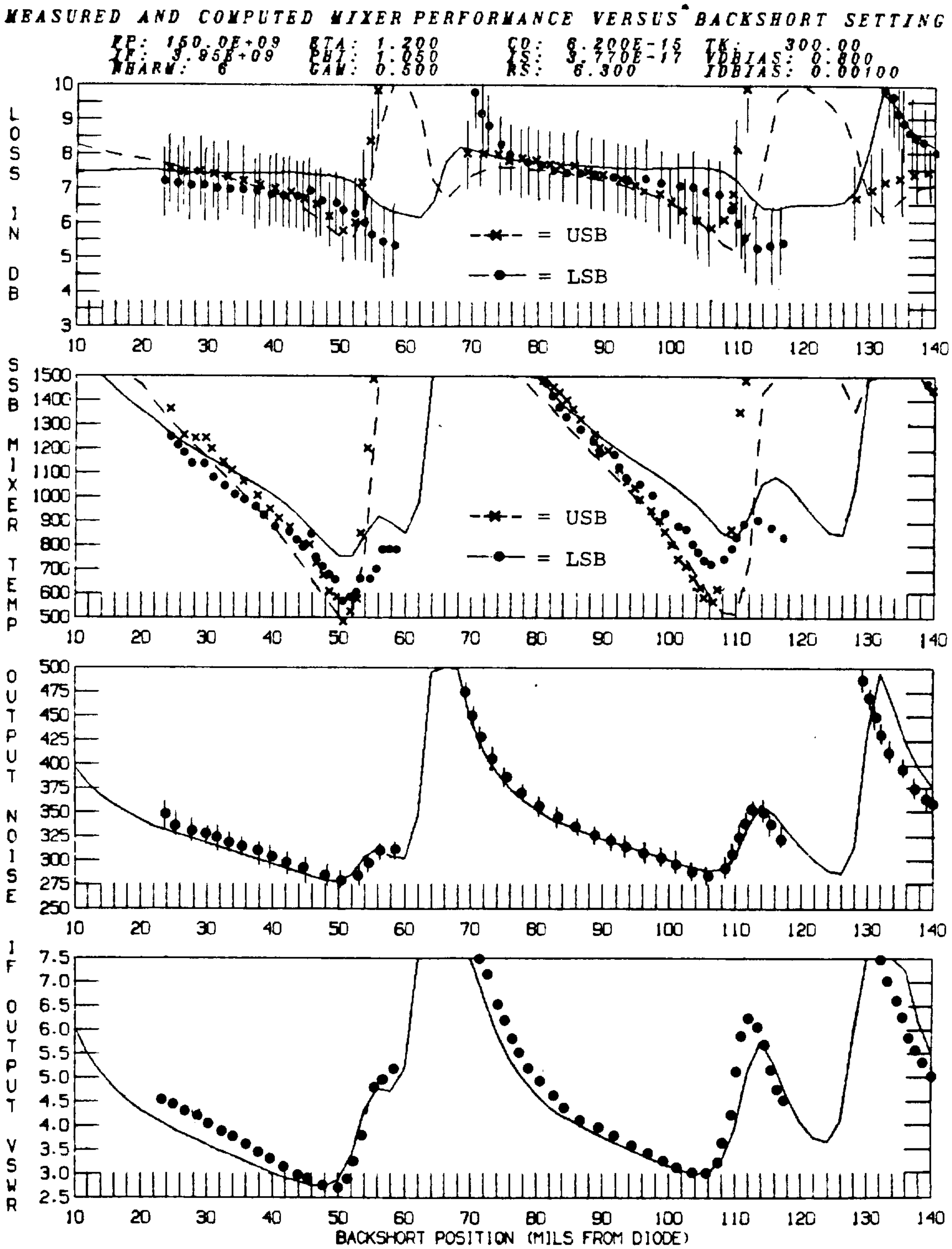

Fig. 4-11 A comparison of the measured (points) and computed (lines) mixer performance at 150 GHz. Error bars reflect uncertainties in the input signal power level and in the IF readings (error bars for the input noise temperature are typically +400,-200K and are not shown).

where the backshort is very close to the diode. Here differences between the backshorts in the scale model and the actual mixer may be significant, especially at the higher harmonic frequencies. One also notices a slight compression of the x-axis in the measured performance parameters. This is more apparent at 150 GHz (Fig.4-11) and is the result of a small increase in the width of the mixer waveguide over its nominal value. Much of the discrepancy between the measured and computed input noise temperature is due to uncertainties in the upper and lower sideband conversion loss. The measured and computed output noise temperatures, which do not involve a separate measurement of the loss, are in much better agreement.

At 150 GHz there is a significant (but consistent) discrepancy between the measured and computed upper sideband conversion loss. This has been attributed to an error in the calibration of the 140-220 GHz power sensor used to measure the signal level at the input of the mixer. The error can be seen in the input noise temperature curves but does not effect the output noise temperature which is not a function of the measured conversion loss. As expected, the compression of the x-axis, due to the width of the waveguide in the actual mixer being slightly greater than its nominal value, is more pronounced at 150 GHz than at 180 GHz.

In conclusion, it is clear from Figs. 4-10 and 4-11 that the mixer analysis program can be used to predict the performance of an actual device with a high degree of accuracy. The excellent agreement between the theory and the measurements suggests that there is no significant amount of scattering or hot electron noise at 180 GHz under the chosen mixer operating conditions. At least at room temperature we can safely say that the conduction mechanism in these mixer diodes is entirely thermionic emission. The results also justify our choice of η, γ and ϕ_{bi} and suggest that the mixer analysis program might be useful in deriving more accurate values for these parameters then can be determined by other measurement techniques.

In the next chapter we will examine the sensitivity of the mixer performance to the derived diode parameters and then go on to suggest an optimum diode for this particular mixer.

CHAPTER 5. MIXER OPTIMIZATION

5.1 Introduction

One of the goals of this research is to establish some criteria which could be applied to the design of future millimeter wave mixers. In this chapter the mixer analysis program is used to examine the importance of various diode parameters as they effect the overall mixer performance at 180 GHz. Some general guidelines for the fabrication of an improved diode for this mixer are then proposed. The effects of the diode mount impedances, particularly the whisker inductance, on the mixer performance are also investigated.

5.2 Effect of Diode Parameters on the Mixer Performance

Before we can specify the optimum diode for a given mixer it is useful to establish the sensitivity of the mixer performance to particular diode parameters. We will take as our reference diode the one described in Section 4.5. Each of the diode parameters η, ϕ_{bi}, γ, R_s, T, c_0, and i_s, will be varied in turn and the changes produced in the mixer performance will be examined. (In all cases the DC bias voltage and diode rectified current are maintained constant at 0.8 V and 1 mA). The results are summarized in Fig. 5-8. Individual performance curves are given separately in Figs. 5-1 to 5-7 and are discussed below.

(1). η: The diode ideality factor has a fairly strong effect on the mixer input and output noise temperatures and, to a lesser extent, on the conversion loss and IF output VSWR. Varying η while i_s is held constant is equivalent to changing the slope of the log I-V curve and, in a sense, the operating point of the diode. In Fig. 5-1 the computed mixer performance at 180 GHz is plotted for three values of η (η = 1.2 is the value used in Fig.

4-11). An increase in η (decrease in the log I-V curve slope) of only 3% causes a 250 degree increase in the minimum input noise temperature, a slight decrease (< 0.5dB) in the conversion loss and a moderate increase in the output VSWR. Note that an increase in η causes an increase in the amount of required LO power if the DC current is to be maintained at the same level, which is the case for the results presented here.

(2). ϕ_{bi}: The built in potential becomes an important parameter when the voltage across the intrinsic diode swings close to ϕ_{bi} at some point during the LO cycle, causing the depletion layer capacitance to become very large [see equation (2.5)]. When this occurs the noise temperature of the mixer is the most affected parameter (increasing substantially as v_d gets very close to ϕ_{bi}). At other operating points ϕ_{bi} acts inversely with η, however with a less pronounced effect. Fig. 5-2 contains plots of the mixer performance when ϕ_{bi} is varied by $\pm 5\%$ from its nominal value of 1.05. The lowest value of the built in potential shown in the figure (1.01) corresponds to an operating point at which the maximum value of v_d in an LO cycle is 99.3% of ϕ_{bi}.

(3). γ: A decrease in the capacitance law exponent most strongly affects the mixer noise temperature as can be seen in the plots of Fig. 5-3 (γ=0 corresponds to a diode with a constant capacitance equal to c_0). In all instances studied, a decrease in γ improved the mixer noise performance (this is not to say that a constant capacitance diode always gives better mixer performance as is evidenced in the plots of Appendix 4).

(4). R_s(dc): Much effort has been placed in trying to reduce the diode series resistance as much as possible. As shown in the plots of Fig. 5-4 the series resistance affects the thermal noise component and the conversion loss. Notice however, that a fairly substantial change in R_s(dc) is required to obtain any significant improvement in performance.

(5). T: A change in diode temperature, while i_s is fixed, has the same effect as a proportional change in η. (There will be a small additional change in the thermal noise component but it is not noticeable in Fig. 5-5 where T has been varied -5 K and +10 K from its nominal value of 300K).

(6). c_0: The zero bias capacitance is one physical parameter which is relatively simple to alter and, as shown in the plots of Fig. 5-6, it has a very strong affect on the mixer performance. The decrease in conversion loss and noise temperature from a 30% drop in capacitance more than makes up for any increase in series resistance which might result from using a smaller area diode (that is, assuming the increased current density in the smaller area diode does not give rise to effects which degrade the mixer performance).

(7). i_s: Changing the saturation current while η and ϕ_{bi} remain fixed is equivalent to a shift of the diode log I-V curve (Fig.4-7) along the V axis. Fig. 5-7 shows the resulting change in mixer performance when i_s is varied by $\pm 50\%$ from its nominal value of 3.8×10^{-17} A.

A summary of the effects of the 7 aforementioned diode parameters on the mixer noise, loss and output VSWR can be found in Fig. 5-8.

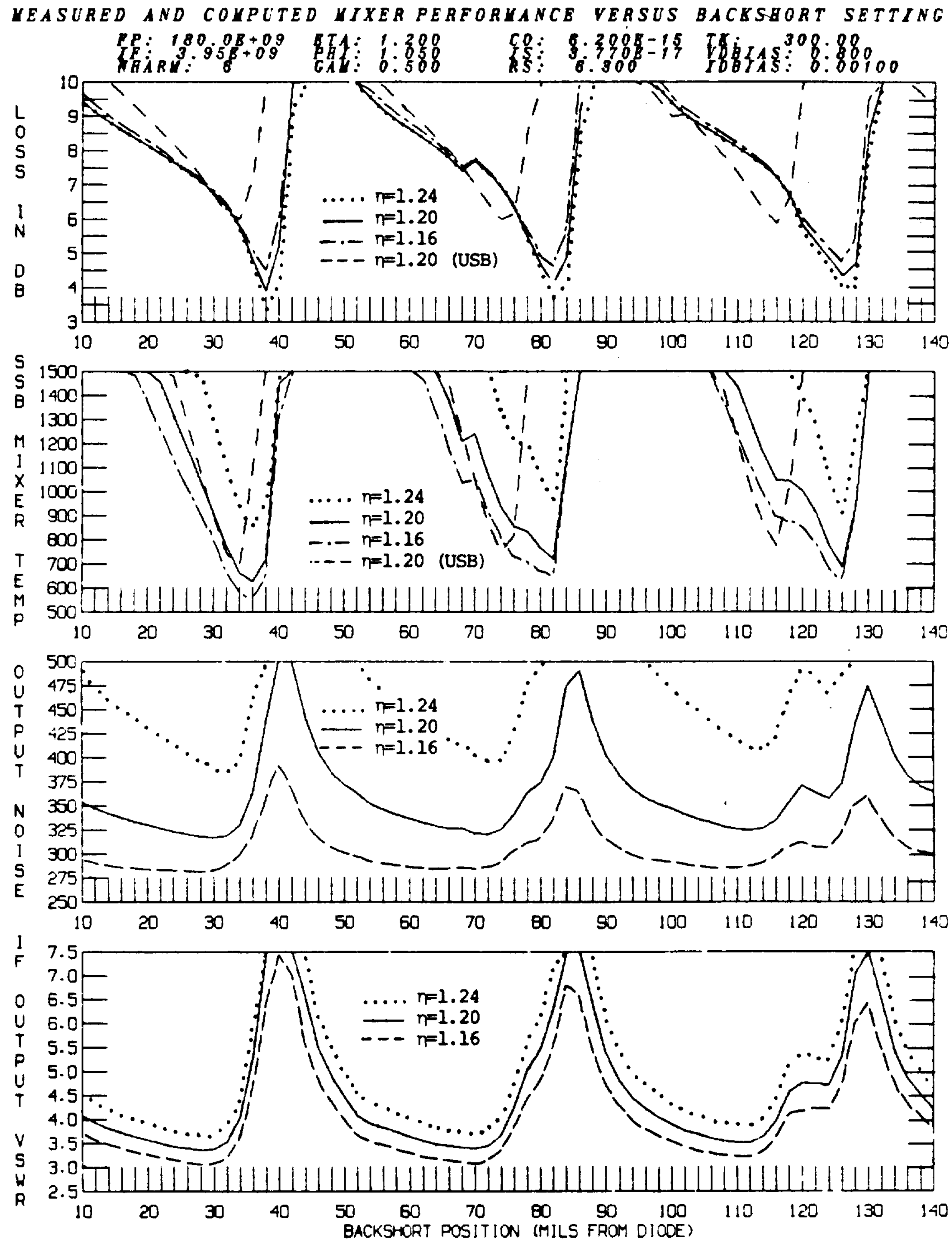

Fig. 5-1 Computed mixer performance at 180 GHz when $\eta = 1.16$, 1.20 and 1.24. In the top two graphs only the lower sidebands are compared (except for the plain dashed line which represents the upper sideband performance for $\eta = 1.2$, our standard value).

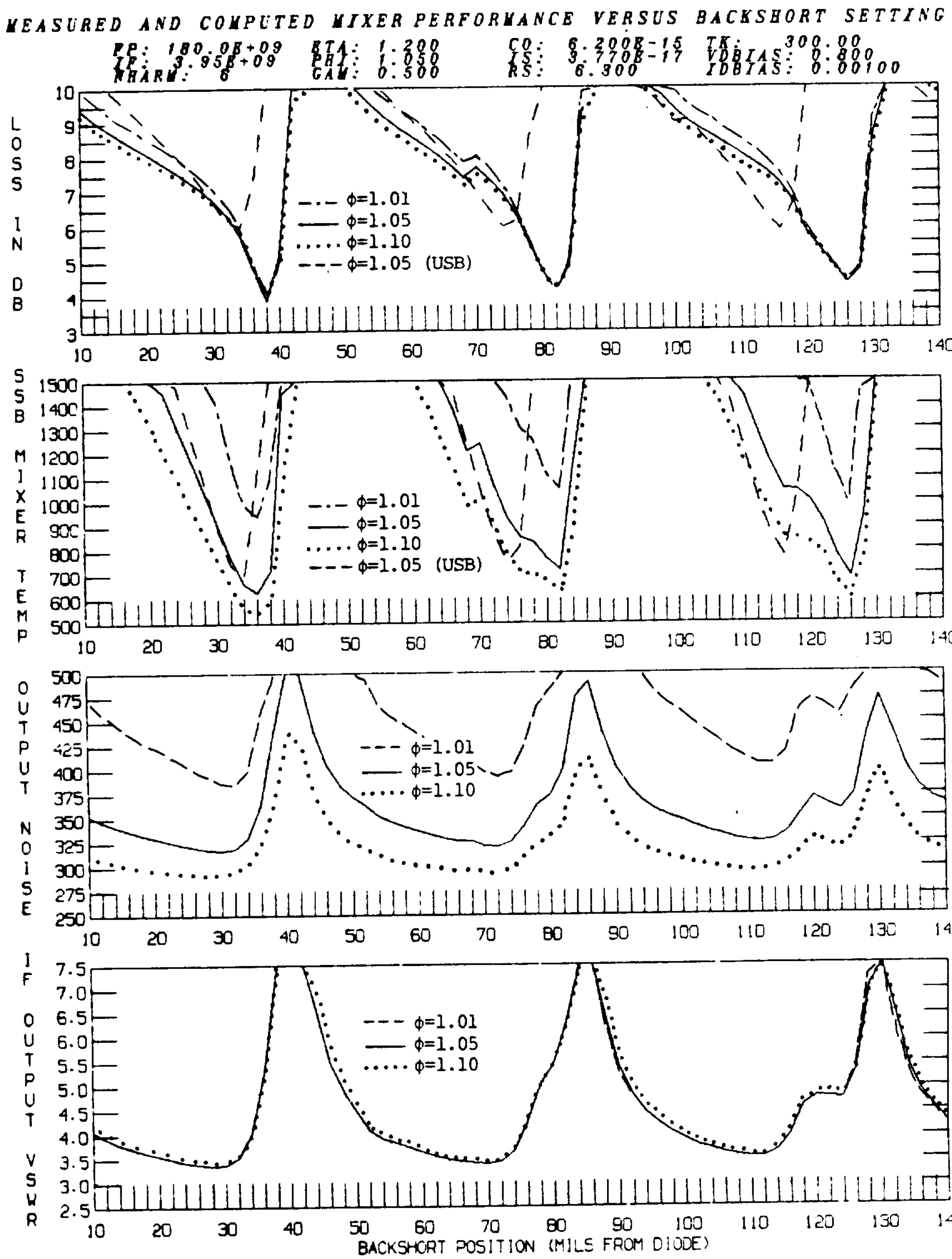

Fig. 5-2 Computed mixer performance at 180 GHz when ϕ_{bi}= 1.01, 1.05 and 1.1 V. In the top two graphs only the lower sidebands are compared (except for the plain dashed line which represents the upper sideband performance for ϕ_{bi}=1.05, our standard value).

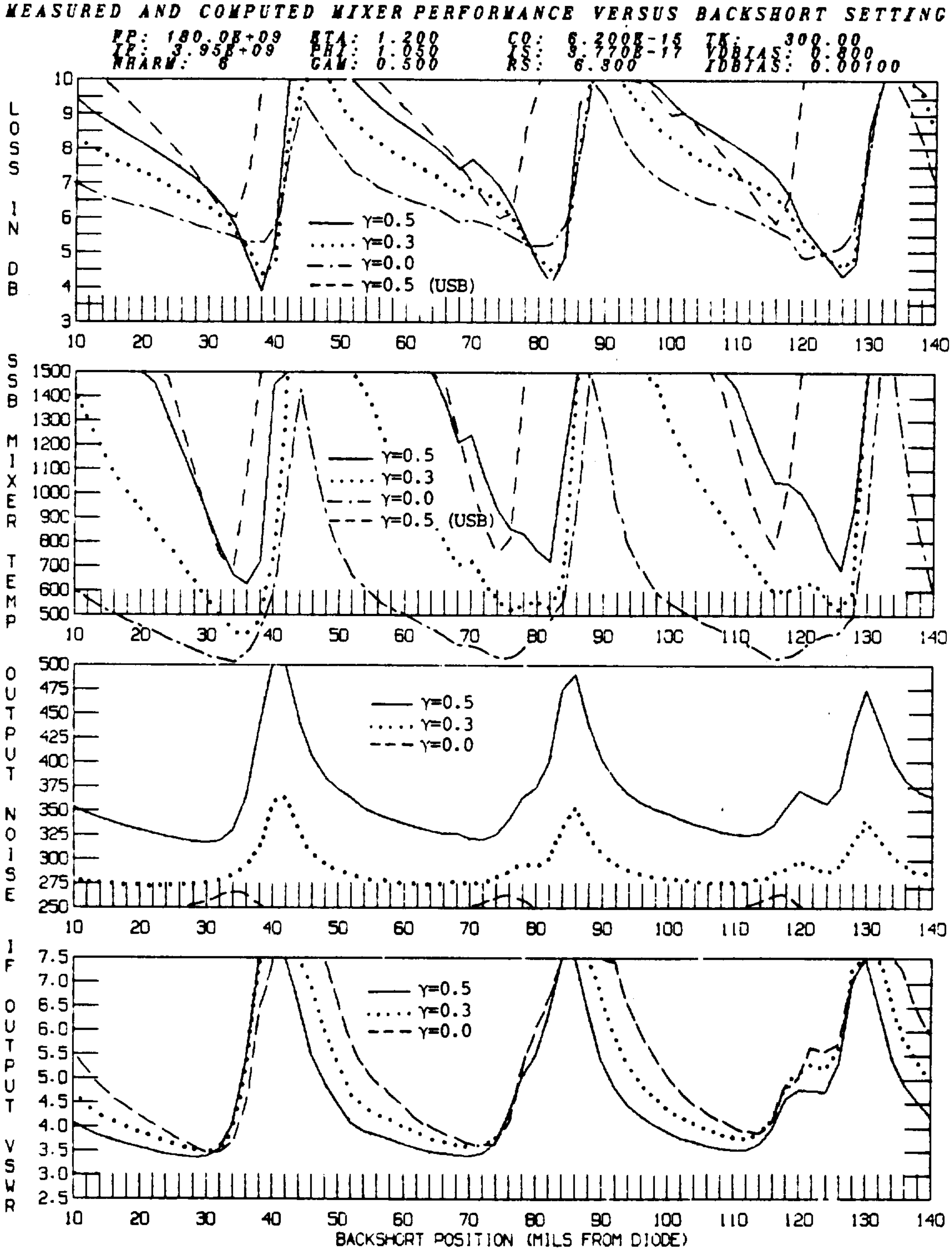

Fig. 5-3 Computed mixer performance at 180 GHz when γ = 0.0, 0.3 and 0.5. In the top two graphs only the lower sidebands are compared (except for the plain dashed line which represents the upper sideband performance for γ = 0.5, our standard value).

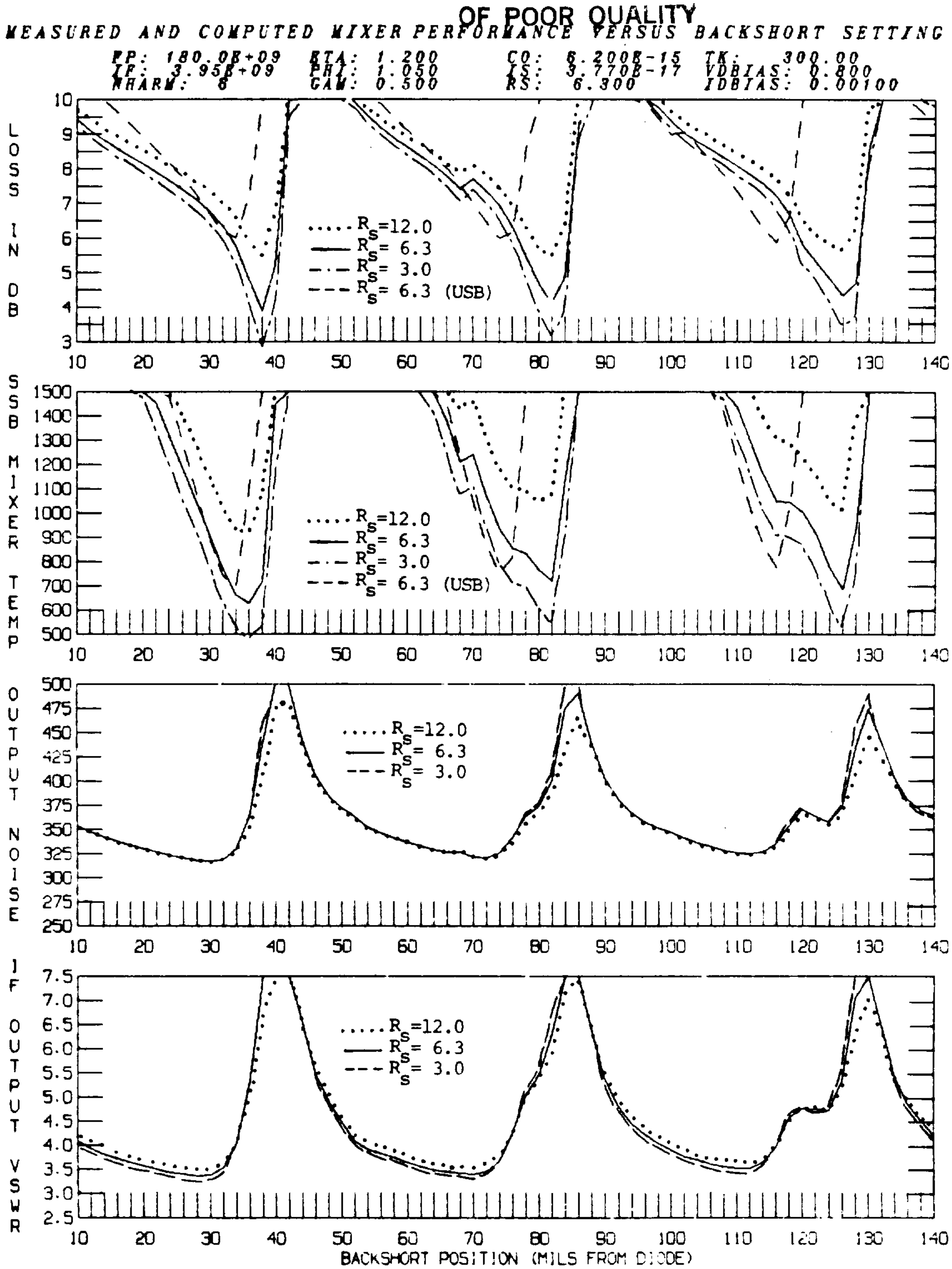

Fig. 5-4 Computed mixer performance at 180 GHz when R_s(dc) = 3, 6.3 and 12 ohms. In the top two graphs only the lower sidebands are compared (except for the plain dashed line which represents the upper sideband performance for R_s(dc) = 6.3, our standard value).

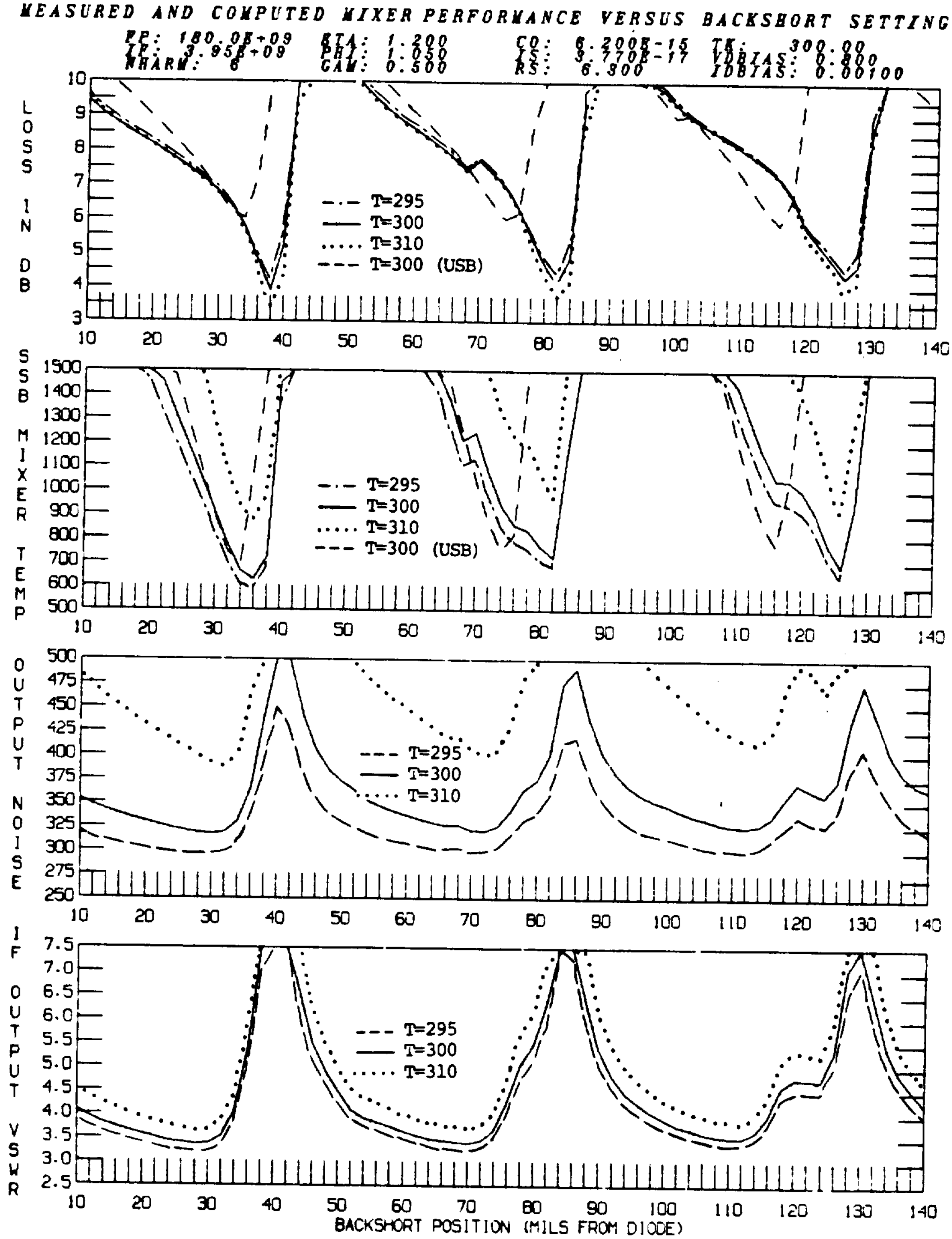

Fig. 5-5 Computed mixer performance at 180 GHz when T = 295, 300 and 310 K. In the top two graphs only the lower sidebands are compared (except for the plain dashed line which represents the upper sideband performance for T = 300K, our standard value).

ORIGINAL PAGE IS
OF POOR QUALITY

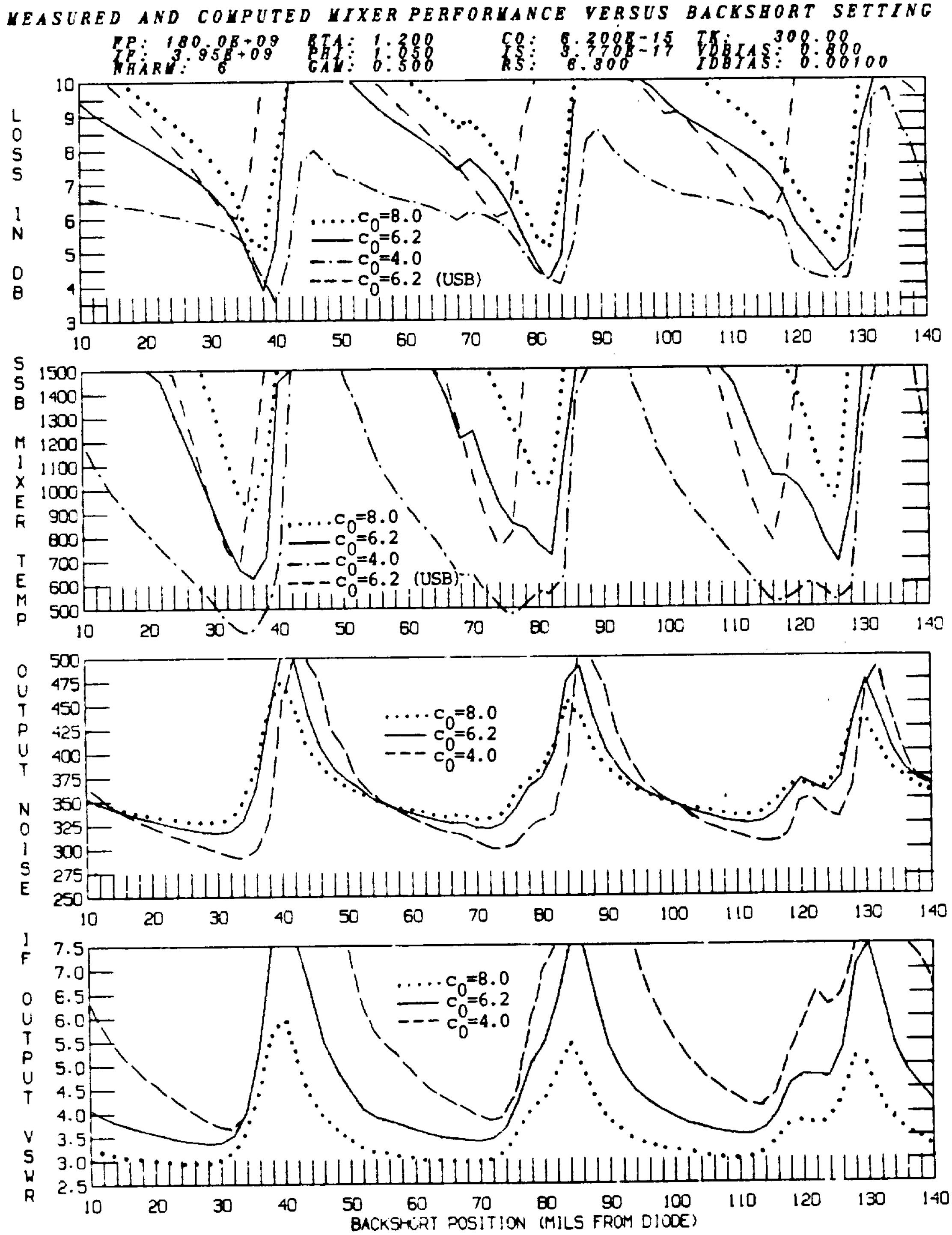

Fig. 5-6 Computed mixer performance at 180 GHz when c_0 = 4, 6.2 and 8 fF. In the top two graphs only the lower sidebands are compared (except for the plain dashed line which represents the upper sideband performance for c_0 = 6.2 fF, our standard value).

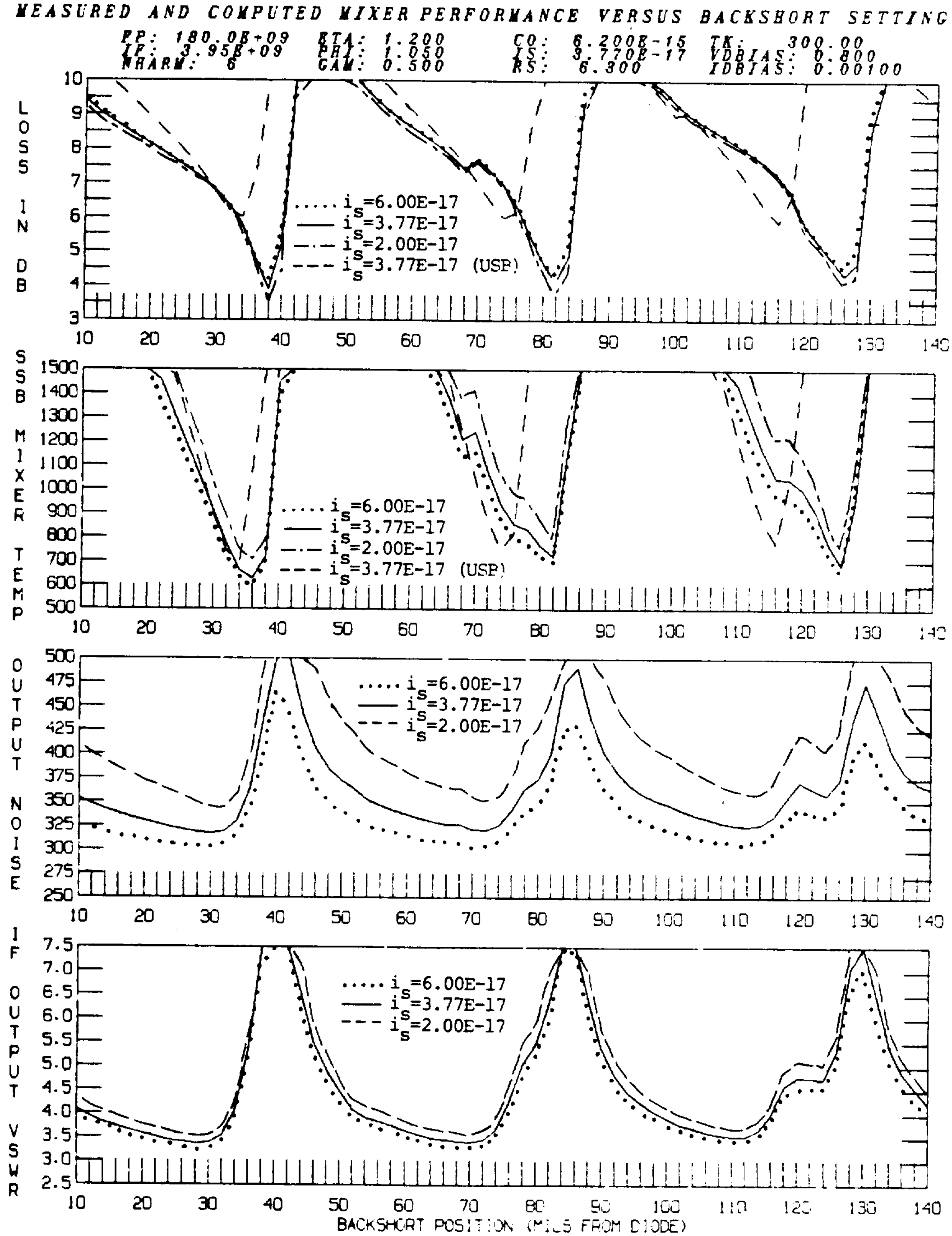

Fig. 5-7 Computed mixer performance at 180 GHz when i_s = 2, 3.77 and 6×10^{-17} A. In the top two graphs only the lower sidebands are compared (except for the plain dashed line which represents the upper sideband performance for $i_s = 3.77\times10^{-17}$, our standard value).

ORIGINAL PAGE IS
OF POOR QUALITY

% increase in diode parameter (max-min)/min	η 1.16-1.24	ϕ 1.01-1.10	γ .3-.5	R_s(dc) 3 - 12Ω	T 295-310K	c_0 4-8 fF	i_s 2-6x10^{-17}
Associated change in mixer performance	+7%	+9%	+67%	+300%	+5%	+100%	+200%
% Change in LOSS	-32%	0%	-10%	+44%	-20%	+29%	+14%
% Change in T_{SSB}	+55%	-43%	+58%	+84%	+47%	+130%	-14%
% Change in T_o	+38%	-23%	+18%	0%	+30%	+12%	-11%
% Change in $\|\Gamma\|$, $\|\Gamma\| = \frac{VSWR-1}{VSWR+1}$	+12%	+1%	-4%	+11%	+8%	-13%	-5%

Fig. 5-8 A chart summarizing the effects of the diode parameters on the mixer performance. The numbers in the boxes show whether an increase in the particular diode parameter increases (+) or decreases (−) the mixer conversion loss (LSB), equivalent input noise temperature (LSB), output noise temperature and voltage reflection coefficient at the IF port (referred to 50 ohms). The data is taken from the graphs in Figs. 5-1 to 5-7.

5.2.1 Optimum Diode Operating Point

The mixer analysis program can be used to search for the optimum diode operating point, that is the combination of DC bias and diode rectified current which results in the best mixer performance. These parameters are limited by the available LO power and also by the power handling capacity of the diode.

In Fig. 5-9 the mixer performance is plotted for 3 values of the DC bias setting (VDBIAS in the mixer analysis program) between 0.65 and 0.85 volts (0.8 V is the setting which was used for all of the mixer measurements). In all cases the LO power is adjusted until 1 mA of rectified current flows in the diode. The mixer noise and conversion loss decrease as the bias voltage is lowered (note however that the IF VSWR increases). There is even a point at which the single sideband conversion loss is less than 3 dB due to parametric effects associated with the nonlinear diode capacitance. Bear in mind that the required LO power at an operating point of 0.65 V is much higher than that at 0.8 V and is above 4 mW at the backshort setting with the lowest conversion loss (compared with 0.6 mW at 0.8 V bias).

Fig 5-10 shows the predicted mixer performance when the rectified current in the diode (IDBIAS in the mixer analysis program) is varied. Slight improvements in performance are obtained when IDBIAS is higher than its nominal value of 1 mA (greater required LO power).

With the limited amount of data presented in this thesis it is difficult to make any definitive statements concerning the most desirable operating point for mixers in general. Although in the plots of Figs. 5-9 and 5-10 the loss and noise vary together, experience has shown that this is not always the case. The most that can be said is that the mixer performance is a strong function of both the DC operating point and the incident LO power level and that the upper and lower sidebands are affected very differently.

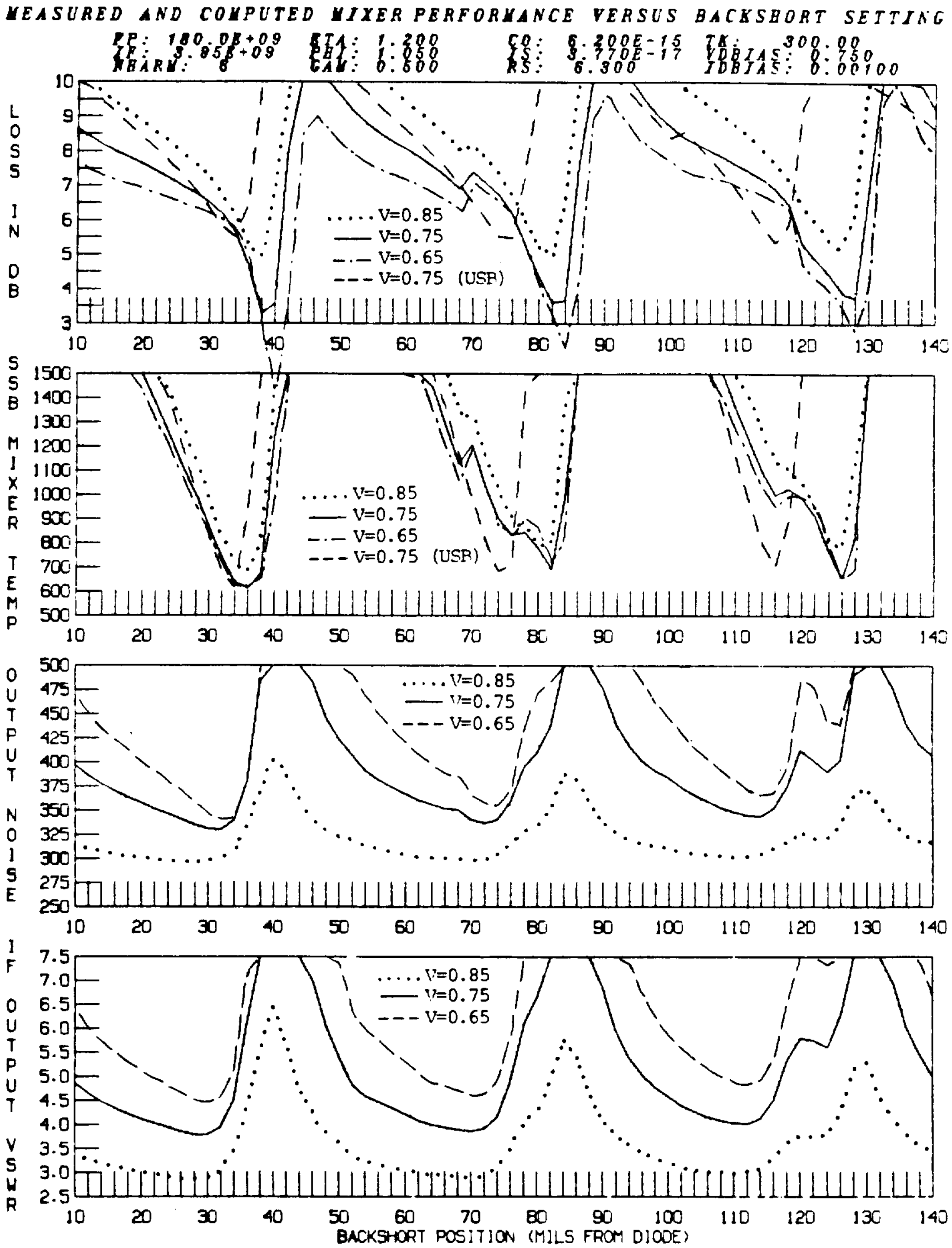

Fig. 5-9 Computed mixer performance at 180 GHz when VDBIAS = .65, .75 and .85 V. In the top two graphs only the lower sidebands are compared (except for the plain dashed line which represents the upper sideband performance for VDBIAS = 0.75).

ORIGINAL PAGE IS
OF POOR QUALITY

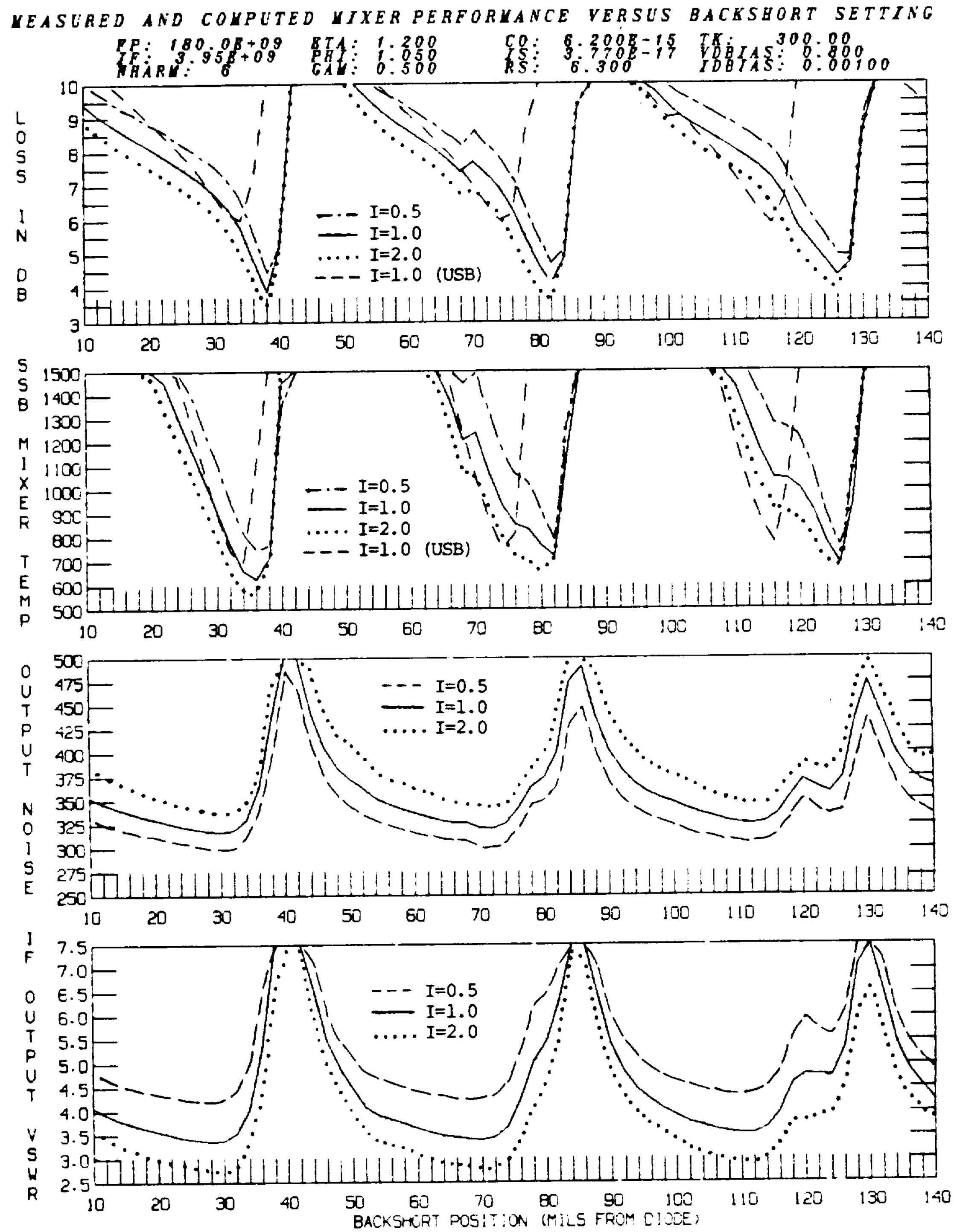

Fig. 5-10 Computed mixer performance at 180 GHz when IDBIAS = 0.5, 1 and 2 mA. In the top two graphs only the lower sidebands are compared (except for the plain dashed line which represents the upper sideband performance for IDBIAS = 1 mA, our standard value).

5.3 Diode Optimization

We are now in a position to make some statements about the optimum diode for this particular mixer mount. Clearly some trade-offs will have to be made, however several trends emerge from the results of Section 5.2:

(1). Using a lower capacitance diode should improve the mixer performance even if the series resistance is increased.

(2). For this mixer mount a diode with little or no capacitance variation is preferred.

(3). The diode series resistance should be kept as low as possible but not at the expense of higher capacitance.

(4). Although these parameters can not be optimized independently, the diode ideality factor, barrier height and saturation current strongly affect the mixer performance. In addition, the magnitudes of their effects are tied to the diode bias point and LO power level.

(5). There is a clear difference between the upper and lower sideband performance even when the intermediate frequency is only 2% of the LO. For our particular mixer the upper sideband is preferred at 150 GHz but the lower sideband gives better performance at 180 GHz.

(6). At certain tuning positions it is possible to get a conversion loss which is less than 3 dB due to the parametric effects associated with the diode capacitance. These operating points are a strong function of the bias voltage applied to the mixer.

(7). For the mixer studied in this thesis it appears that higher incident LO power levels (lower VDBIAS or higher IDBIAS) improve performance.

It would not be fair to generalize the above results in an attempt to steer the course of future mixer diode development. What we can do is offer the mixer designer a chance to determine the optimum diode parameters for use in a particular mixer mount. Clearly more than one approach may be taken in trying to design a better mixer diode and only with an extensive analysis (such as the one presented in this thesis) can the competing effects be sorted out.

Thus far we have looked at the effect of the diode on the mixer performance, but the design of the mixer block (mount embedding impedances) is also very important. This problem is examined in the next section.

5.4 Effects of the Mixer Embedding Impedances

Up until this point we have only considered the effects of the diode on the mixer performance. Equally important is the effect of the diode mount, usually designed by attempting to optimize the impedance at the signal frequency with little or no consideration being given to the higher harmonics.

As a first step we will examine the sensitivity of the mixer performance to the higher harmonic embedding impedances. Fig. 5-11 contains graphs of computed performance versus backshort position for our 180 GHz mixer when the embedding impedances (LO and sideband harmonics) at all frequencies above 184 GHz are: (i) open circuited, (ii) short circuited and (iii) set to 50 ohms outside the diode series resistance.

The plots show that the higher harmonic impedances do effect the mixer performance and must be considered in any accurate analysis. For the mixer analyzed in this thesis it was found that the impedances above the second harmonic (above 364 GHz) had no significant effect, however results from the analysis of a cooled 115 GHz mixer did show small

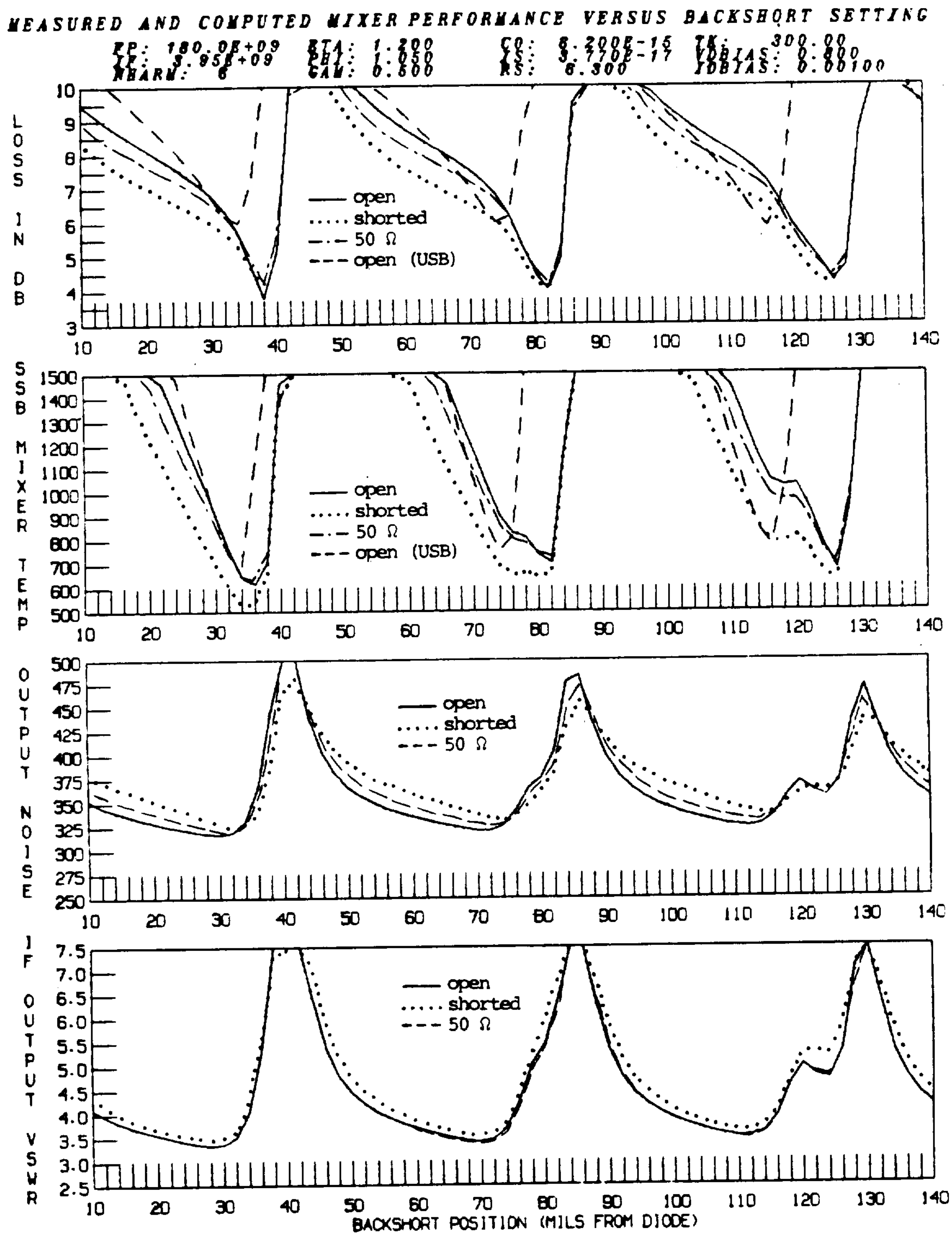

Fig. 5-11 Computed mixer performance at 180 GHz when the embedding impedances are (a) open circuited, (b) short circuited and (c) set to 50 ohms above the upper sideband. Curves (a) are indistinguishable from the standard run (Fig. 4-11). In the top two graphs only the lower sidebands are compared (except for the plain dashed line which represents the upper sideband performance for Z_e open circuited).

small changes in mixer performance when the third harmonic impedance was altered. It is probably fair to assume that for most millimeter-wave mixers an accurate analysis can be performed when the embedding impedances at only the first 3 LO harmonics (ω_p, $2\omega_p$ and $3\omega_p$) and the first 2 harmonic sideband pairs ($\omega_p \pm\omega_0$ and $2\omega_p \pm\omega_0$) are known. Note however, that we must also specify a value for the embedding impedance at $4\omega_p$ in order to correctly perform the large signal mixer analysis [85].

Keeping the above considerations in mind, it should be possible to design a mixer mount which at least approximates a desired set of embedding impedances. One physical parameter which can usually be varied quite easily on most waveguide mixers is the length of the diode contact whisker. Increasing the length of the contact whisker on our 140-220 GHz mixer is approximately equivalent to adding an inductance in series with the measured embedding impedances.

Fig. 5-12 shows what happens to the 180 GHz mixer performance when all the embedding impedances are increased by $j\omega\, \Delta L_s$, where ΔL_s=0.03 and 0.06nH (0.03 nH is equivalent to about a 1 mil change in whisker length). The effect of shortening the whisker length is shown in Fig. 5-13 where $j\omega\Delta L_s$ has been subtracted from the embedding impedances. Notice that there is an optimum value

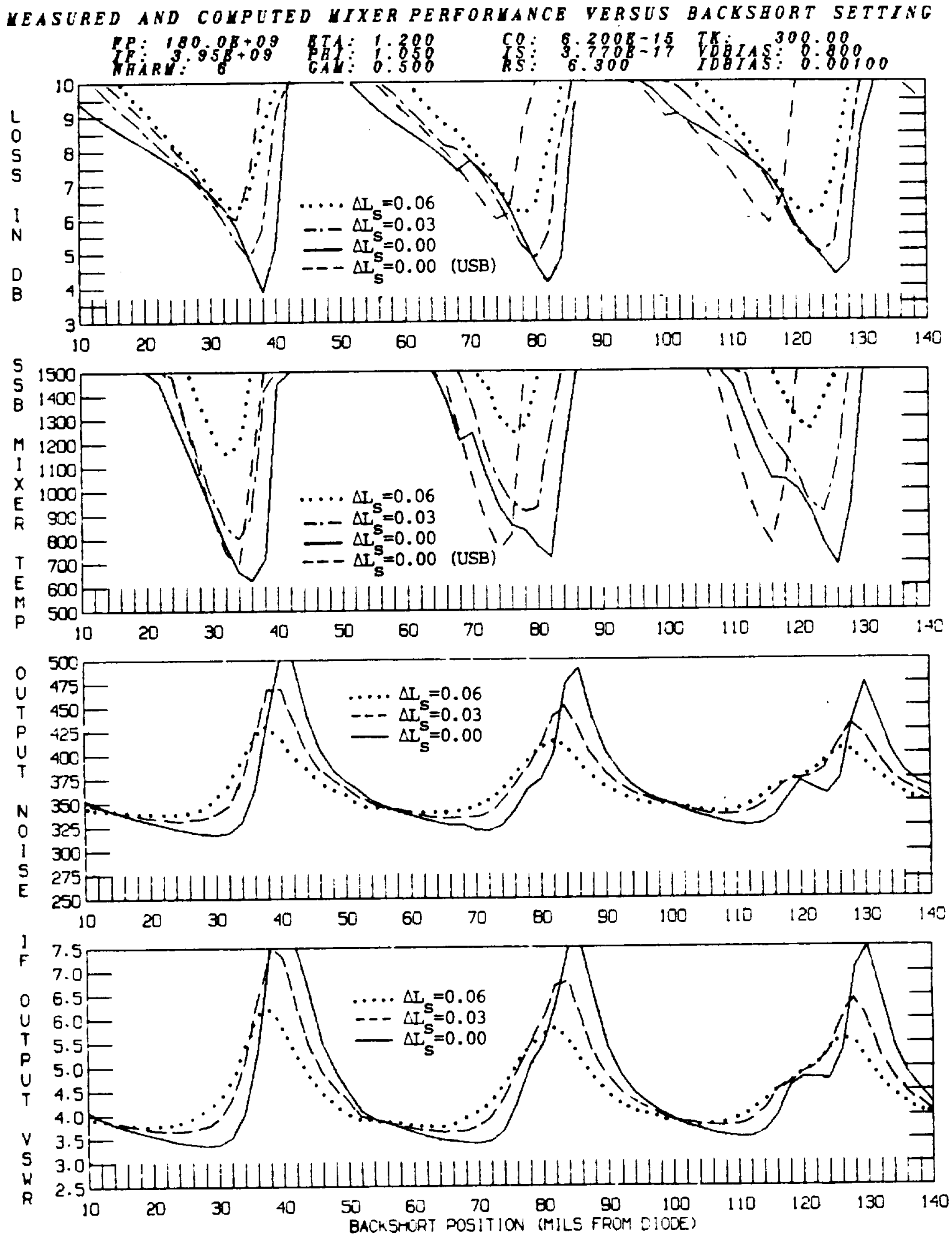

Fig. 5-12 Computed mixer performance at 180 GHz when the diode contact whisker length is increased (ΔL_s = 0.0, 0.03 and 0.06 nH). In the top two graphs only the lower sidebands are compared (except for the plain dashed line which represents the upper sideband performance for our standard diode).

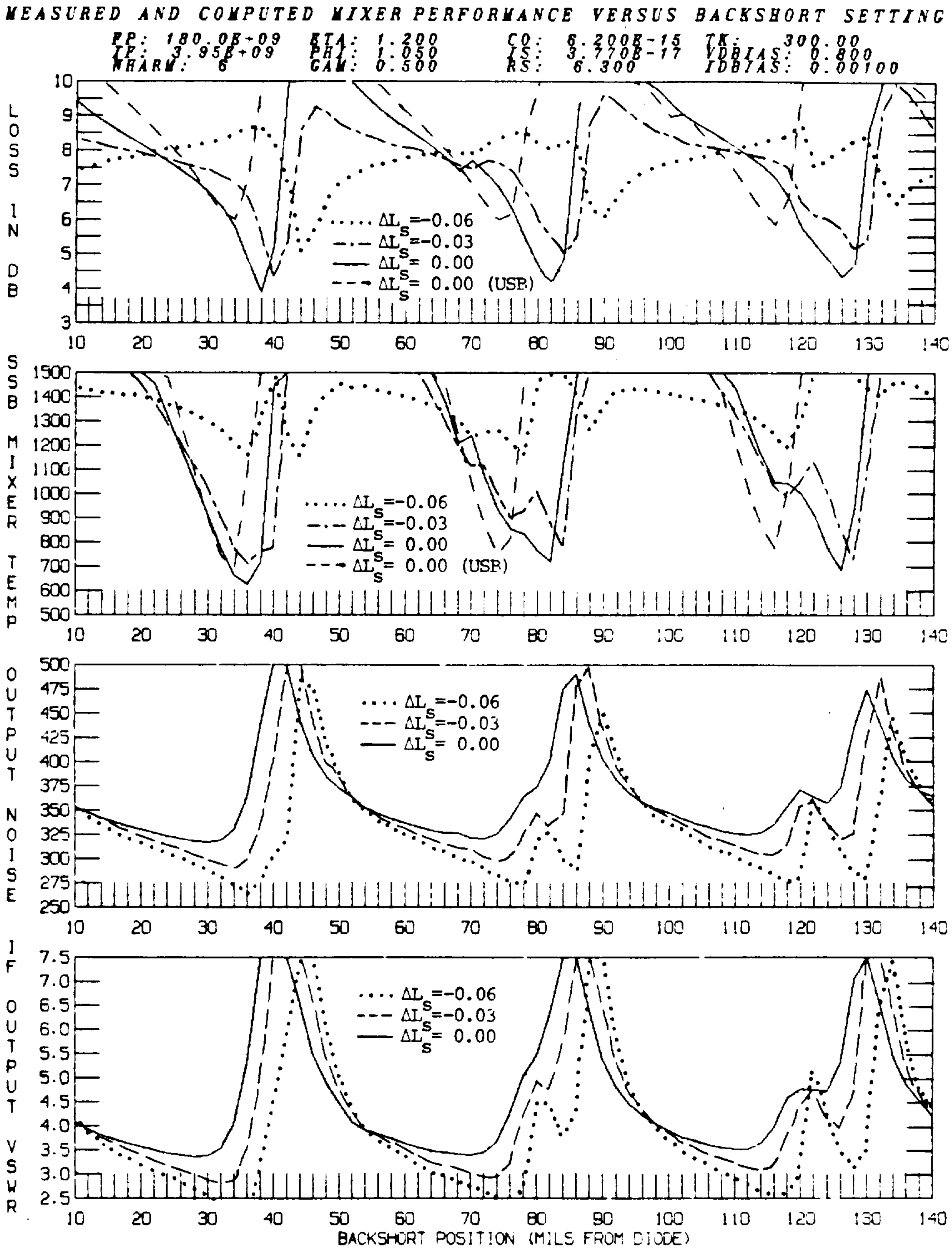

Fig. 5-13 Computed mixer performance at 180 GHz when the diode contact whisker length is decreased (ΔL_s = 0.0, -0.03 and -0.06 nH). In the top two graphs only the lower sidebands are compared (except for the plain dashed line which represents the upper sideband performance for our standard diode).

of whisker length for a particular diode (as we saw in Section 2.7).

Working with our scale model, it is possible to measure the effect, on the diode embedding impedances, of changing various aspects of the mixer mount. In this way one could design a more optimum mixer block to be used with a particular diode. Such an approach was not taken in this thesis. However, it is hoped that future investigators will find this a helpful method to use in the design of other millimeter wave mixers.

5.5 Summary of Mixer Optimization

In concluding this chapter it is helpful to summarize what we have learned about the mixer optimization process.

(1). Much can be gained by tailoring a diode to a particular mixer block. All of the diode physical properties we have looked at in this thesis have a significant effect on the mixer performance and some of these, such as the series resistance and junction capacitance, may be varied more or less independently.

(2). In a given mixer there is a strong connection between overall performance and the diode operating point. The important parameter appears to be the difference between the peak instantaneous forward voltage and the built in potential, i.e. $\phi_{bi} - v_d(\max)$ in an LO cycle. We should also note that the mixer noise and loss are not equally affected by a change of bias voltage or LO power level.

(3). The upper and lower sideband performance are generally quite different. As shown in Section 5.2.1 the upper sideband may have better performance at one frequency while the lower sideband is preferred at another frequency.

(4). It is important to consider the embedding impedances up to at least 3 LO harmonics (up to $3\omega_p$) and 2 sideband harmonic frequencies (up to $2\omega_p \pm \omega_0$) to perform an accurate mixer analysis.

(5). The behavior of a room temperature Schottky diode at 180 GHz is described quite accurately by the thermionic emission theory.

(6). It seems possible to use the mixer analysis program to determine some of the less accessible properties of the diode, namely the barrier height and C-V law exponent (especially if it is approximately constant with voltage), by careful comparison of the theoretical and measured conversion loss and noise temperature.

(7). At least some potential for improvement lies in the design of the mixer block. A more complete study than is performed in this thesis would be extremely beneficial in this regard.

(8). Although it is not yet possible to give a complete set of design guidelines for millimeter-wave mixers it is possible to use the mixer analysis program to explore a new design before any fabrication steps have been taken (apart from building a scale model).

In conclusion, we still have much to learn before we can make any general statements concerning the preferred directions of future diode fabrication efforts or mixer mount design. It is hoped that the approach presented in this thesis will help to increase our understanding of mixer design and eventually lead to devices with improved performance.

CHAPTER 6. ANALYSIS AND DESIGN OF DIODE MULTIPLIERS

6.1 Introduction

The measurement of the conversion loss of a mixer is greatly facilitated if a swept frequency source of millimeter-wave power is available. Klystrons, the traditional source of millimeter-wave power, can only be swept over very narrow ranges and are very costly at high frequencies. Lower frequency oscillators coupled with broad-band harmonic generators offer a more satisfactory means of supplying the LO and signal power required for mixer measurements.

This chapter is concerned with the design and analysis of millimeter-wave varactor diode multipliers. In the first half of the chapter a computer program is described for predicting the performance of varactor multipliers given the diode and mount characteristics. In the second half of the chapter a design for a high efficiency solid-state frequency doubler with its output in the 140-220 GHz waveguide band is given.

The analysis of a diode multiplier is very similar to that of a diode mixer. The nonlinear analysis techniques developed in Chapter 2 can be readily adapted to the multiplier resulting in a useful program for the optimization of these devices.

The multiplier analysis program described in this chapter is more general than past analyses in that it allows the diode to operate in the reverse biased varactor mode or the forward conduction region where resistive multiplication may take place. The program determines the conversion efficiency and the input and output impedances of a multiplier given its diode characteristics and the embedding impedances at the pump and higher harmonic frequencies.

In the second half of this chapter a design for a varactor diode multiplier with a fundamental input of 75-110 GHz is given. The multiplier is based on one described by J.W. Archer [1] but contains a new waveguide transformer developed as part of this work (discussed in Chapter 7) which greatly simplifies fabrication. As a doubler, the device provides 10-15% efficiency in up converting to the 140-220 GHz waveguide band with an instantaneous 3 dB bandwidth of approximately 3%, sufficient for mixer testing or for use as a local oscillator. The varactor diodes were made by R.J. Mattauch at the University of Virginia.

Following a brief historical introduction, the varactor multiplier nonlinear analysis is discussed and the relevant performance parameters are given. The multiplier analysis program is described in Section 6.3 and appears in Appendix 5. Finally, in Section 6.4 the design of the 140-220 GHz frequency doubler is given along with some typical performance data.

6.1.1 Harmonic Generators: A Brief Historical Look

Frequency multiplication occurs whenever a nonlinear impedance is driven by a periodic source. Two types of millimeter-wave harmonic generators are in general use; one based on the nonlinear resistance of a forward biased Schottky barrier diode and the other which makes use of the nonlinear capacitance variation of a reverse biased varactor diode.

Resistive multipliers have been used to produce millimeter-wave power since the early 1940's [15]. The most common arrangement is the crossed waveguide structure, a hypothetical version of which is shown in Fig. 6-1. The diode is mounted in the output waveguide and is contacted by a long whisker which extends through a hole in the wall of the lower frequency input waveguide. The

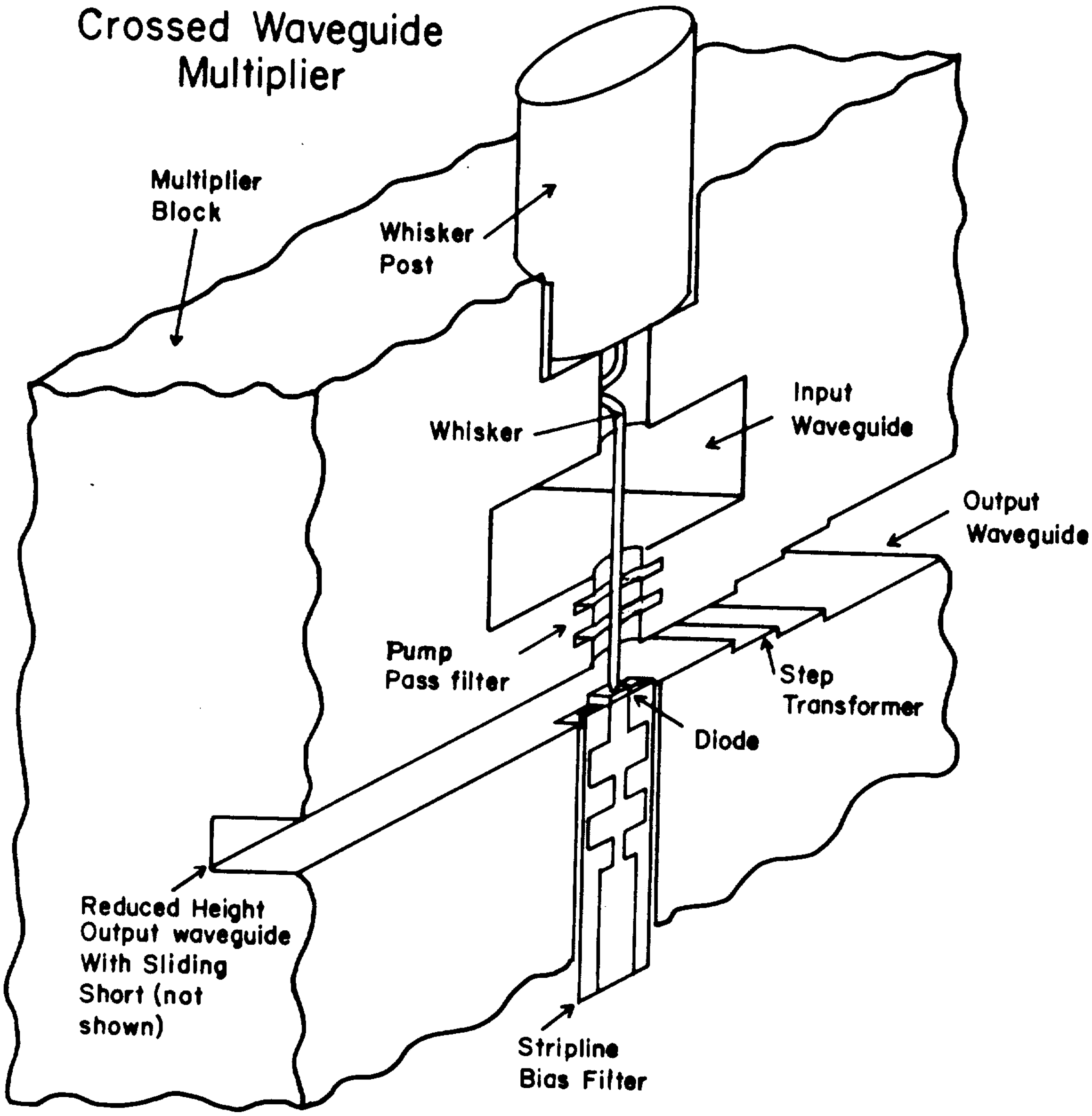

Fig. 6-1 Isometric view of a hypothetical crossed waveguide multiplier in the region near the diode. Only one half of a split-block structure is shown. The region between the input and output waveguides contains a coaxial pump-pass filter. The diode is bonded to a low pass stripline filter which allows DC biasing of the diode. Sliding shorts in each waveguide (not illustrated) can be used for tuning. A step transformer is included in the output waveguide for reducing the guide impedance to a value which more closely matches the input impedance of the diode.

whisker acts as an antenna, coupling energy from the local oscillator into the diode. Tuning shorts are usually included in both the input and output waveguides and a low pass filter may be placed between the two waveguides to allow the bias and pump power to reach the diode while at the same time preventing any of the harmonic power from leaking back into the input path.

Many investigators have produced resistive diode multipliers with varying degrees of success [14,45,54, 76,91,106,118,120,136] to name but a few. C.H. Page [121,122] showed that purely resistive multipliers can attain conversion efficiencies of at most n^{-2} where n is the output harmonic number. As far as the author knows, this limit has not been exceeded experimentally. Typical measured conversion efficiencies for millimeter-wave doublers are shown in Fig. 6-2 (an exhaustive search for published data has not been conducted and there are undoubtedly results from other laboratories which have not been included in the figure).

In 1956, J.M. Manley and H.E. Rowe [104] derived the equations relating the power flow in nonlinear reactive elements at different frequencies. Their results showed that it was theoretically possible to convert all of the signal power exciting a nonlinear reactive element to any higher harmonic of the input frequency. Two years later,

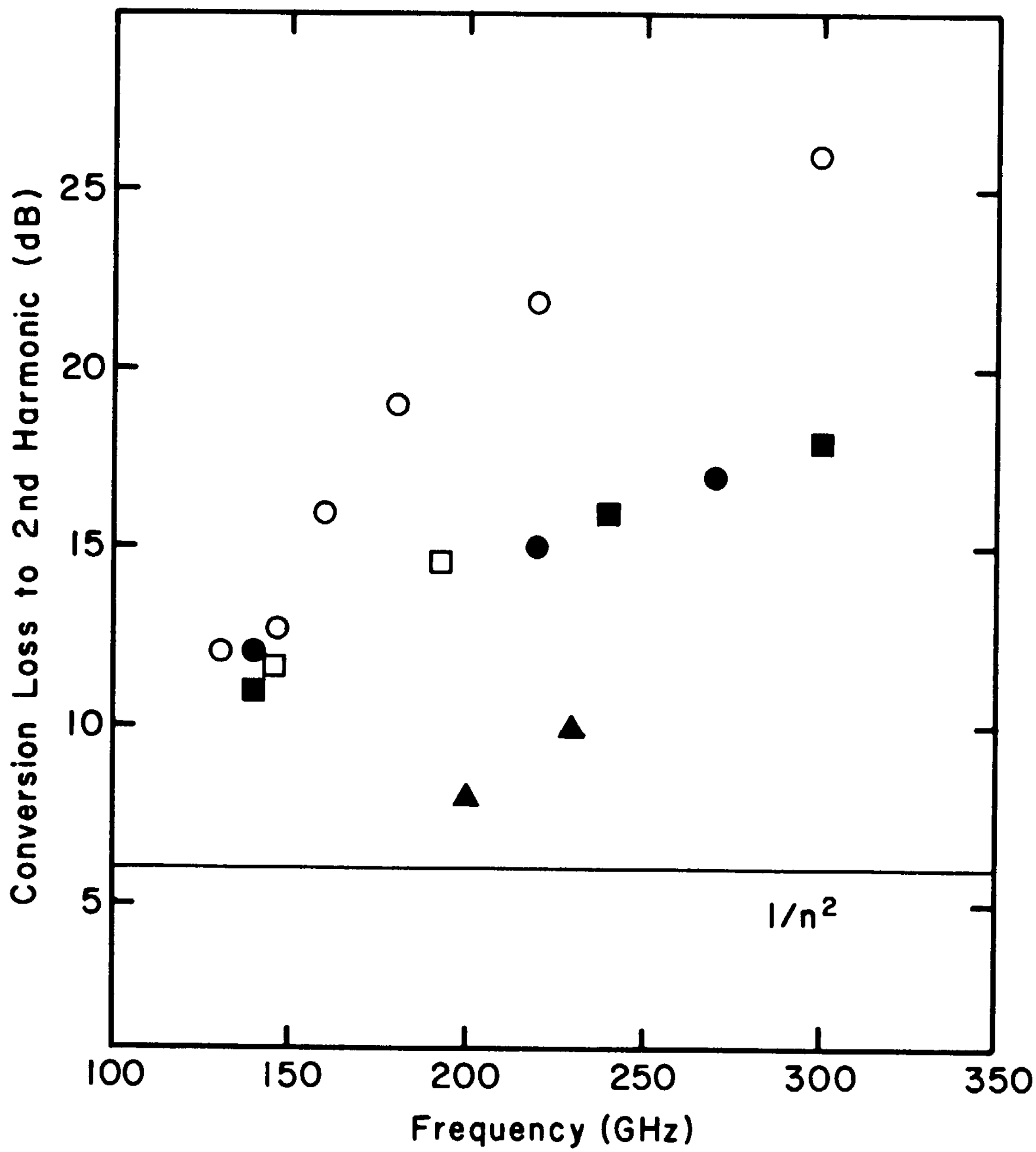

References

- ● Bauer et. al. [12]
- ■ Bauer in ref. [106]
- □ Horvath in ref. [106]
- ○ Marden in ref. [106]
- ▲ Schneider et.al.[143]*

* This result is for a forward biased varactor diode which is probably operating in a mixed resistive-reactive mode.

Fig. 6-2

Reported conversion efficiencies for resistive diode doublers with outputs between 100 and 350 GHz.

A. Uhlir and M.E. Hines, coined the term "varactor" to describe "any device whose operating principle is nonlinear reactance" [ref. 166, page 1100]. Uhlir [166], drawing on the results of Manley and Rowe, proposed using the nonlinear capacitance variation of a reverse biased diode as a more efficient harmonic generator than the nonlinear resistance. Uhlir obtained experimental conversion efficiencies of approximately 30% in frequency doubling to 860 MHz with silicon diodes operated in the varactor mode. At the same time both S. Kita [92] and K.K.N. Chang [22] reported harmonic generation in the microwave region using point contact germanium diodes. Subsequent theoretical treatment of the ideal varactor multiplier (extensively discussed in the text by Penfield and Rafuse [125]) yielded predictions of maximum multiplier efficiencies approaching 100%.

Despite the excellent performance of some early varactor multipliers in the microwave region [34,73,114] the efficiencies of devices in the millimeter-wave band fell far below the levels predicted by theory [18]. It was not until very recently that millimeter-wave multipliers began to achieve respectable output power levels and much of the improvement is due to advances in diode fabrication technology. The crossed waveguide mount is still extensively used although other successful configurations have been proposed [1,25,162,177]. Fig. 6-3 shows the varactor doubler efficiencies which are now being obtained in many laboratories (again, the list is not meant to be all inclusive).

In the millimeter-wave band varactor diode multipliers help to fill the gap between 200 and 1000 GHz in which there are relatively few readily available sources of power. In the 100 to 200 GHz region, they can replace costly narrow band klystrons. When coupled with lower frequency traveling wave tubes, harmonic generators can provide swept sources of power across a moderate portion of a millimeter waveguide band, greatly facilitating mixer measurements.

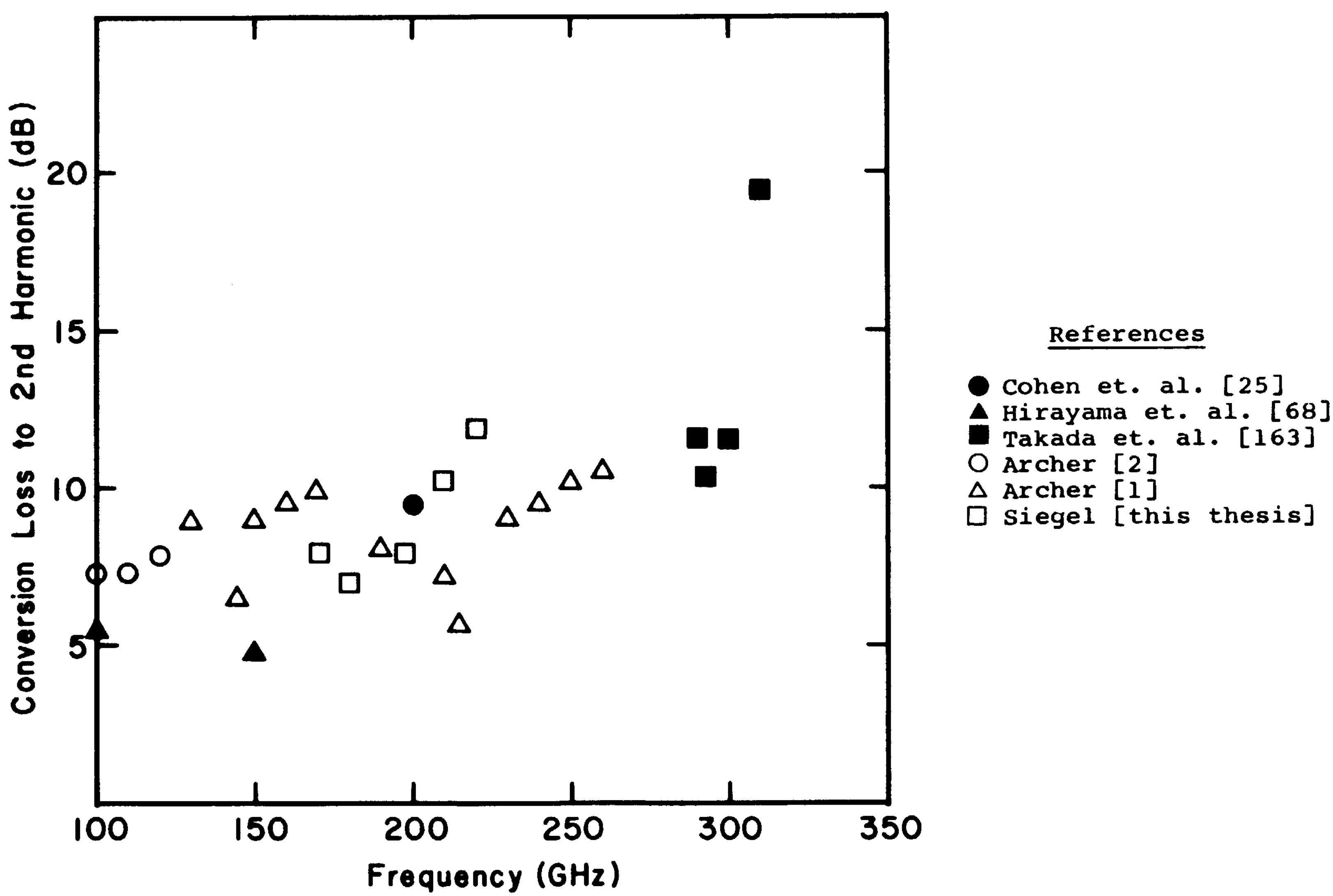

Fig. 6-3 Reported conversion efficiencies for varactor diode doublers with outputs between 100 and 350 GHz.

6.2 Multiplier Analysis

Unlike the analysis of mixers, the multiplier problem involves only large signals. A great deal of information is needed to obtain a complete picture of the performance of a multiplier; which is a function of pump power, bias setting, and input and output tuning. Therefore, the following procedures are suggested if one wishes to use the analysis presented here to study the behavior of a diode multiplier:

(1). Measure the embedding impedance of the multiplier at the pump and at least 2 higher harmonic frequencies as a function of the output tuning.

(2). Choose a set of bias voltages at which the multiplier is to be operated.

(3). Settle on a range of available pump powers for driving the multiplier.

(4). Use the multiplier analysis program (given in Appendix 5) to calculate the input and output impedance and the conversion properties of the multiplier as a function of pump power and output tuning.

(5). From the computed input impedance at each operating point, calculate the absorbed power. This is the power required from a source whose impedance is conjugate matched to the input impedance of the multiplier.

(6). Try to obtain the appropriate source impedance at the optimum operating point by tuning at the multiplier input frequency port.

(7). Repeat the procedures from step (2) with a new bias setting.

In optimizing a particular multiplier it must be remembered that any physical changes at the output port will affect all the harmonic frequency impedances unless they are electrically isolated from one another. In addition it may not be possible to obtain a given source impedance with just one degree of tuning (e.g. a single backshort) at the input port of the multiplier. Finally, if the output circuit is not isolated (by filtering) from the harmonic circuits then tuning at the input port will alter the embedding impedances at the other multiplier ports. This means that the embedding impedances would have to be known as a function of <u>both</u> the output and the input tuning in order to solve the multiplier problem completely. In the discussion to follow, we assume that the input and output ports are fully isolated at all harmonics.

6.2.1 Large Signal Analysis

In this section we apply the large signal mixer theory of Chapter 2 to the analysis of a varactor diode multiplier. We assume, as we did in the mixer analysis, that the multiplier embedding impedances at the harmonics of the pump frequency are given and that the diode electrical characteristics are known. The mixer program described in Section 2.6 can then be used for analyzing diode multipliers with only slight modifications to the Fortran code.

The equivalent circuit of the varactor multiplier is shown in Fig. 6-4. $Z_e(n\omega_p)$ represents the embedding network impedances at the pump and harmonic frequencies. Under reverse bias the diode conductance tends towards zero and the more familiar varactor model of Uhlir [166] and Penfield and Rafuse [125] is obtained. In the more general analysis presented here the diode is allowed to swing into the forward conduction region where it becomes predominantly resistive. Although the multiplier analysis program can handle a diode with any I-V and C-V law we will base the discussion to follow on the relationships

MULTIPLIER EQUIVALENT CIRCUIT

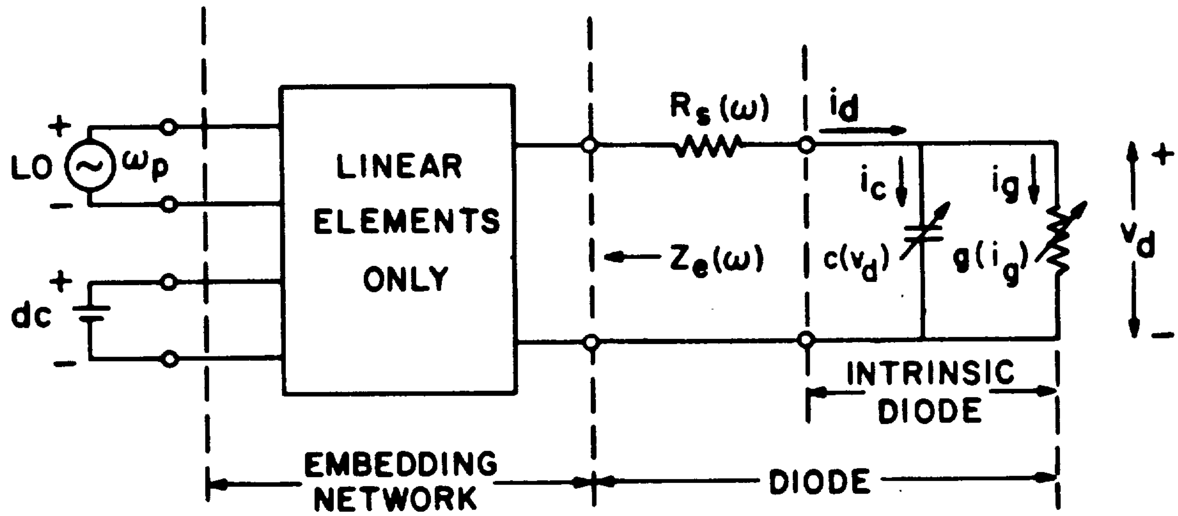

Fig. 6-4 The equivalent circuit used in the analysis of the diode multiplier. The circuit is exactly the same as that of the Schottky diode mixer (Fig.2-1) studied in this thesis. If the diode is operated in a pure varactor mode then $g(i_g)$ goes to zero and the more familiar equivalent circuit of Uhlir[166] is obtained.

used in the mixer analysis of Chapter 2, that is:

$$i_c = c\ dv_d/dt \ , \quad \text{with} \tag{6.1}$$

$$c = c_0\ (1 - v_d/\phi_{bi})^{-\gamma} \ , \tag{6.2}$$

and

$$i_g = i_s\ [\exp\ (\alpha v_d) - 1] \ , \tag{6.3}$$

$$g = \alpha\ (i_g + i_s) \ , \tag{6.4}$$

where the following identifications are made:

c_0 = capacitance at zero bias,

ϕ_{bi} = built in potential (see eqn 2.6),

i_s = reverse bias current (see eqn. 2.3),

$\alpha = q/\eta kT$, where η = diode ideality factor,

γ = .3 to .5 and is a function of the doping profile.

6.2.1.1 Differences Between the Mixer and Multiplier Large Signal Analyses

The multiplier analysis follows closely the large signal mixer theory of Chapter 2 with one basic alteration; the incident pump (LO) power and not the DC bias current is taken to be the independent variable for the multiplier.

In normal mixer operation the LO power is adjusted until a desired rectified current flows in the diode. Since this current is known beforehand it allows us to speed up the mixer nonlinear analysis routine by artificially setting the embedding impedances at DC and f_{LO} to Z_O, the characteristic impedance of the hypothetical transmission line used in the multiple reflection technique of Kerr [83]. The reason we can do this is that V_{DC} and V_{LO} (see Fig.2-3) can be changed to compensate for any effects the new impedances will have on the diode terminal currents. The only change to the final mixer analysis results occurs in the calculation of the required mixer LO power. Instead of finding the power from the LO voltage arrived at in the program (VLO) we must use the actual VLO which would have been obtained had the embedding impedance not been set to Z_0. This correction is discussed in Appendix 3.

Frequency multipliers are usually operated with a fixed incident pump power level while the DC bias voltage is varied to obtain the optimum conversion efficiency. Because the DC current in the diode is not generally prescribed in advance, it is not practical to set the embedding impedance at the LO (pump) frequency to Z_0 as was done in the mixer analysis. As a consequence we may require more reflection cycles for convergence of the nonlinear analysis. However, we can still set the embedding impedance at DC to Z_0 if we keep in mind one point. When we perform the nonlinear analysis with $Z_e(0) + R_s(0)$ set to Z_0, the DC bias voltage (VDBIAS) used in the program will in general be different from that which would have to be applied to the actual multiplier (VDBIAS') in order to obtain the same rectified current in the diode. VDBIAS' can be found from the DC current calculated in the program [IDCOS(1)], and the DC embedding impedance. The principle is illustrated in Fig.6-5. Since IDCOS(1) will generally be small (< 1 mA), the actual bias voltage which must be applied to the multiplier and that specified in the program will be nearly equal. If we wish to analyze the multiplier at a specific DC bias voltage, we can use the program to adjust VDBIAS and home in on the value

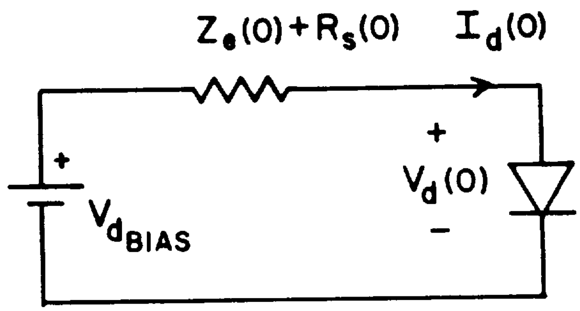

(a)

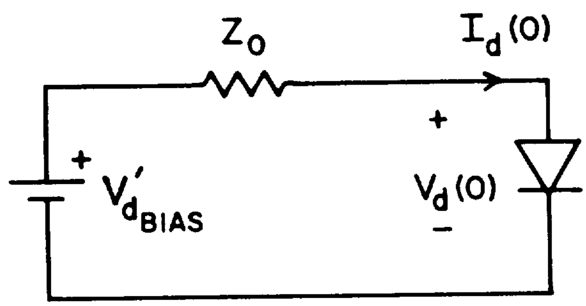

(b)

$$V_{d_{BIAS}} = I_d(0)\ (Z_e(0) + R_s(0)) + V_d(0)$$

$$V'_{d_{BIAS}} = I_d(0)\ Z_0 + V_d(0)$$

Therefore:

$$V_{d_{BIAS}} = I_d(0)\ (Z_e(0) + R_s(0) - Z_0) + V'_{d_{BIAS}}$$

Fig. 6-5 (a) The equivalent circuit of the actual multiplier at DC. (b) The circuit solved in the multiplier analysis program.

which results in a calculated DC current, IDCOS(1), equal to that measured in the actual device.

To summarize; the changes which must be made to the large signal analysis section of the mixer program in order to use it for predicting the performance of a diode multiplier are as follows:

(1). Do not set the LO embedding (source) impedance equal to the characteristic impedance Z_0 of the hypothetical transmission line used in the multiple reflection technique.

(2). Eliminate the loop which adjusts the LO power to give a specified rectified current in the diode.

(3). With a given set of harmonic embedding impedances and a given bias voltage, repeat the analysis over a range of values of pump power, P_{avail}.

(4). After each run determine the multiplier conversion properties, i.e. the input and output impedances and efficiency.

(5). From the input impedance, find the absorbed power at the pump frequency and hence the drive power required from an oscillator with a conjugate matched source impedance.

(6). From the calculated DC bias current and the chosen DC embedding impedance find the actual bias voltage which must be applied to the multiplier to obtain the predicted performance.

(7). Proceed to the next set of embedding impedances (new output tuning position) and repeat from step (3).

In the next section the equations used in the program to determine the input and output impedances and the conversion properties of the multiplier will be given. It must be remembered however, that these properties are nonlinear functions of the incident power level and can not be generalized in the same way as in a mixer.

6.2.2 Port Impedances and Conversion Properties

From the multiplier nonlinear analysis we obtain the diode voltage, current, capacitance and conductance waveforms at a particular available pump power level and DC bias setting. These waveforms can be used to derive the input and output impedances of the multiplier and the conversion efficiencies.

Input Impedance:

Let V_n and I_n be the single ended complex Fourier series coefficients of the intrinsic diode* voltage and current at frequency $n\omega_p$. Referring to Fig. 6-6, the input impedance of the multiplier at any port i is simply:

$$Z_{in}(i) = R_s(i) + V_i/I_i \ , \tag{6.5}$$

where I_i = [IDCOS(i+1) - j IDSIN(i+1)] and V_i = [VDCOS(i+1) - j VDSIN(i+1)] in the multiplier analysis program. The minus sign is present because the program calculates the trigonometric Fourier series and the single ended complex Fourier series is being used here.

Available Input Power:

The power available from the pump at port 1 is (from Fig. 6-6):

---

* The intrinsic diode includes the nonlinear capacitance and conductance but not the series resistance.

Circuit for Multiplier Conversion Loss Calculation

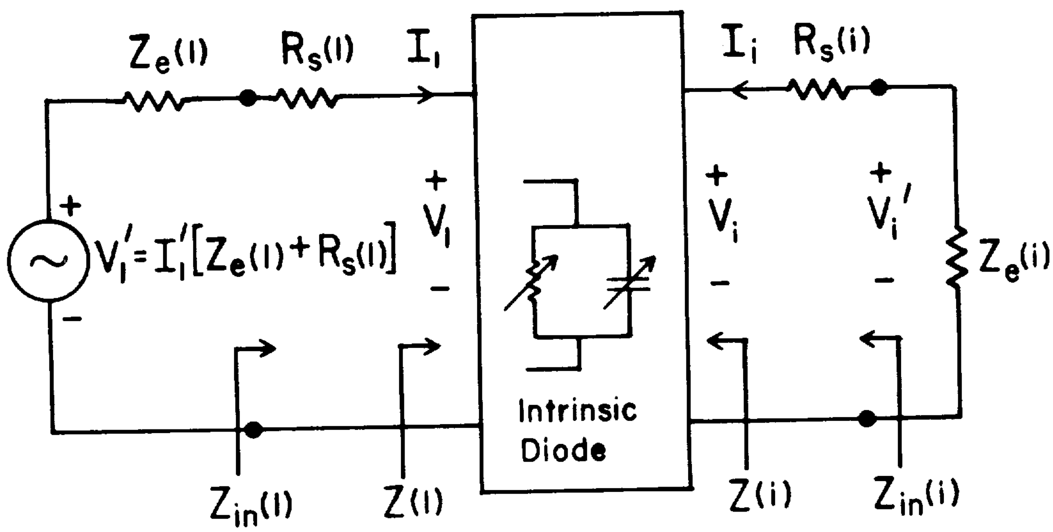

Fig. 6-6 The equivalent circuit used in the calculation of the multiplier conversion loss. The signal is assumed to be incident at port 1 and the converted power is removed at port i.

$$P_{avail} = |V_1'|^2 \,/\, 8\, \mathrm{Re}[Z_e(1)] \,. \qquad (6.6)$$

In the multiplier analysis program P_{avail} is an input quantity [PAVAIL] and V_1' [VLO] is calculated from (6.6).

Absorbed Power:

Since the source impedance is not in general matched to the input impedance only a portion of the available power will be absorbed. Referring to Fig. 6-6 we have:

$$P_{abs} = 1/2\ \mathrm{Re}[\{V_1+I_1R_s(1)\}I_1^*] = 1/2\ \mathrm{Re}[Z_{in}(1)]|I_1|^2 \qquad (6.7)$$

where the series resistance has been included in the input impedance term.

Output Power:

The power delivered to output port i with impedance $Z_e(i)$ is simply (referring to Fig. 6-6):

$$P_{out} = 1/2\ |I_i|^2\ \mathrm{Re}[Z_e(i)] \,, \qquad (6.8)$$

or in terms of V_i, the voltage across the diode without the series resistance:

$$P_{out} = 1/2 \ |V_i|^2 \ Re[Z_e(i)] \ / \ |Z_e(i)+R_s(i)|^2 \ . \qquad (6.9)$$

In the program V_i = [VDCOS(i+1) - j VDSIN(i+1)] and I_i = [IDCOS(i+1)-jIDSIN(i+1)].

Conversion Efficiency:

The conversion efficiency will be defined here as the ratio of the output power to the absorbed power. Hence the efficiency in converting from input port j to output port i is:

$$Eff(i) = \frac{P_{abs}(j)}{P_{out}(i)} = \frac{|I_j|^2 \ Re[Z_{in}(j)]}{|I_i|^2 \ Re[Z_e(i)]} \ , \qquad (6.10)$$

where I_i is given by [IDCOS(i+1) - j IDSIN(i+1)] in the program.

6.3 Multiplier Analysis Program

The multiplier analysis can readily be incorporated into the mixer analysis program listed in Appendix 1. The changes which must be made to the Fortran code are given in Appendix 5. Line numbers indicate where to replace or insert the corresponding statements in the listing of Appendix 1.

The multiplier program begins with a call to subroutine LGSIG which is slightly modified from the version used to solve the mixer problem. The loop, which varies the LO voltage in an attempt to home in on the correct DC bias current, and subroutine ADJVLO have been eliminated. The embedding impedance at the LO frequency $Z_e(1)$ is no longer set to Z_0, the transmission line characteristic impedance, and so a convergence parameter at the pump frequency [ZQMAG (1)] has been added to the reflection cycle loop (see equation (2.29)). Both the DC bias voltage applied to the diode and the available pump power are independent variables, therefore, two more loops [JPUMP and JVDC] have been added to LGSIG.

As discussed in Section 6.2.1, the bias voltage input in the program does not correspond to the bias voltage which would have to be applied to an actual multiplier to obtain the same diode rectified current. Therefore, in general one cannot predict the performance of a particular device under a particular set of operating conditions from a single run of the program. However, in many cases, a varactor multiplier will have the highest efficiency when it is back biased, i.e. when there is negligible current flow. Under this condition the bias voltage input in the program will have very nearly the same value as that applied to the actual multiplier.

The multiple reflection technique is executed within the JPUMP and JVDC loops and the large signal diode waveforms (voltage, current, conductance and capacitance) are found and plotted over a pump cycle just as in the mixer analysis program. An additional subroutine, BIAS, uses the calculated DC current IDCOS(1) and DC embedding impedance to find the difference between the bias voltage used in the program and the DC bias voltage which must be applied to the actual multiplier in order to realize the same diode rectified current and terminal voltage. After each complete nonlinear analysis, subroutine MLTPER is called to calculate the multiplier port impedances and conversion efficiency using the equations in Section 6.2.2.

The multiplier analysis is now complete for a particular input frequency, available pump power, DC bias voltage, and a given set of embedding impedances. The entire analysis must be repeated every time the embedding impedances are changed (for instance by tuning at the multiplier output port), whenever the input power is altered and at each new DC bias voltage (VDBIAS). A typical set of output results is shown in Appendix 5, Section A5.4 for a single loop over PAVAIL and VDBIAS.

The multiplier program just described has not as yet been used for any extensive device analysis. To do so requires a knowledge of the multiplier embedding impedances at a number of higher pump harmonic frequencies and entails a good deal of scale modelling work. It is hoped that the multiplier analysis program can be used as the basis for an optimization study similar to that presented in this thesis for Schottky barrier diode mixers.

In the next section we present a design for a varactor doubler with an output in the 140-220 GHz band. As a complete scale model was not constructed for this particular design the multiplier analysis program was not used for the calculation of the expected performance or for any optimization.

6.4 140-220 GHz Doubler

Above 150 GHz swept sources of millimeter-wave power are not readily available. The varactor diode multiplier design to be given in this section has greater than 10% conversion efficiency in doubling to the 140-220 GHz band and, when coupled with a lower frequency backward wave oscillator, the doubler provides enough output power to be used as the LO for the room temperature Schottky diode mixer which is the subject of this thesis. In addition, the fixed tuned bandwidth of $\approx 3\%$ is large enough that the doubler can be used as a swept signal source, covering both the upper and lower sidebands, greatly facilitating the mixer conversion loss measurements described in Chapter 4.

6.4.1 Block Design

The multiplier is fabricated in two halves with the input and output waveguides split along the center of their broad walls (where there is no lateral current flow). The lower block contains the diode and filter structures as well as the DC bias connector. A third bolt-on section houses two micrometers used to position sliding shorts in the input and output waveguides. A view of the lower block, with the diode chip and filters in place is shown in Fig. 6-7. Complete machinists drawings of the multiplier appear at the end of the chapter in Figs. 6-15 through 6-20.

The electrical layout is largely based on a design by Archer [1] but differs in three respects:

(1). The crossed waveguide structure has been replaced by a planar design which we feel is somewhat easier to fabricate.

(2). The pump pass filter between the input and output waveguides and the bias filter have been redesigned using low frequency scale modelling to conform better to our particular requirements.

(3). The electroformed quarter wavelength step transformer in the output waveguide has been replaced by a new type of H-plane transformer (discussed in detail in Chapter 7) which can be fabricated quickly and easily with a standard slitting saw.

The varactor diodes used in the doubler were of the notch-front type [142], with ohmic contacts on the sides. They were made by R.J. Mattauch at the University of

ORIGINAL PAGE IS
OF POOR QUALITY

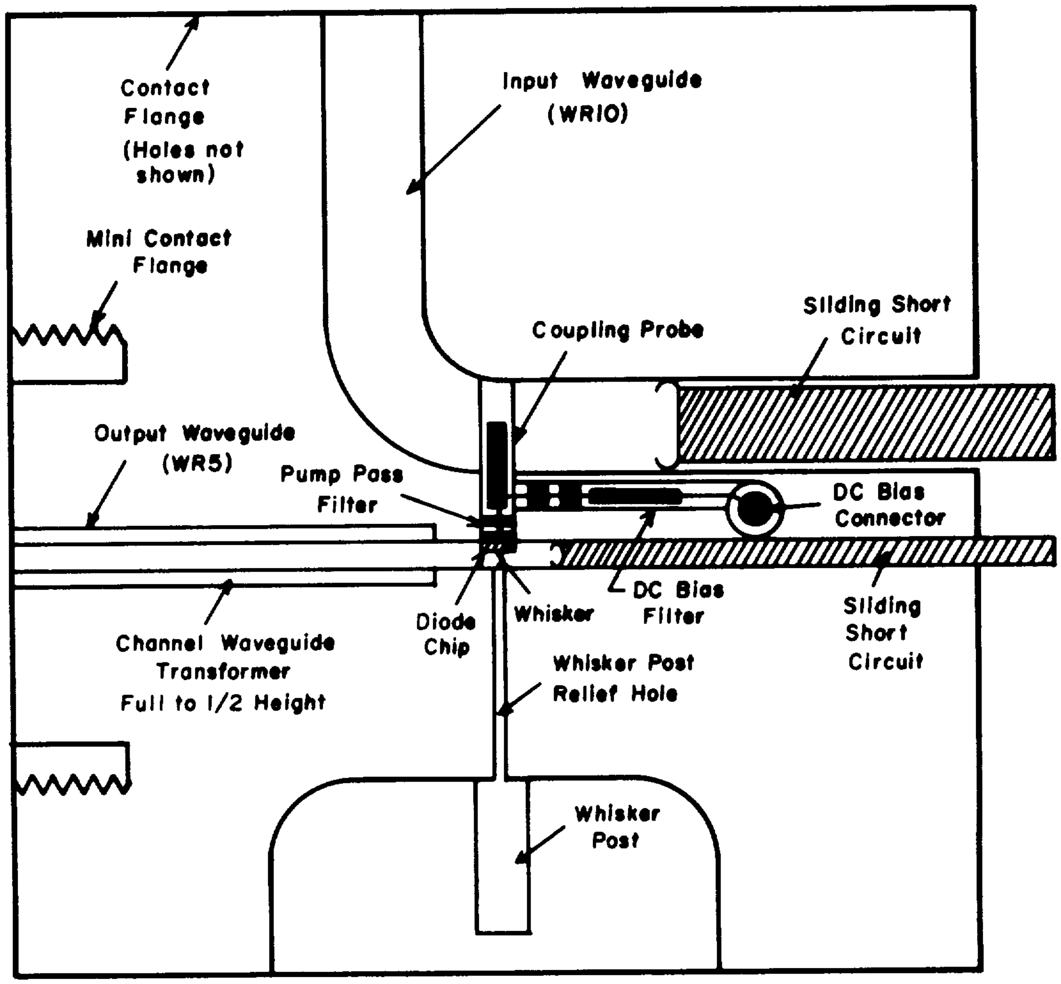

Fig. 6-7 A view looking down on the lower half of the multiplier block showing the pump pass and DC bias filters, the whisker contacted diode chip and the two spring-finger sliding short circuits. The drawing is scaled up roughly 5x.

Virginia and are designated type 5M4. The substrate is composed of n-type GaAs with a doping concentration of 10^{18} atoms/cm^3. The epitaxial layer is 1.5 microns thick and is doped with silicon to a density of $3x10^{16}$ atoms/cm^3. The anodes, composed of electroplated gold over platinum, are 5 microns in diameter and spaced 7 microns center to center on the front face of a 3x5x5 mil GaAs chip. Typically the diodes have a DC series resistance of 5 ohms, a zero bias junction capacitance of 17 fF and a reverse breakdown voltage of 14 V. The diode saturation current and ideality factor, as determined from the log I-V curve, are $1.4x10^{-17}$ A and 1.06 respectively.

The GaAs chip butts up against the front edge of a pump pass stripline filter which lies between the input and output waveguides (see Fig. 6-8). The filter is a lumped element Tchebychev design with 11 alternating low and high impedance sections ending in a long 50 ohm segment. It is photolithographically produced on a 150x20x3 mil thick fuzed quartz substrate which rests on a ledge milled into the walls of a channel 18 mils wide and 9 mils high. Individual section widths and lengths were calculated using the equations developed by Yamashita and Atsuki [183] and Matthaei, Young and Jones [107] and were then empirically adjusted using an 83x scale model at

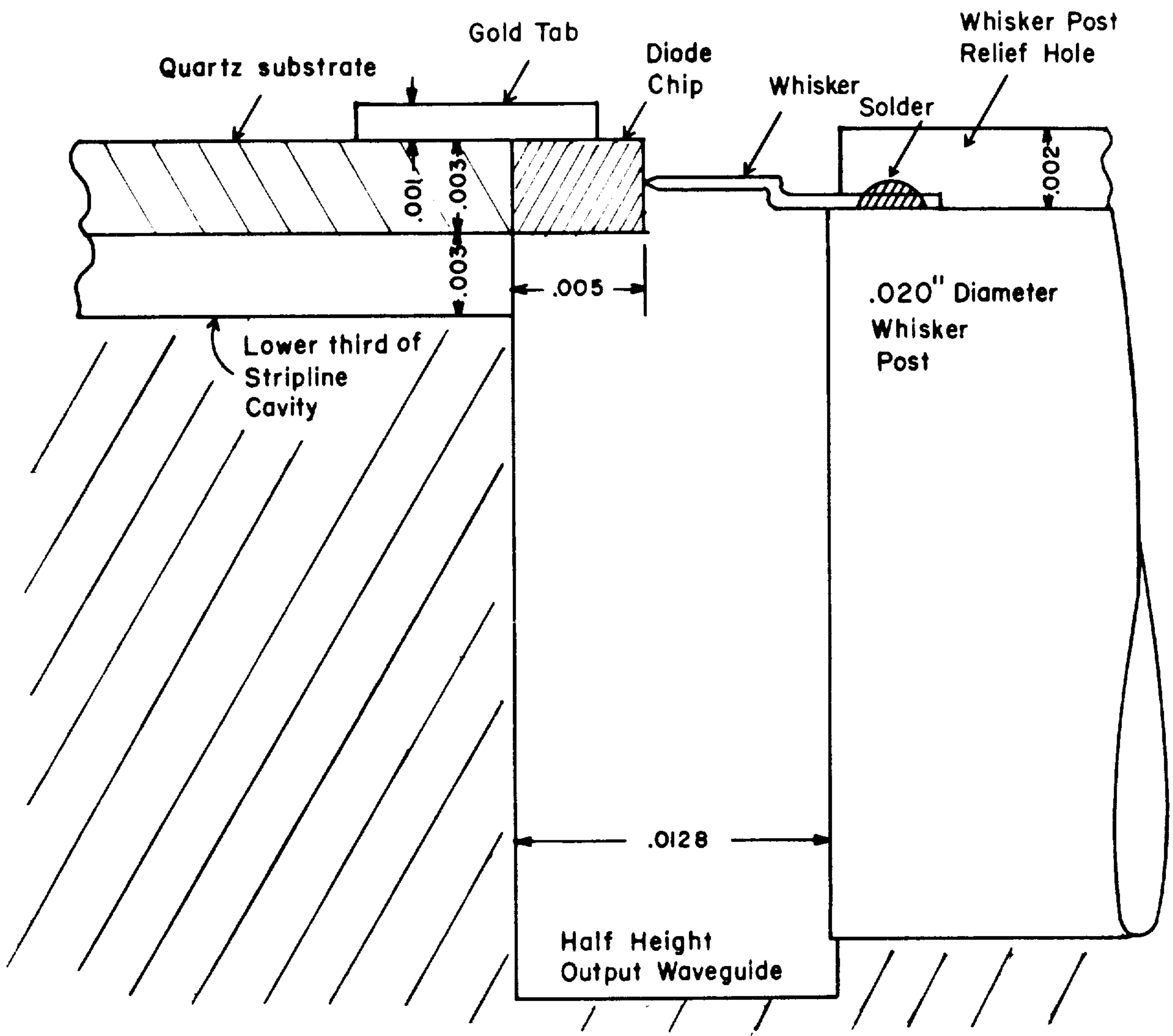

Fig. 6-8 A sectional view looking down the reduced height output waveguide which shows the orientation of the diode chip and whisker.

0.9-4 GHz to obtain the desired filter characteristics. The long 50 ohm section of the filter extends roughly halfway across the input waveguide of the multiplier to couple the pump power into the diode [1,53,93]. The length of the probe is adjusted to maximize the coupling efficiency and the bandwidth of the doubler. The quartz substrate itself extends across the full width of the input waveguide and butts up against the far wall to provide positive location.

A second stripline filter (4 element quarter-wave design), placed in a channel perpendicular to the pump pass filter, is used to pass DC bias to the diode while preventing pump power from returning via the same path. The two stripline channels are joined by a 1 mil diameter gold wire through a common wall in the pump pass filter cavity. This wire forms the first high impedance section of the bias filter. The spacing between the two filters (approximately one-quarter wavelength at the pump frequency) is such that there is an effective short circuit for the pump at the slot in the stripline cavity wall where the two filter channels meet. The section lengths of the bias filter were determined empirically using a low frequency scale model.

The signal and bias filters are shown in Fig. 6-9. The transmission characteristics with both filters in place (as measured on a scale model at a frequency 83.3 times lower than that of the actual multiplier) are shown in Fig.6-10.

The bias voltage for the diode is applied through an SMA connector whose center conductor is bonded to the 50 ohm section at the rear of the bias filter using a 1 mil diameter gold wire. Applying a positive voltage to the center conductor of the connector reverse biases the diode.

The multiplier input waveguide contains a 90 degree bend so as to accommodate a standard WR-10 contact flange. A contacting spring-finger short circuit slides in the waveguide behind the coupling probe for varying the input impedance at the pump frequency.

The diode chip extends fully into the output waveguide which has been reduced to half height in accordance with the design of Archer [1] who found that this improved the RF match to the diode. A contacting spring-finger short circuit in the reduced height waveguide behind the diode allows tuning at the output frequency.

Rather than use an electroformed step transformer to bring the multiplier output waveguide up to full height, an H-plane transformer designed specifically for this type of application was employed. The transformer (hereafter

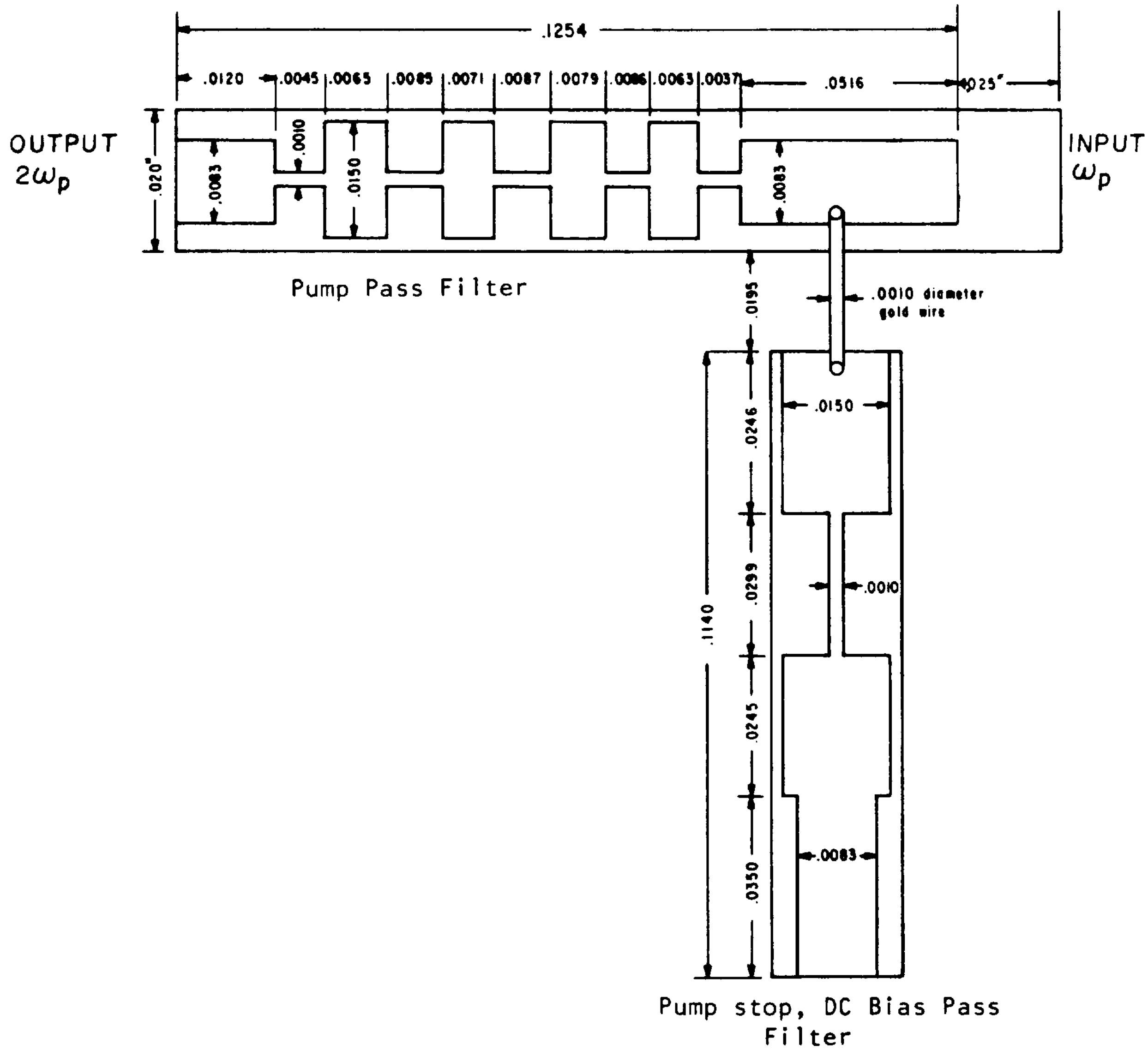

Fig. 6-9 The section dimensions of the two multiplier filters. The substrate of the pump pass filter extends 25 mils beyond the edge of the metalization so as to butt up against the far wall of the input waveguide. The two filters are shown as they are oriented in their respective stripline cavities in the actual multiplier block.

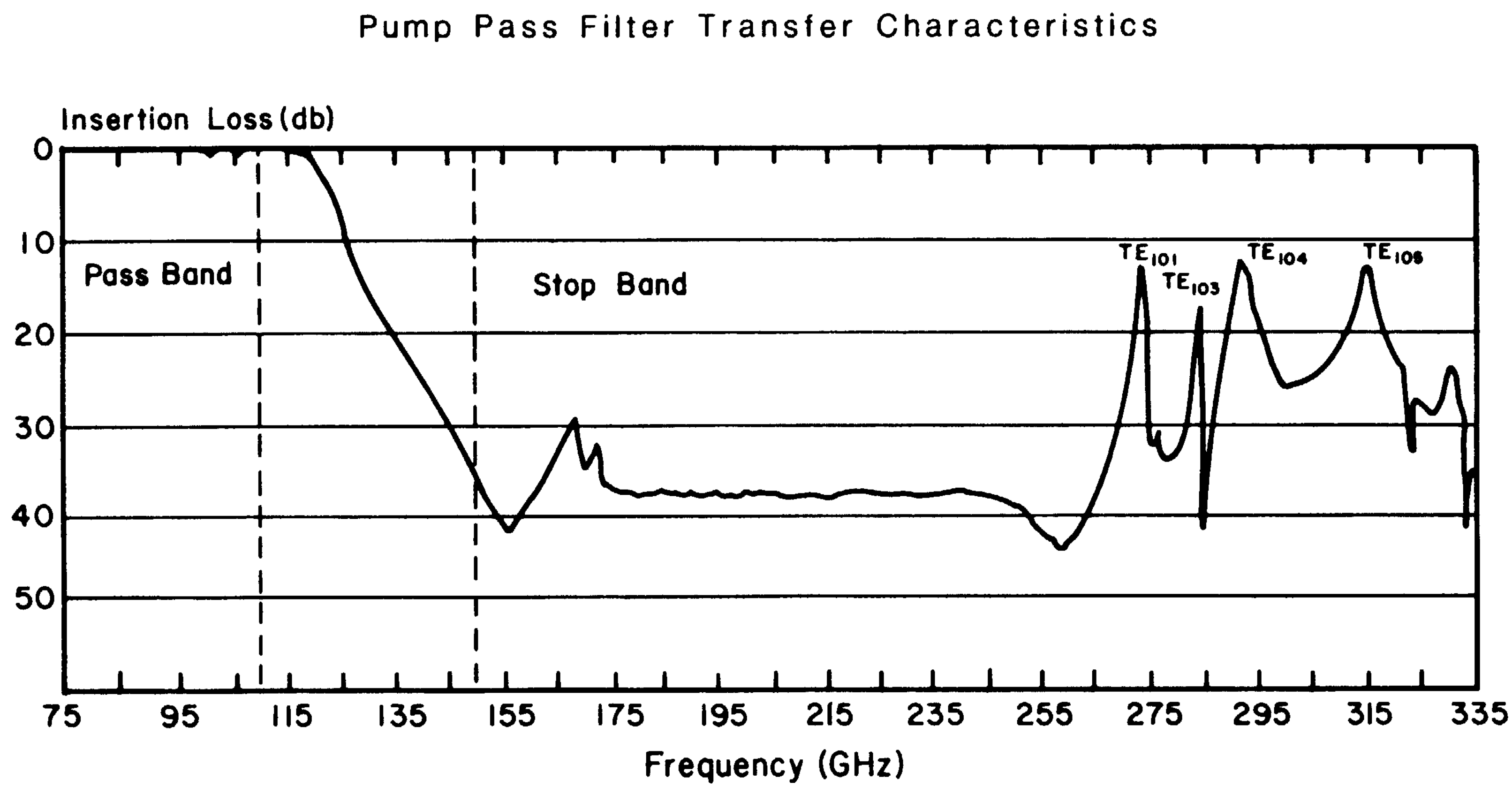

Fig. 6-10 The transfer characteristics of the combined pump pass and bias filters looking from the 50 ohm section which forms the coupling probe for the input waveguide. The measurements were made on an 83.3 times scale model of the filters over a frequency range of 0.9 to 4 GHz. The resonances in the third harmonic stop band are identified as various stripline cavity modes.

referred to as the channel waveguide transformer) is much easier to fabricate than the more conventional electroformed designs [107] and is discussed in Chapter 7. The position of the transformer in relation to the diode may affect the impedance at the harmonic frequencies and some degree of optimization can be obtained if this distance is properly chosen. For the multiplier described here the spacing between the diode and the transformer was simply kept as short as possible so as to minimize waveguide loss.

Two micrometers with nonrotating spindles (Starrett model no.261) are used for positioning the sliding shorts in the input and output waveguide and they are housed in a separate bolt-on structure which can be seen in Fig. 6-15. The two shorts, composed of heavily gold plated beryllium copper, lie adjacent to one another. Short flexible spring fingers, cut into the end of each backshort, make the electrical contact to the waveguide walls.

The multiplier assembly procedures are quite simple and can be carried out in a couple of hours. A small gold tab is soldered to the ohmic contact on the top surface of the notch-front diode chip. The rear of the chip is then butted up against the front edge of the signal filter and the gold tab is soldered to the first low impedance section (see Fig. 6-8). The chip will thus rest about midway between the top and bottom walls of the stripline channel. Next the two filters are epoxied into place in their appropriate channels in the lower block, one third of the way up from the bottom and resting on a 1 mil ledge machined into the side walls. The rear edge of the pump pass filter substrate butts up against the far wall of the input waveguide and the front edge is flush with the opening in the wall of the output waveguide. The diode chip thus protrudes fully (5 mils) into the output waveguide. The bias filter (positioned 19.5 mils from the near edge of the pump pass filter substrate) is now electrically connected to the pump pass filter with a 1 mil gold wire. The bias connection is then made by soldering a gold wire between the SMA center conductor and the 50 ohm section of the bias filter. The whole lower block assembly is now placed in a special jig for contacting the diode. A pointed phosphor bronze whisker, bent into a bayonet shape (see Fig. 6-8), is soldered to a steel post and pressed into a 20 mil reamed hole in the multiplier block. The hole breaks through the output waveguide wall directly opposite the diode chip. A differential micrometer is used to push the tight fitting whisker post towards the diode chip until the whisker contacts one of the diode anodes. The procedure is monitored both electrically (with a capacitance bridge) and under a specially equipped optical microscope. The capacitance is measured while the whisker is being advanced and, as described in Section 4.5.1, the zero bias diode junction capacitance can be determined after contact has been made. The upper half of the block is then screwed in place and the backshorts slid into their respective slots. Finally, the backshort tuning support structure is added and the multiplier is ready for use.

6.4.2 Performance

The test set used for measuring the conversion efficiency of the doubler is shown in Fig. 6-11. No filters were used to isolate the second harmonic output power and therefore the measured efficiencies include the conversion to all the higher harmonics of the signal frequency as well. Independent tests by C. Gottlieb [55] indicate that the power converted to the third and fourth harmonics is at least 10 dB below the doubled output. Following a suggestion by Archer [4], the length of the coupling probe in the input waveguide was shaved down with a scalpel blade until the best doubling performance was obtained.

A plot of the doubling efficiency versus frequency using a 75-110 GHz backward wave oscillator as the pump source is shown in Fig. 6-12. Note that the input power level varies between 10 and 40 mW over the indicated frequency range. Fig. 6-13 shows the doubling efficiency as a function of input power level at 3 frequencies; 172, 188 and 200 GHz. The fixed tuned bandwidth of the doubler is indicated at a number of frequencies in the 140-220 GHz band in Fig. 6-14 where the dark line represents the input

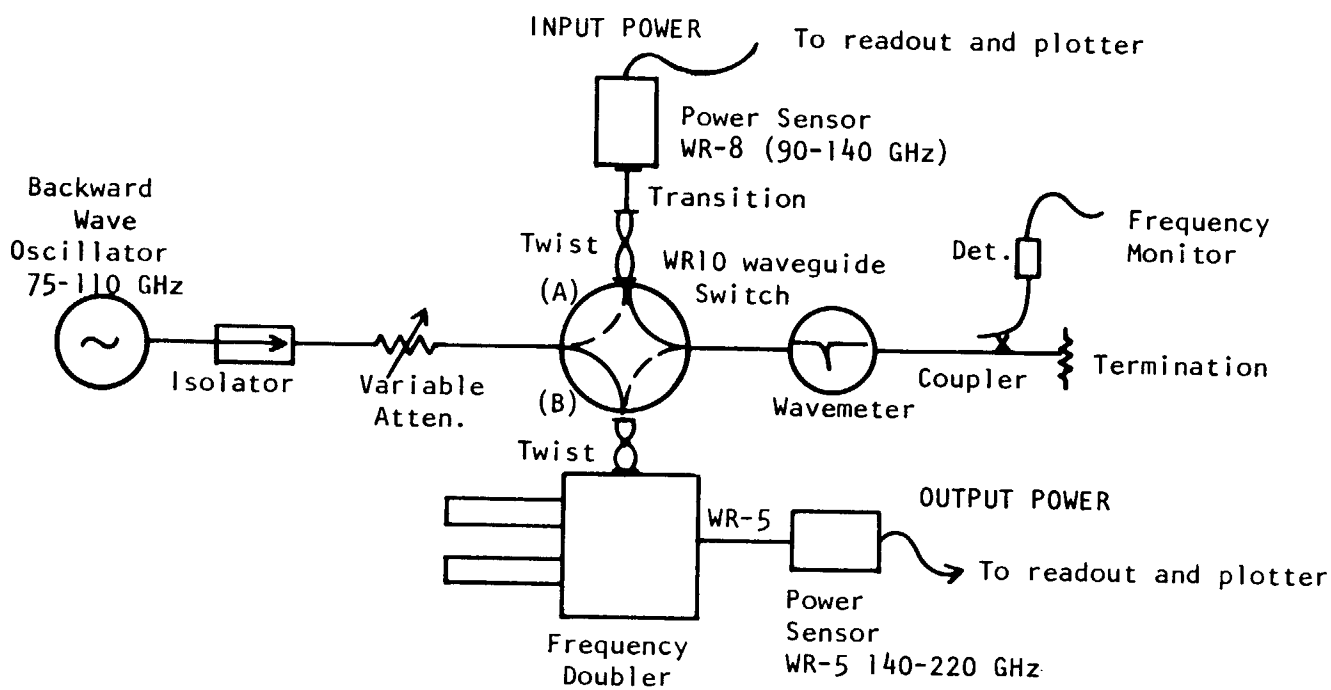

Fig. 6-11 The test set used to determine the conversion efficiency of the 140-220 GHz doubler. With the waveguide switch at position A, the backward wave oscillator is swept over a range of frequencies and its output power recorded by a plotter. The sweep is then repeated with the switch at position B and the doubled power times 10 dB is plotted on the same page. The two curves cross at 10% efficiency. The multiplier is retuned for maximum efficiency at a number of frequencies within the 140-220 GHz band so that an envelope of maximum output versus input power can be obtained with the available pump source.

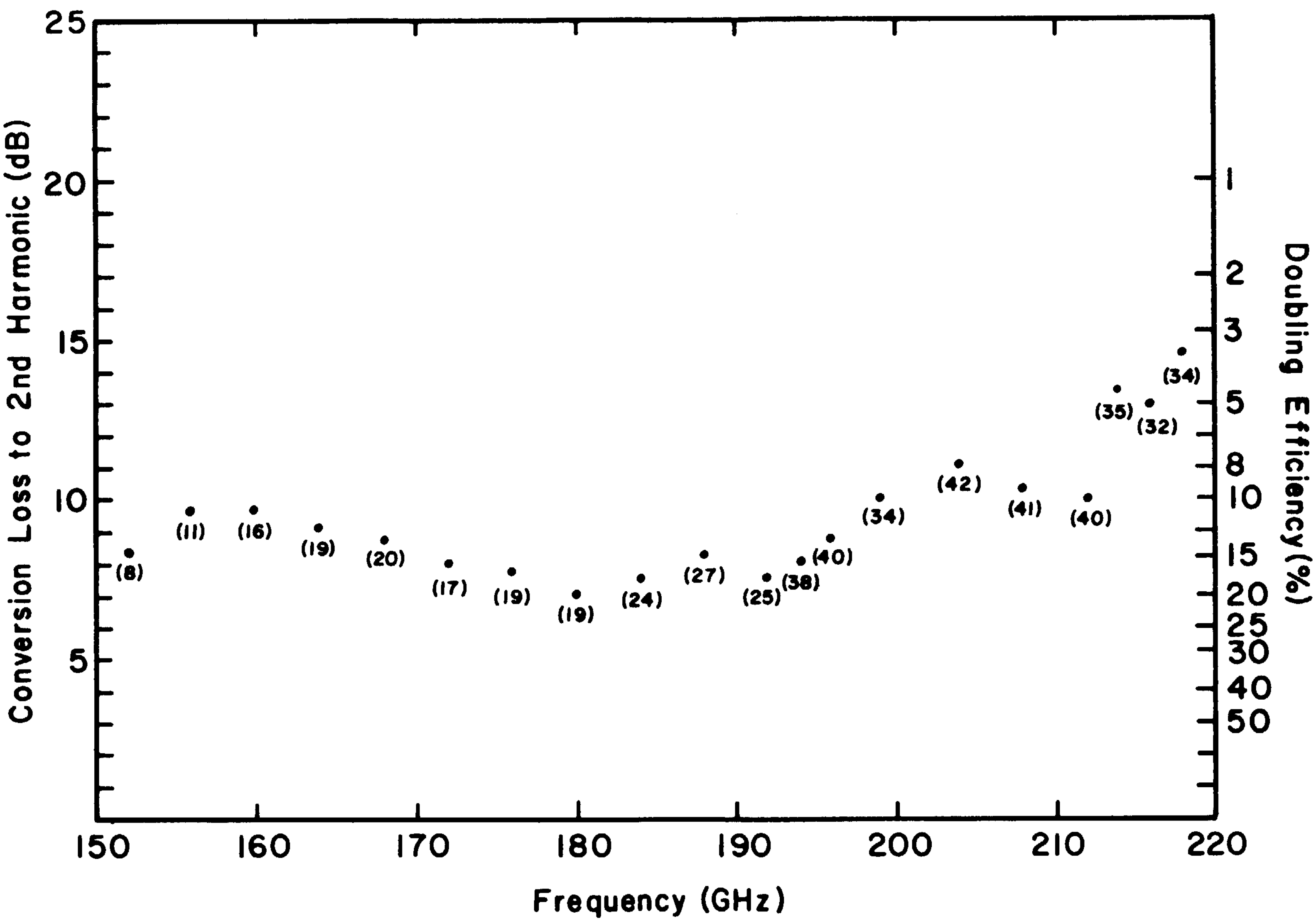

Fig. 6-12 A plot of doubling efficiency versus frequency using a Siemens RWO 170, 75-110 GHz backward wave oscillator as the pump source. Note that the available power from the backward wave oscillator varies from 10 to 40 mW across the frequency band. The multiplier tuning shorts and DC bias voltage were adjusted for peak power output at each frequency (the input power in mW is noted below each point).

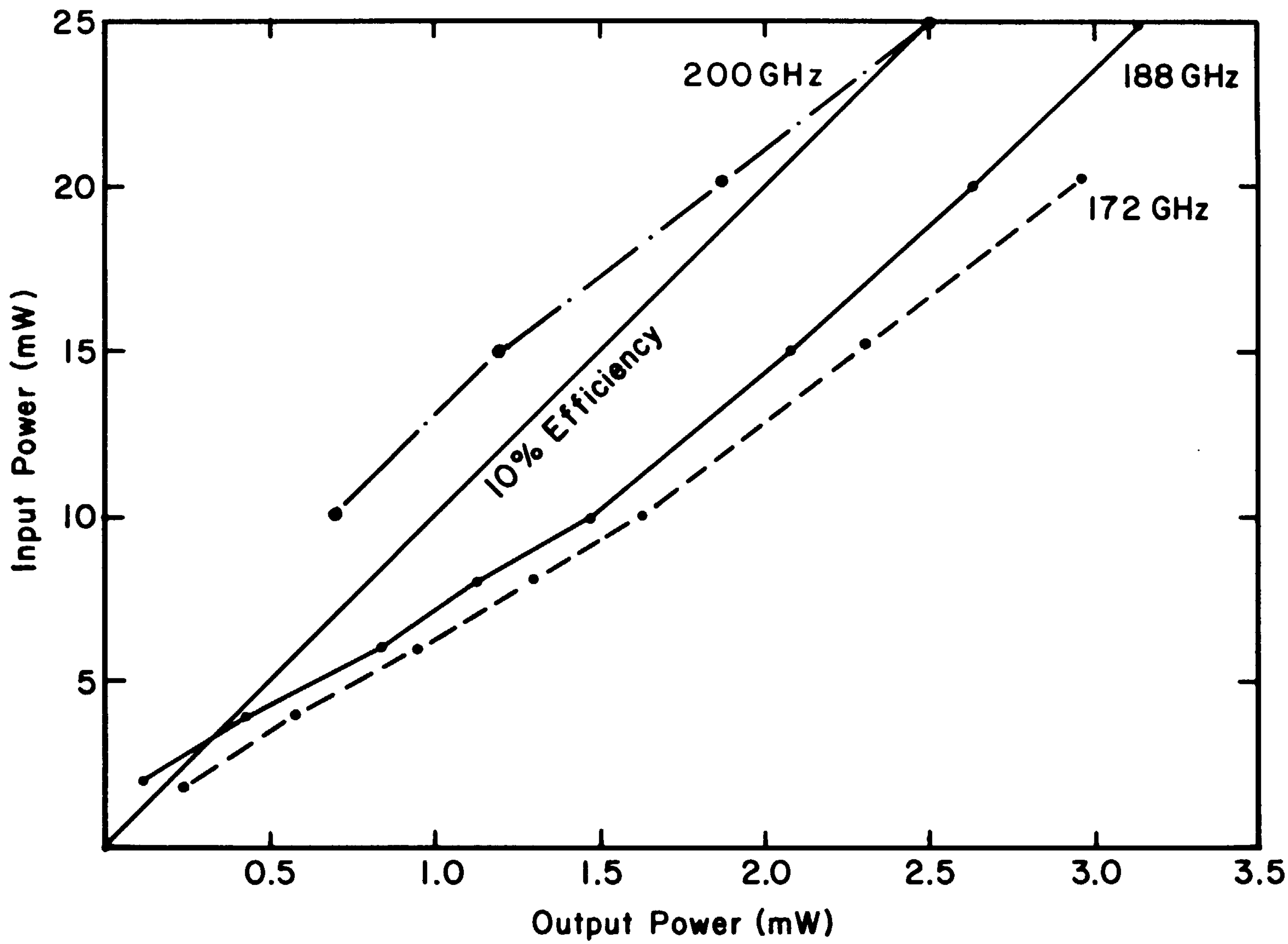

Fig. 6-13 Plots of doubled output power versus input power at 172, 188 and 200 GHz. The DC bias and multiplier tuning shorts were adjusted to give maximum output power at each point.

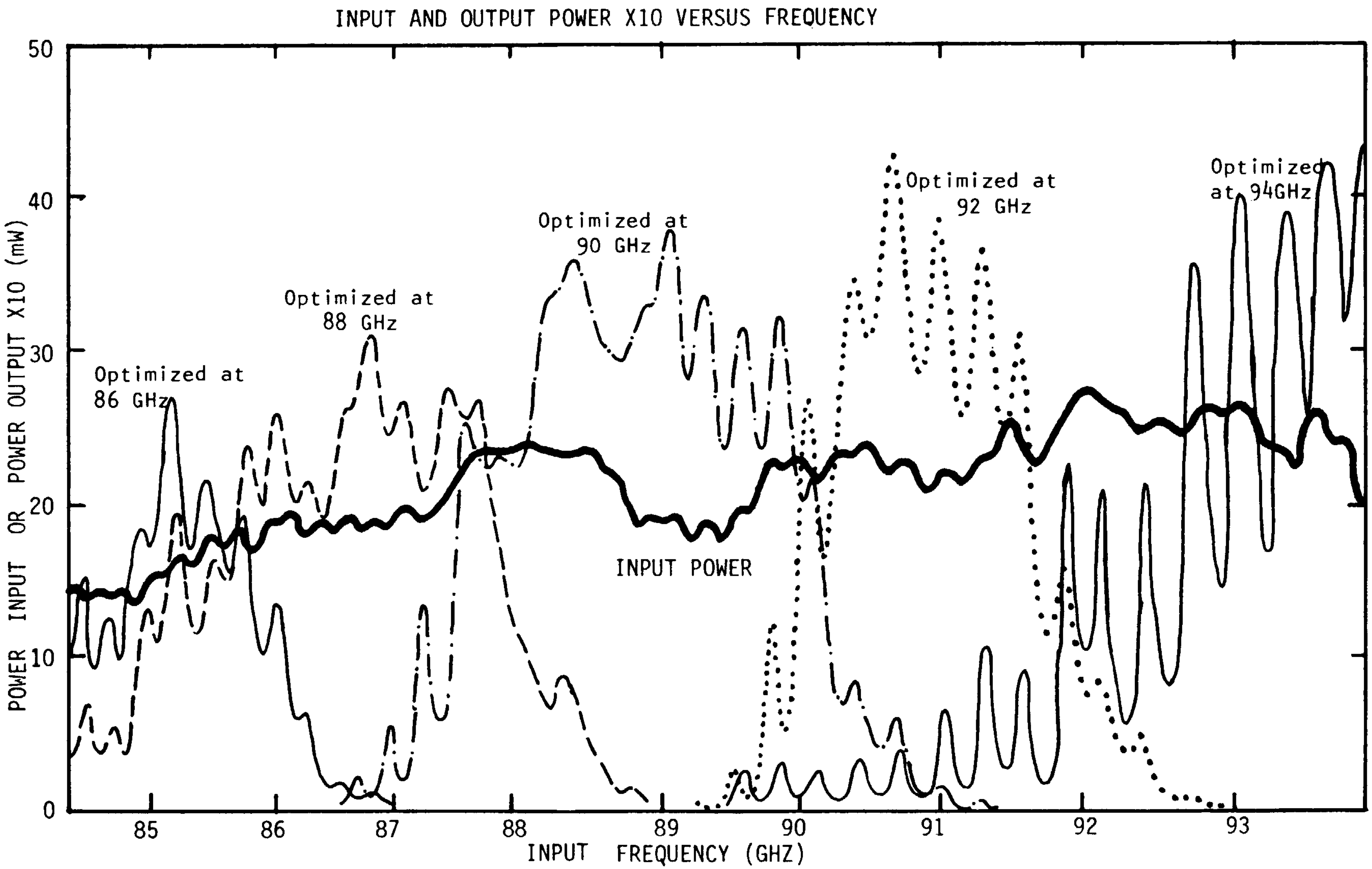

Fig. 6-14 A plot taken directly from the measurement test set in Fig.6-11 showing the fixed tuned bandwidth of the doubler at a number of frequencies in the 140-220 GHz band. The bold line is the input power and the superposed traces represent the frequency doubled output power x10. The curves cross at 10% efficiency. Each output curve was measured with the multiplier DC bias and tuning shorts adjusted for maximum power at the frequency indicated.

power and the superposed curves are the output power times 10.

No extensive optimization was performed on these multipliers since the primary motivation for their development was to facilitate the mixer performance measurements. A scaled down version of the 140-220 GHz multiplier was constructed for use as an LO source in a 115 GHz receiver. In doubling up from 57.5 GHz, the measured efficiency exceeded 40%.

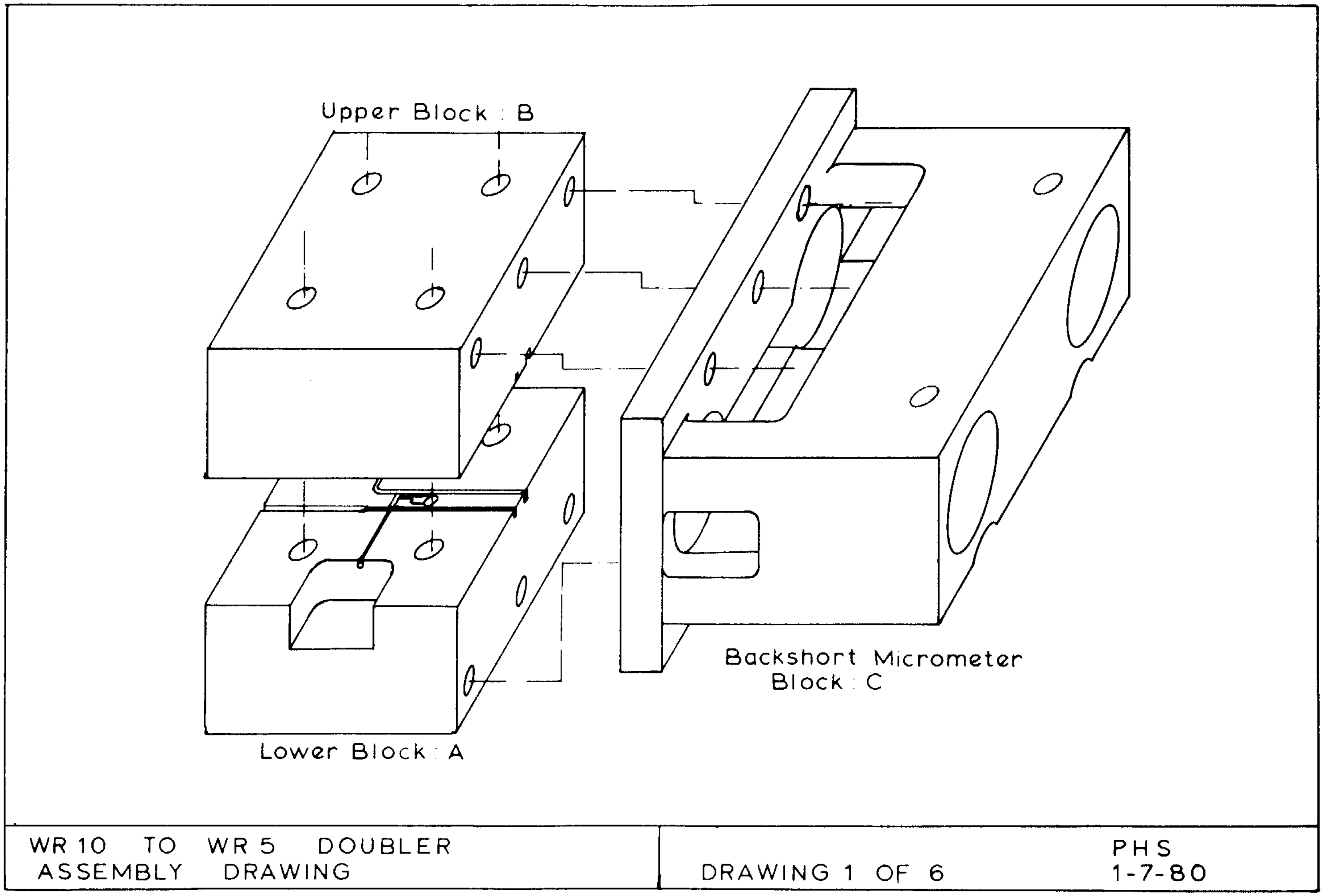

Fig. 6-15 An assembly drawing for the 140-220 GHz multiplier. Block "C" holds two micrometers with nonrotating spindles which are used to adjust the sliding shorts in the input and output waveguides.

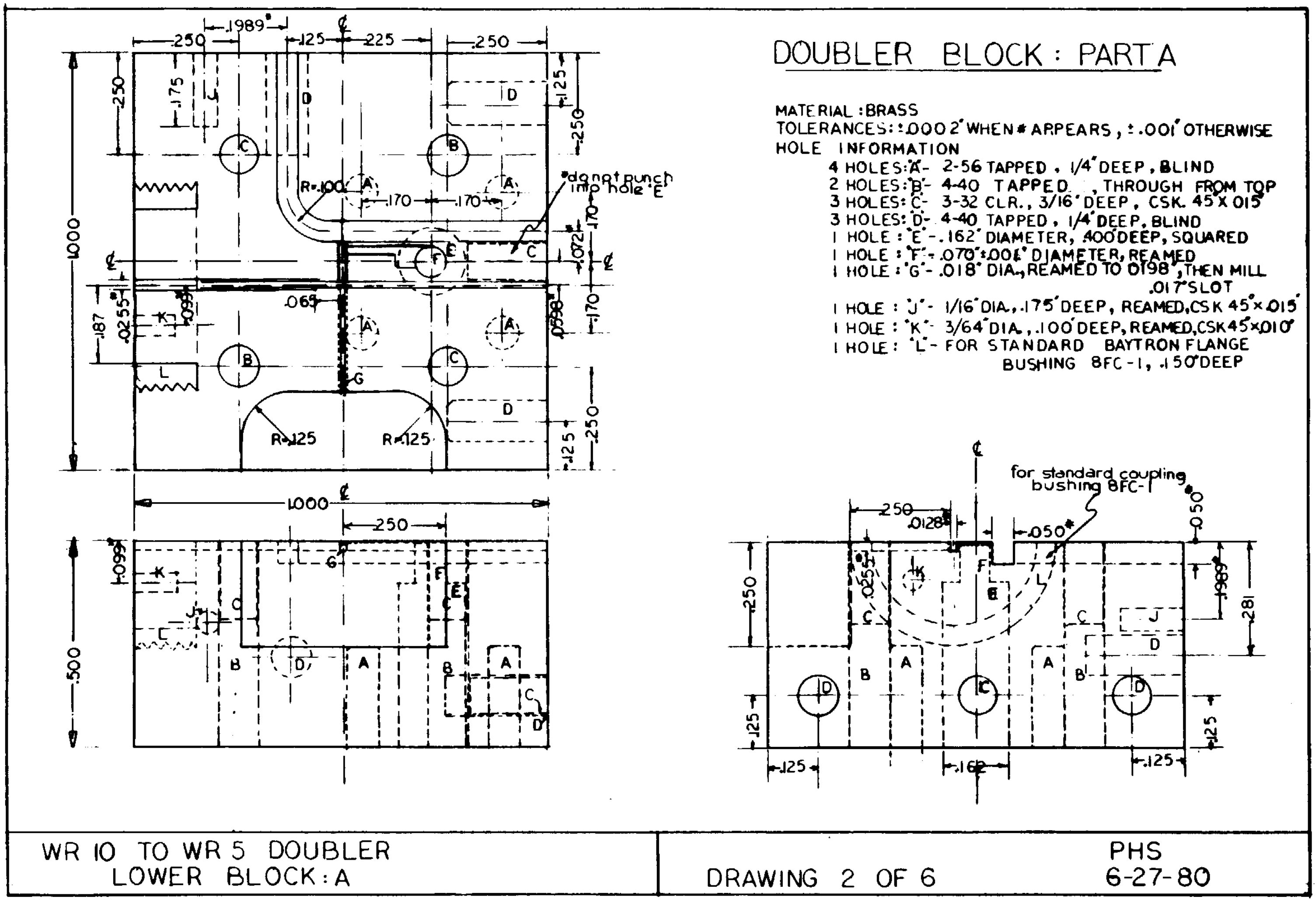

Fig. 6-16 A machinists drawing of the lower half of the multiplier block. This section will contain the diode chip, whisker post, bias connector and stripline filter structures.

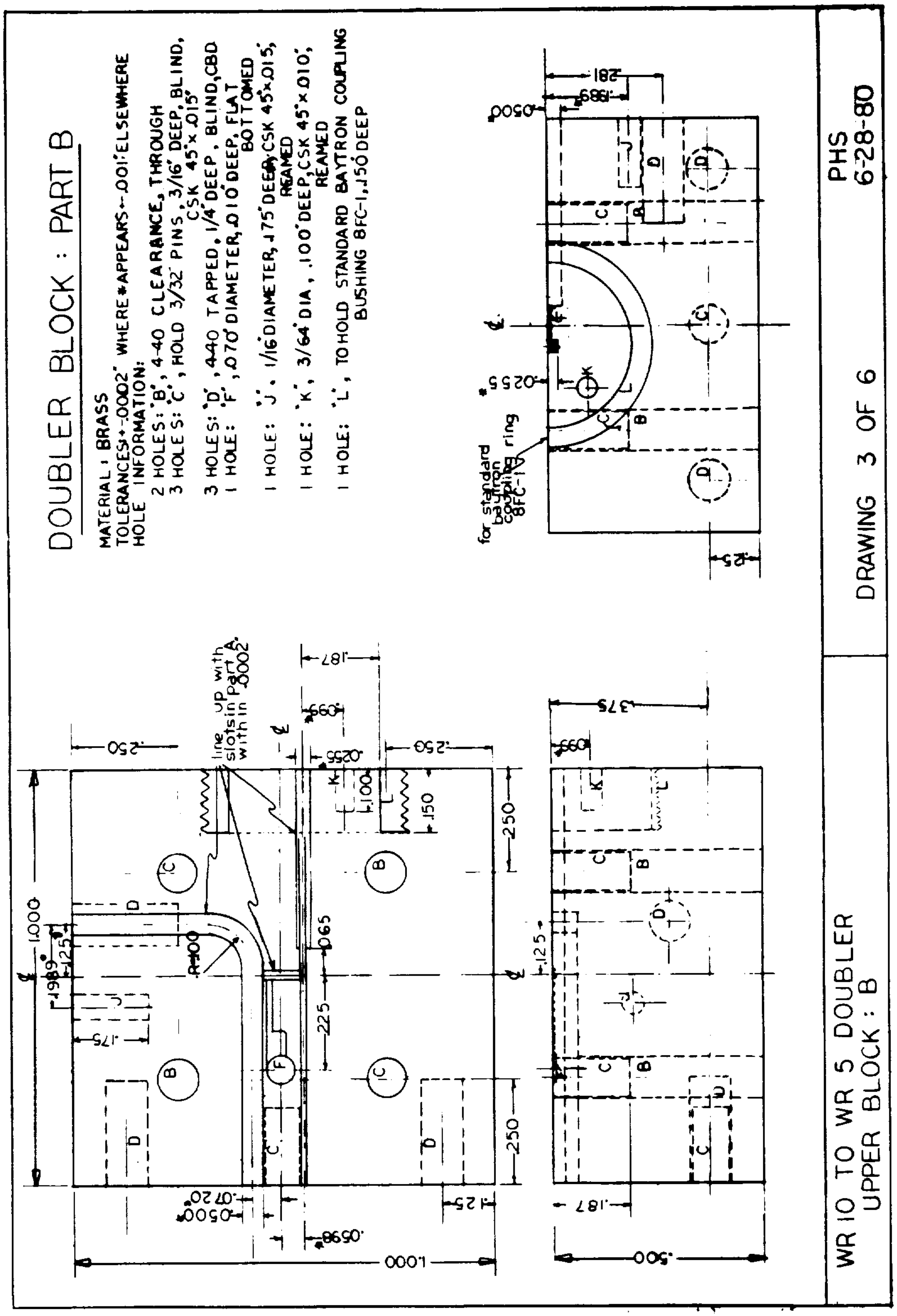

Fig. 6-17 A machinists drawing of the upper half of the multiplier block.

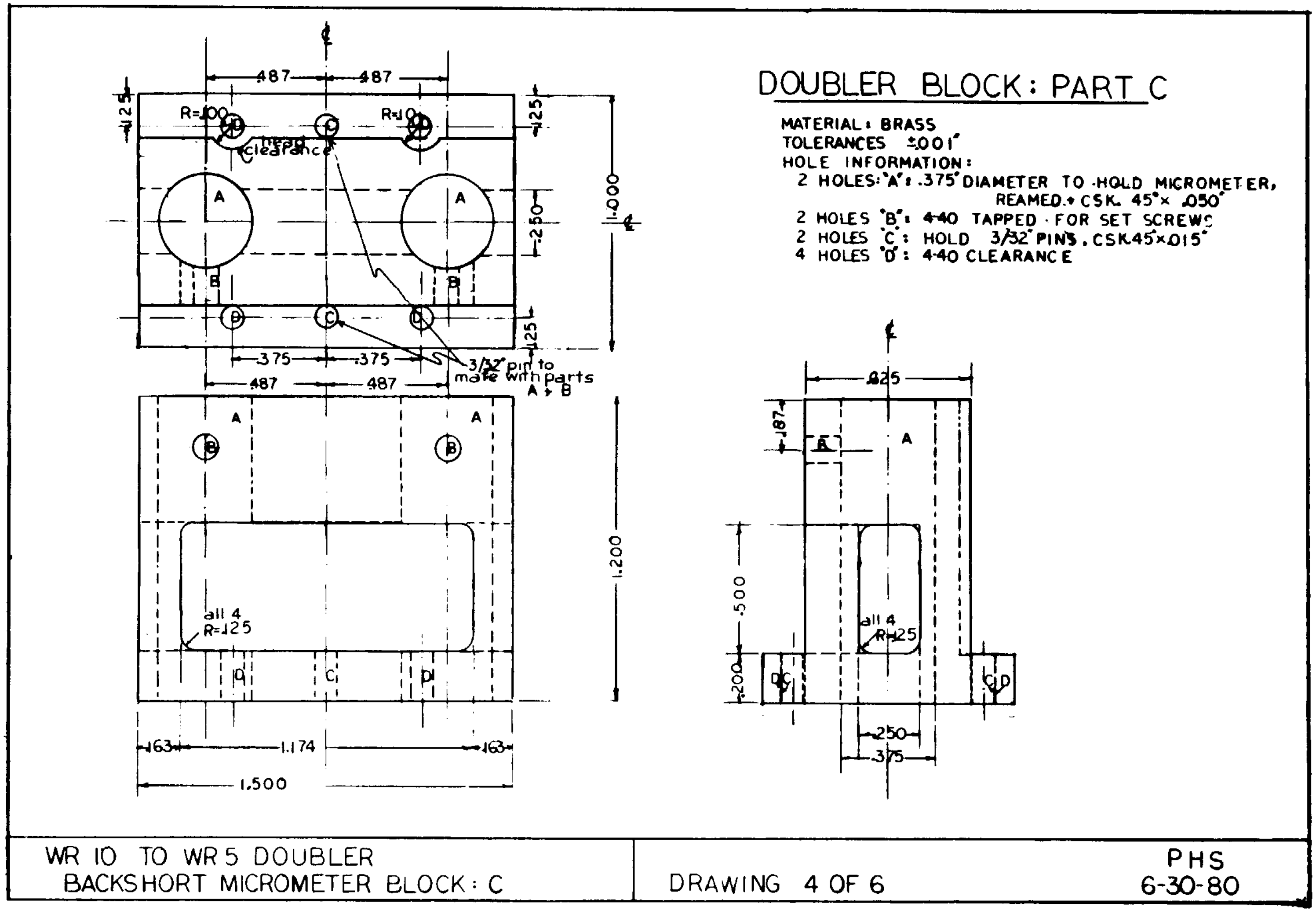

Fig. 6-18 A machinists drawing of the micrometer housing which will be clamped on to the multiplier block after the two halves have been assembled.

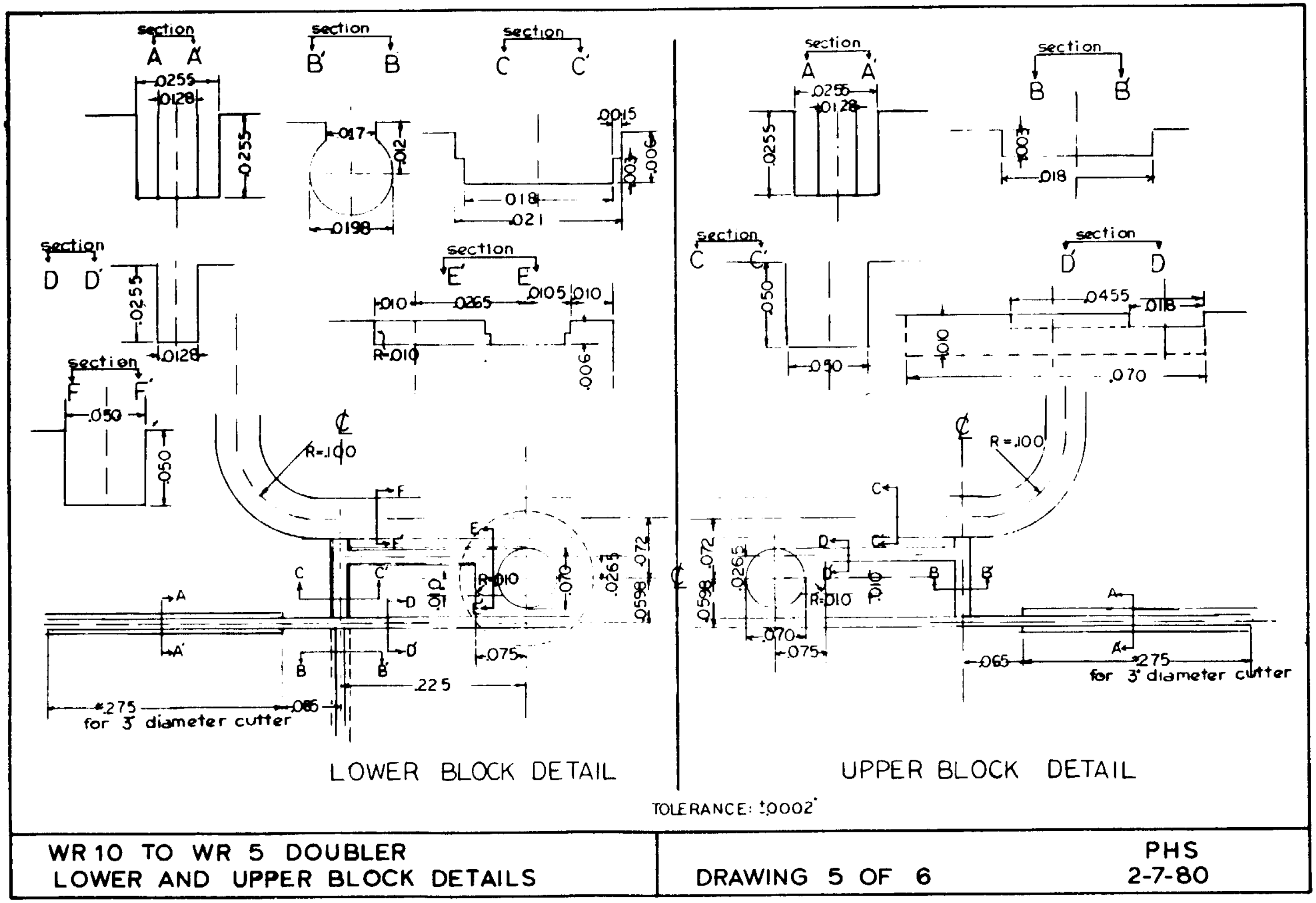

Fig. 6-19 A blow up of the region in the vicinity of the diode. Views for both the upper and lower multiplier blocks are shown.

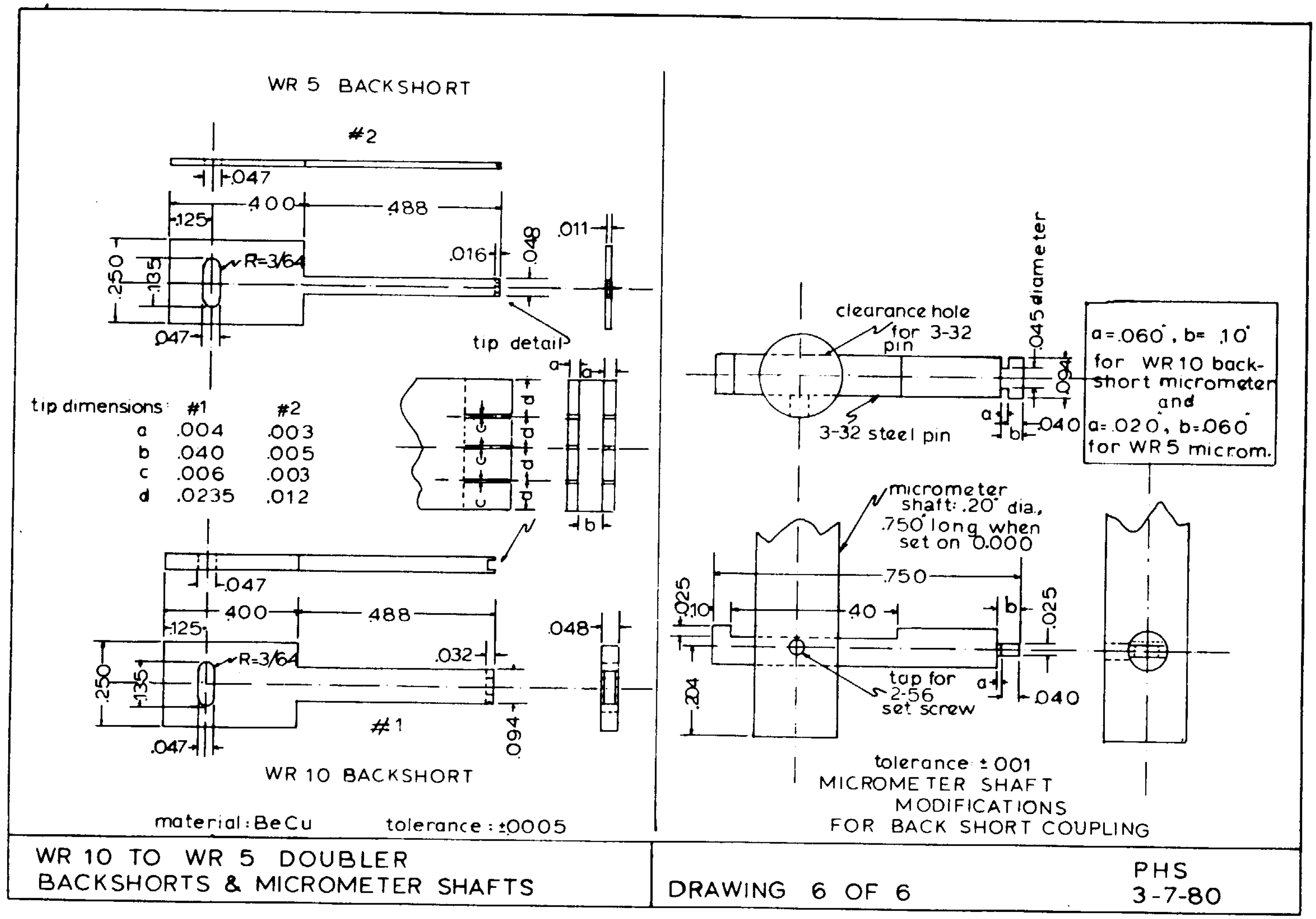

Fig. 6-20 Machinists drawings for the multiplier backshort and micrometer coupling pin. One end of the pin fits loosley into the hole in the backshort and the other is fed through a hole drilled into the shaft of the micrometer.

CHAPTER 7. THE CHANNEL WAVEGUIDE TRANSFORMER

7.1 Introduction

Waveguide mixers and frequency multipliers often use reduced height waveguide for improved impedance matching to the nonlinear element. A stepped or tapered transformer is generally employed between the full and reduced height sections to minimize the mismatch. These transformers are especially difficult to fabricate at millimeter wavelengths where the guide dimensions are very small. Copper electroforming has been used successfully; however this process is time consuming and usually requires the production of a disposable mandrel for each finished piece.

This chapter contains a description and an analysis of a new form of H-plane transformer, particularly suitable for use in split-block rectangular waveguide, which can be made quickly and easily with a slitting saw or single point cutting tool. The transformer was used in the 140-220 GHz frequency multipliers described in Chapter 6 and has been employed successfully in mixers operating at 115 GHz.

A physical description of the transformer and detailed fabrication procedures are given in Section 7.2. Section 7.3 outlines an approximate theoretical analysis for the determination of the reflection coefficient. The accuracy of the analysis is considered in Section 7.4 where VSWR measurements of three X-band transformers are compared with computed values. In Section 7.5 the theory is applied to two transformer configurations and design curves are given for transitions from full to one-half, one-third, and one-quarter height waveguide. Finally, in Section 7.6 two modifications are described which increase the bandwidth of the transformer. All detailed equations and derivations appear in Appendix 6.

7.2 Description of the Transformer

The channel waveguide transformer is shown in Fig. 7-1. It is most easily fabricated as a split-block structure in which the two halves are joined along a plane of zero transverse current (Fig. 7-1d). A slitting saw or single point tool is used to cut the reduced height waveguide completely along the two blocks (Fig. 7-1a). The full height waveguide and transition region are then formed by moving the saw to each side of the centerline, producing a sloping channel in part of the block (Figs. 7-1b and 7-1c). The result is a length of full height waveguide with sections of its narrow walls tapering in a circular arc towards the center until only the desired reduced height waveguide remains (Fig. 7-1e). Fig. 7-2a shows a series of cross sections along the longitudinal axis of the transformer, corresponding to the numbered positions in Fig. 7-1d. The length of the taper is determined by the radius, R, of the slitting saw and the depth of cut (waveguide half-width), a , according to $L = (2aR-a^2)^{\frac{1}{2}}$.

A taper with a linear rather than circular-arc-shaped profile can be formed by tilting the workpiece and moving it longitudinally under the slitting saw while the

2-4

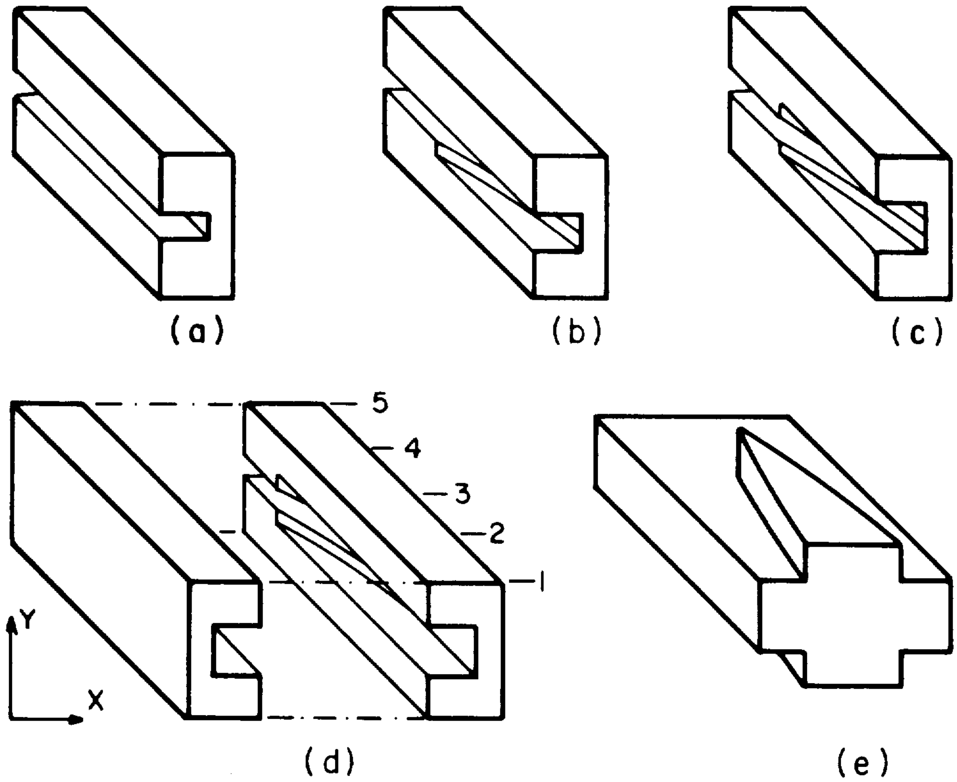

Fig. 7-1. (a) View of the right half of the transformer after machining the reduced height waveguide, (b) after slitting saw has been used to produce one side of the the transition from full to reduced height, and (c), the complete right half. (d) An exploded view of the finished transformer. (e) A solid view of the transition region beginning about midway down the length of the taper.

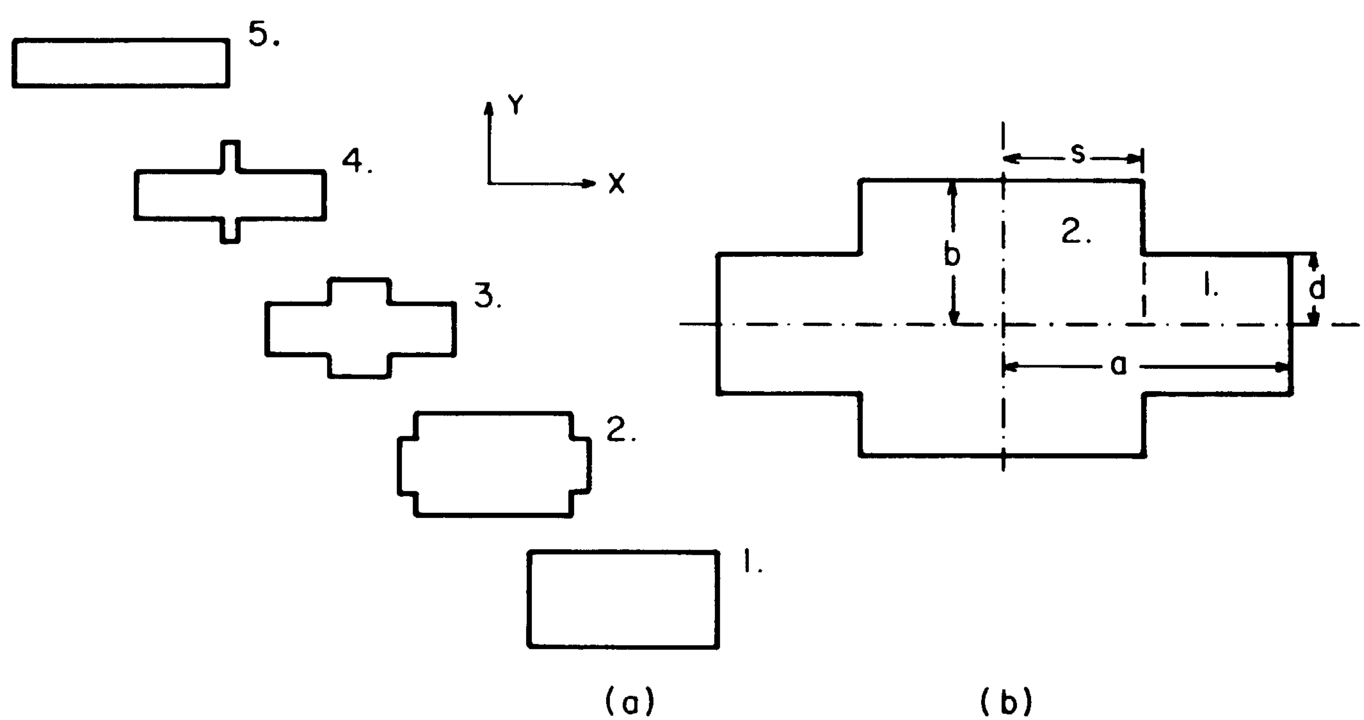

Fig. 7-2. (a) A series of cross sections taken along the length of the transformer. The numbers correspond to the positions indicated in Fig. 1(d). (b) A typical cross section defining the variables used in the theoretical analysis.

transition is being machined.

In cross section the device resembles a symmetrical form of the channel waveguide described by Vilmur and Ishii [171]. An equivalent structure has also been termed cross-shaped [96] and crossed [100, 164] rectangular waveguide in the literature. We have chosen to use the term channel waveguide as it contrasts well with the more familiar ridged guide; one can think of the ridge as having been inverted to form a channel along the axis of propagation.

7.3 Theory and Analysis

7.3.1 The Characteristic Impedance Method

An approximate analysis of a taper of arbitrary cross section between two uniform waveguides propagating a single mode has been given by Johnson [78]. The tapered region is replaced by a series of short butt-jointed uniform waveguides each having its own propagation constant and guide impedance. Letting the number of sections become large and neglecting higher order modes and multiple reflections, Johnson arrived at the following expression for the reflection coefficient of the dominant mode:

$$\Gamma\Big|_{z=0} = \frac{1}{2} \int_0^L \frac{d[\ln(Z_C)]}{dz} \exp \left[-2\int_0^z \gamma(z')dz'\right] dz \ , \qquad (7.1)$$

where the integration is over the length, L, of the transformer. For a gradual transition, $Z_C(z)$ can be equated with the characteristic impedance of a uniform waveguide having the same cross sectional dimensions as the transformer at position z. $\gamma(z) = \alpha(z) + j\beta(z)$ is the propagation constant of the mode in each short section of guide and reduces simply to $j\beta(z)$ for a lossless transition. $\beta(z)$ is related to the cutoff wavenumber, $k_c(z)$ via:

$$\beta = (\omega^2 \mu\varepsilon - k_c^2)^{\frac{1}{2}}, \tag{7.2}$$

where $\omega = 2\pi f$ is the radian frequency of the incident wave and μ and ε are the permeability and permittivity of the medium in the transition. Considering each cross section in Fig. 7-2a to be that of a uniform waveguide, the value of the cutoff wavenumber, $k_c(z)$, and hence the propagation phase constant, $\beta(z)$, can be determined using the method of transverse resonance (see Appendix 6, Section A6.1). Approximate expressions for the transverse fields in the cross section can then be used to derive a waveguide characteristic impedance.

A second, though more laborious means of calculating k_c and Z_c along the length of the transition is to solve the wave equation in each section of uniform waveguide subject to the appropriate boundary conditions. Such an analysis was performed on the channel waveguide by Kuz'min and Makarov [96] and later by Tham [164] and Lin [100]. By breaking the cross section into two regions, expanding the fields in each region in a series of orthogonal functions, and matching the solutions across the boundary line, a matrix eigenvalue problem is set up. The lowest order eigenvalue is the wavenumber for the dominant mode in the guide and the corresponding eigenvector contains the coefficients in the series expansion of the field. The latter can be integrated to determine the equivalent voltage and current used in calculating the characteristic impedance. The relevant equations are given in Appendix 6, Section A6.2 where a comparison is made between the different methods of calculating k_c and Z_c.

Once the values of $k_c(z)$ and $Z_c(z,f)$ have been determined, eq. (7.1) can be integrated numerically to find Γ at a particular frequency.

The concept of a characteristic impedance for waveguides propagating a single mode is discussed by Schelkunoff [139]. For certain special cases, such as rectangular waveguide, there are three equally useful definitions which differ only by constant factors. However, for non-TEM waveguides generally, and specifically for the channel waveguide structure, there is no obvious choice of expression for the characteristic impedance. The equivalent circuit of a junction between two waveguides with different cross sections can be described by a transformer, which couples between the wave impedances of the propagating mode in the two guides, and a shunt susceptance. To analyze the tapered channel waveguide rigorously by the characteristic impedance method it is necessary to find a definition which results in a unity transformer ratio at each incremental change of cross section (as would be the case for a TEM or rectangular TE_{10} waveguide taper using the conventional characteristic impedance definitions). Cohn [28] used a particular definition of characteristic impedance in analyzing ridged waveguide. As shown in Section 7.4 we have found that an analogous definition for channel waveguide gives acceptable agreement with experiment. However, we know of no way to prove that this definition actually does result in a unity transformer ratio.

7.3.2 The Method of Mode Coupling

The method of mode coupling* is a more general approach to the analysis of waveguides with slowly varying tapers. Early work by Schelkunoff [140] on a system of generalized Telegraphist's equations, and subsequent applications by Reiter [134], Solymar [155] and Katzenelenbaum [80] resulted in a general theory of coupled wave equations. This theory avoids using the concept of a characteristic guide impedance, and is not

---

* A useful discussion of the method of mode coupling is given in the monograph by Sporleder and Unger [157].

restricted to single mode propagation. It was shown by Solymar [155], that the reflection coefficient of the dominant mode of a sufficiently gradual taper depends only upon the variation of two quantities along the taper: the wave impedance, and one of a set of mode coupling coefficients. The appropriate coupling coefficient, which describes coupling from the forward-traveling wave into the backward-traveling wave, is calculated from the transverse electric or magnetic field at each cross section of the transformer.

Since analytic expressions for the fields were available from [100] or [164] a concerted effort was made to apply Solymar's theory to the channel waveguide transformer. However, we found that it was not practical to predict the transformer performance with reasonable accuracy using this method. The problem appears to be the slow convergence of the series representing the fields in the channel waveguide.

Both the mode matching method of [164] and the Ritz-Galerkin method of [96] and [100] express the fields in the waveguide as infinite series satisfying the boundary conditions at each cross section. In any practical computation these series must be truncated. It was found that the matrix eigenvector problem could not be solved accurately unless the matrix was truncated at 5 x 5 or fewer elements. It is clear from Fig. 7-3 that the resulting electric field expressions are a poor approximation to the full series solution near the start of the channel, and especially in the region of the singularity at the obtuse corner. Montgomery [115] made the same observations when he used the Ritz-Galerkin method to find the fields of the ridged waveguide. It so happens that the backward wave coupling coefficient for the dominant mode of the channel waveguide is governed only by the fields along the side wall of the channel ($x = s$), where they are most poorly represented by the truncated series. One might expect that the value of the coupling coefficient as determined from this series would be too small. Indeed, it was found that one could get the mode coupling theory to agree with measured values of reflection coefficient if the coupling coefficient, as calculated from the truncated series expansions, was increased from two to four times.

An alternative approach to the mode coupling method would be to use a numerical finite difference scheme to determine the fields in the channel waveguide transformer more accurately, and then to use the small coupling theory of Solymar to calculate the reflection coefficient. Such an approach was used by Saad, Davies and Davies [137] in the design of a Marie mode transformer.

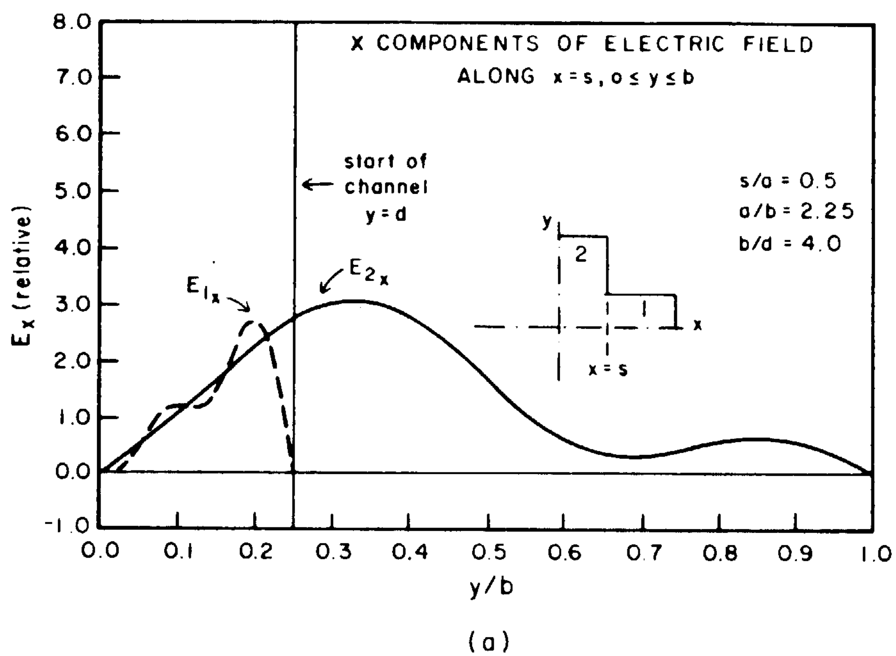

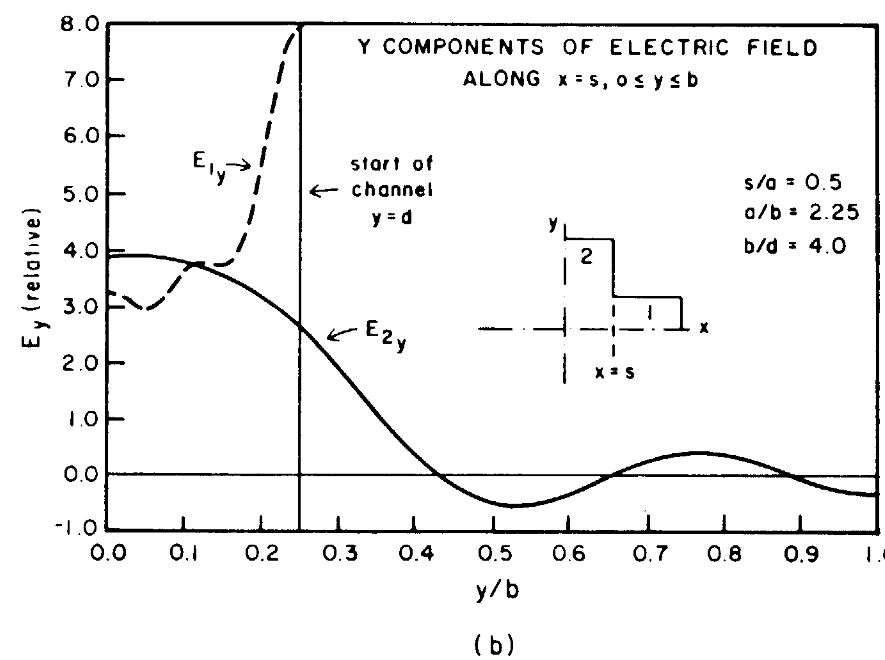

Fig. 7-3 (a) A plot of the x component of the electric field along x=s, from y=0 to y=b when s/a=0.5. This includes the boundary line at which the fields in the two regions of the cross section are matched, and the side wall of the channel. The plot has been made using the field expansions given in Appendix 6, Section A6.2 with the series truncated to five terms. Ideally E_{2_x} should become infinite as y approaches d.

(b) A similar plot of the y component of the electric field. E_{1_y} and E_{2_y} should be equal from y=0 to y=d and should become infinite as y approaches d. E_{2_y} must go to zero when y>d.

7.3.4. Choice of Method

For the reasons described in the previous section, the characteristic impedance method was used in deriving the theoretical results given in this thesis.

The following steps summarize the algorithm used for determining the reflection coefficient of the channel waveguide transformer:

(1) The input and output waveguide sizes are specified, together with expressions for the cross sectional dimensions at any point along the length of the transition.

(2) The transcendental equation (A6.1) Appendix 6, or the eigenvalue equation (A6.10) is solved at each of a series of cross sections along the length of the transformer. The lowest order roots from either solution yield the TE_{10} mode cutoff wavenumbers, $k_c(z)$. For the results presented in this thesis, the transverse resonance method was used, as it requires much less computing time than the solution of the eigenvalue problem.

(3) The waveguide characteristic impedance $Z_c(z)$ is obtained using either the transverse resonance method (Appendix 6, Section A6.1) or the eigenvalue method (Section A6.2). Again, in this thesis the transverse

resonance method was used because of the saving in computer time.

(4) The propagation phase constant, $\beta(z)$, is found from the wavenumber, and the logarithmic derivative of the characteristic impedance is determined at each cross section along the length of the transformer.

(5) The reflection coefficient, Γ, at the start of the taper, is calculated from (6.1) by numerical integration.

(6) Steps (4) and (5) are repeated at each frequency of interest.

7.4 Comparison with Experiment

To check the accuracy of the analysis, three channel waveguide transformers having input to output height ratios of 2, 3, and 4 were fabricated in X-band waveguide (8.2-12.4 GHz). The transitions used linear tapers with half angles of 8 and 10 degrees, and lengths approximately one guide wavelength (as measured in X-band rectangular waveguide) at 8 GHz. The voltage standing wave ratio over the entire waveguide band was measured using a slotted line and a well matched sliding load in the reduced height guide.* A comparison of the measured and computed VSWR for each of the transformers appears in Fig. 7-4. Calculated values of the normalized cutoff wavenumber, k_c/k_{c_0} ($k_{c_0}=2\pi/4a$) versus position along the length of the taper are shown in Fig. 7-5 for the three transformer ratios. Notice that the cutoff frequency in the full-to one-quarter-height transition increases to 1.35 times its value in rectangular waveguide (s/a=1). This effect reduces the usefulness of the transformer near the low end of the waveguide band. Two simple remedies to this problem are given in Section 7.6.

---

* The load was fabricated from LDV Radite #75 tapered to a single point at the side wall of the reduced height

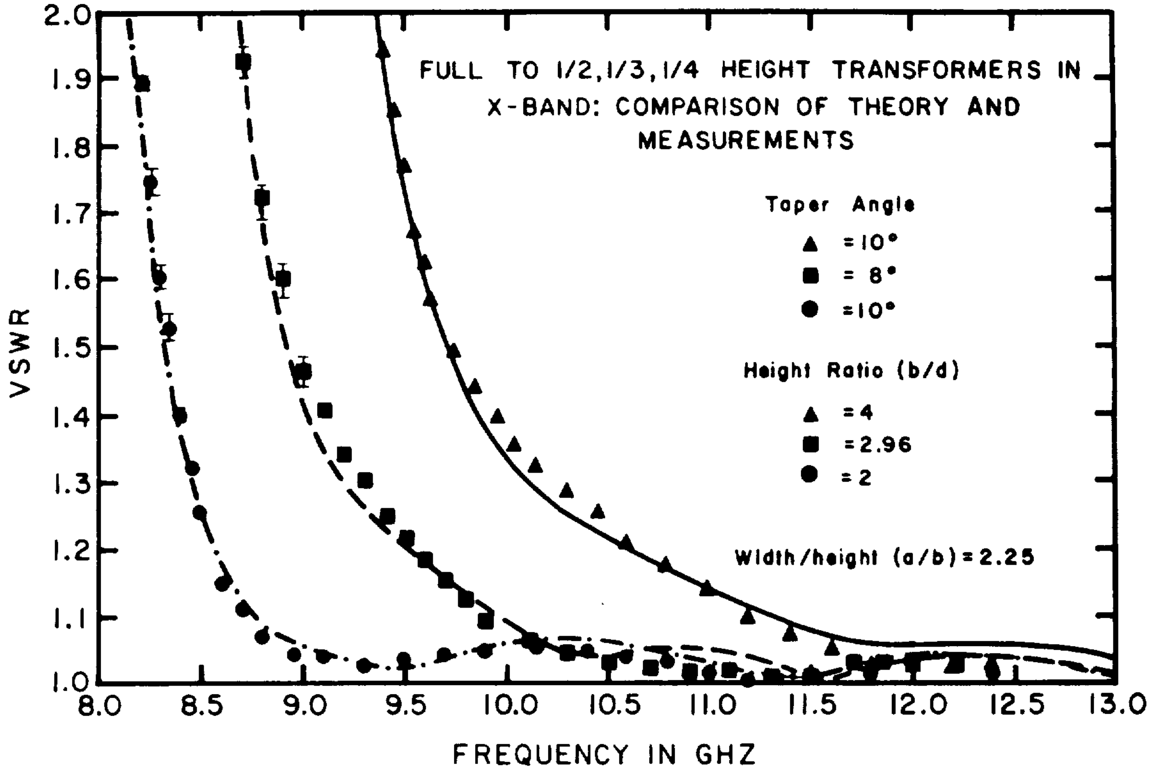

ORIGINAL PAGE IS
OF POOR QUALITY

Fig. 7-4. Comparison of measured and predicted VSWR for three X-band transformers with linear tapers. The lines are the computed values; points, the measured values. Error bars reflect the mismatch uncertainties of the sliding load.

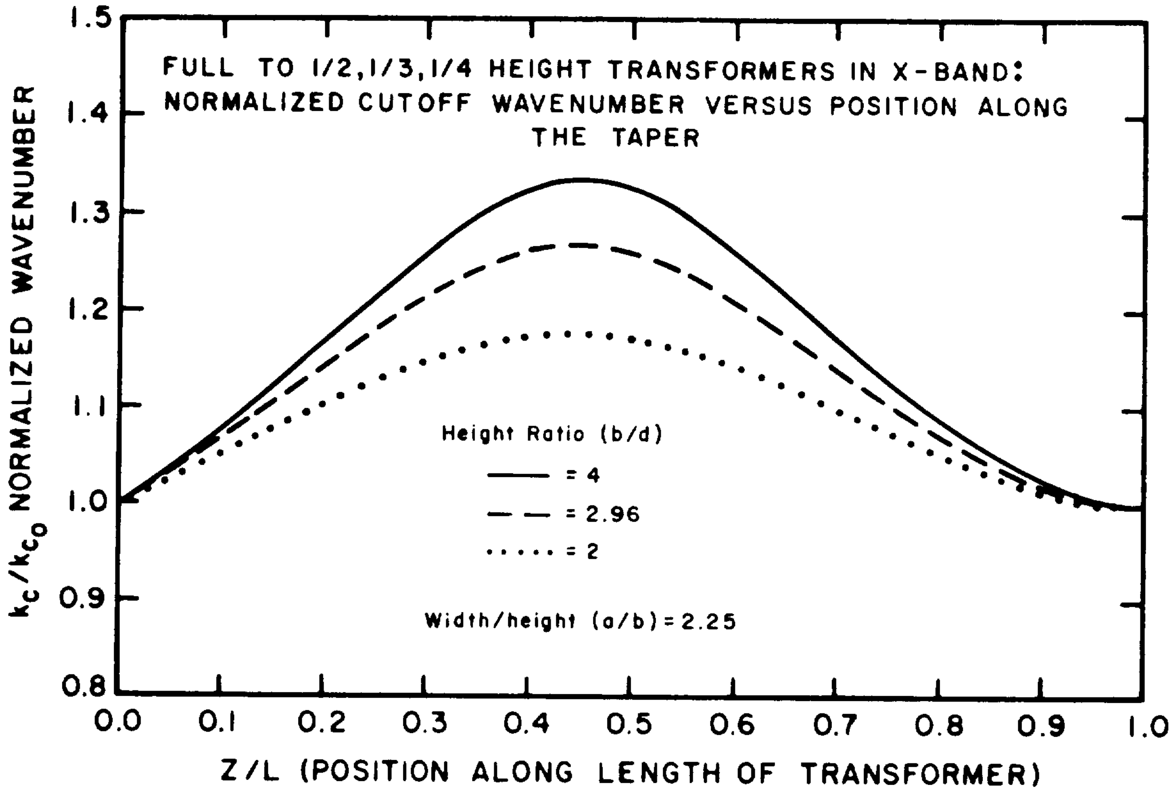

Fig. 7-5. Predicted values of the normalized cutoff wavenumber versus position along the taper for the transformers of Fig. 7-4. The cutoff wavenumber of the channel waveguide, k_c is normalized to that of standard X-band waveguide, $k_{c_0}=2\pi/4a$, where a is the waveguide half width.

The agreement between the theory and the experimental data is fairly good except at very low values of VSWR. This discrepancy cannot be accounted for by measurement errors and is especially noticeable in the full-to one-quarter-height design. As can be seen in Fig. 7-6, the only higher order TE mode able to propagate in any portion of the transition is the TE_{20} mode which, being asymmetrical, should not be excited in this structure. Although the magnitude of the reflection coefficient is particularly sensitive to the value of k_c, an error in this variable would show up at all frequencies and not simply when the VSWR is low. The calculation of C_d, the discontinuity capacitance associated with the edge of the channel (see Section A6.1 of Appendix 6) takes into account proximity effects when the channel width is small but not when it approaches the outer dimensions of the guide ($s \approx a$). It was found that an increase in the value of C_d in the region where s is close to a will have a noticeable effect on the VSWR wherever the reflection coefficient is small. The effect to bring the measured and predicted performance into closer agreement.

Because of the observed discrepancies between the theory and measurements for small values of VSWR, the design curves given in the next section must be used with a degree of caution. Clearly, if one does not deviate significantly from the three prototypes in this section

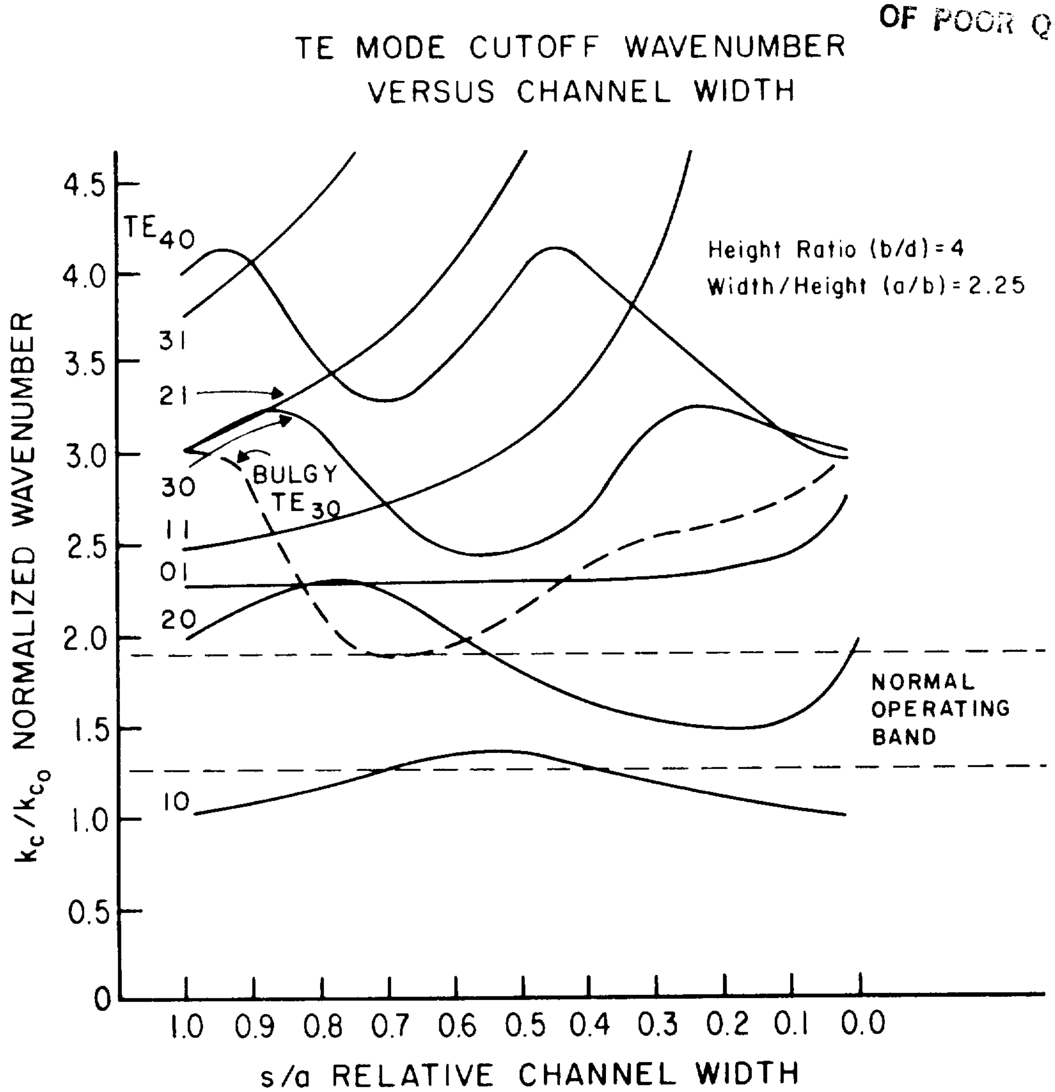

Fig. 7-6. The TE-mode wavenumbers, normalized to those of X-band rectangular waveguide, along the length of the full to one-quarter height transformer of Fig. 7-4. The normal operating band is bounded by the horizontal broken lines. The broken curve represents the TE_{30} mode of a bulgy transformer, discussed in Section 6.6.

the theory will adequately predict the transformer performance. For transformer ratios and taper angles which are substantially different, the design curves in Section 7.5 should not be relied on to give precise VSWR values below 1.1. For general use, however, the curves should enable the designer to select an easily fabricated transformer to meet his other needs.

7.5 Design Curves

The algorithm described in Section 7.3 and A6.1 was used to analyze two different types of channel waveguide transformer. Those of the first type have circular-arc-shaped tapers which could be produced with slitting saws of various diameters, while those of the second type have linear tapers with various half angles. The former design is somewhat easier to fabricate at millimeter wavelengths, whereas the latter configuration is more suitable for use at lower frequencies where the required slitting saw diameters would be prohibitively large. Transformers with input to output height ratios of 2, 3, and 4 were examined. In every case the taper was divided into 50 cross sections for the analysis. Increasing this number had no significant effect on the results.

Plots of the predicted VSWR versus normalized frequency for the transformers with the circular-arc-shaped tapers are shown in Figs. 7-7 to 7-9. The three curves represent transformers whose lengths are 1.5, 2 and 2.5 times the guide wavelength in standard rectangular waveguide at the center of the band. The design data for transformers with linear tapers are given in Figs. 7-10 to 7-12, where the predicted VSWR for transitions with different half angles are shown. The half angles are chosen to yield taper lengths equal to those of the circular-arc-shaped transformers in Figs. 7-7 to 7-9. The expected rise in the wavenumber as a function of position along the taper is plotted in Figs. 7-13 and 7-14 for both sets of transformers.

The overall performance of the transformers with linear tapered transitions is slightly better than those with a circular-arc-shaped profiles. Transformers of large input to output height ratios do not perform well at the low end of their waveguide bands regardless of their length. Fairly good performance can be expected, however, if one operates far enough above the maximum cutoff frequency in the transition. In the next section methods of increasing the bandwidth of the transformers are described which lead to designs having useful performance over the full waveguide band.

ORIGINAL PAGE IS
OF POOR QUALITY

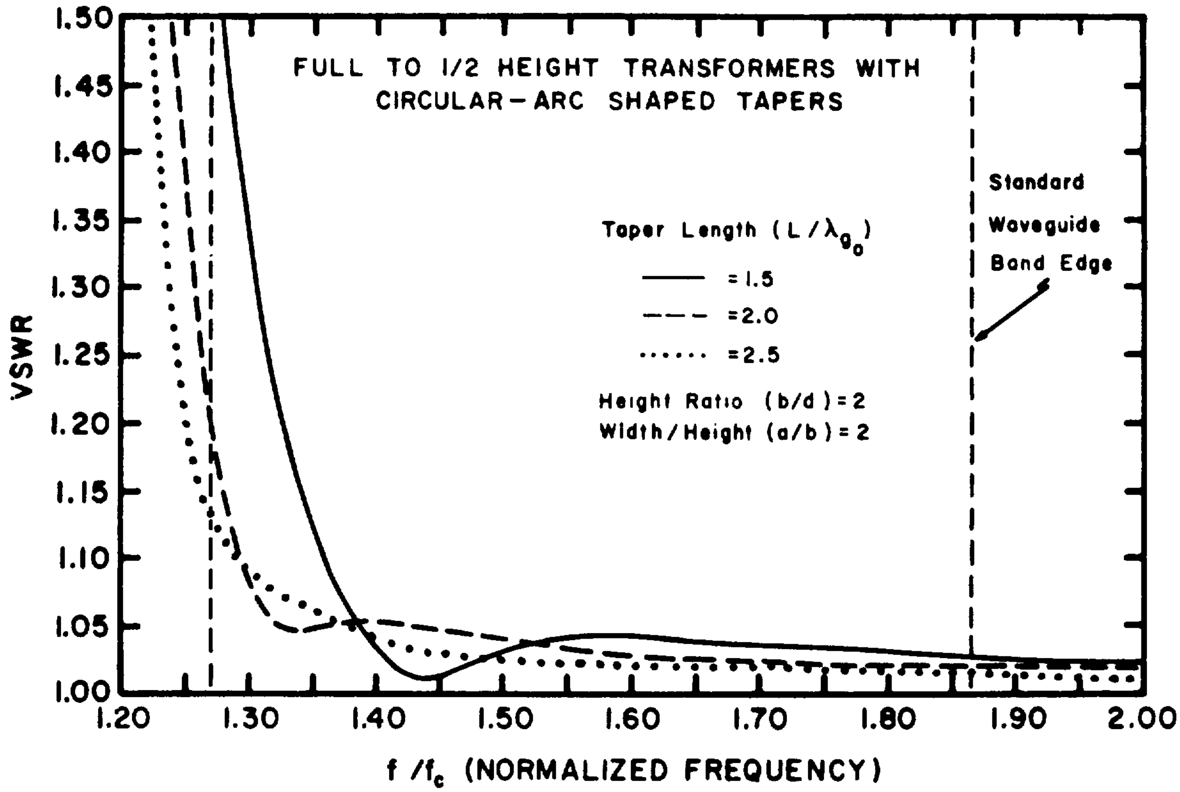

Fig. 7-7. Predicted VSWR versus normalized frequency for three full to 1/2 height transformers with circular-arc shaped tapers. The curves represent transformers whose lengths are 1.5, 2 and 2.5 times the guide wavelength in rectangular waveguide at the center of the band ($\lambda_{g_0} = 4a/[1-(f_c/f_0)^2]^{\frac{1}{2}}$, with $f_0/f_c = 1.57$). The frequency is normalized to the cutoff frequency of the rectangular waveguide, f_c=c/4a. The slitting saw radius used to produce a particular taper is given by $R/a = 13.461(L/\lambda_{g_0})^2 + 0.5$.

The width to height ratio (a/b) of the full-height waveguide is 2:1, which is characteristic of most millimeter waveguides. The two vertical lines indicate the normal operating band.

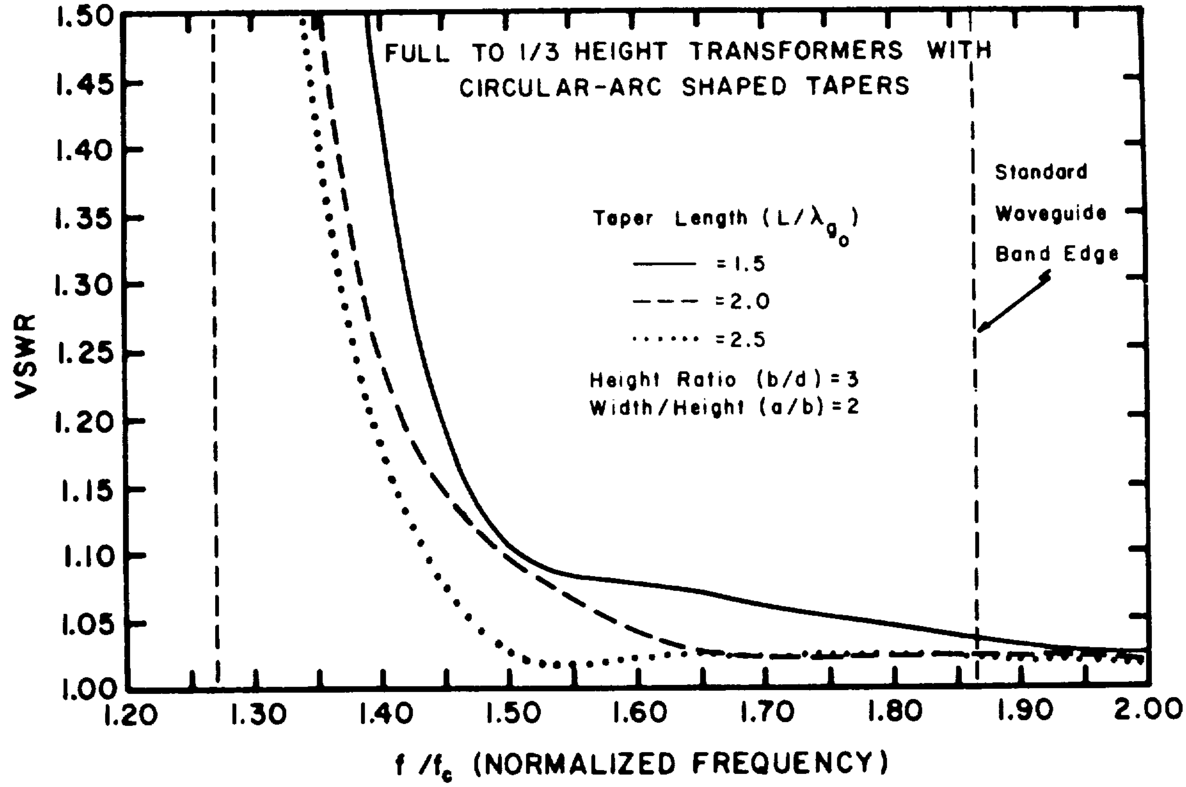

Fig. 7-8. Predicted VSWR versus normalized frequency for three full to 1/3 height transformers with circular-arc shaped tapers. The transformers have the same lengths and width to height ratio as in Fig. 7-7.

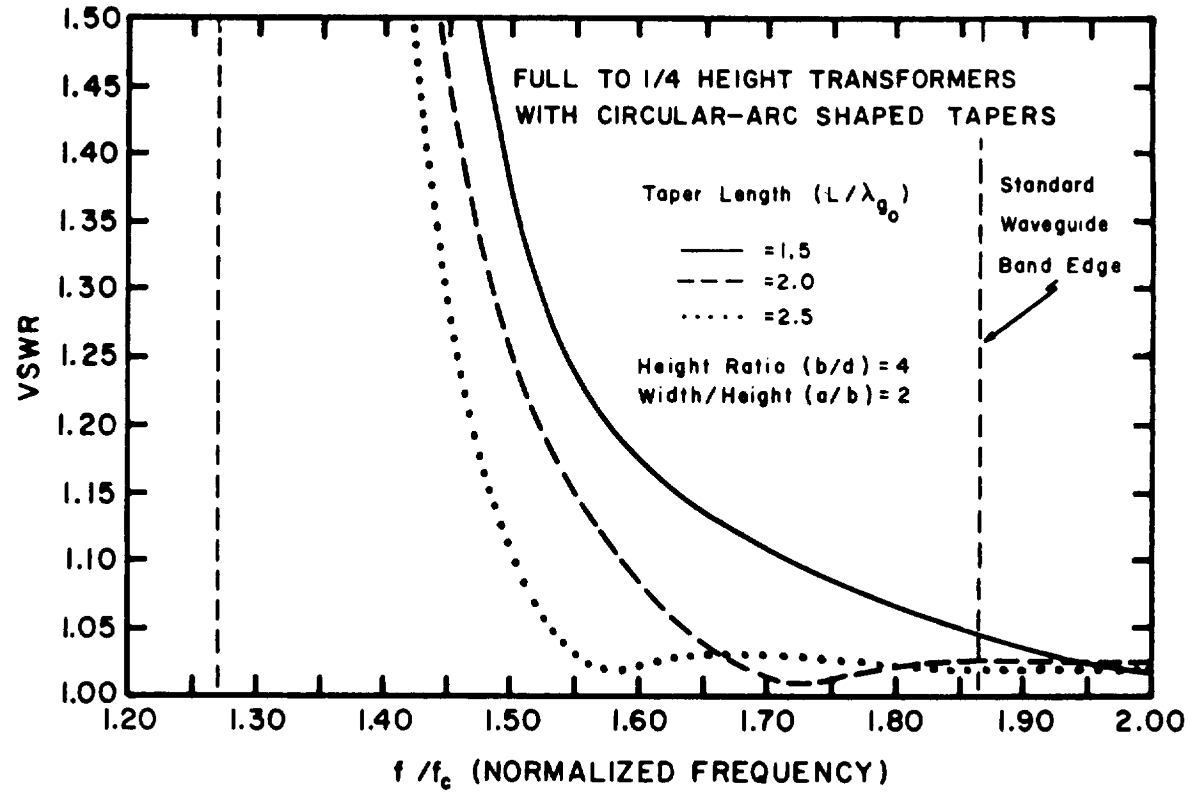

Fig. 7-9. Predicted VSWR versus normalized frequency for three full to 1/4 height transformers with circular-arc shaped tapers. The same conditions apply as in Fig. 7-7 and Fig. 7-8.

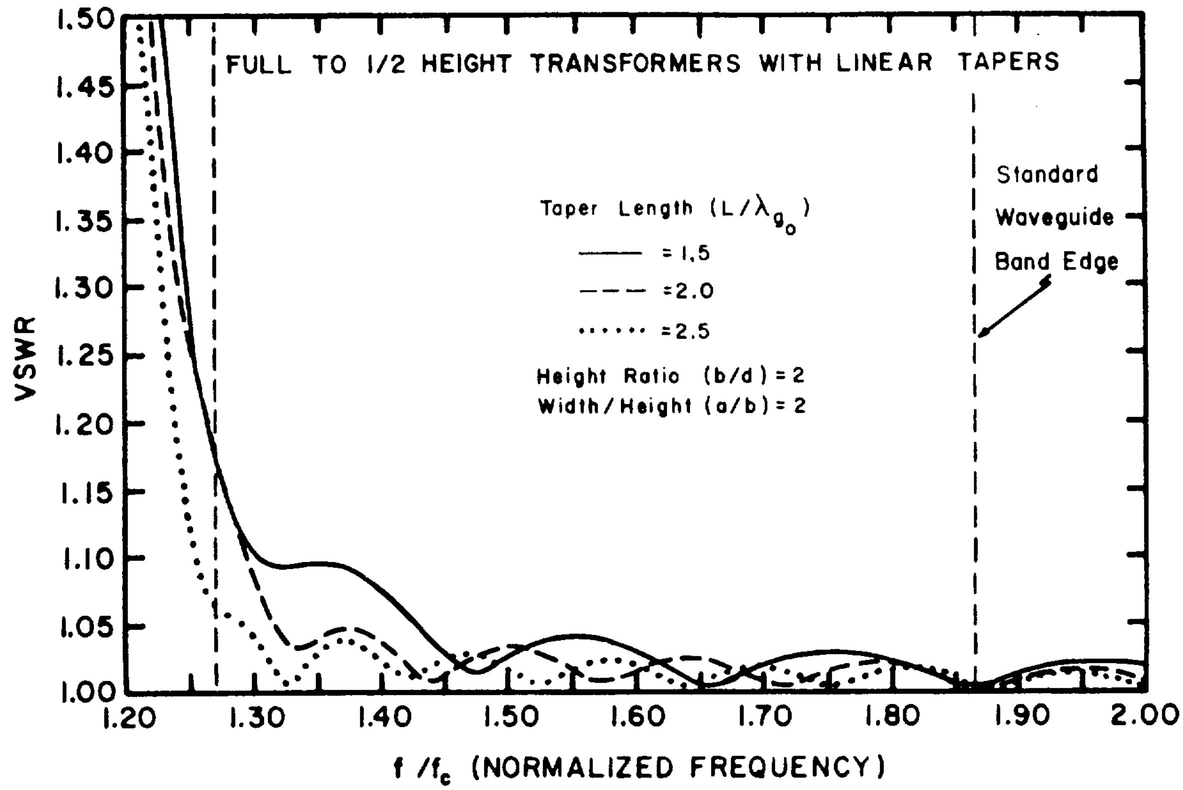

Fig. 7-10. Predicted VSWR versus normalized frequency for three full to 1/2 height transformers with linear tapers. The curves represent tapers with half angles chosen to give the same overall length as those of Figs. 7-7 to 7-9, i.e. $\Theta = \arctan\left[.1927/(L/\lambda_{g_0})\right]$. All other conditions are the same as in Figs. 7-7 to 7-9.

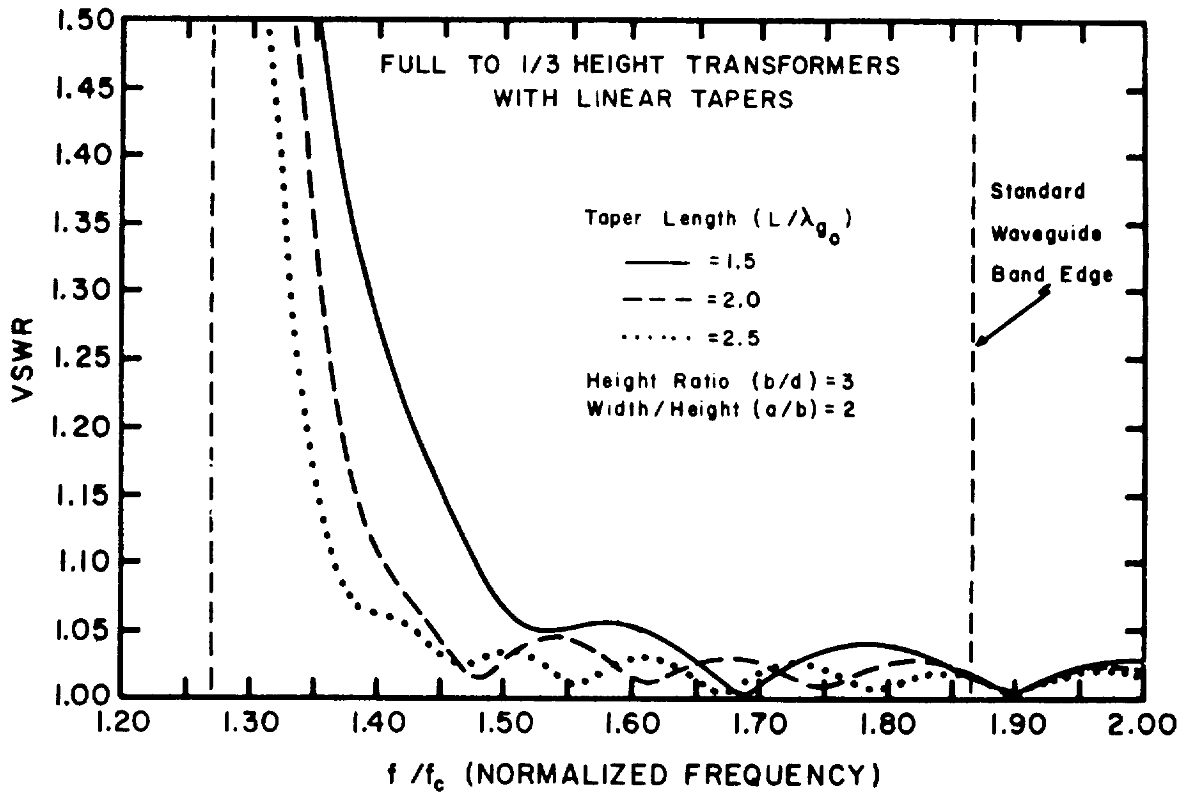

Fig. 7-11. Predicted VSWR versus normalized frequency for three full to 1/3 height transformers with linear tapers. The taper half angles are chosen to give transition lengths identical to those of Figs. 7-7 to 7-10. All other conditions are the same as in Figs. 7-7 to 7-10.

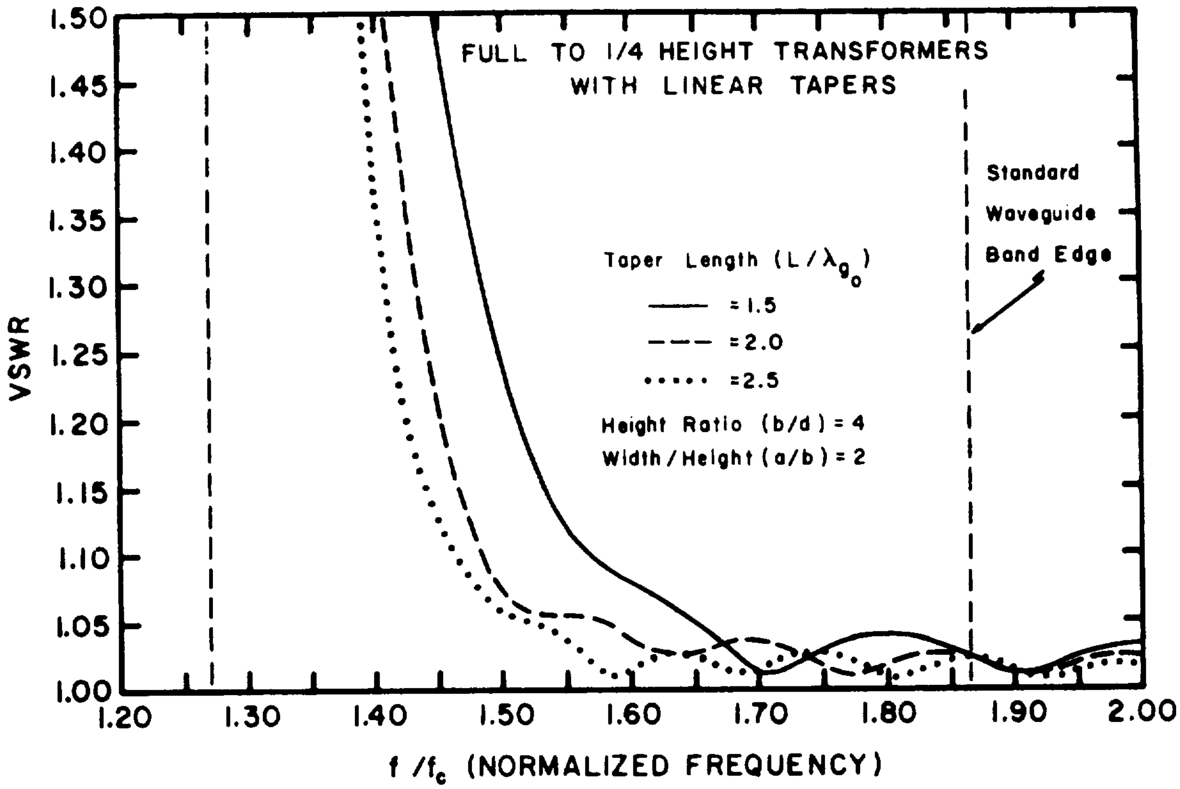

Fig. 7-12. Predicted VSWR versus normalized frequency for three full to 1/4 height transformers with linear tapers. All other conditions are identical to those of Figs. 7-10 and 7-11.

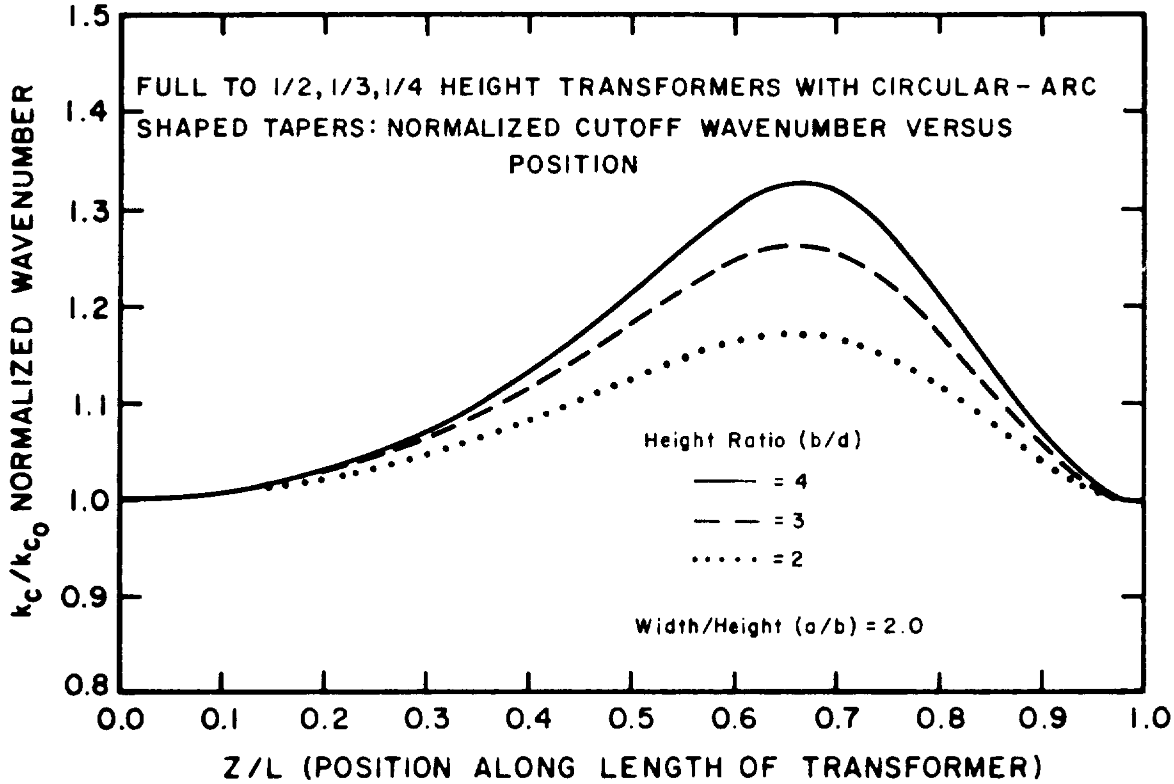

Fig. 7-13. Predicted values of the normalized wavenumber versus position along the transition for the three circular-arc shaped transformers in Figs. 7-7 to 7-9. The wavenumber is normalized to that in the rectangular waveguide at the start of the taper ($k_{c_0}=2\pi/4a$), and the ratio of guide width to full height is assumed to be 2:1, characteristic of standard millimeter waveguides.

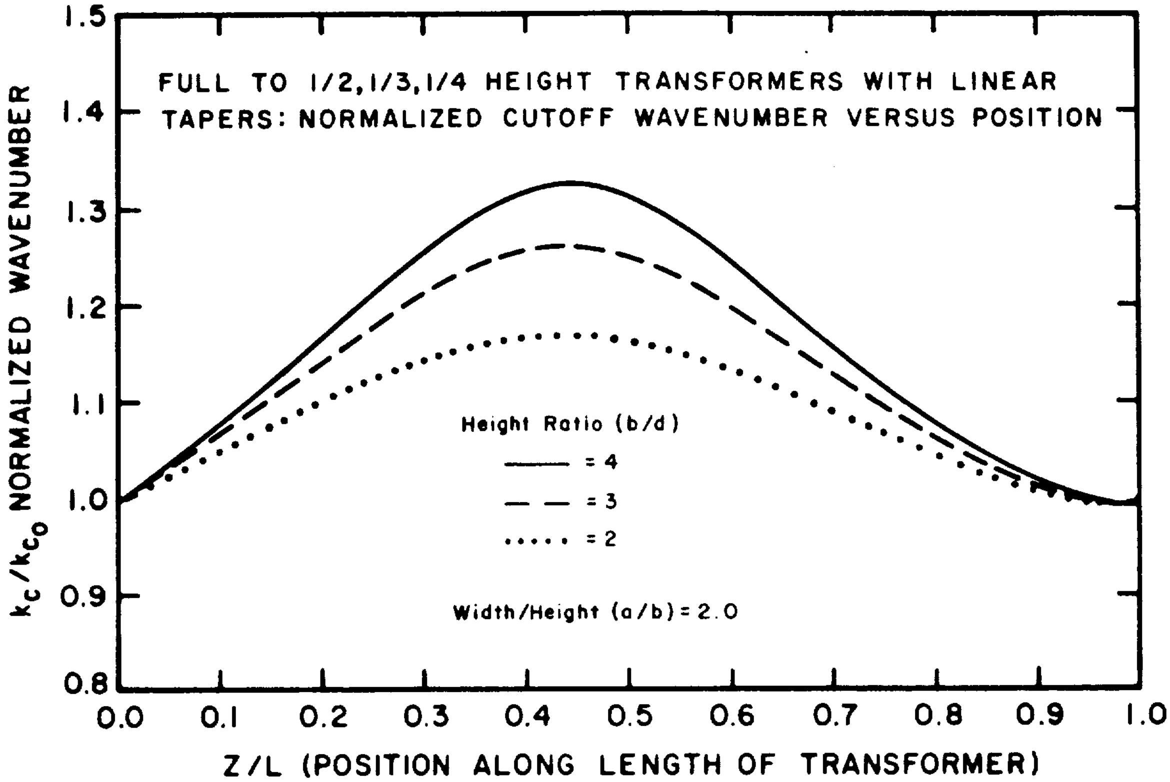

Fig. 7-14. Predicted values of the normalized wavenumber versus position along the length of the transition for the three linearly tapered transformers of Figs. 7-10 to 7-12. The same conditions apply as in Fig. 7-13.

7.6 Broadband Transformers

Two approaches for improving the low frequency performance of channel waveguide transformers were investigated. The first is to use two transformers with low height ratios in series to achieve the desired overall ratio. It is clear from Figs. 7-13 and 7-14 that the cutoff frequency of a channel waveguide transformer is related to the input and output waveguide heights. Two transformers of low height ratio in series should have a lower VSWR than a single high ratio transition.

A second way of improving the low frequency performance is to vary the waveguide width along the transformer, which can be done without significantly complicating the fabrication procedure. This approach is suggested by the observation, based on Figs. 7-13 and 7-14, that the cutoff frequency of a channel waveguide transformer is governed by the dimensions of the cross section with the highest value of k_c/k_{c_0}, which occurs when $s/a \approx 0.55$.

7.6.1 Two Stage Transformers

The analysis of a transformer from full-to half-height in series with a half-to quarter-height transformer indicates a substantial improvement in performance across the waveguide band. The maximum cutoff frequency in the transition is reduced to that of the full-to half-height transformer design. Measurements on a transformer of this type in WR-10 (75-110 Ghz) waveguide confirmed the theoretical results.

The approach could be extended to produce a transformer with many steps in height. If the individual tapers were to overlap, the resulting structure could be analyzed using the same method as in Appendix 6, Section A6.1. No design curves are offered here because of the large number of free parameters.

7.6.2 Bulgy Transformers

To make a channel waveguide transformer with increased width near the middle of its length, the same set-up and cutting tool can be used as for the unmodified design. Upon completing the reduced height waveguide section (as in Fig. 7-1a) one simply moves the slitting saw to the center of what is to be the transition region, and plunges downwards, producing a circular-arc shaped bulge in the narrow wall of the guide. The length of the bulge is determined by the slitting saw radius, R, and the depth of the cut according to: $L_B = (2hR-h^2)^{\frac{1}{2}}$ where h is the depth at the midpoint of the bulge.

Figs. 7-15 and 7-16 show the results of the theoretical analysis on a group of full-to one-quarter-height bulgy channel waveguide transformers in which the bulges extend the full length of the transition. The transformer lengths correspond to those of Figs. 7-7 to 7-12 and the bulge depths, fixed by the slitting saw radii, increase the reduced height waveguide by ~25% at the midpoint of the transition.

Figs. 7-17 and 7-18 show the normalized wavenumber along the longitudinal axis of the transformers. The

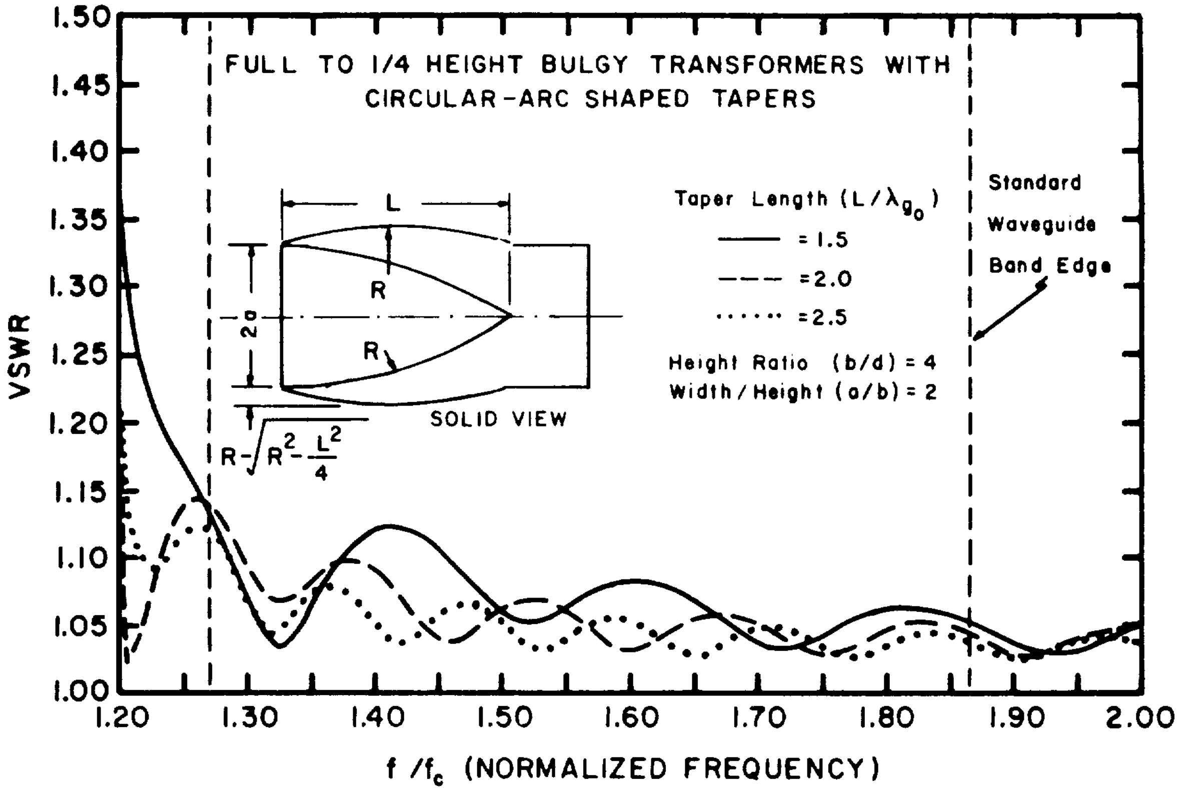

Fig. 7-15. Predicted VSWR versus normalized frequency for three full to 1/4 height bulgy transformers with circular-arc shaped tapers. Each curve corresponds to one of the transformers in Fig. 7-9, modified with a bulge in the width of the reduced height waveguide. The bulges are made with the same slitting saw used to produce the rest of the transformer and extend the full length of the transition. The reduced height waveguide width is increased by a maximum of ~25% at the midpoint of the taper.

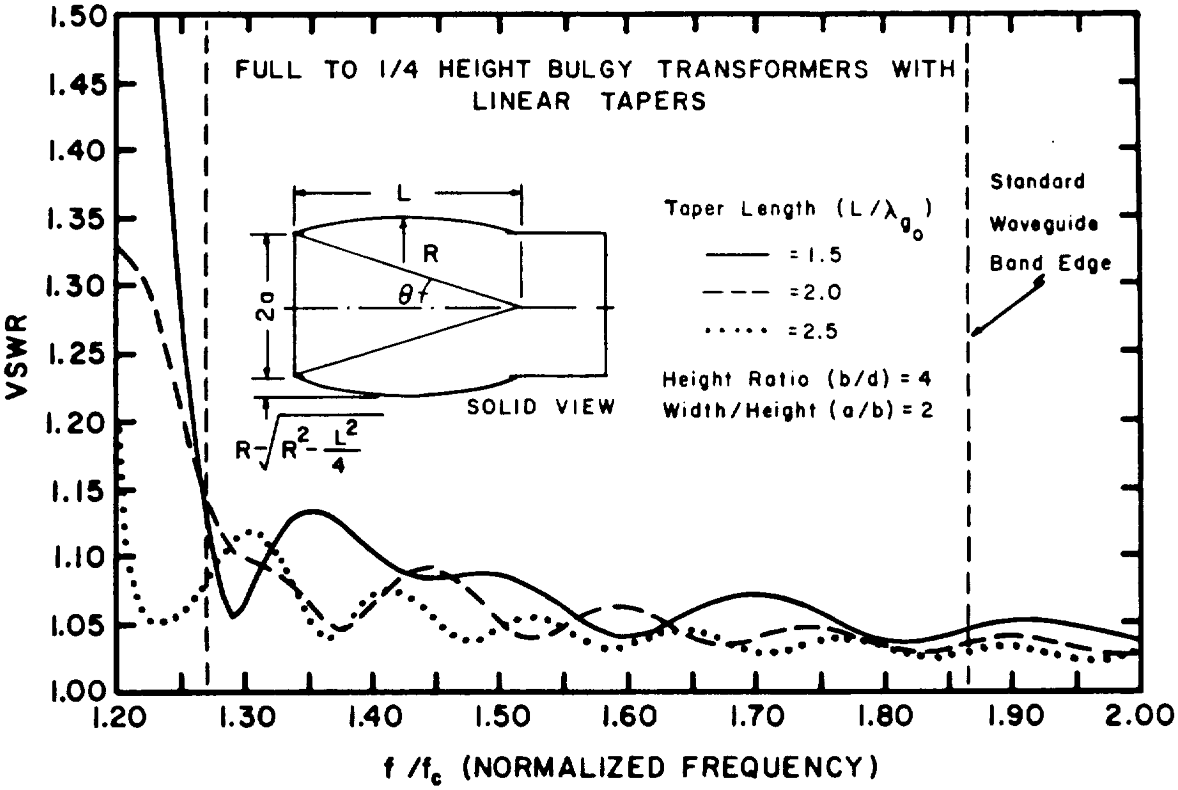

Fig. 7-16. Predicted VSWR versus normalized frequency for three full to 1/4 height bulgy transformers with linear tapers. Each curve corresponds to one of those in Fig. 7-12. All other conditions are the same as in Fig. 7-15.

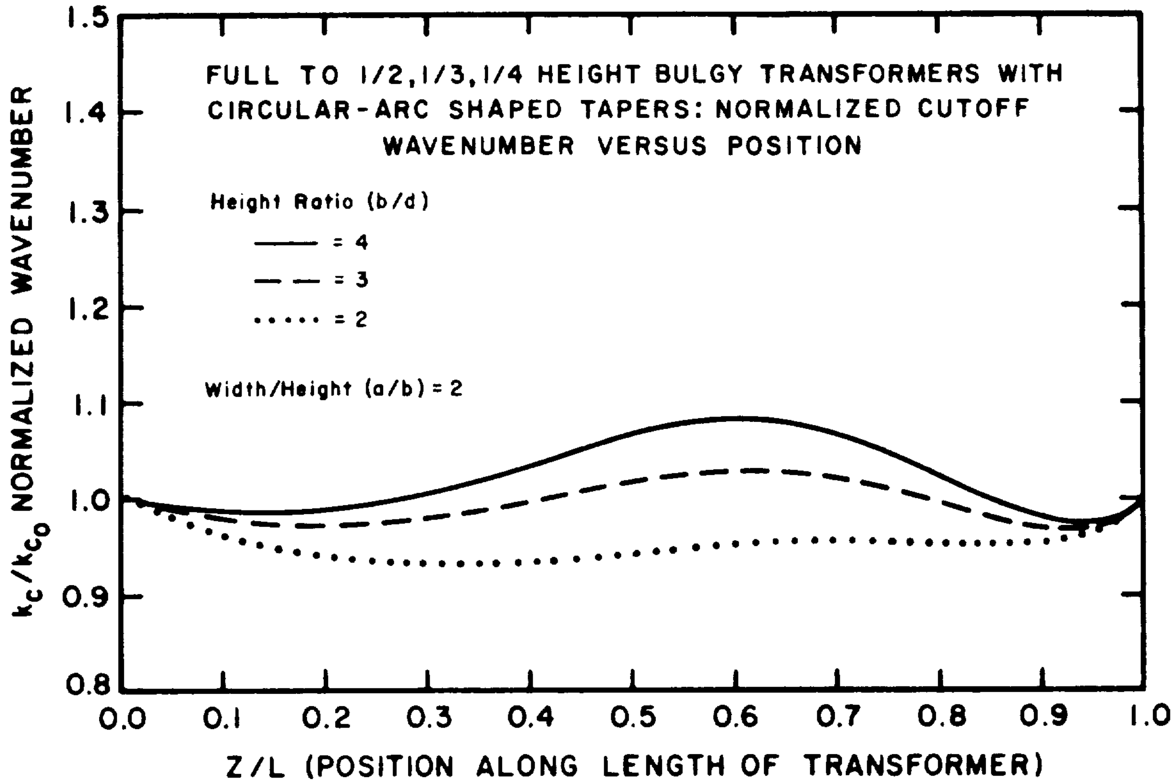

Fig. 7-17. Predicted normalized cutoff wave number versus position along the transition for three bulgy circular-arc shaped transformers with different height ratios. The cutoff wavenumber is normalized to that in the rectangular guide at the start of the taper ($k_{c_0}=2\pi/4a$) where the width to height ratio (a/b) is 2:1. The curves should be compared to the corresponding bulgeless designs of Fig. 7-13.

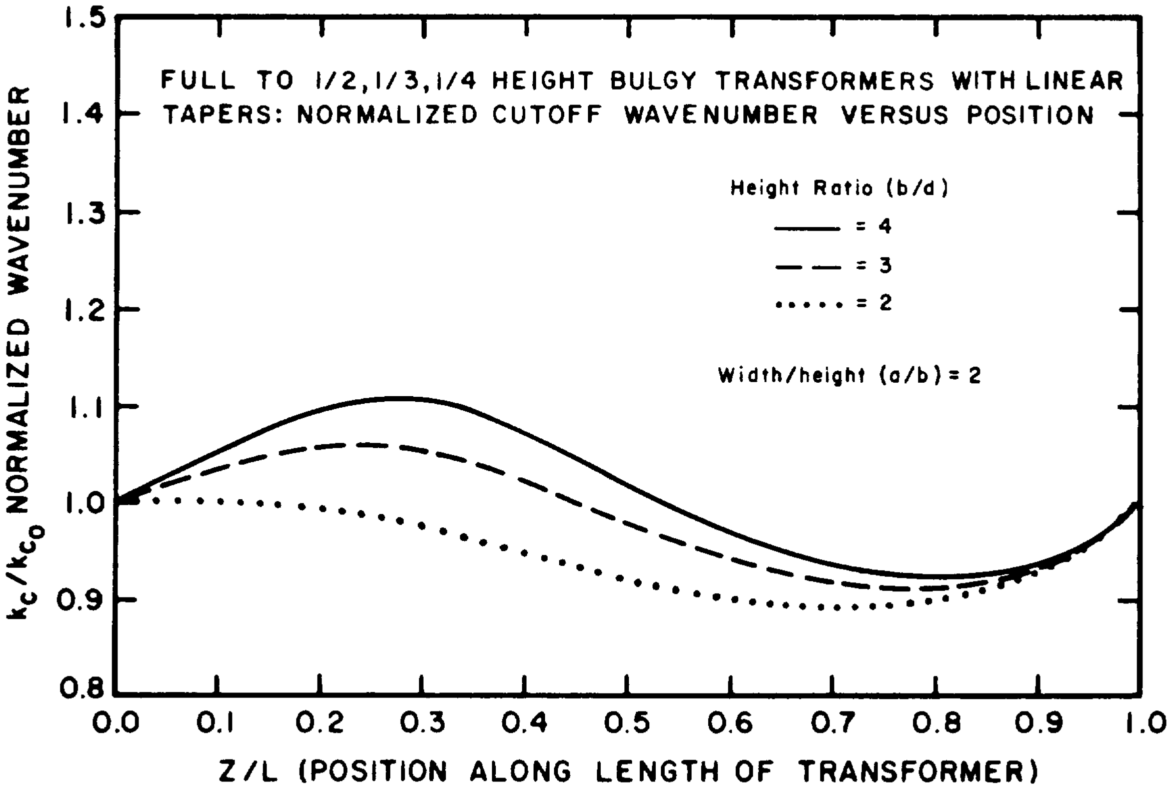

Fig. 7-18. Predicted values of the normalized cutoff wavenumber versus position along the transition for three linearly tapered, bulgy transformers with different height ratios. The same conditions apply as those of Fig. 7-17. These curves should be compared to the corresponding bulgeless designs in Fig. 7-14.

maxima have been reduced significantly compared with the corresponding bulgeless transformers of Figs. 7-13 and 7-14. The analysis indicates that transformers with circular-arc shaped tapers will perform better than those with linear tapers when a bulge is added to the width of the reduced height section. Using this design it is possible to reduce the VSWR to less than 1.2 over the full waveguide band.

To check the accuracy of the analysis of the bulgy transformer a bulge was made in the full to one-quarter-height X-band channel waveguide transformer described in Section 7.4. The bulge increased the waveguide width by 37% at the maximum and extended over the full length of the taper. The measured and predicted performance are compared in Fig. 7-19.

The difference between the experimental and theoretical curves here is greater than in the non-bulgy cases. This may be due to the fact that coupling between the fundamental and higher order evanescent modes, especially the TE_{30} mode (see Fig. 7-6), from one section of the taper to the next, ignored in the analysis, has a greater affect in the bulgy tranformers. It is clear, nonetheless, that the addition of a bulge to the transformer results in a significant improvement in low frequency performance.

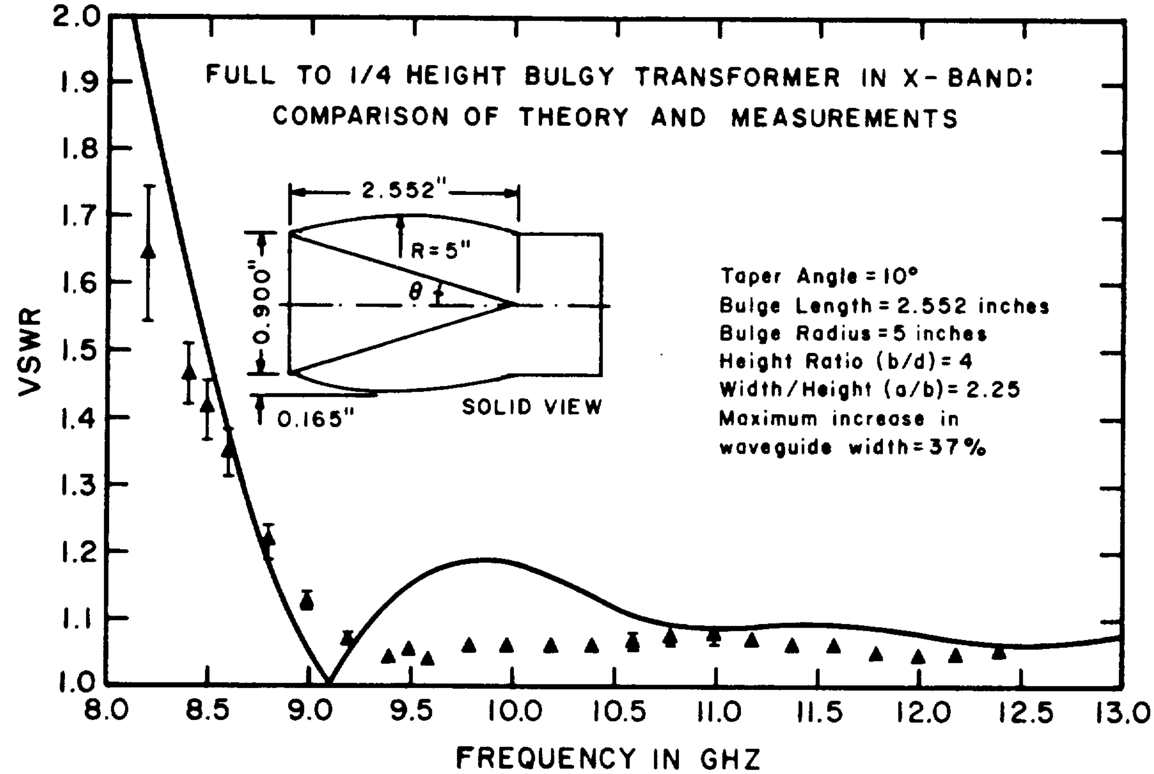

Fig. 7-19. Measured and predicted VSWR versus frequency for a full to 1/4 height bulgy transformer at X-band. The transformer is the same as that shown in Fig. 7-4 with the addition of a bulge in the reduced height waveguide which extends over the full length of the taper. The bulge was made with a rotary milling head, whose effective cutting radius was 5 inches, and increases the width of the guide by 37% at the midpoint of the transformer. The taper half angle of the linear transition is 10 degrees, yielding a transformer length of 6.482 cm. Note that at the high frequency end of the band the TE_{30} mode can propagate in part of this transition (see Fig. 7-6). The error bars reflect the mismatch uncertainties of the sliding load.

7.7 Summary

In this chapter we have described a new type of easily fabricated H-plane waveguide transformer. The results of a theoretical analysis of the structure agree fairly well with measurements made on X-band transformers with input to output height ratios of 2, 3, and 4. Two basic versions of the new design were analyzed and the results presented graphically. The analysis indicates that in its simplest form the transformer is not usable at the lower end of its waveguide band when the height ratio is large. For high-ratio transitions a two-stage transformer gives better results. The bandwidth of the single-stage transformer can be increased to cover the full waveguide band by increasing the width of the reduced height waveguide in the tapered region. Analysis indicates that the performance of transitions with high impedance ratios could be improved dramatically with only a small increase in waveguide width. Using the same slitting saw to form the reduced height waveguide, the transition section, and the bulge in the width, no additional complication is added to the fabrication process. Measurements of the VSWR of a bulgy full-to one-quarter-height transformer at X-band confirmed the predictions of the computer analysis although agreement with theoretical results was not as close as it was for the unmodified transformers.

7.8 Approximations in the Analysis

The design curves given here should be sufficient in most cases to achieve transformers with a VSWR < 1.2 over a full waveguide band. However it is important to ask why the measured and computed results showed consistent discrepancies at low VSWR's, and in the case of the bulgy transformer, why the low frequency results were not in closer agreement. As mentioned in Section 7.6.2 the assumption that there is no coupling between the fundamental and higher order evanescent modes in the transition is a possible source of error.

The somewhat arbitrary choice of the voltage and current variables used to define the characteristic impedance of the channel waveguide, discussed in Section 7.3.1 is justified only in that it gives good agreement between theory and experiment. The same definition was used by [28] and [113] in their analysis of ridged waveguides.

The approximations inherent in the transverse resonance and characteristic impedance methods lead to errors whose magnitude are difficult to estimate. These uncertainties might be circumvented if a finite difference technique [137] for determining the fields in the transformer were combined with the complete mode coupling theory of Solymar [155].

7.9 Applications

The channel waveguide transformer is particularly suitable for use at millimeter wavelengths where the fabrication of conventional step and tapered transformers is difficult and expensive. The transformer can be formed in a split-block waveguide structure using a single set up on a milling machine. The block is split in the E-plane which has zero transverse current, and hence poor contact along the joint line will cause no loss.

The full-to one-half-height channel waveguide transformer with a circular-arc shaped taper was used in the solid state frequency multiplier described in Chapter 6. The equivalent full to one-quarter height design has been used in a mixer at 115 GHz. Fabrication time for these devices was reduced dramatically by employing the new transformer. The design is also useful as a transition from the crossed or channel waveguide [96, 100, 164, 171] to conventional rectangular waveguide.

APPENDIX 1. MIXER ANALYSIS PROGRAM

Program Statistics

Language: Fortran IV H Extended (enhanced)

Program Size: 36K (compiled code with library routines)

Execution Time: 2 seconds on an Amdahl 470/V6-II

Special Requirements: Complex Arithmetic
132 column printout

A1.1 Introduction

This appendix contains a listing of the mixer analysis program along with the output results from a sample run. The program implementation follows the theory of Chapter 2 and Appendices 2 and 3. The Fortran code is further elucidated in the many comment cards which adorn the program. Every effort has been made to make this program both flexible and user friendly, occasionally sacrificing both core space and execution speed.

The problem to be solved in the listing which follows is the analysis of a 180 GHz mixer with a known set of embedding impedances at six LO harmonic frequencies. The diode characteristics are typical of those found in the 140-220 GHz mixer which is the subject of this thesis.

A1.2 Listing of the Mixer Analysis Program

The following is a listing of the mixer analysis program in card image format (72 columns of text with 8 columns reserved for line numbers). The modifications to the program which are discussed in later appendices are numbered so as to fit between or replace the appropriate statements listed here.

```
C
C
C
C                          MIXER ANALYSIS PROGRAM
C
C    GENERAL INFORMATION
C
C    THIS PROGRAM ANALYZES MIXERS WITH A SINGLE SCHOTTKY-BARRIER DIODE
C  WHOSE I-V AND C-V CHARACTERISTICS ARE KNOWN. ARBITRARY EMBEDDING
C  IMPEDANCES AT THE SIDEBAND AND LO HARMONIC FREQUENCIES ARE ALLOWED.
C  THE DIODE MOUNT IS ASSUMED LOSSLESS AND RECIPROCAL.
C
C    THE PROGRAM IS SPLIT INTO TWO MAIN SECTIONS. THE FIRST PER-
C  FORMS A NONLINEAR ANALYSIS TO DETERMINE THE DIODE WAVEFORMS PRO-
C  DUCED BY THE LOCAL OSCILLATOR. THE SECOND PERFORMS A SMALL-SIGNAL
C  AND NOISE ANALYSIS TO COMPUTE THE CONVERSION LOSS, PORT IMPEDANCES,
C  AND NOISE TEMPERATURE OF THE MIXER.
C
C     THE NONLINEAR ANALYSIS IS BASED ON THE MULTIPLE REFLECTION
C   TECHNIQUE OF KERR (IEEE TRANS. MTT, MTT-23, NO.10, PP.828-831,
C   OCT.1975) , MODIFIED TO TAKE INTO ACCOUNT THE NONLINEAR CAPACITANCE
C   OF THE DIODE.
C
C     THE SMALL-SIGNAL AND NOISE ANALYSES ARE BASED ON THE WORK OF
C   HELD AND KERR (IEEE TRANS. MTT, MTT-26, NO.2, PP.49-61, FEB. 1978).
C
C
C    PROGRAM NOTES
C
C    TWO SUBROUTINES CONTROL THE ANALYSIS: LGSIG WHICH PERFORMS
C  THE NONLINEAR ANALYSIS AND SMSIG WHICH COMPUTES THE SMALL-
C  SIGNAL AND NOISE PROPERTIES OF THE MIXER. BOTH CALL A NUMBER OF
C  SECONDARY SUBROUTINES TO PERFORM SPECIFIC CALCULATIONS
C  OR CONTROL THE OUTPUTTING OF RESULTS.
C
C    ALL DATA IS INPUT VIA THE BLOCK DATA SUBPROGRAM. THE FOLLOWING
C  INFORMATION MUST BE SUPPLIED BY THE USER:
C
C  1) THE EMBEDDING IMPEDANCES AT THE LO FREQUENCY AND THE HIGHER
C     HARMONICS AS REAL AND IMAGINARY PARTS (ZER,ZEI) IN OHMS.
C  2) THE SIDEBAND IMPEDANCES IN COMPLEX FORM (ZEMBSB) IN OHMS,WHERE
C     SIDEBAND M IS ARRAY ELEMENT (NH/2+1-M) AND THERE ARE NH+1 ARRAY
C     ELEMENTS IN ALL.NOTE THAT,BECAUSE ALL LOWER SIDEBANDS ARE TREATED
C     AS NEGATIVE FREQUENCIES,VALUES OF ZEMBSB FOR LOWER SIDEBANDS MUST
C     BE THE CONJUGATES OF THEIR USUAL POSITIVE FREQUENCY VALUES.
C  3) THE LO FREQUENCY (FP) AND THE INTERMEDIATE FREQUENCY (IF) IN HZ.
C  4) THE DC OPERATING CURRENT (IDBIAS) OF THE MIXER IN AMPERES.
C  5) THE DC BIAS VOLTAGE ACROSS THE DIODE (VDBIAS) IN VOLTS.
C  6) THE MIXER OPERATING TEMPERATURE (TK) IN DEGREES K.
C  7) THE DIODE REVERSE SATURATION CURRENT (IS) IN AMPERES.
C  8) THE DIODE CAPACITANCE AT ZERO VOLTS (C0) IN FARADS.
```

```
C   9) THE DIODE BUILT IN POTENTIAL (PHI) IN VOLTS.
C   10) THE DIODE CAPACITANCE LAW EXPONENT (GAM).
C   11) THE DIODE IDEALITY FACTOR (ETA)
C   12) THE DIODE SERIES RESISTANCE AT DC OR THE FOLLOWING DIODE
C       CHARACTERISTICS FROM WHICH THE SERIES RESISTANCE WILL BE
C       CALCULATED: THE ANODE RADIUS (AR) IN CM, THE DIODE CHIP
C       DIMENSIONS (CW,CL,CT) IN CM, THE SUBSTRATE AND EPI LAYER
C       DOPING DENSITIES (NDS,NDE) IN CM-3, THE SUBSTRATE AND EPI LAYER
C       CARRIER MOBILITIES (SMOB,EMOB) IN CM2/V-S, THE DIELECTRIC
C       CONSTANT OF THE SEMICONDUCTOR (ER), AND THE WHISKER PLUS
C       OHMIC CONTACT RESISTANCE (RC) IN OHMS.
C
C     THERE ARE SEVERAL OTHER VARIABLES WHICH MAY BE ADJUSTED TO
C   CONTROL THE OPERATION OF THE PROGRAM. THEIR VALUES HAVE BEEN
C   OPTIMIZED FOR THE LISTING WHICH FOLLOWS AND MAY BE ALTERED
C   WHEN THE PROGRAM IS USED TO SOLVE OTHER CIRCUITS.
C   THESE VARIABLES ARE:
C
C   ACC:THE ACCURACY OF THE RUNGE KUTTA INTEGRATION USED TO SOLVE THE
C       STATE EQUATION OF THE DIODE NETWORK.
C   IDCACC:THE ACCURACY WITH WHICH THE CALCULATED DC CURRENT MUST
C          APPROACH THE DESIRED VALUE (IDBIAS).
C   NCURR:THE NUMBER OF REFLECTION CYCLES BEFORE THE CALCULATED DC
C         CURRENT (IDCOS(1)) IS COMPARED TO THE DESIRED VALUE (IDBIAS).
C   NLO:THE NUMBER OF LO CYCLES NEEDED TO REACH A STEADY STATE IN THE
C       NONLINEAR ANALYSIS ROUTINE. SINCE SETTLING OCCURS IN SUCCESSIVE
C       REFLECTION CYCLES NLO CAN USUALLY BE SET TO ONE.
C   NPRINT:THE NUMBER OF CYCLES BETWEEN PRINTOUTS OF THE INTERMEDIATE
C          RESULTS IN THE NONLINEAR ANALYSIS.
C   NPTS:THE NUMBER OF INTERVALS+1 INTO WHICH THE LO CYCLE IS DIVIDED
C        FOR THE INTEGRATION AND STORAGE OF DATA POINTS. TO AVOID
C        ALIASING NPTS SHOULD BE CHOSEN CONSIDERABLY LARGER THAN
C        (2*NH+1), THE VALUE REQUIRED BY THE SAMPLING THEOREM.
C   VLO:THE INITIAL VALUE OF THE LOCAL OSCILLATOR VOLTAGE.
C   VLOINC:THE INITIAL INCREMENT SIZE USED TO ZERO IN ON THE DESIRED
C          DC RECTIFIED CURRENT (IDBIAS).
C   ZQACC: THE DEGREE OF CONVERGENCE OF THE FINAL SOLUTION IN THE NON-
C          LINEAR ANALYSIS.
C   Z0:THE CHARACTERISTIC IMPEDANCE OF THE HYPOTHETICAL TRANSMISSION
C      LINE INSERTED BETWEEN THE DIODE AND EMBEDDING NETWORK. Z0 MAY
C      HAVE A SIGNIFIGANT EFFECT ON THE RATE OF CONVERGENCE OF THE
C      NONLINEAR ANALYSIS.
C
C     THE USER MAY FIND IT NECESSARY TO ALTER OTHER PROGRAM VARIABLES
C   FOR SPECIFIC PROBLEMS. FOR THIS REASON A LIST OF THE
C   VARIABLES (EXCEPT THOSE INTERNAL TO THE IBM SSP ROUTINES),
C   SUBROUTINES AND COMMON BLOCKS USED IN THE PROGRAM FOLLOWS.
C
C
C     LIST OF VARIABLES
C
C   A: THE SMALL-SIGNAL AUGMENTED ADMITTANCE (Y') OR IMPEDANCE (Z')
C      MATRIX OF THE MIXER.
C   ACC: THE INTEGRATION ACCURACY USED IN DRKGS.
C   ALP: THE DIODE I-V LAW EXPONENT (Q/NKT).
```

```
C  AR: THE DIODE ANODE RADIUS IN CM.
C  AUX: DRKGS STORAGE ARRAY OF DIMENSION (8,NDIM).
C  BLANK: A NUMERIC USED FOR PLOTTING A BLANK.
C  BOLTZ: BOLTZMANN'S CONSTANT.
C  CJ: FREQUENCY SCALED DIODE JUNCTION CAPACITANCE USED IN LGSIG.
C  CJCOS: FOURIER COSINE COEFFICIENTS OF THE DIODE CAPACITANCE.
C  CJDATA: STORAGE ARRAY CONTAINING THE DIODE CAPACITANCE FOR EACH
C          OF THE NPTS POINTS IN THE LOCAL OSCILLATOR CYCLE.
C  CJMAG: THE MAGNITUDES OF THE FOURIER CAPACITANCE COEFFICIENTS.
C  CJPHA: PHASES OF THE FOURIER CAPACITANCE COEFFICIENTS (IN DEGREES).
C  CJPOS: POSITION OF CJ IN THE PLOT OF DIODE CAPACITANCE.
C  CJSIN: FOURIER SINE COEFFICIENTS OF THE DIODE CAPACITANCE.
C  CL: THE DIODE CHIP LENGTH IN CM.
C  COR: THE NOISE CURRENT CORRELATION MATRIX.
C  CR1: THE EQUIVALENT RADIUS OF THE DIODE CHIP FACE IN CM.
C  CR2: THE EQUIV. RADIUS OF THE CYLINDER REPRESENTING THE DIODE CHIP
C  CT: THE THICKNESS (HEIGHT) OF THE DIODE CHIP IN CM.
C  CW: THE WIDTH OF THE DIODE CHIP IN CM.
C  CØ: THE DIODE CAPACITANCE AT ZERO VOLTS (IN FARADS).
C  CØPOS: POSITION OF CØ IN THE GRAPH OF THE DIODE CAPACITANCE.
C  DERY: INITIALLY THE RKGS ERROR PARAMETER AND LATER THE DERIVATIVE
C        IN THE NETWORK STATE EQUATION (DY(1)/DT).
C  DET: DETERMINANT OF  A (Y')  AS RETURNED BY THE CMINV ROUTINE.
C  DOT: A NUMERIC USED FOR PLOTTING A DOT.
C  EMOB: THE CARRIER MOBILITY IN THE DIODE EPI LAYER (CM2/V-S).
C  EPS:  THE ELECTRIC PERMITTIVITY OF FREE SPACE.
C  ER: THE RELATIVE DIELECTRIC CONSTANT OF THE DIODE SEMICONDUCTOR.
C  ETA: THE DIODE IDEALITY FACTOR.
C  FC: COMPLEX FOURIER COEFFICIENTS OF THE DIODE CAPACITANCE.
C  FG: COMPLEX FOURIER COEFFICIENTS OF THE DIODE CONDUCTANCE.
C  FP: THE LOCAL OSCILLATOR OR PUMP FREQUENCY IN HERTZ.
C  GAM: THE DIODE CAPACITANCE EXPONENT.
C  GJ: THE DIODE CONDUCTANCE.
C  GJCOS: FOURIER COSINE COEFFICIENTS OF THE DIODE CONDUCTANCE.
C  GJDATA: STORAGE ARRAY CONTAINING THE VALUES OF THE DIODE
C          CONDUCTANCE FOR EACH OF THE NPTS POINTS IN THE LO CYCLE.
C  GJMAG: MAGNITUDES OF THE FOURIER CONDUCTANCE COEFFICIENTS.
C  GJPHA: PHASES OF THE FOURIER CONDUCTANCE COEFFICIENTS (IN DEGREES).
C  GJSIN: FOURIER SINE COEFFICIENTS OF THE DIODE CONDUCTANCE.
C  ICJ: THE CURRENT THROUGH THE DIODE CAPACITANCE
C  ICJDAT: STORAGE ARRAY FOR ICJ AT EACH POINT IN THE LO CYCLE.
C  ID: THE CURRENT AT THE DIODE TERMINALS.
C  IDBIAS: DESIRED RECTIFIED CURRENT AT WHICH THE MIXER IS TO BE
C          OPERATED (IN AMPS).
C  IDCACC: DESIRED ACCURACY OF THE CALCULATED DC CURRENT,MEASURED AS
C          THE MAXIMUM TOLERABLE DEVIATION FROM THE DESIRED DC CURRENT,
C          IDBIAS.
C  IDCOS: FOURIER COSINE COEFFICIENT OF THE TOTAL DIODE CURRENT.
C  IDDATA: STORAGE ARRAY CONTAINING THE VALUES OF THE TOTAL DIODE
C          CURRENT FOR EACH OF THE NPTS POINTS IN THE LO CYCLE.
C  IDPOS: POSITION OF ID ON THE GRAPH OF TOTAL CURRENT IN THE DIODE.
C  IDSIN: FOURIER SINE COEFFICIENT OF THE TOTAL DIODE CURRENT.
C  IER: THE ERROR MESSAGE CODE OF SUBROUTINE DFORIT.
C  IF: THE INTERMEDIATE FREQUENCY IN HERTZ.
C  IGJ: THE CURRENT THROUGH THE DIODE CONDUCTANCE.
```

```
C   IGJDAT: STORAGE ARRAY CONTAINING VALUES OF THE DIODE CONDUCTANCE
C           CURRENT FOR EACH OF THE NPTS POINTS IN THE LO CYCLE.
C   IGJPOS: POSITION OF IGJ ON THE GRAPH OF DIODE CONDUCTANCE CURRENT.
C   IHLF: DRKGS PARAMETER GIVING THE NUMBER OF TIMES THE INTEGRATION
C         INTERVAL HAS BEEN HALVED OR DOUBLED.
C   IMZIN: IMAGINARY PART OF THE INPUT IMPEDANCE AT EACH SIDEBAND.
C   IPT: A COUNTING VARIABLE USED TO DETERMINE THE POSITION ALONG AN
C        LO CYCLE. IPT COUNTS THE NUMBER OF LO CYCLE INTERVALS WHICH
C        HAVE PASSED SINCE THE RKGS INTEGRATION BEGAN.
C   IS: DIODE SATURATION CURRENT (IN AMPS).
C   ITER: LOOP REPRESENTING THE REFLECTION CYCLES IN THE NONLINEAR
C         ANALYSIS .
C   IVLO: COUNTING VARIABLE USED TO SIGNAL THE END OF THE JLO LOOP.
C   JH: LOOP OVER THE LO HARMONICS
C   JLO: LOOP OVER THE NUMBER OF LO CYCLES REQUIRED TO REACH
C        A STEADY STATE.
C   JPRINT: KEEPS TRACK OF THE CYCLES WHOSE RESULTS ARE TO BE PRINTED.
C   JPT: LOOP OVER THE NUMBER OF POINTS IN AN LO CYCLE
C   JVLO: LOOP FOR ZEROING IN ON THE DESIRED RECTIFIED CURRENT (IDBIAS).
C   LIJ: CONVERSION LOSS FROM SIDEBAND J TO SIDEBAND I.
C   LOFLAG: A FLAG TO KEEP COUNT OF THE NUMBER OF TIMES VLO HAS BEEN
C           LOWERED TO TRY AND OBTAIN THE DESIRED RECTIFIED CURRENT.
C   LOPWR: THE REQUIRED LO POWER FOR A RECTIFIED CURRENT OF IDBIAS.
C   LOVLO: THE LOWER BOUND OF THE VLO ADJUSTMENT DONE IN SUBROUTINE
C          ADJVLO.
C   MAXCJ: MAXIMUM VALUE OF CJ IN AN LO CYCLE (USED FOR PLOTTING).
C   MAXID: MAXIMUM VALUE OF ID IN AN LO CYCLE (USED FOR PLOTTING).
C   MAXIGJ: MAXIMUM VALUE OF IGJ IN AN LO CYCLE (USED FOR PLOTTING).
C   MAXVD: MAXIMUM VALUE OF VD IN AN LO CYCLE (USED FOR PLOTTING).
C   MINCJ: MINIMUM VALUE OF CJ IN AN LO CYCLE (USED FOR PLOTTING).
C   MU: THE MAGNETIC PERMEABILITY OF FREE SPACE.
C   NCURR: THE NUMBER OF REFLECTION CYCLES DURING THE VLO ADJUSTMENT
C          LOOP BEFORE WHICH IDCOS(1) IS COMPARED TO IDBIAS.
C   NDE: THE DOPING CONCENTRATION IN THE DIODE EPI LAYER IN CM-3.
C   NDIM: THE NUMBER OF DIFFERENTIAL EQUATIONS TO BE SOLVED BY DRKGS.
C   NDS: THE DOPING CONCENTRATION IN THE DIODE SUBSTRATE IN CM-3.
C   NH: NUMBER OF LO HARMONICS CONSIDERED (MUST BE EVEN)
C   NHARM: USED IN PRINT1 AS THE TOTAL NUMBER OF LO HARMONICS.
C   NHD2: THE NUMBER OF LO HARMONICS DIVIDED BY TWO (UPPER SIDEBAND).
C   NHD2P1: THE NUMBER OF LO HARMONICS/2 + 1 (IF=SIDEBAND 0).
C   NHD2P2: THE NUMBER OF LO HARMONICS/2 + 2 (LOWER SIDEBAND).
C   NHP1: THE TOTAL NUMBER OF LO HARMONICS PLUS ONE (# OF SIDEBANDS).
C   NHP2: THE NUMBER OF LO HARMONICS PLUS 2.
C   NITER: TOTAL NUMBER OF ITERATIONS ALLOWED FOR ACHIEVING FULL CONVER-
C          GENCE AFTER THE DESIRED RECTIFIED CURRENT HAS BEEN OBTAINED.
C   NLO: THE TOTAL NUMBER OF LOCAL OSCILLATOR CYCLES TO BE INTEGRATED
C        THROUGH IN ORDER TO REACH A STEADY STATE.
C   NPRINT: CONTROLS THE REFLECTION CYCLE NUMBER AT WHICH THE PRINTING
C           OF THE INTERMEDIATE RESULTS OCCURS.
C   NPTS: THE NUMBER OF INTERVALS + 1 IN AN LO CYCLE.
C   NSB: SIDEBAND TO WHICH THE EQUIVALENT NOISE TEMPERATURE OF THE
C        MIXER IS REFERRED TO IN SUBROUTINE TMIX.
C   NVLO: THE LIMIT ON THE NUMBER OF TIMES THE LO VOLTAGE IS ADJUSTED.
C   PHI: DIODE CONTACT POTENTIAL (IN VOLTS).
C   PI: THE CONSTANT PI.
```

```
C  PRMT: ARRAY USED BY RKGS CONTAINING THE FOLLOWING VARIABLES:
C         PRMT(1): THE LOWER BOUND OF THE INTEGRATION INTERVAL.
C         PRMT(2): THE UPPER BOUND OF THE INTEGRATION INTERVAL.
C         PRMT(3): THE INITIAL INTEGRATION INTERVAL STEP SIZE.
C         PRMT(4): THE INTEGRATION ACCURACY.
C         PRMT(5): ALLOWS HALTING OF THE RKGS ROUTINE IF SET TO Ø.
C  QEL: THE ELECTRONIC CHARGE.
C  RC: THE WHISKER AND OHMIC CONTACT RESISTANCE (USED IN RESIST).
C  REF: THE MAGNITUDE OF THE REFLECTION COEFFICIENT AT THE IF PORT
C       OF THE MIXER REFERRED TO 5Ø OHMS.
C  REPI: THE RESISTANCE OF THE DIODE EPI LAYER (USED IN RESIST).
C  REZIN: REAL PART OF THE INPUT IMPEDANCE AT EACH SIDEBAND.
C  RHO: THE COMPLEX VOLTAGE REFLECTION COEFFICIENT OF THE EMBEDDING
C       NETWORK (INCLUDING RS) AT EACH LO HARMONIC.
C  RHODC: THE REFLECTION COEFFICIENT OF THE EMBEDDING NETWORK
C         PLUS SERIES RESISTANCE, AT DC.
C  R1SUB:  AC RESISTANCE OF DIODE TO LATERAL CURRENT FLOW.
C  RS: LOW FREQUENCY DIODE SERIES RESISTANCE. RS IS EITHER INPUT IN
C      BLOCK DATA OR FORMED IN SUBROUTINE RESIST.
C  RSB: THE REAL PART OF THE DIODE SERIES RESISTANCE AT THE
C       SIDEBAND FREQUENCIES (USED IN RESIST).
C  RSLO: THE REAL PART OF THE DIODE SERIES RESISTANCE AT THE LO
C        HARMONIC FREQUENCIES.
C  RSSB: COMPLEX DIODE SERIES RESISTANCE AT THE SIDEBAND FREQUENCIES.
C  RSUB: THE DIODE SUBSTRATE RESISTANCE (USED IN RESIST).
C  R2SUB:  AC RESISTANCE TO CURRENT FLOW DOWN SIDES OF DIODE.
C  SEPI: THE CONDUCTIVITY IN THE DIODE EPI LAYER (USED IN RESIST)
C  SHLSB: THE SHOT NOISE TEMPERATURE REFERRED TO THE LOWER SIDEBAND
C  SHUSB: THE SHOT NOISE TEMPERATURE REFERRED TO THE UPPER SIDEBAND
C  SKIN: THE SKIN DEPTH IN THE DIODE SUBSTRATE (USED IN RESIST).
C  SMOB:  THE CARRIER MOBILITY IN THE DIODE SUBSTRATE (CM2/V-S).
C  SSUB: THE CONDUCTIVITY IN THE DIODE SUBSTRATE (USED IN RESIST).
C  STAR: A NUMERIC USED FOR PLOTTING AN ASTERISK.
C  T: INTERMEDIATE VARIABLE IN THE MIXER TEMPERATURE CALCULATION.
C  TE: THE THICKNESS OF THE DIODE EPI LAYER IN CM.
C  THLSB: THE THERMAL NOISE TEMPERATURE REFERRED TO THE LOWER SIDEBAND.
C  THUSB: THE THERMAL NOISE TEMPERATURE REFERRED TO THE UPPER SIDEBAND.
C  TK: THE MIXER OPERATING TEMPERATUR IN KELVIN.
C  TMLSB: THE SINGLE SIDEBAND MIXER NOISE TEMPERATURE AT THE IMAGE.
C  TMUSB: THE SINGLE SIDEBAND MIXER NOISE TEMPERATURE AT THE SIGNAL.
C  TX: USED IN OUTP TO TEST THE CURRENT POSITION IN THE LO CYCLE
C      DURING THE DRKGS INTEGRATION. IF THIS POSITION IS AN INTEGRAL
C      NUMBER OF 1/(NPTS-1), THE INTERVAL USED IN DIVIDING UP THE
C      LO CYCLE, THEN THE DIODE WAVEFORM DATA IS STORED FOR SUBSEQUENT
C      USE.
C  UPFLAG: A FLAG TO KEEP COUNT OF THE NUMBER OF TIMES VLO HAS BEEN
C          RAISED TO TRY AND GET THE DESIRED RECTIFIED CURRENT IDBIAS.
C  UPVLO: THE UPPER BOUND OF VLO DURING ADJUSTMENTS DONE IN ADJVLO.
C  VD: THE VOLTAGE ACROSS THE DIODE (WITHOUT THE SERIES RESISTANCE).
C  VDBIAS: THE DC BIAS VOLTAGE ACROSS THE DIODE AND SERIES RESISTANCE.
C  VDC: THE THEVENIN EQUIVALENT DC VOLTAGE SEEN BY THE DIODE.
C  VDCOS: FOURIER COSINE COEFFICIENTS OF THE VOLTAGE ACROSS THE DIODE.
C  VDDATA: STORAGE ARRAY CONTAINING Y(1),THE VOLTAGE ACROSS THE DIODE
C          AT EACH OF THE NPTS POINTS IN THE LO CYCLE.
C  VDINIT: INITIAL GUESS FOR THE VOLTAGE ACROSS THE DIODE.
```

```
C   VDPOS: POSITION OF VD ON THE GRAPH OF THE VOLTAGE ACROSS THE DIODE.
C   VDSIN: FOURIER SINE COEFFICIENTS OF THE VOLTAGE ACROSS THE DIODE.
C   VL: LEFT TRAVELING WAVE ON THE TRANSMISSION LINE
C   VLDC: LEFT TRAVELING DC WAVEFORM ON THE TRANSMISSION LINE
C   VLO: THEVENIN EQUIVALENT LO VOLTAGE SOURCE SEEN BY THE DIODE.
C   VLOINC: AMOUNT BY WHICH THE LO VOLTAGE IS INCREMENTED WHEN TRYING
C           TO OBTAIN THE DESIRED DC CURRENT IDBIAS.
C   VR: RIGHT TRAVELING WAVEFORM ON THE TRANSMISSION LINE.
C   VRDC: RIGHT TRAVELING DC WAVE ON THE TRANSMISSION LINE
C   VS: THE SUM OF THE VOLTAGES WHICH MAKE UP THE EQUIVALENT CIRCUIT
C       OF THE HYPOTHETICAL TRANSMISSION LINE WHEN THE RIGHT TRAVELING
C       WAVE IS INCIDENT ON THE DIODE TERMINALS.
C   VSQ: MEAN SQUARE OUTPUT NOISE VOLTAGE.
C   VSWR: THE STANDING WAVE RATIO AT THE MIXER IF PORT REFERRED TO
C         50 OHMS.
C   WIF: 2*PI*INTERMEDIATE FREQUENCY.
C   WK1: WORK SPACE USED IN THE MATRIX INVERSION ROUTINE CMINV.
C   WK2: WORK SPACE USED IN THE MATRIX INVERSION ROUTINE CMINV.
C   WN: THE DIODE DEPLETION LAYER WIDTH AT VDBIAS.
C   WP: 2*PI*PUMP FREQUENCY.
C   X: THE DEPENDENT VARIABLE IN DRKGS (X=2*PI*FP*TIME).
C   XLMAT: THE CONVERSION LOSS MATRIX WHICH GIVES THE CONVERSION
C          LOSSES BETWEEN PAIRS OF SIDEBANDS.
C   XSB: THE IMAGINARY PART OF THE DIODE SERIES RESISTANCE AT THE
C        SIDEBAND FREQUENCIES (USED IN RESIST).
C   XSLO: THE IMAGINARY PART OF THE DIODE SERIES RESISTANCE AT THE
C         LO AND HARMONIC FREQUENCIES.
C   Y: DRKGS VARIABLE TO BE FOUND (Y=VOLTAGE ACROSS THE DIODE WITHOUT
C      THE SERIES RESISTANCE).
C   YCPOS: USED FOR PLOTTING THE DIODE CAPACITANCE.
C   YGPOS: USED FOR PLOTTING THE CURRENT THROUGH THE DIODE CONDUCTANCE.
C   YIDPOS: USED FOR PLOTTING THE TOTAL DIODE CURRENT.
C   YPT: A DO LOOP VARIABLE USED FOR PLOTTING POINTS ACROSS A PAGE.
C   YVDPOS: USED FOR PLOTTING THE VOLTAGE ACROSS THE DIODE.
C   ZEI: IMAGINARY PART OF THE EMBEDDING IMPEDANCE AT EACH LO HARMONIC.
C   ZEMB: COMPLEX EMBEDDING IMPEDANCE AT EACH LO HARMONIC INCLUDING
C         THE DIODE SERIES RESISTANCE.
C   ZEMBSB: THE EMBEDDING IMPEDANCES AT THE SIDEBAND FREQUENCIES
C           WITHOUT THE DIODE SERIES RESISTANCE.
C   ZER: REAL PART OF THE EMBEDDING IMPEDANCE AT EACH LO HARMONIC.
C   ZIFOUT: IMPEDANCE AT THE MXER IF PORT.
C   ZIN: INPUT IMPEDANCES AT THE MIXER SIDEBAND PORTS.
C   ZQ: IMPEDANCE QUOTIENT (VD/ID)/(ZE+RS) AT EACH HARMONIC
C       USED TO CALCULATE THE LARGE SIGNAL CONVERGENCE PARAMETER.
C   ZQACC: DESIRED DEGREE OF CONVERGENCE MEASURED AS THE DEVIATION FROM
C          UNTIY OF (THE IMPEDANCE AT THE DIODE/EMBEDDING IMPEDANCE).
C   ZQFLAG: THE NUMBER OF HARMONICS WHICH HAVE NOT YET CONVERGED IN A
C           PARTICULAR CYCLE OF THE NONLINEAR ANALYSIS.
C   ZQMAG: MAGNITUDE OF THE IMPEDANCE QUOTIENT (ZQ).
C   ZQPHA: PHASE OF THE IMPEDANCE QUOTIENT (ZQ) IN DEGREES.
C   Z0: CHARACTERISTIC IMPEDANCE OF THE HYPOTHETICAL TRANSMISSION LINE
C       INSERTED BETWEEN THE DIODE AND THE EMBEDDING NETWORK.
C
C
C     LIST OF SUBROUTINES
```

```
C
C  ADJVLO: SUBROUTINE FOR ADJUSTING THE LOCAL OSCILLATOR VOLTAGE UNTIL
C          THE CALCULATED DC CURRENT EQUALS IDBIAS.
C  CMINV: IBM SSP PROGRAM SLIGHTLY MODIFIED TO INVERT A COMPLEX MATRIX.
C  CORREL: SUBROUTINE FOR FORMING THE NOISE CORRELATION MATRIX.
C  DFORIT: DOUBLE PRECISION VERSION OF AN IBM SSP PROGRAM WHICH
C          PERFORMS A FOURIER ANALYSIS ON A PERIODIC WAVEFORM.
C  DRKGS: AN IBM SSP PROGRAM WHICH SOLVES A SYSTEM OF DIFFERENTIAL
C         EQUATIONS USING A RUNGE-KUTTA ALGORITHM.
C  FCT: SUBROUTINE,FOR USE WITH DRKGS,CONTAINING THE NETWORK STATE
C       EQUATION.
C  LGSIG: CONTROL PROGRAM FOR THE LARGE-SIGNAL,NONLINEAR ANALYSIS.
C  OUTP: OUTPUT ROUTINE REQUIRED BY DRKGS AND USED TO SAVE THE DIODE
C        WAVEFORM RESULTS AT EACH OF THE POINTS ALONG AN LO CYCLE.
C  PLOT: SUBROUTINE FOR PLOTTING THE LARGE-SIGNAL DIODE WAVEFORMS.
C  POWER: CALCULATES THE LO POWER REQUIRED TO MAINTAIN AN OPERATING
C         CURRENT OF IDBIAS.
C  PRINT1: CONTROLS THE PRINTING OF INITIAL VALUES.
C  PRINT2: CONTROLS THE PRINTING OF VARIABLES FOR A PARTICULAR CYCLE
C          OF THE NONLINEAR ANALYSIS.
C  PRINT3: WRITES THE FOURIER COEFFICIENTS OF THE DIODE CONDUCTANCE
C          AND CAPACITANCE.
C  PRINT4: PRINTS THE RESULTS OF THE SMALL-SIGNAL AND NOISE ANALYSES.
C  RESIST: CALCULATES THE COMPLEX DIODE SERIES RESISTANCE AT THE LO
C          AND HARMONIC SIDEBANDS. RESIST WILL ALSO CALCULATE THE DC
C          RESISTANCE IF RS IS NOT KNOWN FROM MEASUREMENTS.
C  SMSIG: CONTROL PROGRAM FOR THE SMALL-SIGNAL AND NOISE ANALYSES.
C  TMIX: SUBROUTINE FOR CALCULATING THE EQUIVALENT NOISE TEMPERATURE
C        OF THE MIXER.
C  TNOISE: ADDS THE THERMAL NOISE COMPONENT TO THE CORRELATION MATRIX.
C  YPRIME: SUBROUTINE FOR FORMING THE AUGMENTED MATRIX Y'.
C  ZEMBED: FORMS THE EMBEDDING IMPEDANCES AT THE HARMONICS OF THE LO
C          AND AT THE HARMONIC SIDEBANDS.
C
C
C     LIST OF COMMON BLOCKS
C
C  COMMON/CONST/:CONTAINS CONSTANTS USED IN THE PROGRAM.
C  COMMON/DATA/:CONTAINS THE LARGE SIGNAL DIODE WAVEFORM DATA AT EACH
C               OF THE POINTS ALONG AN LO CYCLE (NPTS IN ALL).
C  COMMON/DIODE/:CONTAINS DIODE PARAMETERS.
C  COMMON/FORITS/:CONTAINS VARIABLES RETURNED BY DFORIT.
C  COMMON/IMPED/:CONTAINS INPUT EMBEDDING IMPEDANCES AND THE DIODE
C                SERIES RESISTANCE AT THE VARIOUS FREQUENCIES.
C  COMMON/IVMAG/:CONTAINS THE FOURIER COEFFICIENTS OF THE DIODE CON-
C                DUCTANCE AND CAPACITANCE IN MAGNITUDE AND PHASE.
C  COMMON/LOOPS/:CONTAINS THE LIMITS OF THE VARIOUS PROGRAM LOOPS.
C  COMMON/RES/:CONTAINS DATA USED IN THE CALCULATION OF THE DIODE
C              SERIES RESISTANCE.
C  COMMON/RKG/:CONTAINS THE INITIAL VALUES FOR THE DRKGS INTEGRATION.
C  COMMON/TLINE/:CONTAINS PARAMETERS EFFECTING THE CONVERGENCE OF THE
C                NONLINER ANALYSIS.
C  COMMON/VLODAT/:CONTAINS VARIABLES USED IN THE ADJUSTMENT OF THE LO
C                 VOLTAGE TO GIVE A DC CURRENT OF IDBIAS.
C  COMMON/VOLTS/:CONTAINS VALUES OF THE CIRCUIT VOLTAGES AND CURRENTS.
```

```
C
C
C     BEGIN THE MIXER ANALYSIS.
C
C
C---CALL LGSIG TO DO THE LARGE SIGNAL ANALYSIS
      CALL LGSIG
C---CALL SMSIG TO DO THE SMALL-SIGNAL AND NOISE ANALYSES
      CALL SMSIG
      STOP
      END



      SUBROUTINE LGSIG
C
C     LGSIG PERFORMS THE NONLINEAR ANALYSIS OF THE MIXER TO DETERMINE
C   THE DIODE CONDUCTANCE AND CAPACITANCE WAVEFORMS PRODUCED BY THE
C   LOCAL OSCILLATOR.
C     THE OUTPUT INCLUDES:
C   1) VALUES OF THE INITIALIZED VARIABLES AND INPUT DATA.
C   2) THE EMBEDDING IMPEDANCES AND DIODE SERIES RESISTANCE AT THE
C      LO HARMONICS AND SIDEBAND FREQUENCIES.
C   3) THE RESULTS OF SOME OR ALL OF THE REFLECTION CYCLES.
C   4) THE RESULTS OF THE FINAL REFLECTION CYCLE.
C   5) THE REQUIRED LO POWER OF THE MIXER.
C   6) THE FOURIER COEFFICIENTS OF THE DIODE CONDUCTANCE AND
C      CAPACITANCE.
C   7) PLOTS OF THE DIODE VOLTAGE, TOTAL CURRENT, CONDUCTANCE CURRENT,
C      AND CAPACITANCE OVER A SINGLE LO CYCLE.
C
C      IF ARRAY DIMENSIONS ARE ALTERED BE SURE TO CHANGE THEM (IF
C   NEED BE) IN SUBROUTINES FCT,OUTP,SMSIG AND BLOCK DATA AS WELL.
C
C---THE VARIABLES USED IN THIS SUBROUTINE ARE AS FOLLOWS:
C---FOR COMMON/CONST/:
      REAL*8 QEL,BOLTZ,PI,TK,MU,EPS
C---FOR COMMON/DATA/:
      REAL*8 ICJDAT(51),IGJDAT(51),CJDATA(51),GJDATA(51)
      REAL*8  VDDATA(51),IDDATA(51)
C---FOR COMMON/DIODE/:
      REAL*8 ALP,ETA,PHI,GAM,C0,IS,RS,FP,WP,IF,IGJ,ICJ,GJ,CJ
C---FOR COMMON/FORITS/:
      REAL*8 GJCOS(7),GJSIN(7),CJCOS(7),CJSIN(7),VDCOS(7),VDSIN(7)
      REAL*8 IDCOS(7),IDSIN(7)
      INTEGER IER
C---FOR COMMON/IMPED/:
      COMPLEX*16 ZEMBSB(7),RSSB(7)
      REAL*8 LOPWR,ZER(6),ZEI(6),ZERDC,RSLO(6),XSLO(6)
C---FOR COMMON/LOOPS/:
      INTEGER NH,NLO,JLO,NVLO,NPTS,NCURR,IPT,NPRINT,NITER
C---FOR COMMON/RES/:
      REAL*8 ER,NDS,NDE,SMOB,EMOB,TE,AR,CL,CW,CT,RC
C---FOR COMMON/RKG/:
      REAL*8 ACC,VDINIT
```

```
      INTEGER NDIM
C---FOR COMMON/TLINE/:
      REAL*8 ZØ,ZQACC
      INTEGER ZQFLAG
C---FOR COMMON/VLODAT/:
      REAL*8 LOVLO,UPVLO,VLOINC,IDCACC
      INTEGER UPFLAG,LOFLAG
C---FOR COMMON/VOLTS/:
      COMPLEX*16 VR(6)
      REAL*8 VRDC,VLO,VDBIAS,IDBIAS
C---FOR VARIABLES NOT IN ANY COMMON BLOCKS:
      COMPLEX*16 RHO(6),ZEMB(6),VL(6),ID,VD,ZQ
      REAL*8 Y(1),DERY(1),PRMT(5),AUX(8,1)
      REAL*8 VLDC,VDC,RHODC,ZEMBDC
      REAL*8  ZQMAG(6),ZQPHA(6)
      INTEGER IHLF,ITER,IVLO,JVLO,JLO,JPT,JH,NHP1,NHD2,NHD2P1
C---THE COMMON BLOCKS USED ARE:
      COMMON/CONST/QEL,BOLTZ,PI,TK,MU,EPS
      COMMON/DATA/ICJDAT,IGJDAT,CJDATA,GJDATA,VDDATA,IDDATA
      COMMON/DIODE/ALP,ETA,PHI,GAM,CØ,IS,RS,FP,WP,IF,IGJ,ICJ,GJ,CJ
      COMMON/FORITS/GJCOS,GJSIN,CJCOS,CJSIN,VDCOS,VDSIN,IDCOS,IDSIN,IER
      COMMON/IMPED/LOPWR,ZER,ZEI,ZERDC,RSLO,XSLO,ZEMBSB,RSSB
      COMMON/LOOPS/NH,NLO,JLO,NVLO,NPTS,NCURR,IPT,NPRINT,NITER
      COMMON/RES/ER,NDS,NDE,SMOB,EMOB,TE,AR,CL,CW,CT,RC
      COMMON/RKG/ACC,VDINIT,NDIM
      COMMON/TLINE/ZØ,ZQACC,ZQFLAG
      COMMON/VLODAT/LOVLO,UPVLO,LOFLAG,UPFLAG,VLOINC,IDCACC
      COMMON/VOLTS/VR,VRDC,VLO,VDBIAS,IDBIAS
C---SINCE THE FCT AND OUTP SUBPROGRAMS ARE CALLED BY DRKGS THEY MUST BE
C---DEFINED EXTERNALLY
      EXTERNAL FCT,OUTP
C---DEFINE SOME USEFUL CONSTANTS
      NHP1=NH+1
      NHD2=NH/2
      NHD2P1=NH/2+1
      WP=2.ØDØ*PI*FP
      ALP=QEL/(ETA*BOLTZ*TK)
C---CALL ZEMBED TO FORM THE EMBEDDING IMPEDANCES
      CALL ZEMBED(ZER,ZEI,ZERDC,ZEMBSB,NH,NHP1,NHD2P1)
C---CALL RESIST TO FIND THE SERIES RESISTANCE AS A FUNCTION OF FREQ
      CALL RESIST(RSSB,RSLO,XSLO,VDBIAS,NH,NHP1,NHD2P1)
C---SET THE IMPEDANCE AT DC AND THE FIRST HARMONIC TO ZØ TO SPEED THE
C---ANALYSIS. THIS DOES NOT AFFECT THE DIODE WAVEFORMS.
      ZEMB(1)=DCMPLX(ZØ,Ø.ØDØ)
      ZEMBDC=ZØ
C---FORM THE SET OF COMPLEX IMPEDANCES WITH THE SERIES RESISTANCE ADDED
      DO 1 JH=2,NH
    1 ZEMB(JH)=DCMPLX(ZER(JH)+RSLO(JH),ZEI(JH)+XSLO(JH))
C---CALCULATE THE REFLECTION COEFFICIENT OF THE EMBEDDING NETWORK AT
C---EACH LO HARMONIC
      RHODC=(ZEMBDC-ZØ)/(ZEMBDC+ZØ)
      DO 13 JH=1,NH
   13 RHO(JH)=(ZEMB(JH)-ZØ)/(ZEMB(JH)+ZØ)
C---INITIALIZE THE VARIABLES FOR THE VLO ADJUSTMENT LOOP
      JVLO=1
```

```
      IVLO=NVLO
      UPFLAG=0
      LOFLAG=0
C---INITIALIZE VARIABLES FOR THE INTEGRATION BY DRKGS
      PRMT(1)=0.0D0
      PRMT(2)=2.0D0*PI
      PRMT(3)=PRMT(2)/DFLOAT(NPTS)
      PRMT(4)=ACC
      Y(1)=VDINIT
C---CALCULATE THE DC SOURCE VOLTAGE FROM THE GIVEN BIAS VOLTAGE,VDBIAS,
C---ACROSS THE DIODE PLUS SERIES RESISTANCE
      VDC=VDBIAS+IDBIAS*(ZEMBDC-RS)
C---THE INITIAL LEFT AND RIGHT TRAVELING WAVES ON THE TRANSMISSION LINE
      DO 2 JH=1,NH
      VL(JH)=DCMPLX(0.0D0,0.0D0)
    2 VR(JH)=DCMPLX(0.0D0,0.0D0)
C---THE DC TERMS
      VLDC=0.0D0
      VRDC=VDC*Z0/(Z0+ZEMBDC)
C---RETURN HERE IF THE LO VOLTAGE HAS BEEN ADJUSTED
   15 ITER=0
      VR(1)=VLO*Z0/(ZEMB(1)+Z0)
      IF(JVLO.NE.1) GOTO 3
C---INITIALIZE DRKGS ERROR WEIGHT
      DERY(1)=1.0D0
C---CALL PRINTI TO WRITE THE INITIAL CONDITIONS
      CALL PRINTI(ZEMB,ZERDC,ZEMBDC,ZER,ZEI,ZEMBSB,PRMT,Y,DERY,
     1VLO,VDBIAS,IDBIAS,RSSB,RSLO,XSLO,NH,NHP1,NHD2)
C---START THE REFLECTION CYCLE
    3 ITER=ITER+1
C---PRINT ONLY AFTER MULTIPLES OF NPRINT CYCLES HAVE BEEN COMPLETED
      JPRINT=MOD(ITER,NPRINT)
C---SOLVE THE NETWORK STATE EQUATION OVER ONE LO CYCLE
C---THE LOOP OVER THE NUMBER OF LO CYCLES TO REACH STEADY STATE
      DO 6 JLO=1,NLO
      IPT=1
      DERY(1)=1.0D0
      CALL DRKGS(PRMT,Y,DERY,NDIM,IHLF,FCT,OUTP,AUX)
    6 CONTINUE
C---CALL DFORIT TO FORM THE FOURIER COEFFICIENTS OF THE DIODE CURRENT
C---AND VOLTAGE. NOTE THAT THE COEFFICIENTS ARE THOSE OF THE
C---TRIGONOMETRIC FOURIER SERIES AND MUST BE CONVERTED INTO THE
C---SINGLE OR DOUBLE ENDED COMPLEX FOURIER SERIES COEFFICIENTS
C---FOR USE IN THE REST OF THE ANALYSIS. ALSO NOTE THAT THE FIRST
C---FOURIER COEFFICIENT HAS ALREADY BEEN MULTIPLIED BY 1/2 IN DFORIT.
      CALL DFORIT(VDDATA,NPTS/2,NH,VDCOS,VDSIN,IER)
      CALL DFORIT(IDDATA,NPTS/2,NH,IDCOS,IDSIN,IER)
C---SET THE FLAG FOR THE CONVERGENCE TESTS
      ZQFLAG=0
C---CALCULATE THE LEFT TRAVELING WAVE  ON THE TRANSMISSION LINE
C---THE MINUS SIGN COMES FROM THE CONVERSION OF THE TRIGONOMETRIC
C---FOURIER SERIES REPRESENTATION RETURNED BY DFORIT INTO THE SINGLE
C---ENDED COMPLEX EXPONENTIAL SERIES REPRESENTATION USED IN THE
C---LARGE SIGNAL ANALYSIS.
      DO 7 JH=1,NH
```

```
      VD=DCMPLX(VDCOS(JH+1),-VDSIN(JH+1))
      ID=DCMPLX(IDCOS(JH+1),-IDSIN(JH+1))
      VL(JH)=Ø.5DØ*(VD-ID*ZØ)
C---CALCULATE THE IMPEDANCE RATIOS AT EACH LO HARMONIC TO DETERMINE
C---THE DEGREE OF CONVERGENCE
      ZQ=VD/ID/ZEMB(JH)
      ZQMAG(JH)=CDABS(ZQ)
      ZQPHA(JH)=DATAN2(DIMAG(ZQ),DREAL(ZQ))*57.29577951DØ
      IF(JH.EQ.1) GOTO 7
      IF(ZQMAG(JH).GT.1.ØDØ+ZQACC) ZQFLAG=ZQFLAG+1
      IF(ZQMAG(JH).LT.1.ØDØ-ZQACC) ZQFLAG=ZQFLAG+1
    7 CONTINUE
C---THE LEFT TRAVELING WAVE AT DC
      VLDC=Ø.5DØ*(VDCOS(1)-ZØ*IDCOS(1))
      IF(JPRINT.NE.Ø) GOTO 9
C---CALL PRINT2 TO WRITE THE RESULTS OF THIS REFLECTION CYCLE
      IF(JVLO.NE.IVLO) GOTO 9
      CALL PRINT2(RHO,VL,VR,VDCOS,VDSIN,IDCOS,IDSIN,ZQMAG,ZQPHA,
     1VLDC,VRDC,RHODC,ITER,ZQFLAG,JVLO,NH,NHP1)
    9 CONTINUE
C---THE NEW RIGHT TRAVELING WAVE INCIDENT ON THE DIODE
      DO 1Ø JH=2,NH
   1Ø VR(JH)=VL(JH)*RHO(JH)
C---THE RIGHT TRAVELING WAVE AT DC AND THE FIRST HARMONIC
      VR(1)=RHO(1)*VL(1)+VLO*ZØ/(ZØ+ZEMB(1))
      VRDC=RHODC*VLDC+VDC*ZØ/(ZØ+ZEMBDC)
C---DON'T ADJUST THE DC CURRENT UNTIL WE HAVE RUN FOR ENOUGH CYCLES TO
C---REACH A STEADY STATE
      IF(ITER.NE.NCURR) GOTO 11
C---ADJUST THE DC CURRENT TO THE DESIRED VALUE BY CHANGING VLO
      CALL ADJVLO(JVLO,IVLO,VLO,IDCOS,IDBIAS,NHP1)
C---WAS THIS THE LAST VLO ADJUSTMENT LOOP?
      IF(JVLO.EQ.IVLO) GOTO 11
C---REPEAT THE ANALYSIS WITH A NEW VALUE OF VLO
      JVLO=JVLO+1
      GOTO 15
C---WAS THIS THE LAST REFECTION CYCLE ALLOWED?
   11 IF(ITER.EQ.NITER) GOTQ 12
C---HAS THE SOLUTION CONVERGED?
      IF(ZQFLAG.EQ.Ø.AND.JVLO.EQ.IVLO) GOTO 12
C---GO ON TO THE NEXT REFLECTION CYCLE
      GOTO 3
C---CALL PRINT2 TO WRITE THE RESULTS OF THE FINAL REFLECTION CYCLE
   12 CALL PRINT2(RHO,VL,VR,VDCOS,VDSIN,IDCOS,IDSIN,ZQMAG,ZQPHA,
     1VLDC,VRDC,RHODC,ITER,ZQFLAG,JVLO,NH,NHP1)
C---CALL POWER TO FIND THE REQUIRED LO POWER
      CALL POWER(IDCOS(2),IDSIN(2),ZER(1),ZEI(1),
     1RSLO(1),XSLO(1),VLO,ZØ,LOPWR)
C---UNSCALE THE CAPACITANCE VALUES (THEY WERE SCALED IN SUBROUTINE FCT
C---WHICH IS CALLED BY THE DRKGS INTEGRATION ROUTINE).
      DO 19 JPT=1,NPTS
   19 CJDATA(JPT)=CJDATA(JPT)/WP
C---FINISH THE ANALYSIS BY OBTAINING THE FOURIER COEFFICIENTS OF THE
C---DIODE CONDUCTANCE AND CAPACITANCE.
      CALL DFORIT(GJDATA,NPTS/2,NH,GJCOS,GJSIN,IER)
```

```
602.       CALL DFORIT(CJDATA,NPTS/2,NH,CJCOS,CJSIN,IER)
6Ø3. C---CALL PLOT TO PRINT THE DIODE WAVEFORMS IN THE TIME DOMAIN
6Ø4.       CALL PLOT (IGJDAT,CJDATA,VDDATA,IDDATA,NPTS,ITER,CØ)
6Ø5.       RETURN
6Ø6.       END
6Ø7.
6Ø8.
6Ø9.
61Ø.       SUBROUTINE ZEMBED(ZER,ZEI,ZERDC,ZEMBSB,NH,NHP1,NHD2P1)
611. C
612. C    ZEMBED FORMS THE EMBEDDING IMPEDANCES AT THE HARMONICS OF THE
613. C  LO AND AT THE SIDEBAND FREQUENCIES (ASSUMING THEY HAVE NOT BEEN
614. C  INPUT VIA THE BLOCK DATA PROGRAM).
615. C    NOTE THAT IF YOU WISH TO INPUT THE SIDEBAND EMBEDDING IMPEDAN-
616. C  CES THROUGH THE BLOCK DATA SUBPROGRAM THE SIDEBAND FREQUENCY NO-
617. C  TATION MUST BE TAKEN INTO ACCOUNT. ALL LOWER SIDEBAND EMBEDDING
618. C  IMPEDANCES (ZEMBSB(I) , I.GT.(NH/2)+1 ) SHOULD BE FORMED AS THE
619. C  COMPLEX CONJUGATES OF THEIR POSITIVE FREQUENCY VALUES. THIS IS
62Ø. C  CONSISTANT WITH THE USE OF NEGATIVE FREQUENCIES FOR ALL LOWER
621. C  SIDEBANDS. NOTE THAT SIDEBAND I IS ARRAY ELEMENT (NH/2 + 1 -I)
622. C  IN THIS FREQUENCY NOTATION.
623. C
624. C---THE VARIABLE TYPES USED IN THIS SUBROUTINE ARE AS FOLLOWS:
625.       COMPLEX*16 ZEMBSB(NHP1)
626.       REAL*8 ZER(NH),ZEI(NH),ZERDC
627.       INTEGER NH,NHP1,NHD2P1,K,I
628. C---IN THIS EXAMPLE THE EMBEDDING IMPEDANCES AT THE LO HARMONICS
629. C---AND AT THE SIDEBAND FREQUENCIES HAVE BEEN INPUT VIA THE BLOCK DATA
63Ø. C---SUBPROGRAM AND THUS THEY WILL NOT BE FORMED IN THIS SUBROUTINE
631.       RETURN
632.       END
633.
634.
635.       SUBROUTINE RESIST(RSSB,RSLO,XSLO,VDBIAS,NH,NHP1,NHD2P1)
636. C
637. C     RESIST CALCULATES THE DIODE SERIES RESISTANCE AT DC AND AT THE
638. C  LO AND SIDEBAND HARMONIC FREQUENCIES. IF THE DC RESISTANCE (RS)
639. C  IS TO BE CALCULATED REMOVE THE 'C*****' IN LINE 68Ø, OTHERWISE
64Ø. C  THE VALUE OF RS INPUT IN BLOCK DATA WILL BE USED.
641. C     THE RESISTANCE IS DEPENDENT ON DIODE GEOMETRY AND HERE A
642. C  RECTANGULAR CHIP WITH A CIRCULAR ANODE AT THE CENTER IS ASSUMED.
643. C  THE AC RESISTANCE IS CALCULATED UNDER THE ASSUMPTIONS THAT THE
644. C  FRONT FACE OF THE DIODE CHIP HAS A CYLINDRICAL SHAPE WHICH IS
645. C  EQUAL IN AREA TO THE ACTUAL RECTANGULAR SURFACE. IN ADDITION THE
646. C  RESISTANCE DUE TO THE CURRENT FLOW DOWN THE SIDE WALLS OF THE
647. C  DIODE CHIP IS FOUND BY ASSUMING THE CHIP IS CYLINDRICAL AND HAS A
648. C  RADIUS CR2 WHICH PRODUCES A CYLINDER OF SURFACE AREA EQUAL TO
649. C  THAT OF THE ACTUAL RECTANGULAR CHIP.
65Ø. C
651. C  THE VARIABLE TYPES USED ARE AS FOLLOWS:
652. C---FOR COMMON/CONST/:
653.       REAL*8 QEL,BOLTZ,PI,TK,MU,EPS
654. C---FOR COMMON/DIODE/:
655.       REAL*8 ALP,ETA,PHI,GAM,CØ,IS,RS,FP,WP,IF,IGJ,ICJ,GJ,CJ
656. C---FOR COMMON/RES/:
```

```
      REAL*8 ER,NDS,NDE,SMOB,EMOB,TE,AR,CL,CW,CT,RC
C---FOR VARIABLES NOT IN ANY COMMON BLOCKS:
      COMPLEX*16 RSSB(NHP1)
      REAL*8 RSB,XSB,RSLO(NH),XSLO(NH)
      REAL*8 WN,SSUB,SEPI,REPI,RSUB,R1SUB,R2SUB,SKIN,CR1,CR2
      INTEGER I,J,K,NH,NHP1,NHD2P1
C---THE COMMON BLOCKS USED ARE:
      COMMON/CONST/QEL,BOLTZ,PI,TK,MU,EPS
      COMMON/DIODE/ALP,ETA,PHI,GAM,CØ,IS,RS,FP,WP,IF,IGJ,ICJ,GJ,CJ
      COMMON/RES/ER,NDS,NDE,SMOB,EMOB,TE,AR,CL,CW,CT,RC
C  EQUIVALENT RADIUS OF THE FRONT FACE OF THE RECTANGULAR CHIP
      CR1=DSQRT(CL*CW/PI)
C  EQUIVALENT RADIUS OF A CYLINDER REPRESENTING CHIP'S SIDE WALLS
      CR2=(CL+CW)/PI
C DEPLETION LAYER WIDTH AT VDBIAS
      WN=DSQRT(2.ØDØ*ER*EPS*(PHI-VDBIAS-BOLTZ*TK/QEL)/QEL/NDE)
C  SUBSTRATE AND EPI LAYER CONDUCTIVITIES
      SEPI=QEL*EMOB*NDE
      SSUB=QEL*SMOB*NDS
C  CALCULATED DC RESISTANCE IN EPI LAYER AND SUBSTRATE
      RSUB=8.ØDØ/(SSUB*3.ØDØ*PI*PI*AR)
      REPI=DMAX1((TE-WN)/(SEPI*PI*AR*AR),Ø.ØDØ)
C  TOTAL DC RESISTANCE
C*****RS=REPI+RSUB+RC
C  AC RESISTANCE AT THE HARMONIC SIDEBANDS
      DO 4Ø I=1,NHP1
      K=NHD2P1-I
C  SKIN DEPTH
      SKIN=DSQRT(1.ØDØ/(PI*DABS(FP*K+IF)*MU*SSUB))
C  SPREADING RESISTANCE FROM ANODE TO EDGE OF CHIP (LATERAL FLOW)
      R1SUB=Ø.5DØ/(PI*SSUB*SKIN)*(DLOG(CR1/AR)+SKIN/AR*DATAN(CR1/AR))
C  RESISTANCE DUE TO FLOW DOWN THE SIDES OF THE CHIP(REAL PART)
      R2SUB=CT/(2.ØDØ*PI*CR2*SSUB*SKIN)
C  TOTAL RESISTANCE = DC(MEAS)*(AC(CALC)/DC(CALC))
      RSB=RS*(R1SUB+R2SUB+RC+REPI)/(REPI+RC+RSUB)
C  THE IMAGINARY PART OF THE RESISTANCE DUE TO FLOW DOWN THE SIDE
C  WALLS OF THE CHIP IS THE SAME AS THE REAL PART, R2SUB.
      XSB=R2SUB+DLOG(CR1/AR)/(2.ØDØ*PI*SSUB*SKIN)
      RSSB(I)=DCMPLX(RSB,XSB)
C---CONJUGATE THE LOWER SIDEBAND TERMS
      IF(K.GE.Ø) GOTO 4Ø
      RSSB(I)=DCONJG(RSSB(I))
   4Ø CONTINUE
C  AC RESISTANCE AT THE LO HARMONIC FREQUENCIES
      DO 5Ø I=1,NH
      SKIN=DSQRT(1.ØDØ/(PI*FP*I*MU*SSUB))
      R1SUB=Ø.5DØ/(PI*SSUB*SKIN)*(DLOG(CR1/AR)+SKIN/AR*DATAN(CR1/AR))
      R2SUB=CT/(2.ØDØ*PI*CR2*SSUB*SKIN)
      RSLO(I)=RS*(R1SUB+R2SUB+RC+REPI)/(REPI+RSUB+RC)
      XSLO(I)=R2SUB+DLOG(CR1/AR)/(2.ØDØ*PI*SSUB*SKIN)
   5Ø CONTINUE
      RETURN
      END
```

```
      SUBROUTINE POWER(IDCOS,IDSIN,ZER,ZEI,RSLO,XSLO,VLO,ZØ,LOPWR)
C
C     POWER CALCULATES AND PRINTS THE REQUIRED LO POWER USED BY THE
C  MIXER WITH ITS ORIGINAL VALUE OF ZE(1) (BEFORE IT WAS SET TO ZØ).
C
C---THE VARIABLE TYPES USED IN THIS SUBROUTINE ARE AS FOLLOWS:
      COMPLEX*16 VN
      REAL*8 ZER,ZEI,IDCOS,IDSIN,RSLO,XSLO,VLO,ZØ,LOPWR
C---THE COMPLEX PORTION OF THE NUMERATOR IN THE POWER EXPRESSION
      VN=VLO+DCMPLX(IDCOS,-IDSIN)*(DCMPLX(RSLO,XSLO)+
     1DCMPLX(ZER,ZEI)-ZØ)
C---THE REQUIRED LO POWER FOR AN LO IMPEDANCE OF ZER(1),JZEI(1)
      LOPWR=(CDABS(VN)**2)/8.ØDØ/ZER
C---PRINT THE RESULTS
      WRITE(6,1ØØ) LOPWR
  1ØØ FORMAT(//2X,'REQUIRED LO POWER:',1PE1Ø.3//)
      RETURN
      END




      SUBROUTINE ADJVLO(JVLO,IVLO,VLO,IDCOS,IDBIAS,NHP1)
C
C     SUBROUTINE ADJVLO ADJUSTS THE LOCAL OSCILLATOR VOLTAGE UNTIL
C   THE RECTIFIED CURRENT IS WITHIN IDCACC OF THE DESIRED VALUE,IDBIAS.
C
C---THE VARIABLE TYPES USED IN THIS SUBROUTINE ARE AS FOLLOWS:
C---FOR COMMON/VLODAT/:
      REAL*8 LOVLO,UPVLO,VLOINC,IDCACC
      INTEGER UPFLAG,LOFLAG
C---FOR VARIABLES NOT IN ANY COMMON BLOCKS:
      REAL*8 IDCOS(NHP1),VLO,IDBIAS
      INTEGER JVLO,IVLO,NHP1
C---THE COMMON BLOCKS USED ARE:
      COMMON/VLODAT/LOVLO,UPVLO,LOFLAG,UPFLAG,VLOINC,IDCACC
C---IF THIS IS ALREADY THE LAST VLO LOOP THEN DON'T OUTPUT
      IF(JVLO.EQ.IVLO) GOTO 25
      WRITE(6,1ØØ) JVLO,IDBIAS
  1ØØ FORMAT(/'  VALUES OF THE DC CURRENT AND LO VOLTAGE FOR CYCLE ',
     1I2,' OF THE LOOP FOR ADJUSTING VLO TO GIVE ',F8.6,' AMPS ARE:')
      WRITE(6,11Ø) IDCOS(1),VLO
  11Ø FORMAT(1ØX,'  IDCOS(1)=',F8.6,T35,' VLO BEFORE ADJUSTMENT:',F8.5)
      IF(IDCOS(1).GT.IDBIAS+(IDBIAS*IDCACC)) GOTO 1Ø
      IF(IDCOS(1).LT.IDBIAS-(IDBIAS*IDCACC)) GOTO 15
      IVLO=JVLO
      GOTO 2Ø
   1Ø UPVLO=VLO
C---KEEP TRACK OF THE NUMBER OF TIMES VLO IS GREATER THAN ITS DESIRED
C---VALUE
      UPFLAG=UPFLAG+1
C---IF WE HAVE NOT YET PASSED THE DESIRED VLO CHANGE VLO
      IF(LOFLAG.EQ.Ø) GOTO 11
      VLO=VLO-(UPVLO-LOVLO)/2.ØDØ
      GOTO 2Ø
```

```
   11 VLO=VLO-VLOINC
      IF(VLO.LT.Ø.Ø) VLO=Ø.ØDØ
      GOTO 2Ø
   15 LOVLO=VLO
C---KEEPING TRACK OF THE NUMBER OF TIMES VLO IS LESS THAN ITS DESIRED
C---VALUE
      LOFLAG=LOFLAG+1
C---IF WE HAVE NOT YET PASSED THE DESIRED VLO,CHANGE VLO
      IF(UPFLAG.EQ.Ø) GOTO 16
      VLO=VLO+(UPVLO-LOVLO)/2.ØDØ
      GOTO 2Ø
   16 VLO=VLO+VLOINC
   2Ø WRITE(6,12Ø) VLO
  12Ø FORMAT( T35,' VLO AFTER ADJUSTMENT: ',F8.5)
   25 RETURN
      END



      SUBROUTINE DRKGS(PRMT,Y,DERY,NDIM,IHLF,FCT,OUTP,AUX)
C
C   DRKGS IS AN IBM SSP PROGRAM WHICH SOLVES A SYSTEM OF DIFFERENTIAL
C EQUATIONS BY THE RUNGE-KUTTA ALGORITHM. IT HAS NOT BEEN ALTERED
C FOR THIS ANALYSIS.
C
      DIMENSION Y(1),DERY(1),AUX(8,1),A(4),B(4),C(4),PRMT(1)
      DOUBLE PRECISION PRMT,Y,DERY,AUX,A,B,C,X,XEND,H,AJ,BJ,CJ,R1,R2,
     1DELT
      DO 1 I=1,NDIM
    1 AUX(8,I)=.Ø66666666666666667DØ*DERY(I)
      X=PRMT(1)
      XEND=PRMT(2)
      H=PRMT(3)
      PRMT(5)=Ø.DØ
      CALL FCT(X,Y,DERY)
      IF(H*(XEND-X))38,37,2
    2 A(1)=.5DØ
      A(2)=.29289321881345248DØ
      A(3)=1.7Ø71Ø67811865475DØ
      A(4)=.16666666666666667DØ
      B(1)=2.DØ
      B(2)=1.DØ
      B(3)=1.DØ
      B(4)=2.DØ
      C(1)=.5DØ
      C(2)=.29289321881345248DØ
      C(3)=1.7Ø71Ø67811865475DØ
      C(4)=.5DØ
      DO 3 I=1,NDIM
      AUX(1,I)=Y(I)
      AUX(2,I)=DERY(I)
      AUX(3,I)=Ø.DØ
    3 AUX(6,I)=Ø.DØ
      IREC=Ø
      H=H+H
```

```
      IHLF=-1
      ISTEP=Ø
      IEND=Ø
    4 IF((X+H-XEND)*H)7,6,5
    5 H=XEND-X
    6 IEND=1
    7 CALL OUTP(X,Y,DERY,IREC,NDIM,PRMT)
      IF(PRMT(5))4Ø,8,4Ø
    8 ITEST=Ø
    9 ISTEP=ISTEP+1
      J=1
   1Ø AJ=A(J)
      BJ=B(J)
      CJ=C(J)
      DO 11 I=1,NDIM
      R1=H*DERY(I)
      R2=AJ*(R1-BJ*AUX(6,I))
      Y(I)=Y(I)+R2
      R2=R2+R2+R2
   11 AUX(6,I)=AUX(6,I)+R2-CJ*R1
      IF(J-4)12,15,15
   12 J=J+1
      IF(J-3)13,14,13
   13 X=X+.5DØ*H
   14 CALL FCT(X,Y,DERY)
      GOTO 1Ø
   15 IF(ITEST)16,16,2Ø
   16 DO 17 I=1,NDIM
   17 AUX(4,I)=Y(I)
      ITEST=1
      ISTEP=ISTEP+ISTEP-2
   18 IHLF=IHLF+1
      X=X-H
      H=.5DØ*H
      DO 19 I=1,NDIM
      Y(I)=AUX(1,I)
      DERY(I)=AUX(2,I)
   19 AUX(6,I)=AUX(3,I)
      GOTO 9
   2Ø IMOD=ISTEP/2
      IF(ISTEP-IMOD-IMOD)21,23,21
   21 CALL FCT(X,Y,DERY)
      DO 22 I=1,NDIM
      AUX(5,I)=Y(I)
   22 AUX(7,I)=DERY(I)
      GOTO 9
   23 DELT=Ø.DØ
      DO 24 I=1,NDIM
   24 DELT=DELT+AUX(8,I)*DABS(AUX(4,I)-Y(I))
      IF(DELT-PRMT(4))28,28,25
   25 IF (IHLF-1Ø)26,36,36
   26 DO 27 I=1,NDIM
   27 AUX(4,I)=AUX(5,I)
      ISTEP=ISTEP+ISTEP-4
      X=X-H
```

```
      IEND=Ø
      GOTO 18
   28 CALL FCT(X,Y,DERY)
      DO 29 I=1,NDIM
      AUX(1,I)=Y(I)
      AUX(2,I)=DERY(I)
      AUX(3,I)=AUX(6,I)
      Y(I)=AUX(5,I)
   29 DERY(I)=AUX(7,I)
      CALL OUTP(X-H,Y,DERY,IHLF,NDIM,PRMT)
      IF(PRMT(5))4Ø,3Ø,4Ø
   3Ø DO 31 I=1,NDIM
      Y(I)=AUX(1,I)
   31 DERY(I)=AUX(2,I)
      IREC=IHLF
      IF(IEND)32,32,39
   32 IHLF=IHLF-1
      ISTEP=ISTEP/2
      H=H+H
      IF(IHLF)4,33,33
   33 IMOD=ISTEP/2
      IF(ISTEP-IMOD-IMOD)4,34,4
   34 IF(DELT-.Ø2DØ*PRMT(4))35,35,4
   35 IHLF=IHLF-1
      ISTEP=ISTEP/2
      H=H+H
      GOTO 4
   36 IHLF=11
      CALL FCT(X,Y,DERY)
      GOTO 39
   37 IHLF=12
      GOTO 39
   38 IHLF=13
   39 CALL OUTP(X,Y,DERY,IHLF,NDIM,PRMT)
   4Ø RETURN
      END


      SUBROUTINE FCT(X,Y,DERY)
C
C     FCT IS REQUIRED BY DRKGS AND SETS UP THE NETWORK STATE EQUATION
C  FOR THE DIODE AND TRANSMISSION LINE.
C     NOTE THAT THE JUNCTION CAPACITANCE HAS BEEN FREQUENCY
C  SCALED BY 2*PI*FP SO THAT ONE LO CYCLE OCCURS IN 2*PI SECONDS
C
C---THE VARIABLE TYPES USED IN THIS SUBROUTINE ARE AS FOLLOWS:
C---FOR COMMON/CONST/:
      REAL*8 QEL,BOLTZ,PI,TK,MU,EPS
C---FOR COMMON/DIODE/:
      REAL*8 ALP,ETA,PHI,GAM,CØ,IS,RS,FP,WP,IF,IGJ,ICJ,GJ,CJ
C---FOR COMMON/LOOPS/:
      INTEGER NH,NLO,JLO,NVLO,NPTS,NCURR,IPT,NPRINT,NITER
C---FOR COMMON/TLINE/:
      REAL*8 ZØ,ZQACC
      INTEGER ZQFLAG
```

```
C---FOR COMMON/VOLTS/:
      COMPLEX*16 VR(6)
      REAL*8 VRDC,VLO,VDBIAS,IDBIAS
C---FOR VARIABLES NOT IN ANY COMMON BLOCKS:
      REAL*8 X,Y(1),DERY(1),VS
      REAL*8 CN,SN,CNØ,SNØ,CN1,SN1
      INTEGER JH
C---THE COMMON BLOCKS USED ARE:
      COMMON/CONST/QEL,BOLTZ,PI,TK,MU,EPS
      COMMON/DIODE/ALP,ETA,PHI,GAM,CØ,IS,RS,FP,WP,IF,IGJ,ICJ,GJ,CJ
      COMMON/LOOPS/NH,NLO,JLO,NVLO,NPTS,NCURR,IPT,NPRINT,NITER
      COMMON/TLINE/ZØ,ZQACC,ZQFLAG
      COMMON/VOLTS/VR,VRDC,VLO,VDBIAS,IDBIAS
C---CALCULATE THE TOTAL VOLTAGE ON THE TRANSMISSION LINE INCIDENT ON
C---THE DIODE USING A FAST TRIG ALGORITHM TO FIND SINES AND COSINES.
C---THE AUTHOR IS INDEBTED TO ROBERT O. GRONDIN OF THE UNIVERSITY OF
C---MICHIGAN FOR POINTING OUT THIS ALGORITHM WHICH GREATLY SPEEDS UP
C---THE PROGRAM.
      VS=VRDC
      SN1=DSIN(X)
      CN1=DCOS(X)
      SNØ=Ø.ØDØ
      CNØ=1.ØDØ
      DO 1 JH=1,NH
      SN=SN1*CNØ+CN1*SNØ
      CN=CN1*CNØ-SN1*SNØ
      VS=VS+DREAL(VR(JH))*CN-DIMAG(VR(JH))*SN
      CNØ=CN
    1 SNØ=SN
C---MULTIPLY BY 2 TO CONVERT VS INTO AN EQUIVALENT TRANSMISSION LINE
C---VOLTAGE SOURCE
      VS=VS*2.ØDØ
      CNØ=(1.ØDØ-Y(1)/PHI)
      IF(CNØ.LT.Ø.ØDØ) CNØ=1.ØD-8
      SNØ=ALP*Y(1)
      IF(DABS(SNØ).GT.174.ØDØ) SNØ=DSIGN(174.ØDØ,Y(1))
C---FIND THE FREQUENCY SCALED JUNCTION CAPACITANCE.
      CJ=WP*CØ/(CNØ**GAM)
C---FIND THE CURRENT THROUGH THE DIODE CONDUCTANCE
      IGJ=IS*(DEXP(SNØ)-1.ØDØ)
C---DVD/DT
      DERY(1)=((VS-Y(1))/ZØ-IGJ)/CJ
      RETURN
      END



      SUBROUTINE OUTP(X,Y,DERY,IHLF,NDIM,PRMT)
C
C     OUTP IS REQUIRED BY DRKGS AND IS USED TO OUTPUT THE RESULTS
C  OF THE INTEGRATION AT THE PROPER POINT ALONG AN LO CYCLE. WHEN
C  THE X VARIABLE IN THE DRKGS INTEGRATION REACHES THE END OF AN
C  INTERVAL OF LENGTH 1/(NPTS-1) THEN ALL THE WAVEFORM DATA (DIODE
C  CURRENTS AND VOTAGE) ARE SAVED IN DATA ARRAYS. OTHERWISE THE
C  INTEGRATION IS ALLOWED TO CONTINUE. THIS ROUTINE IS NEEDED SINCE
```

```
C  DRKGS AUTOMATICALLY HALVES AND DOUBLES THE INTEGRATION STEP SIZE
C  TO OBTAIN A GIVEN ACCURACY.
C---THE VARIABLE TYPES USED IN THIS SUBROUTINE ARE AS FOLLOWS:
C---FOR COMMON/CONST/:
      REAL*8 QEL,BOLTZ,PI,TK,MU,EPS
C---FOR COMMON/DATA/:
      REAL*8 ICJDAT(51),IGJDAT(51),CJDATA(51),GJDATA(51)
      REAL*8 VDDATA(51),IDDATA(51)
C---FOR COMMON/DIODE/:
      REAL*8 ALP,ETA,PHI,GAM,C0,IS,RS,FP,WP,IF,IGJ,ICJ,GJ,CJ
C---FOR COMMON/LOOPS/:
      INTEGER NH,NLO,JLO,NVLO,NPTS,NCURR,IPT,NPRINT,NITER
C---FOR VARIABLES NOT IN ANY COMMON BLOCKS:
      REAL*8 TX,D,X,Y(1),DERY(1),PRMT(5)
      INTEGER IHLF,NDIM
C---THE COMMON BLOCKS USED ARE:
      COMMON/CONST/QEL,BOLTZ,PI,TK,MU,EPS
      COMMON/DATA/ICJDAT,IGJDAT,CJDATA,GJDATA,VDDATA,IDDATA
      COMMON/DIODE/ALP,ETA,PHI,GAM,C0,IS,RS,FP,WP,IF,IGJ,ICJ,GJ,CJ
      COMMON/LOOPS/NH,NLO,JLO,NVLO,NPTS,NCURR,IPT,NPRINT,NITER
C---TEST X TO SEE IF WE HAVE REACHED THE END OF AN INTERVAL
      TX=X-PRMT(1)-DFLOAT(IPT)*PRMT(3)
C---DON'T STORE RESULTS IF WE ARE STILL ADJUSTING THE LO VOLTAGE
      IF(JLO-NLO) 6,1,6
C---DON'T STORE ANYTHING IF THIS IS NOT THE END OF AN LO CYCLE INTERVAL
    1 IF(DABS(TX).GT.1.0D-7) GOTO 6
C---INCREMENT THE LO CYCLE INTERVAL COUNTER
    2 IPT=IPT+1
      D=1.0D0-Y(1)/PHI
C---IF THE DIODE VOLTAGE EXCEEDS PHI, CLAMP IT.
      IF(D.LT.0.0D0) D=1.0D-8
      CJ=WP*C0/(D**GAM)
      D=ALP*Y(1)
C---IF THE DIODE EXPONENT IS TOO LARGE, CLAMP IT.
      IF(DABS(D).GT.174.0D0) D=DSIGN(174.0D0,Y(1))
      IGJ=IS*(DEXP(D)-1.0D0)
      ICJ=DERY(1)*CJ
      GJ=IGJ*ALP
C---SAVE THE LAST POINT (NPTS) AS THE FIRST LO CYCLE POINT.
      IF(IPT-NPTS-1) 3,4,6
    3 VDDATA(IPT)=Y(1)
      IDDATA(IPT)=IGJ+ICJ
      IGJDAT(IPT)=IGJ
      ICJDAT(IPT)=ICJ
      GJDATA(IPT)=GJ
      CJDATA(IPT)=CJ
      GOTO 6
    4 VDDATA(1)=Y(1)
      IDDATA(1)=IGJ+ICJ
      GJDATA(1)=GJ
      CJDATA(1)=CJ
      IGJDAT(1)=IGJ
      ICJDAT(1)=ICJ
    6 CONTINUE
      RETURN
```

```
      END



      SUBROUTINE DFORIT(FNT,N,M,A,B,IER)
C
C     DFORIT IS A DOUBLE PRECISION VERSION OF FORIT,AN IBM SSP ROUTINE
C   THAT PERFORMS A FOURIER ANALYSIS ON A PERIODIC FUNCTION.
C   IT COMPUTES THE COEFFICIENTS OF THE TERMS IN THE SERIES WHICH
C   IS GIVEN BY:A(1)+SUM(A(N)COS((N-1)X)+B(N)SIN((N-1)X)) N=2,3,4...
C     NOTE THAT THESE SINGLE ENDED SERIES COEFFICIENTS MUST BE CONVERTED
C   INTO THEIR EQUIVALENT COMPLEX DOUBLE ENDED FOURIER COEFFICIENTS
C   FOR USE IN THE REST OF THE ANALYSIS. IN DOING SO A(N) BECOMES A(N)/2
C   AND B(N) BECOMES -B(N)/2 FOR N>1. FOR N=1, A(N) REMAINS UNCHANGED
C   SINCE THE FACTOR OF 1/2 IS ALREADY INCLUDED IN THE VALUE RETURNED
C   BY THIS ROUTINE (SEE LABEL 1ØØ).
C
C---THE PARAMETERS USED ARE:
C---FNT/: TABULATED VALUES OF THE FUNCTION TO BE ANALYSED
C---       NOTE THAT FNT(1) CORRESPONDS TO TIME T=Ø
C---M/: THE MAXIMUM ORDER OF THE HARMONICS TO BE FITTED
C---N/: DEFINES THE INTERVAL OVER WHICH THE POINTS ARE TAKEN. THE
C---    INTERVAL GOES FROM Ø TO 2*PI AND 2N+1 POINTS ARE TAKEN AS DATA.
C---A/: THE FOURIER COSINE COEFFICIENTS
C---B/: THE FOURIER SINE COEFFICIENTS
C---IER/: THE RESULTANT ERROR  MESSAGE CODE WHERE IER=Ø MEANS NO ERROR.
C---       IER=1 MEANS N IS LESS THAN M.  IER=2 MEANS M IS LESS THAN Ø
C---
      REAL*8 A(1),B(1),FNT(1),CONST
      REAL*8 COEF,C,S,C1,S1,AN,FNTZ,UØ,U1,U2,Q
      INTEGER N,M
      IER=Ø
   2Ø IF(M) 3Ø,4Ø,4Ø
   3Ø IER=2
      RETURN
   4Ø IF(M-N) 6Ø,6Ø,5Ø
   5Ø IER=1
      RETURN
   6Ø AN=N
      COEF=2.ØDØ/(2.ØDØ*AN+1.ØDØ)
      CONST=3.14159265358979DØ*COEF
      S1=DSIN(CONST)
      C1=DCOS(CONST)
      C=1.ØDØ
      S=Ø.ØDØ
      J=1
      FNTZ=FNT(1)
   7Ø U2=Ø.ØDØ
      U1=Ø.ØDØ
      I=2*N+1
   75 UØ=FNT(I)+2.ØDØ*C*U1-U2
      U2=U1
      U1=UØ
      I=I-1
      IF(I-1) 8Ø,8Ø,75
```

```
   8Ø A(J)=COEF*(FNTZ+C*U1-U2)
      B(J)=COEF*S*U1
      IF(J-(M+1)) 9Ø,1ØØ,1ØØ
   9Ø Q=C1*C-S1*S
      S=C1*S+S1*C
      C=Q
      J=J+1
      GO TO 7Ø
  1ØØ A(1)=A(1)*Ø.5DØ
      RETURN
      END



      SUBROUTINE SMSIG
C
C     SMSIG PERFORMS THE SMALL-SIGNAL AND NOISE ANALYSES OF THE MIXER
C   TO DETERMINE THE CONVERSION LOSS BETWEEN ALL PAIRS OF SIDEBANDS,
C   THE INPUT AND OUTPUT IMPEDANCES, AND THE EQUIVALENT INPUT NOISE
C   TEMPERATURE.
C     THE OUTPUT INCLUDES:
C   1) THE CONVERSION LOSS BETWEEN ALL PAIRS OF SIDEBANDS (PRINTED
C      AS A CONVERSION LOSS MATRIX).
C   2) THE INPUT IMPEDANCES OF THE MIXER AT EACH SIDEBAND.
C   3) THE OUTPUT IMPEDANCE AT THE IF.
C   4) THE EQUIVALENT INPUT NOISE TEMPERATURE AT THE UPPER AND LOWER
C      SIDEBANDS WITH THE THERMAL AND SHOT NOISE COMPONENTS.
C     THE SUBSCRIPT NOTATION USED IN THE PROGRAM TO IDENTIFY THE NH+1
C   SMALL-SIGNAL SIDEBANDS IS THAT OF A.A.M. SALEH,'THEORY OF RESISTIVE
C   MIXERS',M.I.T. PRESS,CAMBRIDGE,MASS.,1971. SIDEBAND FREQUENCY
C   (IF+N*LO) IS DENOTED BY THE ARRAY SUBSCRIPT (NH/2 + 1 - N). THE
C   LOWER SIDEBANDS ARE TREATED AS NEGATIVE FREQUENCIES CONSIDERABLY
C   SIMPLIFYING THE EQUATIONS IN THE ANALYSIS.
C     IF ARRAY DIMENSIONS ARE ALTERED THEY MUST BE CHANGED HERE, IN
C   SUBROUTINE LGSIG AND IN THE BLOCK DATA PROGRAM. IN ADDITION THE
C   PRINT FORMAT OF THE CONVERSION LOSS MATRIX MUST BE ALTERED IF
C   A DIFFERENT NUMBER OF LO HARMONICS IS USED.
C
C---THE VARIABLE TYPES USED IN THIS SUBROUTINE ARE AS FOLLOWS:
C---FOR COMMON/CONST/:
       REAL*8 QEL,BOLTZ,PI,TK,MU,EPS
C---FOR COMMON/DIODE/:
       REAL*8 ALP,ETA,PHI,GAM,CØ,IS,RS,FP,WP,IF,IGJ,ICJ,GJ,CJ
C---FOR COMMON/FORITS/:
       REAL*8 GJCOS(7),GJSIN(7),CJCOS(7),CJSIN(7),VDCOS(7),VDSIN(7)
       REAL*8 IDCOS(7),IDSIN(7)
       INTEGER IER
C---FOR COMMON/IMPED/:
       COMPLEX*16 ZEMBSB(7),RSSB(7)
       REAL*8 LOPWR,ZER(6),ZEI(6),ZEMBDC,RSLO(6),XSLO(6)
C---FOR COMMON/LOOPS/:
       INTEGER NH,NLO,JLO,NVLO,NPTS,NCURR,IPT,NPRINT,NITER
C---FOR VARIABLES NOT IN ANY COMMON BLOCKS:
       COMPLEX*16 A(7,7),COR(7,7),FG(7),FC(7)
       COMPLEX*16 T(7),ZIN(7),ZIFOUT,DET
```

```
      REAL*8 XLMAT(7,7),TMUSB,TMLSB,THLSB,THUSB,SHLSB,SHUSB,SHOT
      REAL*8 REF,LIJ,VSWR,GJMAG(7),GJPHA(7),CJMAG(7),CJPHA(7)
      INTEGER JH,NHP1,NHD2P1,NHD2,NHD2P2,WK1(7),WK2(7),I,J
C---THE COMMON BLOCKS USED ARE:
      COMMON/CONST/QEL,BOLTZ,PI,TK,MU,EPS
      COMMON/DIODE/ALP,ETA,PHI,GAM,CØ,IS,RS,FP,WP,IF,IGJ,ICJ,GJ,CJ
      COMMON/FORITS/GJCOS,GJSIN,CJCOS,CJSIN,VDCOS,VDSIN,IDCOS,IDSIN,IER
      COMMON/IMPED/LOPWR,ZER,ZEI,ZEMBDC,RSLO,XSLO,ZEMBSB,RSSB
      COMMON/IVMAG/GJMAG,GJPHA,CJMAG,CJPHA
      COMMON/LOOPS/NH,NLO,JLO,NVLO,NPTS,NCURR,IPT,NPRINT,NITER
C---DEFINE SOME USEFUL CONSTANTS
      NHP1=NH+1
      NHD2=NH/2
      NHD2P1=NHD2+1
      NHD2P2=NHD2+2
C---FORM THE COMPLEX FOURIER COEFFICIENTS OF THE DIODE CONDUCTANCE
C---AND CAPACITANCE
C---THE MINUS SIGN AND FACTOR OF 1/2 COME FROM THE CONVERSION OF
C---THE TRIGONOMETRIC FOURIER SERIES COEFFICIENTS RETURNED BY DFORIT
C---INTO THE DOUBLE ENDED COMPLEX FOURIER COEFFICIENTS USED IN THE
C---SMALL SIGNAL ANALYSIS.
      DO 1Ø JH=2,NHP1
      FG(JH)=DCMPLX(GJCOS(JH),-GJSIN(JH))*Ø.5DØ
   1Ø FC(JH)=DCMPLX(CJCOS(JH),-CJSIN(JH))*Ø.5DØ
      FG(1)=DCMPLX(GJCOS(1),Ø.ØDØ)
      FC(1)=DCMPLX(CJCOS(1),Ø.ØDØ)
C---CALL PRINT3 TO WRITE THE FOURIER COEFFICIENTS
      CALL PRINT3(FG,FC,GJMAG,GJPHA,CJMAG,CJPHA,NH,NHP1)
C---OPEN CIRCUIT THE IF LOAD TO FIND THE IF PORT IMPEDANCE
      ZEMBSB(NHD2P1)=DCMPLX(1.ØD1Ø,Ø.ØDØ)
C---FORM THE Y' MATRIX WITH THE OPEN CIRCUITED IF BY CALLING YPRIME
      CALL YPRIME(FG,FC,NHD2,NHD2P1,NHP1,FP,IF,A,ZEMBSB,RSSB)
C---TAKE THE INVERSE OF THE Y' MATRIX TO FIND THE OUTPUT IMPEDANCE
      CALL CMINV(A,NHP1,DET,WK1,WK2,NHP1*NHP1)
C---THE IF OUTPUT IMPEDANCE IS THE CENTER ELEMENT OF THE Z' MATRIX+RS
      ZIFOUT=A(NHD2P1,NHD2P1)+RSSB(NHD2P1)
C---CONJUGATE MATCH THE IF LOAD IMPEDANCE TO THE IF PORT IMPEDANCE
      ZEMBSB(NHD2P1)=DCONJG(ZIFOUT)
C---FORM THE Y' MATRIX WITH A MATCHED IF LOAD
      CALL YPRIME(FG,FC,NHD2,NHD2P1,NHP1,FP,IF,A,ZEMBSB,RSSB)
C---INVERT THE Y' MATRIX TO OBTAIN THE Z' MATRIX
      CALL CMINV(A,NHP1,DET,WK1,WK2,NHP1*NHP1)
C---FORM THE LOSS MATRIX AND INPUT IMPEDANCE AT EACH SIDEBAND
      DO 5Ø I=1,NHP1
      ZIN(I)=RSSB(I)+A(I,I)*(RSSB(I)+ZEMBSB(I))/(RSSB(I)+ZEMBSB(I)
     1-A(I,I))
      DO 4Ø J=1,NHP1
      IF(I-J) 2Ø,3Ø,2Ø
   2Ø LIJ=((CDABS(RSSB(I)+ZEMBSB(I))*CDABS(RSSB(J)+ZEMBSB(J))/
     1(2.ØDØ*CDABS(A(I,J))))**2)/(DREAL(ZEMBSB(I))*DREAL(ZEMBSB(J)))
C---CONVERT TO DB WHEN FORMING THE LOSS MATRIX
      XLMAT(I,J)=1Ø.ØDØ*DLOG1Ø(LIJ)
      GOTO 4Ø
C---THE DIAGONAL ELEMENTS HAVE NO OBVIOUS MEANING AND ARE ZEROED FOR
C---CONVENIENCE
```

```
   3Ø XLMAT(I,J)=Ø.ØDØ
   4Ø CONTINUE
   5Ø CONTINUE
C---BEGIN THE NOISE ANALYSIS BY FORMING THE SHOT NOISE CORRELATION
C---MATRIX
      CALL CORREL(ALP,FG,COR,NHP1)
C---CALCULATE THE EQUIVALENT INPUT NOISE TEMPERATURE AT THE LOWER
C---SIDEBAND CONSIDERING THE SHOT NOISE COMPONENT ONLY.
      CALL TMIX(NHD2P2,SHLSB,T,COR,A,RSSB,ZEMBSB,NHP1,NHD2P1)
C---ADD THE THERMAL NOISE TO THE SHOT NOISE CORRELATION MATRIX
      CALL TNOISE(COR,RSSB,ZEMBSB,NHP1,NHD2P1)
C---RECALCULATE THE EQUIVALENT NOISE TEMPERATURE NOW INCLUDING BOTH
C---SHOT AND THERMAL NOISE CONTRIBUTIONS
      CALL TMIX(NHD2P2,TMLSB,T,COR,A,RSSB,ZEMBSB,NHP1,NHD2P1)
      THLSB=TMLSB-SHLSB
C---REPEAT THE ABOVE PROCEDURE FOR THE UPPER SIDEBAND
      CALL CORREL(ALP,FG,COR,NHP1)
      CALL TMIX(NHD2,SHUSB,T,COR,A,RSSB,ZEMBSB,NHP1,NHD2P1)
      CALL TNOISE(COR,RSSB,ZEMBSB,NHP1,NHD2P1)
      CALL TMIX(NHD2,TMUSB,T,COR,A,RSSB,ZEMBSB,NHP1,NHD2P1)
C---FIND THE THERMAL NOISE COMPONENT REFERRED TO THE UPPER SIDEBAND
      THUSB=TMUSB-SHUSB
C---CALCULATE THE REFLECTION COEFFICIENT REFERRED TO 5Ø OHMS AT THE IF
      REF=CDABS(DCMPLX(DREAL(ZIFOUT)-5Ø.ØDØ,DIMAG(ZIFOUT)))/
     1CDABS(DCMPLX(DREAL(ZIFOUT)+5Ø.ØDØ,DIMAG(ZIFOUT)))
C---FIND THE VSWR REFERRED TO 5Ø OHMS AT THE IF
      VSWR=(1.ØDØ+REF)/(1.ØDØ-REF)
C---CALL PRINT4 TO PRINT THE RESULTS OF THE SMALL-SIGNAL AND NOISE
C---ANALYSIS
      CALL PRINT4(XLMAT,ZIN,ZIFOUT,VSWR,TMUSB,TMLSB,THUSB,THLSB,
     1SHUSB,SHLSB,NHD2,NHP1,NHD2P1,NHD2P2)
      RETURN
      END



      SUBROUTINE YPRIME(FG,FC,NHD2,NHD2P1,NHP1,FP,IF,A,ZEMBSB,RSSB)
C
C   YPRIME FORMS THE AUGMENTED ADMITTANCE MATRIX Y' (A) OF THE MIXER
C
C---THE VARIABLE TYPES USED IN THIS SUBROUTINE ARE AS FOLLOWS:
C---FOR COMMON/CONST/:
      REAL*8 QEL,BOLTZ,PI,TK,MU,EPS
C---FOR VARIABLES NOT IN ANY COMMON BLOCKS:
      COMPLEX*16 ZEMBSB(NHP1),RSSB(NHP1),A(NHP1,NHP1),FG(NHP1),FC(NHP1)
      REAL*8 FP,IF,WP,WIF
      INTEGER NHD2,NHD2P1,NHP1,I,J
C---THE COMMON BLOCKS USED ARE:
      COMMON/CONST/QEL,BOLTZ,PI,TK,MU,EPS
      WIF=2.ØDØ*PI*IF
      WP=2.ØDØ*PI*FP
C---FORM THE ADMITTANCE MATRIX Y OF THE INTRINSIC DIODE
      DO 6Ø I=1,NHP1
      DO 5Ø J=1,NHP1
   2Ø IF(J-I) 3Ø,4Ø,4Ø
```

```
C---FIND THE LOWER HALF OF THE Y MATRIX
   3Ø A(I,J)=DCONJG(FG(I-J+1))+DCMPLX(Ø.ØDØ,WIF+WP*(NHD2P1-I))
     1*DCONJG(FC(I-J+1))
      GOTO 5Ø
C---FIND THE UPPER HALF OF THE Y MATRIX
   4Ø A(I,J)=FG(J-I+1)+DCMPLX(Ø.ØDØ,WIF+WP*(NHD2P1-I))*FC(J-I+1)
   5Ø CONTINUE
   6Ø CONTINUE
C---ADD 1/(RS+ZEMBSB) TO THE DIAGONAL ELEMENTS OF Y TO FORM THE
C---AUGMENTED ADMITTANCE MATRIX Y' OF THE MIXER
      DO 7Ø I=1,NHP1
   7Ø A(I,I)=A(I,I)+1.ØDØ/(ZEMBSB(I)+RSSB(I))
      RETURN
      END



      SUBROUTINE CORREL(ALP,FG,COR,NHP1)
C
C     CORREL FORMS THE NOISE CURRENT CORRELATION MATRIX FOR THE SHOT
C   NOISE. THE THERMAL NOISE COMPONENTS ARE ADDED IN SUBROUTINE
C   TNOISE.
C
C---THE VARIABLE TYPES USED IN THIS SUBROUTINE ARE AS FOLLOWS:
      COMPLEX*16 FG(NHP1),COR(NHP1,NHP1)
      REAL*8 QEL,BOLTZ,PI,TK,MU,EPS,ALP
      INTEGER NHP1,I,J
C---THE COMMON BLOCKS USED ARE:
      COMMON/CONST/QEL,BOLTZ,PI,TK,MU,EPS
C---FORM THE SHOT NOISE CORRELATION MATRIX USING I=FG/ALP
      DO 1Ø I=1,NHP1
      DO 2Ø J=1,I
      COR(J,I)=2.ØDØ*QEL*FG(I-J+1)/ALP
   2Ø COR(I,J)=DCONJG(COR(J,I))
   1Ø CONTINUE
      RETURN
      END



      SUBROUTINE TNOISE(COR,RSSB,ZEMBSB,NHP1,NHD2P1)
C
C     TNOISE FORMS THE THERMAL NOISE CURRENT CORRELATION MATRIX AND
C   ADDS IT TO THE SHOT NOISE CORRELATION MATRIX.
C
C---THE VARIABLE TYPES USED IN THIS SUBROUTINE ARE AS FOLLOWS:
      COMPLEX*16 COR(NHP1,NHP1),ZEMBSB(NHP1),RSSB(NHP1)
      REAL*8 QEL,BOLTZ,PI,TK,MU,EPS
C---THE COMMON BLOCKS USED ARE:
      COMMON/CONST/QEL,BOLTZ,PI,TK,MU,EPS
C---SINCE THE THERMAL NOISE MATRIX IS DIAGONAL ADD THESE ELEMENTS TO
C---THE DIAGONAL TERMS OF THE SHOT NOISE CORRELATION MATRIX
      DO 35 I=1,NHP1
      IF(I.EQ.NHD2P1) GOTO 3Ø
      COR(I,I)=COR(I,I)+4.ØDØ*BOLTZ*TK*RSSB(I)/
```

```
     1(CDABS(ZEMBSB(I)+RSSB(I)))**2
      GOTO 35
C---AT THE IF THE THERMAL NOISE TERM IS GIVEN BY:
   3Ø COR(I,I)=COR(I,I)+4.ØDØ*BOLTZ*TK*RSSB(I)/
     1(CDABS(ZEMBSB(I)-RSSB(I)))**2
   35 CONTINUE
      RETURN
      END



      SUBROUTINE TMIX(NSB,TM,T,COR,A,RSSB,ZEMBSB,NHP1,NHD2P1)
C
C     TMIX COMPUTES THE EQUIVALENT SINGLE SIDEBAND INPUT NOISE
C   TEMPERATURE OF THE MIXER REFERRED TO SIDEBAND NSB.
C   NOTE THAT SIDEBAND NSB IS ARRAY SUBSCRIPT NH/2 + 1 - NSB.
C
C---THE VARIABLE TYPES USED IN THIS SUBROUTINE ARE AS FOLLOWS:
C   FOR COMMON/CONST/:
      REAL*8 QEL,BOLTZ,PI,TK,MU,EPS
C   FOR VARIABLES NOT IN ANY COMMON BLOCKS:
      COMPLEX*16 COR(NHP1,NHP1),A(NHP1,NHP1),ZEMBSB(NHP1),VSQ
      COMPLEX*16 RSSB(NHP1),T(NHP1)
      REAL*8 TM
      INTEGER I,J,NSB,NHP1,NHD2P1
C---THE COMMON BLOCKS USED ARE:
      COMMON/CONST/QEL,BOLTZ,PI,TK,MU,EPS
C---POST MULTIPLY COR BY THE CONJUGATE TRANSPOSE OF THE CENTER ROW
C---OF THE Z' MATRIX (ROW Ø)
      DO 1Ø I=1,NHP1
      T(I)=Ø.ØDØ
      DO 2Ø J=1,NHP1
   2Ø T(I)=T(I)+COR(I,J)*DCONJG(A(NHD2P1,J))
   1Ø CONTINUE
C---PREMULTIPLY COR BY THE CENTER ROW OF THE MIXER Z' MATRIX
      VSQ=Ø.ØDØ
      DO 3Ø I=1,NHP1
   3Ø VSQ=VSQ+A(NHD2P1,I)*T(I)
C---COMPUTE THE EQUIVALENT INPUT NOISE TEMPERATURE OF THE MIXER
      TM=(DREAL(VSQ)*(CDABS(ZEMBSB(NSB)+RSSB(NSB)))**2)/
     1(BOLTZ*4.ØDØ*DREAL(ZEMBSB(NSB))*(CDABS(A(NHD2P1,NSB))**2))
      RETURN
      END



      SUBROUTINE CMINV(A,N,D,L,M,NSQ)
C
C     CMINV IS A SLIGHTLY MODIFIED VERSION OF THE IBM SSP ROUTINE MINV
C   FOR INVERTING A COMPLEX MATRIX. ONLY THE FIRST TWO STATEMENTS AND
C   THOSE NUMBERED 1Ø AND 45 HAVE BEEN ALTERED.
C
      COMPLEX*16 A,D,BIGA,HOLD
      DIMENSION A(NSQ),L(N),M(N)
      D=1.ØDØ
```

```
      NK=-N
      DO 80 K=1,N
      NK=NK+N
      L(K)=K
      M(K)=K
      KK=NK+K
      BIGA=A(KK)
      DO 20 J=K,N
      IZ=N*(J-1)
      DO 20 I=K,N
      IJ=IZ+I
   10 IF(CDABS(BIGA)-CDABS(A(IJ))) 15,20,20
   15 BIGA=A(IJ)
      L(K)=I
      M(K)=J
   20 CONTINUE
      J=L(K)
      IF(J-K) 35,35,25
   25 KI=K-N
      DO 30 I=1,N
      KI=KI+N
      HOLD=-A(KI)
      JI=KI-K+J
      A(KI)=A(JI)
   30 A(JI) =HOLD
   35 I=M(K)
      IF(I-K) 45,45,38
   38 JP=N*(I-1)
      DO 40 J=1,N
      JK=NK+J
      JI=JP+J
      HOLD=-A(JK)
      A(JK)=A(JI)
   40 A(JI) =HOLD
   45 IF(CDABS(BIGA)) 48,46,48
   46 D=0.0D0
      RETURN
   48 DO 55 I=1,N
      IF(I-K) 50,55,50
   50 IK=NK+I
      A(IK)=A(IK)/(-BIGA)
   55 CONTINUE
      DO 65 I=1,N
      IK=NK+I
      HOLD=A(IK)
      IJ=I-N
      DO 65 J=1,N
      IJ=IJ+N
      IF(I-K) 60,65,60
   60 IF(J-K) 62,65,62
   62 KJ=IJ-I+K
      A(IJ)=HOLD*A(KJ)+A(IJ)
   65 CONTINUE
      KJ=K-N
      DO 75 J=1,N
```

```
      KJ=KJ+N
      IF(J-K) 70,75,70
   70 A(KJ)=A(KJ)/BIGA
   75 CONTINUE
      D=D*BIGA
      A(KK)=1.0D0/BIGA
   80 CONTINUE
      K=N
  100 K=(K-1)
      IF(K) 150,150,105
  105 I=L(K)
      IF(I-K) 120,120,108
  108 JQ=N*(K-1)
      JR=N*(I-1)
      DO 110 J=1,N
      JK=JQ+J
      HOLD=A(JK)
      JI=JR+J
      A(JK)=-A(JI)
  110 A(JI) =HOLD
  120 J=M(K)
      IF(J-K) 100,100,125
  125 KI=K-N
      DO 130 I=1,N
      KI=KI+N
      HOLD=A(KI)
      JI=KI-K+J
      A(KI)=-A(JI)
  130 A(JI) =HOLD
      GO TO 100
  150 RETURN
      END



      SUBROUTINE PRINT1(ZEMB,ZERDC,ZEMBDC,ZER,ZEI,ZEMBSB,PRMT,Y,
     1DERY,VLO,VDBIAS,IDBIAS,RSSB,RSLO,XSLO,NHARM,NHP1,NHD2)
C
C     PRINT1 WRITES THE VALUES OF THE INPUT VARIABLES AND THE INITIAL
C   CONDITIONS FOR THE NONLINEAR ANALYSIS SECTION OF THE PROGRAM.
C
C---THE VARIABLE TYPES USED IN THIS SUBROUTINE ARE AS FOLLOWS:
C---FOR COMMON/CONST/:
      REAL*8 QEL,BOLTZ,PI,TK,MU,EPS
C---FOR COMMON/DIODE/:
      REAL*8 ALP,ETA,PHI,GAM,C0,IS,RS,FP,WP,IF,IGJ,ICJ,GJ,CJ
C---FOR COMMON/LOOPS/:
      INTEGER NH,NLO,JLO,NVLO,NPTS,NCURR,IPT,NPRINT,NITER
C---FOR COMMON/RES/:
      REAL*8 ER,NDS,NDE,SMOB,EMOB,TE,AR,CL,CW,CT,RC
C---FOR COMMON/RKG/:
      REAL*8 ACC,VDINIT
      INTEGER NDIM
C---FOR COMMON/TLINE/:
      REAL*8 Z0,ZQACC
```

```
      INTEGER ZQFLAG
C---FOR COMMON/VLODAT/:
      REAL*8 LOVLO,UPVLO,VLOINC,IDCACC
      INTEGER LOFLAG,UPFLAG
C---FOR VARIABLES NOT IN ANY COMMON BLOCKS:
      COMPLEX*16 ZEMB(NHARM),ZEMBSB(NHP1),RSSB(NHP1)
      REAL*8 VDBIAS,IDBIAS,VLO,ZQACC,Z0,ZEMBDC,ZERDC,FSB,FLO
      REAL*8 PRMT(5),Y(1),DERY(1)
      REAL*8 ZER(NHARM),ZEI(NHARM),XSLO(NHARM),RSLO(NHARM)
      INTEGER NHARM,NHP1,NHD2,I,K,J
C---THE COMMON BLOCKS USED ARE:
      COMMON/CONST/QEL,BOLTZ,PI,TK,MU,EPS
      COMMON/DIODE/ALP,ETA,PHI,GAM,C0,IS,RS,FP,WP,IF,IGJ,ICJ,GJ,CJ
      COMMON/LOOPS/NH,NLO,JLO,NVLO,NPTS,NCURR,IPT,NPRINT,NITER
      COMMON/RES/ER,NDS,NDE,SMOB,EMOB,TE,AR,CL,CW,CT,RC
      COMMON/RKG/ACC,VDINIT,NDIM
      COMMON/TLINE/Z0,ZQACC,ZQFLAG
      COMMON/VLODAT/LOVLO,UPVLO,LOFLAG,UPFLAG,VLOINC,IDCACC
C---PRINT THE TITLE
      WRITE(6,50) FP
   50 FORMAT(1H1,1X,' ANALYSIS OF A ',-9PF6.2,' GHZ MICROWAVE MIXER'/
     *1X,50('-'))
C---WRITE THE VALUES OF THE RELEVANT VARIABLES.
      WRITE (6,75)
   75 FORMAT(/1X,'INPUT DATA')
      WRITE(6,100)
  100 FORMAT(//1X,' DIODE PARAMETERS:',T25,'ALP',T41,'PHI',T56,'GAM',
     1T70,'C0',T85,'IS',T99,'RS',T111,'ETA')
      WRITE(6,110) ALP,PHI,GAM,C0,IS,RS,ETA
  110 FORMAT(19X,3(F10.3,5X),2(1PE10.3,5X),0PF8.4,5X,F8.4)
      WRITE(6,112)
  112 FORMAT(//2X,'CHIP PARAMETERS:',T21,'LENGTH',T30,'WIDTH',
     1T39,'HEIGHT',T50,'ANODE RAD',T66,'SUB DOP',T81,'EPI DOP',
     2T94,'SUB MOB',T106,'EPI MOB')
      WRITE(6,116) CL,CW,CT,AR,NDS,NDE,SMOB,EMOB
  116 FORMAT(19X,3(F6.3,3X),2X,3(1PD10.3,5X),2(0PF7.1,5X))
      WRITE(6,120) FP,IF,TK
  120 FORMAT(/1X,' OPERATING FREQUENCIES AND TEMPERATURE:',T50,'FP',
     1T65,'IF',T81,'TK'/T45,2(1PE10.3,5X),0PF10.1)
      WRITE(6,130) VDBIAS,IDBIAS
  130 FORMAT(/1X,' BIAS SETTINGS:',T24,'VDBIAS',T38,'IDBIAS'/T20,
     1F10.3,5X,F10.6)
      WRITE(6,140) VLO,VLOINC,IDCACC
  140 FORMAT(/1X,' VLO ADJUST VARIABLES:',T28,'VLO',T42,'VLOINC',T57,
     1'IDCACC'/T24,3(F10.6,5X))
      WRITE(6,150) PRMT(1),PRMT(2),PRMT(3),PRMT(4),Y(1),DERY(1),NDIM
  150 FORMAT(/1X,' DRKGS VARIABLES:',T21,'PRMT(1)',T35,'PRMT(2)',T50,
     1'PRMT(3)',T65,'PRMT(4)',T80,'Y(1)',T95,'DERY(1)',T110,'NDIM'/
     2T20,'(LOW LIM)',T35,'(UP LIM)',T50,'(INCR)',T66,'(ACC)',T80,
     3'(VD)',T95,'(DV/DT)',T109,'(NEQS)'/
     4T22,F10.8,1X,2( F10.8,5X),1PE10.3,2X,2(0PF10.3,6X),4X,I2)
      WRITE(6,160) NITER,NLO,NVLO,NPTS,NHARM,NPRINT
  160 FORMAT(/1X,' LOOP LIMITS:',T21,'NITER',T31,'NLO',T40,'NVLO',
     1T51,'NPTS',T62,'NHARM',T72,'NPRINT'/T21,I4,6X,2(I2,8X),1X,
     2I2,09X,I2,8X,I3)
```

```
      WRITE(6,17Ø) ZØ,ZQACC
  17Ø FORMAT(/1X,' CONVERGENCE PARAMETERS:',T4Ø,'ZØ',T57,'ZQACC'/
     1T34,F1Ø.2,1ØX,1PE1Ø.3)
      WRITE(6,18Ø) ZERDC,ZEMBDC,NHD2,ZEMBSB(1)
  18Ø FORMAT(///1X,' EMBEDDING IMPEDANCES:',T48,'HARMONICS OF THE LO',
     1T1Ø5,'HARMONIC SIDEBANDS'/T25,'HARM#',T37,'ZER',T5Ø,
     *'ZEI',T71,'ZEMB',T92,'SIDEBAND#',T112,'ZEMBSB'/T26,'DC',T33,
     *1PE1Ø.3,T61,1PE1Ø.3,T95,I2,T1Ø3,1PE1Ø.3,T116,1PE1Ø.3)
      DO 1Ø I=1,NHARM
      K=NHD2-I
      J=I+1
   1Ø WRITE(6,19Ø) I,ZER(I),ZEI(I),ZEMB(I),K,ZEMBSB(J)
  19Ø FORMAT(1X,T26,I2,T33,2(1PE1Ø.3,3X),T61,2(1PE1Ø.3,3X),T95,I2,
     *T1Ø3,1PE1Ø.3,T116,1PE1Ø.3)
      FSB=(FP*NHD2+IF)*1.ØD-9
      WRITE(6,2ØØ) RS,FSB,NHD2,RSSB(1)
  2ØØ FORMAT(///1X,' DIODE SERIES RESISTANCES:',T49,'HARMONICS OF THE '
     1,' LO',T1Ø4,'HARMONIC SIDEBANDS'/T33,'FGHZ',T42,'HARM#',
     *T52,'RSLO',T63,'XSLO',T82,'FGHZ',T91,'SIDEBAND#',
     2T111,'RSSB'/T34,'DC',T43,'Ø',T49,F8.4,
     3T79,F8.2,T94,I2,T1Ø3,F8.4,T113,F8.4)
      DO 2Ø I=1,NHARM
      K=NHD2-I
      J=I+1
      FLO=FP*I*1.ØD-9
      FSB=(FP*IABS(K)+ISIGN(1,K)*IF)*1.ØD-9
   2Ø WRITE(6,21Ø) FLO,I,RSLO(I),XSLO(I),FSB,K,RSSB(J)
  21Ø FORMAT(1X,T3Ø,F8.2,T42,I2,T49,F8.4,T6Ø,F8.4,T79,
     1F8.2,T94,I2,T1Ø3,F8.4,T113,F8.4)
      WRITE(6,22Ø)
  22Ø FORMAT(1H1,'RESULTS OF THE VLO ADJUSTMENTS'//)
      RETURN
      END



      SUBROUTINE PRINT2(RHO,VL,VR,VDCOS,VDSIN,IDCOS,IDSIN,ZQMAG,
     1ZQPHA,VLDC,VRDC,RHODC,ITER,ZQFLAG,JVLO,NH,NHP1)
C
C     PRINT2 WRITES THE RESULTS OF EACH REFLECTION CYCLE OF THE LOOP
C   ITER IN SUBROUTINE LGSIG.
C---
C---THE VARIABLE TYPES USED IN THIS SUBROUTINE ARE AS FOLLOWS:
      COMPLEX*16 RHO(NH),VR(NH),VL(NH)
      REAL*8 VDCOS(NHP1),VDSIN(NHP1),IDCOS(NHP1),IDSIN(NHP1),ZQMAG(NH)
      REAL*8 ZQPHA(NH),VLDC,VRDC,RHODC
      INTEGER ITER,JVLO,NH,NHP1
C---WRITE THE RESULTS OF THE REFLECTION CYCLE
      WRITE(6,1ØØ) ITER,JVLO
  1ØØ FORMAT(////1X,'NONLINEAR ANALYSIS RESULTS:  REFLECTION CYCLE #'
     1,I4,' IN VLO ADJUSTMENT LOOP NUMBER',I3/)
      WRITE(6,11Ø)
  11Ø FORMAT(/2X,'VL(I)')
      WRITE(6,12Ø) (I,VL(I),I=1,NH)
  12Ø FORMAT(1H+,6(8X,4(I7,1PE12.3,1PE12.3)/1X))
```

```
      WRITE(6,130)
  130 FORMAT(/2X,'VR(I)')
      WRITE(6,120) (I,VR(I),I=1,NH)
      WRITE(6,150)
  150 FORMAT(/2X,'VDCOS,VDSIN')
      WRITE(6,120) (I,VDCOS(I+1),VDSIN(I+1),I=1,NH)
      WRITE(6,160)
  160 FORMAT(/2X,'IDCOS,IDSIN')
      WRITE(6,120) (I,IDCOS(I+1),IDSIN(I+1),I=1,NH)
      WRITE(6,170)
  170 FORMAT(/2X,'ZQMAG,ZQPHA')
      WRITE(6,180) (I,ZQMAG(I),ZQPHA(I),I=1,NH)
  180 FORMAT(1H+,6(8X,4(I7,1PE12.3,0PF7.0,5X)/1X))
      WRITE(6,190) VDCOS(1),IDCOS(1),VLDC,VRDC,ZQFLAG
  190 FORMAT(//2X,'DC TERMS:  VDCOS=',1PE10.3,T35,'IDCOS=',1PE10.3,
     1T54,'VLDC=',1PE10.3,T76,'VRDC=',1PE10.3///2X,'ZQFLAG=',I2)
      RETURN
      END



      SUBROUTINE PRINT3(FG,FC,GJMAG,GJPHA,CJMAG,CJPHA,NH,NHP1)
C
C     PRINT3 WRITES THE FOURIER COEFFICIENTS OF THE DIODE CONDUCTANCE
C   AND CAPACITANCE WHICH ARE USED IN THE SMALL-SIGNAL ANALYSIS.
C
C---THE VARIABLE TYPES USED IN THIS SUBROUTINE ARE AS FOLLOWS:
      COMPLEX*16 FG(NHP1),FC(NHP1)
      REAL*8 GJMAG(NHP1),GJPHA(NHP1),CJMAG(NHP1),CJPHA(NHP1)
      INTEGER NHP1,NH
C---TRANSFORM THE FOURIER COEFFICIENTS TO MAGNITUDE AND PHASE (DEGREES)
      DO 10 I=1,NHP1
      GJMAG(I)=CDABS(FG(I))
      CJMAG(I)=CDABS(FC(I))
      GJPHA(I)=DATAN2(DIMAG(FG(I)),DREAL(FG(I)))*57.29577951D0
   10 CJPHA(I)=DATAN2(DIMAG(FC(I)),DREAL(FC(I)))*57.29577951D0
      WRITE(6,50)
   50 FORMAT(1H1,1X,'RESULTS OF THE SMALL-SIGNAL ANALYSIS'/)
      WRITE(6,100)
  100 FORMAT(/1X,' FOURIER COEFFICIENTS OF THE DIODE',
     1' CONDUCTANCE AND CAPACITANCE WAVEFORMS'/)
      WRITE(6,110)
  110 FORMAT(/2X,'GJMAG,GJPHA')
      WRITE(6,120) (I,GJMAG(I+1),GJPHA(I+1),I=1,NH)
  120 FORMAT(1H+,6(8X,4(I7,1PE12.3,0PF7.0,5X)/1X))
      WRITE(6,130)
  130 FORMAT(/2X,'CJMAG,CJPHA')
      WRITE(6,120) (I,CJMAG(I+1),CJPHA(I+1),I=1,NH)
      WRITE(6,140) GJMAG(1),CJMAG(1)
  140 FORMAT(//2X,'DC TERMS:  GJMAG = ',1PE10.3,4X,'CJMAG = '
     1,1PE10.3/)
      RETURN
      END
```

```
      SUBROUTINE PRINT4(XLMAT,ZIN,ZIFOUT,VSWR,TMUSB,TMLSB,THUSB,THLSB
     1,SHUSB,SHLSB,NHD2,NHP1,NHD2P1,NHD2P2)
C
C     SUBROUTINE PRINT4 WRITES THE RESULTS OF THE SMALL-SIGNAL
C   AND NOISE ANALYSES. THESE INCLUDE THE CONVERSION LOSS MATRIX,
C   THE INPUT IMPEDANCE AT EACH SIDEBAND, THE IF OUTPUT IMPEDANCE,
C   AND THE EQUIVALENT INPUT NOISE TEMPERATURE OF THE MIXER WITH ITS
C   THERMAL AND SHOT NOISE COMPONENTS.
C
C---THE VARIABLE TYPES USED IN THIS SUBROUTINE ARE AS FOLLOWS:
      COMPLEX*16 ZIN(NHP1),ZIFOUT
      REAL*8 XLMAT(NHP1,NHP1),REZIN(7),IMZIN(7)
      REAL*8 TMUSB,TMLSB,THUSB,THLSB,SHUSB,SHLSB,VSWR
      INTEGER NHP1,I,J,K,NHD2P1,NHD2P2,NHD2
C---DEFINE THE ARRAY ELEMENT WHICH CORRESPONDS TO THE LOWER SIDEBAND
      NHD2P2=NHD2P1+1
      WRITE(6,1ØØ)
  1ØØ FORMAT(//44X,'CONVERSION  LOSS  MATRIX (DB)'/)
      WRITE(6,2ØØ)
  2ØØ FORMAT(1X,T25,'3',T35,'2',T45,'1',T55,'Ø',T65,'-1',T74,'-2',
     1T84,'-3'//)
      DO 1Ø I=1,NHP1
      K=NHD2P1-I
   1Ø WRITE(6,3ØØ) K,(XLMAT(I,J),J=1,NHP1)
  3ØØ FORMAT(9X,I4,4X,9F1Ø.2/)
      WRITE(6,35Ø) XLMAT(NHD2P1,NHD2),XLMAT(NHD2P1,NHD2P2)
  35Ø FORMAT(//2X,'UPPER SIDEBAND CONVERSION LOSS:  L(Ø,1)  =',F7.2,
     *' DB'//2X,'LOWER SIDEBAND CONVERSION LOSS:  L(Ø,-1) =',F7.2,
     *' DB'/)
      WRITE (6,39Ø)
  39Ø FORMAT(2X,'INPUT IMPEDANCES',T25,'3',T35,'2',T45,'1',T55,'Ø',
     1T65,'-1',T74,'-2',T84,'-3')
      DO 2Ø I=1,NHP1
      REZIN(I)=DREAL(ZIN(I))
   2Ø IMZIN(I)=DIMAG(ZIN(I))
      WRITE(6,4ØØ) (REZIN(I),I=1,NHP1)
  4ØØ FORMAT (/3X,' REAL(ZIN):',3X,9F1Ø.2)
      WRITE(6,5ØØ) (IMZIN(I),I=1,NHP1)
  5ØØ FORMAT (/3X,' IMAG(ZIN):',3X,9F1Ø.2)
      WRITE (6,55Ø) ZIFOUT
  55Ø FORMAT(//2X,'IF OUTPUT IMPEDANCE:   ZIFOUT = ',F8.2,' + J'
     *F8.2)
      WRITE(6,575) VSWR
  575 FORMAT(/2X,'VSWR OF IF PORT REFERRED TO 5Ø OHMS:',F12.4)
      WRITE(6,6ØØ) TMUSB,THUSB,SHUSB,TMLSB,THLSB,SHLSB
  6ØØ FORMAT(//2X,'EQUIVALENT INPUT NOISE TEMPERATURES:',T4Ø,
     1'TSSB(USB)',T55,'SHOT(USB)',T69,'THERM(USB)',T85,'TSSB(LSB)',
     2T1ØØ,'THERM(LSB)',T115,'SHOT(LSB)'/1X,T38,F1Ø.2,T53,F1Ø.2,
     3T68,F1Ø.2,T83,F1Ø.2,T98,F1Ø.2,T113,F1Ø.2)
      RETURN
      END
```

```
      SUBROUTINE PLOT(IGJDAT,CJDATA,VDDATA,IDDATA,NPTS,ITER,CØ)
C
C     SUBROUTINE PLOT GRAPHS THE CURRENT THROUGH THE DIODE CONDUCTANCE
C   (IGJ),THE DIODE CAPACITANCE (CJ),THE TOTAL CURRENT THROUGH THE
C   DIODE (IGJ+ICJ), AND THE VOLTAGE ACROSS THE INTRINSIC DIODE TER -
C   MINALS (Y(1)) (WHICH DOES NOT INCLUDE THE DIODE SERIES RESISTANCE)
C   AS FUNCTIONS OF TIME,OVER ONE LOCAL OSCILLATOR CYCLE.
C
C---THE VARIABLE TYPES USED IN THIS SUBROUTINE ARE AS FOLLOWS:
      REAL*8 IGJDAT(NPTS),CJDATA(NPTS),VDDATA(NPTS),IDDATA(NPTS)
      REAL*8 MAXIGJ,MAXCJ,MAXVD,MAXID,MINCJ,CØ
      INTEGER ITER,JPT,YPT,NPTS,IGJPOS,CJPOS,CØPOS,VDPOS,IDPOS,C,ZERO
      INTEGER BLANK,DOT,STAR,YGPOS(5Ø),YCPOS(5Ø),YIDPOS(5Ø),YVDPOS(5Ø)
C---DEFINE THE NUMERICS USED IN THE GRAPHS
      DATA BLANK,DOT,STAR,C,ZERO/' ','.','*','C','Ø'/
C---DETERMINE THE GRAPH SCALES
      MAXIGJ=DABS(IGJDAT(1))
      MAXCJ=DABS(CJDATA(1))
      MINCJ=CJDATA(1)
      MAXVD=DABS(VDDATA(1))
      MAXID=DABS(IDDATA(1))
      DO 1Ø JPT=2,NPTS
      IF(MAXIGJ.LT.DABS(IGJDAT(JPT))) MAXIGJ=DABS(IGJDAT(JPT))
      IF(MAXCJ.LT.DABS(CJDATA(JPT))) MAXCJ=DABS(CJDATA(JPT))
      IF(MINCJ.GT.CJDATA(JPT)) MINCJ=CJDATA(JPT)
      IF(MAXVD.LT.DABS(VDDATA(JPT))) MAXVD=DABS(VDDATA(JPT))
      IF(MAXID.LT.DABS(IDDATA(JPT))) MAXID=DABS(IDDATA(JPT))
   1Ø CONTINUE
C---THE GRAPH HEADINGS
      WRITE(6,1ØØ) ITER
  1ØØ FORMAT(1H1,1X,'GRAPHS FOR REFLECTION CYCLE NUMBER ',I4/)
      WRITE(6,11Ø)
  11Ø FORMAT(/3X,'IGJ(MA)',5X,'DIODE CONDUCTANCE CURRENT VS TIME FOR',
     1' ONE LO CYCLE',T67,'  CJ(PF)',5X,'DIODE CAPACITANCE VS',
     2' TIME FOR ONE LO CYCLE'/)
C---THE LOOP FOR THE POINTS TO PLOTTED VERTICALLY DOWN THE PAGE
C---PREVENT A DIVISION BY Ø IF THE CAPACITANCE DOES NOT VARY
      IF(MAXCJ.EQ.MINCJ) MAXCJ=MAXCJ+1.ØDØ
C---LET CØ BE THE Y AXIS IF IT IS NOT IN THE RANGE MINCJ TO MAXCJ
      IF(CØ.LT.MINCJ) MINCJ=CØ
      IF(CØ.GT.MAXCJ) MAXCJ=CØ
      CØPOS=Ø1+DINT(5Ø.ØDØ/(MAXCJ-MINCJ)*(CØ-MINCJ)+DSIGN(Ø.5DØ,CØ))
      DO 2 JPT=1,NPTS
      IGJPOS=Ø1+DINT(5Ø.ØDØ/MAXIGJ*IGJDAT(JPT)+
     1DSIGN(Ø.5DØ,IGJDAT(JPT)))
      CJPOS=Ø1+DINT(5Ø.ØDØ/(MAXCJ-MINCJ)*(CJDATA(JPT)-MINCJ)+DSIGN(
     1Ø.5DØ,CJDATA(JPT)))
C---SET THE GRAPH LIMITS
      IF(IGJPOS.LT.1) IGJPOS=1
      IF(IGJPOS.GT.5Ø) IGJPOS=5Ø
      IF(CJPOS.LT.1) CJPOS=1
      IF(CJPOS.GT.49) CJPOS=49
C---CLEAR THE HORIZONTAL LINE
      DO 1 YPT=1,5Ø
      YCPOS(YPT)=BLANK
```

```
    1 YGPOS(YPT)=BLANK
C---SET THE GRAPH'S Y AXIS
      YGPOS(1)=DOT
      YCPOS(CØPOS)=DOT
C---THE PLOTTED POINTS ARE REPRESENTED AS ASTERIKS
      YGPOS(IGJPOS)=STAR
      YCPOS(CJPOS)=STAR
C---WRITE 'CØ' ON THE Y AXIS OF THE CAPACITANCE GRAPH
      IF(CØPOS.EQ.5Ø) GOTO 6
      IF(JPT.EQ.1) YCPOS(CØPOS)=C
      IF(JPT.EQ.1) YCPOS(CØPOS+1)=ZERO
      GOTO 7
    6 IF(JPT.EQ.1) YCPOS(CØPOS-1)=C
      IF(JPT.EQ.1) YCPOS(CØPOS)=ZERO
    7 CONTINUE
C---PRINT THIS LINE OF THE GRAPHS
      WRITE(6,12Ø) IGJDAT(JPT),(YGPOS(YPT),YPT=1,5Ø),CJDATA(JPT),
     1(YCPOS(YPT),YPT=1,5Ø)
  12Ø FORMAT(3PF9.3,2X,5ØA1,3X,12PF9.4,2X,5ØA1)
    2 CONTINUE
      WRITE(6,1ØØ) ITER
      WRITE(6,13Ø)
  13Ø FORMAT(//3X,'ID(MA)',5X,'TOTAL DIODE CURRENT VS TIME FOR ONE LO',
     1' CYCLE',T67,' VD(VOLTS)',8X,' DIODE VOLTAGE VS TIME FOR',
     2' ONE LO CYCLE'/)
C---THE DO LOOP FOR THE POINTS TO BE PLOTTED VERTICALLY DOWN THE PAGE
      DO 4 JPT=1,NPTS
      IDPOS=25+DINT(25.ØDØ/MAXID*IDDATA(JPT)+DSIGN(Ø.5DØ,IDDATA(JPT)))
      VDPOS=25+DINT(25.ØDØ/MAXVD*VDDATA(JPT)+DSIGN(Ø.5DØ,VDDATA(JPT)))
C---SET THE GRAPH LIMITS
      IF(IDPOS.LT.1) IDPOS=1
      IF(IDPOS.GT.5Ø) IDPOS=5Ø
      IF(VDPOS.LT.1) VDPOS=1
      IF(VDPOS.GT.5Ø) VDPOS=5Ø
C---CLEAR THE HORIZONTAL LINE
      DO 5 YPT=1,5Ø
      YIDPOS(YPT)=BLANK
      YVDPOS(YPT)=BLANK
    5 CONTINUE
C---SET THE Y AXIS
      YIDPOS(25)=DOT
      YVDPOS(25)=DOT
C---THE PLOTTED POINTS ARE REPRESENTED AS ASTERIKS
      YIDPOS(IDPOS)=STAR
      YVDPOS(VDPOS)=STAR
C---PRINT THIS LINE OF THE GRAPHS
      WRITE(6,14Ø) IDDATA(JPT),(YIDPOS(YPT),YPT=1,5Ø),VDDATA(JPT),
     1(YVDPOS(YPT),YPT=1,5Ø)
  14Ø FORMAT(3PF9.3,2X,5ØA1,3X,ØPF9.3,2X,5ØA1)
    4 CONTINUE
    3 RETURN
      END
```

```
      BLOCK DATA
C
C---FOR COMMON/CONST/:
      REAL*8 QEL,BOLTZ,PI,TK,MU,EPS
C---FOR COMMON/DIODE/:
      REAL*8 ALP,ETA,PHI,GAM,C0,IS,RS,FP,WP,IF,IGJ,ICJ,GJ,CJ
C---FOR COMMON/IMPED/:
      COMPLEX*16 ZEMBSB(7),RSSB(7)
      REAL*8 LOPWR,ZER(6),ZEI(6),ZERDC,RSLO(6),XSLO(6)
C---FOR COMMON/LOOPS/:
      INTEGER NH,NLO,JLO,NVLO,NPTS,NCURR,IPT,NPRINT,NITER
C---FOR COMMON/RES/:
      REAL*8 ER,NDS,NDE,SMOB,EMOB,TE,AR,CL,CW,CT,RC
C---FOR COMMON/RKG/:
      REAL*8 ACC,VDINIT
      INTEGER NDIM
C---FOR COMMON/TLINE/:
      REAL*8 Z0,ZQACC
      INTEGER ZQFLAG
C---FOR COMMON/VLODAT/:
      REAL*8 LOVLO,UPVLO,VLOINC,IDCACC
      INTEGER LOFLAG,UPFLAG
C---FOR COMMON/VOLTS/:
      COMPLEX*16 VR(6)
      REAL*8 VRDC,VLO,VDBIAS,IDBIAS
C---THE COMMON BLOCKS USED ARE:
      COMMON/CONST/QEL,BOLTZ,PI,TK,MU,EPS
      COMMON/DIODE/ALP,ETA,PHI,GAM,C0,IS,RS,FP,WP,IF,IGJ,ICJ,GJ,CJ
      COMMON/IMPED/LOPWR,ZER,ZEI,ZERDC,RSLO,XSLO,ZEMBSB,RSSB
      COMMON/LOOPS/NH,NLO,JLO,NVLO,NPTS,NCURR,IPT,NPRINT,NITER
      COMMON/RES/ER,NDS,NDE,SMOB,EMOB,TE,AR,CL,CW,CT,RC
      COMMON/RKG/ACC,VDINIT,NDIM
      COMMON/TLINE/Z0,ZQACC,ZQFLAG
      COMMON/VLODAT/LOVLO,UPVLO,LOFLAG,UPFLAG,VLOINC,IDCACC
      COMMON/VOLTS/VR,VRDC,VLO,VDBIAS,IDBIAS
C---VARIABLES ARE INITIALIZED AS FOLLOWS:
C---COMMON/CONST/VARIABLES:
      DATA QEL,BOLTZ,PI/1.602192D-19,1.38062D-23,3.14159265358979D0/
      DATA MU,EPS/12.56637061435917D-9,8.854185336732028D-14/
      DATA TK/300.0D0/
C---COMMON/DIODE/VARIABLES:
      DATA ETA,PHI,GAM/1.18D0,1.05D0,0.5D0/
      DATA C0,IS,RS/6.2D-15,3.77D-17,6.3D0/
      DATA FP,IF/180.0D9,3.95D9/
C---COMMON/IMPED/VARIABLES:
      DATA ZERDC/1.0D0/
      DATA ZER(1),ZER(2),ZER(3)/15.216D0,549.419D0,36.848D0/
      DATA ZER(4),ZER(5),ZER(6)/25.249D0,10.735D0,61.657D0/
      DATA ZEI(1),ZEI(2),ZEI(3)/93.576D0,-302.2027D0,-166.141D0/
      DATA ZEI(4),ZEI(5),ZEI(6)/-73.613D0,17.426D0,17.533D0/
      DATA ZEMBSB(1),ZEMBSB(2)/(28.7D0,-166.3D0),(481.6D0,-196.62D0)/
      DATA ZEMBSB(3),ZEMBSB(4)/(9.46D0,119.36D0),(50.0D0,0.0D0)/
      DATA ZEMBSB(5),ZEMBSB(6)/(25.25D0,-67.83D0),(291.4D0,-62.2D0)/
      DATA ZEMBSB(7)/(61.8D0,195.5D0)/
C---COMMON/LOOPS/VARIABLES:
```

```
      DATA  NH,NLO,NPTS,NCURR,NVLO,NITER,NPRINT/6,1,51,10,50,500,100/
C---COMMON/RES/VARIABLES:
      DATA ER,NDS,NDE,SMOB,EMOB/13.1D0,2.0D18,2.0D17,3.125D3,2.5D3/
      DATA TE,AR,CL,CW,CT/8.0D-6,1.000D-4,0.02286D0,0.0127D0,0.0127D0/
      DATA RC/0.5D0/
C---COMMON/RKG/VARIABLES:
      DATA VDINIT,ACC,NDIM/0.0D0,1.0D-6,1/
C---COMMON/TLINE/VARIABLES:
      DATA Z0,ZQACC/200.0D0,0.01D0/
C---COMMON/VLODAT/ VARIABLES:
      DATA VLOINC,IDCACC/0.20D0,0.01D0/
C---COMMON/VOLTS/VARIABLES:
      DATA VDBIAS,IDBIAS/0.8D0,0.001D0/
      DATA VLO/0.9625D0/
      END
```

A1.3 Printout from the Mixer Analysis Program of Section A1.2

The following 5 pages contain the output which results from the execution of the mixer analysis program listed in Section A1.2.

The embedding impedances are those at backshort setting 38 (see Figs. 3-17 to 3-22 and Figs. 3-29 to 3-34). The diode parameters are discussed in Section 4.5 of Chapter 4.

ANALYSIS OF A 180.00 GHZ MICROWAVE MIXER

INPUT DATA

DIODE PARAMETERS:	ALP	PHI	GAM	C0	IS	RS	ETA	
	32.782	1.050	0.500	6.200D-15	3.770D-17	6.3000	1.1800	
CHIP PARAMETERS:	LENGTH	WIDTH	HEIGHT	ANODE RAD	SUB DOP	EPI DOP	SUB MOB	EPI MOB
	0.023	0.013	0.013	1.0000D-04	2.0000D+18	2.0000D+17	3125.0	2500.0
OPERATING FREQUENCIES AND TEMPERATURE:	FP	IF	TK					
	1.8000D+11	3.9500D+09	300.0					
BIAS SETTINGS:	VDBIAS	IDBIAS						
	0.800	0.001000						
VLO ADJUST VARIABLES:	VLO	VLOINC	IDCACC					
	0.962500	0.200000	0.010000					
DRKGS VARIABLES:	PRMT(1) (LOW LIM)	PRMT(2) (UP LIM)	PRMT(3) (INCR)	PRMT(4) (ACC)	Y(1) (VD)	DERY(1) (DV/DT)	NDIM (NEQS)	
	0.0	6.28318531	0.12319971	1.0000D-06	0.0	1.000	1	
LOOP LIMITS:	NITER	NLO	NVLO	NPTS	NHARM	NPRINT		
	500	1	50	51	6	100		
CONVERGENCE PARAMETERS:	Z0	ZOACC						
	200.00	1.000D-02						

EMBEDDING IMPEDANCES:

	HARMONICS OF THE LO					HARMONIC SIDEBANDS	
HARM#	ZER	ZEI	ZEMB		SIDEBAND#	ZEMBSB	
DC	1.000D+00		2.000D+02		3	2.870D+01	-1.663D+02
1	1.522D+01	9.358D+01	2.000D+02	0.0	2	4.816D+02	-1.966D+02
2	5.494D+02	-2.022D+02	5.599D+02	-2.988D+02	1	9.460D+00	1.194D+02
3	3.685D+01	-1.661D+02	4.837D+01	-1.620D+02	0	5.000D+01	0.0
4	2.525D+01	-7.361D+01	3.762D+01	-6.879D+01	-1	2.525D+01	-6.783D+01
5	1.074D+01	1.743D+01	2.386D+01	2.282D+01	-2	2.914D+02	-6.220D+01
6	6.166D+01	1.753D+01	7.546D+01	2.344D+01	-3	6.180D+01	1.955D+02

DIODE SERIES RESISTANCES:

	HARMONICS OF THE LO					HARMONIC SIDEBANDS	
FGHZ	HARM#	RSLO	XSLO	FGHZ	SIDEBAND#	RSSB	
DC	0	6.3000		543.95	3	11.5416	4.1920
180.00	1	9.1930	2.4114	363.95	2	10.5351	3.4290
360.00	2	10.5104	3.4103	183.95	1	9.2277	2.4378
540.00	3	11.5214	4.1767	3.95	0	6.4834	0.3572
720.00	4	12.2737	4.8229	176.05	-1	9.1579	-2.3848
900.00	5	13.1245	5.3921	356.05	-2	10.4857	-3.3915
1080.00	6	13.8033	5.9068	536.05	-3	11.5012	-4.1614

ORIGINAL PAGE IS
OF POOR QUALITY

```
RESULTS OF THE VLO ADJUSTMENTS

 VALUES OF THE DC CURRENT AND LO VOLTAGE FOR CYCLE  1 OF THE LOOP FOR ADJUSTING VLO TO GIVE 0.001000 AMPS ARE:
           IDCOS(1)=0.000999       VLO BEFORE ADJUSTMENT: 0.96250
                                   VLO AFTER ADJUSTMENT:  0.96250

NONLINEAR ANALYSIS RESULTS:  REFLECTION CYCLE #  26 IN VLO ADJUSTMENT LOOP NUMBER  1

 VL(I)
             1  -3.469D-01  -1.950D-01     2   2.187D-02   2.631D-02     3  2.073D-04   3.858D-03     4  2.433D-04   3.453D-03
             5   5.064D-03   1.273D-03     6   5.529D-04   4.803D-04

 VR(I)
             1   4.812D-01   0.0           2   1.662D-02   1.039D-02     3  2.816D-03  -6.541D-04     4  1.418D-03  -2.020D-03
             5  -4.121D-03  -6.562D-05     6  -3.031D-04  -1.443D-04

 VDCOS,VDSIN
             1   1.344D-01   1.950D-01     2   3.849D-02  -3.671D-02     3  3.067D-03  -3.201D-03     4  1.666D-03  -1.434D-03
             5   9.265D-04  -1.229D-03     6   2.510D-04  -3.354D-04

 IDCOS,IDSIN
             1   4.141D-03  -9.751D-04     2  -2.627D-05   7.956D-05     3  1.326D-05   2.257D-05     4  5.897D-06   2.736D-05
             5  -4.601D-05   6.587D-06     6  -4.274D-06   3.126D-06

 ZQMAG,ZQPHA
             1   2.784D-01  -69.           2   1.0000D+00  180.          3  1.002D+00   179.          4  1.002D+00   180.
             5   1.003D+00  -179.          6   1.001D+00   180.

 DC TERMS:  VDCOS= 7.936D-01     IDCOS= 1.000D-03   VLDC= 2.968D-01       VRDC= 4.968D-01

 ZQFLAG= 0

 REQUIRED LO POWER: 5.858D-04
```

ORIGINAL PAGE IS
OF POOR QUALITY

GRAPHS FOR REFLECTION CYCLE NUMBER 26

DIODE CONDUCTANCE CURRENT VS TIME FOR ONE LO CYCLE

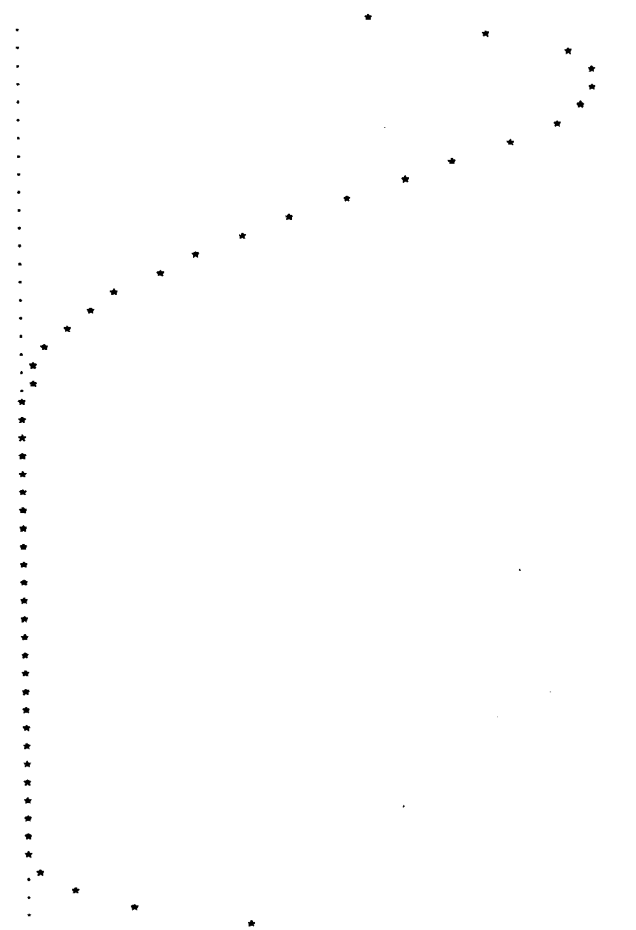

DIODE CAPACITANCE VS TIME FOR ONE LO CYCLE

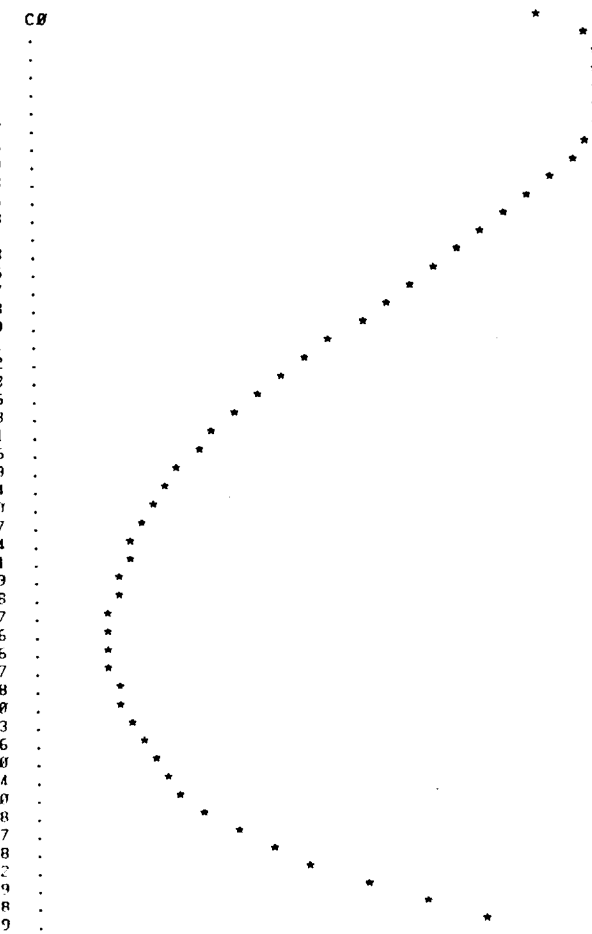

IGJ(MA)	CJ(PF)
2.662	0.0229
3.555	0.0243
4.136	0.0251
4.403	0.0255
4.433	0.0256
4.296	0.0254
4.041	0.0250
3.706	0.0245
3.320	0.0239
2.907	0.0233
2.488	0.0226
2.081	0.0218
1.697	0.0211
1.344	0.0203
1.027	0.0195
0.750	0.0187
0.518	0.0178
0.335	0.0169
0.200	0.0161
0.109	0.0152
0.054	0.0143
0.024	0.0135
0.010	0.0128
0.004	0.0121
0.001	0.0115
0.001	0.0109
0.000	0.0104
0.000	0.0100
0.000	0.0097
0.000	0.0094
0.000	0.0091
0.000	0.0089
0.000	0.0088
0.000	0.0087
0.000	0.0086
0.000	0.0086
0.000	0.0087
0.000	0.0088
0.000	0.0090
0.000	0.0093
0.000	0.0096
0.000	0.0100
0.000	0.0104
0.001	0.0110
0.002	0.0118
0.009	0.0127
0.032	0.0138
0.105	0.0152
0.321	0.0169
0.807	0.0188
1.641	0.0209

GRAPHS FOR REFLECTION CYCLE NUMBER 26

ID(MA)	VD(VOLTS)
5.082	0.973
4.989	0.982
4.840	0.986
4.673	0.988
4.330	0.988
3.960	0.987
3.522	0.985
3.030	0.983
2.505	0.979
1.968	0.975
1.434	0.971
0.915	0.965
0.412	0.959
-0.076	0.952
-0.555	0.944
-1.025	0.934
-1.484	0.923
-1.922	0.909
-2.324	0.894
-2.672	0.875
-2.953	0.854
-3.155	0.830
-3.274	0.803
-3.316	0.774
-3.286	0.743
-3.196	0.711
-3.054	0.680
-2.864	0.648
-2.625	0.618
-2.336	0.589
-1.992	0.563
-1.593	0.542
-1.142	0.525
-0.650	0.514
-0.132	0.509
0.396	0.510
0.918	0.519
1.425	0.533
1.910	0.554
2.375	0.579
2.820	0.609
3.247	0.643
3.652	0.680
4.028	0.719
4.363	0.759
4.645	0.799
4.865	0.838
5.018	0.875
5.107	0.908
5.141	0.936
5.131	0.958

TOTAL DIODE CURRENT VS TIME FOR ONE LO CYCLE

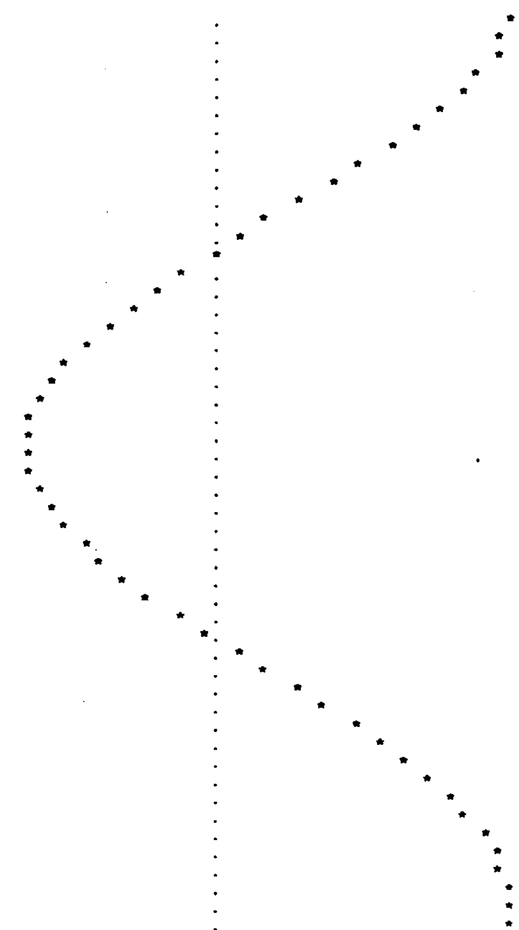

DIODE VOLTAGE VS TIME FOR ONE LO CYCLE

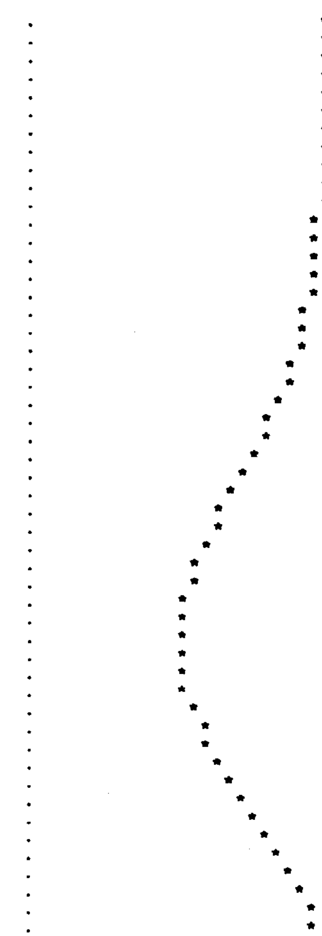

RESULTS OF THE SMALL-SIGNAL ANALYSIS

FOURIER COEFFICIENTS OF THE DIODE CONDUCTANCE AND CAPACITANCE WAVEFORMS

GJMAG,GJPHA	1	2.81ØD-Ø2	-4Ø.	2	1.758D-Ø2	-75.	3	8.32ØD-Ø3	-94.	4	4.184D-Ø3	-89.
	5	2.599D-Ø3	-86.	6	1.5Ø1D-Ø3	-81.						
CJMAG,CJPHA	1	4.Ø89D-15	-49.	2	9.21ØD-16	-61.	3	4.Ø54D-16	-47.	4	1.976D-16	-5Ø.
	5	8.851D-17	-41.	6	5.2Ø7D-17	-35.						

DC TERMS: GJMAG = 3.28ØD-Ø2 CJMAG = 1.548D-14

CONVERSION LOSS MATRIX (DB)

	3	2	1	Ø	-1	-2	-3
3	Ø.Ø	31.62	4Ø.62	36.7Ø	49.39	52.23	63.83
2	36.13	Ø.Ø	21.21	2Ø.33	28.54	46.99	48.86
1	36.Ø8	24.94	Ø.Ø	1Ø.4Ø	18.82	37.1Ø	42.66
Ø	31.34	29.92	11.67	Ø.Ø	4.31	35.6Ø	31.Ø8
-1	38.69	31.11	2Ø.56	3.63	Ø.Ø	15.5Ø	28.34
-2	47.75	43.85	32.91	19.4Ø	11.67	Ø.Ø	3Ø.77
-3	67.98	61.46	45.Ø2	36.57	36.Ø1	26.37	Ø.Ø

UPPER SIDEBAND CONVERSION LOSS: L(Ø,1) = 11.67 DB

LOWER SIDEBAND CONVERSION LOSS: L(Ø,-1) = 4.31 DB

INPUT IMPEDANCES	3	2	1	Ø	-1	-2	-3
REAL(ZIN):	16.26	13.24	31.94	238.57	23.72	19.16	16.57
IMAG(ZIN):	-13.62	-29.85	-63.1Ø	-171.32	61.88	3Ø.94	13.69

IF OUTPUT IMPEDANCE: ZIFOUT = 238.57 + J -171.32

VSWR OF IF PORT REFERRED TO 5Ø OHMS: 7.3Ø45

EQUIVALENT INPUT NOISE TEMPERATURES:	TSSB(USB)	SHOT(USB)	THERM(USB)	TSSB(LSB)	THERM(LSB)	SHOT(LSB)
	3983.36	1ØØ7.57	2975.79	731.35	184.99	546.36

APPENDIX 2. CALCULATION OF THE DIODE SERIES RESISTANCE

A2.1 Introduction

The series resistance of a Schottky barrier diode is a function of geometry and frequency.* The equations which will be given here apply to diodes having circular shaped anodes and an ohmic contact at the rear of the semiconductor chip. The arrangement is shown in Fig.A2-1. Other anode geometries are discussed in [102,141,182].

---

* The series resistance in the undepleted epitaxial layer is also a function of applied voltage. This effect has been neglected in the mixer analysis program since in most cases the diode series resistance is only a small fraction of the overall dynamic resistance of the mixer. In order to include a voltage dependent series resistance in the mixer analysis program substantial modifications are required. In the large signal analysis R_s could no longer be considered as part of the embedding network and we would require two state equations to solve the diode equivalent circuit. In the noise calculations the thermal noise components would now be correlated due to the dependence on applied voltage and a more complete theory than is presented in Chapter 2 is needed to take this effect into account.

ORIGINAL PAGE IS
OF POOR QUALITY

Geometry of Diode Chip Used in 140-220 GHz Mixer

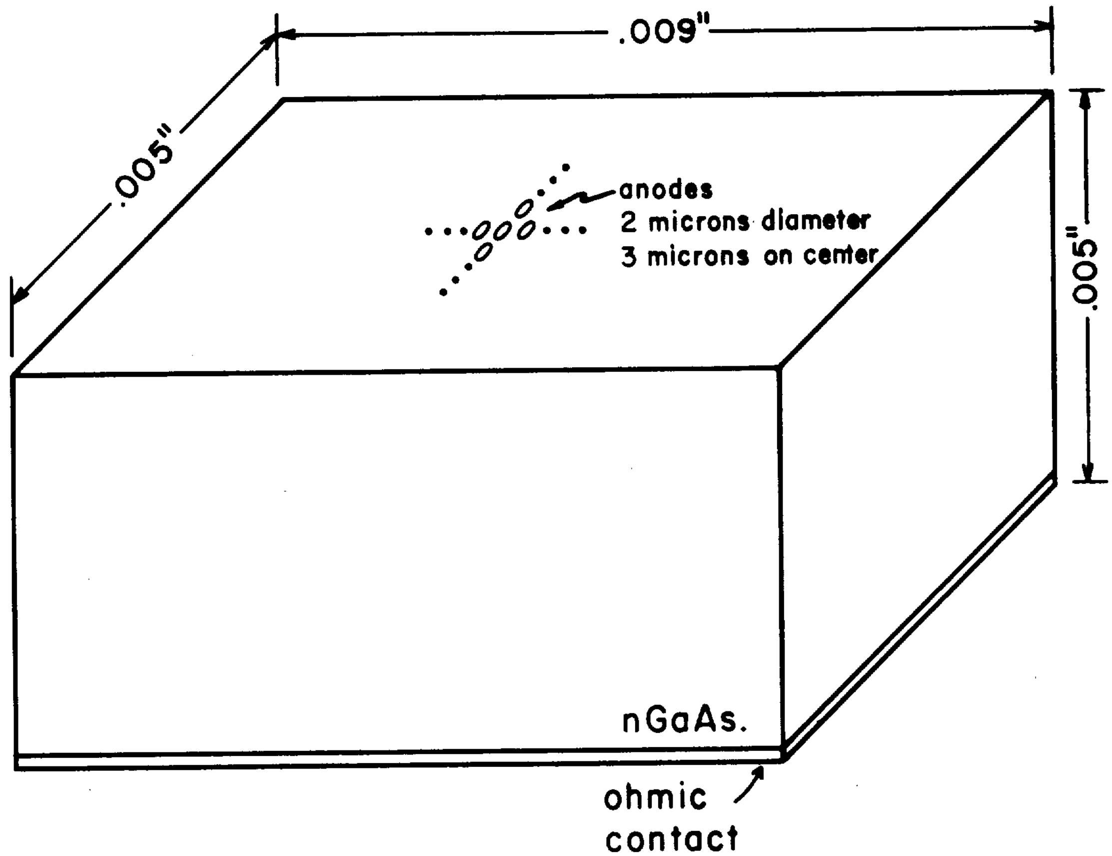

Fig. A2-1 An isometric view of the diode chip used in the 140-220 GHz mixer. The anodes on the front face are 2 microns in diameter and spaced 3 microns on center. The ohmic contact is at the rear of the chip. In the analysis it is assumed that the anode which is contacted by the whisker is near the center of the chip.

A2.2 DC Resistance

The DC resistance of a diode is given by the resistance in the undepleted epitaxial layer plus the resistance of the semiconductor bulk. To these must be added the whisker and ohmic contact resistance and the DC loss through the microstrip filter structure of the mixer. Symbolically:

$$R_s(dc) = R_{epi}(dc) + R_{sub}(dc) + R_c \ , \tag{A2.1}$$

where R_c represents the contributions from the ohmic contact and filter loss.

$R_s(dc)$ can be measured from the diode I-V curve. However the DC I-V curve gives a value of R_s which is too low [86]. This is due to the fact that as current flows into the diode the temperature rises and continually changes the exponent in the I-V relation (see equations (2.1) and (2.2)). The true resistance can be measured only if the bias voltage is applied at a high enough frequency so that the diode temperature rise cannot follow the rapid changes in voltage. Generally the difference in the measured resistance at DC and the actual value is 1-2 ohms. $R_s(dc)$ can also be calculated and the appropriate equations are developed in the next two subsections.

A2.2.1 DC Resistance of the Epitaxial Layer

If the diode current is considered to flow vertically down from the anode through the undepleted epitaxial layer as shown in Fig.A2-2 then the series resistance is easily shown to be:

$$R_{epi}(dc) = \frac{t_{epi} - w_n(v_d)}{\sigma_{epi}\, a^2} , \qquad \text{(A2.2)}$$

where t_{epi} and w_n are the epi and depletion layer widths respectively, σ_{epi} is the epi layer conductivity in $(\text{ohm-cm})^{-1}$, and a is the anode radius in cm. σ_{epi}, for a material of mobility μ_n (cm^2/V-s) is:

$$\sigma_{epi} = q\mu_n n_{d_{epi}} , \qquad \text{(A2.3)}$$

where $n_{d_{epi}}$ is the carrier concentration in cm^{-3}.

At room temperature in GaAs, $n_{d_{epi}}$ is equal to the

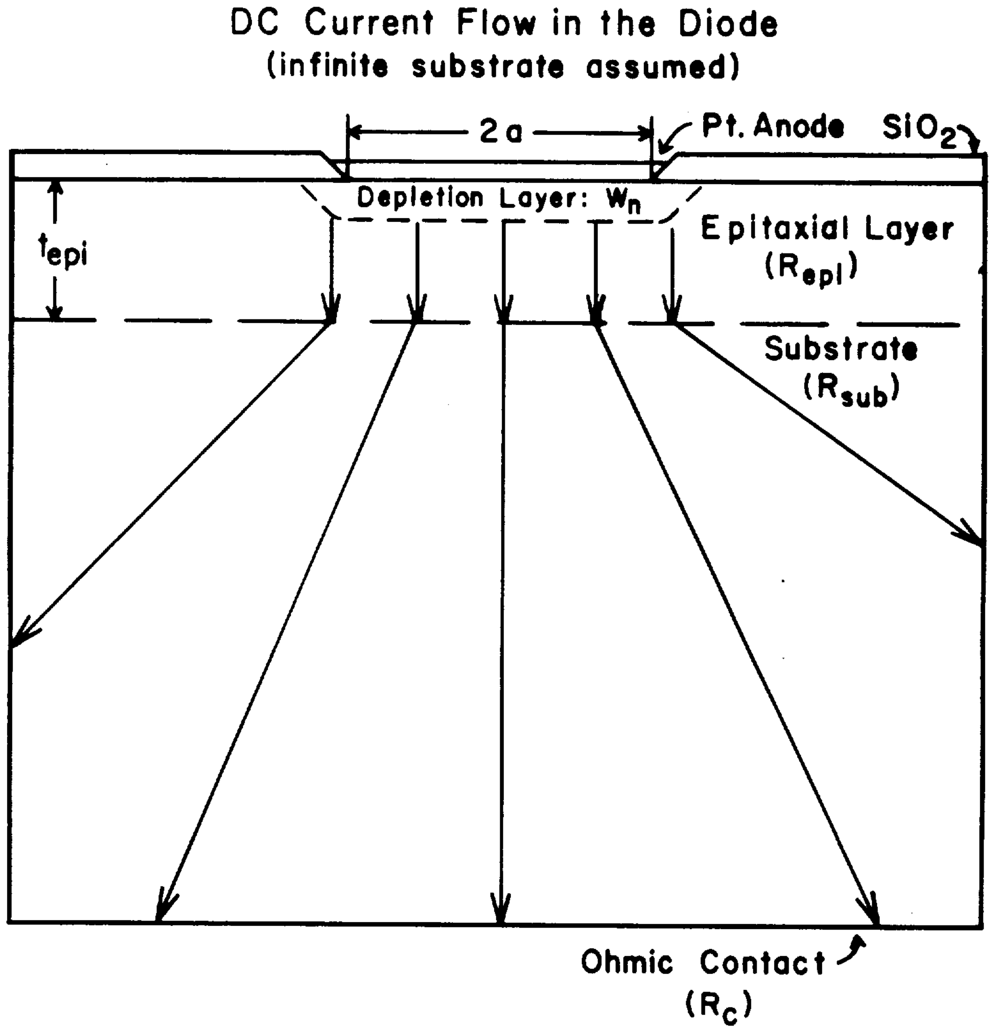

Fig. A2-2 An illustration of the DC current path in the diode chip. The current is assumed to flow vertically down through the epitaxial layer and then to spread spheroidally through the substrate. The diode dc resistance is the sum of the three components shown in the figure: R_{epi}, R_{sub} and R_c.

electron donor concentration, $N_{d_{epi}}$. At low temperatures, when all the donor atoms are not ionized [161]:

$$n_{d_{epi}} = N_{d_{epi}} \{1-(1+ 0.5 \exp[(E_d-E_f)/kT])^{-1}\} \quad \text{(A2.4)}$$

E_d is the difference in energy between the conduction band E_c and the donor dopant level (E_d=0.03 eV for Tellurium in GaAs for instance). The Fermi level must be determined by solving the following expression for E_f [161]:

$$N_c \exp[(E_f-E_c)/kT] = N_v \exp[(E_v-E_f)/kT] + N_{d_{epi}} \{1+2 \exp[(E_f-E_d)/kT]\} , \quad \text{(A2.5)}$$

where N_c and N_v are the conduction and valance band state densities, and E_v is the valance band energy level. In the mixer analysis program of Appendix 1, $n_{d_{epi}}$ has been set equal to $N_{d_{epi}}$ since only room temperature performance is being examined.

In (A2.2) we see that R_{epi} is a function of the diode voltage through $w_n(v_d)$. For most mixers w_n will be much less than t_{epi} at any point in an LO cycle and we can neglect w_n in the series resistance calculation. However, in diodes with very thin epitaxial layers w_n may be equal to t_{epi} for a substantial portion of an LO cycle and R_{epi} will then be negligible. As a compromise v_d is taken to be the DC bias voltage (VDBIAS in the mixer analysis program) and w_n is then [161]:

$$w_n = [(\phi_{bi}-v_d-kT/q)\ 2\varepsilon_0\varepsilon_r/qN_{d_{epi}}]^{1/2} , \qquad (A2.6)$$

where ε_r is the relative dielectric constant in the semiconductor and ϕ_{bi} is the built in potential given in equation (2.6).

A2.2.2 DC Resistance of the Substrate

The DC spreading resistance of the semiconductor substrate was calculated by, among others, Dickens [36]. Using oblate spherical coordinates and assuming a circular anode on an infinite dielectric Dickens obtained (for the current flow pattern of Fig.A2-2):

$$R_{sub}(dc) = 1/(4a\sigma_{sub}) , \qquad (A2.7)$$

where the substrate conductivity σ_{sub} is calculated from:

$$\sigma_{sub} = q\mu_n n_{d_{sub}} . \tag{A2.8}$$

At room temperature $n_{d_{sub}}$ is equal to $N_{d_{sub}}$, the substrate donor concentration. For low temperatures (A2.4) and (A2.5) should be used with $N_{d_{sub}}$ replacing $N_{d_{epi}}$.

Expression (A2.7) has been in use since at least 1948 [165] and inherent in its calculation is the assumption of an infinite conductivity for the metallic anode. When this restriction is lifted (thereby changing the boundary conditions used in the determination of the electromagnetic fields) the following formula results [128]:

$$R_{sub}(dc) = 8/(3a\pi^2\sigma_{sub}) , \tag{A2.9}$$

which is roughly 8% higher than the value obtained using (A2.7).

A2.3 AC Resistance

Under AC conditions the current flow in the diode is restricted to a narrow region around the edge of the semiconductor chip as shown in Fig.A2-3. This skin depth δ_s is given by:

$$\delta_s = [2/(\omega\mu\sigma)]^{1/2} \quad , \tag{A2.10}$$

where μ is the magnetic permeability of the semiconductor, σ is its conductivity and ω is the incident radian frequency.

For GaAs doped with 2×10^{18} atoms/cm^3, δ_s is 3 microns at 100 GHz. At 1000 GHz (the sixth harmonic of the local oscillator in the 140-220 GHz mixer) δ_s drops to about one micron. This confinement of the current flow increases the series resistance in the diode over its DC value.

AC Current Flow in the Diode
(cylindrical geometry assumed)

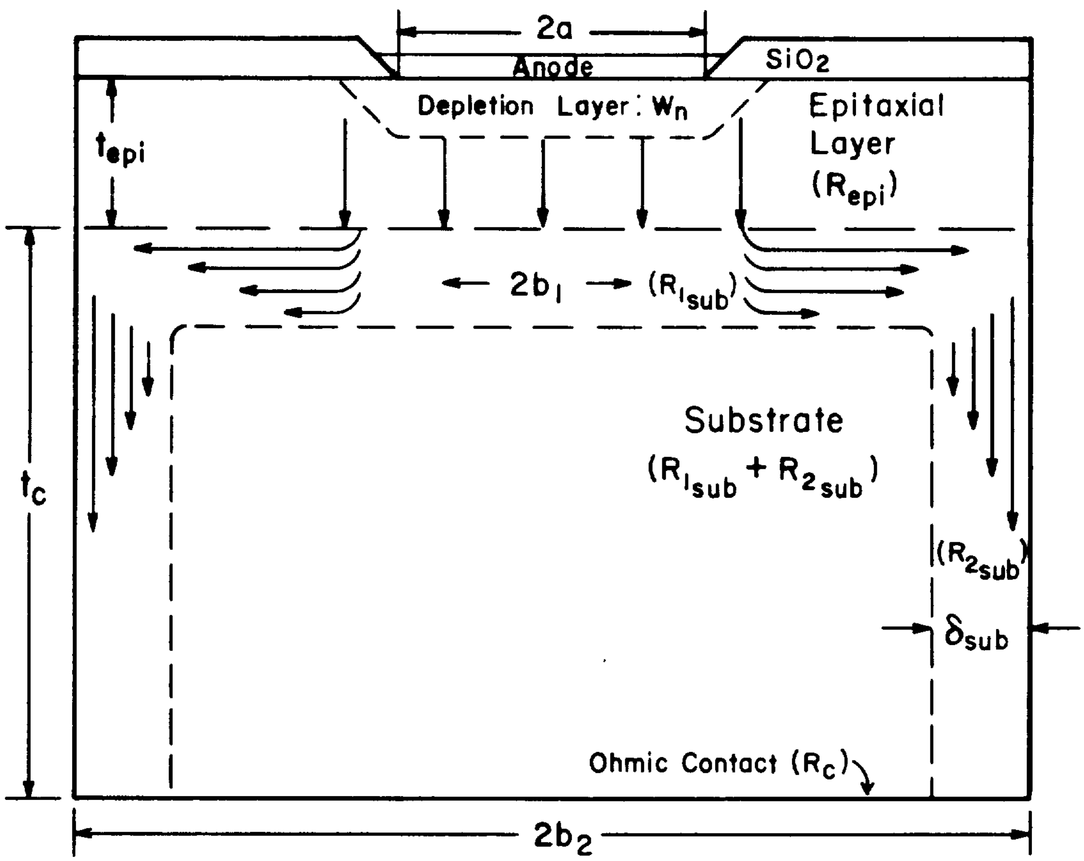

Fig. A2-3 An illustration of the AC current path in the diode chip. The current is assumed to flow vertically down through the epitaxial layer, laterally outwards along the top surface of the substrate and vertically down the side walls of the chip. In the series resistance calculation the diode chip is taken to be a cylinder of radius b_1 for one skin depth at the substrate surface and radius b_2 throughout the remainder of the substrate. b_1 is the radius of a circle whose area is the same as that of the actual rectangular chip face and b_2 is the radius of a cylinder whose surface area is equal to that of the four sides of the actual rectangular chip.

A2.3.1 AC Resistance of the Epitaxial Layer

Even at 1000 GHz the skin depth in the lightly doped epitaxial layer is much larger than the epi thickness. Therefore the AC series resistance of the epitaxial layer is still governed by (A2.2).

A2.3.2 AC Resistance of the Substrate

The AC series resistance of the substrate is a function both of anode and diode chip geometry. The current is assumed to flow laterally outward from the circular anode to the edge of the chip and then down the side walls as shown in Fig.A2-3. Dickens [36] calculated the resistance due to the lateral portion of the current flow and obtained:

$$R_{1_{sub}} = \frac{(1 + j)}{2\pi\sigma_{sub}\delta_s} \left[\ln(b_1/a)+(\delta_s/a)\tan^{-1}(b_1/a)\right], \quad (A2.11)$$

where b_1 is the chip radius (which we will take to be the radius of a circle whose area is equal to that of the rectangular chip face). Notice that $R_{1_{sub}}$ is complex.

After reaching the edge the current is assumed to flow down the sides of the diode chip to the back contact. If we represent the chip by a cylinder of radius b_2 whose surface area is equal to the total area of all four sides of the actual rectangular chip then $R_{2_{sub}}$ can be approximated as:

$$R_{2_{sub}} = (1 + j)\, t_c/(2\pi b_2 \sigma_{sub} \delta_s) \; , \tag{A2.12}$$

t_c being the thickness of the chip. The total AC resistance of the diode substrate is then the sum of (A2.11) and (A2.12).

A2.4 Total Series Resistance

The total diode series resistance at any frequency is calculated from the equations in Sections A2.2 and A2.3:

$$R_s = R_{epi}(ac) + R_c + R_{1_{sub}}(ac) + R_{2_{sub}}(ac) \; . \qquad (A2.13)$$

It is very likely that $R_s(dc)$ will be available from measurements and therefore it will not be necessary to use the less accurate form obtained in Section A2.2. In this instance, rather than use (A2.13) to calculate R_s we can make use of the measured DC resistance by writing:

$$R_s = R_s(dc)\ [R_s/R_s(dc)] \; . \qquad (A2.14)$$

Now if we substitute the measured DC resistance for the first term on the right hand side of (A2.14) we obtain:

$$R_s = R_s(\overset{dc}{measured})\ \frac{R_s[\text{calculated using (A2.13)}]}{R_s[\text{calculated using (A2.1)}]} \; . \qquad (A2.15)$$

Using (A2.15) the measured value of the DC resistance is increased at AC frequencies by the percentage change that would have been incurred if only the calculated values of the resistance were used. This is the preferred format employed in the mixer analysis program, R_s(measured at DC) being entered in the BLOCK DATA routine.

APPENDIX 3. CALCULATION OF THE AVAILABLE MIXER LOCAL OSCILLATOR POWER

The local oscillator power available to a mixer with an LO frequency source impedance of $Z_e(\omega_p)$ is:

$$P_{LO} = |V_{LO}|^2 \; / \; \{8 \; \mathrm{Re}[Z_e(\omega_p)] \} \; , \tag{A3.1}$$

where V_{LO} is the amplitude of the Thevenin equivalent LO voltage source at radian frequency ω_p. Referring to Fig.A3-1a (or using equation (2.11)):

$$V_{LO} = V_{d_1} + I_{d_1} \; [R_s(\omega_p) + Z_e(\omega_p)] \; , \tag{A3.2}$$

where V_{d_1} and I_{d_1} are the diode current and voltage amplitudes at the first LO harmonic, i.e. at radian frequency ω_p.

In the mixer analysis program described in Chapter 2, the local oscillator voltage (VLO) is adjusted until a desired DC rectified current (IDCOS(1)) appears in the diode. This LO voltage is not the same as that given in

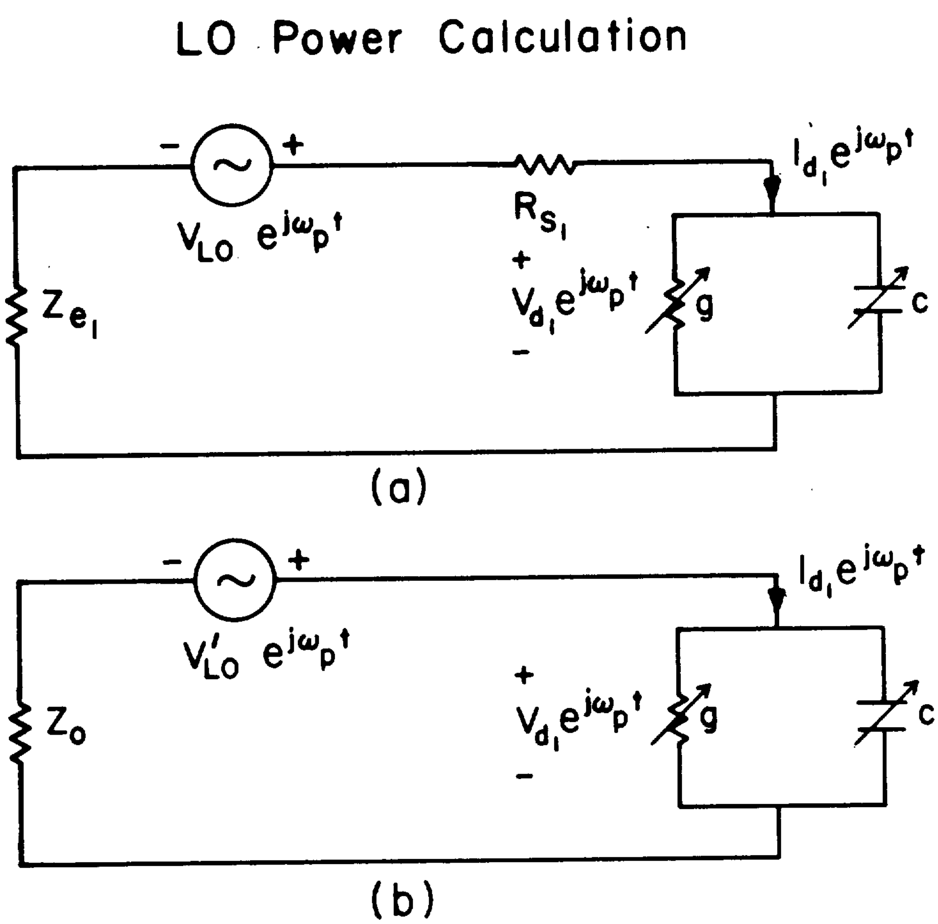

Fig. A3-1 (a) The equivalent circuit of the actual mixer at the LO frequency and, (b) the circuit which is solved by the mixer analysis program. Since we know that V_{d_1} and I_{d_1} in the two circuits are the same, the actual LO voltage V_{LO} (and hence the available power) can be determined from the computed value V'_{LO} and Z_0.

(A3.2) because the embedding impedance of the mixer at the LO frequency is artificially set to Z_0 (ZO), the characteristic impedance of the hypothetical transmission line in the large signal mixer equivalent circuit. The LO voltage returned by the mixer analysis program is actually given by the circuit shown in Fig.A3-1b, where the diode series resistance plus first harmonic embedding impedance (ZEMB(1)) have been set to Z_0 (ZO). The available LO power for this mixer circuit is:

$$P'_{LO} = |V'_{LO}|^2 \, / \, \{8 \, \mathrm{Re}[Z_0] \} \, , \qquad (A3.3)$$

where V'_{LO} is the final value of VLO returned in the mixer analysis program and is given by (referring to Fig.A3-1b):

$$V'_{LO} = I_{d_1} \, Z_0 + V_{d_1} \; . \qquad (A3.4)$$

Using (A3.4) in (A3.2):

$$V_{LO} = V'_{LO} + I_{d_1} [R_s(\omega_p) + Z_e(\omega_p) - Z_0] \, , \qquad (A3.5)$$

and therefore the actual power available for a source impedance of $Z_e(\omega_p)$ is:

$$P_{LO} = \frac{|V'_{LO} + I_{d_1}[R_s(\omega_p) + Z_e(\omega_p) - Z_0]|^2}{8\ \mathrm{Re}[Z_e(\omega_p)]}\ , \tag{A3.6}$$

which is the form used in the mixer analysis program (in subroutine POWER). I_{d_1} is the n=1 term in the complex exponential Fourier series representation of $i_d(t)$ and is given by I_{d_1}=IDCOS(2)-jIDSIN(2) in the mixer analysis program. The minus sign results from the conversion of the coefficients in the trigonometric Fourier series representation of $i_d(t)$ (returned by DFORIT) into the single ended complex exponential series coefficients used in the large signal mixer theory of Chapter 2. The small signal analysis makes use of the double ended complex exponential Fourier series which adds an additional factor of one-half to the conversion from the trigonometric series given by DFORIT.

APPENDIX 4. A STUDY OF THE EFFECTS OF SERIES INDUCTANCE AND DIODE CAPACITANCE ON THE PERFORMANCE OF SOME SIMPLE MIXERS

This appendix contains graphs of the equivalent input noise temperature, upper sideband conversion loss and the real part of the IF output impedance as a function of series inductance and diode capacitance for the two simple mixer circuits given in Figs. 2-12 and 2-13.

The mixer analysis program described in [151] was used for each of three diodes in the two mixer circuits, (1) a Schottky diode with a varying capacitance (GAM=.5), (2) a Schottky diode with a constant capacitance (GAM=0) and (3) a Mott diode with an experimentally determined C-V relationship (see Fig. 2-14). In all cases the diodes were forward biased to 0.4 V and the LO power was adjusted to give a rectified current of 2 mA. The signal, LO and IF frequencies were 119 GHz, 115 GHz and 4 GHz respectively. No account was taken for skin effect in these results, i.e. the diode series resistance was assumed constant at 4.4 ohms.

Section A4.1 contains a plot showing the effect on the mixer performance of varying the series inductance (LS) while the zero bias junction capacitance (CO) is kept constant. Section A4.2 contains graphs showing the mixer performance as a function of the zero bias junction capacitance at nine different values of series inductance. In all cases the graph labelled (a) contains the results of the analysis of the circuit in Fig. 2-12 (higher harmonics short circuited outside the series inductance) and the graph labelled (b) contains the results of the analysis of the circuit in Fig. 2-13 (higher harmonics open circuited outside the series inductance).

A4.1 Graphs of Mixer Performance as a Function of Series Inductance

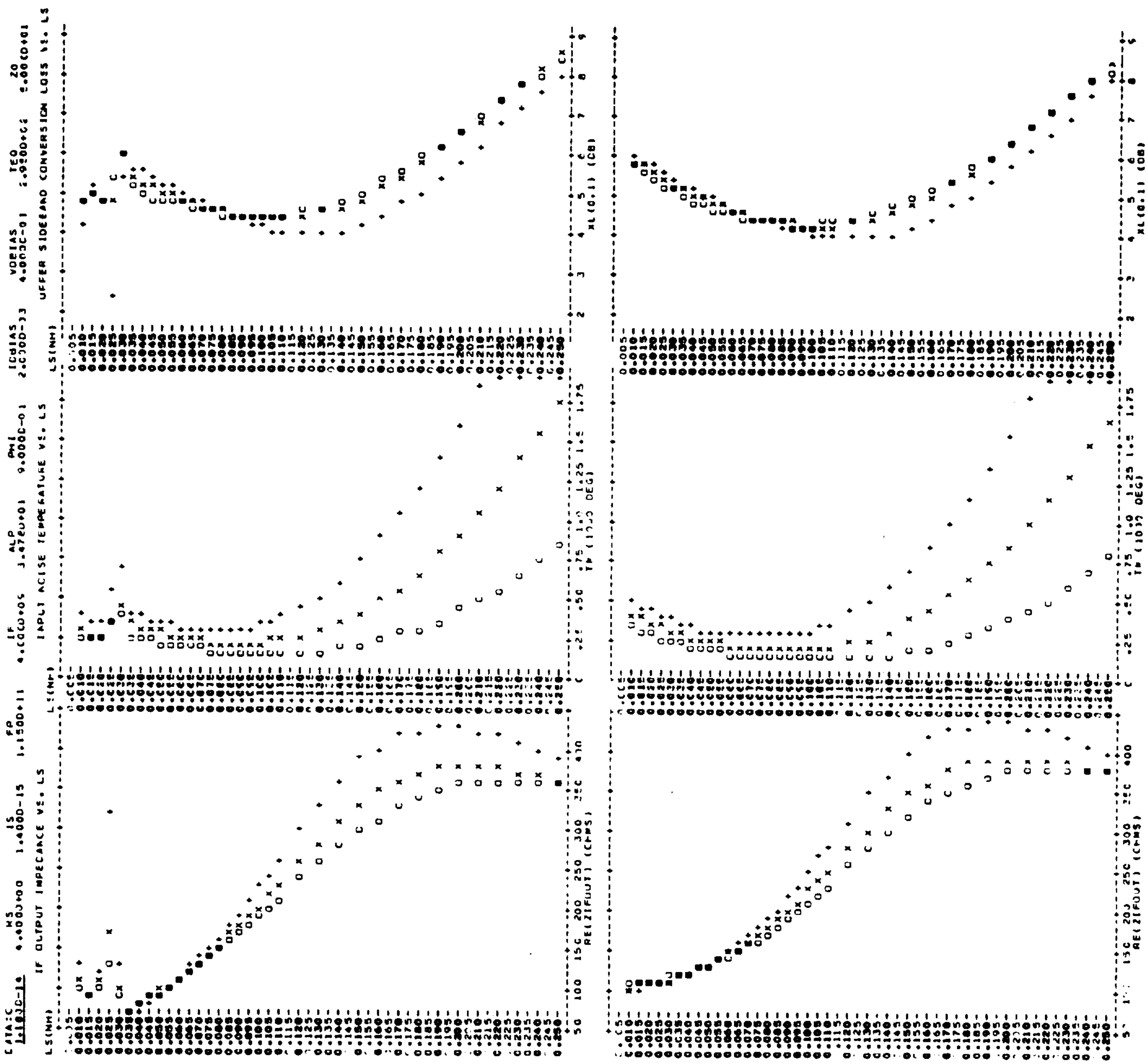

(a)
s/c harmonics

(b)
o/c harmonics

C0 = 11.8 fFd.

+ = Schottky diode with varying capacitance (GAM=0.5)

O = Schottky diode with constant capacitance (GAM=0)

x = Mott diode with a realistic C-V variation

ORIGINAL PAGE IS
OF POOR QUALITY

A4.2 Graphs of Mixer Performance as a Function of Diode Capacitance at Nine Different Values of Series Inductance

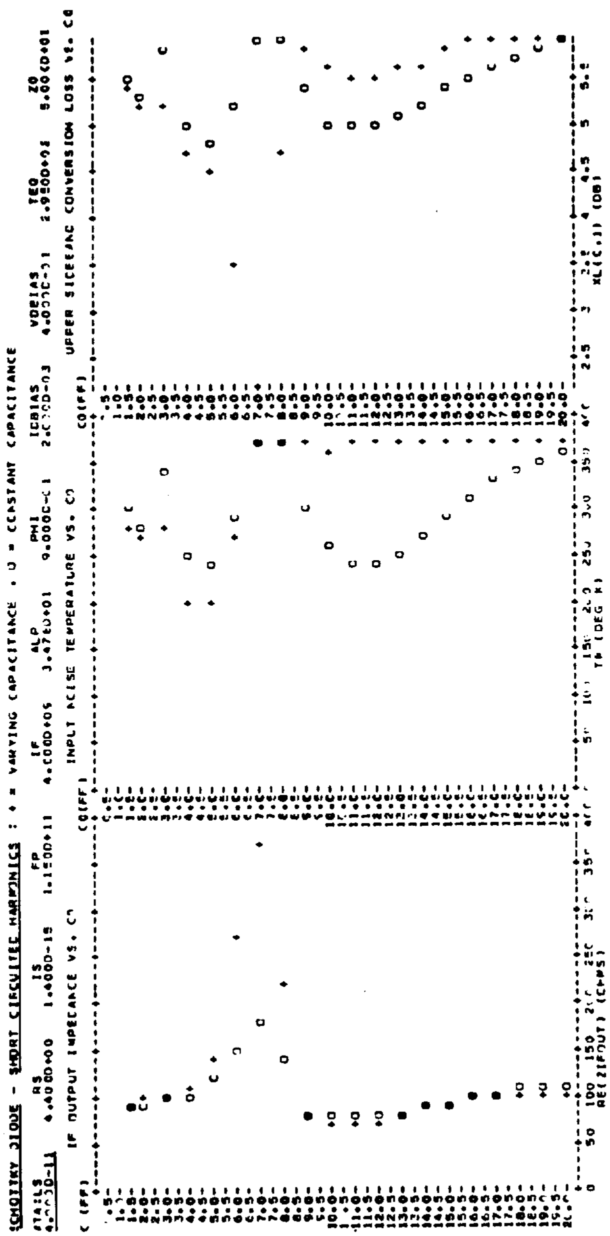

(a)

s/c harmonics

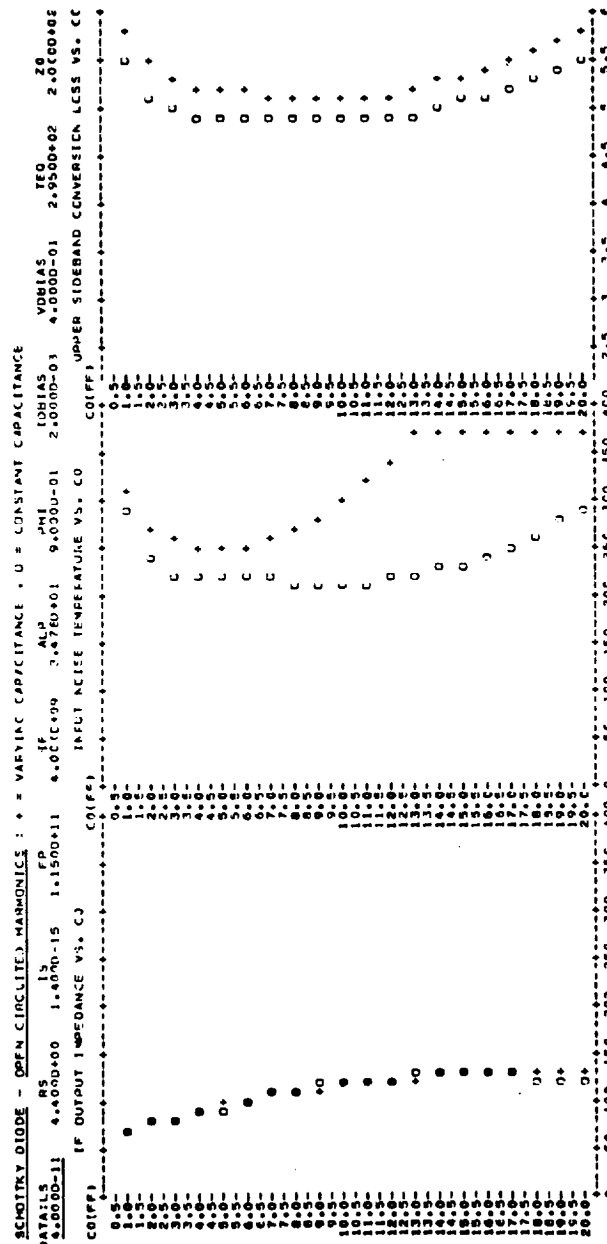

(b)

o/c harmonics

LS = 0.04 nH.

+ = varying capacitance (GAM=0.5)

O = constant capacitance (GAM=0)

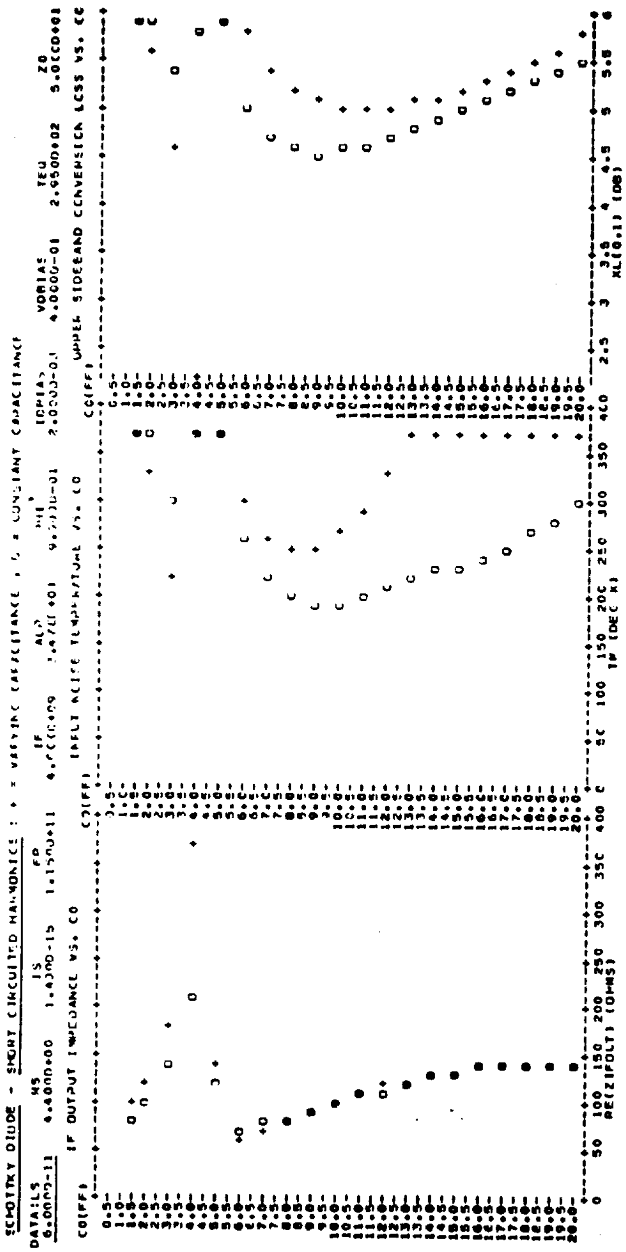

(a)

s/c harmonics

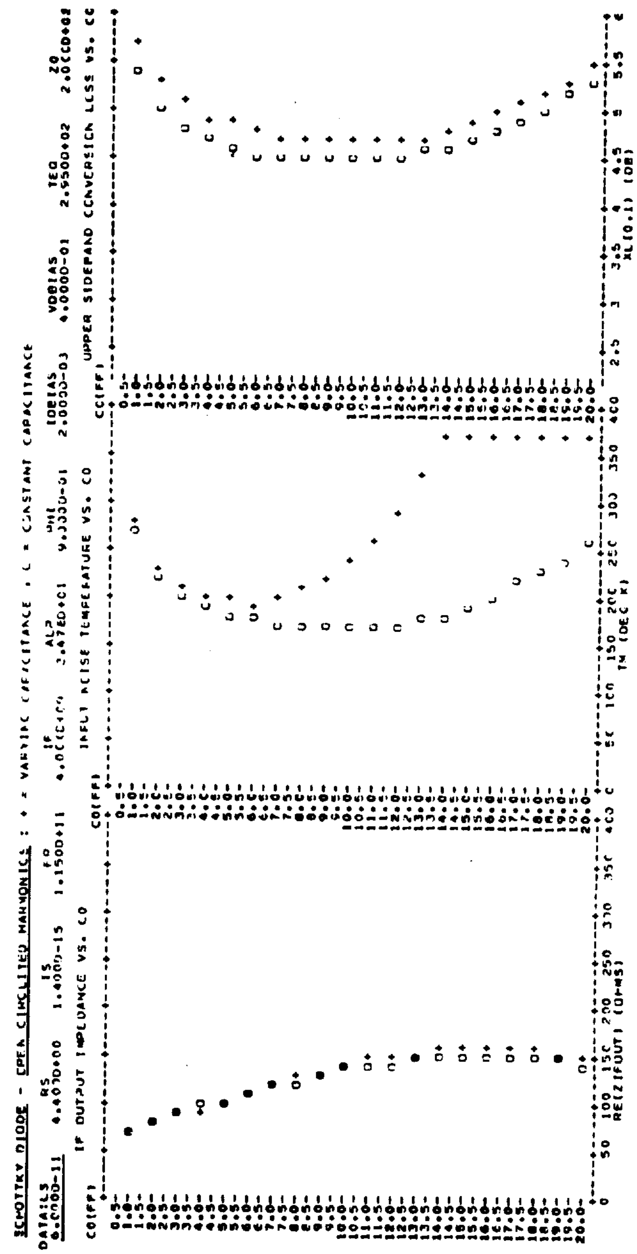

(b)

o/c harmonics

LS = 0.06 nH.

+ = varying capacitance (GAM=0.5)

O = constant capacitance (GAM=0)

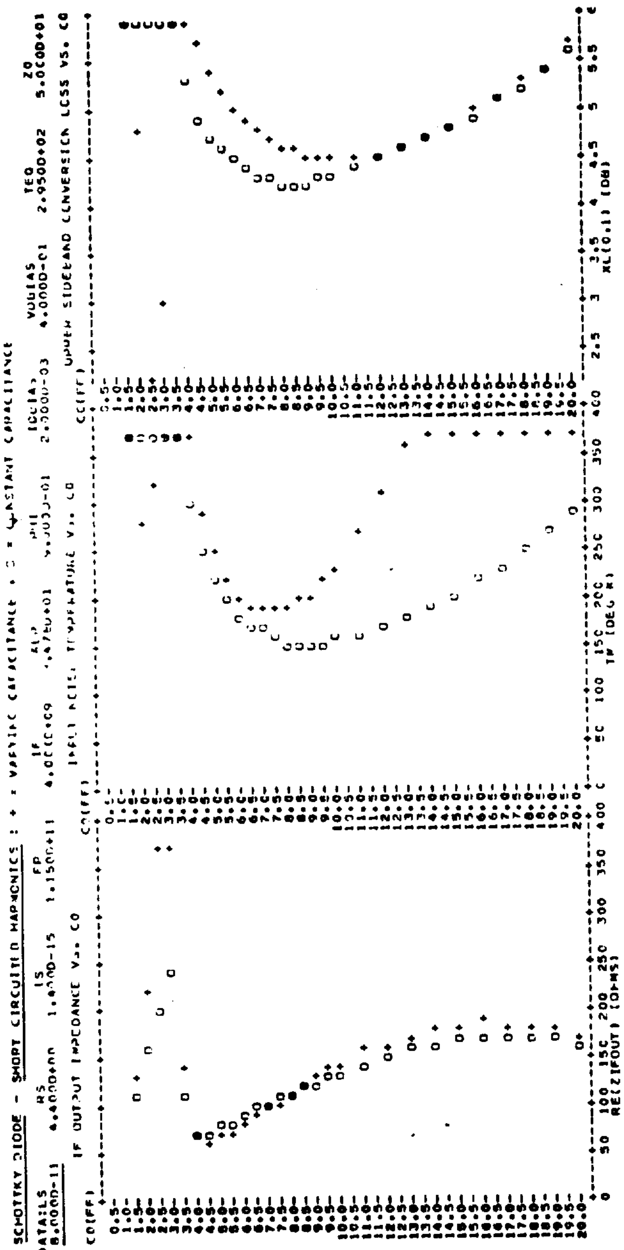

(a)

s/c harmonics

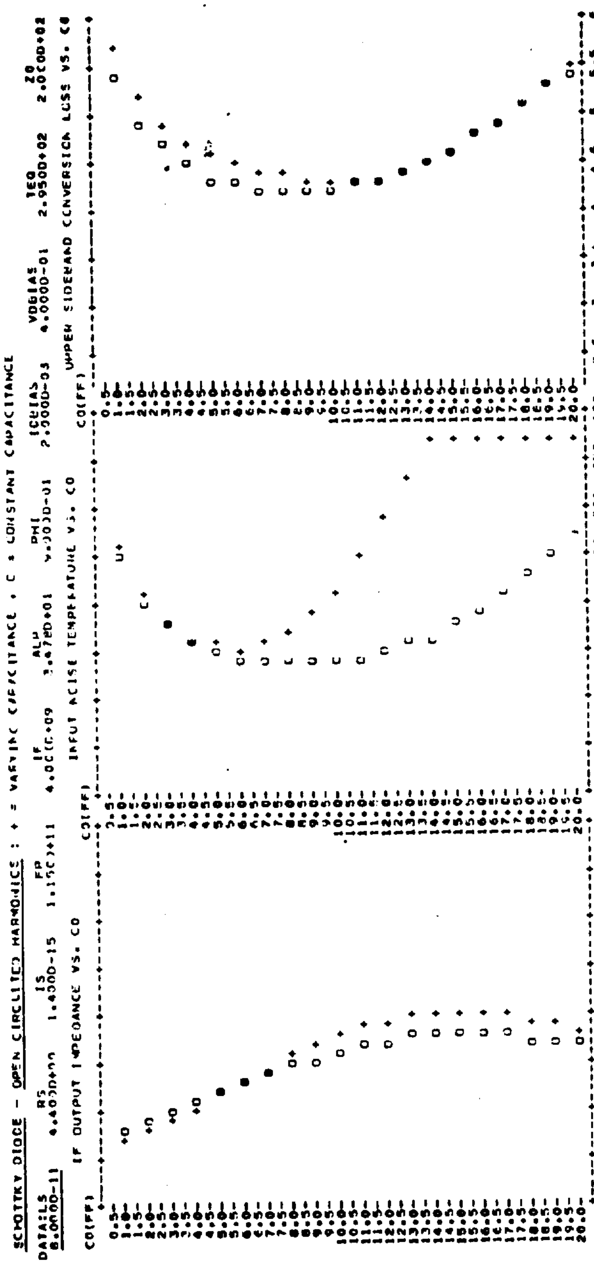

(b)

o/c harmonics

LS = 0.08 nH.

+ = varying capacitance (GAM=0.5)

O = constant capacitance (GAM=0)

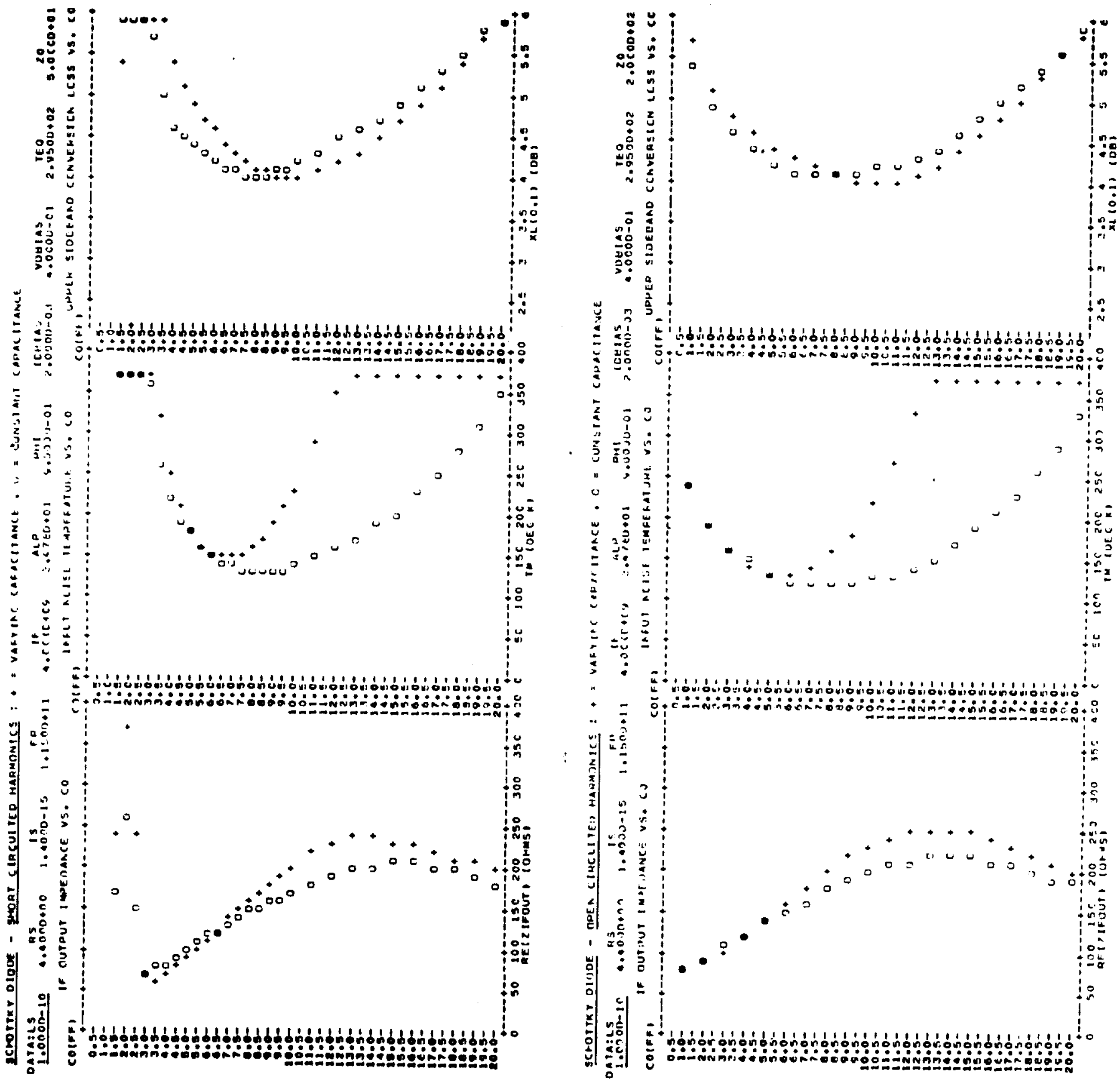

(a) s/c harmonics

(b) o/c harmonics

LS = 0.10 nH.

+ = varying capacitance (GAM=0.5)

O = constant capacitance (GAM=0)

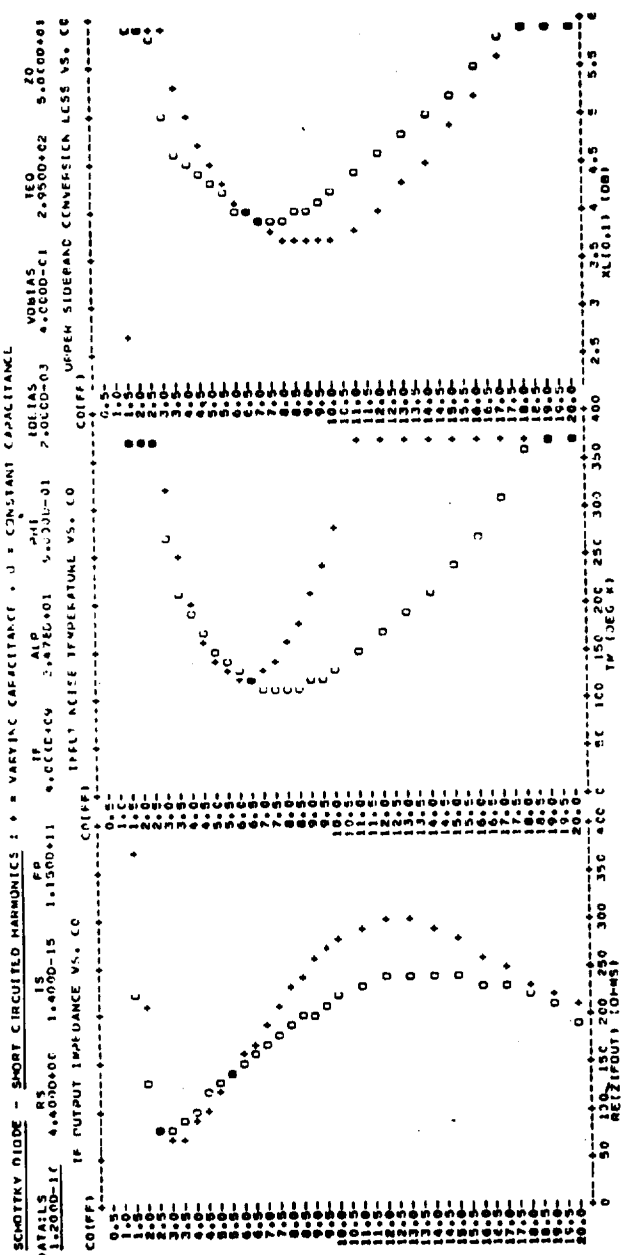

(a)

s/c harmonics

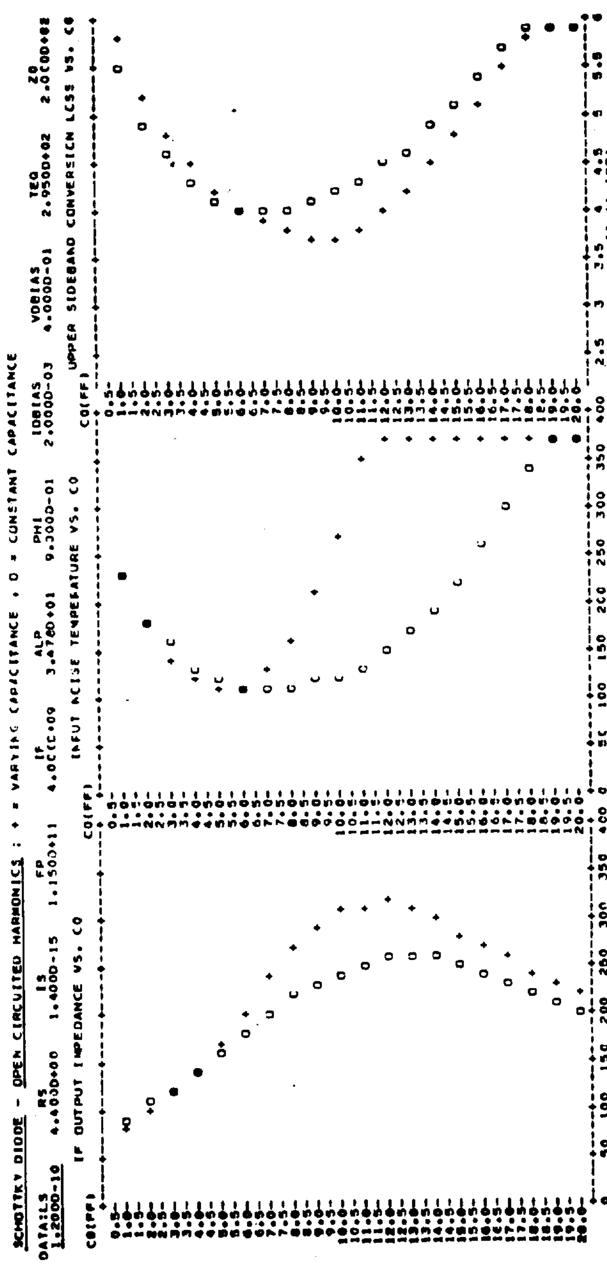

(b)

o/c harmonics

LS = 0.12 nH.

+ = varying capacitance (GAM=0.5)

O = constant capacitance (GAM=0)

ORIGINAL PAGE IS
OF POOR QUALITY

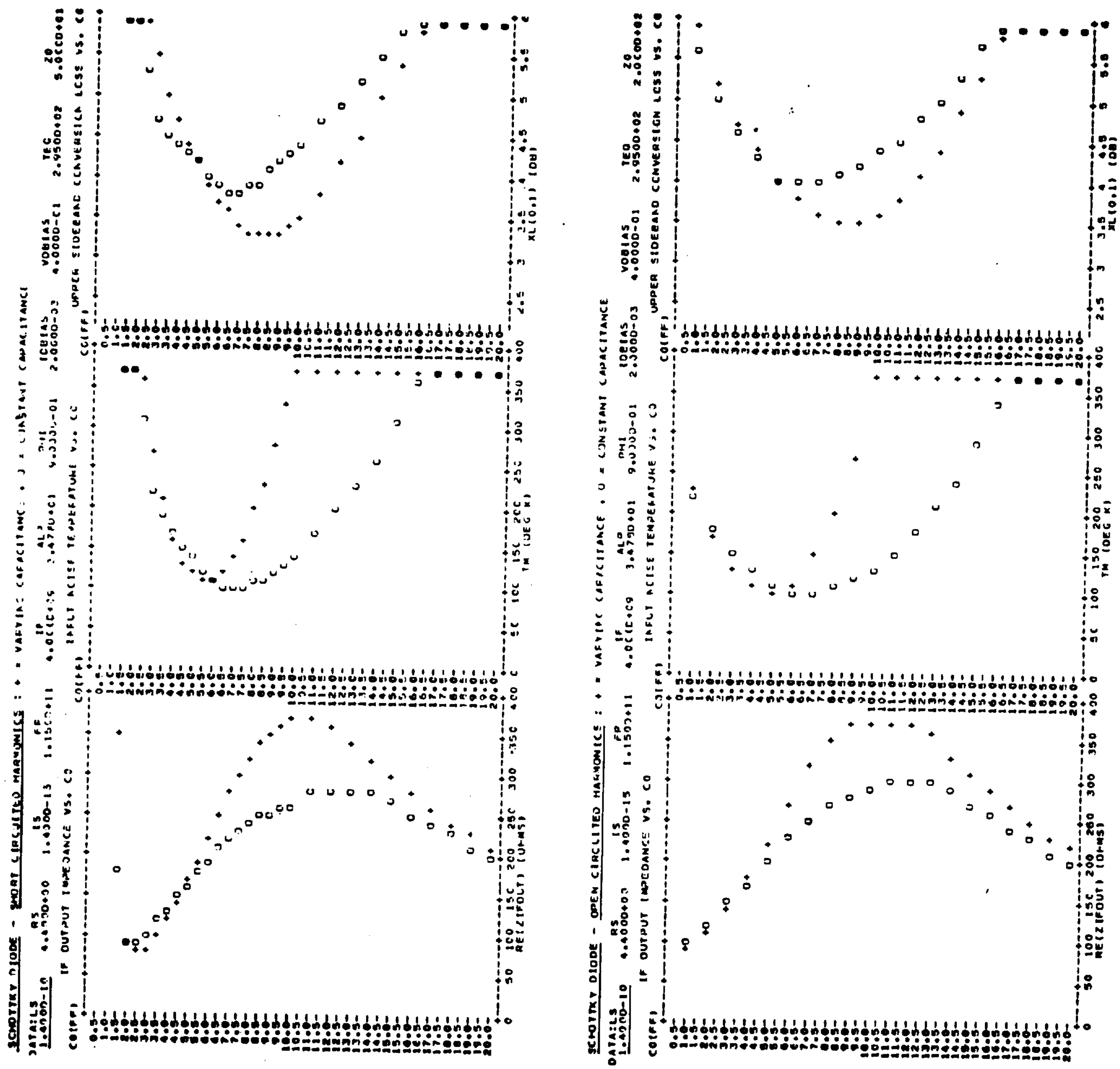

(a)
s/c harmonics

(b)
o/c harmonics

LS = 0.14 nH.

+ = varying capacitance (GAM=0.5)

O = constant capacitance (GAM=0)

ORIGINAL PAGE IS
OF POOR QUALITY

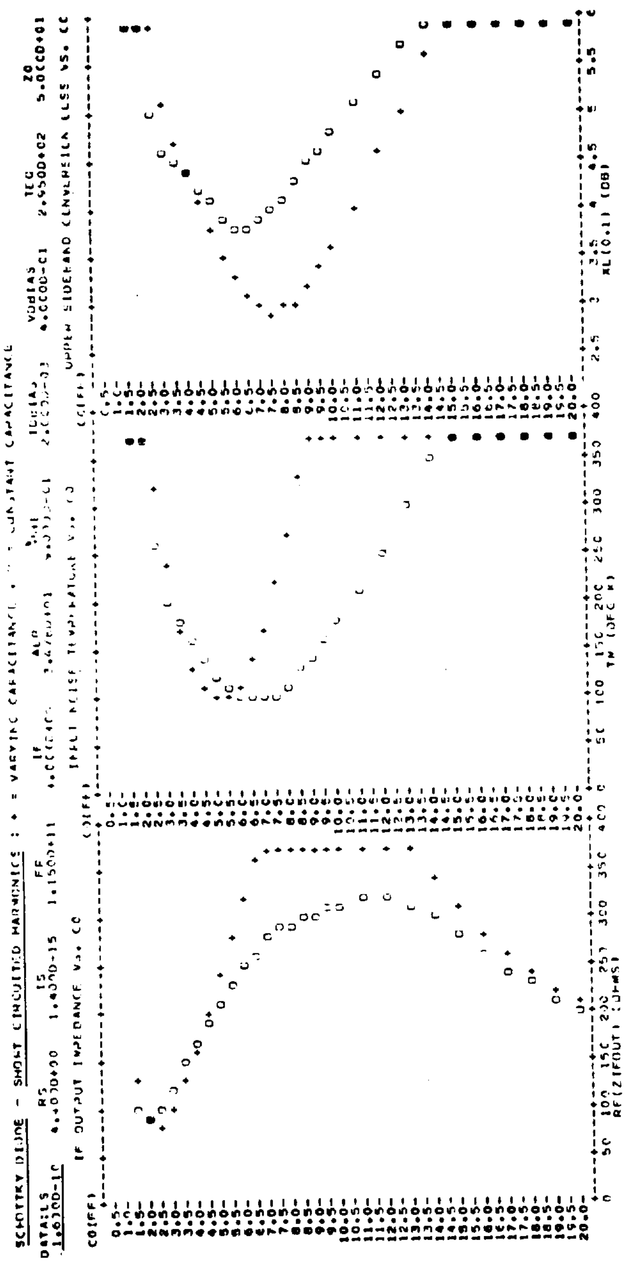

(a)

s/c harmonics

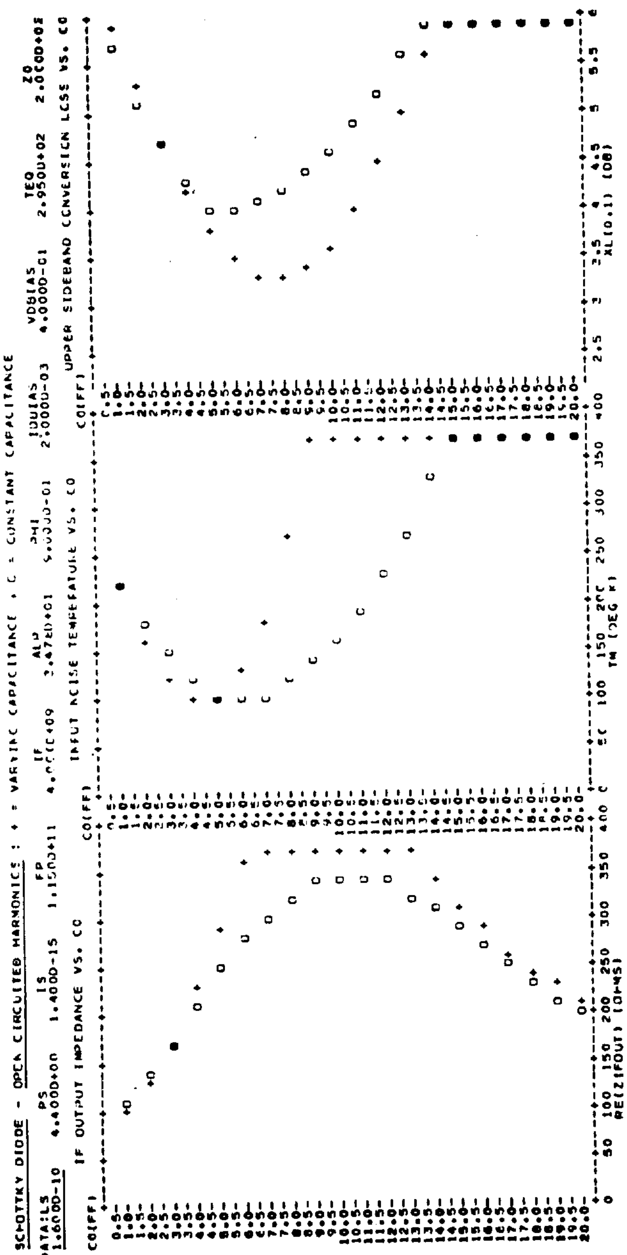

(b)

o/c harmonics

LS = 0.16 nH.

+ = varying capacitance (GAM=0.5)

O = constant capacitance (GAM=0)

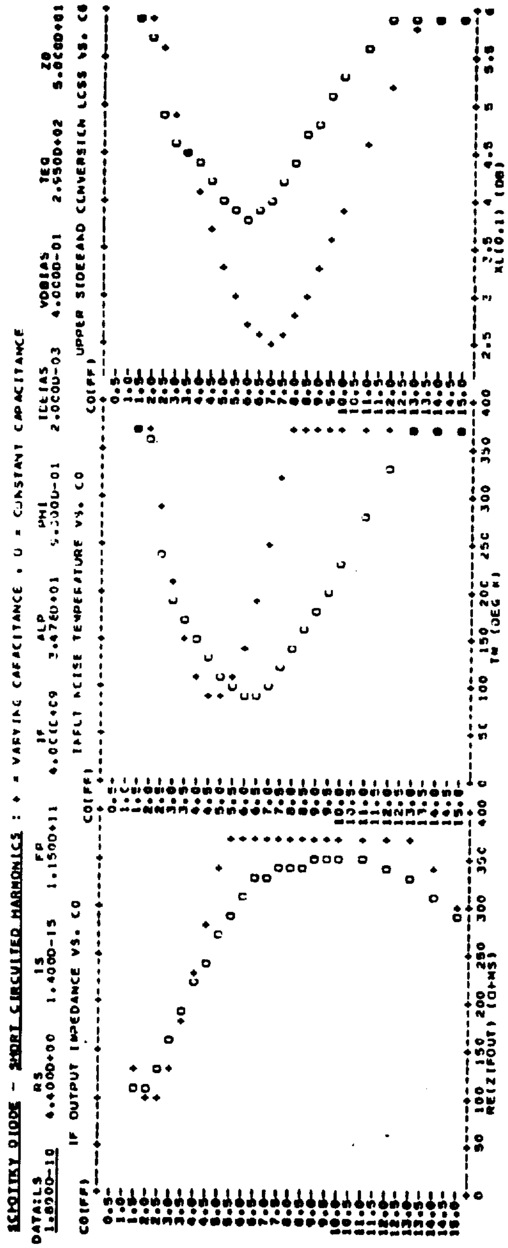

(a)

s/c harmonics

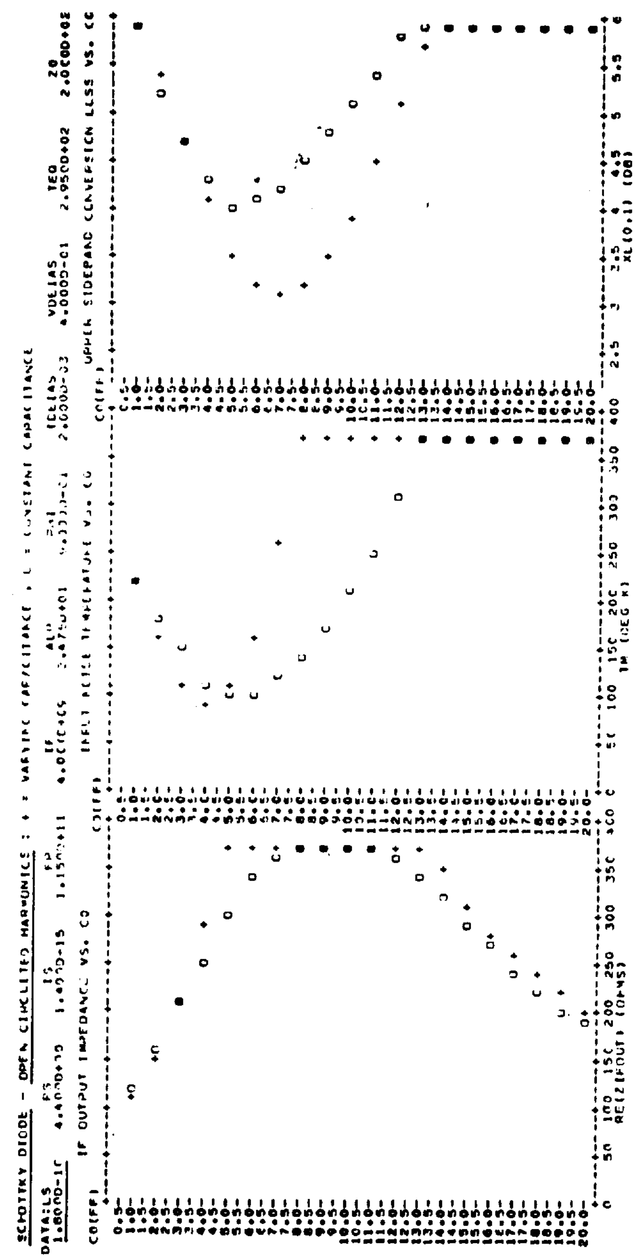

(b)

o/c harmonics

LS = 0.18 nH.

+ = varying capacitance (GAM=0.5)

O = constant capacitance (GAM=0)

ORIGINAL PAGE IS
OF POOR QUALITY

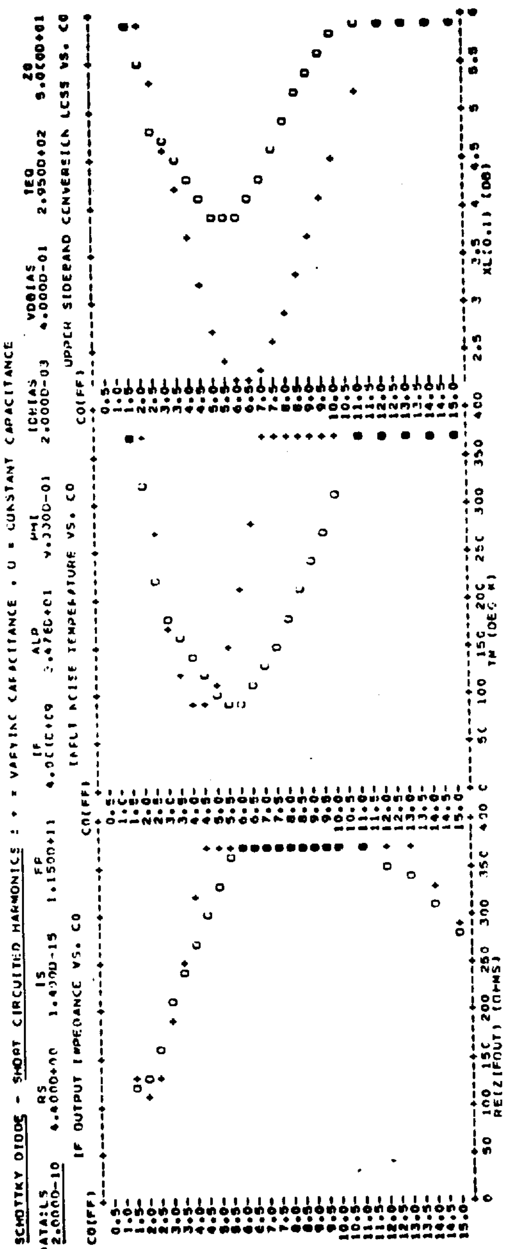

(a)

s/c harmonics

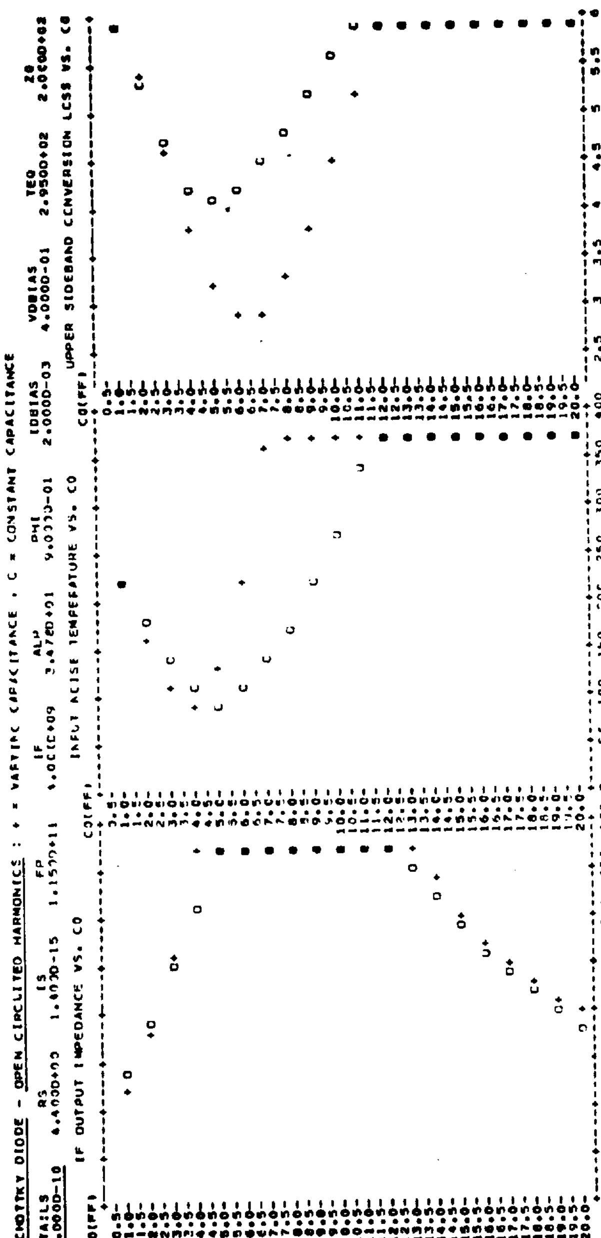

(b)

o/c harmonics

LS = 0.2 nH.

+ = varying capacitance (GAM=0.5)

O = constant capacitance (GAM=0)

APPENDIX 5. MULTIPLIER ANALYSIS PROGRAM

A5.1 Introduction

This appendix contains a computer program for the analysis of varactor diode multipliers. The program performs a nonlinear analysis on the multiplier equivalent circuit to obtain the large signal voltage, current, capacitance and conductance waveforms of the diode. The equations given in Chapter 6 are then used to calculate the multiplier port impedances and the conversion efficiencies from the pump to the higher harmonic frequencies.

The multiplier program is identical to that used for the analysis of mixers (Appendix 1) except for a few cosmetic changes. The available pump power (PAVAIL) and DC bias voltage (VDBIAS) are input rather than the diode rectified current. The embedding impedance at the pump frequency is not artificially set to the characteristic impedance of the transmission line (ZO) in the multiple reflection technique, resulting in one additional convergence parameter [ZQMAG(1)]. A new common block (MULT) is used to contain the chosen multiplier input and output ports (NIN,NOUT) and the available, absorbed and output ports (NIN,NOUT) and the available, absorbed and output powers (PAVAIL, PABS, POUT). Subroutine BIAS has been added to calculate the difference between the bias voltage used in the program and that which must be applied to the actual multiplier to obtain the same diode rectified current IDCOS(1). Finally, subroutine MLTPER has been included to calculate the multiplier port impedances and conversion efficiencies from the large signal currents and voltages.

The listing of the multiplier analysis program which follows is only a partial one since most of the subroutines are identical to those used in the mixer program in Appendix 1. The following subprograms (from Appendix 1) should be added after subroutine MLTPER: ZEMBED, RESIST, DRKGS, FCT, OUTP, DFORIT and PLOT. Subroutines PRINT1, PRINT2, PRINT3 and BLOCK DATA should also be added but with the statement substitutions listed in Section A5.3.

In Section A5.4 the output from a run of the multiplier analysis program, as listed in A5.2-A5.3 is given.

A5.2 Partial Listing of the Multiplier Analysis Program

```
C*************** MULTIPLIER ANALYSIS PROGRAM ********************
C
C    MAIN DRIVER PROGRAM
C---CALL LGSIG TO DO THE LARGE SIGNAL ANALYSIS
      CALL LGSIG
      STOP
      END



      SUBROUTINE LGSIG
C
C    LGSIG PERFORMS A NONLINEAR ANALYSIS ON THE MULTIPLIER
C   EQUIVALENT CIRCUIT TO DETERMINE THE DIODE WAVEFORMS.
C
C---THE VARIABLES USED IN THIS SUBROUTINE ARE AS FOLLOWS:
C---FOR COMMON/CONST/:
      REAL*8 QEL,BOLTZ,PI,TK,MU,EPS
C---FOR COMMON/DATA/:
      REAL*8 ICJDAT(51),IGJDAT(51),CJDATA(51),GJDATA(51)
      REAL*8  VDDATA(51),IDDATA(51)
C---FOR COMMON/DIODE/:
      REAL*8 ALP,ETA,PHI,GAM,C0,IS,RS,FP,WP,IF,IGJ,ICJ,GJ,CJ
C---FOR COMMON/FORITS/:
      REAL*8 GJCOS(7),GJSIN(7),CJCOS(7),CJSIN(7),VDCOS(7),VDSIN(7)
      REAL*8 IDCOS(7),IDSIN(7)
      INTEGER IER
C---FOR COMMON/IMPED/:
      COMPLEX*16 ZEMBSB(7),RSSB(7)
      REAL*8 LOPWR,ZER(6),ZEI(6),ZERDC,RSLO(6),XSLO(6)
C---FOR COMMON/LOOPS/:
      INTEGER NH,NLO,JLO,NVLO,NPTS,NCURR,IPT,NPRINT,NITER
C---FOR COMMON/MULT/:
      INTEGER NIN,NOUT
      REAL*8 PAVAIL,PABS,POUT
C---FOR COMMON/RES/:
      REAL*8 ER,NDS,NDE,SMOB,EMOB,TE,AR,CL,CW,CT,RC
C---FOR COMMON/RKG/:
      REAL*8 ACC,VDINIT
      INTEGER NDIM
C---FOR COMMON/TLINE/:
      REAL*8 Z0,ZQACC
      INTEGER ZQFLAG
C---FOR COMMON/VOLTS/:
      COMPLEX*16 VR(6)
      REAL*8 VRDC,VLO,VDBIAS,IDBIAS
C---FOR VARIABLES NOT IN ANY COMMON BLOCKS:
      COMPLEX*16 RHO(6),ZEMB(6),VL(6),ID,VD,ZQ
      REAL*8 Y(1),DERY(1),PRMT(5),AUX(8,1)
      REAL*8 VLDC,VDC,RHODC,ZEMBDC,VDCMLT
      REAL*8  ZQMAG(6),ZQPHA(6)
      INTEGER IHLF,ITER,IVLO,JPUMP,JLO,JPT,JH,NHP1,NHD2,NHD2P1
C---THE COMMON BLOCKS USED ARE:
      COMMON/CONST/QEL,BOLTZ,PI,TK,MU,EPS
      COMMON/DATA/ICJDAT,IGJDAT,CJDATA,GJDATA,VDDATA,IDDATA
```

```
      COMMON/DIODE/ALP,ETA,PHI,GAM,CØ,IS,RS,FP,WP,IF,IGJ,ICJ,GJ,CJ
      COMMON/FORITS/GJCOS,GJSIN,CJCOS,CJSIN,VDCOS,VDSIN,IDCOS,IDSIN,IER
      COMMON/IMPED/LOPWR,ZER,ZEI,ZERDC,RSLO,XSLO,ZEMBSB,RSSB
      COMMON/LOOPS/NH,NLO,JLO,NVLO,NPTS,NCURR,IPT,NPRINT,NITER
      COMMON/RES/ER,NDS,NDE,SMOB,EMOB,TE,AR,CL,CW,CT,RC
      COMMON/MULT/NIN,NOUT,PAVAIL,PABS,POUT
      COMMON/RKG/ACC,VDINIT,NDIM
      COMMON/TLINE/ZØ,ZQACC,ZQFLAG
      COMMON/VOLTS/VR,VRDC,VLO,VDBIAS,IDBIAS
C---SINCE THE FCT AND OUTP SUBPROGRAMS ARE CALLED BY DRKGS THEY MUST BE
C---DEFINED EXTERNALLY
      EXTERNAL FCT,OUTP
C---DEFINE SOME USEFUL CONSTANTS
      NHP1=NH+1
      NHD2=NH/2
      NHD2P1=NH/2+1
      WP=2.ØDØ*PI*FP
      ALP=QEL/(ETA*BOLTZ*TK)
C---CALL ZEMBED TO FORM THE EMBEDDING IMPEDANCES (THE SIDEBAND
C---IMPEDANCES ARE NOT USED IN THE MULTIPLIER ANALYSIS)
      CALL ZEMBED(ZER,ZEI,ZERDC,ZEMBSB,NH,NHP1,NHD2P1)
C  BEGIN THE LOOP OVER THE DC BIAS VOLTAGE
      DO 3Ø JVDC=4,4
      VDBIAS=-DFLOAT(JVDC)
C---CALL RESIST TO FIND THE SERIES RESISTANCE AS A FUNCTION OF FREQ
C---(THE RESISTANCES AT THE SIDEBAND FREQUENCIES ARE NOT USED)
      CALL RESIST(RSSB,RSLO,XSLO,VDBIAS,NH,NHP1,NHD2P1)
C---SET THE IMPEDANCE AT DC TO ZØ TO SPEED THE ANALYSIS
      ZEMBDC=ZØ
C---FORM THE SET OF COMPLEX IMPEDANCES WITH THE SERIES RESISTANCE ADDED
      DO 1 JH=1,NH
    1 ZEMB(JH)=DCMPLX(ZER(JH)+RSLO(JH),ZEI(JH)+XSLO(JH))
C---CALCULATE THE REFLECTION COEFFICIENT OF THE EMBEDDING NETWORK AT
C---EACH LO HARMONIC
      RHODC=(ZEMBDC-ZØ)/(ZEMBDC+ZØ)
      DO 13 JH=1,NH
   13 RHO(JH)=(ZEMB(JH)-ZØ)/(ZEMB(JH)+ZØ)
C---BEGIN THE LOOP OVER THE PUMP POWER, PAVAIL IN WATTS
      DO 2Ø JPUMP=1,1
      PAVAIL=DFLOAT(JPUMP)*35.ØDØ/1ØØØ.ØDØ
C---INITIALIZE VARIABLES FOR THE INTEGRATION BY DRKGS
      VLO=DSQRT(PAVAIL*8.ØDØ*ZER(NIN))
      PRMT(1)=Ø.ØDØ
      PRMT(2)=2.ØDØ*PI
      PRMT(3)=PRMT(2)/DFLOAT(NPTS)
      PRMT(4)=ACC
      Y(1)=VDINIT
C---VDBIAS IS THE DC VOLTAGE APPLIED TO THE CIRCUIT IN WHICH
C---ZE(Ø)=ZØ.  THE TRUE MULTIPLIER BIAS WILL BE FOUND LATER.
      VDC=VDBIAS
C---THE INITIAL LEFT AND RIGHT TRAVELING WAVES ON THE TRANSMISSION LINE
      DO 2 JH=1,NH
      VL(JH)=DCMPLX(Ø.ØDØ,Ø.ØDØ)
    2 VR(JH)=DCMPLX(Ø.ØDØ,Ø.ØDØ)
C---THE DC TERMS
```

```
      VLDC=Ø.ØDØ
      VRDC=VDC*ZØ/(ZØ+ZEMBDC)
      ITER=Ø
      VR(1)=VLO*ZØ/(ZEMB(1)+ZØ)
C---INITIALIZE DRKGS ERROR WEIGHT
      DERY(1)=1.ØDØ
C---CALL PRINT1 TO WRITE THE INITIAL CONDITIONS
      CALL PRINT1(ZEMB,ZERDC,ZEMBDC,ZER,ZEI,ZEMBSB,PRMT,Y,DERY,
     1VLO,VDBIAS,IDBIAS,RSSB,RSLO,XSLO,NH,NHP1,NHD2)
C---START THE REFLECTION CYCLE
    3 ITER=ITER+1
C---PRINT ONLY AFTER MULTIPLES OF NPRINT CYCLES HAVE BEEN COMPLETED
      JPRINT=MOD(ITER,NPRINT)
C---SOLVE THE NETWORK STATE EQUATION OVER ONE LO CYCLE
C---THE LOOP OVER THE NUMBER OF LO CYCLES TO REACH STEADY STATE
      DO 6 JLO=1,NLO
      IPT=1
      DERY(1)=1.ØDØ
      CALL DRKGS(PRMT,Y,DERY,NDIM,IHLF,FCT,OUTP,AUX)
    6 CONTINUE
C---CALL DFORIT TO FORM THE FOURIER COEFFICIENTS OF THE DIODE CURRENT
C---AND VOLTAGE.
      CALL DFORIT(VDDATA,NPTS/2,NH,VDCOS,VDSIN,IER)
      CALL DFORIT(IDDATA,NPTS/2,NH,IDCOS,IDSIN,IER)
C---SET THE FLAG FOR THE CONVERGENCE TESTS
      ZQFLAG=Ø
C---CALCULATE THE LEFT TRAVELING WAVE  ON THE TRANSMISSION LINE
C---THE MINUS SIGN COMES FROM THE CONVERSION OF THE TRIGONOMETRIC
C---FOURIER SERIES REPRESENTATION RETURNED BY DFORIT INTO THE SINGLE
C---ENDED COMPLEX EXPONENTIAL SERIES REPRESENTATION USED IN THE
C---LARGE SIGNAL ANALYSIS.
      DO 7 JH=1,NH
      VD=DCMPLX(VDCOS(JH+1),-VDSIN(JH+1))
      ID=DCMPLX(IDCOS(JH+1),-IDSIN(JH+1))
      VL(JH)=Ø.5DØ*(VD-ID*ZØ)
C---CALCULATE THE IMPEDANCE RATIOS AT EACH LO HARMONIC TO DETERMINE
C---THE DEGREE OF CONVERGENCE
      ZQ=VD/ID/ZEMB(JH)
      IF(JH.GT.1) GOTO 5
C---AT THE PUMP FREQUENCY THE CONVERGENCE PARAMETER IS MODIFIED BY VLO
      ZQ=(VLO-VD)/ID/ZEMB(1)
    5 ZQMAG(JH)=CDABS(ZQ)
      ZQPHA(JH)=DATAN2(DIMAG(ZQ),DREAL(ZQ))*57.29577951DØ
      IF(ZQMAG(JH).GT.1.ØDØ+ZQACC) ZQFLAG=ZQFLAG+1
      IF(ZQMAG(JH).LT.1.ØDØ-ZQACC) ZQFLAG=ZQFLAG+1
    7 CONTINUE
C---THE LEFT TRAVELING WAVE AT DC
      VLDC=Ø.5DØ*(VDCOS(1)-ZØ*IDCOS(1))
C---CALL PRINT2 TO WRITE THE RESULTS OF THIS REFLECTION CYCLE
      IF(JPRINT.NE.Ø) GOTO 9
      CALL PRINT2(RHO,VL,VR,VDCOS,VDSIN,IDCOS,IDSIN,ZQMAG,ZQPHA,
     1VLDC,VRDC,RHODC,ITER,ZQFLAG,JPUMP,NH,NHP1)
    9 CONTINUE
C---THE NEW RIGHT TRAVELING WAVE INCIDENT ON THE DIODE
      DO 1Ø JH=2,NH
```

```
   1Ø VR(JH)=VL(JH)*RHO(JH)
C---THE RIGHT TRAVELING WAVE AT DC AND THE FIRST HARMONIC
      VR(1)=RHO(1)*VL(1)+VLO*ZØ/(ZØ+ZEMB(1))
      VRDC=RHODC*VLDC+VDC*ZØ/(ZØ+ZEMBDC)
C---WAS THIS THE LAST REFECTION CYCLE ALLOWED?
   11 IF(ITER.EQ.NITER) GOTO 12
C---HAS THE SOLUTION CONVERGED?
      IF(ZQFLAG.EQ.Ø) GOTO 12
C---GO ON TO THE NEXT REFLECTION CYCLE
      GOTO 3
C---CALL PRINT2 TO WRITE THE RESULTS OF THE FINAL REFLECTION CYCLE
   12 CALL PRINT2(RHO,VL,VR,VDCOS,VDSIN,IDCOS,IDSIN,ZQMAG,ZQPHA,
     1VLDC,VRDC,RHODC,ITER,ZQFLAG,JPUMP,NH,NHP1)
C---UNSCALE THE CAPACITANCE VALUES (THEY WERE SCALED IN SUBROUTINE FCT
C---WHICH IS CALLED BY THE DRKGS INTEGRATION ROUTINE).
      DO 19 JPT=1,NPTS
   19 CJDATA(JPT)=CJDATA(JPT)/WP
C---FINISH THE ANALYSIS BY OBTAINING THE FOURIER COEFFICIENTS OF THE
C---DIODE CONDUCTANCE AND CAPACITANCE.
      CALL DFORIT(GJDATA,NPTS/2,NH,GJCOS,GJSIN,IER)
      CALL DFORIT(CJDATA,NPTS/2,NH,CJCOS,CJSIN,IER)
C---CALL PRINT3 TO PRINT THE FOURIER COEFFICIENTS
      CALL PRINT3(GJCOS,GJSIN,CJCOS,CJSIN,NHP1,NH)
C---CALL BIAS TO CALCULATE THE ACTUAL BIAS WHICH MUST BE APPLIED
C---TO THE DIODE TO OBTAIN THE PERFORMANCE CALCULATED HERE
      CALL BIAS(VDCOS(1),IDCOS(1),ZERDC,RS,ZØ,VDCMLT,VDBIAS)
C---CALL MLTPER TO CALCULATE AND PRINT THE MULTIPLIER PERFORMANCE
      CALL MLTPER(ZER,RSLO,XSLO,VDCOS,VDSIN,IDCOS,IDSIN,NH,NHP1)
C---CALL PLOT TO PRINT THE DIODE WAVEFORMS IN THE TIME DOMAIN
      CALL PLOT (IGJDAT,CJDATA,VDDATA,IDDATA,NPTS,ITER,CØ)
C---REPEAT THE ANALYSIS WITH A NEW PUMP POWER
   2Ø CONTINUE
C---REPEAT THE ANALYSIS WITH A NEW BIAS VOLTAGE
   3Ø CONTINUE
      RETURN
      END



C
      SUBROUTINE BIAS(VDØ,IDØ,ZERDC,RS,ZØ,VDCMLT,VDBIAS)
C
C    BIAS CALCULATES THE ACTUAL DC VOLTAGE WHICH SHOULD BE APPLIED
C   TO THE MULTIPLIER IN ORDER TO OBTAIN THE DIODE RECTIFIED
C   CURRENT CALCULATED IN THIS PROGRAM
C
      REAL*8 VDØ,IDØ,ZERDC,RS,ZØ,VDCMLT
      VDCMLT=IDØ*(ZERDC+RS-ZØ)+VDBIAS
      WRITE(6,1ØØ) VDBIAS,IDØ,VDCMLT
  1ØØ FORMAT(//1X,'THE DC BIAS VOLTAGE USED IN THIS PROGRAM WAS ',
     1F9.4//1X,'THIS VALUE OF BIAS VOLTAGE RESULTED IN A DIODE',
     2' RECTIFIED CURRENT OF ',3PF9.4,' MA'//1X,'THE VOLTAGE WHICH',
     3' MUST BE APPLIED TO THE MULTIPLIER TO OBTAIN THIS SAME CURRENT'
     4' IS ',ØPF8.4//)
      RETURN
```

```fortran
      END
C
C
      SUBROUTINE MLTPER(ZER,RSLO,XSLO,VDCOS,VDSIN,IDCOS,IDSIN,NH,NHP1)
C
C    MLTPER CALCULATES AND PRINTS THE MULTIPLIER INPUT AND OUTPUT
C   IMPEDANCES AND THE CONVERSION EFFICIENCY FROM THE INPUT TO EACH
C   OUTPUT PORT.
C
      COMPLEX*16 ID(6),VD(6),ZIN(6)
      REAL*8 ZER(NH),RSLO(NH),XSLO(NH),EFF(6),PABS,PAVAIL,POUT
      REAL*8 VDCOS(NHP1),VDSIN(NHP1),IDCOS(NHP1),IDSIN(NHP1)
      INTEGER NIN,NOUT
      COMMON/MULT/NIN,NOUT,PAVAIL,PABS,POUT
C---INPUT IMPEDANCES
      DO 10 I=1,NH
      VD(I)=DCMPLX(VDCOS(I+1),-VDSIN(I+1))
      ID(I)=DCMPLX(IDCOS(I+1),-IDSIN(I+1))
      ZIN(I)=VD(I)/ID(I)+DCMPLX(RSLO(I),XSLO(I))
   10 CONTINUE
C---ABSORBED POWER
      PABS=0.5D0*DREAL(ZIN(NIN))*ID(NIN)*DCONJG(ID(NIN))
C---OUPUT POWER
      POUT=0.5D0*ZER(NOUT)*ID(NOUT)*DCONJG(ID(NOUT))
C---EFFICIENCY
      DO 20 I=1,NH
      EFF(I)=0.5D0*ZER(I)*ID(I)*DCONJG(ID(I))/PABS
   20 CONTINUE
C---PRINT RESULTS
      WRITE(6,100) NIN,PAVAIL,PABS,NOUT,POUT
  100 FORMAT(//1X,'THE AVAILABLE POWER AT INPUT PORT ',I2,
     1' IS: ',3PF8.3,' MW.'//1X,'THE ABSORBED POWER IS: ',3PF8.3,
     2' MW.'//1X,'THE POWER DELIVERED TO PORT ',I2,' IS: ',3PF8.3,
     3' MW.'//)
      DO 30 I=1,NH
      IF(I.EQ.NIN) GOTO 30
      WRITE(6,200) NIN,I,EFF(I)
  200 FORMAT(1X,'THE CONVERSION EFFICIENCY IN % FROM PORT ',I2,
     1' TO PORT ',I2,' IS: ',2PF7.2/)
   30 CONTINUE
      WRITE(6,250)
  250 FORMAT(//1X)
      DO 40 I=1,NH
      WRITE(6,300) I,ZIN(I)
  300 FORMAT(1X,'INPUT IMPEDANCE (REAL,IMAG) AT PORT ',I2,
     1' : (',0PF9.3,',',0PF9.3,')'/)
   40 CONTINUE
      RETURN
      END
```

A5.3 Statement Substitutions for Subroutines PRINT1, PRINT2, PRINT3 and BLOCK DATA from Appendix 1

Line 683.5 should be inserted into subroutine RESIST.

```
683.5        IF(K.EQ.Ø) GOTO 4Ø
1474.1 C---FOR COMMON/MULT/:
1474.2       INTEGER NIN,NOUT
1474.3       REAL*8 PAVAIL,PABS,POUT
1483.  C
1484.  C
1485.  C
1495.1       COMMON/MULT/NIN,NOUT,PAVAIL,PABS,POUT
1499.  C
15Ø1.        WRITE(6,5Ø) FP,NOUT
15Ø2.     5Ø FORMAT(1H1,1X,' ANALYSIS OF A ',-9PF6.2,' GHZ X',I2,' MULTIPLIER'/
1521.        WRITE(6,13Ø) VDBIAS
1522.    13Ø FORMAT(/1X,' BIAS VOLTAGE:',T23,'VDBIAS'/T25,F1Ø.3)
1523.  C
1524.  C
1525.  C
1526.  C
154Ø.        WRITE(6,18Ø) ZERDC,ZEMBDC
1541.    18Ø FORMAT(///1X,' EMBEDDING IMPEDANCES:',T48,'PUMP HARMONICS'/
1542.       1/T25,'HARM#',T37,'ZER',T5Ø,
1543.       *'ZEI',T71,'ZEMB'/T26,'DC',T33,
1544.       *1PE1Ø.3,T61,1PE1Ø.3)
1545.        DO 1Ø I=1,NHARM
1546.  C
1547.  C
1548.     1Ø WRITE(6,19Ø) I,ZER(I),ZEI(I),ZEMB(I)
1549.    19Ø FORMAT(1X,T26,I2,T33,2(1PE1Ø.3,3X),T61,2(1PE1Ø.3,3X))
1552.        WRITE(6,2ØØ) RS
1553.    2ØØ FORMAT(///1X,' DIODE SERIES RESISTANCES:'
1554.       1/T33,'FGHZ',T42,'HARM#',
1555.       *T52,'RSLO',T63,'XSLO'
1556.       2/T34,'DC',T43,'Ø',T49,F8.4)
1558.        DO 2Ø I=1,NHARM
1559.  C
156Ø.  C
1561.        FLO=FP*I*1.ØD-9
1563.     2Ø WRITE(6,21Ø) FLO,I,RSLO(I),XSLO(I)
1564.    21Ø FORMAT(1X,T3Ø,F8.2,T42,I2,T49,F8.4,T6Ø,F8.4)
1565.  C
1566.  C
1567.  C
1585.        WRITE(6,1ØØ) ITER,JPUMP
1586.    1ØØ FORMAT(////1X,'NONLINEAR ANALYSIS RESULTS:  REFLECTION CYCLE #'
1587.       1,I4,' IN PUMP POWER LOOP NUMBER ',I3/)
1613.        SUBROUTINE PRINT3(GJCOS,GJSIN,CJCOS,CJSIN,NHP1,NH)
1616.  C   AND CAPACITANCE.
162Ø.        REAL*8 GJCOS(NHP1),GJSIN(NHP1),CJCOS(NHP1),CJSIN(NHP1)
```

```
C
C
C
C
C
C
C
C
  110 FORMAT(/2X,'GJCOS,GJSIN')
      WRITE(6,120) (I,GJCOS(I+1),GJSIN(I+1),I=1,NH)
  120 FORMAT(1H+,6(8X,4(I7,1PE12.3,1PE12.3)/1X))
  130 FORMAT(/2X,'CJCOS,CJSIN')
      WRITE(6,120) (I,CJCOS(I+1),CJSIN(I+1),I=1,NH)
      WRITE(6,140) GJCOS(1),CJCOS(1)
  140 FORMAT(//2X,'DC TERMS:  GJCOS(1) = ',1PE10.3,4X,'CJCOS(1) =
     1,1PE10.3/)
C---FOR COMMON/MULT/:
      INTEGER NIN,NOUT
      REAL*8 PAVAIL,PABS,POUT
C
C
C
      COMMON/MULT/NIN,NOUT,PAVAIL,PABS,POUT
C
      DATA ETA,PHI,GAM/1.20D0,1.10D0,0.5D0/
      DATA C0,IS,RS/17.0D-15,1.4D-17,7.0D0/
      DATA FP,IF/100.0D9,0.0D0/
C---COMMON/IMPED/VARIABLES:
      DATA ZERDC/1.0D0/
      DATA ZER(1),ZER(2),ZER(3)/200.0D0,100.0D0,30.0D0/
      DATA ZER(4),ZER(5),ZER(6)/10.0D0,5.0D0,1.0D0/
      DATA ZEI(1),ZEI(2),ZEI(3)/250.0D0,150.0D0,20.0D0/
      DATA ZEI(4),ZEI(5),ZEI(6)/10.0D0,5.0D0,1.0D0/
C
C
C
C
C---COMMON/MULT/VARIABLES
      DATA NIN,NOUT/1,2/
C---COMMON/RES/VARIABLES:
      DATA ER,NDS,NDE,SMOB,EMOB/13.1D0,1.0D18,3.0D16,3.125D3,5.5D3/
      DATA TE,AR,CL,CW,CT/1.5D-4,2.5D-4,0.02286D0,0.0127D0,0.0127D0/
      DATA RC/1.0D0/
C---COMMON/RKG/VARIABLES:
C
C
C
C
C
```

A5.4 Output from the Multiplier Analysis Program of Sections A5.2-A5.3

```
ANALYSIS OF A 100.00 GHZ X 2 MULTIPLIER
--------------------------------------------------------------
INPUT DATA

DIODE PARAMETERS:     ALP          PHI         GAM        C0          IS          RS        ETA
                     32.236       1.100       0.500    1.7000D-14  1.4000D-17   7.0000    1.2000

CHIP PARAMETERS:  LENGTH   WIDTH   HEIGHT   ANODE RAD    SUB DOP     EPI DOP    SUB MOB   EPI MOB
                  0.023    0.013   0.013    2.5000D-04  1.0000D+18  3.0000D+16  3125.0    5500.0

OPERATING FREQUENCIES AND TEMPERATURE:   FP           IF          TK
                                      1.0000D+11    0.0         300.0

BIAS AND PUMP SETTINGS:     VDBIAS     VLO
                            -4.000     7.483315

DRKGS VARIABLES:  PRMT(1)     PRMT(2)      PRMT(3)      PRMT(4)      Y(1)      DERY(1)    NDIM
                  (LOW LIM)   (UP LIM)     (INCR)       (ACC)        (VD)      (DV/DT)    (NEQS)
                  0.0         6.28318531   0.12319971   1.0000D-06   -1.000    1.000      1

LOOP LIMITS:      NITER     NLO     NVLO     NPTS     NHARM     NPRINT
                  500       1       50       51       6         100

CONVERGENCE PARAMETERS:        Z0          ZQACC
                               50.00       1.0000D-02


EMBEDDING IMPEDANCES:                     PUMP HARMONICS

                 HARM#     ZER          ZEI                   ZEM
                  DC     1.0000D+00                    5.0000D+01
                  1      2.0000D+02   2.5000D+02       2.076D+02   2.521D+02
                  2      1.0000D+02   1.5000D+02       1.079D+02   1.530D+02
                  3      3.0000D+01   2.0000D+01       3.009D+01   2.369D+01
                  4      1.0000D+01   1.0000D+01       1.827D+01   1.426D+01
                  5      5.0000D+00   5.0000D+00       1.342D+01   9.768D+00
                  6      1.0000D+00   1.0000D+00       9.563D+00   6.223D+00


DIODE SERIES RESISTANCES:
                     FGHZ     HARM#     RSLO      XSLO
                      DC        0       7.0000
                     100.00     1       7.6023    2.1324
                     200.00     2       7.8769    3.0156
                     300.00     3       8.0875    3.6934
                     400.00     4       8.2651    4.2648
                     500.00     5       8.4215    4.7682
                     600.00     6       8.5630    5.2233
```

```
NONLINEAR ANALYSIS RESULTS:  REFLECTION CYCLE #  24 IN PUMP POWER LOOP NUMBER   1

VL(I)
                1  -1.606D+00  -2.638D+00     2   7.892D-01  -3.322D-01     3  -1.681D-01   1.330D-01     4   1.018D-01  -4.198D-02
                5  -6.784D-02   6.025D-03     6   3.315D-02   1.433D-02

VR(I)
                1  -3.373D-02  -3.152D+00     2   6.366D-01   2.607D-02     3  -2.802D-02  -5.566D-02     4  -2.876D-02   4.679D-02
                5   3.522D-02  -1.935D-02     6  -2.439D-02  -3.720D-03

VDCOS,VDSIN
                1  -1.642D+00   5.787D+00     2   1.423D+00   3.074D-01     3  -1.960D-01  -7.779D-02     4   7.347D-02  -4.529D-03
                5  -3.284D-02   1.352D-02     6   8.838D-03  -1.061D-02

IDCOS,IDSIN
                1   3.139D-02   1.024D-02     2  -3.096D-03  -7.141D-03     3   2.803D-03   3.765D-03     4  -2.602D-03  -1.770D-03
                5   2.057D-03   5.113D-04     6  -1.149D-03   3.612D-04

ZQMAG,ZQPHA
                1   1.002D+00   -0.           2   9.993D-01   180.          3   1.002D+00   180.          4   1.009D+00   180.
                5   1.009D+00  -180.          6   1.005D+00   180.

DC TERMS:  VDCOS=-4.000D+00    IDCOS= 6.227D-06   VLDC=-2.000D+00      VRDC=-2.000D+00

ZQFLAG= 0

FOURIER COEFFICIENTS OF THE DIODE CONDUCTANCE AND CAPACITANCE WAVEFORMS

GJCOS,GJSIN
                1  -6.165D-08   7.720D-08     2  -1.949D-08  -8.853D-08     3   6.953D-08   3.603D-08     4  -5.911D-08   2.302D-08
                5   1.859D-08  -4.426D-08     6   1.069D-08   3.242D-08

CJCOS,CJSIN
                1  -4.206D-15   9.479D-15     2  -1.492D-15  -3.242D-15     3   7.197D-16   6.894D-16     4  -2.232D-16  -4.518D-16
                5   2.932D-16   3.500D-16     6  -3.230D-16  -9.524D-17

DC TERMS:  GJCOS(1) =  5.002D-08    CJCOS(1) =  1.272D-14
```

ORIGINAL PAGE IS
OF POOR QUALITY

ORIGINAL PAGE IS
OF POOR QUALITY

```
THE DC BIAS VOLTAGE USED IN THIS PROGRAM WAS    -4.0000
THIS VALUE OF BIAS VOLTAGE RESULTED IN A DIODE RECTIFIED CURRENT OF     0.0062 MA
THE VOLTAGE WHICH MUST BE APPLIED TO THE MULTIPLIER TO OBTAIN THIS SAME CURRENT IS  -4.0003


THE AVAILABLE POWER AT INPUT PORT  1 IS:    35.000 MW.
THE ABSORBED POWER IS:     7.998 MW.
THE POWER DELIVERED TO PORT  2 IS:     3.029 MW.

THE CONVERSION EFFICIENCY IN % FROM PORT  1 TO PORT  2 IS:   37.88
THE CONVERSION EFFICIENCY IN % FROM PORT  1 TO PORT  3 IS:    4.13
THE CONVERSION EFFICIENCY IN % FROM PORT  1 TO PORT  4 IS:    0.62
THE CONVERSION EFFICIENCY IN % FROM PORT  1 TO PORT  5 IS:    0.14
THE CONVERSION EFFICIENCY IN % FROM PORT  1 TO PORT  6 IS:    0.01


INPUT IMPEDANCE (REAL,IMAG) AT PORT  1 : (   14.672, -179.928)
INPUT IMPEDANCE (REAL,IMAG) AT PORT  2 : ( -101.108, -149.059)
INPUT IMPEDANCE (REAL,IMAG) AT PORT  3 : (  -30.142,  -19.912)
INPUT IMPEDANCE (REAL,IMAG) AT PORT  4 : (  -10.232,  -10.058)
INPUT IMPEDANCE (REAL,IMAG) AT PORT  5 : (   -5.078,   -5.161)
INPUT IMPEDANCE (REAL,IMAG) AT PORT  6 : (   -1.077,   -0.980)
```

GRAPHS FOR REFLECTION CYCLE NUMBER 24

IGJ(MA)	CJ(PF)
-0.000	0.0076
-0.000	0.0082
-0.000	0.0089
-0.000	0.0096
-0.000	0.0105
-0.000	0.0116
-0.000	0.0127
-0.000	0.0140
-0.000	0.0154
-0.000	0.0170
0.000	0.0187
0.000	0.0205
0.000	0.0223
0.000	0.0238
0.000	0.0249
0.000	0.0256
0.000	0.0259
0.000	0.0261
0.000	0.0263
0.000	0.0265
0.000	0.0265
0.000	0.0258
0.000	0.0240
0.000	0.0212
0.000	0.0180
-0.000	0.0150
-0.000	0.0125
-0.000	0.0106
-0.000	0.0092
-0.000	0.0081
-0.000	0.0074
-0.000	0.0068
-0.000	0.0063
-0.000	0.0059
-0.000	0.0057
-0.000	0.0054
-0.000	0.0053
-0.000	0.0052
-0.000	0.0051
-0.000	0.0051
-0.000	0.0051
-0.000	0.0051
-0.000	0.0052
-0.000	0.0053
-0.000	0.0054
-0.000	0.0056
-0.000	0.0058
-0.000	0.0060
-0.000	0.0064
-0.000	0.0067
-0.000	0.0071

DIODE CONDUCTANCE CURRENT VS TIME FOR ONE LO CYCLE

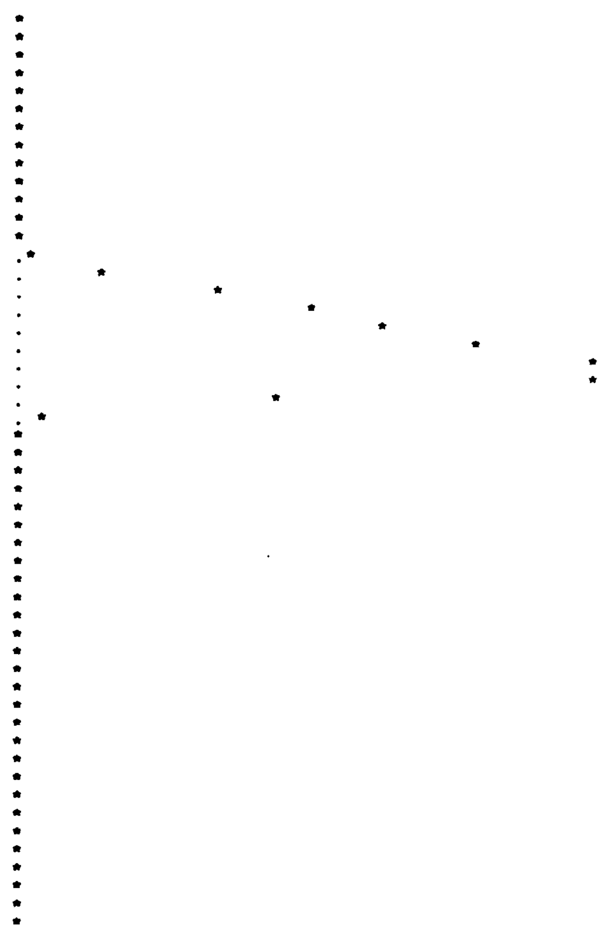

DIODE CAPACITANCE VS TIME FOR ONE LO CYCLE

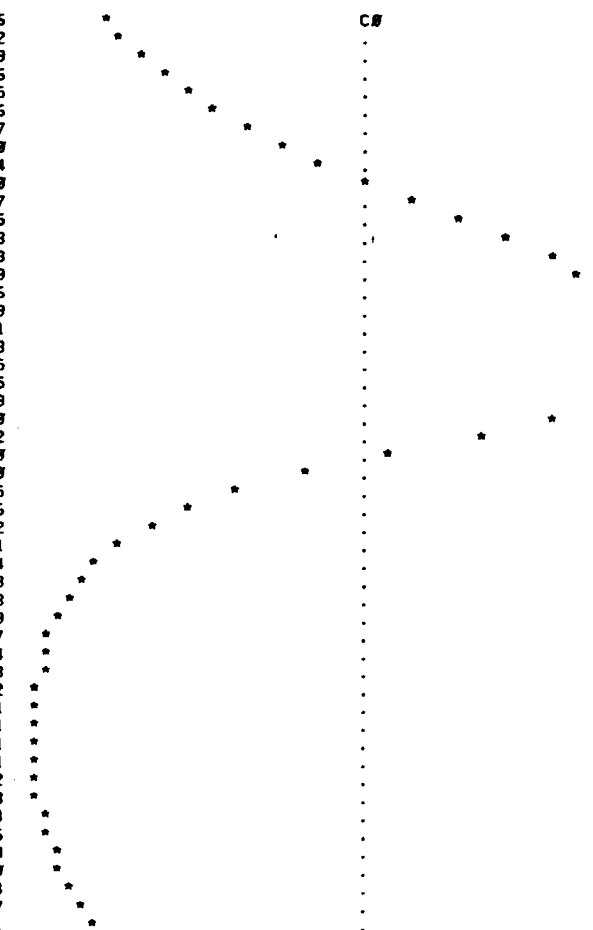

GRAPHS FOR REFLECTION CYCLE NUMBER 24

TOTAL DIODE CURRENT VS TIME FOR ONE LO CYCLE

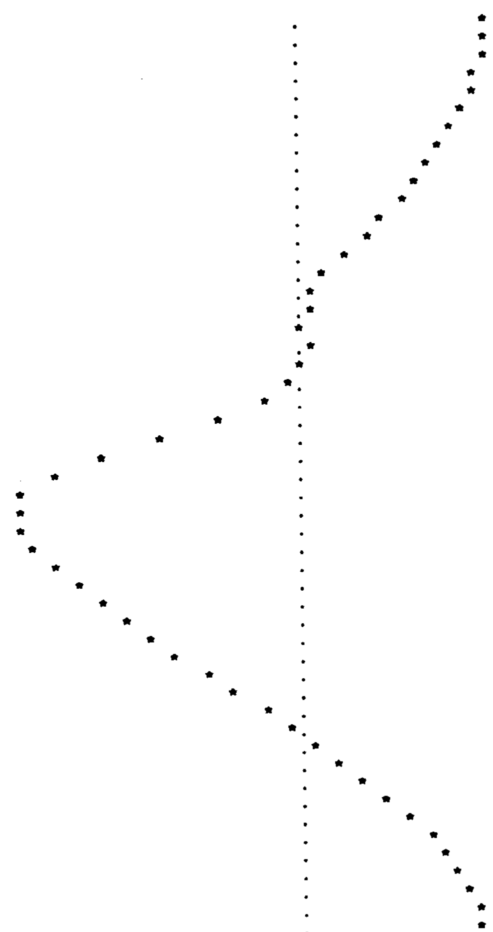

ID(MA)
29.561
30.055
29.916
29.222
27.955
26.237
24.285
22.317
20.437
18.573
16.511
14.025
11.040
7.758
4.646
2.272
1.022
0.832
1.091
0.764
-1.277
-5.856
-13.129
-22.379
-32.092
-40.390
-45.751
-47.626
-46.552
-43.691
-40.158
-36.584
-33.065
-29.394
-25.347
-20.869
-16.095
-11.259
-6.568
-2.121
2.099
6.160
10.106
13.900
17.427
20.538
23.122
25.157
26.715
27.917
28.861

DIODE VOLTAGE VS TIME FOR ONE LO CYCLE

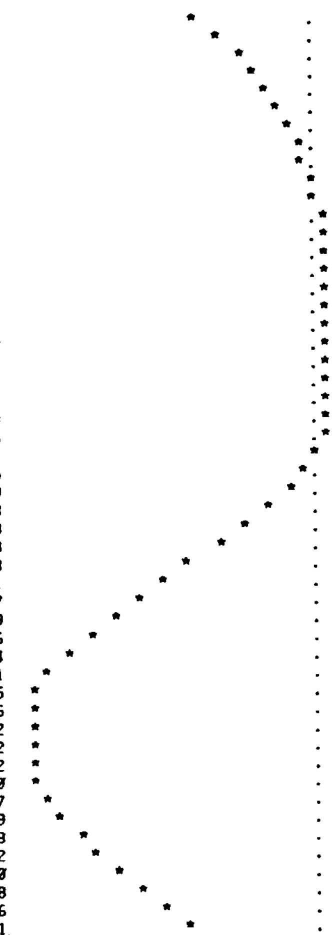

VD(VOLTS)
-4.373
-3.640
-2.948
-2.319
-1.762
-1.279
-0.870
-0.527
-0.241
-0.004
0.190
0.343
0.459
0.539
0.589
0.615
0.627
0.633
0.640
0.648
0.647
0.622
0.549
0.396
0.121
-0.315
-0.939
-1.743
-2.688
-3.718
-4.783
-5.851
-6.897
-7.899
-8.826
-9.644
-10.321
-10.835
-11.175
-11.342
-11.342
-11.182
-10.870
-10.417
-9.839
-9.158
-8.402
-7.600
-6.778
-5.956
-5.151

APPENDIX 6. EQUATIONS USED IN THE ANALYSIS OF THE CHANNEL WAVEGUIDE TRANSFORMER

A6.1 Transverse Resonance Solution for $k_{c_{10}}$ and the Determination of $Z_{c_{10}}$

A6.1.1 Cutoff Wavenumbers by Transverse Resonance

The method of transverse resonance [133] was applied by Cohn [28] to calculate the TE_{m0}-mode wavenumbers of ridged waveguide. It was later used by Vilmur and Ishii [171] for the determination of the TE_{10} mode cutoff frequencies of single channel waveguide. Precisely the same technique can be employed on the double-channel waveguide to obtain the equivalent circuit of Fig. A6-1 and the following relation involving $k_{c_{10}}$:

$$1 - \frac{d}{b} \tan(k_{c_{10}} s)\tan(k_c(a-s)) -$$

$$dk_{c_{10}} \frac{C_d}{\epsilon} \tan(k_{c_{10}}(a-s)) = 0. \qquad \text{(A6.1)}$$

This equation has the same form as that derived by Pyle [130] for ridged waveguide when the following identifications are made:

PRECEDING PAGE BLANK NOT FILMED

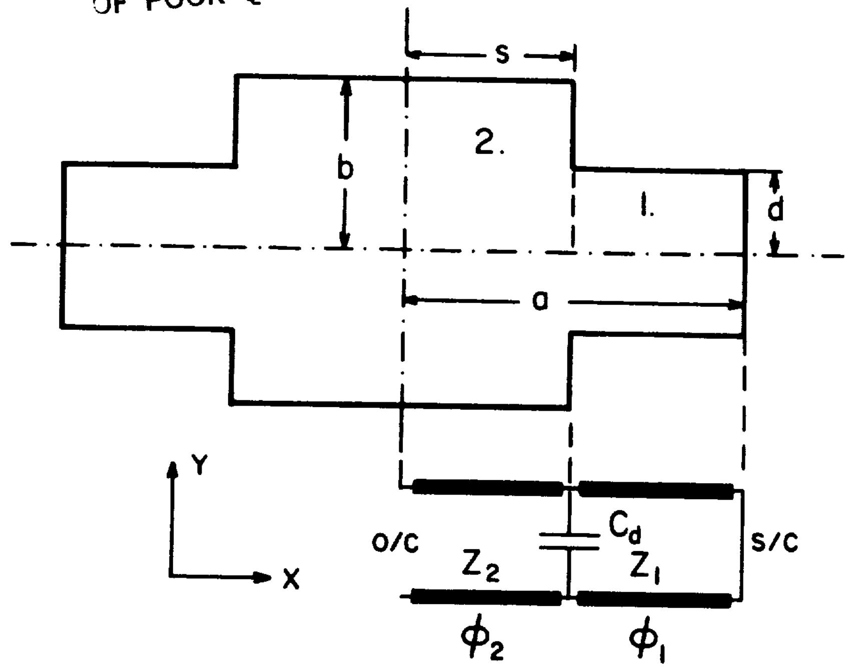

Fig. A6-1. A cross sectional view of the channel waveguide with the equivalent circuit used to derive the wavenumbers by the transverse resonance method of Section A6.1 For the wave equation solutions described in Section A6.2 the cross section is divided into the two regions indicated in the figure and the fields in each are expanded as a series of orthogonal functions. The final solutions are determined after the application of the boundary conditions, which require matching of the tangential fields at the line dividing regions 1 and 2.

$$Z_1 = \left(\frac{\mu}{\varepsilon}\right)^{\frac{1}{2}} \frac{b}{\ell} \,, \tag{A6.2a}$$

$$Z_2 = \left(\frac{\mu}{\varepsilon}\right)^{\frac{1}{2}} \frac{d}{\ell} \,, \tag{A6.2b}$$

$$\alpha = \frac{d}{b} \quad , \tag{A6.2c}$$

$$\Phi_1 = k_{c_{10}} s, \tag{A6.2d}$$

$$\Phi_2 = k_{c_{10}}(a-s), \tag{A6.2e}$$

$$B = \frac{k_{c_{10}} C_d \;\ell}{\sqrt{\mu\varepsilon}} \quad . \tag{A6.2f}$$

C_d is a discontinuity capacitance which accounts for the generation of higher order modes at the edge of the channel. Whinnery and Jamieson [178] approximated C_d to a high degree of accuracy by:

$$\frac{C_d}{\varepsilon} = G \cdot \frac{1}{\pi} \left[\frac{\alpha^2+1}{\alpha} \cosh^{-1} \left(\frac{1+\alpha^2}{1-\alpha^2}\right) - 2 \ln \left(\frac{4\alpha}{1-\alpha^2}\right)\right] \quad . \tag{A6.3}$$

The multiplier, G, is a proximity effect term which decreases the value of C_d when the channel width becomes small ($s/a \approx 0$) and the discontinuities can no longer be considered as being isolated from one another. It is given, for two values of α, by Whinnery and Jamieson's

Fig. 15. When the channel height, 2b, approaches a half wavelength the value of C_d must be increased. The effect is small, <10% for operation in the standard waveguide band, but can be incorporated into (A6.3) by multiplying C_d by a correction factor given in Fig. 16 of Whinnery and Jamieson. The additional term makes C_d in (A6.1) a function of k_c.

A computer program was written to solve the transcendental equation (A6.1) iteratively for the lowest order root. The resulting values of $k_{c_{10}}$ for 10 positions along the length of a full to one-quarter height transformer in X-band waveguide are listed in Table A6-2. The program is given in Appendix 7, Section A7.2.

A6.1.2 Characteristic Impedance

As discussed in Section 7.3.1, the characteristic impedance in the channel waveguide is not unique. Cohn [28] and Mihran [113] defined a characteristic impedance in ridged waveguide using the transverse voltage at the center of the guide divided by the total longitudinal current on the top face. We have found that this definition, when applied to the channel waveguide transformer, gives acceptable agreement with experiment.

In a manner analogous to that of Mihran [156] we obtain for the channel waveguide:

$$Z_{c_{IV}} = \frac{Z_W}{\frac{C_d}{\varepsilon}\cos(k_{c_{10}}s) + \frac{1}{bk_{c_{10}}}\left[\sin(k_{c_{10}}s) + \frac{b}{d}\cos(k_{c_{10}}s)\tan\left(k_{c_{10}}\left(\frac{a-s}{2}\right)\right)\right]} \tag{A6.4}$$

where

$$Z_W = \frac{\omega\mu}{\beta} = \left(\frac{\mu}{\varepsilon}\right)^{\frac{1}{2}}\left[1-\left(\frac{f_c}{f}\right)^2\right]^{-\frac{1}{2}} \quad , \tag{A6.5}$$

is the TE mode wave impedance. The equation has the same form as Mihran's eq. (2). Note that C_d contains a frequency dependent term which should be included in the solution of (A6.4).

A6.2 Wave Equation Solution for $k_{c_{10}}$ and the Determination of $Z_{c_{10}}$

A6.2.1 Cutoff Wavenumbers from the Wave Equation

The field relations derived by Tham [164] for the channel waveguide are given in equations (A6.6)-(A6.14). The unnormalized expressions for the TE_{10} magnetic fields at any cross section along the length of the channel waveguide transformer are (referring to Fig. A6-1):

$$H_{z_1} = \sum_{r=0,2,4...}^{\infty} \Phi_{1_r} \cosh\left[p_{1_r} \left(\frac{x}{2a} - \frac{1}{2}\right)\right]\cos\left[\frac{r\pi}{2d}(d-y)\right] \quad \text{(A6.6)}$$

and

$$H_{z_2} = \sum_{m=0,2,4...}^{\infty} \Phi_{2_m} \sinh\left[p_{2_m} \frac{x}{2a}\right]\cos\left[\frac{m\pi}{2b}(b-y)\right], \quad \text{(A6.7)}$$

where Φ_{1_r} and Φ_{2_m} are complex constants. Also

$$p_{1_r}^2 = \left[-4k_{c_{10}}^2 a^2 + \left(\frac{r\pi a}{d}\right)^2\right] \quad \text{and} \quad \text{(A6.8)}$$

$$p_{2_m}^2 = \left[-4k_{c_{10}}^2 a^2 + \left(\frac{m\pi a}{b}\right)^2 \right] \quad . \tag{A6.9}$$

Subscript 1 refers to the region $s < x < a$, $0 < y < d$ and subscript 2 refers to the region $0 < x < s$, $0 < y < b$. The eigenvalue equation which must be solved to find the wavenumbers, $k_{c_{10}}$, is:

$$\sum_{n=0,2,\ldots}^{\infty} \; \sum_{m=0,2\ldots}^{\infty} \Phi_{2_m} \; a_{nm} = 0. \tag{A6.10}$$

This has a solution if:

$$\det \left[\underset{\approx}{a} \right] = 0. \tag{A6.11}$$

a_{nm} is given by:

$$a_{nm} = \sinh \left[p_{2_m} \frac{s}{2a} \right] \cdot \left[\left\{ \frac{4d}{b} \sum_{r=0,2\ldots}^{\infty} p_{1_r} \frac{C_{rn} C_{rm}}{\Delta_r} \tanh \left[p_{1_r} \left(\frac{s}{2a} - \frac{1}{2} \right) \right] \right\} - \frac{p_{2_m} \Delta_m \delta_{nm}}{\tanh \left[p_{2_m} \frac{s}{2a} \right]} \right] \tag{A6.12}$$

where

$$C_{mn} = \frac{1}{d} \int_0^d \cos\left[\frac{m\pi}{2d}(d-y)\right] \cos\left[\frac{n\pi}{2b}(b-y)\right] dy \quad . \qquad \text{(A6.13)}$$

Φ_{1_m} and Φ_{2_m} are related by:

$$\Phi_{1_m} = \frac{2}{\Delta_m \cosh\left[p_{1_m}\left(\frac{s}{2a} - \frac{1}{2}\right)\right]} \sum_{n=0,2...}^{\infty} \Phi_{2_n} C_{mn} \sinh\left(p_{2_n} \frac{s}{2a}\right), \qquad \text{(A6.14)}$$

where $\Delta_m = 2$ if $m = 0$

$= 1$ otherwise.

A computer program was written to solve (A6.6)-(A6.14) for $k_{c_{10}}$ and $H_{z_{10}}$ (see Appendix 7, Section A7.3). It was found that the infinite sums could be truncated to the first three terms without appreciable loss of accuracy. The solutions to equation (A6.11) provide all the $TE_{odd,even}$ mode wave numbers, but only the lowest nonzero value is required for calculating $k_{c_{10}}$. An initial guess for $k_{c_{10}}$ is taken to be the TE_{10} rectangular guide wave number, (A6.8), (A6.9), and (A6.13) are calculated, the matrix terms in (A6.2) are formed, and (A6.1) is solved using the IBM SSP program MINV. There is no effect on the solution of (A6.11) if a_{nm} in (A6.12) is divided through by the sinh term outside the brackets.

The terms in the matrix will then all be real, since p_1 and p_2 are always pure real or pure imaginary, and the evaluation of the determinant is considerably faster. If the solution of (A6.11) is greater than a specified limit then $k_{c_{10}}$ is incremented, $\underset{\approx}{a}$ is reformed, and the determinant reevaluated. Following the suggestion in [100], if a sign change occurs in the value of the determinant, then the increment for $k_{c_{10}}$ is halved and its sign is reversed. Usually $k_{c_{10}}$ converges to 8 decimal places within 40 iterations when a 3x3 matrix is used. When more than five terms are used in the series in (A6.6)-(A6.14) the solution of (A6.11) becomes a very sensitive function of $k_{c_{10}}$ and the eigenvectors in (A6.10) are then difficult to determine accurately. In Table A6-2, the values of $k_{c_{10}}$ as found from (A6.11) are compared with those obtained from the solution by the transverse resonance method (eq. (A6.1)) for ten values of the channel width. Results are shown with the series truncated at 3 and 7 terms. The two methods agree to within 0.5%.

Once the values of $k_{c_{10}}$ at each cross section have been determined they are used in (A6.10) to find the values of the TE_{10} mode eigenvectors. The IBM SSP program MFGR can be used for this purpose since $\underset{\approx}{a}$ is now a real matrix. The rank of $\underset{\approx}{a}$ is always the number of rows -1 and therefore the eigenvectors for the terms

Normalized Channel Width (s/a)	Position Along Taper in cm. (z)	Cutoff Wavenumber by Transverse Resonance (k_c)	Cutoff Wavenumber by 3x3 Matrix Solution (k_c)	Cutoff Wavenumber by 7x7 Matrix Solution (k_c)	Impedance by TEM Approx. (Z_c/Z_w)	Impedance by Field Solutions (Z_c/Z_w)
1.0	0.0000	1.3743	1.3743	1.3743	0.6981	0.6981
0.9	0.6482	1.4845	1.4845	1.4845	0.7360	0.7313
0.8	1.2965	1.6073	1.6075	1.6073	0.7446	0.7310
0.7	1.9447	1.7323	1.7330	1.7321	0.6982	0.6766
0.6	2.5929	1.8248	1.8264	1.8240	0.5792	0.5541
0.5	3.2411	1.8275	1.8307	1.8261	0.4273	0.4057
0.4	3.8894	1.7380	1.7430	1.7375	0.3136	0.2975
0.3	4.5376	1.6137	1.6210	1.6157	0.2473	0.2355
0.2	5.1858	1.4972	1.5050	1.5002	0.2096	0.2009
0.1	5.8340	1.4107	1.4162	1.4122	0.1876	0.1822

ORIGINAL PAGE IS
OF POOR QUALITY

Table A6-2 A table comparing the cutoff wavenumbers and the characteristic impedances obtained by the method of transverse resonance and by the method of matrix solution at a series of cross sections along the transformer length.

n>0 are expressed as multiples of the n=0 term. This causes no difficulty in determining the characteristic impedance since the arbitrary constant divides out. The sinh factor taken out of equation (A6.12) must now be replaced to obtain the desired eigenvectors. If required, a value for the arbitrary constant can be established by normalizing the transverse fields in some way, usually so that the power flow at each cross section is unity. When the Φ_{2_m}'s have been determined the Φ_{1_r}'s can be found from (A6.14). Substitution into (A6.6)-(A6.7) then gives the expressions for the longitudinal field components in the two regions of the channel waveguide cross section. Similar expressions can be obtained using the Ritz-Galerkin method as in [100] or by breaking the cross section along the y=d line rather than along x=s.

A6.2.2 Characteristic Impedance

The characteristic impedance is derived from the equivalent voltage and current as discussed in Section A6.1. The maximum transverse voltage at the center of the channel is determined by integrating the electric field, $E_y \propto \partial H_z/\partial x$, from -b to b (by symmetry $E_x = 0$ along this line). The total longitudinal current along the upper half (y>0) of the channel waveguide is then found by integrating the transverse magnetic field along the walls and Z_c is calculated by dividing V by I.

The steps leading to the calculation of Z_c are as follows:

$$Z_c \equiv V/I, \text{ with} \tag{A6.15}$$

$$V = -\int \underline{E}_t \cdot d\underline{\ell}_1 = \text{transverse voltage, and} \tag{A6.16}$$

$$I = \int \underline{H}_t \cdot d\underline{\ell}_2 = \text{longitudinal current.} \tag{A6.17}$$

$\underline{E}_t$ and $\underline{H}_t$ are transverse field vectors in the waveguide. They are related to the TE_{10} orthogonal mode vector functions by:

$$\underline{E}_t \equiv V_{10}\underline{e}_{10} \tag{A6.18}$$

$$\underline{H}_t \equiv I_{10}\underline{h}_{10}. \tag{A6.19}$$

$\underline{e}_{10}$ and $\underline{h}_{10}$ are derived from the transverse scalar wave equation:

$$\underline{\nabla}_t^2 \Psi_{10} + k_{c_{10}}^2 \Psi_{10} = 0 \qquad \text{using} \tag{A6.20}$$

$$\underline{e}_{10} = \hat{z} \times \underline{\nabla}_t \Psi_{10} \qquad \text{and} \tag{A6.21}$$

$$\underline{h}_{10} = \hat{z} \times \underline{e}_{10}, \tag{A6.22}$$

with

$$\iint \underline{e}_{10} \cdot \underline{e}_{10} \, d\underline{A} = 1. \tag{A6.23}$$

The longitudinal fields in (A6.6) and (A6.7) are related to Ψ_{10} by:

$$H_z = \frac{V_{10} k_{c_{10}}^2 \Psi_{10}}{jk_0 \sqrt{\frac{\mu}{\varepsilon}}} \tag{A6.24}$$

where $k_{c_{10}}$ is the wavenumber in the guide at cutoff and k_0 is the wavenumber in free space.

The transverse fields in (A6.18) and (A6.19) can be expressed in terms of H_z using Maxwell's equations:

$$\underline{E}_t = V_{10}\underline{e}_{10} = V_{10}(e_{10_x}\hat{x} + e_{10_y}\hat{y}) = \frac{-jk_0}{k_{c_{10}}^2}\sqrt{\frac{\mu}{\varepsilon}} \left(\frac{\partial H_z}{\partial y}\hat{x} - \frac{\partial H_z}{\partial x}\hat{y}\right) \tag{A6.25}$$

$$\begin{aligned} \underline{H}_t &= I_{10}\underline{h}_{10} = I_{10}(-e_{10_y}\hat{x} + e_{10_x}\hat{y}) \\ &= \frac{-jk_0}{k_{c_{10}}^2}\sqrt{\frac{\mu}{\varepsilon}} \; \frac{I_{10}}{V_{10}} \left(\frac{\partial H_z}{\partial x}\hat{x} + \frac{\partial H_z}{\partial y}\hat{y}\right) \end{aligned} \tag{A6.26}$$

The transverse voltage at the center of the channel waveguide is found from:

$$V = -2\int_0^b \underline{E}t_2 dy = \frac{-j2k_0\sqrt{\frac{\mu}{\varepsilon}}}{k^2_{c_{10}}} \int_0^b \left(\frac{\partial H_{z_2}}{\partial x}\right)dy \tag{A6.27}$$

where H_{z_2} is obtained from (A6.6).

The total longitudinal current along the upper half of the channel waveguide is given by:

$$I = 2\left[\int_0^s \underline{H}t_2 dx + \int_s^a \underline{H}t_1 dx + \int_d^b \underline{H}t_2 dy + \int_0^d \underline{H}t_1 dy\right] \tag{A6.28}$$

$$= -j\frac{2k_0}{k^2_{c_{10}}}\sqrt{\frac{\mu}{\varepsilon}}\ \frac{I_{10}}{V_{10}}\left[\int_0^s \left(\frac{\partial H_{z2}}{\partial y}\right)dx + \int_s^a \left(\frac{\partial H_{z1}}{\partial y}\right)dx + \right. \tag{A6.29}$$

$$\left.\int_d^b \left(\frac{\partial H_{z2}}{\partial x}\right)dy + \int_0^d \frac{\partial H_{z1}}{\partial x}\,dy\right].$$

Substituting for H_{z_1} and H_{z_2} from (A6.6) and (A6.7) and carrying out the integrations we obtain:

$$Z_c = \frac{V}{I} = \frac{Z_w \Phi 2_0 \, p 2_0 \left(\frac{b}{a}\right)}{\sum_{m=0,2,4,\ldots}^{\infty} \phi 2_m \sinh\left(p2_m \frac{s}{2a}\right) \; + } \qquad \text{(A6.30)}$$

$$\phi 1_m \left[1-\cosh\left\{p1_m\left(\frac{s}{2a}-\frac{1}{2}\right)\right\}\right] -$$

$$\Phi 2_m \sinh\left(p2_m \frac{s}{2a}\right) \left[1-\cos\left(\frac{m\pi(b-d)}{2b}\right)\right] +$$

$$\Phi_1 \left(1-\cos\left(\frac{m\pi}{2}\right)\right)$$

where $Z_W = \frac{V_{10}}{I_{10}} = \frac{\omega\mu}{\beta}$ is the wave impedance for TE modes. Z_c is real and positive above cutoff.

In Table A6-2 the value of Z_c at infinite frequency (before multiplying through by Z_W), as determined from (A6.30), is compared with the value obtained from (A6.4). The results agree to within ~5.0%.

As discussed in Chapter 7, Section 7.3.2, the field expressions in (A6.6)-(A6.7) converge very slowly in the region near the start of the channel. If we plot the x and y components of the transverse electric field along the line x=s, we see (Fig. 7-3 in Chapter 7) that the truncated series expressions are a poor approximation to the actual fields. The tangential fields in regions 1 and 2 of Fig. 7-2 (Chapter 7) should be identical along the line y=0 to d, and for larger y values E_y in region 2 must go to zero. At the corner x=s, y=d both field components should become infinite.

Fortunately, the determination of the characteristic impedance is most strongly dependent on the fields along y=d and y=b and is not affected greatly by the integral along the side wall of the channel. The same statement cannot be made for the calculation of the terms in the mode coupling theory discussed in Chapter 7, Section 7.3.2.

APPENDIX 7. COMPUTER PROGRAMS FOR THE ANALYSIS OF THE CHANNEL WAVEGUIDE TRANSFORMER

A7.1 Introduction

This appendix contains three different Fortran programs for the analysis of the channel waveguide transformer.

The first program employs the method of transverse resonance (see Appendix 6, Section A6.1.1) to find the cutoff wavenumbers along the length of the transition and then uses the characteristic impedance method (Section A6.1.2) to calculate the reflection coefficient as a function of frequency.

The second program solves the wave equation (Appendix 6, Section A6.2.1) to find the cutoff wavenumbers and then uses the characteristic impedance method (Section A6.2.2) to determine the reflection coefficients.

The third program calculates the cutoff wavenumbers from the wave equation as in program (2) but determines the reflection coefficients of the transformer using the mode coupling theory of Solymar [155] (the relevant equations will be given in Section A7.4).

Each program is used to calculate the performance of a linearly tapered channel waveguide transformer in X-band and the results follow the Fortran listings. Comment cards help to clarify the programming operations and the reader is referred to Appendix 6 for the mathematical details.

A7.2 Solution by Transverse Resonance and Characteristic Impedance

The program listing which follows was used as a basis in generating all the design data presented in Chapter 6. The particular problem analyzed here is that of a linearly tapered channel waveguide transformer in X-band. The taper half-angle is 10 degrees and the input to output height ratio is 4:1.

After the initialization of variables the program calculates the discontinuity capacitance CD given in A6.1.1 (without the proximity effect term G in that equation). The loop which finds the cutoff wavenumbers in each of 50 intervals along the length of the transformer is then begun. An initial guess for the TE_{10} mode cutoff wavenumber $k_{c_{10}}$ (KC) is taken to be the value in rectangular waveguide ($2\pi/4a$). This guess is updated after each cycle. The proximity effect term G, which is a function of position along the transformer through the channel width s, is found in subroutine GAM4 which contains a polynomial fit to the appropriate curve (b/d=4) in Whinnery and Jamieson's [178] figure 15. When G has been determined at a particular point, the transcendental equation A6.1 (set up in subroutine ROOT) is evaluated using the current value of KC. If the solution (DKC) is not zero (less than DKLIM) KC is incremented by KCINC and the procedure is repeated. The size and direction of the increment in KC is determined by the sign of DKC on successive cycles. When a sign change occurs in DKC, KCINC is halved and imaged. Convergence to the proper value of KC is usually reached within 40 cycles.

The propagation constant (BETA), wave impedance (ZW), cutoff frequency (FC) and characteristic impedance (ZCZ) are now calculated as functions of position from A6.4 and A6.5. CD is corrected for proximity effects and a frequency dependent effect which becomes significant when the channel dimensions approach a half wavelength. The input frequency range (IFO to EFO) is adjusted so that no calculations are performed at frequencies which fall below the maximum cutoff frequency in the transformer (FCMAX).

We now have all the terms required for the solution of equation 6.1 which gives the reflection coefficient at the onset of the transition. Equation 6.1 is implemented in differential form in the program with 51 points along the transformer length. The reflection coefficient (RHO) is calculated at each cross section and summed to obtain the final result (AMAG,APHA). The return loss (RLOSS) and voltage standing wave ratio (VSWR) at each frequency are then determined and plotted through subroutine LOCPLT.

```
C
C
C
C      CHANNEL WAVEGUIDE TRANSFORMER ANALYSIS USING THE METHOD
C   OF TRANSVERSE RESONANCE TO DETERMINE THE CUTOFF WAVENUMBERS
C   AND THE CHARACTERISTIC IMPEDANCE TO CALCULATE THE REFLECTION
C   COEFFICIENT.
C
C      IN THIS PROGRAM AN X-BAND LINEARLY TAPERED CHANNEL WAVE-
C   GUIDE TRANSFORMER WITH A 4:1 INPUT TO OUTPUT HEIGHT RATIO
C   IS ANALYZED.  THE TAPER HALF-ANGLE IS 1Ø DEGREES YIELDING
C   A TRANSFORMER LENGTH OF 6.48 CM.
C
C      THE PROGRAM CONTAINS THE ADDITIONAL VARIABLES AND STATEMENTS
C   WHICH ARE USED IN THE ANALYSIS OF A BULGY TRANSFORMER WITH THE
C   SAME PHYSICAL CHARACTERISTICS.  STATEMENTS WHICH REFER TO THE
C   BULGY TRANSFORMER ARE INDICATED BY A C*** IN THE FIRST 4 COLUMNS.
C
C      TO ANALYZE A TRANSFORMER WITH A CIRCULAR-ARC SHAPED PROFILE
C   SIMPLY CHANGE L=AZ/TANW TO L=DSQRT(2.Ø*AZ*RSAW-AZ*AZ) AND
C   S=(L-Z)*TANW TO S=AZ-RSAW+DSQRT(RSAW*RSAW-Z*Z) WHERE RSAW IS
C   THE RADIUS OF THE SLITTING SAW (IN CM) USED TO FORM THE
C   TRANSITION.
C
C
C                MAIN  DRIVER  PROGRAM
C
C   VARIABLES USED IN THE PROGRAM:
      COMPLEX*16 BZ,RHO
      REAL*8 ZW,SB1,AMAG,APHA,DZC,D1,D2,D3,D4,D5,D6,D7
      REAL*8 A,B,D,S,THETA,TANW,ZINT,L,Z,DKLIM,KCLIM,KCINC
      REAL*8 PI,RAD,C,MU,EPS
      REAL*8 RLOSS(1Ø1),VSWR(1Ø1)
      REAL*8 IFØ,EFØ,SFØ,FCMAX,FØ,FC,ZM,W1,DKC,DKCØ,G(5Ø),CDTOT,CD
      REAL*8 KC(5Ø),ZCZ(5Ø),ZC(51),BETA(5Ø)
      INTEGER*4 NINT,NPTS,LOOP,I,IZ,FPTS,IF,NFØ
C   THE FOLLOWING VARAIBLES ARE USED FOR THE ANALYSIS OF A BULGY
C    TRANSFORMER.
      REAL*8 LB,AZ,H,RSAW,DRW
C    COMMON BLOCKS USED IN THE PROGRAM
      COMMON/CONST/PI,RAD,C,MU,EPS
      COMMON/GUIDE/A,B,D,S,THETA
      COMMON/FREQ/FØ,IFØ,EFØ,SFØ,NINT
C   DEFINITIONS OF SOME CONSTANTS USED IN THE PROGRAM
C    THE TANGENT OF THE TAPER HALF-ANGLE
      TANW=DTAN(THETA/RAD)
C    THE NUMBER OF POINTS AT WHICH THE CUTOFF WAVENUMBER IS CALCULATED
      NPTS=NINT+1
C    THE SMALLEST INCREMENT IN KC WHICH WILL BE ALLOWED BEFORE THE
C     PROGRAM IS CONSIDERED TO HAVE CONVERGED
      KCLIM=1.ØD-12
C    DKLIM IS THE ERROR ALLOWED IN THE SOLUTION OF THE TRANSCENDENTAL
C     EQUATION INVOLVING THE CUTOFF WAVENUMBERS, KC.
      DKLIM=1.ØD-6
C    AZ IS DEFINED FOR USE IN THE ANALYSIS OF A BULGY TRANSFORMER WHERE
```

```
C     A, THE REDUCED HEIGHT WAVEGUIDE HALF-WIDTH VARIES ALONG THE
C     LENGTH OF THE TRANSITION
        AZ=A
C    L IS THE TRANSFORMER LENGTH IN THE CASE OF A LINEAR TAPER
        L=AZ/TANW
C    LB IS USED FOR ANALYZING A BULGY TRANSFORMER AND IS THE LENGTH
C     OF THE BULGE IN THE REDUCED HEIGHT WAVEGUIDE
C***    LB=L
C    RSAW IS USED IN THE BULGY TRANSFORMER ANALYSIS AND IS THE RADIUS
C     OF THE TOOL USED TO FORM THE BULGE IN THE WAVEGUIDE WALL IN CM.
C***    RSAW=5.0D0*2.54D0
C    H IS USED IN THE BULGY TRANSFORMER ANALYSIS AND IS THE MAXIMUM
C     INCREASE IN WIDTH OF THE REDUCED HEIGHT WAVEGUIDE DUE TO THE BULGE
C***    H=RSAW-0.5*DSQRT(4.0D0*RSAW*RSAW-LB*LB)
C    THE LENGTH OF THE INTERVAL AFTER WHICH THE CUTOFF WAVENUMBERS,KC
C     WILL BE CALCULATED
        ZINT=L/DFLOAT(NINT)
C    THE TOTAL NUMBER OF FREQUENCIES AT WHICH THE ANALYSIS WILL BE RUN
        FPTS=IDINT((EF0-IF0)/SF0+0.5D0)+1
C    F0 SAVES THE INITIAL INCIDENT FREQUENCY VALUE FOR LATER MANIPULATION
        F0=IF0
C    KC IS THE CUTOFF WEAVENUMBER ALONG THE TRANSITION
        KC(1)=PI/2.0D0/AZ
        WRITE(6,45)
   45 FORMAT(////5X,'ANALYSIS OF A CHANNEL WAVEGUIDE TRANSFORMER',
     1' USING TRANSVERSE RESONANCE AND CHARACTERISTIC IMPEDANCE')
        WRITE(6,50) A,B,A,D,IF0,EF0,THETA,L
   50 FORMAT(//5X,'TRANSFORMER INPUT DATA'//1X,
     *'INPUT WAVEGUIDE DIMENSIONS (A/2,B/2) IN CM:',
     12(F7.4,2X)/1X,'OUTPUT WAVEGUIDE DIMENSIONS (A/2,D/2) IN CM:'
     2,2(F7.4,2X)/1X,'FREQUENCY RANGE (GHZ):',-9PF8.3,' TO ',-9PF8.3/
     3,1X,'THE TAPER HALF-ANGLE IN DEGREES:',0PF8.3/1X,
     4'TRANSFORMER LENGTH (CM):',F7.4/////)
C    THE BULGY TRANSFORMER INPUT PARAMETERS
C***    WRITE(6,60) RSAW,LB,H
   60 FORMAT(5X,'BULGY TRANSFORMER PARAMETERS'//1X,
     1'EQUIVALENT BULGE RADIUS (CM):',F8.4/1X,
     2'BULGE LENGTH (CM):',F9.4/1X,
     3'MAXIMUM INCREASE IN GUIDE WIDTH DUE TO BULGE (CM):',F8.4///)
C    CALCULATE THE CD TERM WHICH IS A FUNCTION OF B AND D AND DOES
C     NOT CHANGE ALONG THE TRANSITION
        CALL CD1(CD,B,D,PI)
C   LOOP OF VALUES OF Z ALONG TRANSFORMER LENGTH
C    THE VALUE OF KC AT Z=0 IS THAT OF A STANDARD RECTANGULAR GUIDE
        DO 2 IZ=2,NINT
C    GUESS THAT THE INITIAL VALUE OF KC AT THIS POINT IS THE SAME
C     AS THE FINAL VALUE AT THE LAST POINT ALONG Z
        KC(IZ)=KC(IZ-1)
C    RESET THE INCREMENT SIZE FOR KC
        KCINC=0.005D0
C    LOOP COUNTS THE NUMBER OF ITERATIONS UNTIL CONVERGENCE
        LOOP=1
C    THE POSITION ALONG THE TRANSFORMER LENGTH
        Z=DFLOAT(IZ-1)*ZINT
C    THE NEXT TWO LINES ARE USED IN A BULGY TRANSFORMER ANALYSIS WHERE
```

```
C     A CHANGES ALONG THE LENGTH OF THE TRANSITION
C***    DRW=DSQRT(RSAW*RSAW-(LB/2.ØDØ-Z)**2)
C***    A=AZ+H-RSAW+DRW
C     S IS THE HALF-WIDTH OF THE TRANSFORMER CHANNEL
        S=(L-Z)*TANW
C     CALCULATE THE PROXIMITY CORRECTION TO CD
C      G(IZ) IS THE CORRECTION TO CD AT EACH OF THE 51 POINTS ALONG
C      THE LENGTH OF THE TRANSFORMER.  GAM4 CONTAINS A POLYNOMIAL
C      REPRESENTATION OF THE CORRECTION CURVE.
        CALL GAM4(G(IZ),B,S)
C     SOLVE THE TRANSCENDENTAL EQUATION FOR KC
C      DKC IS THE SOLUTION OF THE EQUATION IN KC, WHICH IS ZERO
C       WHEN THE PROPER VALUE OF KC HAS BEEN FOUND
    1 CALL ROOT(KC(IZ),DKC,A,B,D,S,PI,CD,G(IZ))
        IF(DABS(DKC).LE.DKLIM) GOTO 16
C     DON'T ADJUST KC ON THE FIRST ITERATION
        IF(LOOP.EQ.1) GOTO 15
C     DKCØ IS THE VALUE OF DKC RETURNED ON THE LAST ITERATION.
C     IF A SIGN CHANGE HAS OCCURRED IN DKC SINCE THE LAST ITERATION
C     HALVE THE INCREMENT AND ADJUST KC IN THE OPPOSITE DIRECTION.
        IF(DKC*DKCØ.LT.Ø.ØDØ) GOTO 17
C     IF THE SOLUTION IS DIVERGING REVERSE THE SIGN OF THE KC INCREMENT.
        IF(DABS(DKC).GT.DABS(DKCØ)) KCINC=-1.ØDØ*KCINC
        GOTO 14
   17 KCINC=KCINC/2.ØDØ
C     IF THE INCREMENT IN KC IS TOO SMALL STOP.
        IF (DABS(KCINC).LT.KCLIM) GOTO 16
C     INCREMENT KC
   14 KC(IZ)=KC(IZ)-KCINC*DSIGN(1.ØDØ,DKC)
C     SAVE THE PRESENT VALUE OF DKC
   15 DKCØ=DKC
C     INCREMENT THE ITERATION COUNTING VARIABLE.
        LOOP=LOOP+1
        IF(LOOP.GT.1ØØØ) GOTO 16
        GOTO 1
   16 CONTINUE
C     GO ON TO THE NEXT POSITION ALONG THE TRANSFORMER LENGTH.
    2 CONTINUE
C     SET INITIAL VALUES OF ZCZ AND G NOT FOUND IN THE ABOVE LOOP
        G(1)=1.ØDØ
        ZCZ(1)=DSQRT(MU/EPS)*KC(1)*B
C     ADJUST THE INPUT FREQUENCIES SO THAT THEY ARE ABOVE CUTOFF
        FCMAX=C/(4.ØDØ*AZ)
        DO 3 I=1,NPTS
        Z=DFLOAT(I-1)*ZINT
        FC=KC(I)*C/(2.ØDØ*PI)
        IF(FC.LE.FCMAX) GOTO 3
        FCMAX=FC
        ZM=Z
    3 CONTINUE
        WRITE(6,113) FCMAX,ZM
  113 FORMAT(/1X,'THE MAXIMUM VALUE OF THE CUTOFF FREQUENCY IN THE',
     1' TRANSFORMER IS:',-9PF8.4,' GHZ.'/1X,'THIS OCCURS AT',
     2' Z=',ØPF8.4,' CM.'/)
        DO 4 IF=1,FPTS
```

```
C    FØ IS THE FIRST FREQUENCY WHICH FALLS ABOVE THE MAXIMUM CUTOFF
C    IN THE TRANSFORMER, FCMAX.
      FØ=IFØ+DFLOAT(IF-1)*SFØ
C    FOR FREQUENCIES WHICH FALL BELOW FCMAX, ARTIFICIALLY FIX THE
C    VALUES OF THE RETURN LOSS AND STANDING WAVE RATIO
      IF(FØ.GT.FCMAX) GOTO 4
      RLOSS(IF)=Ø.ØDØ
      VSWR(IF)=99.999DØ
C    NFØ COUNTS THE NUMBER OF FREQUENCIES WHICH FALL BELOW FCMAX
      NFØ=IF+1
    4 CONTINUE
C    ONLY CALCULATE THE REFLECTION COEFFICIENTS FOR FREQUENCIES
C    ABOVE FCMAX (POINTS AT OR ABOVE NFØ).
      DO 1Ø IF=NFØ,FPTS
      FØ=IFØ+DFLOAT(IF-1)*SFØ
      W1=(2.ØDØ*PI*FØ/C)**2
C    LOOP OVER Z AND CALCULATE THE RELEVENT VARIABLES AT EACH
C    TRANSFORMER CROSS SECTION.
C     WRITE TITLES FOR SUBSEQUENT PRINTOUT OF RESULTS
      IF (IF.NE.FPTS) GOTO 8
      WRITE(6,25Ø) FØ
  25Ø FORMAT(//1ØX,'VALUES OF SOME KEY VARIABLES AS A FUNCTION',
     1' OF POSITION ALONG THE TRANSFORMER AT',-9PF8.3,' GHZ'//3X,
     2'PT.#',T14,'Z',T24,'A',T34,'S',T44,'KC',T56,'FC',T69,'ZC',T82,
     3'ZW',T95,'BETA',T1Ø3,'CDTOT/EPS')
    8 CONTINUE
      DO 5 IZ=1,NINT
      Z=DFLOAT(IZ-1)*ZINT
      S=(L-Z)*TANW
C    THE NEXT TWO LINES ARE USED FOR THE ANALYSIS OF A BULGY TRANSFORMER
C***  DRW=DSQRT(RSAW*RSAW-(LB/2.ØDØ-Z)**2)
C***  A=AZ+H-RSAW+DRW
C    BETA=PROPAGATION CONSTANT, ZW=WAVE IMPEDANCE, FC=CUTOFF FREQUENCY
      BETA(IZ)=DSQRT(W1-KC(IZ)*KC(IZ))
      FC=KC(IZ)*C/(2.ØDØ*PI)
      ZW=DSQRT(MU/EPS)/DSQRT(1.ØDØ-(FC/FØ)**2)
C    CORRECT CD FOR PROXIMITY EFFECTS AND FOR CASES WHERE THE CHANNEL
C    DIMENSIONS APPROACH HALF A GUIDE WAVELENGTH IN THE TRANSITION
      CDTOT=CD*G(IZ)/DSQRT(1.ØDØ-(2.ØDØ*B*FØ/C)**2)
      D1=CDTOT*DCOS(KC(IZ)*S)
      D2=DSIN(KC(IZ)*S)+B/D*DCOS(KC(IZ)*S)*DTAN(KC(IZ)*(A-S)/2.ØDØ)
C    ZCZ IS THE CHARACTERISTIC IMPEDANCE AT INFINITE FREQUENCY
      ZCZ(IZ)=1.ØDØ/(D2/KC(IZ)/B+D1)
      ZC(IZ)=ZCZ(IZ)*ZW
C    PRINT RESULTS AT THE LAST FREQUENCY POINT ONLY
      IF(IF.NE.FPTS) GOTO 5
      WRITE(6,2ØØ) IZ,Z,A,S,KC(IZ),FC,ZC(IZ),ZW,BETA(IZ),CDTOT
  2ØØ FORMAT(1X,T3,I3,T9,F8.4,T2Ø,F8.4,T3Ø,F8.4,T4Ø,F9.6,T52,
     1-9PF8.3,T64,ØPF1Ø.3,T78,FØ9.3,T91,F9.4,T1Ø3,F8.4)
    5 CONTINUE
C    WE REQUIRE ZC AT THE END OF THE TRANSFORMER
      ZC(NPTS)=ZC(1)*D/B
C    CALCULATE THE REFLECTION COEFFICIENTS
      RHO=DCMPLX(Ø.ØDØ,Ø.ØDØ)
      DO 7 IZ=2,NPTS
```

```
C     CALCULATE THE INTEGRAL OVER BETA IN DIFFERENTIAL FORM
        SB1=0.0D0
        IMAX=IZ-1
        Z=DFLOAT(IMAX)*ZINT
        DO 6 I=1,IMAX
      6 SB1=-2.0D0*BETA(I)*ZINT+SB1
C     THE BETA INTEGRALS ARE EXPONENTIATED
        BZ=DCMPLX(DCOS(SB1),DSIN(SB1))
C     FIND THE REFLECTION COEFFICIENT AT EACH Z
        DZC=(ZC(IZ)-ZC(IZ-1))/(ZC(IZ)+ZC(IZ-1))
C     RHO IS THE SUM OF ALL THE REFLECTION COEFFICIENTS
        RHO=RHO+DZC*BZ
      7 CONTINUE
C     AMAG=MAG(RHO), APHA=PHASE(RHO) IN DEGREES
        AMAG=CDABS(RHO)
        APHA=DATAN(DIMAG(RHO)/DREAL(RHO))*RAD
        IF(DIMAG(RHO).LT.0.D0.AND.DREAL(RHO).LT.0.D0)
     1  APHA=APHA-180.0D0
        IF(DIMAG(RHO).GT.0.D0.AND.DREAL(RHO).LT.0.D0)
     1  APHA=APHA+180.0D0
        IF(AMAG.GE.1.0D0) AMAG=0.99999D0
        IF(AMAG.LE.0.0D0) AMAG=0.00001D0
C     RLOSS=RETURN LOSS IN DB
C     VSWR=STANDING WAVE RATIO REFERRED TO A MATCHED LOAD
        RLOSS(IF)=-20.0D0*DLOG10(AMAG)
        VSWR(IF)=(1.0D0+AMAG)/(1.0D0-AMAG)
        IF(VSWR(IF).GT.999.9D0) VSWR(IF)=999.9D0
     10 CONTINUE
C     PLOT VSWR AND RLOSS VS FREQ
        CALL LOCPLT(VSWR,RLOSS,FPTS)
        STOP
        END
C
C
C
        SUBROUTINE CD1(CD,B,D,PI)
C
C       THIS ROUTINE RETURNS THE VALUE OF THE DISCONTINUITY
C     CAPACITANCE WITHOUT THE PROXIMITY EFFECT CORRECTION
C     OR ANY FREQUENCY DEPENDENT TERMS
C
        REAL*8 CD,B,D,PI,X,A1,A2
        X=D/B
        A1=1.0D0+X*X
        A2=1.0D0-X*X
        CD=(A1/X*DLOG((1.0D0+X)/(1.0D0-X))-2.0D0*DLOG(4.0D0*X/A2))/PI
        RETURN
        END
C
C
C
        SUBROUTINE GAM4(G,B,S)
C
C       THIS ROUTINE CONTAINS A POLYNOMIAL REPRESENTING THE PROXIMITY
C     EFFECT CORRECTION TO THE DISCONTINUITY CAPACITANCE CALCULATED
```

```
C     IN SUBROUTINE CD1.
C
        REAL*8 G,B,S,X,Y(6)
        DATA Y/Ø.ØØ43DØ,2.6825DØ,-4.1571DØ,4.5661DØ,-2.8248DØ,.69Ø4DØ/
        X=2.ØDØ*S/B
        IF(X.GE.1.4DØ) GOTO 1
        G=Y(1)+Y(2)*X+Y(3)*X*X+Y(4)*X**3+Y(5)*X**4+Y(6)*X**5
        RETURN
      1 G=1.ØDØ
        RETURN
        END
C
C
C
        SUBROUTINE ROOT(KC,DKC,A,B,D,S,PI,CD,G)
C
C       THIS ROUTINE SETS UP THE TRANSCENDENTAL EQUATION WHICH IS SOLVED
C     TO FIND KC.
C
        REAL*8 KC,DKC,A,B,D,S,G,CD,PI,CDTOT,A1,A2
C     CDTOT AMENDS THE VALUE OF CD BY ADDING A TERM TO CORRECT FOR
C     PROXIMITY EFFECTS (G) AND ONE TO INCREASE THE VALUE OF CD WHEN
C     THE CHANNEL DIMENSIONS APPROACH A HALF-WAVELENGTH.  IN THIS
C     INSTANCE THE FREQUENCY IS TAKEN TO BE FC=KC*C/2PI, THE CUTOFF
C     FREQUENCY IN THE CROSS SECTION.
        CDTOT=CD*G/DSQRT(1.ØDØ-(B*KC/PI)**2)
        A1=D/B*DTAN(KC*S)*DTAN(KC*(A-S))
        A2=D*KC*CDTOT*DTAN(KC*(A-S))
        DKC=1.ØDØ-A1-A2
        RETURN
        END
C
C
C
        SUBROUTINE LOCPLT(VSWR,RLOSS,FPTS)
C
C       THIS ROUTINE PLOTS THE VSWR AND RETURN LOSS VERSUS INCIDENT
C     FREQUENCY.
C
        REAL*8 VSWR(FPTS),RLOSS(FPTS),FGHZ
        REAL*8 MNVSWR,MNLOSS,MXVSWR,MXLOSS,FØ,IFØ,EFØ,SFØ,DB,VN
        INTEGER JPT,YPT,FPTS,IVSWR,IRLOSS,LPT
        INTEGER BLANK,DOT,STAR,RLDB(1Ø),VS(1Ø),YVSWR(51),YLOSS(51)
        COMMON/FREQ/FØ,IFØ,EFØ,SFØ,NINT
C---DEFINE THE NUMERICS USED IN THE GRAPHS
        DATA BLANK,DOT,STAR/' ','.','*'/
C---DETERMINE THE GRAPH SCALES
        MXVSWR=2.ØDØ
        MXLOSS=DABS(RLOSS(1))
        MNVSWR=1.ØDØ
        MNLOSS=DABS(RLOSS(1))
        DO 1Ø JPT=2,FPTS
        IF(MXLOSS.LT.DABS(RLOSS(JPT))) MXLOSS=DABS(RLOSS(JPT))
        IF(MNLOSS.GT.DABS(RLOSS(JPT))) MNLOSS=DABS(RLOSS(JPT))
     1Ø CONTINUE
```

```
      DO 2Ø I=1,1Ø
      DB=DFLOAT(I-1)*1Ø.ØDØ
      VN=DFLOAT(I-1)*1.ØDØ+1.ØDØ
      RLDB(I)=1+IDINT(5Ø.ØDØ*(DB-MNLOSS)/(MXLOSS-MNLOSS)+.5DØ)
      VS(I)=1+IDINT(5Ø.ØDØ*(VN-MNVSWR)/(MXVSWR-MNVSWR)+.5DØ)
   2Ø CONTINUE
C---THE GRAPH HEADINGS
      WRITE(6,11Ø)
  11Ø FORMAT(///3X,'FGHZ',4X,'VSWR',12X,'VSWR VERSUS FREQUENCY',
     1T72,' RLOSS',12X,'RETURN LOSS VERSUS FREQUENCY'/)
C---THE LOOP FOR THE PTS TO BE PLOTTED VERTICALLY DOWN THE PAGE
      DO 2 LPT=1,FPTS
      JPT=FPTS-LPT+1
      FGHZ=IFØ+(DFLOAT(JPT)-1.ØDØ)*SFØ
      IVSWR=1+IDINT(5Ø.ØDØ/(MXVSWR-MNVSWR)*(VSWR(JPT)-MNVSWR)+Ø.5DØ)
      IRLOSS=1+IDINT(5Ø.ØDØ*(DABS(RLOSS(JPT))-MNLOSS)/
     1(MXLOSS-MNLOSS)+Ø.5DØ)
C---SET THE GRAPH LIMITS
      IF(IVSWR.LT.1) IVSWR=1
      IF(IVSWR.GT.51) IVSWR=51
      IF(IRLOSS.LT.1) IRLOSS=1
      IF(IRLOSS.GT.51) IRLOSS=51
C---CLEAR THE HORIZONTAL LINE
      DO 1 YPT=1,51
      YLOSS(YPT)=BLANK
    1 YVSWR(YPT)=BLANK
C---SET THE GRAPH'S Y AXIS
      DO 4Ø I=1,1Ø
      IF(RLDB(I).GT.51.OR.RLDB(I).LT.1) GOTO 3Ø
      YLOSS(RLDB(I))=DOT
   3Ø IF(VS(I).GT.51.OR.VS(I).LT.1) GOTO 4Ø
      YVSWR(VS(I))=DOT
   4Ø CONTINUE
C---THE PLOTTED POINTS ARE REPRESENTED AS ASTERIKS
      YVSWR(IVSWR)=STAR
      YLOSS(IRLOSS)=STAR
C---PRINT THIS LINE OF THE GRAPH
      WRITE(6,12Ø) FGHZ,VSWR(JPT),(YVSWR(YPT),YPT=1,51),RLOSS(JPT),
     1(YLOSS(YPT),YPT=1,51)
  12Ø FORMAT(1X,-9PF7.2,2X,ØPF6.3,2X,51A1,3X,F7.3,2X,51A1)
    2 CONTINUE
      RETURN
      END
C
C
C
      BLOCK DATA
      REAL*8 A,B,D,S,THETA,PI,RAD,C,MU,EPS,FØ,IFØ,EFØ,SFØ
      INTEGER*4 NINT
      COMMON/CONST/PI,RAD,C,MU,EPS
      COMMON/GUIDE/A,B,D,S,THETA
      COMMON/FREQ/FØ,IFØ,EFØ,SFØ,NINT
      DATA PI,RAD,C/3.14159265358979320Ø,57.29577951DØ,2.997925D1Ø/
      DATA MU,EPS/12.56637Ø614359170-9,8.854185336732Ø28ØD-14/
      DATA IFØ,EFØ,SFØ/8.ØD9,13.ØD9,5.D7/
      DATA A,B,D,S/1.143DØ,Ø.5Ø8DØ,Ø.127DØ,1.143DØ/
      DATA THETA/1Ø.DØ/
      DATA NINT/5Ø/
      END
```

ORIGINAL PAGE IS
OF POOR QUALITY

ANALYSIS OF A CHANNEL WAVEGUIDE TRANSFORMER USING TRANSVERSE RESONANCE AND CHARACTERISTIC IMPEDANCE

TRANSFORMER INPUT DATA

INPUT WAVEGUIDE DIMENSIONS (A/2,B/2) IN CM: 1.1430 0.5080
OUTPUT WAVEGUIDE DIMENSIONS (A/2,D/2) IN CM: 1.1430 0.1270
FREQUENCY RANGE (GHZ): 8.000 TO 13.000
THE TAPER HALF-ANGLE IN DEGREES: 10.000
TRANSFORMER LENGTH (CM): 6.4823

THE MAXIMUM VALUE OF THE CUTOFF FREQUENCY IN THE TRANSFORMER IS: 8.7577 GHZ.
THIS OCCURS AT Z= 2.9818 CM.

VALUES OF SOME KEY VARIABLES AS A FUNCTION OF POSITION ALONG THE TRANSFORMER AT 13.000 GHZ

PT.#	Z	A	S	KC	FC	ZC	ZW	BETA	CDTOT/EPS
1	0.0	1.1430	1.1430	1.374275	6.557	304.593	436.297	2.3526	0.7240
2	0.1296	1.1430	1.1201	1.395174	6.657	309.435	438.596	2.3403	0.7240
3	0.2593	1.1430	1.0973	1.416644	6.759	314.095	441.033	2.3273	0.7240
4	0.3889	1.1430	1.0744	1.438685	6.864	318.523	443.618	2.3138	0.7240
5	0.5186	1.1430	1.0516	1.461290	6.972	322.664	446.359	2.2996	0.7240
6	0.6482	1.1430	1.0287	1.484444	7.083	326.451	449.266	2.2847	0.7240
7	0.7779	1.1430	1.0058	1.508125	7.196	329.812	452.347	2.2691	0.7240
8	0.9075	1.1430	0.9830	1.532295	7.311	332.662	455.610	2.2529	0.7240
9	1.0372	1.1430	0.9601	1.556904	7.429	334.908	459.061	2.2360	0.7240
10	1.1668	1.1430	0.9373	1.581880	7.548	336.442	462.703	2.2184	0.7240
11	1.2965	1.1430	0.9144	1.607127	7.668	337.151	466.535	2.2001	0.7240
12	1.4261	1.1430	0.8915	1.632518	7.789	336.906	470.551	2.1814	0.7240
13	1.5557	1.1430	0.8687	1.657889	7.910	335.574	474.733	2.1621	0.7240
14	1.6854	1.1430	0.8458	1.683027	8.030	333.016	479.056	2.1426	0.7240
15	1.8150	1.1430	0.8230	1.707668	8.148	329.098	483.476	2.1230	0.7240
16	1.9447	1.1430	0.8001	1.731483	8.262	323.694	487.929	2.1037	0.7240
17	2.0743	1.1430	0.7772	1.754075	8.369	316.707	492.329	2.0849	0.7240
18	2.2040	1.1430	0.7544	1.774979	8.469	308.080	496.561	2.0671	0.7240
19	2.3336	1.1430	0.7315	1.793670	8.558	297.820	500.483	2.0509	0.7240
20	2.4633	1.1430	0.7087	1.809585	8.634	286.016	503.930	2.0369	0.7240
21	2.5929	1.1430	0.6858	1.822163	8.694	272.854	506.727	2.0256	0.7240
22	2.7226	1.1430	0.6629	1.830899	8.736	258.621	508.709	2.0177	0.7240
23	2.8522	1.1430	0.6401	1.835407	8.757	243.687	509.745	2.0136	0.7240
24	2.9818	1.1430	0.6172	1.835477	8.758	228.471	509.761	2.0136	0.7240
25	3.1115	1.1430	0.5944	1.831112	8.737	213.392	508.758	2.0175	0.7240
26	3.2411	1.1430	0.5715	1.822523	8.696	198.824	506.808	2.0253	0.7240
27	3.3708	1.1430	0.5486	1.810098	8.637	185.057	504.043	2.0364	0.7240
28	3.5004	1.1430	0.5258	1.794340	8.561	172.283	500.626	2.0503	0.7240
29	3.6301	1.1430	0.5029	1.775809	8.473	160.600	496.732	2.0664	0.7240
30	3.7597	1.1430	0.4801	1.755062	8.374	150.030	492.525	2.0840	0.7240
31	3.8894	1.1430	0.4572	1.732622	8.267	140.539	488.147	2.1027	0.7240
32	4.0190	1.1430	0.4343	1.708951	8.154	132.060	483.711	2.1220	0.7240
33	4.1487	1.1430	0.4115	1.684443	8.037	124.504	479.305	2.1415	0.7240
34	4.2783	1.1430	0.3886	1.659425	7.918	117.779	474.992	2.1610	0.7240
35	4.4079	1.1430	0.3658	1.634161	7.797	111.794	470.816	2.1801	0.7240
36	4.5376	1.1430	0.3429	1.609264	7.678	106.524	466.867	2.1986	0.7218
37	4.6672	1.1430	0.3200	1.584813	7.562	101.865	463.140	2.2163	0.7176
38	4.7969	1.1430	0.2972	1.560554	7.446	97.688	459.584	2.2334	0.7136
39	4.9265	1.1430	0.2743	1.537132	7.334	94.006	456.278	2.2496	0.7065
40	5.0562	1.1430	0.2515	1.514897	7.228	90.790	453.249	2.2646	0.6944
41	5.1858	1.1430	0.2286	1.493987	7.128	87.993	450.494	2.2785	0.6765
42	5.3155	1.1430	0.2057	1.474414	7.035	85.561	447.994	2.2912	0.6523
43	5.4451	1.1430	0.1829	1.456126	6.948	83.445	445.725	2.3029	0.6222
44	5.5748	1.1430	0.1600	1.439077	6.866	81.605	443.665	2.3135	0.5862
45	5.7044	1.1430	0.1372	1.423275	6.791	80.013	441.802	2.3233	0.5438
46	5.8340	1.1430	0.1143	1.408830	6.722	78.655	440.137	2.3321	0.4942
47	5.9637	1.1430	0.0914	1.396004	6.661	77.533	438.689	2.3398	0.4351
48	6.0933	1.1430	0.0686	1.385247	6.609	76.668	437.495	2.3462	0.3630
49	6.2230	1.1430	0.0457	1.377249	6.571	76.099	436.620	2.3509	0.2724
50	6.3526	1.1430	0.0229	1.372994	6.551	75.886	436.158	2.3534	0.1558

VSWR VERSUS FREQUENCY

RETURN LOSS VERSUS FREQUENCY

FGHZ	VSWR	RLOSS
13.00	1.032	36.162
12.95	1.035	35.393
12.90	1.037	34.722
12.85	1.040	34.135
12.80	1.043	33.622
12.75	1.045	33.176
12.70	1.047	32.790
12.65	1.049	32.460
12.60	1.050	32.182
12.55	1.052	31.951
12.50	1.053	31.765
12.45	1.054	31.621
12.40	1.055	31.514
12.35	1.055	31.442
12.30	1.055	31.401
12.25	1.055	31.387
12.20	1.055	31.394
12.15	1.055	31.414
12.10	1.055	31.441
12.05	1.055	31.464
12.00	1.055	31.471
11.95	1.055	31.452
11.90	1.055	31.392
11.85	1.056	31.280
11.80	1.057	31.106
11.75	1.059	30.866
11.70	1.061	30.558
11.65	1.064	30.186
11.60	1.067	29.757
11.55	1.071	29.284
11.50	1.076	28.777
11.45	1.081	28.247
11.40	1.086	27.706
11.35	1.092	27.163
11.30	1.096	26.624
11.25	1.104	26.094
11.20	1.111	25.579
11.15	1.118	25.080
11.10	1.125	24.601
11.05	1.132	24.141
11.00	1.140	23.701
10.95	1.147	23.281
10.90	1.155	22.882
10.85	1.162	22.500
10.80	1.170	22.137
10.75	1.177	21.790
10.70	1.185	21.457
10.65	1.192	21.136
10.60	1.200	20.826
10.55	1.208	20.524
10.50	1.216	20.227
10.45	1.224	19.932
10.40	1.233	19.637
10.35	1.242	19.337
10.30	1.252	19.031
10.25	1.262	18.714
10.20	1.274	18.384
10.15	1.287	18.038
10.10	1.301	17.673
10.05	1.317	17.286
10.00	1.335	16.875
9.95	1.355	16.440
9.90	1.378	15.979
9.85	1.404	15.492
9.80	1.434	14.979
9.75	1.468	14.439
9.70	1.508	13.874
9.65	1.553	13.284
9.60	1.606	12.670
9.55	1.667	12.035
9.50	1.739	11.378
9.45	1.824	10.702
9.40	1.924	10.007
9.35	2.044	9.297
9.30	2.189	8.571
9.25	2.366	7.833
9.20	2.586	7.085
9.15	2.866	6.328
9.10	3.227	5.566
9.05	3.710	4.801
9.00	4.379	4.038
8.95	5.354	3.283
8.90	6.875	2.545
8.85	9.473	1.841
8.80	14.251	1.221
8.75	99.999	0.0
8.70	99.999	0.0
8.65	99.999	0.0
8.60	99.999	0.0
8.55	99.999	0.0
8.50	99.999	0.0
8.45	99.999	0.0
8.40	99.999	0.0
8.35	99.999	0.0
8.30	99.999	0.0
8.25	99.999	0.0
8.20	99.999	0.0
8.15	99.999	0.0
8.10	99.999	0.0
8.05	99.999	0.0
8.00	99.999	0.0

A7.3 Solution Using the Wave Equation and the Characteristic Impedance

In this program the wave equation is solved at each transformer cross section to find the cutoff wavenumbers as a function of position along the transition. The equations are given in Section A6.2.1 of Appendix 6.

After the initialization of variables, subroutine CMN is called to find C1(m,n) [m=0,2,...NRSUM; n=0,2,...NROW] using A6.13. The integrals were evaluated analytically beforehand and the results coded into the subroutine for arbitrary m and n. The loop over the transformer length (IZ) is begun with an initial guess for $k_{c_{10}}$ of $2\pi/4a$ (the value in rectangular waveguide). A6.8 and A6.9 are calculated with this value of $k_{c_{10}}$ (KC) and matrix $\underline{a}$ (ANM) is formed using A6.12. In order to keep matrix $\underline{a}$ real, A6.12 is divided through by sinh $(p_{2_m} s/2a)$.

The IBM SSP routine DMINV is used to find the determinant of $\underline{a}$ (DET) which is then compared to the value on the previous iteration (DETO) (this step is skipped of course on the first cycle). If the determinant is not zero (i.e. it is larger than LIMIT) then the value of $k_{c_{10}}$ (KC) is incremented by KCINC and matrix $\underline{a}$ is reformed. When the determinant changes sign on successive cycles, KCINC is halved and its sign is reversed prior to incrementing KC. If KCINC becomes too small (less than KCLIM) or the determinant (DET) is less than LIMIT the solution is said to have converged.

Matrix $\underline{a}$ is now reformed with the converged value of KC and the IBM SSP routine DMFGR is used to determine the eigenvector of $\underline{a}$ (PHI2) corresponding to the eigenvalue KC. The sinh term which was previously removed from A6.12 must now be put back in order to find the ϕ_2 coefficients in A6.10. The ϕ_1 coefficients (PHI1) can now be calculated from vector PHI2 using A6.14.

The characteristic impedance, defined as the ratio of the transverse voltage at the center of the transformer divided by the total longitudinal current along the top half, is calculated using the equations in Section A6.2.2. Subroutine CURREN finds the longitudinal current (CURR) at position Z in the transformer from A6.29 where H_{z_1} and H_{z_2} are given by A6.6 and A6.7. The integrals in A6.29 were evaluated beforehand for arbitrary NROW and NRSUM so that numerical integration is not required in CURREN. The voltage at the center of the transformer cross section is given by the numerator in A6.30 and $Z_c(z)$ [ZCZ] is calculated (without the frequency dependent wave impedance term Z_w) by dividing the voltage (VMAX) by the current (CURR).

The remainder of the program is the same as that described in the previous section.

```
C
C
C      CHANNEL WAVEGUIDE TRANSFORMER ANALYSIS USING THE WAVE
C    EQUATION TO DETERMINE THE CUTOFF WAVENUMBERS AND THE
C    CHARACTERISTIC IMPEDANCE TO CALCULATE THE REFLECTION
C    COEFFICIENT.
C
C
C      IN THIS PROGRAM AN X-BAND LINEARLY TAPERED CHANNEL WAVE-
C   GUIDE TRANSFORMER WITH A 4:1 INPUT TO OUTPUT HEIGHT RATIO
C   IS ANALYZED.  THE TAPER HALF-ANGLE IS 1Ø DEGREES YIELDING
C   A TRANSFORMER LENGTH OF 6.48 CM.
C
C
C      THE PROGRAM MAY BE ALTERED TO ANALYZE A BULGY TRANSFORMER
C    BY ADDING THE LINES WITH A C*** IN THE FIRST FOUR COLUMNS.
C
C      TO ANALYZE A TRANSFORMER WITH A CIRCULAR-ARC SHAPED PROFILE
C   SIMPLY CHANGE L=AZ/TANW TO L=DSQRT(2.Ø*AZ*RSAW-AZ*AZ) AND
C   S=(L-Z)*TANW TO S=AZ-RSAW+DSQRT(RSAW*RSAW-Z*Z) WHERE RSAW IS
C   THE RADIUS OF THE SLITTING SAW (IN CM) USED TO FORM THE
C   TRANSITION.
C
C
C                 MAIN  PROGRAM
C
C    VARIABLE TYPES USED IN THIS ROUTINE:
C
      COMPLEX*16 P1(3),P2(3),PHI1(3),PHI2(3)
      COMPLEX*16 AØ,A1,A2,A3,A4,BZ,RHO
      COMPLEX*16 CDTANH,CDSINH,CDCOSH,DELTR,DELTA
      REAL*8 ANM(3,3),C1(3,3)
      REAL*8 ZC(51),ZCZ(5Ø),VMAX(5Ø),CURR(5Ø),BETA(5Ø),KC(5Ø)
      REAL*8 RLOSS(1Ø1),VSWR(1Ø1)
      REAL*8 ZW,DET,DETØ,DZC,SB1,AMAG,APHA
      REAL*8 A,B,D,S,THETA,TANW,ZINT,L,Z,KCINC
      REAL*8 PI,RAD,C,MU,EPS,Z,EPS2,ZINT,LIMIT,KCLIM
      REAL*8 IFØ,EFØ,SFØ,FØ,FC,FCMAX,ZM,W1
      INTEGER*4 WK1(3),WK2(3),IROW(3),ICOL(3)
      INTEGER*4 IRANK,NROW,NRSUM,NINT,NPTS,LOOP,CONVER
      INTEGER*4 I,J,K,IZ,M,N,FPTS,IF,NFØ,IMAX
C    BULGY TRANSFORMER VARIABLES
      REAL*8 RSAW,LB,H,DRW
      COMMON/CONST/PI,RAD,C,MU,EPS
      COMMON/GUIDE/A,B,D,S,THETA
      COMMON/LOOPS/NROW,NRSUM,KCINC,LIMIT,KCLIM,NINT
      COMMON/FREQ/FØ,IFØ,EFØ,SFØ
C    DESCRIPTIONS OF SOME VARIABLES USED FOR THE METHOD OF
C    EIGENVALUE SOLUTION AND NOT LISTED IN THE PREVIOUS ANALYSIS.
C   ANM: THE MATRIX WHOSE DETERMINANT WILL BE ZERO WHEN THE CORRECT
C        VALUE OF KC1Ø HAS BEEN FOUND.  THE EIGENVECTOR OF ANM
C        CONTAINS THE COEFFICIENTS IN THE SERIES EXPANSION OF THE
C        FIELD IN REGION 2 OF THE CHANNEL WAVEGUIDE TRANSFORMER.
C        ANM HAS DIMENSIONS OF NROW BY NROW.
C   C1:  THE SOLUTIONS OF THE TRIGONOMETRIC INTEGRATIONS IN CMN.
```

```
C       C1 IS CALCULATED FOR ALL COMBINATIONS OF N AND M (BOTH EVEN)
C       WHERE EACH INTEGRAL HAS BEEN EVALUATED ANALYTICALLY.
C       SINCE C1 DEPENDS ONLY ON D AND B IT NEED BE FOUND ONLY ONCE
C       DURING THE ANALYSIS.
C  CONVER:  A MARKER WHICH IS SET TO ONE WHEN CONVERGENCE HAS BEEN
C           REACHED.  IT ALLOWS ANM TO BE FORMED ONE LAST TIME WITHOUT
C           BEING DESTROYED BY THE MATRIX INVERSION ROUTINE DMINV.
C  CURR: THE TOTAL LONGITUDINAL CURRENT ALONG THE UPPER WALLS
C        OF THE CHANNEL WAVEGUIDE TRANSFORMER AT EACH CROSS
C        SECTION.  CURREN IS CALCULATED FROM THE FIELDS IN THE
C        TRANSFORMER BY INTEGRATING THE SERIES SOLUTIONS TERM BY
C        TERM.
C  EPS2:  A PARAMETER USED BY THE SSP ROUTINE DMFGR WHICH CAN BE
C        ADJUSTED TO HELP THE ROUTINE CONVERGE WHEN THE DIMENSIONS
C        OF ANM ARE GREATER THAN 3 BY 3.
C  IRANK:  THE RANK OF THE MATRIX ANM RETURNED BY DMFGR AND ALWAYS
C          EQUAL RO NROW-1 IF THE PROGRAM HAS RUN PROPERLY.
C  IROW(ICOL):  ROW AND COLUMN MARKERS REQUIRED BY DMFGR.
C  KC:  THE LOWEST NON-ZERO EIGENVALUE OF ANM AND THE TE1Ø MODE
C       CUTOFF WAVENUMBER.
C  KCLIM:  THE MINIMUM VALUE OF THE INCREMENT IN KC WHICH IS ALLOWED
C          BEFORE THE SOLUTION IS SAID TO HAVE CONVERGED.
C  LIMIT:  THE MAXIMUM ALLOWABLE VALUE OF THE DETERMINANT OF ANM.
C  LOOP:  THE MAXIMUM NUMBER OF ALLOWED CONVERGENCE LOOPS.
C  NROW:  THE NUMBER OF TERMS IN THE SERIES EXPANSION REPRESENTING
C         THE LONGITUDINAL MAGNETIC FIELD HZ. NROW IS ALSO THE
C         DIMENSION OF ANM, PHI1, PHI2 AND P2.
C  NRSUM:  THE DIMENSION OF P1 AND THE NUMBER OF TERMS IN ONE OF
C          THE SUMMATIONS USED IN THE FORMATION OF THE MATRIX ANM.
C  P1(P2):  CONSTANTS WHICH SATISFY THE WAVE EQUATION IN REGION 1(2)
C           OF THE TRANSFORMER. P1 (P2) IS A FUNCTION OF A AND D (B)
C           AND IS EVALUATED ONCE FOR A SIMPLE TRANSFORMER BUT AT EVERY
C           CROSS SECTION IN Z FOR A BULGY TRANSFORMER.
C  PHI1(PHI2):  COEFFICIENTS IN THE SERIES EXPANSIONS OF THE
C               LONGITUDINAL MAGNETIC FIELD HZ1 (HZ2) IS REGION 1(2)
C               OF THE TRANSFORMER. PHI1(I) AND PHI2(I>1) ARE GIVEN
C               IN TERMS OF PHI2(1).
C  VMAX:  THE VOLTAGE CALCULATED ACROSS THE CENTER OF THE CHANNEL
C         WAVEGUIDE TRANSFORMER.  VMAX IS FOUND ANALYTICALLY BY
C         INTEGRATING THE ELECTRIC FIELD FROM -B TO B.
C  WK1(WK2):  WORK SPACE REQUIRED BY ROUTINE DMINV.
C   SET THE CONSTANTS USED IN THE ANALYSIS
      NPTS=NINT+1
      AZ=A
      TANW=DTAN(THETA/RAD)
      L=AZ/TANW
C***  LB=L
C***  RSAW=5.ØDØ*2.54DØ
C***  H=RSAW-Ø.5DØ*DSQRT(4.ØDØ*RSAW*RSAW-LB*LB)
      ZINT=L/DFLOAT(NINT)
      FPTS=IDINT((EFØ-IFØ)/SFØ+Ø.5DØ)+1
C  INITIAL GUESS FOR KC
C   AT THE START OF THE TRANSITION KC1Ø IS TAKEN TO BE THE TE1Ø MODE
C   CUTOFF WAVENUMBER OF A RECTANGULAR WAVEGUIDE.  IF ONE WANTS TO
C   FIND THE CUTOFF WAVENUMBERS OF A HIGHER ORDER TE ODD,EVEN MODE
```

```
C   THEN THE VALUE OF KC(1) SHOULD BE SET EQUAL TO THE VALUE THAT THE
C   PARTICULAR CUTOFF WAVENUMBER HAS IN RECTANGULAR WAVEGUIDE.
C   IN SUBSEQUENT CYCLES THE CUTOFF WAVENUMBERS IN THE TRANSFORMER WILL
C   CONVERGE TO THESE HIGHER ORDER EIGENVALUES RATHER THAN THE TE1Ø
C   MODE SOLUTIONS.
      KC(1)=2.ØDØ*PI/(4.ØDØ*A)
      FØ=IFØ
      WRITE(6,45)
   45 FORMAT(////5X,'ANALYSIS OF A CHANNEL WAVEGUIDE TRANSFORMER',
     1' USING THE WAVE EQUATION AND THE CHARACTERISTIC IMPEDANCE')
      WRITE(6,5Ø) A,B,A,D,IFØ,EFØ,THETA,L,NROW,NRSUM,KCLIM,LIMIT
   5Ø FORMAT(//5X,'TRANSFORMER INPUT DATA'//1X,
     *'INPUT WAVEGUIDE DIMENSIONS (A/2,B/2) IN CM:',
     12(F7.4,2X)/1X,'OUTPUT WAVEGUIDE DIMENSIONS (A/2,D/2) IN CM:'
     2,2(F7.4,2X)/1X,'FREQUENCY RANGE (GHZ):',-9PF8.3,' TO ',-9PF8.3/
     3,1X,'TAPER HALF ANGLE (DEGREES):',ØPF8.3/1X,
     4'TRANSFORMER LENGTH (CM):',F7.4/1X,
     5'SERIES DIMENSIONS: NROW=',I3,2X,'NRSUM=',I3/1X,
     6'CONVERSION LIMITS: KCLIM=',1PD1Ø.3,2X,'LIMIT=',1PD1Ø.3////)
C***  WRITE(6,6Ø) RSAW,LB,H
   6Ø FORMAT(5X,'BULGY TRANSFORMER PARAMETERS'//1X,
     1'EQUIVALENT BULGE RADIUS (CM):',F8.4/1X,
     2'BULGE LENGTH (CM):',F9.4/1X,
     3'MAXIMUM INCREASE IN GUIDE WIDTH DUE TO BULGE (CM):',F8.4///)
C   CALCULATE THE CMN INTEGRALS SINCE THEY DEPEND ONLY ON B AND D
      CALL CMN(NROW,NRSUM,C1)
C  LOOP OF VALUES OF Z ALONG TRANSFORMER LENGTH
      DO 6 IZ=1,NINT
      Z=DFLOAT(IZ-1)*ZINT
      S=(L-Z)*TANW
C***  DRW=DSQRT(RSAW*RSAW-(LB/2.ØDØ-Z)**2)
C***  A=AZ+H-RSAW+DRW
      IF(IZ.GT.1) KC(IZ)=KC(IZ-1)
C   RESET KCINC BEFORE PROCEEDING TO FIND THE NEW VALUE OF KC
C   NOTE THAT IF KCINC IS SET TOO LARGE IT IS POSSIBLE THAT THE
C   SOLUTION WILL NOT CONVERGE ON THE LOWEST NON-ZERO EIGENVALUE
C   (KC1Ø) BUT ON A HIGHER TE ODD,EVEN MODE.
      KCINC=Ø.Ø2DØ
      LOOP=1
C   CONVER IS SET TO 1 WHEN THE SOLUTION HAS CONVERGED
      CONVER=Ø
C   SET EPS2 TO ITS RECOMMENDED VALUE.
      EPS2=1.ØD-7
C   CALL P1P2 TO EVALUATE P1 AND P2 AT THIS Z. THE ROUTINE NEED BE
C   CALLED ONLY ONCE IF A IS CONSTANT ALONG THE TRANSFORMER LENGTH.
    1 CALL P1P2(NROW,NRSUM,P1,P2,KC(IZ))
C   FORM THE ANM MATRIX
C   ANM IS REAL BECAUSE WE HAVE DIVIDED THROUGH BY SINH(P2*S/2A)
      DO 1Ø I=1,NROW
      DO 9 J=1,NROW
      A3=P2(J)*S/2.ØDØ/A
      A1=DELTA(I,J)*P2(J)*DELTR(J)*B/(4.ØDØ*D*CDTANH(A3))
      AØ=DCMPLX(Ø.ØDØ,Ø.ØDØ)
      DO 8 K=1,NRSUM
      A4=P1(K)*(S/2.ØDØ/A-Ø.5DØ)
```

```
      A2=P1(K)*C1(K,I)*C1(K,J)*CDTANH(A4)/DELTR(K)
      AØ=AØ+A2
    8 CONTINUE
      ANM(I,J)=DREAL(AØ-A1)
    9 CONTINUE
   1Ø CONTINUE
C   DON'T INVERT ANM IF THE SOLUTION HAS CONVERGED ALREADY.
      IF (CONVER.EQ.1) GOTO 22
C   CALCULATE THE DETERMINANT OF ANM (DMINV DESTROYS ANM)
      CALL DMINV(ANM,NROW,DET,WK1,WK2,NROW*NROW)
C   CHECK FOR Ø EIGENVALUE AND CHANGE KC ACCORDINGLY
      IF(DABS(DET).LE.LIMIT) GOTO 3Ø
C   ON THE FIRST CYCLE DON'T ADJUST KC
      IF(LOOP.EQ.1) GOTO 27
C   IF A SIGN CHANGE HAS OCCURRED SINCE THE LAST ITERATION THEN
C   HALVE THE INCREMENT IN KC AND REVERSE THE DIRECTION OF CHANGE
C   DETØ IS THE VALUE OF THE DETERMINANT FROM THE PREVIOUS ITERATION
      IF(DETØ*DET.LT.Ø.ØDØ) GOTO 2Ø
C   IF THE DETERMINANT IS INCREASING REVERSE THE DIRECTION OF THE
C   CHANGE IN KC FOR THIS CYCLE.
      IF(DABS(DET).GT.DABS(DETØ)) KCINC=-1.ØDØ*KCINC
      GOTO 25
   2Ø KCINC=KCINC/2.ØDØ
C   IF THE INCREMENT IN KC IS TOO SMALL STOP.
      IF (DABS(KCINC).LT.KCLIM) GOTO 3Ø
C   CHANGE KC AND REPEAT THE CYCLE.
   25 KC(IZ)=KC(IZ)-KCINC*DSIGN(1.ØDØ,DET)
C   SAVE THE PRESENT VALUE OF THE DETERMINANT OF ANM
   27 DETØ=DET
      LOOP=LOOP+1
C   IF CONVERGENCE HASN'T BEEN REACHED AFTER 12Ø CYCLES THEN STOP.
      IF(LOOP.GT.12Ø) GOTO 3Ø
C   GO ON TO THE NEXT ITERATION
      GOTO 1
C   AT THIS POINT THE SOLUTION HAS CONVERGED HOWEVER ANM WAS
C   DESTROYED BY DMINV AND MUST BE REFORMED BEFORE CONTINUING.
C   WHEN CONVER IS SET TO 1 ANM WILL BE FORMED BUT DMINV WILL NOT BE
C   CALLED.
   3Ø CONVER=1
      GOTO 1
   22 CONTINUE
C   FIND THE EIGENVECTORS CORRESPONDING TO THE EIGENVALUE KC1Ø.
      CALL DMFGR(ANM,NROW,NROW,EPS2,IRANK,IROW,ICOL)
C   CHECK THE RANK OF ANM TO BE SURE THAT THERE ARE (NROW-1)
C   INDEPENDENT EIGENVECTOR COMPONENTS. IF NOT THEN AN ERROR
C   HAS OCCURRED IN ROUTINE DMFGR.
      IF(IRANK.EQ.NROW-1) GOTO 58
C   IT IS SOMETIMES POSSIBLE TO CORRECT THE ERROR IN DMFGR IF
C   EPS2 IS ADJUSTED APPROPRIATELY.
      EPS2=EPS2/2.ØDØ
      WRITE(6,18Ø) EPS2
  18Ø FORMAT(1X,'EPS2 HAS BEEN CHANGED TO ',1PD1Ø.3)
      IF(EPS2.LT.1.ØD-1Ø) GOTO 58
      GOTO 1
C   SET THE FIRST EIGENVECTOR COMPONENT TO 1
```

```
   58 PHI2(ICOL(1+IRANK))=DCMPLX(1.ØDØ,Ø.ØDØ)
      DO 3 I=1,IRANK
C     THE REMAINING EIGENVECTOR COMPONENTS ARE GIVEN AS MULTIPLES OF
C     PHI2(1).
    3 PHI2(ICOL(I))=ANM(I,IRANK+1)*PHI2(ICOL(1+IRANK))
C     THE ACTUAL PHI2'S ARE FOUND BY MULTIPLYING THROUGH EACH
C     COMPONENT BY THE SINH(P2*S/2A) TERM WHICH WAS DIVIDED
C     OUT WHEN THE ANM MATRIX WAS ORIGINALLY FORMED
      DO 2 I=1,NROW
    2 PHI2(I)=PHI2(I)/CDSINH(P2(I)*S/2.ØDØ/A)
C     CALCULATE THE PHI1 COEFICIENTS FROM THE PHI2 EIGENVECTOR
      DO 31 I=1,NROW
      AØ=DCMPLX(Ø.ØDØ,Ø.ØDØ)
      DO 29 J=1,NROW
      A2=P2(J)*S/A/2.ØDØ
      A1=PHI2(J)*C1(I,J)*CDSINH(A2)
      AØ=AØ+A1
   29 CONTINUE
      A3=P1(I)*(S/2.ØDØ/A-Ø.5DØ)
      PHI1(I)=AØ*2.ØDØ/(DELTR(I)*CDCOSH(A3))
   31 CONTINUE
C     CALCULATE THE CURRENT ALONG THE UPPER WALLS OF THE TRANSFORMER
C     AT THIS PARTICULAR CROSS SECTION
      CALL CURREN(P1,P2,PHI1,PHI2,CURR(IZ),NROW,NRSUM)
C     EVALUATE THE VOLTAGE ACROSS THE CENTER OF THE TRANSFORMER AT THIS
C     CROSS SECTION.
      VMAX(IZ)=CDABS(PHI2(1)*P2(1))*B/A
C     CALCULATE THE CHARACTERISTIC IMPEDANCE AT THIS CROSS SECTION
C     LEAVING OUT THE FREQUENCY DEPENDENCE
      ZCZ(IZ)=VMAX(IZ)/CURR(IZ)
    6 CONTINUE
C     ADJUST THE INPUT FREQUENCIES SO THAT THEY ARE ABOVE CUTOFF
      FCMAX=C/(4.ØDØ*A)
      DO 4Ø I=1,NINT
      Z=DFLOAT(I-1)*ZINT
      FC=KC(I)*C/(2.ØDØ*PI)
      IF(FC.LE.FCMAX) GOTO 4Ø
      FCMAX=FC
      ZM=Z
   4Ø CONTINUE
      WRITE(6,113) FCMAX,ZM
  113 FORMAT(/1X,'THE MAXIMUM VALUE OF THE CUTOFF FREQUENCY IN THE',
     1' TRANSFORMER IS:',-9PF8.4,' GHZ.'/1X,'THIS OCCURS AT',
     2' Z=',ØPF8.4,' CM.'/)
      DO 41 IF=1,FPTS
      FØ=IFØ+DFLOAT(IF-1)*SFØ
      IF(FØ.GT.FCMAX) GOTO 41
      RLOSS(IF)=Ø.ØDØ
      VSWR(IF)=99.999DØ
      NFØ=IF+1
   41 CONTINUE
      DO 19 IF=NFØ,FPTS
      FØ=IFØ+DFLOAT(IF-1)*SFØ
      W1=(2.ØDØ*PI*FØ/C)**2
C     WRITE TITLES FOR SUBSEQUENT PRINTOUT OF RESULTS
```

```
      IF (IF.NE.FPTS) GOTO 48
      WRITE(6,25Ø) FØ
  25Ø FORMAT(//1ØX,'VALUES OF SOME KEY VARIABLES AS A FUNCTION',
     1' OF POSITION ALONG THE TRANSFORMER AT',-9PF8.3,' GHZ'//3X,
     2'PT.#',T14,'Z',T24,'A',T34,'S',T44,'KC',T56,'FC',T69,'ZC',T82,
     3'ZW',T93,'VMAX',T1Ø5,'CURR',T117,'BETA')
   48 CONTINUE
      DO 16 IZ=1,NINT
      Z=DFLOAT(IZ-1)*ZINT
      S=(L-Z)*TANW
C***  DRW=DSQRT(RSAW*RSAW-(LB/2.ØDØ-Z)**2)
C***  A=AZ+H-RSAW+DRW
      BETA(IZ)=DSQRT(W1-KC(IZ)*KC(IZ))
      FC=KC(IZ)*C/(2.ØDØ*PI)
      ZW=DSQRT(MU/EPS)/DSQRT(1.ØDØ-(FC/FØ)**2)
      ZC(IZ)=DABS(ZCZ(IZ))*ZW
C   PRINT RESULTS AT LAST FREQUENCY POINT ONLY
      IF(IF.NE.FPTS) GOTO 16
      WRITE(6,112) IZ,Z,A,S,KC(IZ),FC,ZC(IZ),ZW,VMAX(IZ),CURR(IZ),
     1BETA(IZ)
  112 FORMAT(1X,T3,I3,T9,F8.4,T2Ø,F8.4,T3Ø,F8.4,T4Ø,F9.6,T52,-9PF8.3,
     1T63,ØPF11.4,T77,F9.3,T89,F9.4,T1Ø1,F9.4,T113,F9.4)
   16 CONTINUE
C   WE REQUIRE ZC AT THE END OF THE TRANSFORMER
      ZC(NPTS)=ZC(1)*D/B
C   CALCULATE THE REFLECTION COEFFICIENTS
      RHO=DCMPLX(Ø.ØDØ,Ø.ØDØ)
      DO 5 IZ=2,NPTS
C   CALCULATE THE INTEGRAL OVER BETA IN DIFFERENTIAL FORM
      SB1=Ø.ØDØ
      IMAX=IZ-1
      Z=DFLOAT(IMAX)*ZINT
      DO 7 I=1,IMAX
    7 SB1=BETA(I)*ZINT+SB1
      SB1=2.ØDØ*SB1
C   THE BETA INTEGRALS ARE EXPONENTIATED
      BZ=DCMPLX(DCOS(SB1),-DSIN(SB1))
C   FIND THE REFLECTION COEFFICIENT AT EACH Z
      DZC=(ZC(IZ)-ZC(IZ-1))/(ZC(IZ)+ZC(IZ-1))
C   RHO IS THE SUM OF ALL THE REFLECTION COEFFICIENTS
      RHO=RHO+DZC*BZ
    5 CONTINUE
      AMAG=CDABS(RHO)
      APHA=DATAN(DIMAG(RHO)/DREAL(RHO))*57.2957795
      IF(DIMAG(RHO).LT.Ø.DØ.AND.DREAL(RHO).LT.Ø.DØ)
     1 APHA=APHA-18Ø.ØDØ
      IF(DIMAG(RHO).GT.Ø.DØ.AND.DREAL(RHO).LT.Ø.DØ)
     1 APHA=APHA+18Ø.ØDØ
      IF(AMAG.GE.1.ØDØ) AMAG=Ø.99999ØDØ
      IF(AMAG.LE.Ø.ØDØ) AMAG=Ø.ØØØØ1ØDØ
      RLOSS(IF)=-2Ø.ØDØ*DLOG1Ø(AMAG)
      VSWR(IF)=(1.ØDØ+AMAG)/(1.ØDØ-AMAG)
      IF(VSWR(IF).GT.99.999DØ) VSWR(IF)=99.999DØ
   19 CONTINUE
C   PLOT VSWR AND RLOSS VS FREQ
```

```
      CALL LOCPLT(VSWR,RLOSS,FPTS)
      STOP
      END


C
C
C
      SUBROUTINE DMINV(A,N,D,L,M,NSQ)
C
C
      DOUBLE PRECISION A,D,BIGA,HOLD
      DIMENSION A(NSQ),L(N),M(N)
      D=1.0D0
      NK=-N
      DO 80 K=1,N
      NK=NK+N
      L(K)=K
      M(K)=K
      KK=NK+K
      BIGA=A(KK)
      DO 20 J=K,N
      IZ=N*(J-1)
      DO 20 I=K,N
      IJ=IZ+I
   10 IF(DABS(BIGA)-DABS(A(IJ))) 15,20,20
   15 BIGA=A(IJ)
      L(K)=I
      M(K)=J
   20 CONTINUE
      J=L(K)
      IF(J-K) 35,35,25
   25 KI=K-N
      DO 30 I=1,N
      KI=KI+N
      HOLD=-A(KI)
      JI=KI-K+J
      A(KI)=A(JI)
   30 A(JI) =HOLD
   35 I=M(K)
      IF(I-K) 45,45,38
   38 JP=N*(I-1)
      DO 40 J=1,N
      JK=NK+J
      JI=JP+J
      HOLD=-A(JK)
      A(JK)=A(JI)
   40 A(JI) =HOLD
   45 IF(DABS(BIGA)) 48,46,48
   46 D=0.0D0
      RETURN
   48 DO 55 I=1,N
      IF(I-K) 50,55,50
   50 IK=NK+I
      A(IK)=A(IK)/(-BIGA)
```

```
   55 CONTINUE
      DO 65 I=1,N
      IK=NK+I
      HOLD=A(IK)
      IJ=I-N
      DO 65 J=1,N
      IJ=IJ+N
      IF(I-K) 60,65,60
   60 IF(J-K) 62,65,62
   62 KJ=IJ-I+K
      A(IJ)=HOLD*A(KJ)+A(IJ)
   65 CONTINUE
      KJ=K-N
      DO 75 J=1,N
      KJ=KJ+N
      IF(J-K) 70,75,70
   70 A(KJ)=A(KJ)/BIGA
   75 CONTINUE
      D=D*BIGA
      A(KK)=1.0D0/BIGA
   80 CONTINUE
      K=N
  100 K=(K-1)
      IF(K) 150,150,105
  105 I=L(K)
      IF(I-K) 120,120,108
  108 JQ=N*(K-1)
      JR=N*(I-1)
      DO 110 J=1,N
      JK=JQ+J
      HOLD=A(JK)
      JI=JR+J
      A(JK)=-A(JI)
  110 A(JI) =HOLD
  120 J=M(K)
      IF(J-K) 100,100,125
  125 KI=K-N
      DO 130 I=1,N
      KI=KI+N
      HOLD=A(KI)
      JI=KI-K+J
      A(KI)=-A(JI)
  130 A(JI) =HOLD
      GO TO 100
  150 RETURN
      END
C
C
C
      COMPLEX FUNCTION CDTANH*16(Z)
      COMPLEX*16 Z,CDTANH
C    AVOID OVERFLOWS AND UNDERFLOWS FOR LARGE VALUES OF Z
      IF(DREAL(Z).GT.170.0D0) GOTO 1
      IF (DREAL(Z).LT.-170.0D0) GOTO 2
      CDTANH=(CDEXP(Z)-CDEXP(-Z))/(CDEXP(Z)+CDEXP(-Z))
```

```
      GOTO 3
    1 CDTANH=DCMPLX(1.ØDØ,Ø.ØDØ)
      GOTO 3
    2 CDTANH=DCMPLX(-1.ØDØ,Ø.ØDØ)
    3 RETURN
      END
C
      COMPLEX FUNCTION CDSINH*16(Z)
      COMPLEX*16 Z,CDSINH
      CDSINH=(CDEXP(Z)-CDEXP(-Z))/DCMPLX(2.ØDØ,Ø.ØDØ)
      RETURN
      END
C
      COMPLEX FUNCTION CDCOSH*16(Z)
      COMPLEX*16 Z,CDCOSH
      CDCOSH=(CDEXP(Z)+CDEXP(-Z))/DCMPLX(2.ØDØ,Ø.ØDØ)
      RETURN
      END
C
      COMPLEX FUNCTION DELTA*16(M,N)
      INTEGER*4 M,N
      COMPLEX*16 DELTA
      IF(M.EQ.N) GOTO 1
      DELTA=DCMPLX(Ø.ØDØ,Ø.ØDØ)
      GOTO 2
    1 DELTA=DCMPLX(1.ØDØ,Ø.ØDØ)
    2 RETURN
      END
C
      COMPLEX FUNCTION DELTR*16(M)
      INTEGER*4 M
      COMPLEX*16 DELTR
      IF(M.EQ.1) GOTO 1
      DELTR=DCMPLX(1.ØDØ,Ø.ØDØ)
      GOTO 2
    1 DELTR=DCMPLX(2.ØDØ,Ø.ØDØ)
    2 RETURN
      END
C
C
C
      SUBROUTINE P1P2(NROW,NRSUM,P1,P2,KC)
C
C     THIS ROUTINE CALCULATES THE FUNCTIONS P1 AND P2 WHICH DEPEND
C   ON A,B AND D
C
      COMPLEX*16 P1(NRSUM),P2(NROW)
      REAL*8 A,B,D,S,THETA,PI,RAD,C,MU,EPS,KC,QUAD
      INTEGER*4 R,I,NROW,NRSUM
      COMMON/GUIDE/A,B,D,S,THETA
      COMMON/CONST/PI,RAD,C,MU,EPS
      DO 3 I=1,NRSUM
C   THE SUM OVER R CONTAINS EVEN TERMS ONLY
      R=(I-1)*2
      QUAD=-4.ØDØ*KC*KC*A*A+(DFLOAT(R)*PI*A/D)**2
```

```
      IF (QUAD) 1,2,2
    1 P1(I)=DCMPLX(Ø.ØDØ,DSQRT(DABS(QUAD)))
      GOTO 3
    2 P1(I)=DCMPLX(DSQRT(QUAD),Ø.ØDØ)
    3 CONTINUE
      DO 6 I=1,NROW
      R=(I-1)*2
      QUAD=-4.ØDØ*KC*KC*A*A+(DFLOAT(R)*PI*A/B)**2
      IF (QUAD) 4,5,5
    4 P2(I)=DCMPLX(Ø.ØDØ,DSQRT(DABS(QUAD)))
      GOTO 6
    5 P2(I)=DCMPLX(DSQRT(QUAD),Ø.ØDØ)
    6 CONTINUE
      RETURN
      END
C
C
C
      SUBROUTINE CMN(NROW,NRSUM,C1)
C
C     CMN EVALUATES A SET OF TRIGONOMETRIC INTEGRALS WITH
C   VARYING ARGUMENTS (M AND N) BOTH EVEN.
C     ANALYTIC SOLUTIONS WERE WORKED OUT BEFOREHAND AND CODED
C   INTO THIS ROUTINE.
C
      REAL*8 C1(NRSUM,NROW)
      REAL*8 A,B,D,S,THETA,PI,RAD,C,MU,EPS,Z,X1,Y1
      INTEGER*4 I,J,K,M,N,NROW,NRSUM
      COMMON/GUIDE/A,B,D,S,THETA
      COMMON/CONST/PI,RAD,C,MU,EPS
      DO 4 I=1,NRSUM
      N=(I-1)*2
      DO 3 J=1,NROW
      M=(J-1)*2
C   K IS DEFINED SO THAT THE CONDITION NB=MD CAN BE IDENTIFIED
C   EVEN THOUGH B/D MAY NOT BE
      K=IDINT(B*1ØØØ.ØDØ+Ø.5DØ)*N-IDINT(D*1ØØØ.ØDØ+Ø.5DØ)*M
      IF(M.EQ.Ø.AND.N.EQ.Ø) GOTO 1
      IF(M.EQ.Ø) GOTO 2
      IF(K.EQ.Ø) GOTO 5
      X1=1.ØDØ/((DFLOAT(M)/B-DFLOAT(N)/D)*PI)
      Y1=1.ØDØ/((DFLOAT(N)/D+DFLOAT(M)/B)*PI)
      C1(I,J)=DSIN(DFLOAT(M)*PI*(D-B)/(2.ØDØ*B))*
     1(X1+Y1)/D
      GOTO 3
    1 C1(I,J)=1.ØDØ
      GOTO 3
    2 C1(I,J)=Ø.ØDØ
      GOTO 3
    5 C1(I,J)=Ø.5DØ*DCOS(PI*DFLOAT(N-M)/2.ØDØ)
    3 CONTINUE
    4 CONTINUE
      RETURN
      END
C
```

ORIGINAL PAGE IS
OF POOR QUALITY

```
C
C
      SUBROUTINE CURREN(P1,P2,PHI1,PHI2,CURR,NROW,NRSUM)
C
C       THIS ROUTINE CALCULATES THE TOTAL LONGITUDINAL CURRENT
C     INTEGRATED AROUND THE UPPER HALF OF THE CHANNEL WAVEGUIDE
C     CROSS SECTION.  DUE TO THE SYMMETRY ONLY THE UPPER QUARTER
C     OF THE CROSS SECTION IS CONSIDERED. THE INTEGRATIONS WERE
C     PERFORMED ANALYTICALLY FOR ARBITRARY NROW AND NRSUM (ASSUMED
C     EVEN).
C
      COMPLEX*16 PHI1(NROW),PHI2(NROW),P1(NRSUM),P2(NROW)
      COMPLEX*16 CDSINH,CDCOSH,A1,A2,S1,S2,S3,S4,SUM
      REAL*8 A,B,D,S,THETA,R,PI,RAD,C,MU,EPS,CURR
      INTEGER*4 I,NROW,NRSUM
      COMMON/GUIDE/A,B,D,S,THETA
      COMMON/CONST/PI,RAD,C,MU,EPS
C CALCULATE SUMS INDIVIDUALLY
      SUM=DCMPLX(Ø.ØDØ,Ø.ØDØ)
      DO 1 I=1,NROW
      A1=P1(I)*(S/(2.ØDØ*A)-Ø.5DØ)
      A2=P2(I)*S/(2.ØDØ*A)
      R=DFLOAT(I-1)*2.ØDØ
      S1=PHI1(I)*(1.ØDØ-CDCOSH(A1))
      S2=PHI1(I)*(1.ØDØ-DCOS(R*PI/2.ØDØ))
      S3=PHI2(I)*CDSINH(A2)
      S4=PHI2(I)*CDSINH(A2)*(1.ØDØ-DCOS(R*PI*(B-D)/(2.ØDØ*B)))
      SUM=SUM+S1+S2+S3-S4
    1 CONTINUE
      CURR=DREAL(SUM)*2.ØDØ
      RETURN
      END
C
C
      SUBROUTINE LOCPLT(VSWR,RLOSS,FPTS)
      REAL*8 VSWR(FPTS),RLOSS(FPTS)
      REAL*8 MNVSWR,MNLOSS,MXVSWR,MXLOSS,FGHZ,FØ,IFØ,EFØ,SFØ,DB,VN
      INTEGER JPT,YPT,FPTS,IVSWR,IRLOSS
      INTEGER BLANK,DOT,STAR,RLDB(1Ø),VS(1Ø),YVSWR(51),YLOSS(51)
      COMMON/FREQ/FØ,IFØ,EFØ,SFØ
C---DEFINE THE NUMERICS USED IN THE GRAPHS
      DATA BLANK,DOT,STAR/' ','.','*'/
C---DETERMINE THE GRAPH SCALES
      MXVSWR=2.ØDØ
      MXLOSS=DABS(RLOSS(1))
      MNVSWR=1.ØDØ
      MNLOSS=DABS(RLOSS(1))
      DO 1Ø JPT=2,FPTS
      IF(MXLOSS.LT.DABS(RLOSS(JPT))) MXLOSS=DABS(RLOSS(JPT))
      IF(MNLOSS.GT.DABS(RLOSS(JPT))) MNLOSS=DABS(RLOSS(JPT))
   1Ø CONTINUE
      DO 2Ø I=1,1Ø
      DB=DFLOAT(I-1)*1Ø.ØDØ
      VN=DFLOAT(I-1)*1.ØDØ+1.ØDØ
      RLDB(I)=1+IDINT(5Ø.ØDØ*(DB-MNLOSS)/(MXLOSS-MNLOSS)+.5DØ)
```

```
      VS(I)=1+IDINT(5Ø.ØDØ*(VN-MNVSWR)/(MXVSWR-MNVSWR)+.5DØ)
   2Ø CONTINUE
C---THE GRAPH HEADINGS
      WRITE(6,11Ø)
  11Ø FORMAT(///3X,'FGHZ',4X,'VSWR',12X,'VSWR VERSUS FREQUENCY',
     1T72,' RLOSS',12X,'RETURN LOSS VERSUS FREQUENCY'/)
C---THE LOOP FOR THE PTS TO BE PLOTTED VERTICALLY DOWN THE PAGE
      DO 2 LPT=1,FPTS
      JPT=FPTS-LPT+1
      FGHZ=IFØ+(DFLOAT(JPT)-1.ØDØ)*SFØ
      IVSWR=1+IDINT(5Ø.ØDØ/(MXVSWR-MNVSWR)*(VSWR(JPT)-MNVSWR)+Ø.5DØ)
      IRLOSS=1+IDINT(5Ø.ØDØ*(DABS(RLOSS(JPT))-MNLOSS)/
     1(MXLOSS-MNLOSS)+Ø.5DØ)
C---SET THE GRAPH LIMITS
      IF(IVSWR.LT.1) IVSWR=1
      IF(IVSWR.GT.51) IVSWR=51
      IF(IRLOSS.LT.1) IRLOSS=1
      IF(IRLOSS.GT.51) IRLOSS=51
C---CLEAR THE HORIZONTAL LINE
      DO 1 YPT=1,51
      YLOSS(YPT)=BLANK
    1 YVSWR(YPT)=BLANK
C---SET THE GRAPH'S Y AXIS
      DO 4Ø I=1,1Ø
      IF(RLDB(I).GT.51.OR.RLDB(I).LT.1) GOTO 3Ø
      YLOSS(RLDB(I))=DOT
   3Ø IF(VS(I).GT.51.OR.VS(I).LT.1) GOTO 4Ø
      YVSWR(VS(I))=DOT
   4Ø CONTINUE
C---THE PLOTTED POINTS ARE REPRESENTED AS ASTERIKS
      YVSWR(IVSWR)=STAR
      YLOSS(IRLOSS)=STAR
C---PRINT THIS LINE OF THE GRAPH
      WRITE(6,12Ø) FGHZ,VSWR(JPT),(YVSWR(YPT),YPT=1,51),RLOSS(JPT),
     1(YLOSS(YPT),YPT=1,51)
  12Ø FORMAT(1X,-9PF7.2,2X,ØPF6.3,2X,51A1,3X,F7.3,2X,51A1)
    2 CONTINUE
      RETURN
      END
C
C
      BLOCK DATA
      REAL*8 A,B,D,S,THETA,PI,RAD,C,MU,EPS
      REAL*8 FØ,IFØ,EFØ,SFØ,KCLIM,LIMIT,KCINC
      INTEGER*4 NROW,NRSUM,NINT
      COMMON/CONST/PI,RAD,C,MU,EPS
      COMMON/GUIDE/A,B,D,S,THETA
      COMMON/LOOPS/NROW,NRSUM,KCINC,LIMIT,KCLIM,NINT
      COMMON/FREQ/FØ,IFØ,EFØ,SFØ
      DATA PI,RAD,C/3.14159265358979320Ø,57.29577951DØ,2.997925D1Ø/
      DATA MU,EPS/12.56637061435917D-9,8.854185336732Ø28ØD-14/
      DATA IFØ,EFØ,SFØ/8.ØD9,13.ØD9,5.D7/
      DATA A,B,D,S/1.143DØ,Ø.5Ø8DØ,Ø.127DØ,1.143DØ/
      DATA THETA/1Ø.ØDØ/
      DATA NROW,NRSUM/3,3/
      DATA NINT/5Ø/
      DATA KCLIM,LIMIT/1.ØD-12,1.ØD-Ø4/
      END
```

ORIGINAL PAGE IS
OF POOR QUALITY

ANALYSIS OF A CHANNEL WAVEGUIDE TRANSFORMER USING THE WAVE EQUATION AND THE CHARACTERISTIC IMPEDANCE

TRANSFORMER INPUT DATA

INPUT WAVEGUIDE DIMENSIONS (A/2,B/2) IN CM: 1.1430 0.5000
OUTPUT WAVEGUIDE DIMENSIONS (A/2,D/2) IN CM: 1.1430 0.1270
FREQUENCY RANGE (GHZ): 8.000 TO 13.000
TAPER HALF ANGLE (DEGREES): 10.000
TRANSFORMER LENGTH (CM): 6.4023
SERIES DIMENSIONS: NROW= 3 NRSUM= 3
CONVERSION LIMITS: KCLIM= 1.0000D-12 LIMIT= 1.0000D-04

THE MAXIMUM VALUE OF THE CUTOFF FREQUENCY IN THE TRANSFORMER IS: 8.7895 GHZ.
THIS OCCURS AT Z= 2.9818 CM.

VALUES OF SOME KEY VARIABLES AS A FUNCTION OF POSITION ALONG THE TRANSFORMER AT 13.000 GHZ

PT.#	Z	A	S	KC	FC	ZC	ZW	VMAX	CURR	BETA
1	0.0	1.1430	1.1430	1.374275	6.557	304.5927	436.297	1.3963	2.0000	2.3526
2	0.1296	1.1430	1.1201	1.395175	6.657	310.3750	438.596	1.4175	2.0032	2.3403
3	0.2593	1.1430	1.0973	1.416652	6.759	315.5772	441.034	1.4395	2.0118	2.3273
4	0.3889	1.1430	1.0744	1.438704	6.865	320.2637	443.620	1.4622	2.0254	2.3136
5	0.5186	1.1430	1.0516	1.461327	6.972	324.5762	446.364	1.4856	2.0430	2.2996
6	0.6482	1.1430	1.0287	1.484507	7.083	328.5549	449.274	1.5097	2.0644	2.2847
7	0.7779	1.1430	1.0058	1.508223	7.196	332.1638	452.360	1.5346	2.0899	2.2691
8	0.9075	1.1430	0.9830	1.532441	7.312	335.3269	455.630	1.5602	2.1199	2.2528
9	1.0372	1.1430	0.9601	1.557113	7.430	337.9458	459.091	1.5866	2.1553	2.2356
10	1.1668	1.1430	0.9373	1.582171	7.549	339.9872	462.746	1.6137	2.1969	2.2181
11	1.2965	1.1430	0.9144	1.607522	7.678	341.0862	466.596	1.6416	2.2456	2.1998
12	1.4261	1.1430	0.8915	1.633046	7.792	341.3473	470.636	1.6702	2.3026	2.1810
13	1.5557	1.1430	0.8687	1.658584	7.914	340.5471	474.850	1.6995	2.3697	2.1616
14	1.6854	1.1430	0.8458	1.683932	8.035	338.5369	479.215	1.7294	2.4480	2.1419
15	1.8150	1.1430	0.8230	1.708833	8.153	335.1689	483.689	1.7599	2.5398	2.1221
16	1.9447	1.1430	0.8001	1.732969	8.269	330.3049	488.213	1.7910	2.6472	2.1024
17	2.0743	1.1430	0.7772	1.755952	8.378	323.6291	492.703	1.8226	2.7730	2.0833
18	2.2040	1.1430	0.7544	1.777326	8.480	315.6656	497.046	1.8546	2.9203	2.0651
19	2.3336	1.1430	0.7315	1.796572	8.572	305.7987	501.104	1.8871	3.0923	2.0484
20	2.4633	1.1430	0.7087	1.813128	8.651	294.2947	504.711	1.9201	3.2929	2.0337
21	2.5929	1.1430	0.6858	1.826425	8.715	281.3191	507.690	1.9537	3.5259	2.0218
22	2.7226	1.1430	0.6629	1.835939	8.760	267.1429	509.868	1.9884	3.7950	2.0131
23	2.8522	1.1430	0.6401	1.841258	8.785	252.1306	511.103	2.0245	4.1039	2.0083
24	2.9818	1.1430	0.6172	1.842138	8.789	236.7861	511.308	2.0627	4.4555	2.0075
25	3.1115	1.1430	0.5944	1.838545	8.772	221.3142	510.471	2.1038	4.8525	2.0100
26	3.2411	1.1430	0.5715	1.830658	8.735	206.3492	508.654	2.1469	5.2971	2.0180
27	3.3708	1.1430	0.5486	1.818846	8.678	192.1348	505.983	2.1991	5.7912	2.0286
28	3.5004	1.1430	0.5258	1.803606	8.606	178.8930	502.623	2.2555	6.3372	2.0422
29	3.6301	1.1430	0.5029	1.785502	8.519	166.7473	498.752	2.3196	6.9361	2.0580
30	3.7597	1.1430	0.4801	1.765109	8.422	155.7374	494.543	2.3926	7.5977	2.0755
31	3.8894	1.1430	0.4572	1.742971	8.316	145.8414	490.145	2.4761	8.3217	2.0942
32	4.0190	1.1430	0.4343	1.719579	8.205	136.9975	485.680	2.5717	9.1171	2.1134
33	4.1487	1.1430	0.4115	1.695358	8.089	129.1218	481.244	2.6814	9.9937	2.1329
34	4.2783	1.1430	0.3886	1.670667	7.971	122.1220	476.900	2.8075	10.9638	2.1523
35	4.4079	1.1430	0.3658	1.645800	7.853	115.9058	472.720	2.9529	12.0434	2.1713
36	4.5376	1.1430	0.3429	1.621033	7.735	110.3859	468.714	3.1212	13.2532	2.1899
37	4.6672	1.1430	0.3200	1.596555	7.618	105.4833	464.912	3.3171	14.6198	2.2070
38	4.7969	1.1430	0.2972	1.572556	7.503	101.1270	461.326	3.5465	16.1785	2.2250
39	4.9265	1.1430	0.2743	1.549197	7.392	97.2586	457.966	3.8176	17.9760	2.2413
40	5.0562	1.1430	0.2515	1.526629	7.284	93.8237	454.834	4.1414	20.0764	2.2567
41	5.1858	1.1430	0.2286	1.504995	7.181	90.7794	451.933	4.2201	-21.0095	2.2712
42	5.3155	1.1430	0.2057	1.484440	7.083	88.0893	449.266	4.3369	-22.1289	2.2847
43	5.4451	1.1430	0.1829	1.465116	6.991	85.7234	446.833	4.5272	-23.5977	2.2971
44	5.5748	1.1430	0.1600	1.447183	6.905	83.6577	444.638	4.8137	-25.5844	2.3085
45	5.7044	1.1430	0.1372	1.430814	6.827	81.8725	442.685	5.2470	-28.3707	2.3187
46	5.8340	1.1430	0.1143	1.416195	6.757	80.3520	440.982	5.9153	-32.4637	2.3276
47	5.9637	1.1430	0.0914	1.403527	6.697	79.0831	439.535	6.9947	-38.8750	2.3353
48	6.0933	1.1430	0.0686	1.393005	6.647	78.0531	438.354	8.8966	-49.9644	2.3416
49	6.2230	1.1430	0.0457	1.384758	6.607	77.2447	437.441	12.8546	-72.7962	2.3465
50	6.3526	1.1430	0.0229	1.378691	6.578	76.6277	436.777	25.0379	-142.7156	2.3502

FGHZ	VSWR	RLOSS
13.00	1.016	42.114
12.95	1.018	40.000
12.90	1.021	39.585
12.85	1.024	38.483
12.80	1.027	37.490
12.75	1.030	36.597
12.70	1.033	35.795
12.65	1.036	35.074
12.60	1.039	34.425
12.55	1.041	33.842
12.50	1.044	33.317
12.45	1.047	32.845
12.40	1.049	32.420
12.35	1.051	32.039
12.30	1.053	31.695
12.25	1.055	31.386
12.20	1.057	31.107
12.15	1.059	30.854
12.10	1.061	30.621
12.05	1.062	30.404
12.00	1.064	30.199
11.95	1.065	29.999
11.90	1.067	29.800
11.85	1.069	29.596
11.80	1.070	29.381
11.75	1.072	29.151
11.70	1.074	28.902
11.65	1.077	28.631
11.60	1.080	28.335
11.55	1.083	28.014
11.50	1.086	27.670
11.45	1.090	27.302
11.40	1.094	26.915
11.35	1.099	26.512
11.30	1.104	26.097
11.25	1.110	25.674
11.20	1.116	25.246
11.15	1.122	24.817
11.10	1.128	24.391
11.05	1.135	23.970
11.00	1.142	23.556
10.95	1.150	23.150
10.90	1.157	22.755
10.85	1.165	22.370
10.80	1.173	21.996
10.75	1.181	21.633
10.70	1.189	21.279
10.65	1.197	20.935
10.60	1.206	20.599
10.55	1.215	20.270
10.50	1.224	19.945
10.45	1.233	19.622
10.40	1.243	19.299
10.35	1.254	18.974
10.30	1.265	18.643
10.25	1.277	18.304
10.20	1.290	17.954
10.15	1.304	17.590
10.10	1.320	17.209
10.05	1.338	16.809
10.00	1.357	16.389
9.95	1.380	15.945
9.90	1.405	15.479
9.85	1.433	14.987
9.80	1.466	14.472
9.75	1.503	13.931
9.70	1.546	13.367
9.65	1.596	12.780
9.60	1.654	12.170
9.55	1.721	11.540
9.50	1.799	10.889
9.45	1.891	10.220
9.40	2.001	9.534
9.35	2.133	8.833
9.30	2.294	8.118
9.25	2.491	7.390
9.20	2.738	6.653
9.15	3.053	5.908
9.10	3.467	5.157
9.05	4.027	4.405
9.00	4.821	3.657
8.95	6.008	2.918
8.90	7.925	2.204
8.85	11.283	1.544
8.80	15.789	1.102
8.75	99.999	0.0
8.70	99.999	0.0
8.65	99.999	0.0
8.60	99.999	0.0
8.55	99.999	0.0
8.50	99.999	0.0
8.45	99.999	0.0
8.40	99.999	0.0
8.35	99.999	0.0
8.30	99.999	0.0
8.25	99.999	0.0
8.20	99.999	0.0
8.15	99.999	0.0
8.10	99.999	0.0
8.05	99.999	0.0
8.00	99.999	0.0

VSWR VERSUS FREQUENCY

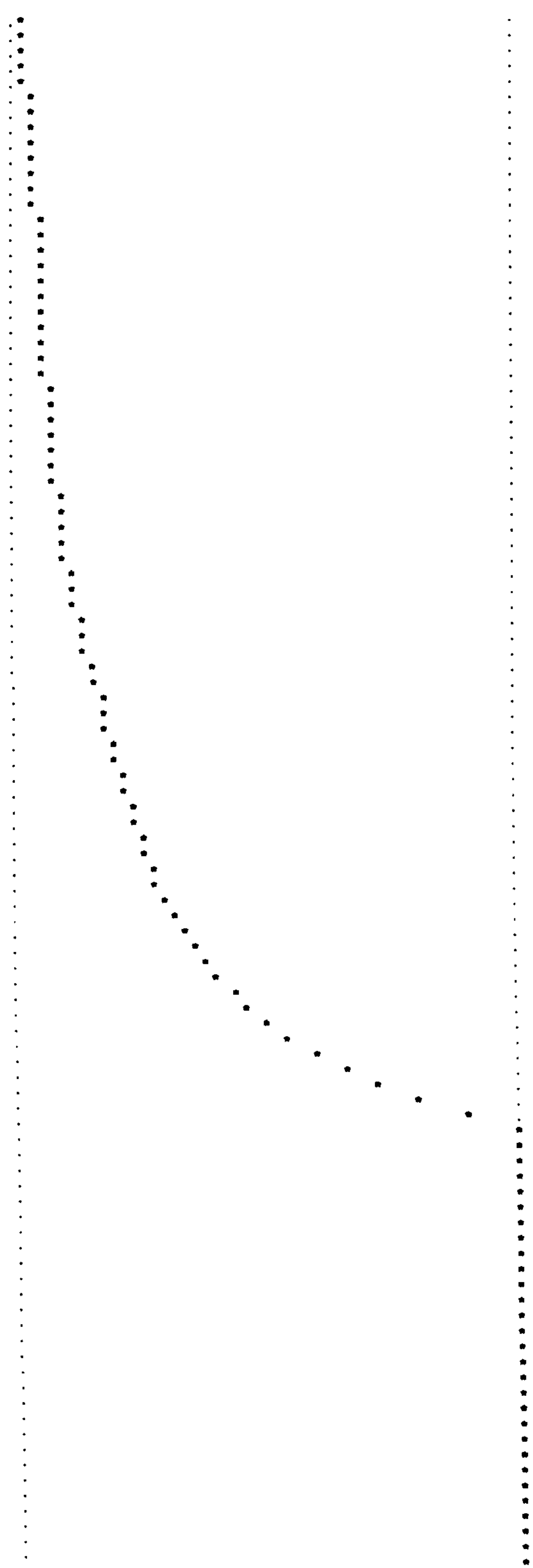

RETURN LOSS VERSUS FREQUENCY

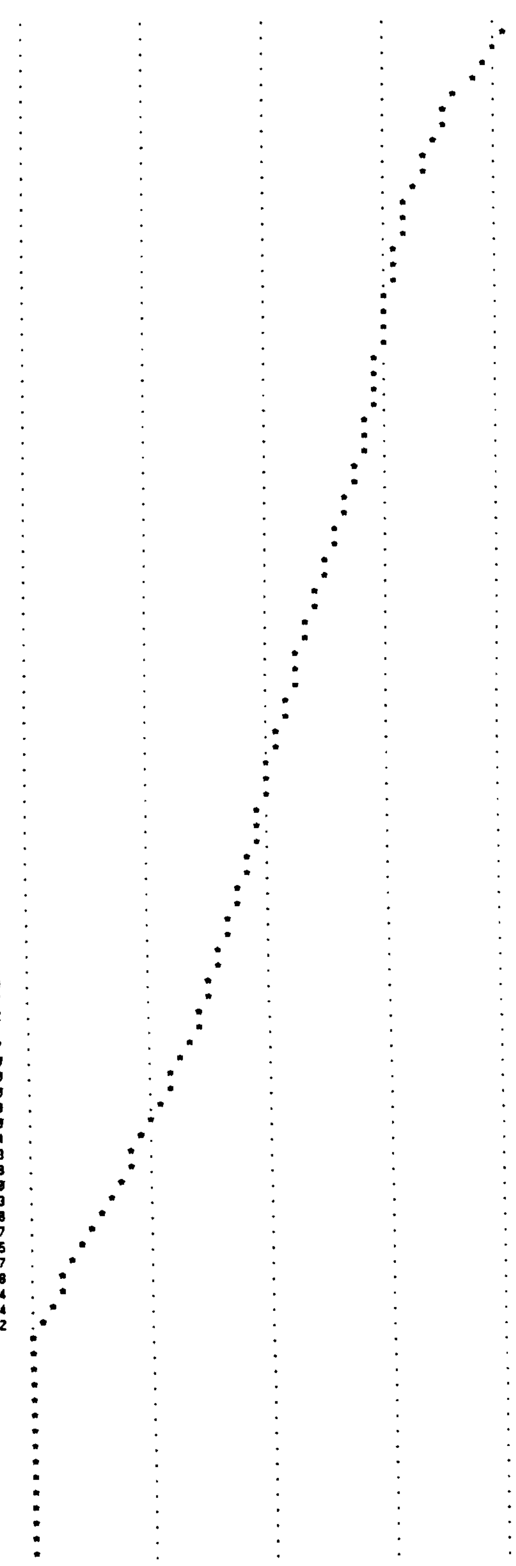

A7.4 Solution Using the Wave Equation and Small Coupling Theory

This program analyzes the channel waveguide transformer using the small coupling theory of Solymar [155]. The small coupling theory avoids the ambiguities associated with the choice of a characteristic waveguide impedance however the author was not able to get accurate predictions of transformer performance using this method. Possible reasons for the lack of agreement with measurements are discussed in Chapter 6. The program is listed here as a starting point for future investigators.

Under the assumptions that (1) coupling occurs only to the backward traveling main mode in the transformer, (2) that this mode is above cutoff everywhere in the transition, and (3) that there is no interaction between this backward traveling mode and the forward traveling main mode, Solymar [155] derived the following expression for the reflection coefficient at the start of the transition:

$$A_{10}\Big|_{z=0} = -\int_0^L \left[S_{\bar{1}010} - 1/2\{d\ln Z_w/dz\} \right] \exp\left[-2j\int_0^z \beta_{10}\,dz'\right] dz \qquad \text{(A7.1)}$$

where β_{10} is the propagation constant, $Z_w = \omega\mu / \beta_{10}$ is the wave impedance and S^-_{1010} is one of a set of mode coupling coefficients which describes coupling from the forward to the backward traveling mode in the transformer. S^-_{1010} is given by [155]:

$$S^-_{1010} = -1/2 \int_{C(z)} \tan\theta \left(\frac{\partial\Psi_{10}}{\partial s}\right)^2 d\underline{s} \ . \qquad (A7.2)$$

θ is the angle between the normal to the surface of the transformer and the normal to the cross sectional plane. It is zero everywhere except along the wall x=s from y=d to y=b as shown in Fig. A7-1 (note that in analyzing a bulgy transformer $\tan\theta$ is also nonzero along x=a from y=0 to y=d). $d\underline{s}$ is a vector which lies along the cross sectional wall of the transformer and is equal to $-d\underline{y}$ for this example (see Fig. A7-1). Ψ_{10} is the solution to the scalar wave equation at a particular cross section as given in A6.20.

Ψ_{10} can be determined from H_z in A6.24 if the eigenvector ϕ_{2_1} is known (recall that ϕ_{2_m}, m>1 is given in terms of ϕ_{2_1}) ϕ_{2_1} can be determined by using the normalization condition given in A6.23 where, because of the symmetry, the integration need be performed over only

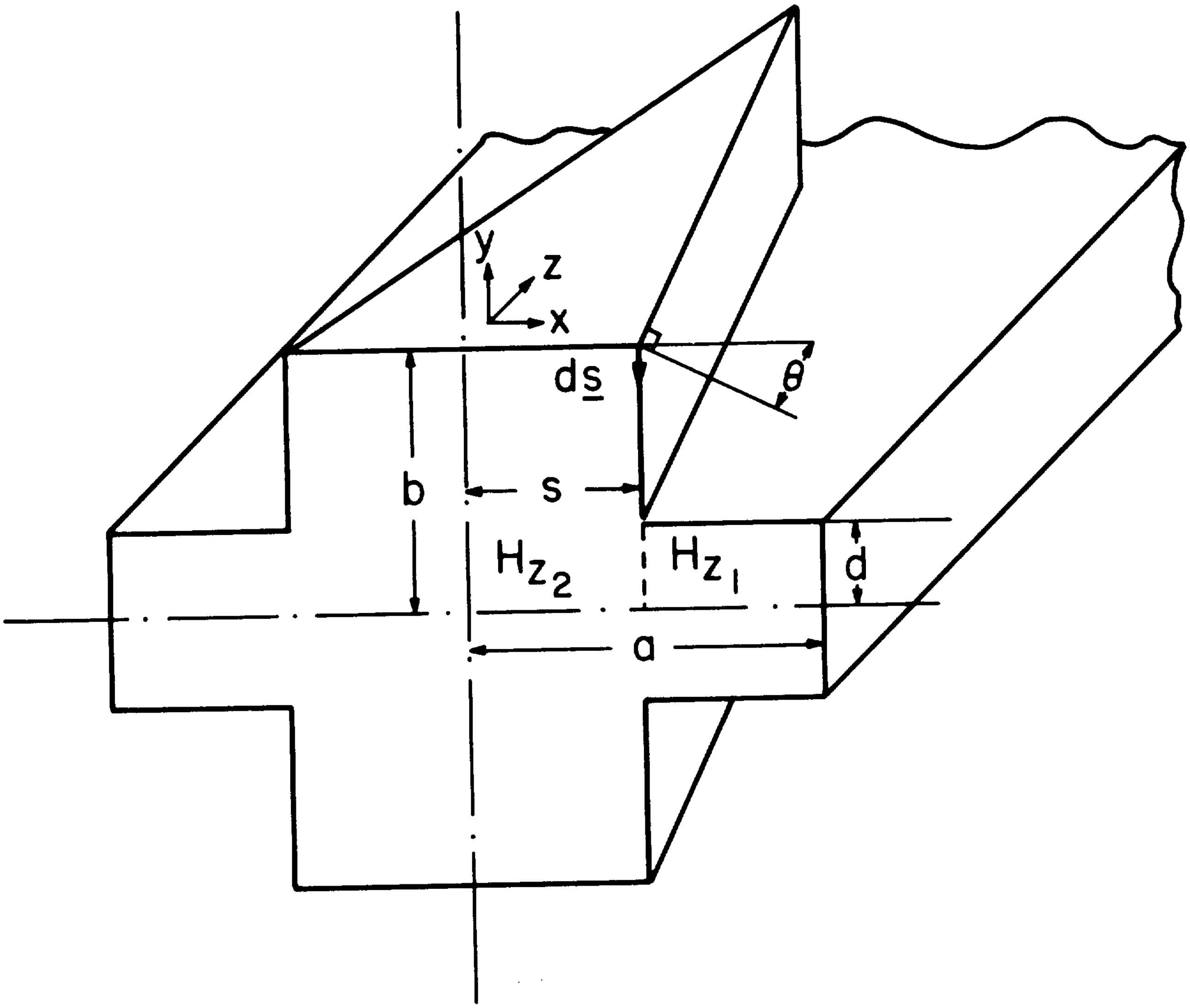

Fig. A7-1 A cross sectional view of a portion of a linearly tapered channel waveguide transformer showing the variables used in the mode coupling analysis. $d\underline{s}$ is the unit vector along the cross sectional wall.

one quarter of the transformer cross section. Separating out the common term ϕ_0 which multiplies all the coefficients in the series expansions for H_z and using A6.23 we have:

$$1/4 = |\phi_0|^2 \int_0^s dx \int_0^b dy \left(\frac{\partial H}{\partial y}z_2\right)^2 + \left(\frac{\partial H}{\partial x}z_2\right)^2$$

$$+ \int_s^a dx \int_0^d dy \left(\frac{\partial H}{\partial y}z_1\right)^2 + \left(\frac{\partial H}{\partial x}z_1\right)^2 \quad . \tag{A7.3}$$

When this equation is solved for $|\phi_0|^2$ and the result replaced in A6.7, the expression for H_{z_2}, S^-_{1010} can be determined from A7.2. β_{10} and Z_w can be calculated in the same manner as the program in Section A7.3 and finally A7.1 can be used to find the reflection coefficient of the transformer. Note that each derivative in A7.3 involves a summation of terms which make up H_{z_1} and H_{z_2}.

In the program which follows the cutoff wavenumbers $k_{c_{10}}$ (KC) along the transformer are found by solving the wave equation as in the program of Section A7.3. The value of ϕ_0 (PHIO) at each cross section along the length of the transformer is determined in subroutine NORM where the integrals in A7.3 have been evaluated analytically and the results coded into the program. After the normalization, S^-_{1010} (S10) is evaluated in subroutine S1010 as a function of position using A7.2. Again, the integrals are evaluated analytically for arbitrary NROW and NRSUM and the results coded into the subroutine.

As in the two previous programs, the frequency is adjusted so that no calculations are performed unless the incident frequency is greater than FCMAX the maximum value of the cutoff frequency in the transition.

In order to evaluate A7.1 it is necessary to determine the derivative of the natural log of $Z_w(z)$ (LNZW) and the integral of $\beta_{10}(z)$ (BZ) at each cross section in the transformer. The IBM SSP routine DDET3 is called to find the derivatives of the log of Z_w (DLNZW) using second degree polynomial interpolation. To determine the β_{10} integrals, BETA(z) is expressed as a Fourier series (coefficients ABETA and BBETA) using the SSP routine DFORIT. The integrals are then evaluated analytically for arbitrary z and the results coded into the program.

$A_{10}(z)$ [A10Z] is then found at each cross section along the transformer length from S10, DLNZW and BZ and the SSP routine CDQSF is called to perform the final integration in A7.1. The resulting value of the reflection coefficient [A10(NPTS)] is now used to calculate the return loss and VSWR which are subsequently plotted in subroutine LOCPLT.

```
C
C
C     CHANNEL WAVEGUIDE TRANSFORMER ANALYSIS USING THE WAVE
C    EQUATION TO DETERMINE THE CUTOFF WAVENUMBERS AND MODE
C    COUPLING THEORY TO CALCULATE THE REFLECTION  COEFFICIENTS.
C
C
C     IN THIS PROGRAM AN X-BAND LINEARLY TAPERED CHANNEL WAVE-
C   GUIDE TRANSFORMER WITH A 4:1 INPUT TO OUTPUT HEIGHT RATIO
C   IS ANALYZED.  THE TAPER HALF-ANGLE IS 1Ø DEGREES YIELDING
C   A TRANSFORMER LENGTH OF 6.48 CM.
C
C
C    COUPLING IS ASSUMED TO EXIST BETWEEN THE FORWARD AND BACKWARD
C    TRAVELING MAIN MODES IN THE TRANSFORMER AND THREE TERMS ARE USED IN
C    THE SERIES REPRESENTING THE FIELDS AT EACH CROSS SECTION.
C      FIVE SUBROUTINES NOT USED IN THE 2 PREVIOUS PROGRAMS ARE REQUIRED:
C    (1) NORM: CALCULATES THE  INTEGRAL OF THE SQUARE MAGNITUDE OF THE
C    ELECTRIC FIELD OVER THE TRANSFORMER CROSS SECTION TO FIND THE VALUE
C    OF PHI2(1). (2) S1Ø1Ø: CALCULATES THE TE1Ø MODE COUPLING
C    COEFFICIENTS. (3) DFORIT: CONVERTS BETA(Z) INTO A FOURIER SERIES
C    SO THAT IT IS ANALYTICALLY INTEGRABLE.  (4) DDET: CALCULATES THE
C    DERIVATIVE OF THE LOG OF THE WAVE IMPEDANCE AS A FUNCTION OF Z.
C    (5) CDQSF: PEFORMS THE FINAL NUMERICAL INTEGRATION TO DETERMINE
C    THE REFLECTION COEFFICIENT.
C
C      TO ANALYZE A BULGY TRANSFORMER AN ADDITIONAL INTEGRATION
C    ALONG X=A FROM Y=Ø TO Y=D. IS REQUIRED IN SUBROUTINE S1Ø1Ø.
C    FOR A TRANSFORMER WITH A CIRCULAR-ARC SHAPED PROFILE THE
C    VALUE OF TANW IN S1Ø1Ø WILL HAVE TO BE CHANGED TO Z/(RSAW-A+S)
C    SINCE THE TAPER ANGLE IS NO LONGER CONSTANT THROUGHOUT THE
C    TRANSITION.
C
C
C                 MAIN  PROGRAM
C
C    DESCRIPTIONS OF SOME VARIABLES NOT USED IN THE TWO PREVIOUS
C    PROGRAMS:
C   ABETA(BBETA):  COSINE (SINE) COEFFICIENTS IN THE FOURIER TRANSFORM
C                  OF BETA(Z).
C   A1Ø:  THE COMPLEX REFLECTION COEFFICIENT AFTER INTEGRATING ALONG
C         THE LENGTH OF THE TRANSFORMER.
C   A1ØZ:  THE REFLECTION COEFFICIENT AT EACH CROSS SECTION ALONG THE
C          TRANSFORMER.  THE POINTS IN A1ØZ ARE INTEGRATED IN CDQSF
C          TO OBTAIN THE A1Ø VECTOR.
C   DLNZW:  THE DERIVATIVE OF THE NATURAL LOG OF THE WAVE IMPEDANCE
C           CALCULATED AT EACH POINT ALONG THE LENGTH OF THE TRANSFORMER.
C   LNZW:  THE NATURAL LOG OF THE WAVE IMPEDANCE AT EACH CROSS SECTION.
C   NH:  THE NUMBER OF TERMS IN THE FOURIER SERIES RESPRESENTATION
C        OF BETA.
C   PHIØ:  THE CONSTANT WHICH MULTIPLIES EACH TERM IN THE SERIES
C          EXPANSIONS OF THE FIELDS IN THE TRANSFORMER.  PHIØ IS
C          DETERMINED BY IMPOSING A NORMALIZING CONDITION ON THE
C          POWER FLOW AT EACH CROSS SECTION ALONG THE LENGTH OF THE
C          TRANSFORMER.
```

```
C   S1Ø:  THE TE1Ø MODE COUPLING COEFFICIENT BETWEEN THE FORWARD
C         AND BACKWARD TRAVELING MODES IN THE TRANSFORMER.  S1Ø
C         INVOLVES THE INTEGRAL OF THE TRANSVERSE FIELDS ALONG THE
C         CROSS SECTIONAL WALLS OF THE TRANSFORMER.
C
C    VARIABLE TYPES USED IN THIS ROUTINE:
      COMPLEX*16 P1(3),P2(3),PHI1(3),PHI2(3),A1ØZ(51),A1Ø(51)
      COMPLEX*16 AØ,A1,A2,A3,A4,SUM
      COMPLEX*16 CDTANH,CDSINH,CDCOSH,DELTR,DELTA
      REAL*8 C1(3,3),ANM(3,3),PHI1Ø(5Ø),ZW(5Ø),KC(5Ø),BETA(5Ø)
      REAL*8 DLNZW(51),LNZW(51),S1Ø(51),ABETA(21),BBETA(21)
      REAL*8 A,B,D,S,THETA,FØ,IFØ,EFØ,SFØ,PI,RAD,C,MU,EPS,TANW,L,Z,W1
      REAL*8 FCMAX,FC,ZM,ZINT,ZPI,KCLIM,KCINC,LIMIT,DET,DETØ,EPS2,R
      REAL*8 AMAG,APHA,SB1,VSWR(1Ø1),RLOSS(1Ø1)
      INTEGER WK1(3),WK2(3),IROW(3),ICOL(3)
      INTEGER IRANK,NROW,NRSUM,NINT,NPTS,NH,LOOP,CONVER
      INTEGER I,J,K,IZ,M,N,IER,FPTS,IF
      COMMON/CONST/PI,RAD,C,MU,EPS
      COMMON/GUIDE/A,B,D,S,THETA
      COMMON/LOOPS/NROW,NRSUM,NINT,NH
      COMMON/FREQ/FØ,IFØ,EFØ,SFØ
C
C    SET THE CONSTANTS USED IN THE ANALYSIS
      NPTS=NINT+1
      LIMIT=1.ØD-4
      KCLIM=1.ØD-12
      TANW=DTAN(THETA/RAD)
      L=A/TANW
      ZINT=L/DFLOAT(NINT)
      FPTS=IDINT((EFØ-IFØ)/SFØ+Ø.5DØ)+1
C   INITIAL GUESS FOR KC
      KC(1)=2.ØDØ*PI/(4.ØDØ*A)
      FØ=IFØ
      WRITE(6,45)
   45 FORMAT(////5X,'ANALYSIS OF A CHANNEL WAVEGUIDE TRANSFORMER'
     1' USING THE WAVE EQUATION AND MODE COUPLING THEORY')
      WRITE(6,5Ø) A,B,A,D,IFØ,EFØ,THETA,L,NROW,NRSUM,KCLIM,LIMIT
   5Ø FORMAT(//5X,'TRANSFORMER INPUT DATA'//1X,
     *'INPUT WAVEGUIDE DIMENSIONS (A/2,B/2) IN CM:',
     12(F7.4,2X)/1X,'OUTPUT WAVEGUIDE DIMENSIONS (A/2,D/2) IN CM:'
     2,2(F7.4,2X)/1X,'FREQUENCY RANGE (GHZ):',-9PF8.3,' TO ',-9PF8.3/
     3,1X,'TAPER HALF ANGLE (DEGREES):',ØPF8.3/1X,
     4'TRANSFORMER LENGTH (CM):',F7.4/1X,
     5'SERIES DIMENSIONS: NROW=',I3,2X,'NRSUM=',I3/1X,
     6'CONVERSION LIMITS: KCLIM=',1PD1Ø.3,2X,'LIMIT=',1PD1Ø.3////)
C    CALCULATE THE CMN INTEGRALS SINCE THEY DEPEND ONLY ON B AND D
      CALL CMN(NROW,NRSUM,C1)
C   LOOP OF VALUES OF Z ALONG TRANSFORMER LENGTH
      DO 6 IZ=1,NINT
      Z=DFLOAT(IZ-1)*ZINT
      S=(L-Z)*TANW
      IF(IZ.GT.1) KC(IZ)=KC(IZ-1)
C    RESET KCINC BEFORE PROCEEDING TO FIND THE NEW VALUE OF KC
C    NOTE THAT IF KCINC IS SET TOO LARGE IT IS POSSIBLE THAT THE
C    SOLUTION WILL NOT CONVERGE ON THE LOWEST NON-ZERO EIGENVALUE
```

```
C    (KC1Ø) BUT ON A HIGHER TE ODD,EVEN MODE.
       KCINC=Ø.Ø1DØ
       LOOP=1
C    CONVER IS SET TO 1 WHEN THE SOLUTION HAS CONVERGED
       CONVER=Ø
C    SET EPS2 TO ITS RECOMMENDED VALUE.
       EPS2=1.ØD-7
C    CALL P1P2 TO EVALUATE P1 AND P2 AT THIS Z. THE ROUTINE NEED BE
C    CALLED ONLY ONCE IF A IS CONSTANT ALONG THE TRANSFORMER LENGTH.
     1 CALL P1P2(NROW,NRSUM,P1,P2,KC(IZ))
C    FORM THE ANM MATRIX
C    ANM IS REAL BECAUSE WE HAVE DIVIDED THROUGH BY SINH(P2*S/2A)
       DO 1Ø I=1,NROW
       DO 9 J=1,NROW
       A3=P2(J)*S/2.ØDØ/A
       A1=DELTA(I,J)*P2(J)*DELTR(J)*B/(4.ØDØ*D*CDTANH(A3))
       AØ=DCMPLX(Ø.ØDØ,Ø.ØDØ)
       DO 8 K=1,NRSUM
       A4=P1(K)*(S/2.ØDØ/A-Ø.5DØ)
       A2=P1(K)*C1(K,I)*C1(K,J)*CDTANH(A4)/DELTR(K)
       AØ=AØ+A2
     8 CONTINUE
       ANM(I,J)=DREAL(AØ-A1)
     9 CONTINUE
    1Ø CONTINUE
C    DON'T INVERT ANM IF THE SOLUTION HAS CONVERGED ALREADY.
       IF (CONVER.EQ.1) GOTO 22
C    CALCULATE THE DETERMINANT OF ANM (DMINV DESTROYS ANM)
       CALL DMINV(ANM,NROW,DET,WK1,WK2,NROW*NROW)
C    CHECK FOR Ø EIGENVALUE AND CHANGE KC ACCORDINGLY
       IF(DABS(DET).LE.LIMIT) GOTO 3Ø
C    ON THE FIRST CYCLE DON'T ADJUST KC
       IF(LOOP.EQ.1) GOTO 27
C    IF A SIGN CHANGE HAS OCCURRED SINCE THE LAST ITERATION THEN
C    HALVE THE INCREMENT IN KC AND REVERSE THE DIRECTION OF CHANGE
C    DETØ IS THE VALUE OF THE DETERMINANT FROM THE PREVIOUS ITERATION
       IF(DETØ*DET.LT.Ø.ØDØ) GOTO 2Ø
C    IF THE DETERMINANT IS INCREASING REVERSE THE DIRECTION OF THE
C    CHANGE IN KC FOR THIS CYCLE.
       IF(DABS(DET).GT.DABS(DETØ)) KCINC=-1.ØDØ*KCINC
       GOTO 25
    2Ø KCINC=KCINC/2.ØDØ
C    IF THE INCREMENT IN KC IS TOO SMALL STOP.
       IF (DABS(KCINC).LT.KCLIM) GOTO 3Ø
C    CHANGE KC AND REPEAT THE CYCLE.
    25 KC(IZ)=KC(IZ)-KCINC*DSIGN(1.ØDØ,DET)
C    SAVE THE PRESENT VALUE OF THE DETERMINANT OF ANM
    27 DETØ=DET
       LOOP=LOOP+1
C    IF CONVERGENCE HASN'T BEEN REACHED AFTER 12Ø CYCLES THEN STOP.
       IF(LOOP.GT.12Ø) GOTO 3Ø
C    GO ON TO THE NEXT ITERATION
       GOTO 1
C    AT THIS POINT THE SOLUTION HAS CONVERGED HOWEVER ANM WAS
C    DESTROYED BY DMINV AND MUST BE REFORMED BEFORE CONTINUING.
```

```
C    WHEN CONVER IS SET TO 1 ANM WILL BE FORMED BUT DMINV WILL NOT BE
C    CALLED.
   3Ø CONVER=1
      GOTO 1
   22 CONTINUE
C    FIND THE EIGENVECTORS CORRESPONDING TO THE EIGENVALUE KC1Ø.
      CALL DMFGR(ANM,NROW,NROW,EPS2,IRANK,IROW,ICOL)
C    CHECK THE RANK OF ANM TO BE SURE THAT THERE ARE (NROW-1)
C    INDEPENDENT EIGENVECTOR COMPONENTS. IF NOT THEN AN ERROR
C    HAS OCCURRED IN ROUTINE DMFGR.
      IF(IRANK.EQ.NROW-1) GOTO 58
C    IT IS SOMETIMES POSSIBLE TO CORRECT THE ERROR IN DMFGR IF
C    EPS2 IS ADJUSTED APPROPRIATELY.
      EPS2=EPS2/2.ØDØ
      WRITE(6,18Ø) EPS2
  18Ø FORMAT(1X,'EPS2 HAS BEEN CHANGED TO ',1PD1Ø.3)
      IF(EPS2.LT.1.ØD-1Ø) GOTO 58
      GOTO 1
C    SET THE FIRST EIGENVECTOR COMPONENT TO 1
   58 PHI2(ICOL(1+IRANK))=DCMPLX(1.ØDØ,Ø.ØDØ)
      DO 3 I=1,IRANK
C    THE REMAINING EIGENVECTOR COMPONENTS ARE GIVEN AS MULTIPLES OF
C    PHI2(1).
    3 PHI2(ICOL(I))=ANM(I,IRANK+1)*PHI2(ICOL(1+IRANK))
C    THE ACTUAL PHI2'S ARE FOUND BY MULTIPLYING THROUGH EACH
C    COMPONENT BY THE SINH(P2*S/2A) TERM WHICH WAS DIVIDED
C    OUT WHEN THE ANM MATRIX WAS ORIGINALLY FORMED
      DO 2 I=1,NROW
    2 PHI2(I)=PHI2(I)/CDSINH(P2(I)*S/2.ØDØ/A)
C    CALCULATE THE PHI1 COEFICIENTS FROM THE PHI2 EIGENVECTOR
      DO 31 I=1,NROW
      AØ=DCMPLX(Ø.ØDØ,Ø.ØDØ)
      DO 29 J=1,NROW
      A2=P2(J)*S/A/2.ØDØ
      A1=PHI2(J)*C1(I,J)*CDSINH(A2)
      AØ=AØ+A1
   29 CONTINUE
      A3=P1(I)*(S/2.ØDØ/A-Ø.5DØ)
      PHI1(I)=AØ*2.ØDØ/(DELTR(I)*CDCOSH(A3))
   31 CONTINUE
C    NORMALIZE THE FIELDS OVER THE TRANSFORMER CROSS SECTION
C    PHIØ IS THE NORMALIZATION CONSTANT WHICH MAKES PHI2(1)=1
      IF(IZ.EQ.1) GOTO 6
      CALL NORM(PHI1,PHI2,P1,P2,PHIØ(IZ),NROW,NRSUM)
C    CALCULATE THE TE1Ø MODE COUPLING COEFFICIENT AT THIS Z
      CALL S1Ø1Ø(P1,P2,PHI1,PHI2,PHIØ(IZ),S1Ø(IZ),TANW,NROW,NRSUM)
    6 CONTINUE
C    WE REQUIRE S1Ø AT THE ENDPOINTS AS WELL
      S1Ø(1)=Ø.ØDØ
      S1Ø(NPTS)=S1Ø(NINT-1)*DEXP(2.ØDØ*DLOG(S1Ø(NINT)/S1Ø(NINT-1)))
C    ADJUST THE INPUT FREQUENCIES SO THAT THEY ARE ABOVE CUTOFF
      FCMAX=C/(4.ØDØ*A)
      DO 4Ø I=1,NINT
      Z=DFLOAT(I-1)*ZINT
      FC=KC(I)*C/(2.ØDØ*PI)
```

```
      IF(FC.LE.FCMAX) GOTO 4Ø
      FCMAX=FC
      ZM=Z
   4Ø CONTINUE
      WRITE(6,113) FCMAX,ZM
  113 FORMAT(/1X,'THE MAXIMUM VALUE OF THE CUTOFF FREQUENCY IN THE',
     1' TRANSFORMER IS:',-9PF8.4,' GHZ.'/1X,'THIS OCCURS AT',
     2' Z=',ØPF8.4,' CM.'/)
      DO 41 IF=1,FPTS
      FØ=IFØ+DFLOAT(IF-1)*SFØ
      IF(FØ.GT.FCMAX) GOTO 41
      RLOSS(IF)=Ø.ØDØ
      VSWR(IF)=99.999DØ
      NFØ=IF+1
   41 CONTINUE
      DO 19 IF=NFØ,FPTS
      FØ=IFØ+DFLOAT(IF-1)*SFØ
      W1=(2.ØDØ*PI*FØ/C)**2
      DO 16 IZ=1,NINT
      BETA(IZ)=DSQRT(W1-KC(IZ)*KC(IZ))
      ZW(IZ)=2.ØDØ*PI*FØ*MU/BETA(IZ)
      LNZW(IZ)=DLOG(ZW(IZ))
   16 CONTINUE
C    FOURIER ANALYZE THE BETA DATA
      CALL DFORIT(BETA,NINT/2,NH,ABETA,BBETA,IER)
C    CALCULATE THE DERIVATIVE OF LOG ZW AT EACH Z
      LNZW(NPTS)=LNZW(1)
      CALL DDET3(ZINT,LNZW,DLNZW,NPTS,IER)
C    WE REQUIRE THE DERIVATIVE AT Z=Ø AND Z=L AS WELL
      DLNZW(1)=2.ØDØ*DLNZW(2)-DLNZW(3)
      DLNZW(NPTS)=2.ØDØ*DLNZW(NINT)-DLNZW(NINT-1)
C     WRITE TITLES FOR SUBSEQUENT PRINTOUT OF RESULTS
      IF (IF.NE.FPTS) GOTO 48
      WRITE(6,25Ø) FØ
  25Ø FORMAT(//1ØX,'VALUES OF SOME KEY VARIABLES AS A FUNCTION',
     1' OF POSITION ALONG THE TRANSFORMER AT',-9PF8.3,' GHZ'//3X,
     2'PT.#',T14,'Z',T24,'KC',T35,'ZW',T46,'BETA',T58,'DLNZW',
     3T7Ø,'S1Ø',T84,'SB1',T98,'A1ØZ(RE,IM)')
   48 CONTINUE
C    EVALUATE THE INTEGRALS OVER BETA
      DO 14 IZ=1,NPTS
      Z=DFLOAT(IZ-1)*ZINT
      ZPI=2.ØDØ*PI*Z/L
      SB1=ABETA(1)*Z
      DO 13 J=1,NH
      R=DFLOAT(J)
      SB1=SB1+L/PI/R/2.ØDØ*(ABETA(J+1)*DSIN(ZPI*R)
     1-BBETA(J+1)*DCOS(ZPI*R)+BBETA(J+1))
   13 CONTINUE
C    CALCULATE A1Ø VALUES AT EACH Z
      A1ØZ(IZ)=-(S1Ø(IZ)-.5DØ*DLNZW(IZ))*
     1CDEXP(DCMPLX(Ø.ØDØ,-2.ØDØ*SB1))
C    PRINT THE RESULTS OF THE LAST FREQUENCY POINT ONLY
      IF(IF.NE.FPTS) GOTO 14
      IF(IZ.EQ.NPTS) GOTO 14
```

```
      WRITE(6,475)IZ,Z,KC(IZ),ZW(IZ),BETA(IZ),DLNZW(IZ),S1Ø(IZ),SB1
     1,A1ØZ(IZ)
  475 FORMAT(1X,T3,I3,T9,F8.4,T19,F9.6,T31,F9.3,T43,F9.5,T55,
     1F9.5,T67,1PD1Ø.3,T8Ø,ØPF9.4,T92,F9.5,T1Ø4,F9.5)
   14 CONTINUE
C  PERFORM THE FINAL INTEGRATION ON A1Ø(Z)
      CALL CDQSF(ZINT,A1ØZ,A1Ø,NPTS)
      AMAG=CDABS(A1Ø(NPTS))
      APHA=DATAN(DIMAG(A1Ø(NPTS))/DREAL(A1Ø(NPTS)))*RAD
      IF(DIMAG(A1Ø(NPTS)).LT.Ø.DØ.AND.DREAL(A1Ø(NPTS)).LT.Ø.DØ)
     1 APHA=APHA-18Ø.ØDØ
      IF(DIMAG(A1Ø(NPTS)).GT.Ø.DØ.AND.DREAL(A1Ø(NPTS)).LT.Ø.DØ)
     1 APHA=APHA+18Ø.ØDØ
      IF(AMAG.GE.1.ØDØ) AMAG=Ø.99999ØDØ
      IF(AMAG.LE.Ø.ØDØ) AMAG=Ø.ØØØØ1ØDØ
      RLOSS(IF)=-2Ø.ØDØ*DLOG1Ø(AMAG)
      VSWR(IF)=(1.ØDØ+AMAG)/(1.ØDØ-AMAG)
      IF(VSWR(IF).GT.99.999DØ) VSWR(IF)=99.999DØ
   19 CONTINUE
C   PLOT VSWR AND RLOSS VS FREQ
      CALL LOCPLT(VSWR,RLOSS,FPTS)
      STOP
      END
C
C
C
      SUBROUTINE DFORIT(FNT,N,M,A,B,IER)
C---
      REAL*8 A(1),B(1),FNT(1),CONST
      REAL*8 COEF,C,S,C1,S1,AN,FNTZ,UØ,U1,U2,Q
      INTEGER N,M
      IER=Ø
   2Ø IF(M) 3Ø,4Ø,4Ø
   3Ø IER=2
      RETURN
   4Ø IF(M-N) 6Ø,6Ø,5Ø
   5Ø IER=1
      RETURN
   6Ø AN=N
      COEF=2.ØDØ/(2.ØDØ*AN+1.ØDØ)
      CONST=3.14159265358979DØ*COEF
      S1=DSIN(CONST)
      C1=DCOS(CONST)
      C=1.ØDØ
      S=Ø.ØDØ
      J=1
      FNTZ=FNT(1)
   7Ø U2=Ø.ØDØ
      U1=Ø.ØDØ
      I=2*N+1
   75 UØ=FNT(I)+2.ØDØ*C*U1-U2
      U2=U1
      U1=UØ
      I=I-1
      IF(I-1) 8Ø,8Ø,75
```

```
   80 A(J)=COEF*(FNTZ+C*U1-U2)
      B(J)=COEF*S*U1
      IF(J-(M+1)) 90,100,100
   90 Q=C1*C-S1*S
      S=C1*S+S1*C
      C=Q
      J=J+1
      GO TO 70
  100 A(1)=A(1)*0.5D0
      RETURN
      END
C
C
      SUBROUTINE DMINV(A,N,D,L,M,NSQ)
C
C
      DOUBLE PRECISION A,D,BIGA,HOLD
      DIMENSION A(NSQ),L(N),M(N)
      D=1.0D0
      NK=-N
      DO 80 K=1,N
      NK=NK+N
      L(K)=K
      M(K)=K
      KK=NK+K
      BIGA=A(KK)
      DO 20 J=K,N
      IZ=N*(J-1)
      DO 20 I=K,N
      IJ=IZ+I
   10 IF(DABS(BIGA)-DABS(A(IJ))) 15,20,20
   15 BIGA=A(IJ)
      L(K)=I
      M(K)=J
   20 CONTINUE
      J=L(K)
      IF(J-K) 35,35,25
   25 KI=K-N
      DO 30 I=1,N
      KI=KI+N
      HOLD=-A(KI)
      JI=KI-K+J
      A(KI)=A(JI)
   30 A(JI) =HOLD
   35 I=M(K)
      IF(I-K) 45,45,38
   38 JP=N*(I-1)
      DO 40 J=1,N
      JK=NK+J
      JI=JP+J
      HOLD=-A(JK)
      A(JK)=A(JI)
   40 A(JI) =HOLD
   45 IF(DABS(BIGA)) 48,46,48
   46 D=0.0D0
```

```
      RETURN
   48 DO 55 I=1,N
      IF(I-K) 50,55,50
   50 IK=NK+I
      A(IK)=A(IK)/(-BIGA)
   55 CONTINUE
      DO 65 I=1,N
      IK=NK+I
      HOLD=A(IK)
      IJ=I-N
      DO 65 J=1,N
      IJ=IJ+N
      IF(I-K) 60,65,60
   60 IF(J-K) 62,65,62
   62 KJ=IJ-I+K
      A(IJ)=HOLD*A(KJ)+A(IJ)
   65 CONTINUE
      KJ=K-N
      DO 75 J=1,N
      KJ=KJ+N
      IF(J-K) 70,75,70
   70 A(KJ)=A(KJ)/BIGA
   75 CONTINUE
      D=D*BIGA
      A(KK)=1.0D0/BIGA
   80 CONTINUE
      K=N
  100 K=(K-1)
      IF(K) 150,150,105
  105 I=L(K)
      IF(I-K) 120,120,108
  108 JQ=N*(K-1)
      JR=N*(I-1)
      DO 110 J=1,N
      JK=JQ+J
      HOLD=A(JK)
      JI=JR+J
      A(JK)=-A(JI)
  110 A(JI) =HOLD
  120 J=M(K)
      IF(J-K) 100,100,125
  125 KI=K-N
      DO 130 I=1,N
      KI=KI+N
      HOLD=A(KI)
      JI=KI-K+J
      A(KI)=-A(JI)
  130 A(JI) =HOLD
      GO TO 100
  150 RETURN
      END
C
C
C
      SUBROUTINE CDQSF(H,Y,Z,NDIM)
```

```
      DIMENSION Y(1),Z(1)
      REAL*8 H,HT
      COMPLEX*16 Y,Z,SUM1,SUM2,AUX1,AUX2,AUX
      HT=.33333333333333333DØ*H
      IF(NDIM-5)7,8,1
    1 SUM1=Y(2)+Y(2)
      SUM1=SUM1+SUM1
      SUM1=HT*(Y(1)+SUM1+Y(3))
      AUX1=Y(4)+Y(4)
      AUX1=AUX1+AUX1
      AUX1=SUM1+HT*(Y(3)+AUX1+Y(5))
      AUX2=HT*(Y(1)+3.875DØ*(Y(2)+Y(5))+2.625DØ*(Y(3)+Y(4))+Y(6))
      SUM2=Y(5)+Y(5)
      SUM2=SUM2+SUM2
      SUM2=AUX2-HT*(Y(4)+SUM2+Y(6))
      Z(1)=DCMPLX(Ø.ØDØ,Ø.ØDØ)
      AUX=Y(3)+Y(3)
      AUX=AUX+AUX
      Z(2)=SUM2-HT*(Y(2)+AUX+Y(4))
      Z(3)=SUM1
      Z(4)=SUM2
      IF(NDIM-6)5,5,2
    2 DO 4 I=7,NDIM,2
      SUM1=AUX1
      SUM2=AUX2
      AUX1=Y(I-1)+Y(I-1)
      AUX1=AUX1+AUX1
      AUX1=SUM1+HT*(Y(I-2)+AUX1+Y(I))
      Z(I-2)=SUM1
      IF(I-NDIM)3,6,6
    3 AUX2=Y(I)+Y(I)
      AUX2=AUX2+AUX2
      AUX2=SUM2+HT*(Y(I-1)+AUX2+Y(I+1))
    4 Z(I-1)=SUM2
    5 Z(NDIM-1)=AUX1
      Z(NDIM)=AUX2
      RETURN
    6 Z(NDIM-1)=SUM2
      Z(NDIM)=AUX1
      RETURN
    7 IF(NDIM-3)12,11,8
    8 SUM2=1.125DØ*HT*(Y(1)+Y(2)+Y(2)+Y(2)+Y(3)+Y(3)+Y(3)+Y(4))
      SUM1=Y(2)+Y(2)
      SUM1=SUM1+SUM1
      SUM1=HT*(Y(1)+SUM1+Y(3))
      Z(1)=DCMPLX(Ø.ØDØ,Ø.ØDØ)
      AUX1=Y(3)+Y(3)
      AUX1=AUX1+AUX1
      Z(2)=SUM2-HT*(Y(2)+AUX1+Y(4))
      IF(NDIM-5)1Ø,9,9
    9 AUX1=Y(4)+Y(4)
      AUX1=AUX1+AUX1
      Z(5)=SUM1+HT*(Y(3)+AUX1+Y(5))
   1Ø Z(3)=SUM1
      Z(4)=SUM2
```

```
      RETURN
   11 SUM1=HT*(1.25DØ*Y(1)+Y(2)+Y(2)-.25DØ*Y(3))
      SUM2=Y(2)+Y(2)
      SUM2=SUM2+SUM2
      Z(3)=HT*(Y(1)+SUM2+Y(3))
      Z(1)=DCMPLX(Ø.ØDØ,Ø.ØDØ)
      Z(2)=SUM1
   12 RETURN
      END
C
C
C
      SUBROUTINE DDET3(H,Y,Z,NDIM,IER)
C
      DIMENSION Y(1),Z(1)
      DOUBLE PRECISION H,HH,Y,Z,YY,B,A
      IF(NDIM-3)4,1,1
    1 IF(H)2,5,2
    2 HH=.5DØ/H
      YY=Y(NDIM-2)
      B=Y(2)+Y(2)
      B=HH*(B+B-Y(3)-Y(1)-Y(1)-Y(1))
      DO 3 I=3,NDIM
      A=B
      B=HH*(Y(I)-Y(I-2))
    3 Z(I-2)=A
      IER=Ø
      A=Y(NDIM-1)+Y(NDIM-1)
      Z(NDIM)=HH*(Y(NDIM)+Y(NDIM)+Y(NDIM)-A-A+YY)
      Z(NDIM-1)=B
      RETURN
    4 IER=-1
      RETURN
    5 IER=1
      RETURN
      END
C
C
C
      SUBROUTINE DMFGR(A,M,N,EPS,IRANK,IROW,ICOL)
C
      DIMENSION A(1),IROW(1),ICOL(1)
      DOUBLE PRECISION A,PIV,HOLD,SAVE
      IF(M)2,2,1
    1 IF(N)2,2,4
    2 IRANK=-1
    3 RETURN
    4 IRANK=Ø
      PIV=Ø.ØDØ
      JJ=Ø
      DO 6 J=1,N
      ICOL(J)=J
      DO 6 I=1,M
      JJ=JJ+1
      HOLD=A(JJ)
```

```
      IF(DABS(PIV)-DABS(HOLD))5,6,6
    5 PIV=HOLD
      IR=I
      IC=J
    6 CONTINUE
      DO 7 I=1,M
    7 IROW(I)=I
      TOL=ABS(EPS*SNGL(DABS(PIV)))
      NM=N*M
      DO 19 NCOL=M,NM,M
    8 IF(ABS(SNGL(DABS(PIV)))-TOL)20,20,9
    9 IRANK=IRANK+1
      JJ=IR-IRANK
      IF(JJ)12,12,10
   10 DO 11 J=IRANK,NM,M
      I=J+JJ
      SAVE=A(J)
      A(J)=A(I)
   11 A(I)=SAVE
      JJ=IROW(IR)
      IROW(IR)=IROW(IRANK)
      IROW(IRANK)=JJ
   12 JJ=(IC-IRANK)*M
      IF(JJ)15,15,13
   13 KK=NCOL
      DO 14 J=1,M
      I=KK+JJ
      SAVE=A(KK)
      A(KK)=A(I)
      KK=KK-1
   14 A(I)=SAVE
      JJ=ICOL(IC)
      ICOL(IC)=ICOL(IRANK)
      ICOL(IRANK)=JJ
   15 KK=IRANK+1
      MM=IRANK-M
      LL=NCOL+MM
      IF(MM)16,25,25
   16 JJ=LL
      SAVE=PIV
      PIV=0.0D0
      DO 19 J=KK,M
      JJ=JJ+1
      HOLD=A(JJ)/SAVE
      A(JJ)=HOLD
      L=J-IRANK
      IF(IRANK-N)17,19,19
   17 II=JJ
      DO 19 I=KK,N
      II=II+M
      MM=II-L
      A(II)=A(II)-HOLD*A(MM)
      IF(DABS(A(II))-DABS(PIV))19,19,18
   18 PIV=A(II)
      IR=J
```

```
      IC=I
   19 CONTINUE
   2Ø IF(IRANK-1)3,25,21
   21 IR=LL
      DO 24 J=2,IRANK
      II=J-1
      IR=IR-M
      JJ=LL
      DO 23 I=KK,M
      HOLD=Ø.ØDØ
      JJ=JJ+1
      MM=JJ
      IC=IR
      DO 22 L=1,II
      HOLD=HOLD+A(MM)*A(IC)
      IC=IC-1
   22 MM=MM-M
   23 A(MM)=A(MM)-HOLD
   24 CONTINUE
   25 IF(N-IRANK)3,3,26
   26 IR=LL
      KK=LL+M
      DO 3Ø J=1,IRANK
      DO 29 I=KK,NM,M
      JJ=IR
      LL=I
      HOLD=Ø.ØDØ
      II=J
   27 II=II-1
      IF(II)29,29,28
   28 HOLD=HOLD-A(JJ)*A(LL)
      JJ=JJ-M
      LL=LL-1
      GOTO 27
   29 A(LL)=(HOLD-A(LL))/A(JJ)
   3Ø IR=IR-1
      RETURN
      END
C
C
C
      COMPLEX FUNCTION CDTANH*16(Z)
      COMPLEX*16 Z,CDTANH
      IF(DREAL(Z).GT.174.ØDØ) GOTO 1
      IF (DREAL(Z).LT.-174.ØDØ) GOTO 2
      CDTANH=(CDEXP(Z)-CDEXP(-Z))/(CDEXP(Z)+CDEXP(-Z))
      GOTO 3
    1 CDTANH=DCMPLX(1.ØDØ,Ø.ØDØ)
      GOTO 3
    2 CDTANH=DCMPLX(-1.ØDØ,Ø.ØDØ)
    3 RETURN
      END
C
      COMPLEX FUNCTION CDSINH*16(Z)
      COMPLEX*16 Z,CDSINH,X
```

```
      X=Z
      IF(DABS(DREAL(X)).GT.174.ØDØ)
     1 X=DCMPLX(174.ØDØ*DSIGN(1.ØDØ,DREAL(Z)),DIMAG(Z))
      CDSINH=(CDEXP(X)-CDEXP(-X))/2.ØDØ
      RETURN
      END
C
      COMPLEX FUNCTION CDCOSH*16(Z)
      COMPLEX*16 X,Z,CDCOSH
      X=Z
      IF(DABS(DREAL(X)).GT.174.ØDØ)
     1 X=DCMPLX(174.ØDØ*DSIGN(1.ØDØ,DREAL(Z)),DIMAG(Z))
      CDCOSH=(CDEXP(X)+CDEXP(-X))/2.ØDØ
      RETURN
      END
C
      COMPLEX FUNCTION DELTA*16(M,N)
      INTEGER M,N
      COMPLEX*16 DELTA
      IF(M.EQ.N) GOTO 1
      DELTA=DCMPLX(Ø.ØDØ,Ø.ØDØ)
      GOTO 2
    1 DELTA=DCMPLX(1.ØDØ,Ø.ØDØ)
    2 RETURN
      END
C
      COMPLEX FUNCTION DELTR*16(M)
      INTEGER M
      COMPLEX*16 DELTR
      IF(M.EQ.1) GOTO 1
      DELTR=DCMPLX(1.ØDØ,Ø.ØDØ)
      GOTO 2
    1 DELTR=DCMPLX(2.ØDØ,Ø.ØDØ)
    2 RETURN
      END
C
C
C
      SUBROUTINE P1P2(NROW,NRSUM,P1,P2,KC)
      COMPLEX*16 P1(NRSUM),P2(NROW)
      REAL *8 A,B,D,S,THETA,PI,RAD,C,MU,EPS,KC,QUAD
      INTEGER R,I,NROW,NRSUM
      COMMON/GUIDE/A,B,D,S,THETA
      COMMON/CONST/PI,RAD,C,MU,EPS
      DO 3 I=1,NRSUM
      R=(I-1)*2
      QUAD=-4.ØDØ*KC*KC*A*A+(DFLOAT(R)*PI*A/D)**2
      IF (QUAD) 1,2,2
    1 P1(I)=DCMPLX(Ø.ØDØ,DSQRT(DABS(QUAD)))
      GOTO 3
    2 P1(I)=DCMPLX(DSQRT(QUAD),Ø.ØDØ)
    3 CONTINUE
      DO 6 I=1,NROW
      R=(I-1)*2
      QUAD=-4.ØDØ*KC*KC*A*A+(DFLOAT(R)*PI*A/B)**2
```

```
      IF (QUAD) 4,5,5
    4 P2(I)=DCMPLX(Ø.ØDØ,DSQRT(DABS(QUAD)))
      GOTO 6
    5 P2(I)=DCMPLX(DSQRT(QUAD),Ø.ØDØ)
    6 CONTINUE
      RETURN
      END
C
C
C
      SUBROUTINE CMN(NROW,NRSUM,C1)
      REAL*8 C1(NRSUM,NROW)
      REAL*8 A,B,D,S,THETA,PI,RAD,C,MU,EPS,X1,Y1
      INTEGER*4 I,J,K,M,N,NROW,NRSUM
      COMMON/GUIDE/A,B,D,S,THETA
      COMMON/CONST/PI,RAD,C,MU,EPS
      DO 4 I=1,NRSUM
      N=(I-1)*2
      DO 3 J=1,NROW
      M=(J-1)*2
      K=IDINT(B*1ØØØ.ØDØ+Ø.5DØ)*N-IDINT(D*1ØØØ.ØDØ+Ø.5DØ)*M
      IF(M.EQ.Ø.AND.N.EQ.Ø) GOTO 1
      IF(M.EQ.Ø) GOTO 2
      IF(K.EQ.Ø) GOTO 5
      X1=1.ØDØ/((DFLOAT(M)/B-DFLOAT(N)/D)*PI)
      Y1=1.ØDØ/((DFLOAT(N)/D+DFLOAT(M)/B)*PI)
      C1(I,J)=DSIN(DFLOAT(M)*PI*(D-B)/(2.ØDØ*B))*
     1(X1+Y1)/D
      GOTO 3
    1 C1(I,J)=1.ØDØ
      GOTO 3
    2 C1(I,J)=Ø.ØDØ
      GOTO 3
    5 C1(I,J)=Ø.5DØ*DCOS(PI*DFLOAT(N-M)/2.ØDØ)
    3 CONTINUE
    4 CONTINUE
      RETURN
      END
C
C
C
      SUBROUTINE NORM(PHI1,PHI2,P1,P2,PHIØ,NROW,NRSUM)
C
C       NORM DETERMINES THE ACTUAL VALUE OF PHI2(1) WHICH HAD BEEN
C     ARBITRARILY SET TO ONE AFTER THE DMFGR ROUTINE.  IT IS DETERMINED
C     BY NORMALIZING THE POWER FLOW AT EACH TRANSFORMER CROSS SECTION
C     SUCH THAT THE INTEGRAL OF THE SQUARE MAGNITUDE OF THE ELECTRIC FIELD
C     IS 1.  THE INTEGRATION IS PERFORMED OVER ONE QUARTER OF THE
C     TRANSFORMER CROSS SECTION AND DUE TO THE SYMMETRY THIS RESULT IS
C     SIMPLY MULTIPLIED BY 4.  THE INTEGRALS WERE EVALUATED ANALYTICALLY
C     FOR ARBITRARY NROW AND NRSUM IN EACH OF THE TWO REGIONS IN THE CROSS
C     SECTION AND THE RESULTS WERE CODED INTO THIS ROUTINE.
C
      COMPLEX*16 PHI1(NROW),PHI2(NROW),P1(NRSUM),P2(NROW)
      COMPLEX*16 CDSINH,A1,A2,SUM,S1,S2,S3,S4
```

```
      REAL*8 A,B,D,S,THETA,PI,RAD,C,MU,EPS,PHIØ,R
      INTEGER I,NROW,NRSUM
      COMMON/GUIDE/A,B,D,S,THETA
      COMMON/CONST/PI,RAD,C,MU,EPS
C CALCULATE SUMS INDIVIDUALLY
      SUM=DCMPLX(Ø.ØDØ,Ø.ØDØ)
      DO 1 I=1,NROW
      A1=P1(I)*DCMPLX(S/A-1.ØDØ,Ø.ØDØ)
      A2=P2(I)*DCMPLX(S/A,Ø.ØDØ)
      R=DFLOAT(I-1)*2.ØDØ
      S1=PHI2(I)*P2(I)*B*(CDSINH(A2)+A2)*PHI2(I)/(16.ØDØ*A)
      IF(I.EQ.1) S1=S1*2.ØDØ
      S2=PHI2(I)*R*R*PI*PI*A*(CDSINH(A2)-A2)*PHI2(I)/(16.ØDØ*B*P2(I))
      S3=PHI1(I)*P1(I)*D*(CDSINH(A1)-A1)*PHI1(I)/(16.ØDØ*A)
      IF(I.EQ.1) S3=2.ØDØ*S3
      S4=PHI1(I)*R*R*PI*PI*A*(CDSINH(A1)+A1)*PHI1(I)/(16.ØDØ*D*P1(I))
      SUM=SUM+S1+S2-S3-S4
C    PHIØ IS THE NORMALIZING CONSTANT WHICH MULTIPLIES EVERY COEFFICIENT
C    IN THE SERIES REPRESENTING THE FIELDS IN THE TRANSFORMER.
    1 CONTINUE
      PHIØ=1.ØDØ/(2.ØDØ*DSQRT(DREAL(SUM)))
      RETURN
      END
C
C
C
      SUBROUTINE S1Ø1Ø(P1,P2,PHI1,PHI2,PHIØ,S1Ø,TANW,NROW,NRSUM)
C
C     S1Ø1Ø CALCULATES THE COUPLING COEFFICIENT INTO THE BACKWARD
C    TRAVELING MAIN MODE.  THE INTEGRALS ALONG THE WAVEGUIDE WALLS HAVE
C    BEEN EVALUATED ANALYTICALLY FOR ARBITRARY NROW AND NRSUM.  THE
C    FINAL SOLUTION (S1Ø) IS MULTIPLIED BY 4 SINCE ONLY ONE QUARTER OF
C    THE CROSS SECTION HAS BEEN CONSIDERED IN THE INTEGRATIONS.
C
      COMPLEX*16 P1(NRSUM),P2(NROW),PHI1(NROW),PHI2(NROW)
      COMPLEX*16 CDSINH,SUM,SØ,S5,S6,S7,S8
      REAL*8 A,B,D,S,THETA,PI,RAD,C,MU,EPS,TANW,M,N,S1Ø,PHIØ
      INTEGER I,J,NROW,NRSUM
      COMMON/CONST/PI,RAD,C,MU,EPS
      COMMON/GUIDE/A,B,D,S,THETA
      SUM=DCMPLX(Ø.ØDØ,Ø.ØDØ)
      DO 1 I=2,NROW
      M=DFLOAT(I-1)*2.ØDØ
      S5=CDSINH(P2(I)*S/(2.ØDØ*A))*PHI2(I)*PHIØ*M*PI/(2.ØDØ*B)
      DO 6 J=2,NROW
      N=DFLOAT(J-1)*2.ØDØ
      S6=CDSINH(P2(J)*S/(2.ØDØ*A))*PHI2(J)*PHIØ*N*PI/2.ØDØ/B
      IF(I.EQ.J) GOTO 3
      S8=DCMPLX(DSIN(PI*(B-D)*(M+N)/(2.ØDØ*B))/(M+N),Ø.ØDØ)
      S7=DCMPLX(DSIN(PI*(B-D)*(M-N)/(2.ØDØ*B))/(N-M),Ø.ØDØ)
      SØ=-S5*S6*(S7+S8)*B/PI
      GOTO 2
    3 S7=DCMPLX(B/(2.ØDØ*M*PI),Ø.ØDØ)
      S8=DCMPLX(M*PI*(B-D)/B-DSIN(M*PI*(B-D)/B),Ø.ØDØ)
      SØ=S5*S6*S7*S8
```

```
    2 SUM=SUM+SØ
    6 CONTINUE
    1 CONTINUE
C   TANW IS CONSTANT ALONG Y AND CAN BE REMOVED FROM THE INTEGRALS.
C   THE FACTOR OF 2 IS FROM MULTIPLYING THE 1/2 IN THE S1Ø EXPRESSION
C   BY 4 SINCE ONLY 1/4 OF THE CROSS SECTION WAS INTEGRATED AROUND.
      S1Ø=-2.ØDØ*TANW*DREAL(SUM)
      RETURN
      END
C
C
C
      SUBROUTINE LOCPLT(VSWR,RLOSS,FPTS)
      REAL*8 VSWR(FPTS),RLOSS(FPTS)
      REAL*8 MNVSWR,MNLOSS,MXVSWR,MXLOSS,FGHZ,FØ,IFØ,EFØ,SFØ,DB,VN
      INTEGER JPT,YPT,FPTS,IVSWR,IRLOSS
      INTEGER BLANK,DOT,STAR,RLDB(1Ø),VS(1Ø),YVSWR(51),YLOSS(51)
      COMMON/FREQ/FØ,IFØ,EFØ,SFØ
C---DEFINE THE NUMERICS USED IN THE GRAPHS
      DATA BLANK,DOT,STAR/' ','.','*'/
C---DETERMINE THE GRAPH SCALES
      MXVSWR=2.ØDØ
      MXLOSS=DABS(RLOSS(1))
      MNVSWR=1.ØDØ
      MNLOSS=DABS(RLOSS(1))
      DO 1Ø JPT=2,FPTS
      IF(MXLOSS.LT.DABS(RLOSS(JPT))) MXLOSS=DABS(RLOSS(JPT))
      IF(MNLOSS.GT.DABS(RLOSS(JPT))) MNLOSS=DABS(RLOSS(JPT))
   1Ø CONTINUE
      DO 2Ø I=1,1Ø
      DB=DFLOAT(I-1)*1Ø.ØDØ
      VN=DFLOAT(I-1)*1.ØDØ+1.ØDØ
      RLDB(I)=1+IDINT(5Ø.ØDØ*(DB-MNLOSS)/(MXLOSS-MNLOSS)+.5DØ)
      VS(I)=1+IDINT(5Ø.ØDØ*(VN-MNVSWR)/(MXVSWR-MNVSWR)+.5DØ)
   2Ø CONTINUE
C---THE GRAPH HEADINGS
      WRITE(6,11Ø)
  11Ø FORMAT(///3X,'FGHZ',4X,'VSWR',12X,'VSWR VERSUS FREQUENCY',
     1T72,' RLOSS',12X,'RETURN LOSS VERSUS FREQUENCY'/)
C---THE LOOP FOR THE PTS TO BE PLOTTED VERTICALLY DOWN THE PAGE
      DO 2 LPT=1,FPTS
      JPT=FPTS-LPT+1
      FGHZ=IFØ+(DFLOAT(JPT)-1.ØDØ)*SFØ
      IVSWR=1+IDINT(5Ø.ØDØ/(MXVSWR-MNVSWR)*(VSWR(JPT)-MNVSWR)+Ø.5DØ)
      IRLOSS=1+IDINT(5Ø.ØDØ*(DABS(RLOSS(JPT))-MNLOSS)/
     1(MXLOSS-MNLOSS)+Ø.5DØ)
C---SET THE GRAPH LIMITS
      IF(IVSWR.LT.1) IVSWR=1
      IF(IVSWR.GT.51) IVSWR=51
      IF(IRLOSS.LT.1) IRLOSS=1
      IF(IRLOSS.GT.51) IRLOSS=51
C---CLEAR THE HORIZONTAL LINE
      DO 1 YPT=1,51
      YLOSS(YPT)=BLANK
    1 YVSWR(YPT)=BLANK
```

```
C---SET THE GRAPH'S Y AXIS
      DO 40 I=1,10
      IF(RLDB(I).GT.51.OR.RLDB(I).LT.1) GOTO 30
      YLOSS(RLDB(I))=DOT
   30 IF(VS(I).GT.51.OR.VS(I).LT.1) GOTO 40
      YVSWR(VS(I))=DOT
   40 CONTINUE
C---THE PLOTTED POINTS ARE REPRESENTED AS ASTERIKS
      YVSWR(IVSWR)=STAR
      YLOSS(IRLOSS)=STAR
C---PRINT THIS LINE OF THE GRAPH
      WRITE(6,120) FGHZ,VSWR(JPT),(YVSWR(YPT),YPT=1,51),RLOSS(JPT),
     1(YLOSS(YPT),YPT=1,51)
  120 FORMAT(1X,-9PF7.2,2X,0PF6.3,2X,51A1,3X,F7.3,2X,51A1)
    2 CONTINUE
      RETURN
      END
C
C
      BLOCK DATA
      REAL*8 A,B,D,S,THETA,PI,RAD,C,MU,EPS,F0,IF0,EF0,SF0
      INTEGER NROW,NRSUM,NINT,NH
      COMMON/CONST/PI,RAD,C,MU,EPS
      COMMON/GUIDE/A,B,D,S,THETA
      COMMON/LOOPS/NROW,NRSUM,NINT,NH
      COMMON/FREQ/F0,IF0,EF0,SF0
      DATA PI,RAD,C/3.1415926535897932D0,57.29577951D0,2.997925D10/
      DATA MU,EPS/12.566370614359170-9,8.854185336732028D-14/
      DATA IF0,EF0,SF0/8.0D9,13.0D9,5.D7/
      DATA A,B,D,S/1.143D0,0.508D0,0.127D0,1.143D0/
      DATA THETA/10.0D0/
      DATA NROW,NRSUM/3,3/
      DATA NINT,NH/50,20/
      END
```

ANALYSIS OF A CHANNEL WAVEGUIDE TRANSFORMER USING THE WAVE EQUATION AND MODE COUPLING THEORY

TRANSFORMER INPUT DATA

INPUT WAVEGUIDE DIMENSIONS (A/2,B/2) IN CM: 1.1430 0.5080
OUTPUT WAVEGUIDE DIMENSIONS (A/2,D/2) IN CM: 1.1430 0.1270
FREQUENCY RANGE (GHZ): 8.000 TO 13.000
TAPER HALF ANGLE (DEGREES): 10.000
TRANSFORMER LENGTH (CM): 6.4823
SERIES DIMENSIONS: NROW= 3 NRSUM= 3
CONVERSION LIMITS: KCLIM= 1.000D-12 LIMIT= 1.000D-04

THE MAXIMUM VALUE OF THE CUTOFF FREQUENCY IN THE TRANSFORMER IS: 8.7895 GHZ.
THIS OCCURS AT Z= 2.9818 CM.

VALUES OF SOME KEY VARIABLES AS A FUNCTION OF POSITION ALONG THE TRANSFORMER AT 13.000 GHZ

PT.#	Z	KC	ZW	BETA	DLNZW	S10	S01	A10Z(RE,IM)	
1	0.0	1.374275	436.297	2.35262	0.03938	0.0	0.0	0.01969	0.0
2	0.1296	1.395175	438.596	2.34028	0.04165	-1.694D-05	0.2660	0.01796	-0.01057
3	0.2593	1.416651	441.034	2.32734	0.04393	-6.927D-05	0.5689	0.00925	-0.02000
4	0.3889	1.438704	443.620	2.31378	0.04633	-1.631D-04	0.8861	-0.00467	-0.02205
5	0.5186	1.461326	446.364	2.29956	0.04884	-3.070D-04	1.1626	-0.01693	-0.01802
6	0.6482	1.484507	449.274	2.28466	0.05146	-5.106D-04	1.4805	-0.02502	-0.00471
7	0.7779	1.508223	452.360	2.26907	0.05418	-7.857D-04	1.7610	-0.02588	0.01035
8	0.9075	1.532441	455.630	2.25279	0.05696	-1.146D-03	2.0597	-0.01655	0.02457
9	1.0372	1.557113	459.091	2.23581	0.05977	-1.609D-03	2.3528	-0.00022	0.03149
10	1.1668	1.582170	462.746	2.21815	0.06254	-2.196D-03	2.6327	0.01758	0.02848
11	1.2965	1.607522	466.596	2.19984	0.06520	-2.932D-03	2.9297	0.03239	0.01461
12	1.4261	1.633046	470.636	2.18096	0.06763	-3.847D-03	3.2029	0.03738	-0.00461
13	1.5557	1.658583	474.850	2.16161	0.06967	-4.978D-03	3.4904	0.03051	-0.02558
14	1.6854	1.683931	479.215	2.14192	0.07113	-6.367D-03	3.7673	0.01316	-0.03981
15	1.8150	1.708833	483.689	2.12210	0.07174	-8.062D-03	4.0395	-0.00980	-0.04283
16	1.9447	1.732968	488.213	2.10244	0.07121	-1.012D-02	4.3196	-0.03232	-0.03233
17	2.0743	1.755951	492.702	2.08328	0.06915	-1.258D-02	4.5820	-0.04557	-0.01216
18	2.2040	1.777326	497.046	2.06508	0.06521	-1.551D-02	4.8570	-0.04612	0.01372
19	2.3336	1.796572	501.104	2.04836	0.05902	-1.894D-02	5.1193	-0.03327	0.03522
20	2.4633	1.813128	504.711	2.03372	0.05036	-2.286D-02	5.3826	-0.01097	0.04677
21	2.5929	1.826425	507.690	2.02178	0.03921	-2.725D-02	5.6493	0.01398	0.04471
22	2.7226	1.835939	509.868	2.01315	0.02584	-3.200D-02	5.9036	0.03258	0.03092
23	2.8522	1.841258	511.103	2.00828	0.01088	-3.696D-02	6.1710	0.04134	0.00943
24	2.9818	1.842138	511.308	2.00748	-0.00477	-4.195D-02	6.4262	0.03796	-0.01116
25	3.1115	1.838545	510.471	2.01077	-0.02007	-4.674D-02	6.6885	0.02529	-0.02660
26	3.2411	1.830658	508.654	2.01795	-0.03406	-5.114D-02	6.9525	0.00785	-0.03320
27	3.3708	1.818846	505.983	2.02860	-0.04600	-5.501D-02	7.2100	-0.00893	-0.03074
28	3.5004	1.803606	502.623	2.04217	-0.05551	-5.826D-02	7.4819	-0.02244	-0.02066
29	3.6301	1.785502	498.752	2.05801	-0.06250	-6.085D-02	7.7423	-0.02806	-0.00655
30	3.7597	1.765109	494.543	2.07553	-0.06714	-6.280D-02	8.0154	-0.02772	0.00927
31	3.8894	1.742972	490.145	2.09416	-0.06974	-6.416D-02	8.2873	-0.01896	0.02232
32	4.0190	1.719580	485.680	2.11341	-0.07067	-6.498D-02	8.5573	-0.00484	0.02925
33	4.1487	1.695358	481.244	2.13288	-0.07030	-6.532D-02	8.8414	0.01106	0.02774
34	4.2783	1.670667	476.908	2.15228	-0.06893	-6.523D-02	9.1127	0.02496	0.01798
35	4.4079	1.645808	472.720	2.17135	-0.06684	-6.473D-02	9.4011	0.03128	0.00148
36	4.5376	1.621033	468.714	2.18991	-0.06423	-6.386D-02	9.6828	0.02761	-0.01566
37	4.6672	1.596555	464.912	2.20781	-0.06127	-6.261D-02	9.9671	0.01494	-0.02827
38	4.7969	1.572556	461.327	2.22497	-0.05805	-6.098D-02	10.2633	-0.00339	-0.03177
39	4.9265	1.549197	457.966	2.24130	-0.05466	-5.893D-02	10.5439	-0.01956	-0.02482
40	5.0562	1.526629	454.834	2.25673	-0.05114	-5.642D-02	10.8477	-0.02951	-0.00899
41	5.1858	1.504995	451.933	2.27122	-0.04751	-5.348D-02	11.1353	-0.02849	0.00817
42	5.3155	1.484440	449.266	2.28470	-0.04378	-4.981D-02	11.4329	-0.01790	0.02142
43	5.4451	1.465116	446.833	2.29714	-0.03993	-4.559D-02	11.7386	-0.00217	0.02553
44	5.5748	1.447183	444.638	2.30848	-0.03596	-4.071D-02	12.0229	0.01057	0.02012
45	5.7044	1.430814	442.685	2.31866	-0.03184	-3.515D-02	12.3448	0.01737	0.00825
46	5.8340	1.416195	440.982	2.32762	-0.02754	-2.893D-02	12.6260	0.01505	-0.00188
47	5.9637	1.403527	439.535	2.33528	-0.02305	-2.211D-02	12.9425	0.00773	-0.00724
48	6.0933	1.393005	438.354	2.34157	-0.01842	-1.491D-02	13.2514	0.00114	-0.00558
49	6.2230	1.384758	437.441	2.34646	-0.01390	-7.873D-03	13.5117	-0.00029	-0.00080
50	6.3526	1.378691	436.777	2.35003	-0.01010	-2.271D-03	14.0811	0.00276	0.00031

ORIGINAL PAGE IS
OF POOR QUALITY

VSWR VERSUS FREQUENCY

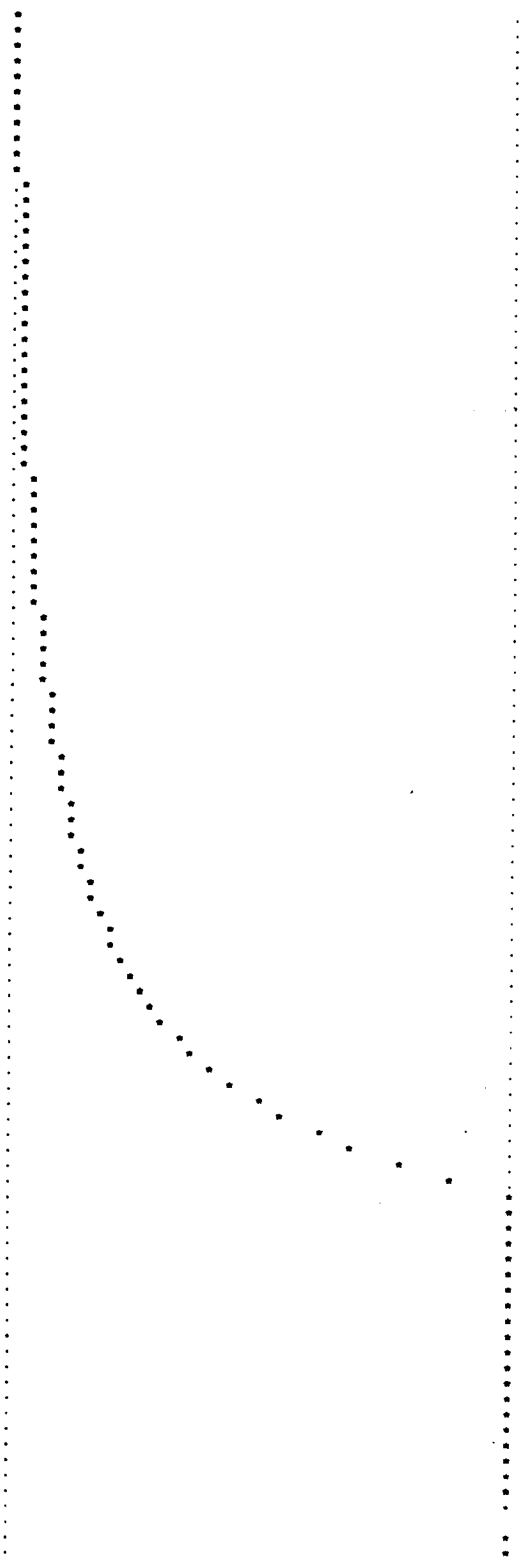

RETURN LOSS VERSUS FREQUENCY

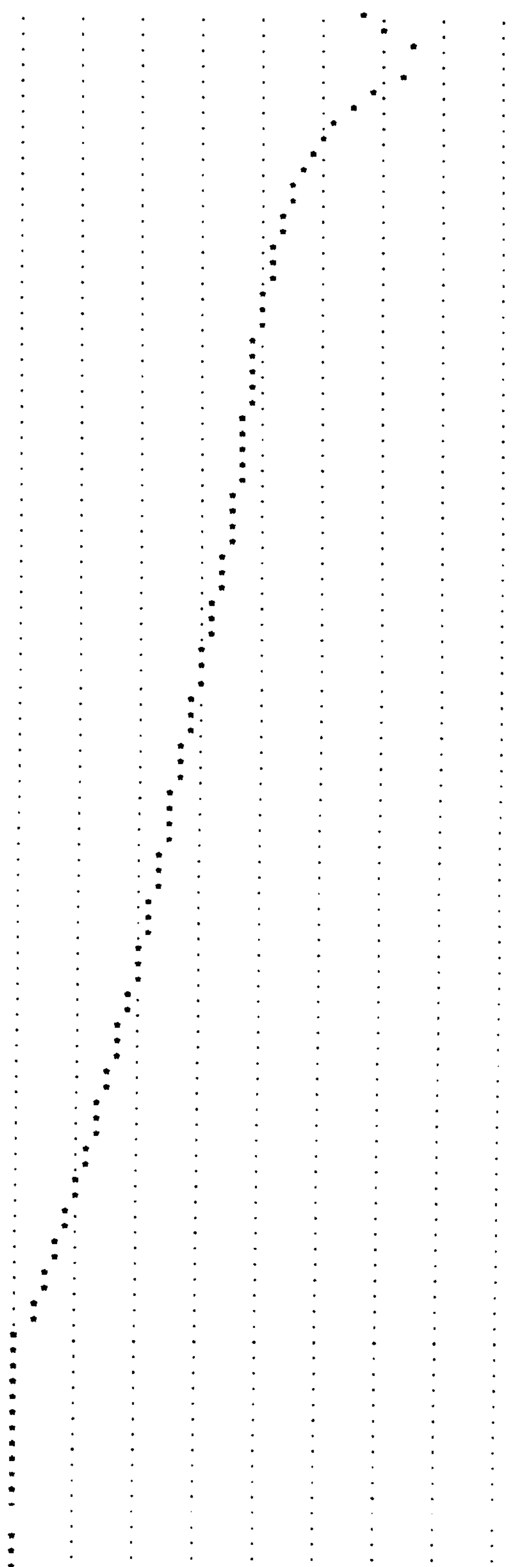

FGHZ	VSWR	RLOSS
13.00	1.003	56.326
12.95	1.002	59.808
12.90	1.001	66.163
12.85	1.000	83.855
12.80	1.001	63.899
12.75	1.002	58.188
12.70	1.004	54.700
12.65	1.005	52.175
12.60	1.006	50.198
12.55	1.007	48.575
12.50	1.009	47.205
12.45	1.010	46.024
12.40	1.011	44.991
12.35	1.013	44.079
12.30	1.014	43.267
12.25	1.015	42.539
12.20	1.016	41.884
12.15	1.017	41.291
12.10	1.019	40.753
12.05	1.020	40.263
12.00	1.021	39.813
11.95	1.022	39.398
11.90	1.023	39.012
11.85	1.024	38.650
11.80	1.025	38.304
11.75	1.026	37.971
11.70	1.027	37.642
11.65	1.028	37.314
11.60	1.029	36.979
11.55	1.030	36.632
11.50	1.031	36.269
11.45	1.033	35.885
11.40	1.034	35.478
11.35	1.036	35.046
11.30	1.038	34.590
11.25	1.040	34.109
11.20	1.043	33.607
11.15	1.045	33.087
11.10	1.048	32.550
11.05	1.052	32.003
11.00	1.055	31.447
10.95	1.059	30.886
10.90	1.063	30.324
10.85	1.067	29.762
10.80	1.072	29.204
10.75	1.077	28.649
10.70	1.082	28.100
10.65	1.087	27.557
10.60	1.093	27.019
10.55	1.099	26.487
10.50	1.106	25.961
10.45	1.113	25.438
10.40	1.120	24.918
10.35	1.128	24.399
10.30	1.137	23.879
10.25	1.146	23.357
10.20	1.156	22.831
10.15	1.166	22.298
10.10	1.178	21.757
10.05	1.191	21.205
10.00	1.205	20.641
9.95	1.220	20.063
9.90	1.238	19.470
9.85	1.257	18.861
9.80	1.279	18.234
9.75	1.304	17.589
9.70	1.332	16.927
9.65	1.364	16.248
9.60	1.401	15.552
9.55	1.442	14.839
9.50	1.491	14.111
9.45	1.546	13.369
9.40	1.611	12.614
9.35	1.687	11.848
9.30	1.776	11.072
9.25	1.882	10.287
9.20	2.008	9.496
9.15	2.161	8.699
9.10	2.340	7.901
9.05	2.580	7.104
9.00	2.872	6.312
8.95	3.245	5.534
8.90	3.723	4.783
8.85	4.321	4.094
8.80	4.855	3.630
8.75	99.999	0.0
8.70	99.999	0.0
8.65	99.999	0.0
8.60	99.999	0.0
8.55	99.999	0.0
8.50	99.999	0.0
8.45	99.999	0.0
8.40	99.999	0.0
8.35	99.999	0.0
8.30	99.999	0.0
8.25	99.999	0.0
[illegible]	[illegible]	[illegible]
[illegible]	[illegible]	[illegible]
8.10	99.999	0.0
8.05	99.999	0.0
8.00	99.999	0.0

APPENDIX 8. THE SYMBOL NOTATION USED IN THIS THESIS

The following symbol notation is generally adhered to throughout this thesis:

(1). Large signal time varying quantities, such as voltage and current, are represented by lower case letters and, if applicable, lower case subscripts (e.g. i_d is the time varying diode current).

(2). Large signal frequency domain quantities appear in upper case and are usually double subscripted (e.g. V_{d_n} is the nth Fourier coefficient of the large signal diode voltage).

(3). Frequency dependent quantities which are used in conjunction with large signals, such as the diode embedding impedances at the LO harmonics, are given by an upper case letter followed by a bracketed term indicating the frequency association (e.g. $Z_e(n)$ is the diode embedding impedance at LO harmonic n). Frequency dependent quantities which are used in conjunction with small signals, such as the diode embedding impedances at the harmonic sidebands, are given by an upper case letter followed by a double subscript (e.g. Z_{e_n} is the diode embedding impedance at sideband n).

(4). Small signal frequency domain quantities are represented by upper case letters preceded by a Greek delta (e.g. δI_{S_n} is the small signal diode shot noise current at sideband n).

(5). Mixer performance parameters are written in upper case, i.e. the single sideband mixer noise temperature, signal to intermediate frequency conversion loss and IF output voltage standing wave ratio are given by T_{SSB}, L_S, and VSWR respectively.

(6). Computer program variables appear in upper case and may or may not be bracketed (e.g. VDBIAS is the variable which represents the DC bias voltage in the mixer analysis program).

(7). MKS units are used except in referring to a few of the diode parameters where, following standard practice, the centimeter has been substituted for the meter (e.g. N_{d_e} is the diode epitaxial layer doping concentration in cm^{-3}). In some places the "mil" (0.001 inches) is used as the unit of length as this is the measure most popularly employed in current U.S. machining practice.

(8). Vector quantities are denoted with an underline as are matrices (except in Appendix A6 where matrices are indicated with a double underline).

(9). Standard symbols have been used wherever possible and definitions either precede or follow the first appearance of a variable. Once a symbol or variable has been defined the convention is adhered to throughout the thesis. If redefinition does occur it is clearly noted.

(10). All of the computer programs included in this thesis contain alphabetical lists of the variables which are used in the various subroutines. In addition Fig. 2-11 contains a table relating the mixer analysis program variables (Appendix 1) to the variables used in the theory of Chapter 2.

ACKNOWLEDGEMENTS

Although only one name appears on the title page of this thesis, next to it belong the names of the many people who have contributed so much to my research over the years. I humbly extend my warmest thanks to all of you.

I would especially like to thank Tony Kerr, who has been my advisor and friend throughout my tenure at the NASA Goddard Institute for Space Studies. Without his constant aid and guidance this thesis would certainly never have been completed. I can only wish that all graduate students had as knowledgeable and as helpful an advisor as he has been to me.

I would also like to individually thank all of the following people who have contributed to my work:

Wei Hwang, my supervisor at Columbia University, who supported me throughout my thesis work and whose faith in my abilities brought me through many rough times.

Patrick Thaddeus, who through Tony Kerr, encouraged my work and provided me with financial support for many of my years as a graduate student.

Bob Mattauch, Gordon Greene and all of the staff at the University of Virginia's Semiconductor Device Laboratory, who fabricated the diodes used for this thesis, and whose excellent research efforts have certainly been the primary reason we have obtained such excellent performance with our mixers and multipliers.

Sandy Weinreb and the staff members at the National Radio Astronomy Observatory in Charlottesville for many useful exchanges, and especially

John Archer of NRAO for his help and advice in the design of the frequency doublers.

Marc Feldman for many helpful discussions and especially for pointing out errors in, and suggesting improvements to, the mixer analysis program.

Dorn Peterson who suggested the idea of the channel waveguide transformer and many of whose helpful suggestions were incorporated into the mixer analysis program.

John Grange, who with his irreplaceable technical skills, has performed minor miracles in fabricating and assembling the mixers and multipliers used in this research.

Charles Burrus, Brian Clifton, Rich Linke, Malcolm McColl, Sandy Weinreb and Bill Wilson who kindly supplied first hand information for the historical section on mixers.

Bill Wilson, Margaret Frerking and Lance Riley at JPL for useful exchanges about frequency multipliers.

Harry Miller and Irving Silverberg, two of the finest machinists I have known, who made practically every noncommercial component used in this thesis.

Kathy McGunigle who made some of the multiplier measurements presented in the thesis.

Jerry Lamb at NASA Goddard for fabricating the mixer and multiplier filter sections.

John Lichtenberger at Meta-Plate who did all of the gold plating and electroforming of the mixers and multipliers.

Robert Grondin at University of Michigan, whose suggestions resulted in a much faster version of the mixer analysis program and Wayne Lam at California Institute of Technology, for pointing out a correction.

Peter Khan at the University of Queensland and Martin Schneider at Bell Telephone Laboratories, whose many visits and helpful discussions have certainly contributed to this work.

Emily Michaud and Andrea Calarco for typing and retyping Chapter 7 and

Lilly Del Valle and Jose Mendoza for their efforts in drawing up many of the figures in the thesis.

In addition all of the following people at GISS who, if they have not contributed directly to the thesis, have supported and helped me in my many years here: Carl Codan, Hong-Ih Cong, Sally Cummins, Mark Dubois, Mike Eilenfeldt, Bob Field, Elaine Gottlieb, Sheldon Green, Dan Held, Ross Hicks, Cornelia Landymore, Dennis Mumma, Barbara Palmer, Hugh Schwartz, Sarah Scott, Alison Smith, David Soll, Yuan Taur, Moy Wong and especially Richard Cohen, Carl Gottlieb, Sam Palmer and Shing-Kuo Pan.

For all those people whom I have not named explicitly or inadvertently left out, thank you.

Finally, I owe my greatest thanks to Ronnie S. Siegel, my wife and closest friend, who for the many years it has taken me to complete this dissertation, has supported me, has been patient with me, has never complained or pressured me, who has stood by me through the good times and the bad and who, more than anyone, has helped me complete this project. To her I dedicate this thesis with the words "per aspera ad astra" and remain forever grateful.

REFERENCES

[1]. Archer, J.W., "Millimeter wavelength frequency multipliers," IEEE Trans. on Microwave Theory and Techniques, vol. MTT-29, no. 6, pp. 552-557, June 1981.

[2]. Archer, J.W., "A high performance frequency doubler for 80-120 GHz," IEEE Trans. Microwave Theory and Tech., vol. MTT-30, no. 5, pp. 824-825, May 1982.

[3]. Archer, J.W., "All solid-state low-noise receivers for 210-240 GHz," IEEE Trans. Microwave Theory and Tech., vol. MTT-30, no. 8, pp. 1247-1252, Aug. 1982.

[4]. Archer, J.W., Private communication.

[5]. Archer, J.W. and R.J. Mattauch, "Low noise single-ended mixer for 230 GHz," Electronics Letters, vol. 17, no. 5, pp. 180-81, March 5, 1981.

[6]. Archer, R.J. and M.M. Atalla, "Metals contacts on cleaned silicon surfaces," in part II of Conference on Clean Surfaces, Annals of the New York Academy of Sciences, vol. 101, art. 3, pp. 697-709, Jan. 23, 1963.

[7]. Armstrong, E.H., "A new system of short wave amplification," Proc. IRE, vol. 9, pp. 539-551, Feb. 1921.

[8]. Armstrong, E.H., "The super-heterodyne - Its origin, development, and some recent improvements," Proc. IRE, vol. 12, pp. 539-551, 1924.

[9]. Baechtold, W. "Noise behavior of GaAs field-effect transistors with short gates," IEEE Trans. on Electron Devices, vol. ED-19, no. 5, pp. 674-680, May 1972.

[10]. Barber, M.R., "Noise figure and conversion loss of the Schottky barrier mixer diode," IEEE Trans. on Microwave Theory and Tech., vol. MTT-15,no. 11, pp. 629-635, Nov. 1967.

[11]. Bauer, R.F. and P. Penfield Jr., "De-embedding and unterminating," IEEE Trans. Microwave Theory and Tech., vol. MTT-22, no. 3, pp.282-288, Mar. 1974.

[12]. Bauer, R.J., M. Cohn, J.M. Cotton Jr. and R.F. Packard, "Millimeter wave semiconductor diode detectors, mixers, and frequency multipliers," Proc. IEEE, vol. 54, no. 4, pp. 595-605, April 1966.

[13]. Becker, L. and R.L. Ernst, "Non-linear-admittance mixers," RCA Review, vol.25, no.4, pp. 662-691, Dec. 1964.

[14]. Benson, F.A. and W.F. Winder, "Harmonic generators and detectors for millimetre wavelengths," Proc. IEE (London), vol. 115, no. 1, pp. 37-42, Jan. 1968.

[15]. Beringer, R., "The absorbtion of one-half centimeter electromagnetic waves in oxygen," Phys. Review, vol. 70, nos. 1 and 2, pp. 53-57, July 1 and 15, 1946.

[16]. Bianco, B., A. Corana, S. Ridella and C. Simicich, "Evaluation of errors in calibration procedures for measurement of reflection coefficient," IEEE Trans. Instrumentation and Measurement, vol. IM-27, no. 4, pp.354-358, Dec. 1978.

[17]. Bracewell, R. The Fourier Transform and Its Applications, N.Y.: McGraw Hill, 1965, p. 197.

[18]. Burrus, C.A., "Millimeter-wave point-contact and junction diodes," Proc. IEEE, vol. 54, no. 4, pp. 575-587, April 1966.

[19]. Burrus, C.A. Private communication.

[20]. Carlson, E.R., M.V. Schneider and T.F. McMaster, "Subharmonically pumped millimeter-wave mixers," IEEE Trans. Microwave Theory and Tech., vol. MTT-26, no. 10, pp. 706-715, Oct. 1978.

[21]. Champlin, K. and G. Eisenstein, "Cutoff frequency of submillimeter Schottky-barrier diodes," IEEE Trans. on Microwave Theory and Tech., vol. MTT-26, no. 1, pp. 31-34, Jan. 1978.

[22]. Chang, K.K.N., "Harmonic generation with nonlinear reactances," RCA Review, vol. 19, no. 3, pp. 455-464, Sept. 1958.

[23]. Clifton, B.J., W.T. Lindley, R.W. Chick and R.A. Cohen, "Materials and processing techniques for the fabrication of high quality millimeter wave diodes," Proc.of the 3rd Bienniel Cornell Conference : High Frequency Generation and Amplification : Devices and Applications, IEEE cat.no.71C71-CORN, pp. 463-475, Aug. 1971.

[24]. Clifton, B.J., Private communication.

[25]. Cohen, L.D., S. Nussbaum, E. Kraemer, J. Calviello and J. Taub, "Varactor frequency doublers and triplers for the 200 to 300 GHz range," IEEE MTT-S Int. Microwave Symposium Digest, pp. 274-276, May 1975.

[26]. Cohn, M., L.E. Dickens, and J.W. Dozier, "Recent developments in millimeter wave components," IEEE G-MTT 1969 International Microwave Symposium Digest, pp. 225-31, May 1969.

[27]. Cohn, M., F.L. Wentworth and J.C. Wiltse, "High sensitivity 100- to 300-Gc radiometers," Proc. IEEE, vol. 51, no. 9, pp. 1227-32, Sept. 1963.

[28]. Cohn, S.B., "Properties of ridge wave guide," Proceedings I.R.E., vol. 35, pp. 783-788, Aug. 1947.

[29]. Coleman, P.D., "State of the art:background and recent developments-millimeter and submillimeter waves," IEEE Trans.on Microwave Theory and Tech., MTT-11, no. 9, pp. 272-288, Sept. 1963.

[30]. Cong, H., A.R. Kerr and R.J. Mattauch, "The low-noise 115-GHz receiver on the Columbia-GISS 4-ft radio telescope," IEEE Trans. on Microwave Theory and Tech., vol. MTT-27, no. 3, pp. 245-248, March 1979.

[31]. Copeland, J.A., "Diode edge effect on doping-profile measurements," IEEE Trans. Electron Devices, vol. ED-17, no. 5, pp. 404-407, May 1970.

[32]. Dalley, J.E., "Computer-aided microwave impedance measurements," IEEE Trans. Microwave Theory and Tech., vol. MTT-17, no. 8, pp. 572-576, Aug. 1969.

[33]. Da Silva, E.F. and M.K. McPhun, "Calibration of microwave network analyzer for computer-corrected S parameter measurements," Electronic Letters, vol. 9, no. 6, pp. 126-128, Mar. 22, 1973.

[34]. DeLoach, B.C. Jr., "Recent advances in solid state microwave generators," in Advances in Microwaves vol. 2, N.Y.: Academic Press, p. 58, 1967.

[35]. Dickens, L.E., "Millimeter wave diodes for harmonic power generation," IEEE Trans. Microwave Theory and Tech., vol. MTT-15, no. 1, pp. 32-37, Jan. 1967.

[36]. Dickens, L.E., "Spreading resistance as a function of frequency," IEEE Trans. on Microwave Theory and Tech., vol. MTT-15, no. 2, pp. 101-109, Feb. 1967.

[37]. Dickens, L.E., "Low conversion loss millimeter wave mixers," 1973 G-MTT International Microwave Symposium Digest, IEEE cat. no. 73CH0736-9MTT, pp. 66-68, June 1973.

[38]. Dickens, L.E., J.M. Cotton Jr. and B.D. Geller, "A mixer and solid state LO for a 60 GHz receiver," 1971 G-MTT International Microwave Symposium Digest, pp. 188-190, May 1971.

[39]. Dragone, C., "Analysis of thermal and shot noise in pumped resistive diodes," Bell System Tech. J., vol. 47, no. 9, pp. 1883-1902, Nov. 1968.

[40]. Edwards, G.F., "Frequency conversion by means of a non-linear admittance," Bell System Tech. Journal, vol. 35, no. 6, pp. 1403-1416, Nov. 1956.

[41]. Egami, S. "Nonlinear, linear analysis and computer aided design of resistive mixers," IEEE Trans. on Microwave Theory and Tech., vol. MTT-22, no. 3, pp. 270-275, March 1974.

[42]. Eisenhart, R.L., P.T. Greiling, L.K. Roberts, and R.S. Robertson, "A useful equivalence for a coaxial-waveguide junction,", IEEE Trans. Microwave Theory and Tech., vol. MTT-26, no.3, pp. 172-174, Mar. 1978.

[43]. Eisenhart, R.L. and P.J. Khan, "Theoretical and experimental analysis of a waveguide mounting structure," IEEE Trans. on Microwave Theory and Tech., vol. MTT-8, no. 8, pp. 706-719, Aug. 1971.

[44]. Erickson, N.R., "A 200-350-GHz heterodyne receiver," IEEE Trans. on Microwave Theory and Tech., vol. MTT-29, no. 6, pp. 557-561, June 1981.

[45]. Erickson, N.R., "A cryogenic receiver for 1 mm wavelength," 6 th International Conference on Infrared and Millimeter Waves: Conference Digest, IEEE cat no. 81CH1645-1MTT, pp. W-3-8, Dec. 1981.

[46]. Evans, J.G., "Measuring frequency characteristics of linear two-port networks automatically," Bell System Tech. Journal, vol. 48, pp. 1313-1338, May-June 1969.

[47]. Evans, J.G., F.W. Kerfoot and R.L. Nichols, "Automated network analyzers for the .9- to 12.4-GHz range," Bell System Tech. Journal, vol. 55, no. 6, pp. 691-721, July-August 1976.

[48]. Fessenden, R.A., U.S. Patent no. 706740, issued Aug.12, 1902.

[49]. Fleri, D.A. and L.D. Cohen, "Nonlinear analysis of the Schottky-barrier mixer diode," IEEE Trans. on Microwave Theory and Tech., vol. MTT-21, no. 1, pp. 39-43, Jan. 1973.

[50]. Frensley, W.R., "High frequency effects of ballistic transport in semiconductors," IEEE Electron Device Letters, vol. EDL-1, no. 7, pp. 137-139, July 1980.

[51]. Frerking, M.A., J.C. Hardy and W.J. Wilson, "A broad band low-noise 205 GHz radiometer for a satellite receiver," IEEE MTT-S 1983 International Microwave Symposium Digest, pp. 110-112, June 1983.

[52]. Getsinger, W.J. ,"The packaged and mounted diode as a microwave circuit," IEEE Trans. Microwave Theory and Tech., vol. MTT-14, no. 2, pp. 58-69, Feb. 1966.

[53]. Glance, B. and R. Trambarulo, "A waveguide to suspended stripline transition," IEEE Trans. on Microwave Theory and Tech., vol. MTT-21, no. 2, pp. 117-118, Feb. 1973.

[54]. Gordy, W., "Millimeter and submillimeter waves in physics," Millimeter Waves, Microwave Res. Inst. Symposium Series vol. IX, Polytechnic Institute of Brooklyn, N.Y.: Polytechnic Press, pp. 1-23, 1959.

[55]. Gottlieb, C.A., Private communication.

[56]. Guillemin, E.A., The Mathematics of Circuit Analysis, New York: John Wiley and Sons, 1949.

[57]. Gupta, M. and R. Lomax, "A self-consistent large signal analysis of a Read-type IMPATT diode oscillator," IEEE Trans. Electron Devices, vol. ED-18, no. 8, pp. 544-550, Aug. 1971.

[58]. Gwarek, W.K., "Nonlinear analysis of microwave mixers," M.S. Thesis, Mass. Institute of Tech., Cambridge, Mass., Sept. 1974.

[59]. Hackam, R. and P. Harrop, "Electrical properties of nickel-doped n-type gallium arsenide Schottky barrier diodes," IEEE Trans. on Electron Devices, vol. ED-19, no. 12, pp. 1231-1238, Dec. 1972.

[60]. Hackborn, R.A., "An automatic network analyzer system," Microwave Journal, vol. 11, no. 5, pp. 45-52, May 1968.

[61]. Hand, B.P., "Developing accuracy specifications for automatic network analyzer systems," Hewlett-Packard Journal, vol. 21, no. 6, pp.16-19, Feb. 1970.

[62]. Held, D.N., "Analysis of room temperature millimeter-wave mixers using GaAs Schottky barrier diodes," NASA Goddard Space Flight Center Report no. X-130-77-6, Jan. 1977.

[63]. Held, D.N. and A.R. Kerr, "Conversion loss and noise of microwave and millimeter-wave mixers : Part I-Theory," and "Part II-Experiment," IEEE Trans. on Microwave Theory and Tech., vol. MTT-26, no.2, pp.49-61, Feb. 1978.

[64]. Hewlett-Packard, "Semi-automated measurements using the 8410B microwave network analyzer and the 9825A desk-top computer," Hewlett-Packard Applications Note 221, 16 pages, Oct. 1977.

[65]. Hicks, R and P.J. Khan, "Numerical technique for determining pumped nonlinear device waveforms," Electronic Letters, vol. 16, no. 10, pp. 375-376, May 8,1980.

[66]. Hicks, R. and P.J. Khan, "Numerical analysis of nonlinear solid-state device excitation in microwave circuits," IEEE Trans. Microwave Theory Tech., vol. MTT-30, no. 3, pp. 251-259, March 1982.

[67]. Hicks, R.G. and P.J. Khan, "Improved waveguide diode mount circuit model using post equivalence factor analysis," IEEE Trans. Microwave Theory and Tech., vol. MTT-30, no. 11, pp. 1914-1920, Nov. 1982.

[68]. Hirayama, M., S. Ogawa and T. Yagasaki, "Doublers and frequency up/down converters in the 100-150 GHz-band," Review of the Electrical Communications Laboratory (Japan), vol. 23, no. 11-12, pp. 1166-1174, Nov.-Dec. 1975.

[69]. Hogan, J.L.Jr., "The heterodyne receiving system, and notes on the recent Arlington-Salem tests," Proc. IRE, vol. 1, pp. 75-102, July 1913.

[70]. Hogan, J.L.Jr., "Developments of the heterodyne receiver," Proc. IRE, vol. 3, pp. 249-259, May 1915.

[71]. "IRE Standards on electron tubes : Definition of terms 1962 (62IRE7.S2)," Proc. IEEE, vol. 51, no. 3, pp. 434-435, March 1963.

[72]. IRE Subcommittee on noise, "Description of the noise performance of amplifiers and receiving systems", Proc. IEEE, vol. 51, no. 3, pp. 436-442, March 1963.

[73]. Irvin, J.C. and N.C. Vanderwal, "Schottky barrier devices," chapter 11 of Microwave Semiconductors and Their Circuit Applications, edited by H.A. Watson, N.Y.: McGraw Hill, pp.340-369, 1969.

[74]. Jenny, D.A., "A gallium arsenide microwave diode," Proc. IRE, vol. 46, no. 4, pp. 717-722, April 1958.

[75]. Johnson, C.M., "Superheterodyne receiver for the 100 to 150 kMc region," IRE Trans.on Microwave Theory and Tech., MTT-2, pp. 27-32, Sept. 1954.

[76]. Johnson, C.M., D.M. Slager and D.D. King, "Millimeter waves from harmonic generators," Rev. of Sci. Instr., vol. 25, no. 3, pp. 213-217, March 1954.

[77]. Johnson, J.B., "Thermal agitation of electricity in conductors," Phys. Rev., vol. 32, p. 97, July 1928.

[78]. Johnson, R.C., "Design of linear double tapers in rectangular waveguide," IRE Transactions on Microwave Theory and Tech., vol. MTT-7, no. 7, pp. 374-78, July 1959.

[79]. Johnson, W.A., T.T. Mori and F.I. Shimabukuro, "Design, development, and initial measurements of a 1.4-mm radiometric system," IEEE Trans. on Antennas and Propagation, AP-18, no. 4, pp. 512-14, July 1970.

[80]. Katzenelenbaum, B.Z., "On the theory of nonuniform waveguides with slowly changing parameters," Congres International Circuits and Antennes Hyperfrequences, Supplement to L'Onde Electrique, no. 376, pp. 124-127, Aug. 1958.

[81]. Keen, N.J., W.M. Kelley and G.T. Wrixon, "Pumped Schottky diodes with noise temperatures of less than 100K at 115 GHz," Electronics Letters, vol. 15, no. 21, pp. 689-690, Oct. 11, 1979.

[82]. Kerr, A.R., "Low-noise room temperature and cryogenic mixers for 80-120 GHz," IEEE Trans.on Microwave Theory and Tech., vol. MTT-23, no. 10, pp. 781-787, Oct. 1975

[83]. Kerr, A.R., "A technique for determining the local oscillator waveforms in a microwave mixer," IEEE Trans.on Microwave Theory and Tech., vol. MTT-23, no. 10, pp. 828-831, Oct. 1975.

[84]. Kerr, A.R., "Shot-noise in resistive-diode mixers and the attenuator noise model," IEEE Trans. on Microwave Theory and Tech., vol. MTT-27, no. 2, pp. 135-140, Feb. 1979.

[85]. Kerr, A.R., "Noise and loss in balanced and subharmonically pumped mixers: Part I-Theory," and "Part II-Experiment," IEEE Trans. on Microwave Theory and Tech., vol. MTT-27, no .12, pp. 938-950, Dec. 1979.

[86]. Kerr, A.R., "On thermal effects in diode series resistance measurements," NASA/Institute for Space Studies Internal Report, 8 pages, July 9, 1982.

[87]. Kerr, A.R. Private communication

[88]. Kerr, A.R., J.A. Grange and J.A. Lichtenberger, "Contact whiskers for millimeter wave diodes," NASA Technical Memorandum no. 79616, Goddard Space Flight Center: Institute for Space Studies, Greenbelt, MD, 33 pages, Aug. 1978.

[89]. Kerr, A.R., R.J. Mattauch and J.A. Grange, "A new mixer design for 140-220 GHz," IEEE Trans. on Microwave Theory and Tech., vol. MTT-25, no. 5, pp. 399-401, May 1977.

[90]. Kim, C.S., "Tunnel diode converter analysis," IRE Trans. Electron Devices, vol. ED-8, no.5, pp.394-405, Sept. 1961.

[91]. King, W.C., "Millimeter wave spectroscopic components," IRE Trans. on Microwave Theory and Tech, vol. MTT-2, no. 3, pp. 13-16, Sept. 1954.

[92]. Kita, S., "A harmonic generator by use of the nonlinear capacitance of germanium diode," Proc. IRE (correspondence), vol. 46, no. 6, p.1307, June 1958.

[93]. Knerr, R.H., "A new type of waveguide-to-stripline transition," IEEE Trans. on Microwave Theory and Tech., vol. MTT-16, no.3, pp. 192-194, March 1968.

[94]. Kollberg, E., "Advances in Mixer Device Technology", Private notes from a paper delivered at the Mixer Workshop of the IEEE MTT-S International Microwave Symposium, Boston, June 30, 1983.

[95]. Kraus, J.D., Radio Astronomy, New York: McGraw Hill, 1966.

[96]. Kuz'min, N.A. and T.V. Makarov, "Electromagnetic waves in a rectangular cross-shaped waveguide," Radio Eng. and Electronic Physics, vol. 6, no. 12, pp. 1781-1789, Dec. 1961.

[97]. Lee, T.P. and C.A. Burrus, "A millimeter-wave quadrupler and an up-converter using planar-diffused gallium arsenide varactor diodes," IEEE Trans.on Microwave Theory and Tech., vol. MTT-16, no. 5, pp. 287-96, May 1968.

[98]. Leedy, H.M., H.L. Stover, H.G. Morehead, R.P. Bryan and H.L. Garvin, "Advanced millimeter-wave mixer diodes,GaAs and silicon, and a broadband low noise mixer," Proc.of the 3rd Bienniel Cornell Elec. Eng. Conference : High Frequency Generation and Amplification : Devices and Applications, IEEE cat. no. 71C71-CORN, pp. 451-62, Aug. 1971.

[99]. Lidholm, S. and Th. de Graauw, "A heterodyne receiver for submillimeter-wave astronomy," Fourth International Conference on Infrared and Millimeter Waves and Their Applications, Post Deadline Digest Contributions, IEEE cat. no. 79CH1384-7 MTT, pp. 38-39, Dec. 1979.

[100]. Lin, F.L.C., "Modal characteristics of crossed rectangular waveguides," IEEE Trans. Microwave Theory and Tech., vol. MTT-25, no. 9, Sept. 1977.

[101]. Linke, R.A. Private communication.

[102]. Linke, R.A., M.V. Schneider and A.Y. Cho, "Cryogenic millimeter-wave receiver using molecular beam epitaxy diodes," IEEE Trans. Microwave Theory and Tech., vol. MTT-26, no. 12, pp. 935-938, Dec. 1978.

[103]. MacPherson, A.C., "An analysis of the diode mixer consisting of a non-linear capacitance and ohmic spreading resistance," IRE Trans. on Microwave Theory and Tech., vol. MTT-5, no. 1, pp. 43-51, Jan. 1957.

[104]. Manley, J.M. and H.E. Rowe, "Some general properties of nonlinear elements - Part I. General energy relations," Proc. IRE, vol. 44, no. 7, pp. 904-913, July 1956.

[105]. Mantena, N.R., and J.S. Barrera, "Measurement of Schottky barrier edge capacitance correction," Solid-State Electronics, vol. 12, Great Britain: Pergamon Press, pp. 1000-1002, 1969.

[106]. Mardon, A, "Non-linear resistance and non-linear reactance devices for harmonic generation," in Millimetre and Submillimetre Waves, edited by F.A. Benson, London: Iliffe Books Ltd., pp. 179-191, 1969.

[107]. Matthaei, G.L., L. Young and E.M.T. Jones, Microwave Filters, Impedance-Matching Networks, and Coupling Structures, New York: McGraw Hill, 1964.

[108]. McColl, M., M.F. Millea, J. Munushian and D.F. Kyser, "Improved 94-GHz GaAs mixer diodes using gold-copper alloy whiskers," Proc. IEEE, vol. 55, no. 12, pp. 2169-70, Dec. 1967.

[109]. McColl, M. and M.F. Millea, "Advantages of Mott barrier mixer diodes," Proc. IEEE, vol. 61, no. 4, pp. 499-500, April 1973.

[110]. Meredith, R. and F.L. Warner, "Superheterodyne radiometers for use at 70 Gc and 140 Gc," IEEE Trans. on Microwave Theory and Tech., vol. MTT-11, no. 9, pp. 397-411, Sept. 1963.

[111]. Messenger, G.C., "New concepts in microwave mixer diodes," Proc. IRE, vol. 46, no. 6, pp. 1116-21, June 1958.

[112]. Messenger, G.C. and C.T. McCoy, "Theory and operation of crystal diodes as mixers," Proc. IRE, vol. 45, no. 9, pp.1269-1283, Sept. 1957.

[113]. Mihran, T.J., "Closed- and open-ridge waveguide," Proceedings I.R.E., vol. 37, pp. 640-644, June 1949.

[114]. Monroe, J. and E. Feldman, "Ka band klystron replacement," IEEE Trans. on Microwave Theory and Tech., vol. MTT-12, no. 9, p.553, Sept. 1964.

[115]. Montgomery, J.P., "On the complete eigenvalue solution of ridged waveguide," IEEE Trans. Microwave Theory and Tech., vol. MTT-19, no. 6, pp.547-555, June 1971.

[116]. Mumford, W.W. and E.H. Scheibe, Noise Performance Factors in Communication Systems, U.S.A.: Horizon House-Microwave, Inc., 1968.

[117]. Nesslage, C.F., E.W. Herold and W.A. Harris, "A new tube for use in superheterodyne frequency conversion systems," Proc. IRE, vol. 24, no. 2, pp. 207-219, Feb. 1936.

[118]. Nethercot, A.H. Jr., "Harmonics at millimeter wavelengths," IRE Trans. on Microwave Theory and Tech, vol. MTT-2, no. 3, pp. 17-19, Sept. 1954.

[119]. Nyquist, H., "Thermal agitation of electric charge in conductors," Phys. Rev., vol. 32, p. 110, July 1928.

[120]. Ohl, R.S., P.P. Budenstein and C.A. Burrus, "Improved diode for harmonic generation of millimeter and submillimeter waves," Rev. of Scientific Instr., vol. 30, no. 9, pp. 765-774, Sept. 1959.

[121]. Page, C.H., "Frequency conversion with positive non-linear resistors," Journal of the National Bureau of Standards, vol. 56, pp. 179-182, April 1956.

[122]. Page, C.H., "Harmonic generation with ideal rectifiers," Proc. IRE, vol. 46, no. 10, pp. 1738-1741, Oct. 1958.

[123]. Page, W.I.G., "New valves," Wireless World, vol. 34, pp. 409, June 9, 1933.

[124]. Pellegrini, B. and T. Di Leo, "Intervalley scattering effect on the current-voltage characteristic of GaAs-metal contacts," Alta Frequenza, vol. 46, no. 8, pp. 345-353, Aug. 1977.

[125]. Penfield, P. and R.P. Rafuse, Varactor Applications. Cambridge, Mass.: MIT Press, 1962.

[126]. Penzias, A.A. and C.A. Burrus, "Millimeter wavelength radio-astronomy techniques," in Annual Review of Astronomy and Astrophysics, vol. 11, pp. 51-71, 1973.

[127]. Peterson, D.W., private communication.

[128]. Polyakov, N.N. and V.L. Kon'kov, "Spreading resistance of a flat circular contact," Translation from Izv. Vys. Uch. Zav., Fizika, no.9, pp. 100-105, Sept. 1970.

[129]. Pound, R.V., Microwave Mixers. MIT Radiation Laboratory Series, vol. 16, N.Y. : McGraw Hill, 1948.

[130]. Pyle, J.R., "The cutoff wavelength of the TE_{10} mode in ridged waveguide of any aspect ratio," IEEE Trans. Microwave Theory and Tech., vol. MTT-14, no. 4, pp. 175-183, April 1966.

[131]. Raisanen, A.V., N.R. Erickson, J.L.R. Marrero, P.F. Goldsmith and C.R. Predmore, "An ultra low-noise Schottky mixer receiver at 80-120 GHz," 6 th International Conference on Infrared and Millimeter Waves: Conference Digest, IEEE cat no. 81CH1645-1MTT, pp. W-3-6, Dec. 1981.

[132]. Raisanen, A.V., C.R. Predmore, P.T. Parrish, P.F. Goldsmith, J.L.R. Marrero, R.A. Kot and M.V. Schneider, "A cooled Schottky-diode mixer for 75-120 GHz," 10th European Microwave Conference Proceedings, Warsaw, Poland, pp. 717-721, Sept. 8-11, 1980.

[133]. Ramo, S., and J.R. Whinnery, Fields and Waves in Modern Radio, N.Y., N.Y. : John Wiley and Sons, 1944.

[134]. Reiter, G., "Generalized Telegraphist's equation for waveguides of varying cross-section," IEE Proceedings, Part B, Supplement no. 13, vol. 106, pp. 54-57, Sept. 1959.

[135]. Rhoderick, E.H., Metal-Semiconductor Contacts. Oxford,England: Clarendon press, 1980.

[136]. Richardson, J.M. and R.B. Riley, "Performance of three-millimeter harmonic generators and crystal detectors," IRE Trans. on Microwave Theory and Tech, vol. MTT-5, no. 2, pp. 131-135, April 1957.

[137]. Saad, S.S., J.B. Davies and O.J. Davies, "Computer analysis of gradually tapered waveguide with arbitrary cross sections," IEEE Trans. Microwave Theory and Tech., vol. MTT-25, no. 5, pp. 437-440, May 1977.

[138]. Saleh, A.A.M., "Theory of resistive mixers," PhD. Dissertation, Mass. Inst. of Tech., Cambridge, Mass., 1970.

[139]. Schelkunoff, S.A., "Impedance concept in wave guides," Quarterly Journal of Applied Math., vol. ii, no.1, pp. 1-15, April 1944.

[140]. Schelkunoff, S.A., "Conversion of Maxwell's equations into generalized Telegraphist's equations," Bell System Tech. J., vol.34, pp. 995-1043, Sept. 1955.

[141]. Schneider, M.V., "Metal-semiconductor junctions as frequency converters," Chapter 4 of Infrared and Millimeter Waves, vol.6, edited by K.J. Button, N.Y.: Academic Press, 1982, pp. 209-275.

[142]. Schneider, M.V., and E.R. Carlson, "Notch front diodes for millimetre-wave integrated circuits," Electronics Letters, vol. 13, no. 24, pp. 745-747, Nov. 24, 1977.

[143]. Schneider, M.V. and T.G. Phillips, "Millimeter-wave frequency multiplier," International Journal of Infrared and Millimeter Waves, vol. 2, no. 1, pp. 15-22, Jan. 1981.

[144]. Schottky, W., "Uber spontane stromschwankungen in verschiedenen elektrizitatsleitern," Ann. Phys. (Leipzig), vol. 57, pp. 541-67, Dec. 1918.

[145]. Schottky, W., "On the origin of the super-heterodyne method," Proc. IRE, vol. 14, pp. 695-698, 1926.

[146]. Sharpless, W.M., "Wafer-type millimeter wave rectifiers," Bell System Tech. Journal, vol. 35, pp. 1385-1402, Nov. 1956.

[147]. Sharpless, W.M., "High-frequency gallium arsenide point-contact rectifiers," Bell System Tech. Journal, vol. 38, pp. 259-69, Jan. 1959.

[148]. Sharpless, W.M., "Gallium arsenide point-contact diodes," IRE Trans.on Microwave Theory and Tech., vol. MTT-9, no. 1, pp. 6-10, Jan. 1961.

[149]. Siegel, P.H., "An IEEE compatible 16 bit D/A converter for the Apple II plus computer," NASA/GISS Internal Report, 15 pages, May 1982.

[150]. Siegel, P.H., "A semi-automated reflectometer test set," NASA/GISS Internal Report, 46 pages, July 1982.

[151]. Siegel, P.H. and A.R. Kerr, "A user oriented computer program for the analysis of microwave mixers, and a study of the effects of the series inductance and diode capacitance on the performance of some simple mixers," NASA Tech. Mem. 80324, National Aeronautics and Space Administration Goddard Space Flight Center, Greenbelt, Maryland, July 1979.

[152]. Siegel, P.H., and A.R. Kerr, "Computer analysis of microwave and millimeter-wave mixers," IEEE Trans. Microwave Theory and Tech., vol. MTT-28, no. 3, pp. 275-276, March 1980.

[153]. Siegel, P.H., D.W. Peterson and A.R. Kerr, "Design and analysis of the channel waveguide transformer," IEEE Trans. Microwave Theory and Tech., vol. MTT-31, no. 6, pp. 473-484, June 1983.

[154]. Siegel, P.H., D.W. Peterson and A.R. Kerr, "The channel waveguide transformer: An easily fabricated transition for the TE-10 mode," 1983 IEEE MTT-S International Microwave Symposium Digest, pp. 169-171, June 1983.

[155]. Solymar, L., "Spurious mode generation in nonuniform waveguide," IRE Trans. Microwave Theory and Tech., vol. MTT-7, no. 7, pp.379-383, July 1959.

[156]. Sowerby, A.L.M., "From triode to double-diode pentode," Wireless World, vol. 35, pp. 350-53, Nov. 2, 1934.

[157]. Sporleder, F. and H.G. Unger, Waveguide Tapers Transitions and Couplers, Stevenage, U.K. : Peter Peregrinus Ltd., 1979.

[158]. Steinbrecher, D.H., "Low-noise microwave mixers," IEEE International Convention Digest, IEEE cat. no. 71C8, pp. 518-19, March 1971.

[159]. Stratton, J.A., Electromagnetic Theory. New York: McGraw Hill, pp. 488-490, 1941.

[160]. Strutt, M.J.O., "Noise figure reduction in mixer stages," Proc. IRE, vol.34, no. 12, pp. 942-950, Dec. 1946.

[161]. Sze, S.M. Physics of Semiconductor Devices. N.Y.: John Wiley and Sons, 1969.

[162]. Takada, T. and M. Hirayama, "Hybrid integrated frequency multipliers at 300 and 450 GHz," IEEE Trans. on Microwave Theory and Tech., vol. MTT-26, no. 10, pp. 733-737, Oct. 1978.

[163]. Takada, T., T. Makimura and M. Ohmori, "Hybrid integrated frequency doublers and triplers to 300 and 450 GHz," IEEE Trans. Microwave Theory and Tech., vol. MTT-28, no. 9, pp. 966-973, Sept. 1980.

[164]. Tham, Q.C., "Modes and cutoff frequencies of crossed rectangular waveguides," IEEE Trans. Microwave Theory and Tech., vol. MTT-25, no. 7, pp. 585-588, July 1977.

[165]. Torrey, H.C. and C.A. Whitmer, Crystal Rectifiers. MIT Radiation Laboratory Series vol. 15, N.Y. : McGraw Hill, 1948.

[166]. Uhlir, A. Jr., "The potential of semiconductor diodes in high-frequency communications," Proc. IRE, vol. 46, no. 6, pp. 1099-1115, June 1958.

[167]. Uhlir, A. Jr., Shot noise in p-n junction frequency converters," Bell System Tech. J., vol. 37, no. 4, pp. 951-988, July 1958.

[168]. Uhlir, A.Jr., Letter to the Editor, Microwaves, vol. 19, no. 9, p. 105, Sept. 1980.

[169]. van der Ziel, A. Noise: Sources, Characterization, and Measurement. Englewood Cliffs, N.J.: Prentice Hall, 1970.

[170]. van der Ziel, A. and R.L. Watters, "Noise in mixer tubes," Proc. IRE, vol. 46, no. 4, pp. 1426-27, July 1958.

[171]. Vilmur, R.J. and K. Ishii, "The channel waveguide," IRE Transactions on Microwave Theory and Techniques, vol. MTT-10, no. 5, pp. 220-221, May 1962.

[172]. Viola, T.J. and R. J. Mattauch, "Unified theory of high frequency noise in Schottky barriers," Journal of Applied Physics, vol. 44, no. 6, pp. 2805-2808, June 1973.

[173]. Vizard, D.L., N.J. Keen and W.M. Wrixon, "Low noise millimeter wave Schottky barrier diodes with extremely low local oscillator power requirements," IEEE MTT-S 1979 International Microwave Symposium Digest, pp. 81-83, April 30 - May 2, 1979.

[174]. Warner, F.L., "Detection of millimetre and submillimetre waves", Millimetre and Submillimetre Waves. Ch.22, Edited by F.A.Benson, London:ILFFE Books Ltd., 1969.

[175]. Wasserstrom, E. and J. McKenna, "The potential due to a charged metallic strip on a semiconductor surface," Bell System Tech. J., vol. 49, pp. 853-877, May-June 1970.

[176]. Weinreb, S. and A.R. Kerr, "Cryogenic cooling of mixers for millimeter and centimeter wavelengths," IEEE Journal of Solid State Circuits, vol. SC-8, no. 1, pp. 58-63, Feb. 1973.

[177]. Wessel, E.G. and R.J. Strain, "Millimeter frequency multiplication with an in-line harmonic generator," IEEE Trans. on Microwave Theory and Tech., vol. MTT-12, no. 1, pp. 139-141, Jan. 1964.

[178]. Whinnery, J.R. and H.W. Jamieson, "Equivalent circuits for discontinuities in transmission lines," Proceedings I.R.E., vol. 32, pp. 98-114, Feb. 1944.

[179]. Wilson, W.J., "The Aerospace low-noise millimeter-wave spectral line receiver," IEEE Trans. on Microwave Theory and Tech., vol. MTT-25, no. 4, pp. 332-335, April 1977.

[180]. Wilson, W.J., Private communication.

[181]. Winderman, J.B., "Perform true DSB-to-SSB noise-figure conversions," Microwaves, vol. 19, no. 7, p. 69, July 1980.

[182]. Wrixon, G.T., "Low-noise diodes and mixers for the 1-2-mm wavelength region," IEEE Trans. on Microwave Theory and Tech., vol. MTT-22, no. 12, pp. 1159-65, Dec. 1974.

[183]. Yamashita, E., and K. Atsuki, "Strip line with rectangular outer conductor and three dielectric layers," IEEE Trans. on Microwave Theory and Tech., vol. MTT-18, no. 5, pp. 238-244, May 1970.

[184]. Young, D.T. and J.C. Irvin, "Millimeter frequency conversion using Au-n-type GaAs Schottky barrier epitaxial diodes with a novel contacting technique," Proc. IEEE, vol. 53, no. 12, pp. 2130-31, Dec. 1965.

[185]. Zimmermann, P. and R.W. Haas, "A broadband low noise mixer for 106-116 GHz," Nachrichtentech. Z., vol. 30, pp. 721-722, Sept. 1977.

BIBLIOGRAPHIC DATA SHEET

1. Report No. NASA TP-2287	2. Government Accession No.	3. Recipient's Catalog No.
4. Title and Subtitle: Topics in the Optimization of Millimeter-Wave Mixers		5. Report Date: March 1984
		6. Performing Organization Code: 980
7. Author(s): Peter H. Siegel, Anthony R. Kerr, and Wei Hwang		8. Performing Organization Report No.
9. Performing Organization Name and Address: Goddard Institute for Space Studies, 2880 Broadway, New York, New York 10025		10. Work Unit No.
		11. Contract or Grant No.
12. Sponsoring Agency Name and Address: National Aeronautics and Space Administration, Washington, D.C. 20546		13. Type of Report and Period Covered: Technical Report
		14. Sponsoring Agency Code
15. Supplementary Notes		

16. Abstract

This report is in three parts:

I. In the first part a user oriented computer program for the analysis of single-ended Schottky diode mixers is described. The program is used to compute the performance of a 140-220 GHz mixer and excellent agreement with measurements at 150 and 180 GHz is obtained. A sensitivity analysis indicates the importance of various diode and mount characteristics on the mixer performance.

II. The second part of this report describes a computer program for the analysis of varactor diode multipliers. The diode may operate in either the reverse biased varactor mode or with substantial forward current flow where the conversion mechanism is predominantly resistive. In addition, a design for a varactor diode doubler, tunable over an output frequency range of 150-220 GHz, is given. The doubler has 10-20% conversion efficiency with an instantaneous bandwidth of 3%.

III. The third section of this report contains a description and analysis of a new H-plane rectangular waveguide transformer. The transformer can be made quickly and easily in split-block waveguide using a standard slitting saw. It is particularly suited for use in the millimeter-wave band, replacing conventional electroformed stepped transformers. A theoretical analysis of the transformer is given and good agreement is obtained with measurements made at X-band. Design curves are included for transitions which have a VSWR <1.2 over a full waveguide band when the impedance ratio is as high as 4 to 1.

17. Key Words (Selected by Author(s)): Millimeter-wave, Mixer, Schottky Diode, Multiplier, Varactor, Waveguide Transformer, Channel Waveguide Transformer		18. Distribution Statement: Unclassified-Unlimited; Subject Category 33	
19. Security Classif. (of this report): Unclassified	20. Security Classif. (of this page): Unclassified	21. No. of Pages: 524	22. Price*: A22

*For sale by the National Technical Information Service, Springfield, Virginia 22161

GSFC 25-44 (10/77)

★U.S. GOVERNMENT PRINTING OFFICE: 1984 -739-010/ 63 REGION NO. 4